

BULGARIAN CHEMICAL COMMUNICATIONS

2014 Volume 46 / Number 1

*Journal of the Chemical Institutes
of the Bulgarian Academy of Sciences
and of the Union of Chemists in Bulgaria*

Aldol condensation of 3-acetylcoumarin derivatives and extraordinary side reactions

S. Stanchev, I. Manolov*

Medical University, Faculty of Pharmacy, Department of Pharmaceutical Chemistry,
2 Dunav St. BG-1000 Sofia, Bulgaria

Received January 18, 2012; Revised April 11, 2013

Aldol reaction of 3-acetylcoumarin derivatives was explored – a derivative without substituents in the aromatic ring (3-acetylcoumarin) (**1**), a derivative containing electron withdrawing substituent (3-acetyl-6-nitrocoumarin) (**1a**) and a derivative containing electron donating substituent (3-acetyl-8-methoxycoumarin) (**1b**). In the first case the typical products of aldol reaction with intact lactone rings were isolated. In the presence of electron donating substituent, a product of aldol reaction was identified, but with opened lactone rings. There was no aldol reaction in the presence of nitro-group and pyran-2-one ring was cleaved.

Key words: 3-acetylcoumarins, aldol reaction, biscoumarins, re-esterification, hemiacetal

INTRODUCTION

The reaction of aldol condensation has been widely used in organic synthesis. In order to synthesize coumarin acidichromic dyes, 7-substituted 3-acetyl-4-hydroxycoumarin has been condensed with 4-*N,N*-dimethylaminobenzaldehyde in benzene, giving products of the aldol reaction with very good yields [1].

The reaction of 3-acetylcoumarin with 3-pyridylaldehyde in butanol in presence of piperidine gave two products - a product of self aldol condensation and a product of mixed condensation [2].

Different coumarin chalcones have been synthesized by aldol reaction of 3-acetyl-4-hydroxy-8-isopropyl-5-methylcoumarin and 3-acetyl-4-hydroxy-6-chloro-7-methylcoumarin with a variety of aromatic aldehydes with very good yields [3, 4]. Microwave-assisted synthesis has been also used for similar reaction intermediates and synthesis of pyrazolinylicoumarins with possible antioxidant activity [5].

Coumarin chalcones and bis-3-coumarinyl-pyridines have been synthesized by a series of two steps of aldol reactions in solventless conditions [6, 7], using the catalyst $\text{Bi}(\text{NO}_3)_3$, immobilized on alumina.

The BF_3 -catalyzed aldol condensations of 5-methyl-2,3-dihydrofuran. The mechanism of formation of hemiacetal group - compound **4** (3-

methoxy-3-hydroxy-2-(2'-hydroxy-5'-nitro)-benzylidenebutanoic acid).

-2-one with RCHO ($\text{R} = \text{Ph}$, halo, nitro, trifluoromethyl, methyl, methoxy or (methylenedioxi)phenyl, thienyl, furyl, cyclohexyl) has given acetyltetrahydrofuranones, which show cardiovascular activity [8].

Efficient aldol dimerization of ketones occurred when the neat ketone is absorbed on basic Al_2O_3 , followed, when necessary, by heating [9]. This could be a reason for forming dimers of acetophenone, 1-indanone and 1-tetralone.

Coumarins containing electron withdrawing group ($-\text{CN}$, $-\text{CONH}_2$, etc.) at third position and tertiary amino group at seventh position in the coumarin ring, usefull as laser dyes, were prepared by Vilsmeier formylation of trimethylsilylated 3-*N,N*-substituted aminophenols, hydrolysis and base-catalyzed aldol condensation with activated methylene compounds [10].

Proline has been used as a catalyst of the aldol reaction for asymmetric direct intermolecular aldol reaction. [11]. Strong solvent influence on the enantiopurity has been observed; anhydrous DMSO has been found to be the most suitable solvent.

4-Hydroxycoumarin has been involved in the aldol type of reaction with benzaldehyde in the presence of NaOH in ultrasonic bath [12]. The product was obtained in high yield.

The aim of the present investigation was to explore the influence of different substituents (electron donating or electron withdrawing) in the benzene ring of 3-acetylcoumarin derivatives on the

* To whom all correspondence should be sent:
E-mail: imanolov@gmx.net

course of the self-aldol condensation and the possible side products.

EXPERIMENTAL

All starting materials were purchased from Merck (Germany), Sigma-Aldrich (USA) and Fluka (Switzerland). They were used without further purification. Melting points were measured in open capillary tubes on a Büchi 535 melting point apparatus (Donau Büchi, Switzerland). The IR spectra were recorded on a Bruker Vertex 70 spectrometer (Bruker, Switzerland) and frequencies were expressed in cm^{-1} . The ^1H NMR spectra were recorded on a Bruker 250 MHz instrument (Bruker, Switzerland) in DMSO-d_6 or CDCl_3 using TMS as an internal standard (chemical shifts were reported in ppm units, coupling constants (J) in Hz).

Mass-spectral analysis was performed by electron ionization on a mass-spectrometer Hewlett-Packard 5973 (USA) at 20 eV.

Synthetic procedure

The 3-acetylcoumarin derivative was dissolved in methanol at reflux. The solution obtained was cooled to room temperature and piperidine was added. The reaction mixture was stirred at ambient temperature for 1.5 h and was concentrated *in vacuo*. The product was crystallized from methanol.

Synthesis of 3-[4-oxo-4-(2-oxo-2H-chromene-3-yl)]-2-butene-2-yl-2H-chromene-2-one /1/ /1/ was obtained from 3-acetylcoumarin (3.76 g, 0.02 mol) and piperidine (0.85 g, 1 mL, 0.01 mol). The product was a white amorphous powder. It was recrystallized from isopropyl alcohol.

Synthesis of 3-[2-hydroxy-4-oxo-3-(2-oxo-2H-chromen-3-yl)isobutyl-2H-chromen-2-one /2/ /2/ was crystallized from the same reaction mixture. It was a white-yellow crystal powder and was recrystallized from ethanol.

Synthesis of dimethyl bis [(3-methoxy-2-hydroxy)-benzylidene] - 3-methyl-5-oxo - 3 - heptenoate /3/

/3/ was synthesized from 3-acetyl-8-methoxycoumarin (1.09 g, 0.005 mol) and piperidine 0.0025 mol (0.21 g, 0.3 mL).

The product was a yellow crystal substance. It was recrystallized from isopropyl alcohol.

Synthesis of 3-methoxy-3-hydroxy-2-(2'-hydroxy-5'-nitro)-benzylidenebutanoic acid /4/

The product */4/* was synthesized from 3-acetyl-6-nitrocoumarin (0.37 g, 0.002 mol) and 0.001 mol (0.09 g, 0.1 mL) of piperidine. The crude product was isolated after removing the methanol and mixing of the viscous substance with water.

The final product was a red - orange amorphous mass. It was recrystallized from water.

The physical and spectral properties of the synthesized compounds are presented in Table 1.

Computational chemistry

All calculations were made with the aid of Horseshoe computer cluster (University of Southern Denmark, Odense). The DFT (Density Functional Theory) calculations about geometry optimization and ESP (Electrostatic Potential) charges were implemented by Gaussian 03 program [13]. B3LYP [14-16] /6-31G(d,p) method was used for geometry optimisation and ESP charges calculations. Gauss View program was used to visualize the results from the calculations.

All initial optimizations and conformational search were implemented by Chem-3-D from ChemOffice package [17], using the MM2 force field.

RESULTS AND DISCUSSION

The aim of this investigation was to study the influence of different types of functional groups on the course of aldol condensation.

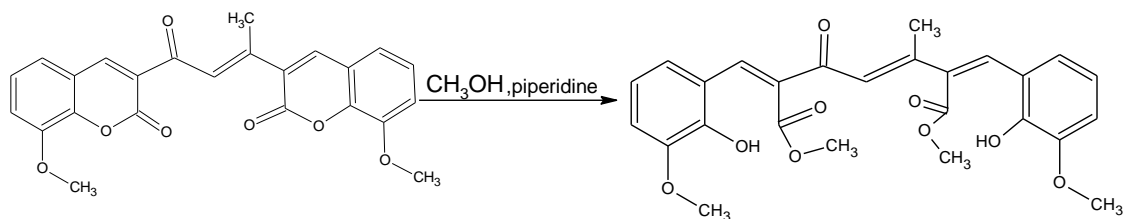
Aldol type of reactions were carried out between two molecules of 3-acetylcoumarin derivatives. The reaction conditions include methanol as solvent and room temperature. The starting compounds were differently substituted 3-acetylcoumarins (3-acetylcoumarin, 3-acetyl-6-nitrocoumarin, 3-acetyl-8-methoxycoumarin), which underwent self condensation to aldol type biscoumarin compounds (**2**, **2a** and **2b**). The latter were dehydrated to unsaturated biscoumarin derivatives (**1**, **1a** and **1b**). The interaction scheme of the aldol reaction is shown in **Scheme 1**.

The probable products are:

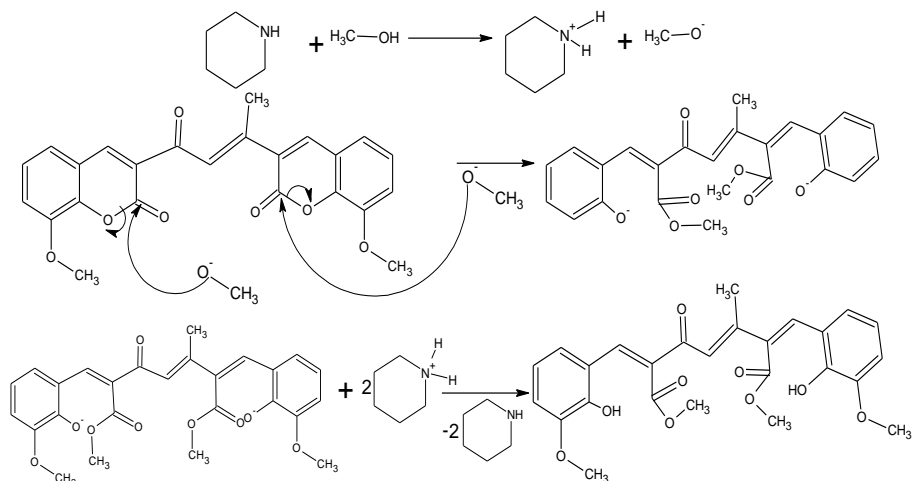
3,3'-[1-oxobut-2-ene-1,2-diyl]-bis(2H-chromene-2-one) /1/; *3,3'-[1-oxobut-2-ene-1,2-diyl]-bis(6-nitro-2H-chromene-2-one) /1a/*; *3,3'-[1-oxobut-2-ene-1,2-diyl]-bis(8-methoxy-2H-chromene-2-one) /1b/*.

These compounds are very convenient for further Michael reaction, because of the activated double bond in one of the coumarin rings.

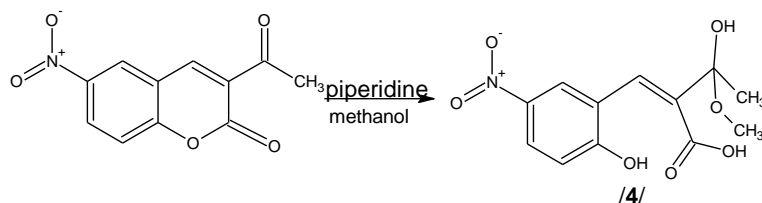
The biscoumarin derivative */1/* was synthesized according to the above mentioned reaction and its structure was proved by spectral methods (IR, MS) and elemental analysis.



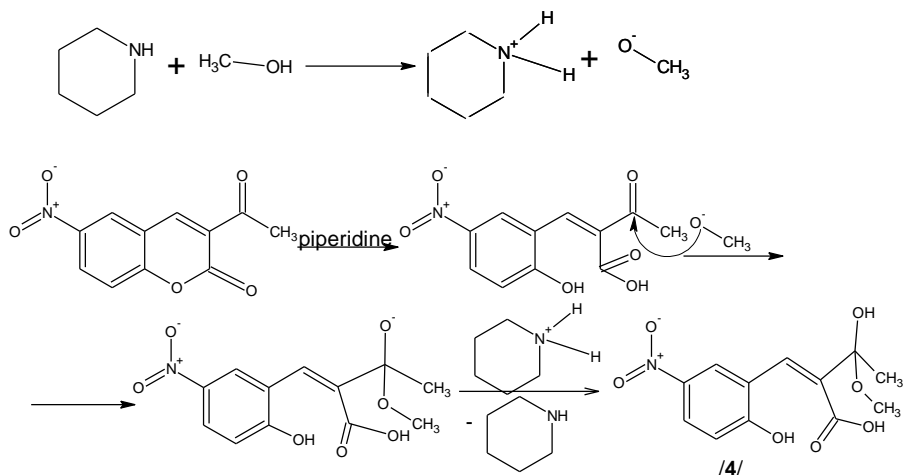
Scheme 2. The reaction of re-esterification of the compound (1) to 3 (dimethyl bis [(3-methoxy-2-hydroxy)-benzylidene]-3-methyl-5-oxo-3-heptenoate).



Scheme 3. Mechanism of re-esterification of the compound 3.



Scheme 4. Mechanism of hydrolysis of lactone group



Scheme 5. The mechanism of formation of hemiacetal group - compound 4 (3-methoxy-3-hydroxy-2-(2'-hydroxy-5'-nitro)-benzylidenebutanoic acid).

Probably, piperidine acts as a base which deprotonates the methanol to a methoxide ion. Thus obtained methoxide ion reacted as a nucleophile, attacked the carbonyl carbon from the lactone ring and opened it. The pyrane-2-one rings were transformed to methyl ester group and a phenol

group was changed to a phenoxide anion. The latter accepts protons from the piperidinium cation and gives back a phenol hydroxyl group, thus a methyl ester being formed. The mechanism of re-esterification for the compound /3/ (dimethyl 2,6-

bis (2-hydroxy-3-methoxybenzylidene)-3-methyl-5-oxohept-3-enedioate) is presented in **Scheme 3**.

No aldol condensation with 3-acetyl-6-nitrocoumarin was performed at all.

There was a reaction of hydrolysis and opening of the lactone ring caused by the basic medium of piperidine. The product is a carboxylic acid containing phenolic group at ortho-position in the aromatic ring. The next step was probably the formation of a methoxide anion, caused by the interaction of piperidine and methanol. Methoxide anion is a strong nucleophile, which attacks and adds to the acetyl carbonyl carbon atom /nucleophilic addition/. In the last step, the protonated piperidine gives its proton, thus the hemiacetal group being formed.

The equation and the probable mechanism of formation of the hemiacetal group - compound **4**/ (3-hydroxy-2-(2-hydroxy-5-nitrobenzylidene)-3-methoxybutanoic acid) are presented in **Schemes 4 and 5**.

CONCLUSIONS

On the basis of the experiments it may be concluded that aldol reaction between two molecules of 3-acetylcoumarin derivatives takes place without any side reactions only when starting from 3-acetylcoumarin non-substituted in the aromatic ring. If there is a methoxy-group (electron donating) at the eighth position in the coumarin ring, a reaction of re-esterification and opening of the lactone ring takes place. If there is a nitro-group (strong electron withdrawing substituent) at sixth position, no aldol interaction is observed. In that case there is only cleavage of the lactone ring, formation of methoxide anion and nucleophilic addition of that anion to the carbonyl group from the acetyl fragment. Finally the hemiacetal structure is observed.

The electron donating substituent in the aromatic ring may facilitate the aldol reaction, but the presence of an electron withdrawing substituent impedes that reaction.

REFERENCES

1. L. Shih, Y. Pey, Y. Ding, *Molecules*, **12**, 1316 (2007).
2. S. El-Morsy, A. Fadda and M. El-Hossini, *J. Ind. Chem. Soc.*, **65**, 699 (1988).
3. T.C. Jalpa, B.B. Jitender, U.D. Kuldip, N.T. Yogesh, J.K. Sudnir, C. Pannecouque, E. DeClercq, A.K. Shah, *Tetrahedron Lett.*, **48**, 8472 (2007).
4. S. Vazquez-Rodriguez, S. Serra, Y. Santos, L. Santana, Lourdes in: Efficient synthesis of coumarin-chalcones hybrids as new scaffold with antibacterial interest (International Electronic Conference on Synthetic Organic Chemistry), J. A. Seijas, T. Vazquez, M. Pilar (eds), 2010.
5. B.S. Jayashree, S. Arora, K.N. Venugopala, *Asian J. Chem.*, **20**, 1 (2008).
6. A.K. Verma, S. Koul, K.K. Kapoor, T.K. Razdan, *Australian J. Chem.*, **60**, 883 (2007).
7. V. Rao, M. Reddy, *Phosphorus, Sulfur and Silicon and the Rel. Elem.* **181**, 461 (2006).
8. J. Coquelet, J.Taoufik, J. Coquelet, P. Tronche, H. Pham, P. Anh, D. Navaro, B. Lassere, *Eur. J. Med. Chem.*, **18**, 301 (1983).
9. J. Muzart, *Synth. Commun.*, **15**, 285 (1985).
10. H. Noack, H. Roemhild, E. Guenther, H. Hartmann, DD Patent 224 592 (1985).
11. Z. Zhang in: Advances in Catalysis, B. Gates, H. Knozinger (eds.), Academic press, Manheim, 2006, p. 188.
12. G. Cravotto, A. Demetri, G. Nano, G. Palmisano, A. Penoni, S. Tagliapetra, *Eur. J. Org. Chem.*, **22**, 4438 (2003).
13. M. Frisch, G. Trucks, H. Schlegel, G. Scuseria, M. Robb, J. Cheeseman, J. Montgomery, T. Vreven, K. Kudin, J. Burant, J. Millam, S. Iyengar, J. Tomasi, V. Barone, B. Mennucci, M. Cossi, G. Scalmani, N. Rega, G. Petersson, H. Nakatsuji, M. Hada, M. Ehara, K. Toyota, R. Fukuda, J. Hasegawa, M. Ishida, T. Nakajima, Y. Honda, O. Kitao, H. Nakai, M. Klene, X. Li, J. Knox, H. Hratchian, J. Cross, V. Bakken, C. Adamo, J. Jaramillo, R. Gomperts, R. Stratmann, O. Yazyev, A. Austin, R. Cammi, C. Pomelli, J. Ochterski, P. Ayala, K. Morokuma, G. Voth, P. Salvador, J. Dannenberg, V. Zakrzewski, S. Dapprich, A. Daniels, M. Strain, O. Farkas, D. Malick, A. Rabuck, K. Raghavachari, J. B. Foresman, J. Ortiz, Q. Cui, A. Baboul, S. Clifford, J. Cioslowski, B. Stefanov, G. Liu, A. Liashenko, P. Piskorz, I. Komaromi, R. Martin, D. Fox, T. Keith, M. Al-Laham, C. Peng, A. Nanayakkara, M. Challacombe, P. Gill, B. Johnson, W. Chen, M. Wong, C. Gonzalez and J. Pople, Gaussian 03. Program for quantum chemistry. Carnegie Mellon University, Pittsburgh (USA) 2003.
14. A. Becke, *Phys. Rev. A* **38**, 3098 (1988).
15. A. Becke, *J. Chem. Phys.*, **96**, 2155 (1992).
16. C. Lee, W. Yang and R. Parr, *Phys. Rev.*, **B 37**, 785 (1988).
17. J. Irwin, ChemOffice 2005, Program for molecular modeling and design, University of California, San Francisco, 2005.

АЛДОЛНА КОНДЕНЗАЦИЯ НА ПРОИЗВОДНИ НА 3-АЦЕТИЛКУМАРИНА С НЕОЧАКВАНИ
СТРАНИЧНИ РЕАКЦИИ

Ст. Станчев, И. Манолов

*Медицински университет, Фармацевтичен факултет, Катедра по фармацевтична химия,
ул. „Дунав” № 2, 1000 София, България*

Постъпила на 18 януари, 2012 г.; коригирана на 11 април, 2013 г.

(Резюме)

Изследвана е алдолната реакция на производни на 3-ацетилкумарина – съединение без заместител в ароматното ядро (3-ацетилкумарин) (**1**), с електроноакцепторен заместител (3-ацетил-6-нитрокумарин) (**1a**) и с електронодонорен заместител (3-ацетил-8-метоксикумарин) (**1b**). При използването на 3-ацетилкумарин се изолират типични продукти на алдолната реакция с непроменен лактонов цикъл. Наличието на електронодонорен заместител в ароматното ядро продуктът на алдолната реакция е с отворен лактонен пръстен. Когато в ароматното ядро има електроноакцепторен заместител (нитро група) алдолна кондензация не протича и изходните продукти остават непроменени.

Synthesis, characterization, antibacterial, antifungal and anthelmintic activities of a new 5 - nitroisatin Schiff base and its metal complexes

R. Rao¹, K.R. Reddy², K.N. Mahendra^{1*}

¹Department of Chemistry, Central College Campus, Bangalore University, Bangalore – 560 001

²Government Science College, Bangalore – 560 001

Received January 23, 2012; Revised October 2, 2012

The copper (II), cobalt (II), nickel (II) and zinc (II) complexes of 5 - nitroisatin Schiff base (L) (L= Schiff base derived from 5-nitroisatin and 2-methyl-4-nitroaniline) were synthesized and characterized. The authenticity of the ligand and its metal complexes has been established by micro analysis, IR, NMR, LC/MS, UV-VIS and electrical conductance measurements. The ligand acts as a bidentate agent in which the carbonyl oxygen and the azomethine nitrogen of 5-nitroisatin are involved in co-ordination. Square planar geometry was proposed for the Cu (II) and Ni (II) complexes and tetrahedral geometry was proposed for the Co (II) and Zn (II) complexes. The ligand and its metal complexes have been screened for antibacterial activity against *Staphylococcus aureus*, *Escherichia coli*, etc. and for antifungal activity against *Aspergillus niger*, *Aspergillus flavous*, etc. The Schiff base and its complexes were also screened for anthelmintic activity on earthworms. Both samples displayed significant activities.

Key words: Schiff base, Isatin, Antibacterial activity, Antifungal activity

INTRODUCTION

Isatin (2,3-dioxindole or indole-2,3-dione) is an endogenous compound identified in humans, and its effect has been studied in a variety of systems. The biological properties of isatin include a range of actions in the brain and offer protection against certain types of infections. Isatin has a range of actions such as CNS-MAO inhibition, anticonvulsant and anxiogenic activities. 5-Nitroisatin with 2-methyl-4-nitro aniline derivatives was found to exhibit interesting applications in physiological studies. Many isatin-derived compounds possess a wide spectrum of medicinal properties and thus have been studied for activity against tuberculosis, leprosy, fungal, viral and bacterial infections, etc. [1– 4].

Z.H. CHOCHAN *et al.* have prepared Schiff bases of isatin with 2-aminothiozoles and its metal complexes. It was observed that such compounds would carry medicinal properties mainly as anticonvulsants. In the present study, we mainly deal with the synthesis and characterization of a novel Schiff base formed by the condensation of 5-nitroisatin with 2-methyl-4-nitroaniline and its complexes with cobalt (II), nickel (II), copper (II)

and zinc (II). Thus another class of isatin incorporating metal-ligand as antibacterials, antifungals and anthelmintics has been introduced. The ligand and its metal complexes have been characterized by IR, NMR, UV-visible, LC/MS, molar conductance, magnetic moment and elemental analysis data.

The resulting Schiff base and its metal complexes were screened for antibacterial activity against *Staphylococcus aureus*, *Escherichia coli*, *Bacillus subtilis*, *S. typhi* and *Pseudomonas aeruginosa* and for antifungal activity against *Aspergillus niger*, *Aspergillus flavous* and *Candida Albicans* by the agar-well diffusion method. The anthelmintic activity on earthworms (*Pheretima posthumous*) of the ligand and its metal complexes was also tested by a reported method [5]. The ligand and its complexes showed varying activity against the strains and their activity was enhanced on coordination/chelation.

EXPERIMENTAL

Material and Methods

All chemicals were purchased from Sigma – Aldrich and used as such. The CHN analysis was carried out by using CHNS analyser of Elementar Vario III. IR spectra were recorded on a Perkin

* To whom all correspondence should be sent:
E-mail: mahendra_kadidal@yahoo.com

Elmer IR spectrometer. NMR spectra were recorded on a Varion FT – NMR apparatus. Mass spectra were recorded using a LC/MS instrument. UV-visible spectra were recorded on the UV-visible spectrophotometer of Shimadzu Hitachi. The melting points were determined in open capillaries and are uncorrected; conductance measurements were measured on a Systronics conductivity meter in DMF. \

Preparation of the Schiff base (L)

Schiff base ligand was prepared according to the following procedure. Ethanolic solutions of 5-nitroisatin (Fig. 1) (0.01 mol, 1.92 g) in 50 ml and 2-methyl-4-nitroaniline (Fig. 2) (0.01 mol, 1.52 g)

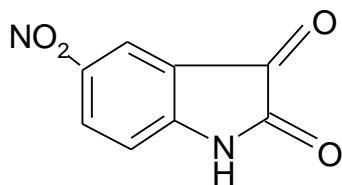


Fig. 1.

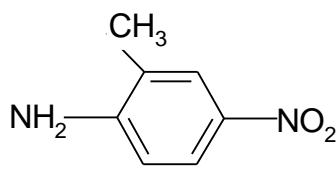


Fig. 2.

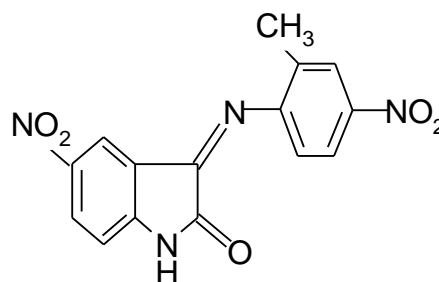


Fig. 3.

Preparation of complexes

The metal complexes were prepared by adding a solution of the metal salt (0.01 mol) in 50 ml absolute ethanol to 100 ml of an ethanolic solution of the ligand (0.01 mol) (1:1 ratio) and heating under reflux conditions at about 80–90°C for 2–4 h. Then the reaction mixture was evaporated to a small volume. On cooling, the metal complexes crystallized and were filtered, washed thoroughly with ethanol and dried under vacuum over fused calcium chloride.

Biological Activity

Antibacterial activity, antifungal activity and anthelmintic activity [in vitro] measurements

The Schiff base and its complexes were screened for antibacterial activity against *Staphylococcus aureus*, *Escherichia coli*, *Bacillus subtilis*, *S. typhi*, and *Pseudomonas aeruginosa*. The antifungal activity against *Aspergillus niger*, *Aspergillus flavus* and *Candida Albicans* was checked by the agar-well diffusion method.

The following strains were used: bacteria - *Staphylococcus aureus* ATCC 25922, *Escherichia coli* ATCC 25923, *B. subtilis* ATCC 6633, *S. typhi* 19430, *Pseudomonas aeruginosa* ATCC 27853 and fungi - *Aspergillus niger* ATCC6275, *Aspergillus flavus* ATCC4797 and *Candida albicans*10231.

in 50 ml were mixed and refluxed for about 1 h. The reaction mixture was evaporated to a small volume and left to cool. The resulting Schiff base ligand (Fig. 3) precipitated on cooling and was filtered off, washed with ethanol and recrystallized from ethanol. The purity of the Schiff base ligand was monitored by TLC using 1:1 ethyl acetate and petroleum ether as an eluent. The product, separated by column chromatography, had a molecular weight of 326, corresponding to the molecular formula of the Schiff base $C_{15}H_{10}N_4O_5$ [L]. The yield of Schiff base was 90%.

The bacteria and fungi were obtained from the Government Science College, Bangalore.

The anthelmintic activity of the ligand and its metal complexes was tested on earthworms (*Pheretima posthumous*) using a reported method.

The bacterial /fungal inoculums of two to six hours containing approximately 10^5 cfu/ml were used in these assays. The wells were dug in the media with the help of a sterile metallic borer with centers at least 24 mm. The recommended amounts of 100 μ l of the test sample were introduced into the corresponding wells. The other wells supplemented with DMF and standard drugs served as negative and positive controls respectively; the plates were incubated immediately at 37°C for 24 h. Activity was determined by measuring the diameter of zones showing the complete inhibition in mm. Gentamycin (positive control) was used as a standard drug for antibacterial activity and nystatin (positive control) was used as a standard for antifungal activity. The positive controls were supplied by the Government Science College, Bangalore.

The Schiff base and its complexes were screened for anthelmintic activity on earthworms (*Pheretima posthumous*) using the standard piperazine citrate.

RESULTS AND DISCUSSION

Chemistry

This section deals with analytical data, conductivity measurements, IR, NMR, UV-visible and mass spectral data. All metal complexes are colored solids stable towards air and have high melting points (above 200°C). The complexes have the general formula $[MLCl_2]$ where M= Co(II) or Zn(II) and $[M LCl.H_2O]Cl$ where M= Cu(II) or Ni(II).

The complexes are insoluble in water and common organic solvents but are soluble in DMF and DMSO. Hence the molecular weights could not be determined. Analytical data of the complexes suggest that the metal to ligand ratio in all complexes is 1:1.

The analytical and physical data of the ligand and its complexes are described as follows.

(a) Ligand ($C_{15}H_{10}N_4O_5$): color yellow, yield % 90.0, M. P. °C 180, elemental analysis %

calc./found C: 55.21/55.01, H: 3.07/3.04, N: 17.18/17.05

IR(cm^{-1}): 3342 (NH isatin), 1715(C=O), 1642(C=N)

1H NMR(δ): isatin: 8.82(s), 7.86(d), 7.83(d); aniline: 7.86(d), 7.83(d), 7.08(d); methyl: 6.47(s)

N-H 11.65 (br)

UV(cm^{-1}): 27777, 36363

Mass spectra (m/z): 325.5

(b) Complex $[CuLCl.H_2O]Cl$: color light brown, yield % 87.4, M.P. °C:230(d), elemental

analysis % calc./found: C 37.66/37.52, H: 2.51/2.47, N: 11.72 /11.68,

molar conductance $\lambda_{MS} cm^2 mol^{-1}$:88

IR(cm^{-1}): 3345(NH isatin), 1700(C=O), 1621(C=N), 535(M-O), 479(M-N), 326(M-Cl)

UV(cm^{-1}): 26315,15748 ESR (μ_{eff} BM): 1.85

(c) Complex $[Co LCl_2]$: color light brown, yield % 89.2, M.P. ° C242(d), elemental analysis %

calc./found: C 39.48/39.33, H: 2.19/2.16, N: 12.28/12.21, molar conductance $\lambda_{MS} cm^2 mol^{-1}$:29

IR(cm^{-1}): 3343 (NH isatin), 1701(C=O), 1622(C=N), 537(M-O), 475(M-N), 327(M-Cl)

UV(cm^{-1}): 27027,15503 ESR (μ_{eff} BM): 4.51

(d) Complex $[NiLCl.H_2O]Cl$: color light brown, yield % 89.8, M.P. °C 236(d), elemental analysis %

calc./found: C: 38.16/38.04, H:2.54/2.50, N: 11.87 /11.81, molar conductance $\lambda_{MS} cm^2 mol^{-1}$: 71

IR(cm^{-1}): 3349(NH isatin), 1704(C=O), 1621(C=N), 536(M-O), 488(M-N), 334(M-Cl)

UV(cm^{-1}): 28571, 14814 ESR (μ_{eff} BM): 3.68

(e) Complex $[Zn LCl_2]$: color: light brown, yield % 86.3, M.P. °C: 224(d), elemental analysis

% calc./found: C: 38.93/38.84, H: 2.16/2.13, N: 12.11/12.05, molar conductance $\lambda_{MS} cm^2 mol^{-1}$: 22

IR (cm^{-1}): 3328(NH isatin), 1705(C=O), 1623(C=N), 542(M-O), 484(M-N), 332(M-Cl)

1H NMR(δ): isatin: 8.90(s), 7.91(d), 7.89(d) aniline: 7.90(d), 7.95(d), 7.21(d) methyl: 6.47(s)

N-H12.65 (br)

UV(cm^{-1}): 28169,21978, ESR: diamagnetic

IR Spectra

The infrared absorption frequencies along with their tentative assignments for the major absorption bands pertaining to the ligand and its complexes are presented in Table 3. In the present investigation the tentative assignments of the infrared bands for most of the major peaks are based on the assignments of previous workers.

The IR spectrum of the free ligand is characterized mainly by the strong bands at 3342, 1715 and 1642 cm^{-1} which were attributed to the stretching frequencies of NH (aromatic), C=O and C=N (azomethine) groups, respectively and reflected in the spectral data of the metal complexes.

The IR spectra of the complexes showed a lower shift of wave numbers of both azomethine (ν C=N) and heteroatomic moieties by about 15 cm^{-1} respectively. The band located at 1700 cm^{-1} in the ligand attributed to (ν C=O) moiety of isatin also moved to the lower frequency side by about 15 cm^{-1} . The ν M-O, ν M-N and ν M-Cl bands in the IR region were also clearly seen. These data on comparison with the spectra of the chelates suggest the azomethine-N and isatin-O of the ligand [7-9].

NMR Spectra

The proton NMR spectral data of the ligand and of the Zn complex are presented in Table 4. The number of protons calculated from the integration of 1H NMR spectra is in accordance with that expected from CHN analyses (Table 2) [10-11].

Mass Spectra

The molecular weight 326 for $C_{15}H_{10}N_4O_5$ and a molecular ion peak is found at 325.5 in the mass spectrum supporting the molecular formula of the Schiff base.

ESR Spectra

The X-band ESR spectrum of the powdered sample of the copper complex was recorded at room temperature in solid state on X-band at a frequency of 9.1 GHz under magnetic field of 3000 G. The spectral profile is typical of axial type

Table 1. Thermo gravimetric analysis of the complexes

Compound	Stage	Temperature °C	Weight Loss (%) Calculated/Found	Species Lost	Residue
[CuLCl.H ₂ O]Cl	1	100	7.43/7.38	Uncoordinated Cl	CuO
	2	210	11.19/11.15	Coordinated Cl+H ₂ O	
	3	320	68.20/68.15	Ligand	
[Co LCl ₂]	1	100	15.60/15.49	Coordinated Cl	Co ₂ O ₃
	2	300	71.50/71.34	Ligand	
[Ni LCl.H ₂ O]Cl	1	100	7.53/7.39	Uncoordinated Cl	NiO
	2	210	11.34/11.18	Coordinated Cl+H ₂ O	
	3	330	69.11/69.05	Ligand	
[Zn LCl ₂]	1	100	15.36/15.24	Coordinated Cl	ZnO
	2	310	70.50/70.32	Ligand	

($g_{\parallel} > g_{\perp}$) implying $d_{x^2-y^2}$ ground state. The g_{\parallel} and g_{\perp} are found to be 2.26 and 2.10, respectively.

The g_{av} is related to g_{\parallel} and g_{\perp} by the equation $g_{av} = (g_{\parallel} + 2g_{\perp}) / (g_{\parallel} + 2)$ and is calculated to be 2.6. Since the value of g_{\parallel} is less than 2.6, a considerable covalent character of the complex in the metal-ligand bond has suggested [12].

Thermogravimetric studies

The TGA studies of the complexes were carried out in nitrogen atmosphere at a rate of 10° per minute up to 700°C. The data are presented in Table 1. In the thermal decomposition studies, a general pattern of uncoordinated chloride, coordinated chloride, water and ligand finally gave the respective oxides at a higher temperature.

UV-visible and magnetic susceptibility measurements

The electronic spectrum of the copper complex exhibits bands at 26315 cm^{-1} and 15748 cm^{-1} which can be assigned to $2B_{1g} \rightarrow 2A_{1g}$ and $2B_{1g} \rightarrow 2E_{1g}$ transitions. These transitions, as well as the measured value of the magnetic moment ($\mu_{\text{eff}} = 1.85 \mu_B$) suggest a square-planar stereochemistry of the compound. The visible electronic absorption spectrum of the cobalt (II) complex is dominated by the highest energy $4A_{2g} \rightarrow 4T_{1g}$ (P) transition, which is a typical one for tetrahedral Co (II) complexes. The magnetic moment value (4.51 μ_B) and the light brown color of the cobalt (II) complex also suggest tetrahedral stereochemistry. The electronic spectrum of the nickel complex shows two bands at 28571 cm^{-1} and 14814 cm^{-1} which are attributed to $1A_{1g} \rightarrow 1A_{2g}$ and $1A_{1g} \rightarrow 1B_{2g}$ transitions. These transitions, as well as the measured value of the magnetic moment (3.68 μ_B) suggest a square-planar stereochemistry of the compound. Since the zinc ion has a d^{10} configuration, the absorption at 28169 cm^{-1} could be assigned to a charge transfer transition. However, taking into account the

spectrum and the configuration of the zinc (II) ion, a tetrahedral geometry could be assumed for its complex [13–14].

BIOLOGICAL ACTIVITIES

A) Antibacterial activity

In view of their potent biological activity, the ligand and its metal complexes were tested against five bacteria, viz., *Staphylococcus aureus* (*S. aureus*) and *Bacillus subtilis* which are representatives of gram positive bacterial groups and *Escherichia coli* (*E. coli*), *Pseudomonas aeruginosa* and *Salmonella Typhi* which are representative of gram negative bacterial groups. These bacterial strains are chosen as they are potential pathogens of human beings. The biological screening was conducted by the disc method according to [5, 15]. The enhancement in the activity can be explained on the basis of the chelation theory and the results obtained are presented in Table 2. The ligand and its metal complexes exhibit more activity at higher concentration.

B) Antifungal Activity

The antifungal activity of the ligand and its metal complexes was tested against the fungi *Aspergillus niger*, *Aspergillus flavus* and *Candida albicans* and the results obtained are presented in Table 3. The ligand and its metal complexes exhibit more activity at higher concentration.

C) Anthelmintic activity [in vitro]

Anthelmintic activity of the ligand and its metal complexes was tested on earthworms (*Pheretima posthuma*) by a reported method [5, 15]. Normal saline has no effect till 10 hours. The standard, piperazine citrate, took 18 minutes till the death of the worms and the results obtained are presented in Table 4. Amongst the complexes under investigation, the complexes of Cu(II), Co(II),

Table 2. Antibacterial activity of the Ligand and its complexes [Concentration(($\mu\text{g/ml}$)]

Compound	50	100	150	200	250	300	350	400	450	500
$\text{C}_{15}\text{H}_{10}\text{N}_4\text{O}_5(\text{L})$ a,b,c,d,e↓	-	-	-	+	++	++	++	++	++	+++
	-	-	+	+	+	++	++	++	++	+++
	+	+	+	+	+	+	++	++	++	+++
	-	-	+	+	+	+	++	++	++	+++
	-	-	+	+	+	+	+	++	++	+++
[CuLClH ₂ O]Cl	+	+	++	++	++	++	++	++	++	+++
	+	+	++	++	++	++	++	++	++	+++
	+	+	+	++	++	++	++	++	++	++
	+	+	+	+	+	+	++	++	++	++
	+	+	+	+	+	+	++	++	++	+++
[Co LCl ₂]	+	+	++	++	++	++	++	++	+++	+++
	+	+	+	++	++	++	++	++	++	+++
	+	+	+	++	++	++	++	++	+++	+++
	+	+	+	+	+	++	++	++	++	+++
	+	+	+	+	++	++	++	++	++	+++
[Ni LClH ₂ O]Cl	+	++	++	++	++	++	++	++	+++	+++
	+	+	+	+	+	++	++	++	+++	+++
	-	-	-	+	+	+	++	++	++	++
	+	+	+	+	+	+	++	++	++	+++
	+	+	+	+	+	++	++	++	++	+++
[Zn LCl ₂]	+	+	+	+	++	++	++	+++	+++	+++
	+	+	+	++	++	++	++	++	++	+++
	-	-	-	-	+	+	++	++	++	++
	+	+	+	+	+	++	++	++	++	+++
	+	+	+	+	++	++	++	++	+++	+++
Negative Control(DMF)	Nil									
Standard(mm)Positive control	a-25,b-26,c-22,d-29,e-27									

(a) Escherichia coli (b); S. aureus; (c) Bacillus subtilis; (d) S. typhi; (e) Pseudomonas aeruginosa ($\mu\text{g/ml}$). DMF(control): Nil, No effect up to 24 hours. Key for interpretation: a) - : Inactive Less than 10 mm; b) + Weakly active between 10 – 14 mm. c) ++ : Moderately active between 15 – 17 mm and d) +++: Highly active above 18 mm

Table 3. Anti fungal activity measurements of the ligand and its complexes[Concentration(($\mu\text{g/ml}$)]

Compound	50	100	150	200	250	300	350	400	450	500
$\text{C}_{15}\text{H}_{10}\text{N}_4\text{O}_5(\text{L})$ a,b,c↓	+	+	+	+	++	++	++	++	++	++
	+	+	+	+	++	++	++	++	++	++
	+	+	+	+	++	++	++	++	++	++
[CuLClH ₂ O]Cl	-	+	+	+	+	++	+++	+++	+++	+++
	-	+	+	+	+	++	+++	+++	+++	+++
	-	+	+	+	+	++	+++	+++	+++	+++
[Co LCl ₂]	-	+	+	+	+	++	++	+++	+++	+++
	-	+	+	+	+	++	++	+++	+++	+++
	-	+	+	+	+	++	++	+++	+++	+++
[Ni LClH ₂ O]Cl	-	-	+	+	+	++	+++	+++	+++	+++
	-	-	+	+	+	++	+++	+++	+++	+++
	-	-	+	+	+	++	+++	+++	+++	+++
[Zn LCl ₂]	-	+	+	+	+	++	+++	+++	+++	+++
	-	+	+	+	+	++	+++	+++	+++	+++
	-	+	+	+	+	++	+++	+++	+++	+++
Negative Control(DMF)	Nil									
Standard(mm)Positive control	a-23,b-21,c-25									

Ni(II) and Zn(II) showed higher activity than the standard.

CONCLUSIONS

The Schiff base acts as a bidentate ligand with azomethine nitrogen and negatively charged oxygen atom as donors. The probable geometry of the structure for the complexes of Co and Zn would be tetrahedral and for those of Cu and Ni - square planar (Figs. 4 and 5, respectively). The antibacterial and antifungal activity of the ligand is greatly enhanced upon complexation with metal ions. Almost all complexes are highly active at higher concentration (500 µg/ml) except a few that are moderately active. The anthelmintic activity of the ligand is greatly enhanced upon

complexation with metal ions, particularly Co, Ni and Zn.

Table 4. Anthelmintic activity of the investigated compounds..

Compound	Time taken for paralysis and death of worms	
	Paralysis (min)	Death (min)
Blank Normal Saline	No effect for 10 hours	
Standard (Piperazine citrate)	10	15
C ₁₅ H ₁₀ N ₄ O ₅ (L)	9	14
[CuLCl.H ₂ O]Cl	8	12
[Co LCl ₂]	11	17
[Ni LCl.H ₂ O]Cl	13	20
[Zn LCl ₂]	21	27

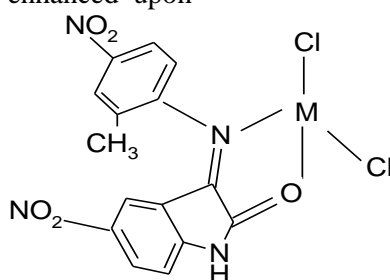


Fig 4. Tetrahedral geometry M= Co and Zn.

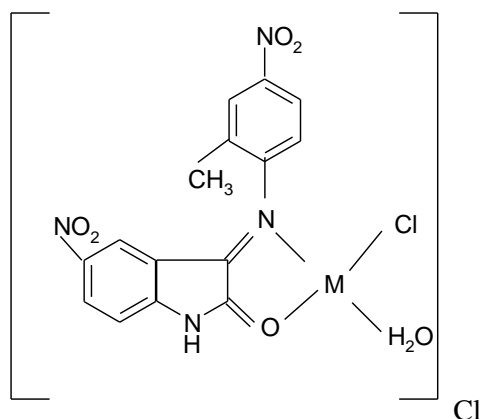


Fig. 5. Square planar geometry. M= Cu and Ni.

REFERENCES

- Z.H. Chohan, H. Perveza, A. Rauf, K.M. Khan, C.T. Supuran, *J. Enzyme Inhibition. Medicinal Chemistry*, **19**, (5) 417-423 (2004),.
- R. Protivinsky, *Antibiotics&Chemotherapy*, **17**, 101 (1971).
- K.C. Joshi, V.N. Pathak, S.K. Jain, *Pharmazie*, **35** 677 (1980).
- R.G. Shepherd, I. Burger, ed., *Medicinal Chemistry*, 1970 (Wiley, New York).
- Atta-ur-Rahman, M.Iqbal Choudhary, W.J. Thomson, *Bioassay Techniques for Drug Development*, Harwood Academic Publishers, The Netherlands. 20, 2001.
- K. Nakamoto, *Infrared Spectra of Inorganic and Coordination Compounds*, 2nd ed. Wiley-Interscience, 1970.
- K. Nakamoto, *Infrared & Raman Spectra of Inorganic & Coordination Compounds. Part-B*, 5th ed., Wiley Interscience Publication, 1997.
- M. Shakir, O.S.M. Nasman, S.P. Varkey, *Polyhedron* **15**, 309 (1996); M. Shakir, K.S. Islam, A.K. Mohamed, M. Shagufa, S.S. Hasan, *Transit. Met. Chem.* **24**(5) 577-580 (1999).
- S. Chandra, R. Kumar, *Transit. Met. Chem.* **29**, 269 (2004).
- W.W. Simmons, *The Sadtler Handbook of Proton NMR Spectra*, Sadtler Research Laboratories, Inc. 1978

11. D. Pado, Organic Structure Determination, Prentice Hall International, London, 1969
12. T.A. Khan, S. Naseem, S.N. Khan, A.U. Khan, M. Shakir, *Spectrochim. Acta*, **73(4)**, 622-629 (2009).
13. F. A. Cotton, G. Wilkinson, Advanced Inorganic Chemistry, 1999, Wiley-Interscience: New York
14. A.I. Vogel, A Text Book of Quantitative Chemical Analysis, 1989, 5th ed., Longman, London
15. K. Rama Krishna Reddy and K. N. Mahendra, *Russ. J. Inorgan. Chem.*, **53(6)** 906-912(2008).

СИНТЕЗА, ОХАРАКТЕРИЗИРАНЕ, АНТИБАКЕРИАЛНИ, ПРОТИВОГЪБИЧНИ И АНТИХЕЛМИНТНИ СВОЙСТВА НА 5-НИТРОИЗАТИН-ШИФОВА БАЗА И НЕЙНИТЕ КОМПЛЕКСИ

Р. Рао¹, К.Р. Реди², К.Н. Махендра¹

¹Департамент по химия, Централен кампус на колежа, Университет в Бангалор, Бангалор – 560 001, Индия

²Правителствен научен колеж, Бангалор – 560 001, Индия

Постъпила на 23 януари, 2012 г.; коригирана на 2 октомври, 2012 г.

(Резюме)

Синтезирани и охарактеризирани са комплексите на медта (II), кобалта (II), никела (II) и цинка (II) на 5 – нитроизатонива Шифова база (L) (L= Шифова база получена от 5-нитроизатин и 2-метил-4-нитроанилин). Автентичността на лигандите и тяхниѐ метални комплекси е установена чрез микроанализ, ИЧ-, ЯМР-, ГХ/МС-, UV-VIS-спектроскопии и измервания на електропроводността. Лигандите действат като би-дентатни агенти в които карбонилния кислород и азо-метиновия азот в 5-нитроизатина участват в координирането. За структурата на комплексите на Cu (II) и (II) е установена планарна квадратна геометрия, а за комплексите на Co (II) и Zn (II) – тетраедрична. Лигандите и тяхните комплекси са изпитани за антибактериална активност спрямо *Staphylococcus aureus*, *Escherichia coli* и др., за противогъбични свойства - спрямо *Aspergillus niger*, *Aspergillus flavous* и др. Шифовата база и нейните комплекси са изпитани и за антихелминтни свойства спрямо земни червеи. И двете групи съединения проявяват значителна активност.

Silica-bonded *N*-propyl sulfamic acid: a recyclable catalyst for microwave-assisted synthesis of various dihydropyrano[3,2-*c*]chromenes

A. Gharib^{1,2*}, N. Noroozi Pesyan³, L. Vojdani Fard⁴, M. Roshani¹

¹Department of Chemistry, Islamic Azad University, Mashhad, IRAN

²Agricultural Researches and Services Center, Mashhad, IRAN

³Department of Chemistry, Faculty of Science, Urmia University, 57159 Urmia, IRAN

⁴Education Ministry, Education Organization of Razavi Khorasan, Mashhad, IRAN

Received March 13, 2012; Revised February 13, 2013

A novel and simple method for the synthesis of dihydropyrano[3,2-*c*]chromenes is reported. The products are obtained in good to excellent yields by a simple, mild and efficient procedure using silica-bonded *N*-propyl sulfamic acid (SBNPSA) as a catalyst under microwave irradiation conditions.

Keywords: Silica-bonded *N*-propyl sulfamic acid (SBNPSA); chromenes; dihydropyrano[3,2-*c*]chromenes; Irradiation microwave

INTRODUCTION

Chromones constitute one of the major classes of naturally occurring compounds, and interest in their chemistry continues unabated because of their usefulness as biologically active agents [1]. Some of the biological activities attributed to chromone derivatives include cytotoxic (anticancer) [2-4], neuroprotective [5], HIV-inhibitory [6], antimicrobial [7,8], antifungal [9] and antioxidant activity [10]. Due to their abundance in plants and their low mammalian toxicity, chromone derivatives are present in large amounts in the diet of humans [11]. The synthesis of chromone derivatives is a research field of great interest and long history [12]. In general, chromones are synthesized by the cyclodehydration of 1-(*o*-hydroxyaryl)-1,3-diketones or equivalent intermediates catalyzed by strong acids or strong bases (Vilsmeier-Haack reaction) [13]. They have been prepared on a large scale by the Allan-Robinson synthesis involving acylation-rearrangement, and subsequent cyclization [14]. This methodology has been followed in the synthesis of chromone derivatives with quaternary ammonium functionalities which show not only activity of cosmetic interest but also for hair sustainability, as well as in the asymmetric synthesis of optically active 4-chromone derivatives [15]. In the Baker-Venkataraman synthesis [16], internal Claisen condensation of 2-aryloxy-1-acetylarenes is employed as a key step. More recently the synthesis of chromone derivatives was

accomplished by intramolecular ester carbonyl olefination [17] or Pd-catalyzed regioselective carbonylative annulation of *o*-iodophenol acetates and acetylenes [1, 18]. 3-Cyanochromones have been synthesized in a mild and facile way from oximes derived from 3-formyl chromones using dimethyl formamide/thionyl chloride complex [19]. As for aminochromones, useful for the prevention of allergic and asthmatic reactions in mammals, as indicated by tests in rats, they have been synthesized either by rearrangement of isoxazoles [20] or from chlorinated salicylic acids and malononitrile in aqueous NaOH or NaH [21]. 2-Amino-4H-chromenes and their derivatives are of considerable interest as they possess a wide range of biological properties [22], such as spasmolytic, diuretic, anticoagulant, anticancer and antianaphylactic activity [23]. In addition, they can be used as cognitive enhancers for the treatment of neurodegenerative diseases, including Alzheimer's disease, amyotrophic lateral sclerosis, Huntington's disease, Parkinson's disease, AIDS associated dementia and Down's syndrome as well as for the treatment of schizophrenia and myoclonus [24]. The development of multi-component reactions (MCRs) has attracted much attention from the vantage point of combinatorial and medicinal chemistry [25]. Many important heterocycle syntheses are multi-component reactions. Recently, the synthesis of 4H-chromenes and dihydropyrano[3,2-*c*]chromenes derivatives has attracted great interest to their biological and pharmacological activities [26]. The 4H-chromene derivatives show various pharmacological properties such as spasmolytic, diuretic,

* To whom all correspondence should be sent:
E-mail: aligharib5@yahoo.com

anticoagulant, anticancer, and antianaphylactic activities [26]. Substituted 4*H*-chromenes are particularly versatile compounds that bind Bcl-2 protein (B-cell lymphoma 2) and induce apoptosis in tumor cells.

EXPERIMENTAL

All materials and solvents were purchased from Merck and Fluka. Melting points were determined in open capillary tubes in an Electrothermal IA 9700 melting point apparatus. ¹H NMR spectra were recorded on a Bruker-300 MHz instrument using tetramethylsilane (TMS) as an internal standard. IR spectra were recorded on a Shimadzu-IR 470 spectrophotometer. The mass spectra were scanned on a Varian Mat CH-7 instrument at 70 eV. Irradiation was carried out in a domestic microwave oven (Electra, 2450 MHz, 700 W) for optimized time. All yields refer to isolated products. Silica bonded *N*-propyl sulfamic acid (SBNPSA) was prepared according to our previously reported procedure [27].

*General procedure for the preparation of 2-amino-5-oxo-dihydropyrano[3,2-*c*]chromenes:*

A mixture of aldehyde (12 mmol), malononitrile (1.5 mmol), 4-hydroxycoumarin (12 mmol) and silica bonded *N*-propyl sulfamic acid (SBNPSA) (0.1 g) in H₂O (5 mL) and EtOH (5 mL) was stirred and irradiated in a microwave oven at 700 W for the appropriate time (Table 1). After completion of the reaction, which was monitored by TLC, the mixture was cooled to room temperature. The solid product was collected by filtration, washed with water and aqueous ethanol and purified by recrystallization from ethanol.

Selected spectral data:

*2-amino-5-oxo-4-(3,4,5-trimethoxyphenyl)-4,5-dihydropyrano[3,2-*c*]chromene-3-carbonitrile* (Table 1, entry 1): m.p. 224-226 °C; (m.p. 224-226 °C [28,29]); IR (KBr) $\nu_{\max}/\text{cm}^{-1}$: 3425, 3321, 2191, 1672, 1595, 1375, 1154. ¹H NMR (DMSO-*d*₆, 300 MHz) δ : 3.63 (s, 3H, CH₃), 3.71 (s, 6H, CH₃), 4.43 (s, 1H, H), 6.52 (s, 2H, NH₂), 7.42 (t, 2H, aromatic), 7.65 (t, 2H, aromatic), 7.87 (2d, 3H, aromatic). ¹³C NMR (DMSO-*d*₆, 250 MHz) δ : 160.1, 158.5, 154.0, 153.3, 152.6, 139.4, 137.1, 133.3, 125.1, 123.0, 119.7, 117.0, 113.6, 105.4, 104.1, 60.4, 58.4, 56.0, 37.7. MS (m/z): 404. Anal. Calc. C, 65.02; H, 4.46; N, 6.89%. Found: C, 65.0; H, 4.27; N, 6.93%.

*2-amino-4-(2,6-dichlorophenyl)-5-oxo-4,5-dihydropyrano[3,2-*c*]chromene-3-carbonitrile* (Table 1, entry 2): m.p. 275-278 °C, (m.p. 274-277 °C [28,29]); IR (KBr) $\nu_{\max}/\text{cm}^{-1}$: 3422, 3320, 2190, 1676, 1595, 1377, 1151. ¹H NMR (DMSO-*d*₆, 300

MHz) δ : 4.29 (s, 1H, H), 6.85 (s, 2H, NH₂), 7.43 (t, 2H, aromatic), 7.66 (t, 2H, aromatic), 7.84 (2d, 3H, aromatic). ¹³C NMR (DMSO-*d*₆, 250 MHz) δ : 161.2, 160.8, 159.3, 152.5, 139.4, 138.4, 135.6, 128.3, 127.5, 123.4, 119.2, 116.4, 115.4, 113.6, 105.3, 58.2. MS (m/z): 384. Anal. Calc. C, 59.24; H, 2.62; N, 7.27%. Found: C, 59.21; H, 2.65; N, 7.25%.

*2-amino-4-(2,3-dichlorophenyl)-5-oxo-4,5-dihydropyrano[3,2-*c*]chromene-3-carbonitrile* (Table 1, entry 3): m.p. 274-276 °C, (m.p. 273-276 °C [29]); IR (KBr) $\nu_{\max}/\text{cm}^{-1}$: 3423, 3320, 2192, 1675, 1595, 1377, 1150. ¹H NMR (DMSO-*d*₆, 300 MHz) δ : 4.29 (s, 1H, H), 6.85 (s, 2H, NH₂), 7.43 (t, 2H, aromatic), 7.66 (t, 2H, aromatic), 7.84 (2d, 3H, aromatic). ¹³C NMR (DMSO-*d*₆, 250 MHz) δ : 161.1, 160.7, 159.4, 152.5, 139.5, 138.4, 135.7, 128.2, 127.4, 123.6, 119.2, 116.6, 115.3, 113.5, 105.4, 58.3. MS (m/z): 384. Anal. Calc. C, 59.24; H, 2.62; N, 7.27%. Found: C, 59.20; H, 2.65; N, 7.26%.

*2-amino-4-(2,4-dichlorophenyl)-5-oxo-4,5-dihydropyrano[3,2-*c*]chromene-3-carbonitrile* (Table 1, entry 4): m.p. 254-256 °C, (m.p. 255-258 °C [29]); IR (KBr) $\nu_{\max}/\text{cm}^{-1}$: 3420, 3322, 2190, 1677, 1595, 1377, 1152. ¹H NMR (DMSO-*d*₆, 300 MHz) δ : 4.27 (s, 1H, H), 6.83 (s, 2H, NH₂), 7.45 (t, 2H, aromatic), 7.67 (t, 2H, aromatic), 7.80 (2d, 3H, aromatic). ¹³C NMR (DMSO-*d*₆, 250 MHz) δ : 161.3, 160.6, 159.4, 152.6, 139.5, 138.4, 135.7, 128.2, 127.4, 123.6, 119.2, 116.6, 115.3, 113.5, 105.4, 58.3. MS (m/z): 384. Anal. Calc. C, 59.24; H, 2.62; N, 7.27%. Found: C, 59.20; H, 2.65; N, 7.26%.

*2-amino-4-(4-bromophenyl)-5-oxo-4,5-dihydropyrano[3,2-*c*]chromene-3-carbonitrile* (Table 1, entry 5): m.p. 254-256 °C, (m.p. 255-257 °C [29]); IR (KBr) $\nu_{\max}/\text{cm}^{-1}$: 3423, 3321, 2190, 1678, 1595, 1375, 1152. ¹H NMR (DMSO-*d*₆, 300 MHz) δ : 4.28 (s, 1H, H), 6.81 (s, 2H, NH₂), 7.42 (t, 2H, aromatic), 7.44 (t, 2H, aromatic), 7.66 (t, 2H, aromatic), 7.81 (2d, 3H, aromatic). ¹³C NMR (DMSO-*d*₆, 250 MHz) δ : 161.9, 160.7, 159.3, 152.6, 139.5, 138.7, 135.4, 128.2, 127.5, 123.6, 120.2, 116.7, 115.1, 113.5, 105.4, 58.3. MS (m/z): 384. Anal. Calc. C, 57.74; H, 2.81; N, 7.09%. Found: C, 57.55; H, 2.75; N, 7.01%.

*2-amino-4-(3-nitrophenyl)-5-oxo-4,5-dihydropyrano[3,2-*c*]chromene-3-carbonitrile* (Table 1, entry 6): m.p. 255-258 °C, (m.p. 256-259 °C [29]); IR (KBr) $\nu_{\max}/\text{cm}^{-1}$: 3423, 3321, 2190, 1678, 1595, 1375, 1152. ¹H NMR (DMSO-*d*₆, 300 MHz) δ : 4.26 (s, 1H, H), 6.82 (s, 2H, NH₂), 7.46 (t, 2H, aromatic), 7.44 (t, 2H, aromatic), 7.68 (t, 2H,

aromatic), 7.81 (2d, 3H, aromatic). ^{13}C NMR (DMSO- d_6 , 250 MHz) δ : 161.9, 160.7, 159.3, 152.6, 139.5, 138.7, 135.4, 128.2, 127.5, 123.6, 120.2, 115.4, 116.7, 113.5, 105.4, 58.3. MS (m/z): 361. Anal. Calc. C, 63.16; H, 3.07; N, 11.63%. Found: C, 63.01; H, 3.12; N, 11.55%.

2-amino-4-(4-nitrophenyl)-5-oxo-4,5-dihydropyrano[3,2-c]chromene-3-carbonitrile (Table 1, entry 7): m.p. 256-259 °C, (m.p. 255-258 °C [29]); IR (KBr) $\nu_{\text{max}}/\text{cm}^{-1}$: 3422, 3320, 2195, 1677, 1591, 1376, 1152. ^1H NMR (DMSO- d_6 , 300 MHz) δ : 4.24 (s, 1H, H), 6.82 (s, 2H, NH_2), 7.44 (t, 2H, aromatic), 7.44 (t, 2H, aromatic), 7.69 (t, 2H, aromatic), 7.83 (2d, 3H, aromatic). ^{13}C NMR (DMSO- d_6 , 250 MHz) δ : 161.7, 160.7, 159.5, 152.8, 139.2, 138.6, 135.6, 128.3, 127.4, 123.6, 120.1, 115.6, 116.7, 113.5, 105.4, 58.3. MS (m/z): 361. Anal. Calc. C, 63.16; H, 3.07; N, 11.63%. Found: C, 63.03; H, 3.14; N, 11.52%.

2-amino-5-oxo-4-p-tolyl-4,5-dihydropyrano[3,2-c]chromene-3-carbonitrile (Table 1, entry 8): m.p. 252-255 °C, (m.p. 252-254 °C [29,30]); IR (KBr) $\nu_{\text{max}}/\text{cm}^{-1}$: 3420, 3325, 2198, 1676, 1591, 1375, 1152. ^1H NMR (DMSO- d_6 , 300 MHz) δ : 2.35 (s, 1H, CH_3), 4.29 (s, 1H, H), 6.81 (s, 2H, NH_2), 7.12 (s, 1H, aromatic), 7.42 (t, 2H, aromatic), 7.65 (t, 2H, aromatic), 7.84 (2d, 3H, aromatic). ^{13}C NMR (DMSO- d_6 , 250 MHz) δ : 161.9, 160.2, 159.2, 152.8, 141.2, 135.5, 128.9, 128.4, 123.3, 125.5, 115.3, 116.4, 105.4, 58.1, 39.8. MS (m/z): 330. Anal. Calc. C, 72.72; H, 4.27; N, 8.48%. Found: C, 72.67; H, 4.31; N, 8.37%.

2-amino-4-(4-methoxyphenyl)-5-oxo-4,5-dihydropyrano[3,2-c]chromene-3-carbonitrile (Table 1, entry 9): m.p. 244-247 °C, (m.p. 246-249 °C [29]); IR (KBr) $\nu_{\text{max}}/\text{cm}^{-1}$: 3421, 3326, 2199, 1676, 1590, 1377, 1154. ^1H NMR (DMSO- d_6 , 300 MHz) δ : 3.83 (s, 1H, CH_3), 4.28 (s, 1H, H), 6.80 (s, 2H, NH_2), 7.14 (s, 1H, aromatic), 7.44 (t, 2H, aromatic), 7.66 (t, 2H, aromatic), 7.82 (2d, 3H, aromatic). ^{13}C NMR (DMSO- d_6 , 250 MHz) δ : 161.9, 160.2, 159.2, 152.8, 141.2, 135.5, 130.1, 128.5, 123.3, 125.4, 115.3, 114.4, 116.5, 105.4, 58.4, 39.9. MS (m/z): 346. Anal. Calc. C, 69.36; H,

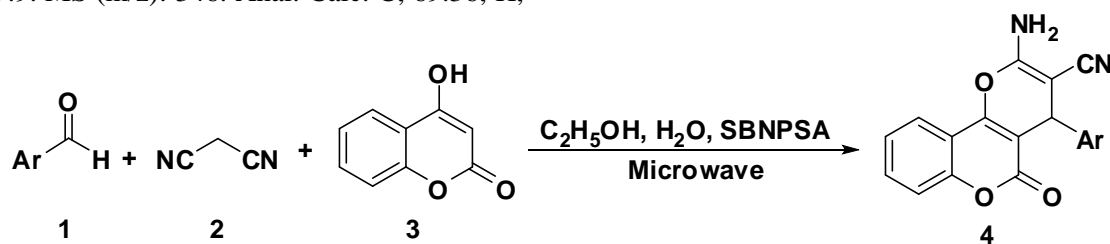
4.07; N, 8.09%. Found: C, 69.21; H, 4.16; N, 8.15%.

2-amino-4-(4-chlorophenyl)-5-oxo-4,5-dihydropyrano[3,2-c]chromene-3-carbonitrile (Table 1, entry 10): m.p. 263-265 °C, (m.p. 265-267 °C [29]); IR (KBr) $\nu_{\text{max}}/\text{cm}^{-1}$: 3422, 3324, 2198, 1676, 1593, 1377, 1154. ^1H NMR (DMSO- d_6 , 300 MHz) δ : 4.29 (s, 1H, H), 6.81 (s, 2H, NH_2), 7.17 (s, 1H, aromatic), 7.37 (2x t, 2H, aromatic), 7.65 (t, 2H, aromatic), 7.84 (2d, 3H, aromatic). ^{13}C NMR (DMSO- d_6 , 250 MHz) δ : 161.9, 160.2, 159.2, 152.8, 142.2, 135.5, 131.3, 130.3, 128.5, 123.3, 125.4, 119.8, 115.3, 114.4, 116.5, 105.4, 58.2, 39.9. MS (m/z): 346. Anal. Calc. C, 65.06; H, 3.16; N, 7.99%. Found: C, 64.93; H, 3.07; N, 7.82%.

2-amino-5-oxo-4-phenyl-4,5-dihydropyrano[3,2-c]chromene-3-carbonitrile (Table 1, entry 11): m.p. 262-264 °C, (m.p. 260-264 °C [29]); IR (KBr) $\nu_{\text{max}}/\text{cm}^{-1}$: 3421, 3324, 2199, 1676, 15935, 1376, 1155. ^1H NMR (DMSO- d_6 , 300 MHz) δ : 4.29 (s, 1H, H), 6.81 (s, 2H, NH_2), 7.17 (s, 1H, aromatic), 7.37 (2x t, 2H, aromatic), 7.65 (t, 2H, aromatic), 7.84 (2d, 3H, aromatic). ^{13}C NMR (DMSO- d_6 , 250 MHz) δ : 161.9, 160.2, 159.2, 152.8, 144.1, 135.5, 127.7, 128.6, 123.3, 125.7, 119.1, 115.3, 116.4, 105.3, 58.1, 39.8. MS (m/z): 316. Anal. Calc. C, 72.15; H, 3.82; N, 8.86%. Found: C, 72.04; H, 3.72; N, 8.94%.

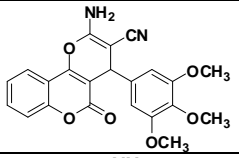
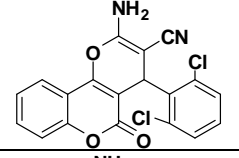
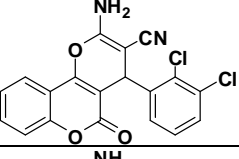
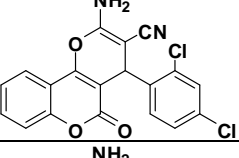
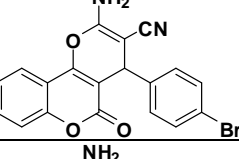
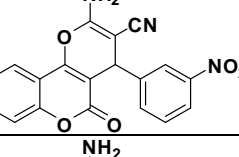
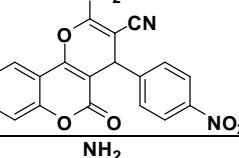
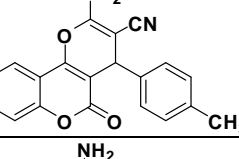
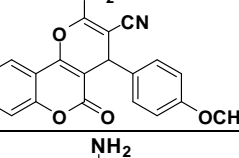
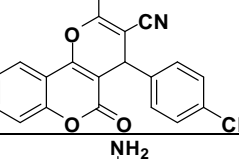
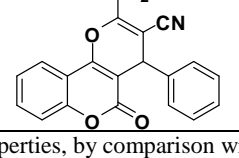
RESULTS AND DISCUSSION

We performed the synthesis of 2-amino-4*H*-chromenes and/or dihydropyrano[3,2-*c*]chromenes through a three-component reaction employing silica-bonded *N*-propyl sulfamic acid (**SBNPSA**) acid as a catalyst. The synthesis of 2-amino-4*H*-chromenes and/or dihydropyrano[3,2-*c*]chromenes was achieved by three-component condensation of an aromatic aldehyde, malononitrile and 4-hydroxycoumarin in the presence of **SBNPSA** as a catalyst. The reaction was carried out in aqueous ethanol under microwave irradiation conditions to give products in good to high yields (Scheme 1 and Table 1).



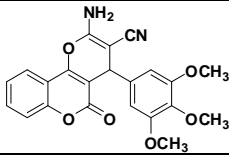
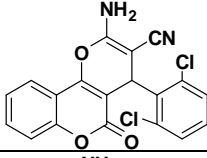
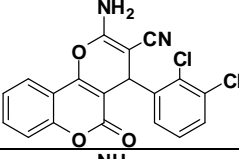
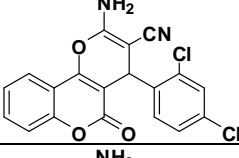
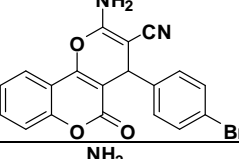
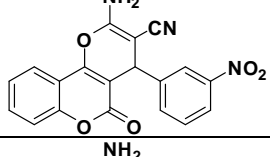
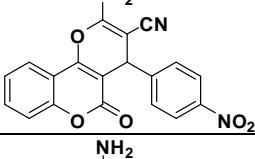
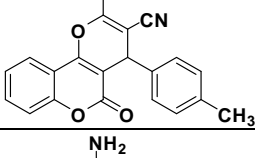
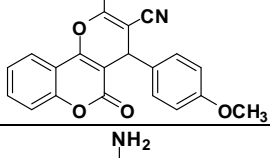
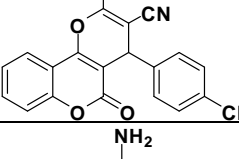
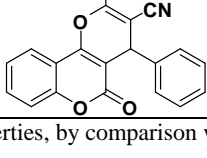
Scheme 1. Synthesis of various dihydropyrano[3,2-*c*]chromenes in the presence of silica-bonded *N*-propyl sulfamic acid (**SBNPSA**) as catalyst under irradiation microwave conditions

Table 1. Synthesis of various dihydropyrano[3,2-*c*]chromenes were run at microwave conditions and in the presence of silica-bonded *N*-propyl sulfamic acid (SBNPSA) as catalyst, H₂O:EtOH (1:1).

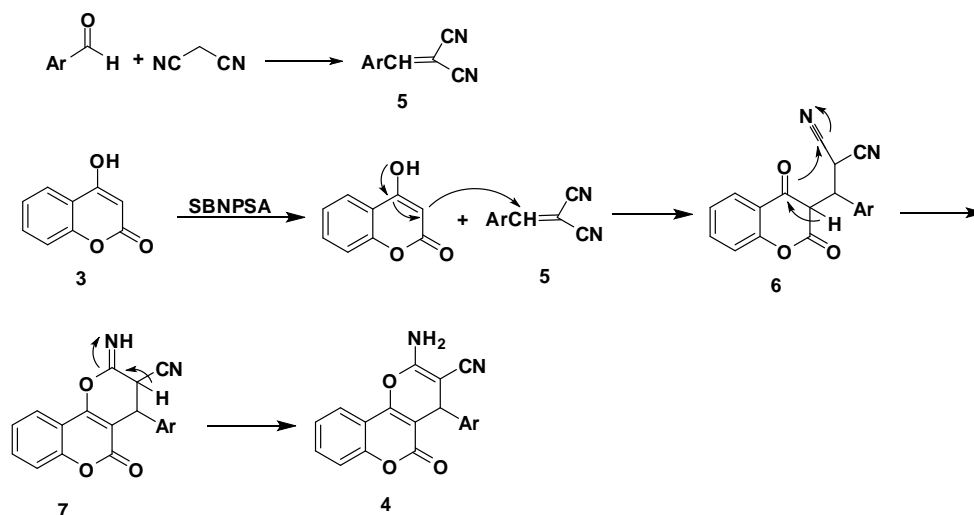
Entry	ArCHO	^a Product	Time (min)	^a Yield(%)	Ref.
1	3,4,5-(OCH₃)₃-C₆H₄CHO		47	94.5	-
2	2,6-Cl₂-C₆H₄CHO		34	96	[28]
3	2,3-Cl₂-C₆H₄CHO		30	92.5	[29]
4	2,4-Cl₂-C₆H₄CHO		32	85	[29]
5	4-Br-C₆H₄CHO		38	95.5	[29]
6	3-NO₂-C₆H₄CHO		40	94.5	[29]
7	4-NO₂-C₆H₄CHO		41	98	[29]
8	4-CH₃-C₆H₄CHO		43	93	[30]
9	4-OCH₃-C₆H₄CHO		24	84.5	[29]
10	4-Cl-C₆H₄CHO		29	83	[29]
11	C₆H₅CHO		44	92.5	[29]

^aProducts were characterized from their physical properties, by comparison with authentic samples, and by spectroscopic methods.

Table 2. Synthesis of various dihydropyrano[3,2-*c*]chromenes were run under reflux (Conventional heating conditions) and in the presence of silica-bonded *N*-propyl sulfamic acid (**SBNPSA**) as catalyst, H₂O:EtOH (1:1).

Entry	ArCHO	^a Product	Time (min)	^a Yield(%)
1	3,4,5-(OCH ₃) ₃ -C ₆ H ₄ CHO		65	88
2	2,6-Cl ₂ -C ₆ H ₄ CHO		47	86.5
3	2,3-Cl ₂ -C ₆ H ₄ CHO		49	83
4	2,4-Cl ₂ -C ₆ H ₄ CHO		51	77
5	4-Br-C ₆ H ₄ CHO		48	74.5
6	3-NO ₂ -C ₆ H ₄ CHO		63	73
7	4-NO ₂ -C ₆ H ₄ CHO		58	82
8	4-CH ₃ -C ₆ H ₄ CHO		61	78
9	4-OCH ₃ -C ₆ H ₄ CHO		47	68.5
10	4-Cl-C ₆ H ₄ CHO		41	68
11	C ₆ H ₅ CHO		59	78.5

^aProducts were characterized from their physical properties, by comparison with authentic samples, and by spectroscopic methods.



Scheme 2. The mechanism of the synthesis of various dihydropyrano[3,2-*c*]chromenes in the presence of silica-bonded *N*-propyl sulfamic acid (**SBNPSA**) as catalyst under irradiation microwave conditions.

As shown in Table 1, the results of the reactions of the aromatic aldehyde, malononitrile with 4-hydroxycoumarin indicate that the application of microwave irradiation can considerably increase the efficiency of these reactions to produce entries 1-11 in satisfactory yields (83-98%) and reduce the reaction times when compared with the conventional thermal conditions (68-88%) (Table 2).

2-Amino-4*H*-chromenes are generally prepared by refluxing malononitrile, aldehyde and activated phenol in the presence of hazardous organic bases like piperidine for several hours [31]. A literature survey revealed that several modified procedures using CTACl [32], TEBA [33], and γ -alumina [34] as catalysts have been recently reported but all these methods require long refluxing hours. Based on previous studies, new heterogeneous catalyst systems for fine chemical preparation were developed [35]. The suggested mechanism for the **SBNPSA**-catalyzed transformations is shown in Scheme 2. As reported in the literature [36], the Knoevenagel coupling of aldehydes with malononitrile gives the intermediate (5). Then, the subsequent 1,4-conjugate addition of 4-hydroxycoumarin to the intermediate (I) followed by cyclization, affords the corresponding products [37,38]. A mechanism for this reaction has been suggested in Scheme 2.

The catalysts were recovered by evaporation of the solvent and washing of the solid with chloroform. When the reaction was completed, the mixture was filtered, the solid residue was washed with warm ethanol and the catalyst was reused in the subsequent reaction. The recycled catalyst could be

reused four times without any additional treatment. No appreciable loss in the catalytic activity of **SBNPSA** was observed (Table 3).

Table 3. Recyclability of **SBNPSA** catalyst for the synthesis of compound (Table 1, 7) (2-amino-4-(4-nitrophenyl)-5-oxo-4,5-dihydropyrano[3,2-*c*]chromene-3-carbonitrile).

Run	Time (min)	^{a,b} Yield (%)
1	41	97
2	41	96
3	41	96
4	41	94

^a Isolated yield.

^b Yield of catalyst recycled four times.

CONCLUSION

In conclusion, we have developed an efficient procedure for the synthesis of 2-amino-4*H*-chromene and/or dihydropyrano[3,2-*c*]chromene derivatives in 1:1 EtOH-water mixture using silica-bonded *N*-propyl sulfamic acid (**SBNPSA**) as a catalyst. This method offers several advantages such as inexpensive catalysts, easy synthetic procedure, high yields, simple work-up procedure and easy product isolation. The microwave irradiation reduced the reaction times in this synthesis.

REFERENCES

1. H. Miao, Z. Yang, *Org. Lett.* **2**, 1765 (2000).
2. P. Valenti, A. Bisi, A. Rampa, F. Belluti, S. Gobbi, A. Zampiron, M. Carrara, *Biorg. Med. Chem.* **8**, 239 (2000).
3. L.-C. Lim, Y.-C. Kuo, C.-J. Chou, *J. Nat. Prod.* **63**, 627 (2000).
4. Y.Q. Shi, T. Fukai, H. Sakagami, W.-J. Chang, P.-Q. Yang, F.-P. Wang, T. Nomura, *J. Nat. Prod.* **64**, 181 (2001).

5. R. Larget, B. Lockhart, P. Renard, M. Largeton, *Biorg. Med. Chem. Lett.* **10**, 835 (2000).
6. A. Groweiss, J. H. Cardellina, II, M. R. Boyd, *J. Nat. Prod.* **63**, 1537 (2000).
7. Y. Deng, J.P. Lee, M. Tianasoa-Ramamonjy, J. K. Synder, S. A. Des Etages, D. Kanada, M. P. Synder, C. J. Turner, *J. Nat. Prod.* **63**, 1082 (2000).
8. I.A. Khan, M.A. Avery, C.L. Burandt, D.K. Goins, J.R. Mikell, T.E. Nash, A. Azadegan, L.A. Walker, *J. Nat. Prod.* **63**, 1414 (2000).
9. K. Mori, G. Audran, H. Monti, H. Synlett. 259 (1998).
10. P.G. Pietta, *J. Nat. Prod.* **63**, 1035 (2000).
11. G. R. Beecher, *J. Nutr.* **133**, 3248S (2003).
12. D.A. Horton, G.T. Bourne, M.L. Smythe, *Chem. Rev.* **103**, 893 (2003).
13. R. Livingstone, In *Rodd's Chemistry of Carbon Compounds*; Coffey, S. Eds.; Elsevier, **IV**, 139 (1977).
14. V. Rossollin, V. Lokshin, A. Samat, R. Guglielmetti, *Tetrahedron.* **59**, 7725 (2003).
15. T. Walenzyk, C. Carola, H. Buchholz, B. Konig, B. *Tetrahedron.* **61**, 7366 (2005).
16. A.K. Ganguly, S. Kaur, P.K. Mahata, D. Biswas, B.N. Pramanik, T.M. Chan, *Tetrahedron Lett.* **46**, 4119 (2005).
17. P. Kumar, M.S. Bodas, *Org. Lett.* **2**, 3821 (2000).
18. V.N. Kalinin, M.V. Shostakovsky, A.B. Ponomaryov, *Tetrahedron Lett.* **31** (1990) 4073
19. G.J. Reddy, D. Latha, K.S. Rao, *Heterocyclic Commun.* **10**, 279 (2004).
20. T. Ghosh, S. Saha, C. Bandyopadhyay, *Synthesis.* **11**, 1845 (2005).
21. R.E. Brown, D.M. Lustgarten, US Patent 3932466 (1976).
22. G.R. Green, J.M. Evans, A.K. Vong, In *Comprehensive Heterocyclic Chemistry II*; Katritzky, A. R., Ress, C. W., Scriven, E. F. V.; Ed.; Pergamon Press: Oxford, **5**, 469 (1995).
23. W.O. Foye, *Principi Di Chemico Farmaceutic*; Piccin: Padova, Italy, 416 (1991).
24. C.S. Konkoy, D. B. Fiseck, S.X. Cai, N.C. Lan, J.F.W. Keana, PCT Int. Appl. WO 0075123, 2000; *Chem. Abstr.* **134**, 29313a (2001).
25. A. Domling, I. Ugi, *Angew. Chem., Int. Ed.* **39**, 3168 (2000).
26. E.C. Witte, P. Neubert. A. Roesch, *Ger. Offen DE. Chem. Abstr.* **104**, 224915f (1986).
27. K. Niknam, D. Saberi, *Tetrahedron Lett.* **50**, 5210 (2009).
28. J.F. Roudier, A. Foucaud, *Synthesis.* 159 (1984).
29. a) R. Ghorbani-Vaghei, Z. Toghraei-Semiromi, R. Karimi-Nami, *J. Braz. Chem. Soc.* **22**, 5, S1-S9 (2011). b) S. Abdolmohammadi, S. Balalaie, *Tetrahedron Lett.* **48**, 3299 (2007).
30. J.M. Khurana, B. Nand, P. Saluja, *Tetrahedron.* **66**, 5637 (2010).
31. F.F. Bamoharram, M.M. Heravi, M. Roshani, M. Jahangir, A. Gharib, *Applied Catal.* **302**, 42 (2006).
32. A.G.A. Elagamey, F.M.A.A. El-Taweel, *Indian J. Chem. B.* **29**, 885 (1990).
33. R. Ballini, G. Bosica, M. L. Conforti, R. Maggi, A. Mazzacani, P. Righi, G. Sartori, *Tetrahedron.* **57**, 1395 (2001).
34. D.Q. Shi, S. Zhang, Q.Y. Zhuang, S.J. Tu, H.W. Hu, *Chinese J. Org. Chem.* **23**, 809 (2003).
35. R. Maggi, R.; Ballini, G. Sartorio, R. Sartorio, R. *Tetrahedron Lett.* **45**, 2297 (2004).
36. N. Bicaç, *J. Mol. Liq.* **116**, 15 (2005).
37. M.M. Heravi, B.A. Jani, F. Derikvand, F.F. Bamoharram, H. A. Oskooie, *Catal. Commu.* **10**, 272 (2008).
38. J.M. Khurana, S. Kumar, *Tetrahedron Lett.* **50**, 4125 (2009).

N-ПРОПИЛ-СУЛФАМИНОВА КИСЕЛИНА ВЪРХУ НОСИТЕЛ ОТ СИЛИЦИЕВ ДИОКСИД: РЕЦИКЛИРУЕМ КАТАЛИЗАТОР ЗА СИНТЕЗИ НА РАЗЛИЧНИ ДИХИДРОПРОПАНОЛ [3,2-С] – ХРОМЕНИ ПРИ МИКРОВЪЛНОВО ЛЪЧЕНИЕ

А. Гариб^{1,2*}, Н. Норузи Песян³, Л. Вождани Фард⁴, М. Рошани¹

¹Департамент по химия, Ислямски университет Азад, Маишад, Иран

²Център за земеделски изследвания и услуги, Маишад, Иран

³Департамент по химия, Научен факултет, Университет в Урмия, 57159 Урмия, Иран

⁴Министерство на образованието, Организация за образованиев Разави, Хоразан, Маишад, Иран

Постъпила на 13 март, 2012 г.; коригирана на 13 февруари, 2013 г.

(Резюме)

Съобщава се за нов и прост метод за синтезата на дихидропропанол [3,2-с] – хромени. Продуктите се получават с добри до отлични добиви с проста и ефективна процедура при меки условия. За катализатор се използва N-пропил-сулфаминова киселина (SBNPSA) върху носител от силициев диоксид при микровълново лъчение.

Antibacterial activity of some newer 1,2,3 – benzotriazole derivatives synthesized by ultrasonication in solvent – free conditions

S.S. Muvvala¹, V.N. Ratnakaram^{2*}

¹ Department of Chemistry, Sri Subbaraya and Narayana College, Narasaraopet – 522 601, India

^{2*} School of Biotechnology, Vignan University, Vadlamudi, Guntur-522213, India

Received July 2, 2012; Accepted January 21, 2013.

Many of the classical synthetic methodologies have broad scope but generate copious amounts of waste. The chemical and pharmaceutical industries have been subjected to increasing pressure to minimize or, preferably, eliminate this waste. In the present study a series of some newer 1,2,3-benzotriazole derivatives were synthesized under ultrasonicated and solvent-free conditions. Newer “1-(1H-benzo[d][1,2,3]triazole-1-carbonyl) derivatives” (**5A** – **5P**) were synthesized from “1H-benzo[d][1,2,3]triazole” (**1**) by optimizing the reaction conditions. The resulting products were isolated and characterized by spectral studies. The anti bacterial activities of these compounds were screened *in vitro* against different strains of bacteria i.e. Gram negative organism (*Pseudomonas aureginosa*, MTCC – 1035) and Gram positive organisms (*Bacillus cereus*, MTCC – 430, *Bacillus subtilis*, MTCC – 441, *Staphylococcus aureus*, MTCC – 737, *Staphylococcus epidermidis*, MTCC – 3086) by paper disc diffusion method. Some of the synthesized compounds showed significant activity against various bacteria.

Key words: Ultrasound irradiation, solvent-free synthesis, 1,2,3 - benzotriazole derivatives, anti bacterial activity.

INTRODUCTION

Heterocyclic compounds containing nitrogen atoms are considered to be one of the most effective antimicrobial drugs used as either single agents or in combination for cancer therapy [1, 2]. Some benzotriazole derivatives have shown anti-inflammatory properties [3]. Touami *et al* [4] reported that the conjugates of benzotriazole derivative photonucleases and DNA minor groove binders exhibit enhanced cleavage efficiency and unique selectivity. It has been proposed that the benzotriazole derivatives have the effect on cancer development [5]. Sparatore and Sparatore reported that 2-(4-(Dialkyl amino alkoxy) phenyl) benzotriazoles and N-oxides works as thromboxane A2 antagonists and as hypocholesterolemic agents, platelet aggregation inhibitors [6], where as benzotriazole carboxylic acid or ester derivatives were found to be effective in the treatment of metabolic related disorders including atherosclerosis, coronary heart disease and type 2 diabetes [7]. Biagi *et al.* [8] reported that 5-(substituted) benzotriazoles and triazolyl benzotriazoles as potential potassium channel activators.

The ultrasound irradiation technique has been increasingly used in organic synthesis for last three

decades. A large number of organic reactions have been carried out in higher yield, shorter reaction time and milder condition under ultrasound irradiation [9-12]. It is well known that ultrasonic irradiation to a liquid phase reaction accelerates the chemical reaction and creates a special reaction field for the preparation of various materials [13-16].

There is a growing awareness that the design of synthetic or chemical processes should follow the basic principles of green chemistry to reduce risks to humans and the environment [17-18]. Large-scale use of organic solvents in synthesis causes environmental hazards [19]. There were several advantages of performing syntheses in solvent-free media, such as, short reaction time, increased safety, and low cost [19-21]. Recently, a few papers reported modern synthetic protocols where solvent-less condition have been used [22-24]. Finally, herein we wish to report the anti-bacterial activity of some newer 1,2,3 – benzotriazole derivatives synthesized by ultrasonication in solvent – free conditions.

EXPERIMENTAL

Reagents of analytical grade were used in the synthesis. The reactions under ultrasonic irradiation were carried out at room temperature in a 40 ml glass reactor. An UP 400S ultrasonic processor equipped with a 12 mm wide and 140 mm long

* To whom all correspondence should be sent:
E-mail: doctornadh@yahoo.co.in

probe was immersed directly into the reaction mixture. The operating frequency was 24 KHz and the output power was 220 W through manual adjustment. The melting points of synthesized derivatives were determined by using an Electrothermal 9100 digital melting point apparatus and were uncorrected. The structures of synthesized derivatives were elucidated by spectral studies. Spectroscopic data were recorded on the following instruments: Perkin Elmer 1600 series Fourier Transformer – Infrared Spectrophotometer in KBr - Pellet method; ¹H NMR, Bruker 400 MHz NMR spectrometer (Bruker Bioscience, Billerica, MA, USA) in MeOD using TMS as internal standard.

Scheme for the synthesis of the compounds: After suitable modifications to the classical synthesis carried out by other workers [25-27], sixteen new benzotriazole derivatives were synthesized under green conditions (viz., ultrasonication and solvent free conditions) by the addition of diazotization step (as shown in the scheme). **Anti – bacterial activity by Disc Diffusion Method and MIC for Bacteria:** All the synthesized compounds of present study were screened for *in-vitro* anti bacterial activity against five different strains of bacteria i.e. Gram negative organism (*Pseudomonas aureginosa* MTCC – 1035) and Gram positive organisms (*Bacillus cereus* MTCC – 430, *Bacillus subtilis* MTCC – 441, *Staphylococcus aureus* MTCC – 737 and *Staphylococcus epidermidis* MTCC – 3086) by paper disc diffusion method [28]. Cotrimoxazole and Cephotaxime were used as reference drugs for bacteria. An additional control disc without any sample but impregnated with an equivalent amount of solvent (DMSO) was also used. The Minimum Inhibitory

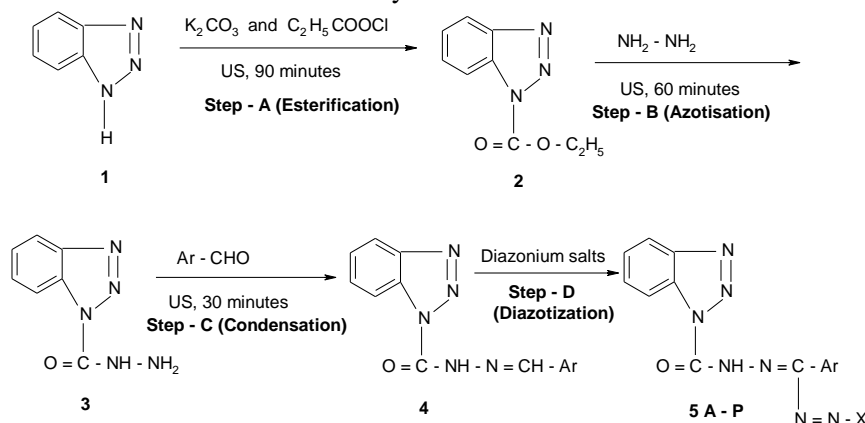
Concentration (MIC) study was carried out at different concentrations of the synthesized compounds such as 15.625, 31.25, 62.5 µg/ml.

RESULTS AND DISCUSSION

Antibacterial activity can be enhanced by addition of aromatic rings / moieties / substituents to the basic structures. Hydrophobic molecules with rigid, planar structures such as aromatic rings have been shown to have the ability to insert into membranes of microbes and induce localized permeability changes leading to leakage out of the membrane leading to their death [29]. Earlier reports revealed that para substituted phenyl compounds containing electron withdrawing groups were found to be more active against microbes [30, 31]. The introduction of the schiff's base moiety enhanced the antibacterial activity of aromatic compounds [32]. Hence, newer 1,2,3-benzotriazole derivatives containing schiff's base with electron withdrawing substituted phenyls at para position were synthesized by ultrasound activation in solvent – free condition (with moderate to good yields in the range of 71 – 82%) and tested for their antibacterial activity.

Characterization of newer 1,2,3 – benzotriazole derivatives: The synthesized derivatives were characterized by following methods.

A. Melting Point: Melting points of the synthesized derivatives were determined by an open-end capillary tube method and were uncorrected. Molecular formulae, molecular weights, melting points and yields of the synthesized derivatives were given in Table 1.



5A – D: Ar = C₆H₅; 5E – H: Ar = C₄H₃O; 5I – L: Ar = C₆H₄NO₂ and 5M – P: Ar = C₆H₄Cl

5A, E, I, M: X = C₆H₅; 5B, F, J, N: X = C₆H₄NO₂; 5C, G, K, O: X = C₆H₄Cl and 5D, H, L, P: X = C₆H₄Br

Note: US = Ultrasonication

Table – 1. Physical data of synthesized 1,2,3 – benzotriazole derivatives.

S. No.	Compound Code	Molecular Formula	Molecular Weight	Melting Point (°C)	Yield (%)
1.	5 A	C ₂₀ H ₁₅ N ₇ O	369.4	99	82
2.	5 B	C ₂₀ H ₁₄ N ₈ O ₃	414.4	96	79
3.	5 C	C ₂₀ H ₁₄ ClN ₇ O	403.8	99	81
4.	5 D	C ₂₀ H ₁₄ BrN ₇ O	448.3	98	82
5.	5 E	C ₁₈ H ₁₃ N ₇ O ₂	359.3	88	79
6.	5 F	C ₁₈ H ₁₂ N ₈ O ₄	404.3	93	72
7.	5 G	C ₁₈ H ₁₂ ClN ₇ O ₂	393.8	95	73
8.	5 H	C ₁₈ H ₁₂ BrN ₇ O ₂	438.2	97	72
9.	5 I	C ₂₀ H ₁₄ N ₈ O ₃	414.4	101	71
10.	5 J	C ₂₀ H ₁₃ N ₉ O ₅	459.4	102	79
11.	5 K	C ₂₀ H ₁₃ ClN ₈ O ₃	448.8	99	75
12.	5 L	C ₂₀ H ₁₃ BrN ₈ O ₃	493.3	103	77
13.	5 M	C ₂₀ H ₁₄ ClN ₇ O	403.8	80	72
14.	5 N	C ₂₀ H ₁₃ ClN ₈ O ₃	448.8	82	77
15.	5 O	C ₂₀ H ₁₃ Cl ₂ N ₇ O	438.3	100	82
16.	5 P	C ₂₀ H ₁₃ BrClN ₇ O	482.7	95	81

B. Infra – Red and ¹H NMR spectral analysis:

The synthesized derivatives were characterized by FTIR and ¹H NMR values measured in cm⁻¹ and δ (ppm) respectively. The data was interpreted with reference to standard values [33, 34] and given below for some of the synthesized compounds.

❖ *1-(1H-benzo[d][1,2,3]triazole-1-carbonyl)-3,5-diphenylformazan (5A):*

IR (KBr, cm⁻¹): 1696.66 (Ar C = C, stretch); 1603.37 (N = N, stretch), 1542.28 (N – H, stretch), 1256.37 (Aryl C – N, stretch), 1007.57 (Aniline C – N, stretch) and 737.28 (CHO – deformation); ¹H NMR (400 MHz) (MeOD) δ □(ppm): 3.33 (1H, s, N-H), 7.06 (1H, d, C-H), 7.33 (2H, d, C-H), 7.40 (2H, d, C-H), 7.45 – 7.48 (2H, m, C-H), 7.56 – 7.59 (3H, m, C-H), 7.83 (2H, d, C-H) and 7.96 (2H, d, C-H).

❖ *1-(1H-benzo[d][1,2,3]triazole-1-carbonyl)-5-(4-nitrophenyl)-3-phenyl formazan (5B):* IR (KBr, cm⁻¹): 1698.47 (Ar C = C, stretch); 1593.99 (N = N, stretch), 1495.50 (Ar – NO₂, stretch), 1301.09 (Aryl C – N, stretch), 1206.78 (Aniline C – N, stretch), 843.07 (p – disubstitution, stretch) and 739.50 (CHO – deformation); ¹H NMR (400 MHz) (MeOD) δ □(ppm): 3.20 (1H, s, N-H), 7.18 (2H, d, C-H), 7.40 (2H, d, C-H), 7.52 – 7.59 (3H, m, C-H), 7.83 (2H, d, C-H), 7.96 (2H, d, C-H) and 8.10 (2H, d, C-H).

❖ *1-(1H-benzo[d][1,2,3]triazole-1-carbonyl)-5-(4-chlorophenyl)-3-(furan-2-yl) formazan (5G):* IR (KBr, cm⁻¹): 3649.31 (Amide – CONH, stretch), 1594.63 (N = N, stretch), 1485.68 (Furan Ring, C = C, stretch), 1206.43 (Aniline C – N, stretch), 1007.96 (C – O – C, stretch), 820.27 (p – disubstitution, stretch), 740.62 (CHO deformation, stretch) and 539.68 (C – Cl); ¹H NMR (400 MHz) (MeOD) δ □(ppm): 3.33 (1H, s, N-H), 6.52 (1H,

m, Furan C-H), 6.54 (1H, d, Furan C-H), 7.0 (1H, s, N-H), 7.27 (2H, d, C-H), 7.40 (2H, d, C-H), 7.49 (2H, d, C-H), 7.75 (1H, d, Furan C-H) and 7.96 (2H, d, C-H).

❖ *1-(1H-benzo[d][1,2,3]triazole-1-carbonyl)-5-(4-bromophenyl)-3-(furan-2-yl)formazan (5H):* IR (KBr, cm⁻¹): 3652.10 (Amide – CONH, stretch), 1722.17 (Furan Ring, stretch), 1622.31 (N = N, stretch), 1511.18 (Ar C = C, stretch), 1457.07 (Furan Ring C = C, stretch), 1202.93 (Aniline C – N, stretch), 1005.36 (C – O – C, stretch), 875.16 (p – disubstitution, stretch), 773.52 (CHO deformation, stretch) and 515.35 (C – Br, stretch); ¹H NMR (400 MHz) (MeOD) δ □(ppm): 3.20 (1H, s, N-H), 6.52 (1H, m, Furan C-H), 6.54 (1H, d, Furan C-H), 7.0 (1H, s, N-H), 7.22 (2H, d, C-H), 7.40 (2H, d, C-H), 7.75 (1H, d, Furan C-H), 7.76 (2H, d, C-H) and 7.96 (2H, d, C-H).

❖ *1-(1H-benzo[d][1,2,3]triazole-1-carbonyl)-3-(4-chlorophenyl)-5-phenyl form--azan (5M):* IR (KBr, cm⁻¹): 3650.62 (Amide – CONH), 1706.94 (Ar, C = C, stretch), 1593.76 (N = N, stretch), 1513.71 (N – H, stretch), 1264.35 (Aryl C – N, stretch), 1204.85 (Aniline C – N, stretch), 820.56 (p – disubstitution, stretch), 772.75 (CHO – deformation, stretch) and 605.30 (C – Cl, stretch); ¹H NMR (400 MHz) (MeOD) δ □(ppm): 3.3 (1H, s, N-H), 7.06 (1H, d, C-H), 7.33 (2H, d, C-H), 7.40 (2H, d, C-H), 7.45 (2H, d, C-H), 7.52 (2H, d, C-H), 7.77 (2H, d, C-H) and 7.96 (2H, d, C-H).

❖ *1-(1H-benzo[d][1,2,3]triazole-1-carbonyl)-3,5-bis(4-chloro-phenyl) formazan (5O):* IR (KBr, cm⁻¹): 1710.45 (Ar, C = C, stretch), 1593.50 (N = N, stretch), 1486.45 (N – H, stretch), 1256.86 (Aryl C – N, stretch), 1143.95 (Aniline C – N, stretch), 827.70 (p – disubstitution, stretch), 773.01 (CHO – deformation, stretch) and 620.81 (C – Cl, stretch);

Table 2. Anti – bacterial activity of 1,2,3 – benzotriazole derivatives.

S.No.	Compound Code	Anti – bacterial activity (in mm)*				
		For disks soaked in 100µg/ml solutions of compounds				
		<i>Pseudomonas aureginosa</i> MTCC – 1035	<i>Bacillus cereus</i> MTCC – 430	<i>Bacillus subtilis</i> MTCC – 441	<i>Staphylococcus aureus</i> MTCC – 737	<i>Staphylococcus epidermidis</i> MTCC – 3086
1.	5 A	10.9	9.0	7.0	--	--
2.	5 B	14.6	10.0	7.0	9.5	--
3.	5 C	8.2	11.0	9.0	11.9	--
4.	5 D	7.4	10.0	8.0	--	10.7
5.	5 E	6.0	10.0	--	--	9.2
6.	5 F	6.8	9.6	15.0	17.1	9.7
7.	5 G	7.0	7.3	7.0	--	8.0
8.	5 H	--	8.0	9.5	--	11.9
9.	5 I	--	19.9	10	9.6	15.1
10.	5 J	8.7	9.0	25	10.4	12.6
11.	5 K	--	11.4	18	--	8.7
12.	5 L	8.1	10.4	8.0	--	--
13.	5 M	7.8	9.5	7.0	7.1	--
14.	5 N	--	12.7	8.0	--	--
15.	5 O	7.5	17.5	9.0	8.5	--
16.	5P	6.7	12.4	--	12.1	8.4
	Cotrimoxazole,	--	10.7	3.3	18	21.8
	Cephotaxime	22	--	--	--	--
	Control	--	--	--	--	--
	(10%DMSO In Methanol)	--	--	--	--	--

(--) indicates No zone of inhibition and * indicates average of triplicate

¹H NMR (400 MHz) (MeOD) δ □(ppm): 3.3 (1H, s, N-H), 7.27 (2H, d, C-H), 7.40 (2H, d, C-H), 7.49 (2H, d, C-H), 7.52 (2H, d, C-H), 7.77 (2H, d, C-H) and 7.96 (2H, d, C-H).

C. Anti bacterial assay of synthesized derivatives: The zones of inhibitions (mm) of tested compounds against bacterial strains were shown in Table 2 and the experimental result indicated variable degree of efficacy of the compounds against different strains of bacteria. Poor activity was shown by 5B, 5A, 5J, 5C and 5L (zone diameters 14.6, 10.9, 8.7, 8.2 and 8.1mm respectively) against Gram positive bacteria (*Pseudomonas aureginosa*, MTCC – 1035) compared to the reference compound – Cephotaxime (zone diameter 22 mm), whereas 5H, 5I, 5K and 5N were completely ineffective.

Exceptionally high antibacterial activity was shown by 5J (zone diameter-25mm, i.e., 7.5 fold activity) against the Gram negative bacteria – *Bacillus subtilis* (MTCC – 441) in comparison to the reference compound Cotrimoxazole (zone diameter-3.3mm), which can be attributed to the nitro substitution on phenyl groups that were attached to cyano and azo groups. The nitro group affects the charge distribution which confers significant improvement in biological effect. The enhanced inhibition observed in the presence of

nitro group is then more likely due to its interaction with some intracellular target. The presence of a strong electron-withdrawing group must alter the nature of the compound in such a way as to promote binding to the target(s) [35]. Even in earlier reports, p-nitro substitution on phenyl group displayed high activity against *B. subtilis* in the case of benzotriazole substituted carboxamides [36] and phenyl methanamine [37]. Other compounds (5A, 5B, 5C, 5D, 5F, 5G, 5H, 5I, 5K, 5L, 5M, 5N, 5O) have shown 5.5 to 2.0 fold activity compared to the reference compound Cotrimoxazole, where as 5E and 5P were inactive.

Compounds 5I and 5O have shown 1.8 and 1.6 fold activity respectively against *Bacillus cereus* (MTCC – 430) compared to the reference compound – Cotrimoxazole, where as all other synthesized compounds were as good as Cotrimoxazole. Better activity of compound 5O might be due to the attachment of chloro phenyl to azo and cyano groups. This result suggested that the introduction of halogen substituent increased the hydrophobicity of the synthesized compounds and lead to the increase of the antibacterial activity [38]. Electron withdrawing groups like halogens will increase bactericidal potential. According to Rajendra Prasad *et al* [39], designing the compounds bearing electron withdrawing

Table 3. Minimum Inhibitory Concentrations for Bacteria ($\mu\text{g/ml}$)

S. No.	Compound Code	<i>Pseudomonas aureginosa</i> MTCC – 1035	<i>Bacillus cereus</i> MTCC – 430	<i>Bacillus subtilis</i> MTCC – 441	<i>Staphylococcus aureus</i> MTCC – 737	<i>Staphylococcus epidermidis</i> MTCC – 3086
1.	5 A	62.5	31.25	31.25	--	--
2.	5 B	62.5	62.5	62.5	31.25	--
3.	5 C	62.5	62.5	31.25	31.25	--
4.	5 D	31.25	62.5	62.5	--	62.5
5.	5 E	62.5	15.625	--	--	15.625
6.	5 F	62.5	31.25	62.5	62.5	62.5
7.	5 G	62.5	62.5	15.625	--	62.5
8.	5 H	--	62.5	62.5	--	62.5
9.	5 I	--	62.5	62.5	15.625	31.25
10.	5 J	31.25	62.5	31.25	62.5	62.5
11.	5 K	--	62.5	62.5	--	31.25
12.	5 L	31.25	62.5	31.25	--	--
13.	5 M	62.5	62.5	62.5	62.5	--
14.	5 N	--	31.25	62.5	--	--
15.	5 O	62.5	62.5	62.5	62.5	--
16.	5 P	62.5	31.25	--	62.5	62.5

substituents and with high degree of binding linearity with groups those results in high molecular weights increases antibacterial activity.

Compounds 5A, 5D, 5E, 5G, 5H, 5K, 5L and 5N were inactive against *Staphylococcus aureus* (MTCC – 737), whereas 5B, 5C, 5F, 5I, 5J, 5M, 5O and 5P have shown approximately half of the activity compared to the reference compound – Cotrimoxazole. 5A, 5B, 5C, 5L, 5M, 5N and 5O were inactive, where as 5D, 5E, 5F, 5G, 5H, 5I, 5J and 5K have shown in the order of half of the activity against *Staphylococcus epidermidis* (MTCC – 3086) compared to the reference compound – Cotrimoxazole.

The Minimum Inhibitory Concentrations (MIC) of the synthesized 1,2,3-benzotriazole derivatives for bacteria were shown in Table 3 and found to be 62.5 $\mu\text{g} / \text{ml}$ for most of the synthesized compounds.

CONCLUSIONS

Excellent antibacterial activity was shown by all the synthesized compounds except 5E and 5P, against the Gram negative bacteria – *Bacillus subtilis* (MTCC – 441) compared to the reference compound - Cotrimoxazole. All the synthesized compounds have shown comparable antibacterial activity to the reference compound – Cotrimoxazole against *Bacillus cereus* (MTCC – 430). Against *Staphylococcus aureus* (MTCC – 737) and *Staphylococcus epidermidis* (MTCC – 3086) some of the compounds were inactive and other were feebly active. In the case of Gram positive bacteria (*Pseudomonas aureginosa*, MTCC – 1035), the activity shown by the

synthesized compounds was not significant compared to the reference compound – Cephotaxime. The Minimum Inhibitory Concentrations (MIC) of the most of the synthesized 1,2,3-benzotriazole derivatives for these bacteria was found to be 62.5 $\mu\text{g} / \text{ml}$.

Finally in conclusion, 1,2,3 – benzotriazole derivatives synthesized under solvent-free and ultrasound irradiation with noteworthy advantages viz., shorter reaction times, operational simplicity, simple work-up, and eco-friendly nature, have shown anti bacterial activities against selected Gram negative organisms.

REFERENCES

1. K. Katarzyna, N. Zelika and Z. Justyna, *Bioorg. Med. Chem.*, **12**, 2617 (2004).
2. H.Q. Li, C. Xu, H.S. Li, Z.P. Xiao, L. Shi and H.L. Zhu, *Chem. Med. Chem.* **2(9)**, 1361 (2007).
3. M.B. Bushuev, A.V. Virovets, Y. Garcia, C. Gieck, L.A. Sheludyakova, V.N. Ikorskii, W. Tremel, P. Gütllich and L.G. Lavrenova, *Polyhedron*, **21**, 797 (2002).
4. S.M. Touami, C.C. Poon and P.A. Wender, *J. Am. Chem. Soc.*, **119(32)**, 7611 (1997).
5. V.D. Handratta, T.S. Vasaitis, A.M.H. Brodie, V.C.O. Njar, L.K. Gediya, R. Kataria, R. Chopra, D. Newman, R. Farquhar, Z. Guo and Y. Qiu, *J. Med. Chem.*, **48**, 2972 (2005).
6. Sparatore, F. Sparatore, *II Farmaco*, **53 (2)**, 102 (1998).
7. G. Semple, P. Skinner, M. Cherrier, P. Webb, S.Y. Tamura, *Benzotriazoles and Methods of Prophylaxis or Treatment of Metabolic-Related Disorders There of*, Patent WO/041274 (2004).

8. G. Biagi, I. Giorgi, O. Livi, V. Scartoni, P.L. Barili, V. Calderone, E. Martinotti, *II Farmaco*, **56**, 827 (2001).
9. B. Hee Han, B.J. Philip, *Tetrahedron Letters*, **23**, 1643 (1982).
10. M.S. Sudhir, R. Venkata Nadh, *J. Pharm. Res.*, **7**, 47 (2013).
11. F. Duss, P.E. Hansen *Molecules*, **12**, 2080 (2007).
12. M.A.E. Naglaa, S.S. Tamer, F.M. Mohamed, *Ultrason. Sonochem.*, **16**, 70 (2009).
13. Gedanken A., *Ultrason Sonochem* **11**, 47 (2004).
14. Y. Zhu, H. Li, Y. Koltypin, Y.R. Hacoheh, A. Gedanken, *Chem. Commun.*, **24**, 2616 (2001).
15. J. Zhang, J. Du, B. Han, Z. Liu, T. Jiang, and Z. Zhang, *Angew. Chem.*, **45**, 1116 (2006).
16. M. Drogenik, M. Kristl, D. Makovec, Z. Jaglicic, D. Hanzel, *Ultrason. Sonochem.*, **15**, 791 (2007).
17. P. Tundo, P. Anastas, D. Black, C. St, J. Breen, T. Collins, S. Memoli, J. Miyamoto, M. Polyakoff, W. Tumas, *Pure Appl. Chem.*, **72**, 1207 (2000).
18. J.J. Heindel, Health Impact of Environmental Chemicals: Need For Green Chemistry, International Seminar On Nuclear War And Planetary Emergencies 42nd Session (135-142), *Erice*, Italy, August 2009, p.19 – 24.
19. R.A. Sheldon, *Green Chemistry.*, **7**, 267 (2005).
20. A. Loupy, A. Petit, J. Hamelin, F. Texier-Boulle, P. Jacquault, D. Mathe, *Synthesis*, **29**, 1213 (1998).
21. W. Leitner, K.R. Seddon, P. Wasserscheid (eds), *Green Chem.*, **5**, 99 (2003).
22. S. Nadeem, A. Munawar, S. Ahmad, M. Smiglak, M.D. Drab, I. Khizar Malik, R.Amjad, M. Chaudhry Ashraf, D. Robin, D. Rogers, *ARKIVOC*, **7**, 19 (2010).
23. S.A. Kothakar, R. Rahul Nagawade, D.B. Shinde, *Ukrainica Bioorganica Acta*, **2**, 17 (2006).
24. R.R. Nagawade, B. Devanand Shinde, *Chinese Chemical Letters*, **17**, 453 (2006).
25. K. C. Asati, S. K. Srivastava, S. Srivastava, *Ind. J. Chem.*, **45B**, 526 (2006).
26. P. Chitre Keyur, P. Jayswal Kejal, D. Patel Hitesh, *Asian J. Chem.*, **17**, 2797 (2005).
27. D.K. Sukla, S.D. Srivatsava, *Ind. J. Chem.*, **47B**, 463 (2008).
28. P. R. Murray, E. J. Baron, M.A. Pfaller, F.C. Tenover, R.H. Yolke, in: *Manual of Clinical Microbiology*, (eds), 7th ed., ASM: Washington, 1999, p.1527.
29. A.T. Kotchevar, P. Ghosh, F.M. Uckun, *J. Phys. Chem. – B*, **102**, 10925 (1998).
30. M.S. Sudhir, R. Venkata Nadh, S Radhika, *Drug Invention Today*, **5**, 126 (2013).
31. P.A. Raj, G. Suddendra, A.S. Shakeel, M. Girish, *Int. J. Drug Formul.Res.*, **3**, 135 (2012).
32. A.K. Nanda, S. Ganguli, R. Chakraborty, *Molecules*, **12**, 2413 (2007).
33. B.K. Sharma, in: *Text book of Spectroscopy*, (eds), Goel Publishing House, 21st edition, Chap. 3, Meerut, India, 2011, p. 283.
34. W. Kemp, in: *Organic spectroscopy*, (eds), Palgrave publishers, 3rd edition, New York, 1991, p.171.
35. M.J. Waring, T. Ben-Hadda, A.T. Kotchevar, A. Ramdani, R. Touzani, S. Elkadiri, A. Hakkou, Md. Bouakka, T. Ellis, *Molecules*, **7**, 641 (2002).
36. R. Sharma, P. Samadhiya, S.D. Srivastava, S.K. Srivastava, *Acta Chimica Slovonica*, **58**, 110 (2011).
37. D. Visagaperumal, V. Praveen, P. Sudeepthi, P. Prasanthi, G.G. Sravani, G. Satyanarayana, *Int. J. Chem. Sci.*, **8**, 1315 (2010).
38. Jun Wan, Peng-Cheng Lv, Na-Na Tian, Hai-Liang Zhu, *J. Chem. Sci.*, **122(4)**, 597 (2010).
39. Y.R. Prasad, P.R. Kumar, D.J. Smiles and P.A. Babu, *ARKIVOC*, **XI**, 266 (2008).

АНТИБАКТЕРИАЛНА АКТИВНОСТ НА НЯКОИ НОВИ ПРОИЗВОДНИ НА 1,2,3 – БЕНЗОТРИАЗОЛА, СИНТЕЗИРАНИ ПРИ УЛТРАЗВУКОВО ВЪЗДЕЙСТВИЕ БЕЗ РАЗТВОРИТЕЛИ

С.С. Муввала¹, В.Н. Ратнакар^{2*}

¹ Департамент по химия, Колеж Сри Суббарая и Нараяна, Нарасарапет – 522 601, Индия

^{2*} Училище по биотехнология, Университет Вигнан, Гунтур-522213, Индия

Постъпила на 2 юли, 2012 г.; приета на 21 януари, 2013 г.

(Резюме)

Много класически методики за синтези генерират големи количества отпадъци. Химичната и фармацевтичната индустрии са под нарастващия натиск да минимизират и дори да избягват тези отпадъци. В настоящата работа се съобщава за синтезирането на нови производни на 1,2,3–бензотриазола при ултразвуково въздействие и без използването на разтворители. Нови “1–(1Н–бензо[d][1,2,3]триазол–1–карбонил)–ови производни (5A – 5P) са синтезирани от “1Н–бензо[d][1,2,3]триазол” (1) оптимизирайки условията на реакцията. Получените продукти са изолирани и охарактеризирани чрез спектрални методи. Антибактериалната активност на тези съединения е изследвана *in vitro* спрямо различни бактериални Грам–отрицателни щамове (*Pseudomonas aureginosa*, МТСС – 1035) and Gram positive organisms (*Bacillus cereus*, МТСС – 430, *Bacillus subtilis*, МТСС – 441, *Staphylococcus aureus*, МТСС – 737, *Staphylococcus epidermidis*, МТСС – 3086). Някои от синтезираните съединения показват значителна активност спрямо различни бактерии.

DFT Study on the Fe, Cu and Zn Complexes of 4-(2-Thiazolylazo) Resorcinol

S. Ali Beyramabadi

Department of Chemistry, Mashhad Branch, Islamic Azad University, Mashhad, Iran

Received August 23, 2012; Revised April 19, 2013

In this work, the Fe(II), Cu(II) and Zn(II) complexes of the 4-(2-thiazolylazo) resorcinol (TAR) ligand were characterized theoretically. Their optimized geometries and theoretical vibrational frequencies were computed using the density functional theory (DFT), where the B3LYP functional was employed. In the structures of octahedral complexes, the deprotonated TAR (TAR⁻) acts as an anionic tridentate ligand *via* azo nitrogen, thiazolyl nitrogen and phenolic O⁻. In the octahedral complexes, the two TAR⁻ ligands are roughly perpendicular to each other. The Cu(TAR)₂ complex is predicted to exhibit the Jahn-Teller distortion.

Keywords: Density functional theory; IR Assignment; Azo-compound; 4-(2-Thiazolylazo) resorcinol; Geometry optimization

1. INTRODUCTION

Due to interesting applications in optical data storage, photoswitching, photochromic materials, dyes and pharmaceuticals, the azo compounds have attracted much attention [1-5]. Among the azo compounds, 4-(2-thiazolylazo) resorcinol (TAR) is a well-known chelating reagent in acid-base titrations [6], separation of trace metal ions from food and environmental samples [7,8], and spectrophotometric determination of metal ions [9].

Now, theoretical investigations are applicable in many areas of chemistry, such as kinetics and mechanism investigations of the reactions, spectroscopic assignments, characterization of molecular structures, and so on [10-17]. They could, at the same time, be considered as complementary to or replacing experimental methods.

Many metal complexes of TAR have been synthesized [7,9,18-20]. Recently, Karipcin *et al.* [21], have synthesized the M(TAR)₂ complexes of TAR, where M is Fe(II), Cu(II) and Zn(II). But as we know, no crystal structure has been reported for these complexes. In this work, we have theoretically investigated the geometrical structures of the complexes. Comparison of the theoretical and experimental vibrational frequencies was used as an evidence for the suitability of the optimized geometries. This method is frequently used for identification of chemical compounds [16,17,22]. The assignment of the IR bands of the studied complexes can be useful in identification of similar compounds.

2. THEORETICAL METHODS

All calculations were performed with the Gaussian 03 software package [23] by using the B3LYP hybrid functional [24] and the 6-31+G(d,p) basis set. First, all degrees of freedom were optimized for all the geometries.

The optimized geometries of the complexes were confirmed to have no imaginary frequency of the Hessian. Then, the gas phase optimized geometries were used to compute their vibrational frequencies. The DFT vibrational frequencies are higher than the experimental ones [17,22], which can be corrected by applying the scaling of frequencies. Here, the scale factor of 0.9614 was used for the calculated frequencies [22].

3. RESULTS AND DISCUSSION

3.1. Geometry optimization

Here, geometries of the deprotonated TAR (TAR⁻) ligand and its M(TAR)₂ complexes (M=Fe^{II}, Cu^{II} and Zn^{II}) were fully optimized in the gas phase. In Table 1, some of the calculated structural parameters are listed, which are in good agreement with the corresponding values reported for similar compounds [7,9,18-20].

The TAR first loses its phenolic proton, which is bonded to the O2 atom. The optimized geometry of the obtained anionic TAR⁻ species is shown in Fig. 1. As seen, the geometry of TAR⁻ is not planar, but the benzene and thiazolyl rings make a dihedral angle of approximately 50° with each other. Although, each of the benzene and thiazolyl rings is planar. For example, the C2-C6-C9-C8 dihedral angle is 49.1° (Fig. 1 and Table 1).

* To whom all correspondence should be sent:
E-mail: beiramabadi@yahoo.com

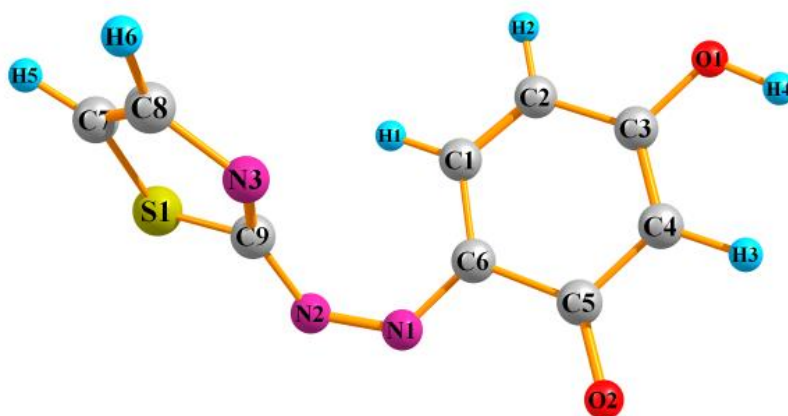


Fig. 1. The B3LYP/6-31+G(d,p) optimized structures of the TAR⁻ ligand.

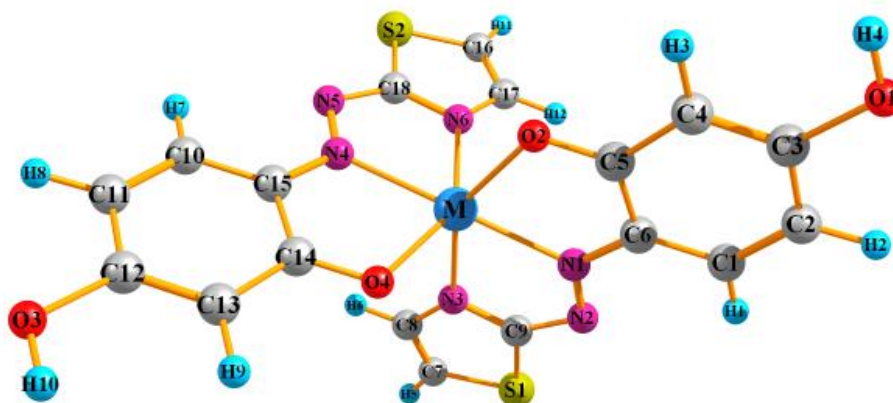


Fig. 2. The B3LYP/6-31+G(d,p) optimized structures of the M(TAR)₂ complexes, where M=Fe(II), Cu(II) and Zn(II).

In the structures of the complexes, the TAR⁻ species acts as a tridentate anionic ligand, which has an N,N,O⁻ binding mode. The optimized geometries of the Fe, Cu and Zn complexes are shown in Fig. 2 and their structural parameters are gathered in Table 1. In the optimized geometries of the complexes, the coordinated TAR⁻ is more planar than its free form. The dihedral angles N2-C9-S1-C7 and C2-C6-C9-C8 confirm this conclusion (Table 1).

The two TAR⁻ ligands, bonded to the central metal, fill six coordination positions of the octahedral complex. In the optimized geometries of the complexes, the TAR⁻ ligands are roughly perpendicular to each other, and form a dihedral angle of approximately 80.0° with each other.

The calculated structural parameters (Table 1) provide confirmation of the Jahn-Teller effect in the octahedral Cu(II) complex, which lengthens the equatorial bonds (Cu-N6 and Cu-O4) and shortens the axial bonds of a tetragonally distorted Cu(II) complex in comparison with the Fe and Zn complexes. In this way, the Cu-O4 bond is longer than the Cu-O2 bond, while the Cu-N3 bond is shorter than the Cu-N6 one.

As expected, the C3-O1 and C12-O2 bond lengths are 136 pm, which corresponds to a single C-O bond. The C5-O2 and C14-O4 bond lengths are 127 pm, corresponding to a C=O double bond.

3.2. Vibrational spectroscopy

Theoretical description of vibrational spectra is of practical importance for the identification of compounds. Here, the IR spectra of the M(TAR)₂ complexes were characterized theoretically. In Table 2, the selected vibrational wavenumbers computed by the B3LYP/6-31+G(d,p) approach are listed.

Overlapping of stretching vibrations of the O-H bonds with the C-H stretching modes leads to band broadening in the 3600-2000 cm⁻¹ spectral region of the IR spectra [17, 25-29]. The deconvolution of this region is given in Table 2. In all IR spectra, the most intensive band is related to the stretching vibrations of the phenolic O-H bonds.

An important diagnostic for coordination of the azo and Schiff-base ligands is the energy value of the very intensive band in the 1660-1500 cm⁻¹ region of the IR spectra [17,21,25-28]. By coordination, the symmetrical stretching modes of

C=N bonds shift to lower energy by 33 cm⁻¹ in comparison with the free TAR ligand (1513 cm⁻¹)

Table 1. Selected structural parameters of the TAR⁻ ligand and its M(TAR)₂ complexes.

	TAR ⁻	M		
		Fe	Cu	Zn
Bond length (PM)				
O1-H4	96.6	96.7	96.7	96.7
O1-C3	138.3	136.2	136.1	136.1
C3-C4	136.8	138.3	137.8	137.9
C5-C6	148.9	145.2	146.5	146.9
C6-N1	135.6	135.5	134.7	134.3
N1-N2	129.5	130.8	129.6	129.6
C9-N2	136.8	136.7	137.2	137.8
C9-N3	132.1	133.5	132.4	132.5
C8-N3	136.9	137.1	136.9	137.2
C7-C8	136.9	136.6	136.8	136.7
C7-S1	174.6	174.4	174.0	174.0
C5-O2	124.7	128.4	127.1	127.5
O2-N1	277.8	258.4	266.1	266.1
M- O2	-	215.9	213.7	212.5
M- O4	-	215.9	218.0	212.5
M- N1	-	215.5	202.0	220.5
M- N3	-	225.6	225.7	230.3
M- N4	-	215.4	202.9	220.5
M- N6	-	227.2	232.0	230.3
M- N2	-	306.8	292.5	310.5
Angle (°)				
C1-C2-C3	118.8	119.5	119.5	119.3
O2-C5-C6	124.1	119.6	120.9	121.3
C1-C6-N1	125.2	127.0	125.2	125.9
C5-C6-N1	115.1	111.4	113.6	113.0
C6-N1-N2	126.7	122.6	122.3	122.6
N1-N2-C9	126.4	107.5	111.2	110.1
N2-C9-N3	130.3	123.4	125.9	126.5
N2-C9-S1	115.7	122.9	120.1	119.5
C9-S1-C7	88.9	89.2	88.9	89.1
C7-C8-N3	117.4	115.1	115.6	115.6
O2-M-O4	-	91.0	96.7	99.1
O2-M-N1	-	82.8	79.5	75.8
O2-M-N3	-	148.2	154.5	146.6
O2-M-N4	-	162.0	99.1	108.7
O2-M-N6	-	90.9	91.3	93.5
N1-M-N4	-	177.6	178.0	173.4
N1-M-N3	-	79.2	75.3	70.9
N1-M-N6	-	102.5	106.8	104.4
N1-M-O4	-	102.3	102.1	108.6
Dihedral angle (°)				
O1-C3-C4-C5	179.8	-179.8	-179.9	-179.8
O2-C5-C6-N1	-9.2	-0.2	-0.5	-0.3
C6-N1-N2-C9	-28.5	178.1	-179.9	-179.9
N2-C9-S1-C7	170.1	179.8	180.0	179.9
S1-C7-C8-N3	0.7	0.1	0.2	0.2
C2-C6- C9-C8	-49.1	177.0	179.8	179.9
M-O2-N1-N3	-	0.2	3.4	2.0
O2- M-N4-N6	-	89.9	88.9	87.3
N3-O2- M-N4	-	178.9	-172.6	-171.1
C6-C9-C15-C18	-	80.8	-86.9	80.0
C3-C6-C15-C12	-	-74.0	-76.0	-79.6
C7-C9-C16-C18	-	80.2	87.8	81.2

Table 2. Some calculated IR vibrational frequencies (cm⁻¹) of the Fe, Cu and Zn complexes of TAR.

TAR	Fe	Cu	Zn	Vibrational assignment
418(89)	422(94)	428(77)	429(95)	δ _{op} (-OH)
-	496(30)	500(14)	496(11)	ν(M-N)
-	516(58)	513(43)	519(56)	ν _{asym} (M-O)
-	527(34)	516(55)	520(52)	ν _{sym} (M-O)
1016(33)	-	-	-	δ _{op} (N1-H5)
1140(376)	1135(467)	1136(428)	1136(468)	ν(C9-S1)
1186(243)	1199(202)	1198(218)	1198(291)	ν(C-O)phenolic
1338(112)	1340(616)	1349(842)	1345(751)	ν _{asym} (N2-C9-N3) + ν _{asym} (C7-C8-N3)
1452(945)	1405(271)	1405(274)	1409(359)	ν(N-N)
1513(60)	1476(76)	1472(232)	1479(194)	ν(C-N)
1617(324)	1521(135)	1528(34)	1524(337)	ν(C5-O2)
1569(177)	1592(486)	1589(935)	1591(1024)	ν(C-C) benzene
3053-3078(11,3)	3069-3104(14,6)	3068-3106(14,8)	3068-3103(14,7)	ν(C-H) benzene
3080(12)	3113(8)	3113(8)	3112(10)	ν(C-H) thiazolyl ring
3100(115)	-	-	-	ν(N1-H5)
3660(133)	3667(126)	3666(125)	3666(122)	ν(O-H) phenolic

The intensity of each absorption is shown in parentheses in front of its computed frequency.

δ_{op}= out-of-plane-rotational vibration.

Computed values suggested that the stretching C5-O2 and C14-O4 vibrations appear as a strong band in the IR spectra at 1550-1500 cm⁻¹, while the C3-O1 and C12-O3 stretching vibrations appear as a strong band at energies lower by 250 cm⁻¹. This is in agreement with their C=O double bond and C-O single bond characteristics, respectively. By complexation, the ν(C5-O2) and ν(C14-O4) bands shift to lower energies in comparison with the free TAR ligand.

An intensive band at about 1140 cm⁻¹ in the IR spectra of the ligand and complexes is attributed to the stretching vibration of the C-S bonds (Table 2). The presented vibrational assignments can be used for analysis of similar compounds, helping to explain their vibrational behaviour.

4. CONCLUSIONS

In this work, the optimized geometries and IR vibrational frequencies of the Fe(II), Cu(II) and Zn(II) complexes of the TAR ligand were calculated by the DFT method. All complexes are octahedral, where the two TAR⁻ act as anionic tridentate ligands. The ligands coordinate to the metal ions *via* the thiazolyl N atom, azo N atom and the deprotonated phenolic O⁻.

The free TAR⁻ ligand is not planar. However, it is more planar in the coordinated form. The two TAR⁻ ligands are roughly perpendicular to each other. The Cu(II) complex exhibits Jahn-Teller distortion.

The important vibrational modes of the TAR ligand and its complexes were assigned theoretically, which can be used for identification of similar compounds.

REFERENCES

1. S. Wu, W. Qian, Z. Xia, Y. Zou, S. Wang, S. Shen, *Chem. Phys. Lett.*, **330**, 535 (2000).
2. H. Kocaokutgen, S. Ozkinali, *Dyes Pigm.*, **63**, 83 (2004).
3. F. Karipcin, B. Dede, S. Percin-Ozkorucuklu, E. Kabalcilar; *Dyes Pigm.*, **84**, 14 (2010).
4. T. Abe, S. Mano, Y. Yamada and A. Tomotake, *J. Imag. Sci. Tech.*, **43**, 339 (1999).
5. S. Wang, S. Shen, H. Xu, *Dyes Pigm.*, **44**, 195 (2000).
6. K. Ueno, T. Imamura, K.L. Cheng, *CRC Handbook of Organic Analytical Reagents*, CRC Press, P. 227, (1992).
7. M. Soylak, E. Yilmaz, *J. Hazard. Mater.*, **182**, 704 (2010).
8. J.B. Ghasemi, B. Hashemi, *Environ. Mod. Assess.* (in press).
9. D.K. Singh, S. Mishra, *Desalination*, **257**, 177 (2010).

10. R.D. Bach, C. Canepa, M.N. Glukhovtsev, *J. Am. Chem. Soc.*, **121**, 6542 (1999).
11. P.J. Gorolomova, R.P. Nikolova, B.L. Shivachev, V.I. Ilieva, D.T. Tsekova, T.D. Tosheva, E.S. Tashev, S.G. Varbanov, G.G. Gencheva, *Bulg. Chem. Commun.*, **43**, 244 (2011).
12. S.A. Beyramabadi, H. Eshtiagh-Hosseini, M.R. Housaindokht, A. Morsali, *Organometallics*, **27**, 72 (2008).
13. S.A. Beyramabadi, H. Eshtiagh-Hosseini, M.R. Housaindokht, A. Morsali, *J. Mol. Struct.: THEOCHEM*, **903**, 108 (2009).
14. A. Jezierska-Mazzarello, R. Vuilleumier, J.J. Panek, G. Ciccotti, *J. Phys. Chem. B*, **114**, 242 (2010).
15. S. Chowdhury, F. Himo, N. Russo, E. Sicilia, *J. Am. Chem. Soc.*, **132**, 4178 (2010).
16. V. Enchev, S. Angelova, N. Markova, I. Wawer, E. Stanoeva, M. Mitewa, *Bulg. Chem. Commun.*, **40**, 532 (2008).
17. H. Eshtiagh-Hosseini, M.R. Housaindokht, S.A. Beyramabadi, S. Beheshti, A.A. Esmaeili, M. Javan-Khoshkholgh, *Spectrochim. Acta Part A*, **71**, 1341 (2008).
18. R.E. Shepherd, *Coord. Chem. Rev.*, **247**, 159 (2003).
19. V.M. Ivanov, O.V. Kuznetsova, *J. Anal. Chem.*, **55**, 899 (2000).
20. R.W. Stanley, G.E. Cheney, *Talanta*, **13**, 1619 (1966).
21. F. Karipcin, E. Kabalcilar, S. Ilican, Y. Caglar, M. Caglar, *Spectrochim. Acta Part A*, **73**, 174 (2009).
22. D.C. Young, *Computational Chemistry: A Practical Guide for Applying Techniques to Real-World Problems*, John Wiley & Sons, Inc., 2001.
23. M.J. Frisch, et al. Gaussian 03, Revision B.03; Gaussian, Inc.: Pittsburgh PA, 2003.
24. C. Lee, W. Yang, R.G. Parr, *Phys. Rev. B*, **37**, 785 (1988).
25. S.A. Beyramabadi, A. Morsali, M. Javan Khoshkholgh, A.A. Esmaeili, *J. Struct. Chem.*, accepted for publication (2012).
26. H. Eshtiagh-Hosseini, M.R. Housaindokht, S.A. Beyramabadi, S.H. Mir Tabatabaie, A.A. Esmaeili, M. Javan Khoshkholgh, *Spectrochim. Acta Part A*, **78**, 1046 (2011).
27. J. Sanmartín, A.M. García-Deibe, M. Fondo, D. Navarro, M.R. Bermejo, *Polyhedron*, **23**, 963 (2004).
28. D.C. Ware, D.S. Mackie, P.J. Brothers, W.A. Denny, *Polyhedron*, **14**, 1641 (1995).
29. S.A. Beyramabadi, A. Morsali, A.A. Esmaeili, M. Javan Khoshkholgh, *Spectrochim. Acta Part A*, **83**, 467 (2011).

DFT-ИЗСЛЕДВАНЕ НА КОМПЛЕКСИТЕ НА ЖЕЛЯЗОТО, МЕДТА И ЦИНКА С 4-(2-ТИАЗОЛИЛАЗО)РЕЗОРЦИНОЛ

С. Али Бейрамабади

Департамент по химия, Клон Маишад, Ислямски университет Азад, Маишад, Иран

Постъпила на 23 август, 2012 г.; коригирана на 19 април, 2013 г.

(Резюме)

В настоящата работа са охарактеризирани теоретично комплексите на Fe(II), Cu(II) и Zn(II) с лиганди от 4-(2-тиазолилазо) резорцинол (TAR). Изчислени са тяхните оптимизирани геометрии и теоретичните вибрационни честоти с помощта на DFT-теорията при използването на B3LYP-функционал. В структурите на октаедричните комплекси депротонирания TAR (TAR⁻) действа като анионен тридентатен лиганд чрез азотния атом, тиазолил-азотния атом и фенолния кислороден атом. В октаедричните комплекси двата TAR-лиганди са почти взаимно перпендикулярни. Предполага се комплексът Cu(TAR)₂ да проявява Jahn-Teller отместваене.

MnSO₄·H₂O: A highly efficient and inexpensive catalyst for the synthesis of benzo-2-pyrones and benzopyrazines

F. Jafari¹, S. Khodabakhshi^{*,2}

¹Department of Chemistry, Dezful Branch, Islamic Azad University, Dezful, Iran

²Young Researchers and Elite Club, Gachsaran Branch, Islamic Azad University, Gachsaran, Iran

Received October 8, 2012; Revised April 17, 2013

Efficient and direct protocols for the preparation of some heterocyclic compounds such as benzo-2-pyrones and benzopyrazines in the presence of manganese (II) sulfate monohydrate (MnSO₄·H₂O) as an inexpensive catalyst have been described. These novel methods are very cheap and they include some advantages, such as excellent yields, use of the safe catalyst and readily available starting materials, and simple work-up procedure.

Keywords: MnSO₄·H₂O; Benzo-2-pyrones, Benzopyrazine; Catalyst.

INTRODUCTION

Development of methods including preparation of heterocycles, which are naturally occurring products, is very significant. A number of heterocyclic compounds, such as benzo-2-pyrones [1] and benzopyrazines [2,3] are found in natural systems.

Some of the substituted benzopyrazines (quinoxalines) have shown antibacterial [4] antifungal [5], anticancer [6], antitubercular [7] antileishmanial [8], and antimalarial activities [9]. For instance, actinomycin (Fig. 1), a substituted quinoxaline, inhibits the growth of gram positive bacteria and it is a blocking agent against various transplantable tumors [10]. Coumarin derivatives also possess diverse biological properties. For example, some polycyclic coumarins such as

calanolides [11] isolated from *Calophyllum* genus, and others have shown potent anti-HIV activity [12]. Numerous coumarins have been also used as drug in contemporary medicine. As can be seen in Fig. 1, warfarin, acenocoumarol, and phenprocoumon are vitamin K antagonists which play anticoagulant role in treatment of thromboembolic disorders [13].

Besides, some coumarins are used as additive in food and cosmetics [14], optical brighteners [15], and dispersed fluorescent and laser dyes [16]. Based on these properties, the synthesis of these heterocycles has attracted much attention of researchers [17-20]. In this work, in regard of some reports on the application of manganese (II) sulfate monohydrate in organic transformations,

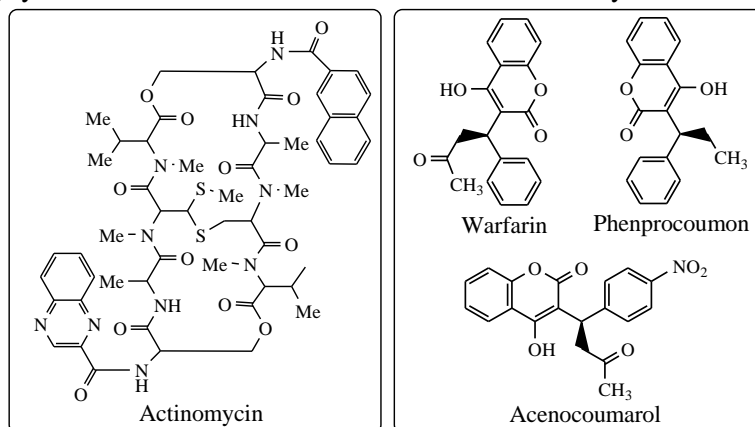


Fig. 1. Some biologically active coumarins and actinomycin.

* To whom all correspondence should be sent:
E-mail: saeidkhm@yahoo.com

we decided to introduce a new application of manganese (II) sulfate monohydrate as a Lewis acid catalyst in synthesis of some benzo fused heterocycles containing nitrogen and oxygen atoms.

RESULTS AND DISCUSSION

Recently, heterogeneous catalysts have gained much attraction, because they are generally inexpensive, easily available and they can conveniently be handled and separated from the reaction mixture, thus the experimental procedure would be simple and eco-friendly [21]. Also, establishing the reaction based on solvent-free conditions obviously reduce pollution, and bring down handling costs due to simplification of experimental procedure, work up technique and saving in labour.

In 1883, Hans von Pechmann and Carl Duisberg found that phenols react with β -keto esters in the presence of sulfuric acid, giving coumarin (benzo-2-pyrone) derivatives [22]. Generally, Pechmann condensation reaction is common method for the synthesis of coumarin derivatives, because it needs simple precursors. In addition, coumarins with substitution on either pyrone or benzene ring or both are affordable in good to excellent yield via the Pechmann condensation. In this study, we found that the Pechmann cyclocondensation of phenols **1** with β -ketoesters **2** in the presence of $MnSO_4 \cdot H_2O$ as an efficient catalyst produces the substituted coumarins **3** under thermal and solvent-free conditions (Scheme 1).

To make optimized conditions, the synthesis of compound **3a** was chosen as a model. As shown in Table 1, it can be concluded that the thermal-assisted model reaction is efficiently carried out by adding catalytic amounts of $MnSO_4 \cdot H_2O$ (20

mol%) in solvent-free conditions at 100 °C. It is noteworthy to not that in the absence of catalyst, the reaction didn't proceed for a long reaction time (12 h) and also using excessive amounts of catalyst cannot improve the product yield.

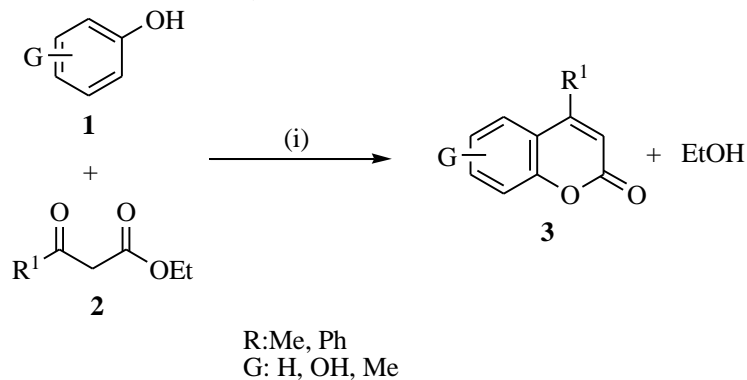
Table 1. The effect of catalyst amount on the synthesis of **3a** at 100°C under solvent-free conditions.

Entry	Catalyst (mol%)	Time (min)	Yield ^a (%)
1	-	720	-
2	5	180	32
3	10	180	66
4	20	45	85
5	30	45	84

^a Refers to isolated yields.

After optimization of the reaction conditions, various phenols such as resorcinol, pyrogallol and phloroglucinol were successfully used for the efficient Pechmann reaction (catalyzed by $MnSO_4 \cdot H_2O$) with different β -ketoesters. A number of coumarins were obtained through this method in good yield and short reaction times (Table 2).

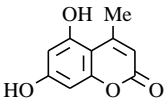
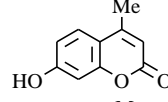
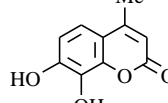
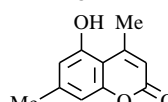
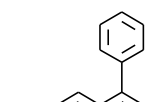
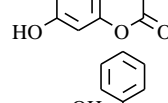
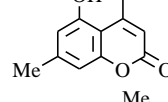
The ¹H NMR spectrum of **3a** exhibited five sharp singlets identified as methyl ($\delta = 2.49$ ppm), olefinic pyrone ring ($\delta = 5.83$ ppm) and two OH group ($\delta = 10.28, 10.51$ ppm), protons. Two singlet signals ($\delta = 6.15$ ppm) and ($\delta = 6.24$ ppm) correspond to the aromatic protons of benzene ring. The proton decoupled ¹³C NMR spectrum of **3a** showed 10 distinct resonances in accord with expected structure. A reasonable mechanism for manganese (II)-catalyzed Pechmann reaction has been proposed in Scheme 2.



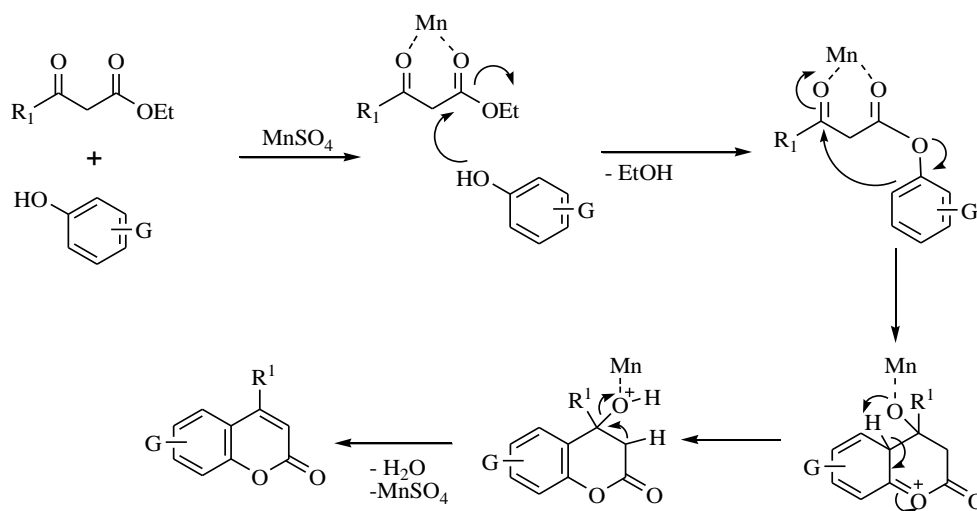
(i): $MnSO_4 \cdot H_2O$ (20 mol%), solvent-free, 100 °C

Scheme 1. Pechmann condensation catalyzed by $MnSO_4 \cdot H_2O$.

Table 2. Synthesis of some coumarin derivatives based on Pechmann condensation using $MnSO_4 \cdot H_2O$ at 100 °C under solvent-free conditions

Entry	Product	Time (min)	Yield (%) ^a	M.p. (°C)
3a		45	85	288-290
3b		60	80	188-190
3c		45	85	243-245
3d		60	90	244-246
3e		100	75	257-259
3f		90	80	243-245
3g		50	90	150-152

^aRefers to isolated yields.

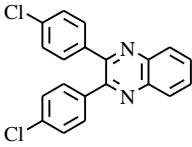
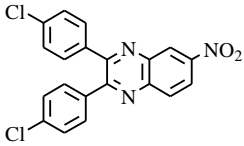
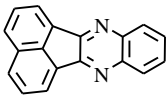
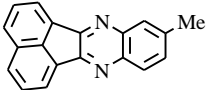
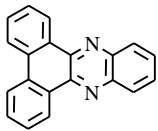
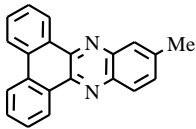


Scheme 2. Suggested mechanism for the Pechmann reaction catalyzed by $MnSO_4$.

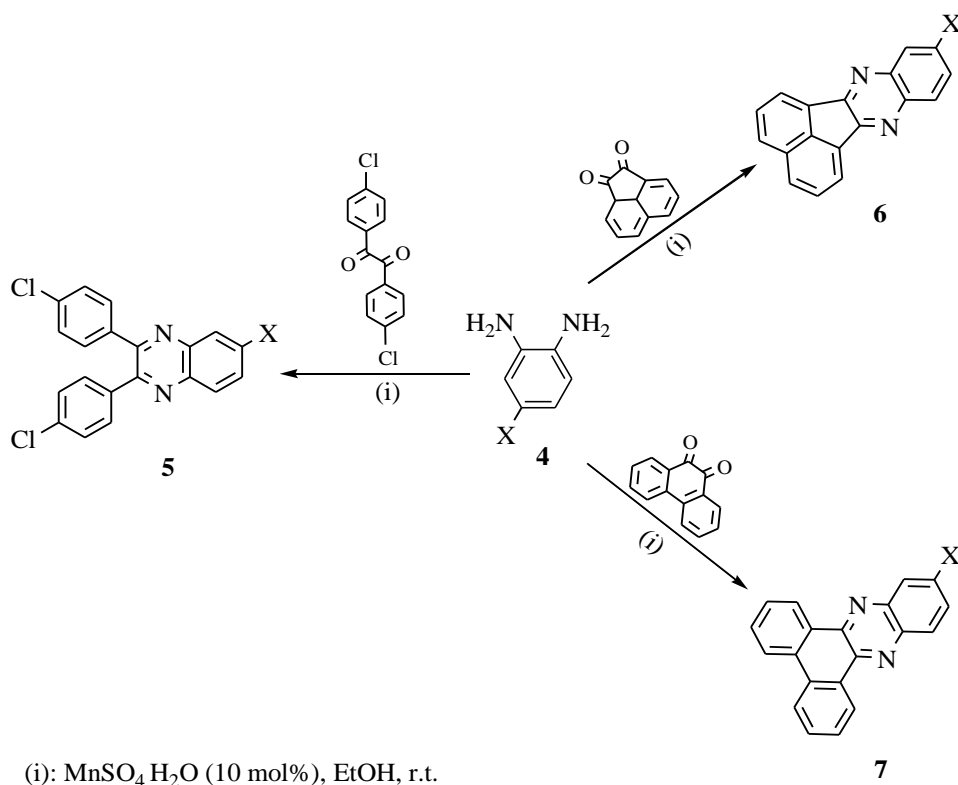
This manganese (II)-catalyzed protocol was also applied for the condensation reactions involving the treatment of *o*-phenylenediamines **4** and three different aromatic 1,2-dicarbonyls to produce bezopyrazines (quinoxalines and phenazines) **5-7** in

excellent yield. In this case, synthesis of **5a** was selected as a model and after optimization through employing several amounts of catalyst, it was found that the results was satisfactory by adding $MnSO_4 \cdot H_2O$ (10 mol%) in EtOH at room

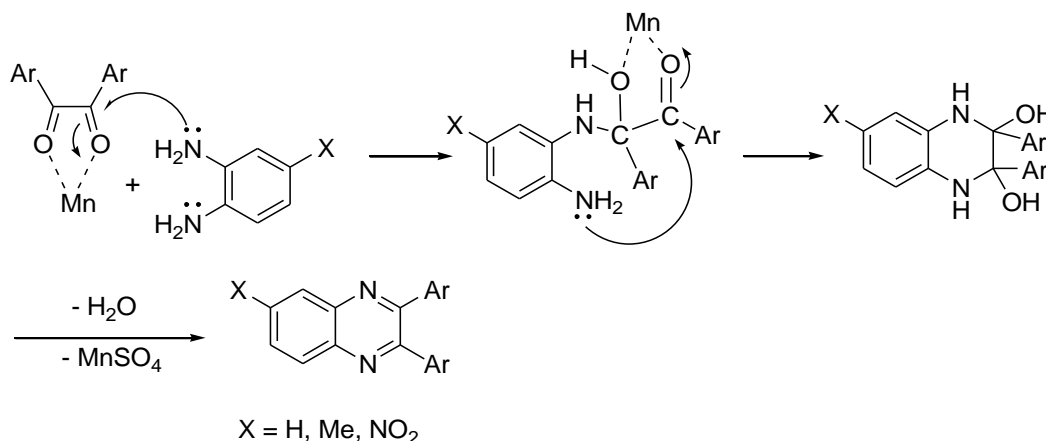
Table 3. Synthesis of benzopyrazine derivatives using $MnSO_4 \cdot H_2O$ in EtOH at room temperature

Entry	Product	Time (min)	Yield (%) ^a	M.p. (°C)
5a		35	95	192-194
5b		120	90	175-177
6a		15	90	238-240
6b		15	95	229-231
7a		12	98	225-227
7b		12	95	218-220

^a Identified by comparison with authentic samples. ^b Refers to isolated yields.



Scheme 3. Synthesis of benzopyrazines by the use of $MnSO_4 \cdot H_2O$.



Scheme 4: Suggested mechanism for the synthesis of phenazines and quinoxalines using $MnSO_4$.

temperature (Scheme 3). Although the generally mechanistic details of this reaction are not yet fully understood, a feasible pathway depicted in Scheme 4. The driving force for all of these reactions is cyclo-aromatization. The catalyst has been applied successfully for the condensation of a variety of aromatic 1,2-dicarbonyl compounds with *o*-phenylenediamines. The results can be seen in Table 3.

It should be mentioned that the reaction of aliphatic 1,2-dicarbonyl compounds with *o*-phenylenediamines in the presence of this catalyst was unsuccessful and after a prolonged reaction time, the TLC of the reaction mixture showed a combination of starting materials and numerous products. It seems that the alkyl aldehydes are enolizable and it is a limiting factor.

EXPERIMENTAL

General

The chemicals were purchased from Merck, Fluka and Aldrich chemical companies. The reactions were monitored by TLC (silica-gel 60 F₂₅₄, hexane: EtOAc). IR spectra were recorded on a FT-IR Shimadzu-470 spectrometer and the ¹H NMR spectra was obtained on a Bruker-Instrument DPX-400 and 500 Avance 2 model.

General procedure for the preparation of coumarin 3

A mixture of phenol **1** (1 mmol), β -ketoesters **2** (1 mmol) and $MnSO_4 \cdot H_2O$ (20 mol%) was stirred at 100 °C for an appropriate time. After completion of the reaction (controlled by TLC), the reaction mixture was cooled to room temperature and poured into crushed ice. Then, the precipitate was separated through simple filtration, washed with ice cold water. The pure product **3**, finally, was obtained after recrystallization from EtOH.

Compound 3a: ¹H NMR (400 MHz, DMSO-*d*₆): δ 10.51 (s, 1H), 10.28 (s, 1H), 6.24 (s, 1H), 6.15 (s, 1H), 5.83 (s, 1H), 2.47 (s, 3H). ¹³C NMR (100 MHz, DMSO-*d*₆): δ 161.51, 160.55, 158.39, 155.43, 109.29, 102.55, 99.54, 94.98, 23.88. Anal. Calcd. For C₁₀H₈O₄: C, 62.50; H, 4.20. Found: C, 62.69, H, 4.15.

Compound 3b: ¹H NMR (500 MHz, CDCl₃): δ 7.49-7.47 (d, *J*=6.8 Hz), 6.85 (d, 1H, *J*=2 Hz), 6.82 (dd, 1H, *J*=6.8, 2.4 Hz), 6.14 (s, 1H), 5.7 (s, 1H), 2.35 (s, 3H). Anal. Calcd. For C₁₀H₈O₃: C, 68.18; H, 4.58. Found: C, 68.36, H, 4.50.

Compound 3c: ¹H NMR (400 MHz, DMSO-*d*₆): δ 10.15 (s, 1H), 9.30 (s, 1H), 7.08 (d, 1H, *J*=8.8 Hz), 6.81 (d, 1H, *J*=8.8 Hz), 6.10 (s, 1H), 2.33 (s, 3H). ¹³C NMR (100 MHz, DMSO-*d*₆): 160.47, 154.35, 149.81, 144.13, 143.74, 132.60, 115.88, 113.23, 112.56, 110.60, 40.42, 40.21, 40.00, 39.79, 39.58, 39.38, 39.17, 1863. Anal. Calcd. For C₁₀H₈O₄: C, 62.50; H, 4.20. Found: C, 62.58, H, 4.27.

Compound 3d: ¹H NMR (400 MHz, DMSO-*d*₆): δ 10.52 (s, 1H), 6.60 (d, 2H), 6.03 (s, 1H), 3.49 (s, 3H), 2.26 (s, 3H). ¹³C NMR (100 MHz, DMSO-*d*₆): 160.29, 156.90, 155.28, 155.04, 143.18, 112.37, 112.30, 108.15, 106.96, 23.91, 21.56. Anal. Calcd. For C₁₁H₁₀O₃: C, 69.46; H, 5.30. Found: C, 69.71, H, 5.25.

Compound 3e: ¹H NMR (400 MHz, DMSO-*d*₆): δ 10.65 (s, 1H), 7.34 (s, 4H), 7.28 (s, 2H), 7.05 (d, 1H, *J*=8.8 Hz), 6.56 (m, 2H). ¹³C NMR (100 MHz, DMSO-*d*₆): 161.80, 160.77, 155.96, 135.52, 130.07, 129.29, 128.79, 128.54, 113.68, 111.08, 110.70. Anal. Calcd. For C₁₅H₁₀O₃: C, 75.62; H, 4.23. Found: C, 75.88, H, 4.18.

Compound 3f: ¹H NMR (400 MHz, DMSO-*d*₆): δ 10.13 (s, 1H), 7.37 (m, 5H), 6.072 (s, 1H), 6.47 (s, 1H), 5.95 (s, 1H), 2.29 (s, 3H). ¹³C NMR (100 MHz, DMSO-*d*₆): 160.09, 156.05, 155.96, 155.91,

143.93, 139.75, 128.34, 127.92, 127.75, 113.88, 112.52, 108.19, 105.44, 21.65. Anal. Calcd. For $C_{16}H_{12}O_3$: C, 76.18; H, 4.79. Found: C, 76.25, H, 4.82.

Compound 3g: 1H NMR (400 MHz, DMSO- d_6): δ 7.96 (s, 1H), 6.97 (s, 2H), 6.20 (s, 1H), 3.85 (s, 3H), 2.39 (s, 3H). ^{13}C NMR (100 MHz, DMSO- d_6): δ 162.83, 160.59, 155.24, 153.86, 126.88, 113.66, 112.54, 111.58, 101.16, 56.36, 18.58. Anal. Calcd. For $C_{11}H_{10}O_3$: C, 69.46; H, 5.30. Found: C, 69.70, H, 4.17.

General procedure for the preparation of benzopyrazines 5-7

A mixture of 1,2-dicarbonyl compound (1 mmol), *o*-phenylenediamine (1.1 mmol) and

$MnSO_4 \cdot H_2O$ (10 mol%) in EtOH (5 mL) was stirred at room temperature. The progress of the reaction was monitored by TLC. After completion of the reaction, the solid was filtered and recrystallized from EtOH to afford the pure product **5-7**.

Compound 5a: 1H NMR (400 MHz, $CDCl_3$): δ 8.20 (m, 2H), 7.830 (m, 2H), 7.521 (m, 4H), 7.39 (m, 4H). ^{13}C NMR (500 MHz, $CDCl_3$): δ 152.34, 141.67, 137.69, 135.78, 131.61, 130.79, 129.63, 129.15. Anal. Calcd. For $C_{10}H_8O_4$: $C_{20}H_{12}Cl_2N_2$: C, 68.39; H, 3.44; N, 7.98. Found: C, 68.61; H, 3.40; N, 8.07.

Compound 5b: 1H NMR (400 MHz, $CDCl_3$): δ 9.08 (d, 1H, $J=2.4$ Hz), 8.58 (dd, 1H, $J=9.2, 4$ Hz), 8.33 (d, 1H, $J=9.2$ Hz), 7.57-7.54 (m, 4H), 7.43-7.30 (m, 4H). ^{13}C -NMR (100 MHz, $CDCl_3$): δ 155.18, 154.57, 148.53, 143.91, 140.40, 136.87, 136.72, 136.67, 136.60, 131.66, 131.58, 131.20, 129.37, 125.99, 124.08. Anal. Calcd. For $C_{20}H_{11}C_{12}N_3O_2$: C, 60.63; H, 2.80; N, 10.61. Found: C, 60.86; H, 2.70; N, 10.75.

Compound 6a: 1H NMR (400 MHz, $CDCl_3$): δ 8.21 (d, 2H, $J=6.8$ Hz), 8.02 (dd, 2H, $J=6.2, 3.2$ Hz), 7.90 (d, 2H, $J=8.4$ Hz), 7.65 (t, 2H, $J=7$ Hz), 7.57 (dd, 2H, $J=6.4, 3.6$ Hz); ^{13}C NMR (100 MHz, $CDCl_3$): δ 155.19, 142.39, 137.60, 132.92, 131.10, 130.47, 130.59, 130.36, 129.78, 122.96. Anal. Calcd. For $C_{18}H_{10}N_2$: C, 85.02; H, 3.96; N, 11.02. Found: C, 85.15; H, 3.90; N, 10.96.

Compound 6b: 1H NMR (400 MHz, $CDCl_3$): δ 8.21 (t, 2H, $J=6.4$ Hz), 7.90 (dd, 3H, $J=8.2$ Hz, 3.2 Hz), 7.79 (s, 1H), 7.64 (t, 2H, $J=7.4$ Hz), 7.40 (dd, 1H, $J=8.4, 1.6$ Hz), 2.43 (s, 3H). ^{13}C NMR (100 MHz, $CDCl_3$): δ 155.15, 154.44, 142.38, 140.82, 140.71, 137.35, 133.08, 132.44, 131.06, 130.46, 130.31, 130.21, 129.89, 129.72, 122.83, 122.68,

22.94. Anal. Calcd. For $C_{19}H_{12}N_2$: C, 85.05; H, 4.51; N, 10.44. Found: C, 85.24; H, 4.40; N, 10.12.

Compound 7a: 1H NMR (400 MHz, $CDCl_3$): δ 9.18 (d, 2H, $J=7.6$ Hz), 8.34 (d, 2H, $J=8.0$ Hz) 8.12 (dd, 2H, $J=6.4, 3.6$ Hz), 7.66-7.51 (m, 6H); ^{13}C NMR (100 MHz, $CDCl_3$): δ 143.54, 143.28, 133.15, 131.42, 130.88, 130.57, 129.04, 127.38, 124.03. Anal. Calcd. For $C_{20}H_{12}N_2$: C, 85.69; H, 4.31; N, 9.99. Found: C, 85.73; H, 4.33; N, 9.95.

Compound 7b: 1H NMR (400MHz, $CDCl_3$): δ 9.14 (dd, 2H, $J=6.00, 1.6$ Hz), 8.32 (2H, d, $J=8$ Hz), 7.97 (1H, d, $J=8.4$ Hz), 7.58 (s, 1H), 7.53-7.52 (m, 5H), 2.54 (s, 3H). ^{13}C NMR (100 MHz, $CDCl_3$): δ 143.29, 143.27, 142.72, 141.81, 141.41, 133.45, 133.06, 132.87, 131.49, 131.45, 131.20, 131.07, 130.01, 129.10, 128.92, 127.29, 127.15, 123.95, 23.20. Anal. Calcd. For $C_{21}H_{14}N_2$: C, 85.69; H, 4.79; N, 9.52. Found: C, 85.73; H, 4.75; N, 9.53

CONCLUSIONS

In summary, this study demonstrated the facile $MnSO_4 \cdot H_2O$ -catalyzed reactions with satisfactory results. Some important advantages of the presented methods are the short reaction time, high yields, simple workup procedures, and the use of inexpensive and available catalyst. These procedures do not involve any hazardous organic solvent, thus, they are they are environmentally friendly methods

Acknowledgement. The authors gratefully acknowledge the partial support of this work by the Islamic Azad University, Dezful Branch, Iran.

REFERENCES

1. A. Cervi, P. Aillard, N. Hazeri, L. Petit, C. L. L. Chai, A. C. Willis, M. G. Banwell, *J. Org. Chem.*, **78**, 9876 (2013).
2. P. Roy, B. K. Ghorai, *Beilstein J. Org. Chem.*, **6**, 1 (2010).
3. A. Dell, D.H. William, H.R. Morris, G.A. Smith, J. Feeney, G. C. K. Roberts, *J. Am. Chem. Soc.*, **97**, 2497 (1975).
4. A.A. El-Gendy, S. El-Meligie, A. El-Ansary, A.M. Ahmedy, *Arch. Pharm. Res.*, **18**, 44 (1995).
5. V. K. Tandon, D. B. Yadav, H. K. Maurya, A. K. Chaturvedi, P. K. S. Design, *Bioorg. Med. Chem.*, **14**, 6120 (2006).
6. A. Monge, F. J. Martinez-Crespo, A. L. Cerain, J. A. Palop, S. Narro, V. Senador, A. Marin, Y. Sainz, M. Gonzalez, E. Hamilton, A. J. Barker, *J. Med. Chem.*, **38**, 4488 (1995).
7. A. Jaso, B. Zarranz, I. Aldana, A. Monge, *Eur. J. Med. Chem.*, **38**, 791 (2003).

8. J. Guillon, I. Forfar, M. Matsuda, V. Desplat, M. Saliege, D. Thiolat, *Bioorg. Med. Chem. Lett.*, **15**, 194 (2007).
9. J.B. Rangisetty, C.N.V. H.B. Gupta, A.L. Prasad, P. Srinivas, N. Sridhar, P. Parimoo, A. Veeranjanyulu, *J. Pharm. Pharmacol.*, **53**, 1409 (2001).
10. S. Sato, O. Shiratori, K. Katagiri, *J. Antibiot.* **20**, 270 (1967).
11. Y. Kashman, K.R. Gustafson, R.W. Fuller, J.H. Cardellina, J.B. McMahon, M.J. Currens, R.W. Buckheit, S.H. Hughes, G.M. Cragg, M.R. Boyd, *J. Med. Chem.*, **35**, 2735, (1992).
12. Y.T. Reddy, V.N. Sonar, P.A. Crooks, P.K. Dasari, P.N. Reddy, B. Rajitha, *Synth. Commun.*, **38**, 2028, (2008).
13. M. Beinema, J.R. Brouwers, T. Schalekamp, B. Wilffert, *Thromb. Haemost.*, **100**, 1052, (2008).
14. R. O'Kennedy, R. D. Thornes, *Coumarins: Biology, Applications, and Mode of Action*, 1997, Wiley: Chichester.
15. M. Zahradnik, *The Production and Application of Fluorescent Brightening Agents*, 1992, Wiley: New York.
16. R.D.H. Murray, J. Mendez, S.A. Brown, *The Natural Coumarins: Occurrence, Chemistry, and Biochemistry*, 1982, Wiley: New York.
17. M. Opanasenko, M. Shamzhy, J. Cejka, *Chem. Cat. Chem.*, **5**, 1024 (2013).
18. B. Karami, S. Khodabakhshi, K. Eskandari, *Tetrahedron Lett.*, **53**, 1445 (2012).
19. N. Ghaffari Khaligh, *Catal. Sci. Technol.*, **2**, 1633 (2012).
20. (a) Aiping Huang, Yimu Chen, Yige Zhou, Wei Guo, Xiaodong Wu, Chen Ma, *Org. Lett.*, **15**, 5480 (2013). (b) S. Biswas, S.Batra, *Eur. J. Org. Chem.* **2013**, 4895 (2013).
21. B. Karami, K. Eskandari, S. Khodabakhshi, S. J. Hoseini, F. Hashemian, *RSC Adv.*, **3**, 23335 (2013).
22. H. V. Pechmann, C. Duisberg, *Ber. Dtsch. Chem. Ges.*, **16**, 2119 (1883).

$MnSO_4 \cdot H_2O$: ВИСОКОЕФЕКТИВЕН И ЕВТИН КАТАЛИЗАТОР ЗА СИНТЕЗА НА БЕНЗО-2-ПИРОНИ И БЕНЗОПИРАЗИНИ

Ф. Джафари¹, С. Ходабахши^{*,2}

¹Департамент по химия, Клон Дезфул, Ислямски университет Азад, Дезфул, Иран

²Клуб за млади изследователи, Клон Гачсаран, Ислямски университет Азад, Гачсаран, Иран

Постъпила на 8 октомври, 2012 г.; коригирана на 17 април, 2013 г.

(Резюме)

Предложена е ефективна и пряка методика за получаването на хетероциклени съединения като бензо-2-пирони и бензопиразини в присъствие на $MnSO_4 \cdot H_2O$ Като евтин катализатор. Тези нови методи са евтини и с предимства, Като отличен добив, използване на безопасен катализатор, достъпни реактиви и проста процедура.

.....

Imine-enamine tautomerism in bicyclic systems in gas phase and solution: a computational study

H. Moghanian¹, A. Mohamadi*²

¹ Young Researchers and Elite Club, Dezful Branch, Islamic Azad University, Dezful, Iran

² Department of Chemistry, Farahan Branch, Islamic Azad University, Farahan, Iran

Received December 17, 2012; Revised April 15, 2013

DFT calculations have been carried out on the bicyclic imines to investigate the influence of ring size on the imine-enamine tautomerisms. Molecular geometries and energetic of imines and enamines in gaseous phase have been obtained using B₃LYP levels of theory, implementing 6-311⁺⁺G(d,p) basis set. Then, important molecular parameters, IR frequencies, NBO and energetic results in the gas phase were extracted. The energetic results show that relative stability of enamine tautomer (versus imine tautomer) increases with the increase of ring size and calculated frequencies show that by decreasing N-containing ring size from 6-membered to 4-membered ring, the frequency of C=N in imine tautomer decreases. In addition variation of NBO charges on atoms in the gas phase are studied.

Key words: DFT study, Tautomerism, Bicyclic, Imine, Enamine, NBO analysis.

INTRODUCTION

Tautomerism is one of the fundamental processes in (bio) organic chemistry that underlies most of the important condensation reactions. It has been extensively studied experimentally and theoretically. For example, tautomerisms in ket-enol [1-5], imine-enamine [6-8], purines [9], pirimidines [10] and many other systems [11-13] have been studied during past two decades. Thereupon, compounds containing different tautomers can be the subject of interest by theoretical chemists.

Imines formations are a particularly important chemical reaction in some biological processes [14, 15] for example, the covalent binding of carbonyl-containing compounds to an enzyme usually involves the formation of an imine. The imine moiety is formed by condensation of carbonyl groups of ketone or aldehyde with a primary or secondary amine. Equilibrium between imine and enamine may be established when at least one hydrogen atom on the imine nitrogen. The relative equilibrium of these species depends on the symmetry of the parent ketone and the substituents on the amine [16].

In this study we focused our research on imine-enamine tautomerism in bicyclic systems. These N-containing heterocycles have three tautomeric forms, one is imine form (I) and others are enamine forms (E_a and E_b). The physicochemical

characteristics of some of the heterocycles were experimentally determined. For example, spectrophotometric data for hexahydroindole that previously expressed as the enamine form (E_b) showed no band in the NH-stretching region in accordance with the imine structure [17]. In the absence of experimental data, it is of special interest to characterize theoretically the imine-enamine tautomeric equilibria to obtain information about the thermodynamic and kinetic aspects.

In this research, molecular parameters, relative energies, NBO analysis and vibrational frequencies of imines and enamines in different ring have been calculated using B₃LYP/6-311⁺⁺G** level of theory. Details of computations and the results obtained in this work are presented below.

COMPUTATIONAL METHODS

The ground-state properties of the all tautomers have been calculated by using B₃LYP method at 6-311⁺⁺G(d,p) basis set level. All computations have been performed on a personal computer using the Gaussian 03 program package [18] and Gauss view molecular visualization program [19]. The B₃LYP method has been validated to give results similar to that of the more computationally expensive MP₂ theory for molecular geometry and frequency calculations [20, 21]. Moreover, several papers have been published on study of tautomerism in similar systems by B₃LYP method [22-28].

* To whom all correspondence should be sent:
E-mail: azin.mohamadi@gmail.com

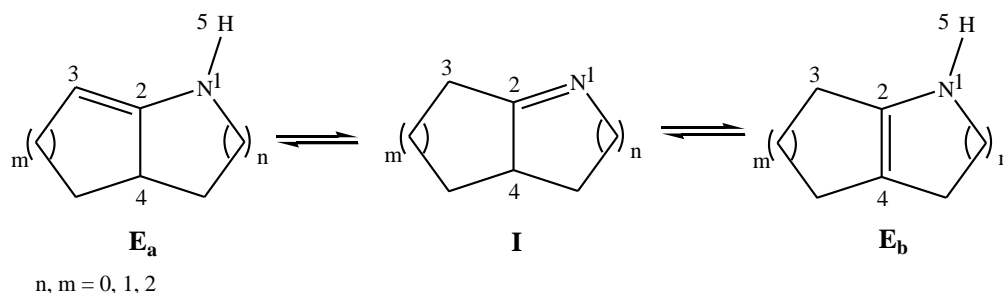


Fig. 1. General structures for possible tautomers

Compound's structures optimized to find stationary point geometries characterized as local minimum on the potential energy surfaces. The absence of imaginary frequency verified that structures were true minima at their respective levels of theory. Atomic charges in all of the structures were obtained using the Natural Population Analysis (NPA) method within the Natural Bond Orbital (NBO) approach [29].

RESULTS AND DISCUSSION

Optimized parameters

The general structures and numbering of possible tautomers are presented in Figure 1. The selected molecules can be presented by three tautomers, imine (I), enamine (E_a) and enamine (E_b).

Because of cyclic structure of these molecules, geometric isomers (cis or trans for double bond) have not been considered in this study (trans endocyclic double bond cannot exist in 4-6-membered rings). Moreover, the most stable conformer was found and used in the calculations. In other word, only the most stable conformer of each structure has been considered in this study. The tautomerism in the selected structures is similar to 1,3-sigmatropic rearrangement. This subject has been attracted considerable attention of scientists especially in cyclic system [30-32]. The optimized structures of tautomers are presented in Figure 2.

Important aspects of molecular structure can be observed in Table 1. The N_1-C_2 bond length, reported in the first column of table, lies in the range of 1.262-1.293 Å in I tautomers, 1.381-1.416 Å in E_a tautomers and 1.386-1.439 Å in E_b tautomers. In I the tautomers, the N_1-C_2 bond length decreases with the increase of N -containing ring size, because of decreasing in ring strain. The C_2-C_3 bond length lies in the range of 1.486-1.523 Å in I tautomers, 1.331-1.351 Å in E_a tautomers and

1.487-1.531 Å in E_b tautomers. The C_2-C_4 bond length lies in the range of 1.496-1.530 Å in I tautomers, 1.484-1.520 Å in E_a tautomers and 1.330-1.348 Å in E_b tautomers. Also, The N_1-H_5 bond length lies in the range of 1.008-1.017 Å in E_a tautomers and 1.011-1.019 Å in E_b tautomers.

According to Table 2, $N_1-C_2-C_3$ angles are in the range of 118.4-137.8 in I tautomers, 122.7-147.8 in E_a tautomers and 114.1-145.7 in E_b tautomers. The $N_1-C_2-C_4$ angles are in the range of 100.3-130.6 in I tautomers, 92.7-122.5 in E_a tautomers and 97.2-127.3 in E_b tautomers. In all tautomers, the $N_1-C_2-C_4$ angles increases with the increase of N -containing ring size, because of decreasing in ring strain.

Moreover, the $C_2-N_1-H_5$ angles, reported in the last column of Table 2, lies in the range of 111.9-119.3 in E_a and E_b tautomers that their amounts are about hybridational angles of central nitrogen.

Energies

Gibbs free energies and other important thermodynamic and kinetic parameters of all structures at 298.15 K and one atmosphere were illustrated in Table 2. The Gibbs free energy difference (ΔG) between I and E_a tautomers at $B_3LYP/6-311^{++}G(d,p)$ level of theory lies between -2.43 and -11.36 kcal/mol and ΔG between I and E_b tautomers lies between -1.23 and -18.82 kcal/mol. These data show that by increasing the N -containing ring size, the relative stability of E_b enamine versus imine I tautomer increase. When the ring size decreases, the ring strain increase and all double bond strengths affect more than single bonds. It is clear that the $C=C$ double bond affect more than $C=N$ double bond by ring strain and its energy decreases more than $C=N$ energy. Therefore, the relative stability of imine tautomer

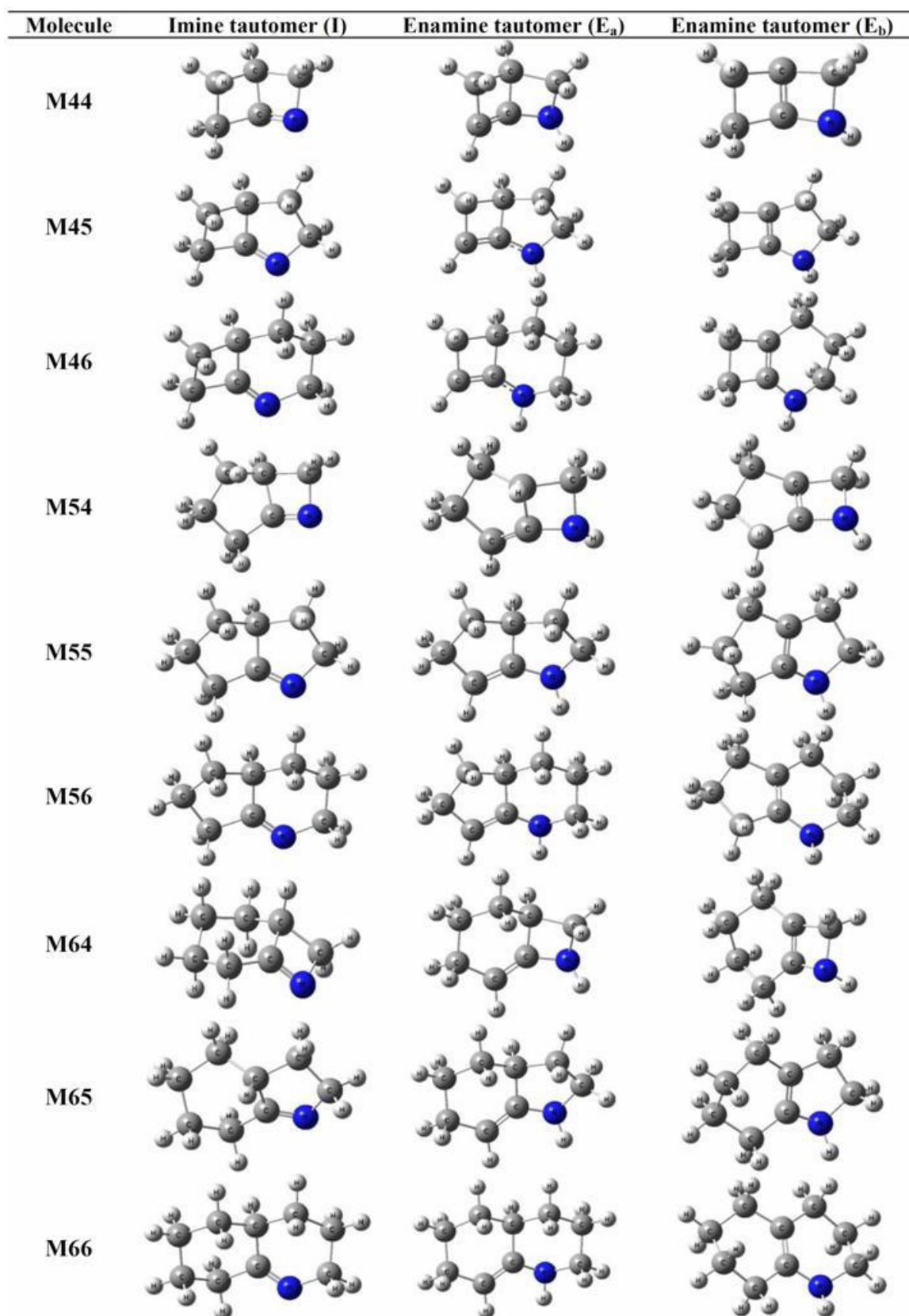


Fig. 2. Optimized structures of the most stable conformer of tautomers.

Table 1. Important molecular parameters of optimized structures at B₃LYP/6-311⁺⁺G(d,p) level of theory.

Molecule	Distance (Å)				Angle (deg)		
	N ₁ -C ₂	N ₁ -H ₅	C ₂ -C ₃	C ₂ -C ₄	N ₁ -C ₂ -C ₃	N ₁ -C ₂ -C ₄	C ₂ -N ₁ -H ₅
M44I	1.293	-	1.504	1.496	134.3	101.9	-
M44E _a	1.416	1.017	1.351	1.484	146.1	97.6	116.8
M44E _b	1.435	1.017	1.531	1.336	144.4	98.7	118.8
M45I	1.266	-	1.511	1.506	137.8	118.9	-
M45E _a	1.381	1.010	1.350	1.492	147.8	112.5	117.4
M45E _b	1.398	1.013	1.518	1.330	145.7	115.5	117.3
M46I	1.262	-	1.516	1.522	132.8	130.6	-
M46E _a	1.382	1.013	1.348	1.505	141.9	122.5	114.3
M46E _b	1.386	1.012	1.511	1.341	137.0	127.3	115.8
M54I	1.288	-	1.498	1.496	137.0	101.4	-
M54E _a	1.409	1.014	1.335	1.498	146.7	94.2	119.2
M54E _b	1.439	1.018	1.496	1.331	143.1	97.9	116.5
M55I	1.269	-	1.508	1.518	131.1	117.2	-
M55E _a	1.383	1.008	1.340	1.509	137.9	108.9	118.9
M55E _b	1.403	1.013	1.498	1.337	131.3	113.9	115.9
M56I	1.267	-	1.523	1.528	123.3	127.6	-
M56E _a	1.392	1.012	1.343	1.518	130.1	117.8	113.5
M56E _b	1.395	1.011	1.506	1.344	122.5	124.6	114.5
M64I	1.289	-	1.486	1.503	133.4	100.3	-
M64E _a	1.415	1.014	1.331	1.509	138.2	92.7	119.3
M64E _b	1.439	1.019	1.487	1.339	134.6	97.2	115.7
M65I	1.273	-	1.506	1.523	125.5	116.1	-
M65E _a	1.396	1.008	1.340	1.515	128.8	107.0	118.1
M65E _b	1.414	1.013	1.498	1.341	121.8	112.7	114.8
M66I	1.274	-	1.515	1.530	118.4	126.5	-
M66E _a	1.408	1.013	1.344	1.520	122.7	114.4	111.9
M66E _b	1.407	1.011	1.512	1.348	114.1	122.7	113.0

Table 2. Relative Energies (ΔE), Relative Zero-Point Energies (ΔE_0), Relative Gibbs Free Energies (ΔG), and equilibrium constant (K_{eq}) for all tautomers.^{a,b}

Molecule	E _a				E _b			
	$\Delta E_{(I-E)}$	$\Delta E_{0(I-E)}$	$\Delta G_{(I-E)}$	$K_{eq(I-E)}$	$\Delta E_{(I-E)}$	$\Delta E_{0(I-E)}$	$\Delta G_{(I-E)}$	$K_{eq(I-E)}$
M44	-11.37	-11.36	-11.35	2.09E+8	-19.24	-19.05	-18.82	6.26E+13
M45	-11.42	-11.36	-11.36	2.13E+8	-13.33	-13.14	-12.92	2.96E+9
M46	-8.45	-8.46	-8.53	1.79E+6	-6.00	-5.85	-5.70	1.51E+4
M54	-3.72	-3.80	-3.98	8.27E+2	-9.94	-9.82	-9.70	1.29E+7
M55	-6.15	-6.06	-6.09	2.91E+4	-7.03	-6.90	-6.84	1.03E+5
M56	-3.31	-3.36	-3.53	3.87E+2	-1.57	-1.40	-1.23	7.97E+0
M64	-4.29	-4.29	-4.30	1.42E+3	-8.50	-8.38	-8.20	1.03E+6
M65	-2.10	-2.11	-2.43	6.04E+1	-1.21	-1.25	-1.57	1.42E+1
M66	-3.78	-3.77	-3.84	6.53E+2	-1.79	-1.40	-1.41	1.08E+1

^a $\Delta E_{(I-E)} = E_I - E_E$, $\Delta E_{0(I-E)} = E_{0I} - E_{0E}$, $\Delta G_{(I-E)} = G_I - G_E$, $K_{eq(I-E)} = [I]/[E]$.^b All energetic data have been reported in kcal/mol.

Table 3. Most important calculated NBO charge and frequencies of tautomers.

Molecule	NBO					Frequency (cm ⁻¹)		
	N ₁	C ₂	C ₃	C ₄	H ₅	C=N	C=C	N-H
M44I	-0.486	0.288	-0.412	-0.301	-	1623	-	-
M44E _a	-0.652	0.215	-0.307	-0.260	0.354	-	1630	3503
M44E _b	-0.654	0.159	-0.400	-0.118	0.359	-	1644	3484
M45I	-0.462	0.295	-0.417	-0.285	-	1739	-	-
M45E _a	-0.646	0.198	-0.300	-0.240	0.373	-	1690	3587
M45E _b	-0.648	0.157	-0.379	-0.114	0.366	-	1727	3539
M46I	-0.464	0.297	-0.418	-0.277	-	1775	-	-
M46E _a	-0.645	0.186	-0.282	-0.232	0.364	-	1697	3548
M46E _b	-0.644	0.160	-0.380	-0.113	0.368	-	1748	3568
M54I	-0.456	0.299	-0.447	-0.301	-	1672	-	-
M54E _a	-0.645	0.200	-0.308	-0.255	0.362	-	1716	3538
M54E _b	-0.646	0.164	-0.418	-0.112	0.351	-	1725	3472
M55I	-0.459	0.305	-0.440	-0.288	-	1735	-	-
M55E _a	-0.643	0.196	-0.310	-0.247	0.377	-	1717	3621
M55E _b	-0.646	0.171	-0.405	-0.109	0.361	-	1719	3542
M56I	-0.472	0.313	-0.435	-0.284	-	1748	-	-
M56E _a	-0.643	0.186	-0.283	-0.245	0.363	-	1697	3564
M56E _b	-0.644	0.177	-0.402	-0.114	0.365	-	1730	3578
M64I	-0.455	0.291	-0.439	-0.287	-	1685	-	-
M64E _a	-0.647	0.195	-0.297	-0.249	0.359	-	1758	3536
M64E _b	-0.649	0.172	-0.423	-0.107	0.345	-	1748	3458
M65I	-0.465	0.308	-0.436	-0.282	-	1714	-	-
M65E _a	-0.647	0.191	-0.390	-0.245	0.373	-	1730	3618
M65E _b	-0.650	0.177	-0.411	-0.103	0.358	-	1730	3539
M66I	-0.474	0.310	-0.423	-0.277	-	1719	-	-
M66E _a	-0.651	0.188	-0.268	-0.246	0.358	-	1706	3551
M66E _b	-0.647	0.176	-0.402	-0.111	0.360	-	1723	3573

versus enamine tautomer increases by decreasing the ring size.

In addition, from Table 2 it is easily seen that relative stability of compounds with more ring strain such as M₄₄, M₄₅, M₅₄, M₅₅ and M₆₄, the enamine tautomer E_a (exocyclic form) will be more stable than enamine tautomer E_b (endocyclic form). Equilibrium constants of tautomeric interconversions were calculated from Gibbs free energies using $\Delta G = -RT \ln K_{eq}$. The equilibrium constant for conversion of tautomer E_a to I and at B₃LYP/6-311⁺⁺G(d,p) level of theory lies between 6.04×10^1 and 2.13×10^8 , and for conversion of tautomer E_b to I lies between 7.97 and 6.26×10^{13} . In accordance with ΔG between tautomers, in compounds with more ring strain, enamine tautomer E_a is major than enamine tautomer E_b (Table 2).

Frequencies

Three important vibrational frequencies of all structures are listed in Table 3. These presented frequencies include imine C=N double bond, enamine C=C double bond and NH bond. In the last column, N₁-H₅ frequency (this frequency only exists in tautomers E_a and E_b) is reported. In tautomers E_b the magnitude of this frequency increases with the increase of N-containing ring size. Also, the C=N frequencies in imine tautomers increases with the increase of N-containing ring size and the C=C frequencies that exists in enamine tautomers lie between 1630 and 1758 cm⁻¹. The C=C frequencies in M₄₄ shows lower magnitude and it correspond to low present of S orbital in these tautomers. The variation of frequencies versus ring size is important because they shows meaningful relation between empirical parameters

(frequency) and simple theories, such as bond angle, ring's strain and hybridation.

NBO analysis

The calculated values NBO charges using the Natural Population Analysis (NPA) of optimized structures of imine-enamine tautomers in the gas phase are listed in Table 3. Nitrogen atom in the all of the tautomers carries the largest negative charge, and among in carbon atoms C₃ carries the largest negative charge. The N₁ and C₃ atoms in all imine-enamine tautomers will most effectively interact with electrophiles.

CONCLUSIONS

In this work, DFT calculation has been applied to study of tautomerism in bicyclic imines and enamines with deferent rings in the gas phase. The following points emerge from the present study:

1. In the title compound imine form was more stable than the other tautomers in the gas phase.
2. The energy data shows that the relative stability of enamine tautomer versus imine tautomer increases with the increase of ring size.
3. Calculated frequencies show that by decreasing N-containing ring size, the frequency of C=N in imine tautomer decreases.

REFERENCES

1. A. Misra, S. Dalai, *J. Mol. Struct. THEOCHEM*, **807**, 33 (2007).
2. K. Zborowski, A. Korenova, *J. Mol. Struct. THEOCHEM*, **683**, 15 (2004).
3. M. Shabaniyan, H. Moghanian, M. Hajibeygi, A. Mohamadi, *E-J. Chem.*, **9**, 107 (2012).
4. M. Shabaniyan, H. Moghanian, M. Hajibeygi, A. Mohamadi, *Orient. J. Chem.*, **28**, 669 (2012).
5. B. Ivanova, A. Chapkanov, M. Arnaudov, I. Petkov, *Spectrosc. Lett.*, **39**, 1 (2006).
6. W. P. Oziminski, J. C. Dobrovolski, A. P. Mazurek, *J. Mol. Struct. THEOCHEM*, **680**, 107 (2004).
7. T. J. Dines, H. Onoh, *Spectrochim. Acta A*, **64**, 891 (2006).
8. M. K. Shukla, S. K. Mishra, *J. Comput. Chem.*, **21**, 826 (2000).
9. J.A. Bonacin, D. Melo, H.E. Toma, *Vib. Spectrosc.*, **44**, 133 (2007).
10. A. Mohamadi, M. Shabaniyan, M. Hajibeygi, H. Moghanian, *J. Chil. Chem. Soc.*, **58**, 1553 (2013).
11. S. Angelova, V. Enchev, *J. Mol. Struct. THEOCHEM*, **711**, 201 (2004).
12. J. Grochowski, P. Serda, B. Kozik, *J. Mol. Struct. THEOCHEM.*, **689**, 43 (2004).
13. S.O. Smith, T.A. Pardeon, P.P.J. Mulder, B. Cuny, J. Lugtenburg, R. Mathies, *Biochemistry*, **22**, 6141 (1983).
14. S.I. Vdovenko, I.I. Gerus, J. Wo'jcik, *J. Phys. Org. Chem.*, **14**, 533 (2001).
15. H. Zhong, E.L. Stewart, M. Kontoyianni, J.P. Bowen, *J. Chem. Theory Comput.*, **1**, 230 (2005).
16. M. Shabaniyan, M. Hajibeygi, H. Moghanian, A. Mohamadi, *Heterocycl. Commun.*, **18**, 161 (2012)
17. B. Witkop, *J. Am. Chem. Soc.*, **78**, 2873 (1956).
18. M.J. Frisch, G.W. Trucks, H.B. Schlegel, *et al.*, Gaussian 03, Revision B.03, Gaussian, Inc. Pittsburgh PA (2003).
19. R. Dengton, T. Keith, J. Millam, K. Eppinnett, W. L. Hovell, R. Gilliland. GaussView, Version 309., Semichem, Inc, Shawnee Mission, KS (2003).
20. B.G. Johnson, P.M.W. Gill, J.A. Pople, *J. Chem. Phys.*, **98**, 5612 (1993).
21. C.W. Bauschlicher, H. Partridge, *J. Chem. Phys.*, **103**, 1788 (1995).
22. V. Jimenez, J.B. Alderete, *J. Mol. Struct. THEOCHEM.*, **775**, 1 (2006).
23. A.A. Mohamed, A.W. El-Harby, *J. Mol. Struct. THEOCHEM.*, **849**, 52 (2008).
24. V. Jimenez, J.B. Alderete, *J. Mol. Struct. THEOCHEM.*, **755**, 209 (2005).
25. K.H. Choa, J. Choob, S.W. Joo, *J. Mol. Struct. THEOCHEM.*, **738**, 9 (2005).
26. S.I. Okovytyy, L.K. Sviatenko, A.A. Gaponov, *Eur. J. Org. Chem.*, **2010**, 280 (2010).
27. G. Alagona, C. Ghio, *Int. J. Quantum Chem.*, **108**, 1840 (2008).
28. L. Hai-Bo, Q. Yong-Qing, S. Shi-Ling, S. Xiao-Na, S. Zhong-Min. *Acta Phys. Chim. Sin.*, **26**, 120 (2010).
29. A. Najafi-Chermahini, M. Nasr-Esfahani, Z. Dalirnasab, H.A. Dabbagh, A. Teimouri, *J. Mol. Struct. THEOCHEM.*, **820**, 7 (2007).
30. J.Y. Choi, C.K. Kim, C.K. Kim, I. Lee, *J. Phys. Chem. A*, **106**, 5709 (2002).
31. S. Erdem, F. Uyar, O. Karahan, K. Yelekc, *J. Mol. Struct. THEOCHEM.*, **814**, 61 (2007).
32. H.R. Tao, D.C. Fang, *Theor. Chem. Acc.*, **121**, 91(2008).

ИМИНО-ЕНАМИННА ТАВТОМЕРИЯ ПРИ БИ-ЦИКЛИЧНИ СИСТЕМИ В ГАЗОВА ФАЗА: ИЗЧИСЛИТЕЛНО ИЗСЛЕДВАНЕ

Х. Моганиан¹, А. Мохамеди*²

¹*Клуб за млади изследователи, Клон Дезфул, Ислямски университет Азад, Дезфул, Иран*

²*Департамент по химия, Клон Фарахан, Ислямски университет Азад, Фарахан, Иран*

Постъпила на 17 декември, 2012; коригирана на 15 април, 2013 г.

(Резюме)

Извършени са DFT-изчисления относно би-цикличните имини за да се изследва влиянието на размера на пръстена върху имин-енамин-тавтомерията. Определени са геометрията на молекулите и енергетиката на имините и енамините в газова фаза при използването на V_3LYP -нива на теорията, прилагайки 6-311⁺⁺G(d,p) базисна мрежа. По този начин са определени важни параметри на молекулите, като ИЧ-честотите, NBO и резултати за енергетиката им в газова фаза. Резултатите за енергетиката показват, че относителната стабилност на енаминната тавтомерна форма (спрямо иминната) нараства с размера на ръстена. Изчислените честоти показват, че намаляването на размера от 6- на 4-атомен пръстен юестотата на C=N връзката в иминния тавтомер намалява. Освен това са изследвани и измененията на NBO-товарите на атомите в газова фаза.

Hybrid materials parameters influencing the enzyme activity of immobilized cells

L. V. Kabaivanova¹, G. E. Chernev², P. V. Markov³, I. M. Miranda Salvado⁴

¹ Institute of Microbiology, Bulgarian Academy of Sciences, 26, Acad. G. Bonchev Str., 1113 Sofia, Bulgaria

² Department of Silicate Technology, University of Chemical Technology and Metallurgy, 8, Kl. Ohridsky Blvd., 1756 Sofia, Bulgaria

³ Institute of General and Inorganic Chemistry, Bulgarian Academy of Sciences, 11, Acad. G. Bonchev Str., 1113 Sofia, Bulgaria

⁴ Department of Materials & Ceramic Engineering, CICECO, University of Aveiro, Portugal.

Received October 29, 2012; Revised February 7, 2013

Hybrid materials, synthesized by the sol-gel method, were used as matrices for immobilization of bacterial cells, producers of the enzyme nitrilase. Different methods were employed for structure investigations of the synthesized hybrids: Fourier transform infrared spectroscopy (FT-IR), BET and atomic force microscopy (AFM). The influence of the structure of these materials on their properties was followed. The obtained hybrid materials were successfully applied for immobilization of live bacterial cells since cell vitality was kept and enzyme systems preserved their functions in the immobilized systems. The influence of different parameters during the cell immobilization procedure was evaluated for optimization of the immobilization process and enhancement of the activity of the studied enzyme. Most favorable effect on *Bacillus sp.* cells had the matrix with 5 wt. % sepharose and the enzyme activity obtained was 0.45 U ml⁻¹ when the process was carried out at 60°C. Increased specific surface area of the matrix was another factor that led to enhanced nitrilase activity.

Keywords: sol-gel; hybrids; parameters; enzyme activity

INTRODUCTION

Inorganic-organic hybrids, synthesized by the sol-gel method, are a remarkable group of amorphous nanocomposites, investigated for application in biotechnology, medicine and other areas due to their mechanical, optical, structural and thermal properties, as a result of combining silicon chemistry with life sciences [1-2]. Such hybrid materials are promising for applications as biocatalysts by immobilization of different biomolecules [3-4]. These biocatalysts are expected to reduce the energy expenses and their employment could lower pollutants dissemination in the environment [5-6]. Nitrilases (EC.3.5.5.1) are the enzymes that convert nitriles to the corresponding acid and ammonia. Nitrilases are thiol enzymes that perform an array of carbon-nitrogen bond hydrolysis and condensation reactions [7]. Enzymes degrading nitriles can be found in many microorganisms [8]. Their high chemical specificity makes them attractive versatile biocatalysts [9]. Nitrile-converting enzymes are becoming commonplace in the synthesis of pharmaceuticals and commodity chemicals,

showing their potential in the synthetic biocatalysis, as well as in bioremediation processes, degrading a broad spectrum of toxic substrates [10].

In this work we report on the influence of temperature, type and quantity of organic material included in the matrix and specific surface area of the hybrid materials on the enzyme activity during the immobilization of the moderate thermophilic strain *Bacillus sp.* UG-5B.

EXPERIMENTAL

Hybrid materials preparation and characterization

The silica hybrids were prepared by the sol-gel method at room temperature. Silica precursor tetraethylortosilicate (TEOS) (Sigma-Aldrich, reagent grade $\geq 98\%$, formula weight 208.33 g/mol) was pre-hydrolyzed with H₂O using a small quantity of hydrochloric acid as a catalyst. The molar ratio between TEOS:H₂O:C₂H₅OH:HCl was (v/v) 1:2:8:1 $\times 10^{-3}$. The content of silica was kept constant and hybrids containing from 5 to 40 wt.% organic part (lactic acid (Sigma-Aldrich, natural $\geq 85\%$, FG, formula weight 90.08 g/mol) or sepharose 4B (Sigma-Aldrich, exclusion limit 60,000 for proteins, 30,000 for dextrans) and combination of poly(ethylene oxide) (Sigma-

* To whom all correspondence should be sent:
E-mail: georgi_chernev@yahoo.com

Aldrich, average M_v 100,000, viscosity 12-50 cP, 5 % in H_2O (25 °C, Brookfield) (lit.)) and agar (Sigma-Aldrich, Type A)) added to SiO_2 were prepared. After gelation, the samples were dried at room temperature. The main steps of the entrapment procedure were previously described [11]. The structure of the synthesized materials was studied using Fourier transform infrared spectroscopy (FT-IR), BET and atomic force microscopy (AFM).

Strain and medium

The bacterial strain involved was *Bacillus sp.* UG-5B (№ 8021) deposited in the National Bank for Industrial Microorganisms and Cell Cultures, Bulgaria. The medium for cultivation contained (g/l): K_2HPO_4 2.0; NaCl 1.0; $MgSO_4$ 0.01; $FeSO_4 \times 7H_2O$ 0.02; biotin 2.9×10^{-5} ; thiamine, 0.004; inositol 0.002 and benzonitrile (20 mM), pH 7.2. The nitrilase activity assay was realized by measuring the ammonia released, following the phenol-hypochloride method of Fawcett and Scott [12]. One enzyme unit is defined as the amount of enzyme producing 1 μmol ammonia min^{-1} at pH 7.2, 45 °C and 20 mM benzonitrile as a substrate. Cells were harvested for 24 h on a rotary shaker in 100 ml flasks with nutrient medium containing 20 mM benzonitrile. Cells were separated from the culture medium by centrifugation and then resuspended in phosphate buffer pH 7.2. Cell suspension with a concentration of 30 $mg\ ml^{-1}$ dry cells and enzyme activity of 0.3 $U\ ml^{-1}$ was used for immobilization. Immobilization procedure comprises the preparation of the gel solution which contains SiO_2 and organic parts in a ratio from 5 to 40 wt.%; 5 ml of the ready cell suspension was introduced before gelation, which took place within 30 min. The gel containing the cells was spread over petri dishes and left to dry overnight at room temperature. Leaching of cells was spectrophotometrically estimated to be 0.02-0.06 %.

RESULTS AND DISCUSSION

The structure of the synthesized hybrid materials was investigated using FT-IR (Fig. 1), which showed characteristic peaks at around 1080 cm^{-1} , 790 cm^{-1} and 460 cm^{-1} , attributed to the SiO_2 network. They are assigned to ν_{as} , ν_s and δ of Si-O-Si vibrations; the band at 1080 cm^{-1} could also be related to the existence of Si-O-C, C-O-C and Si-C bonds. The presence of bands at 950 cm^{-1} reveals

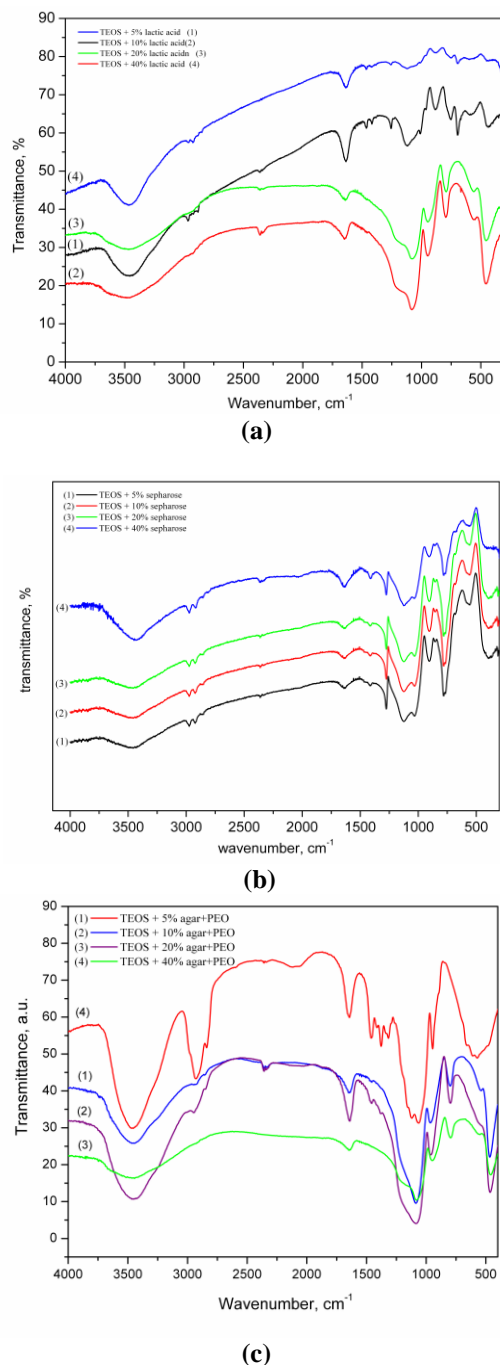


Fig. 1. FT-IR spectra of hybrids containing: a - lactic acid; b - sepharose and c - PEO and agar.

the presence of Si-OH groups. Characteristic bands at around 3460 cm^{-1} and at 1630 cm^{-1} , assigned to H-O-H vibration, can also be detected. The bands around 3460 cm^{-1} could also be associated with ν (OH) ring stretching vibrations.

The results of BET analysis proved that the pore size is about 2 nm, and the specific surface area is in the range from 130 to 310 m^2/g , depending on the hybrid chemical composition. The matrix

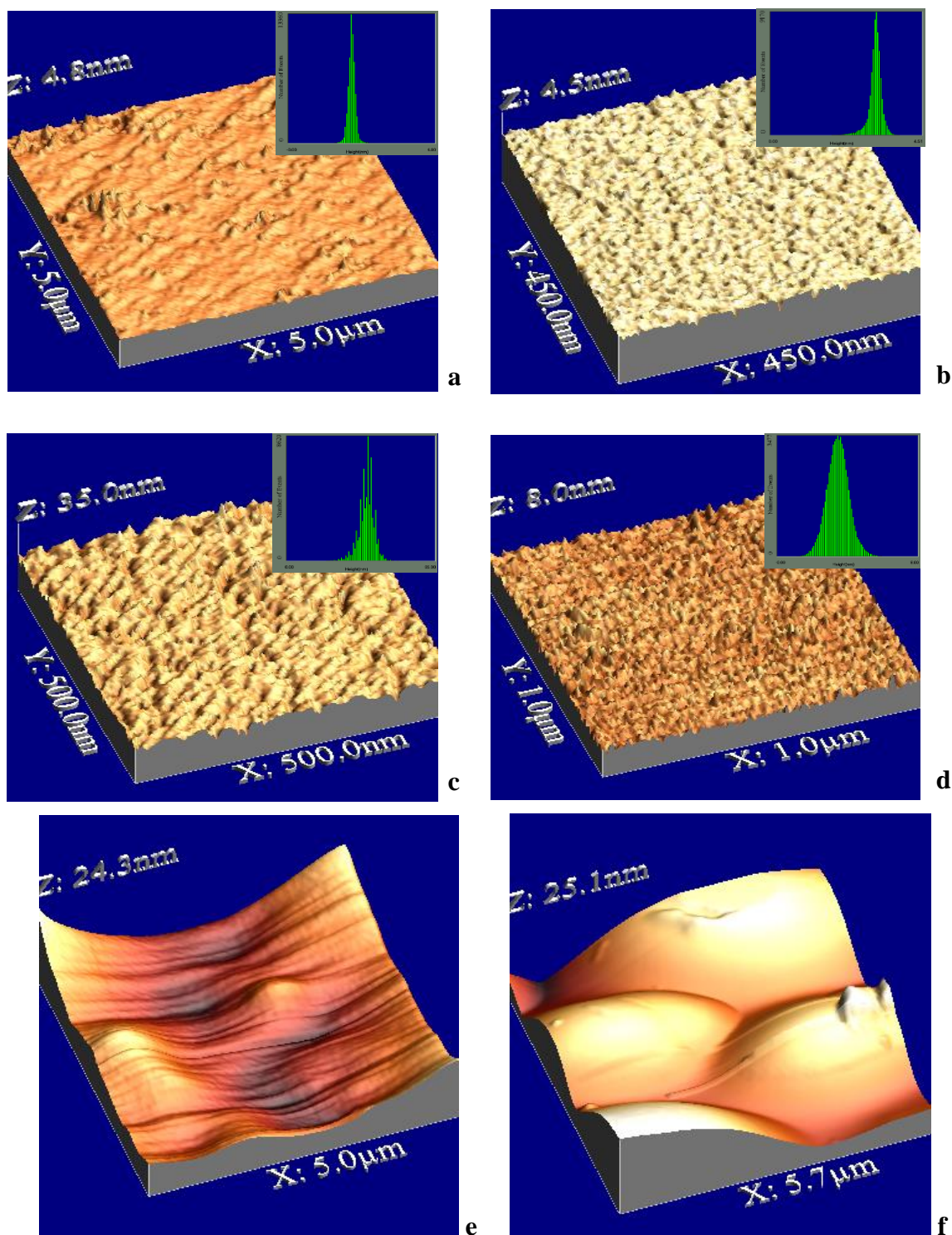
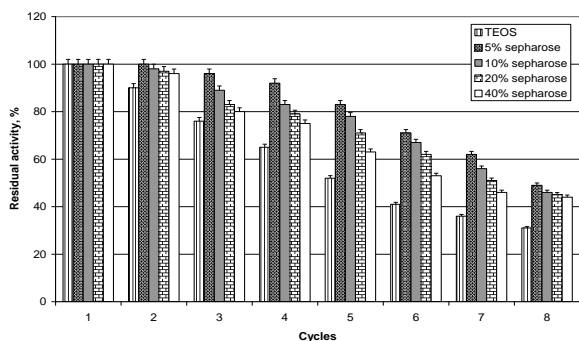


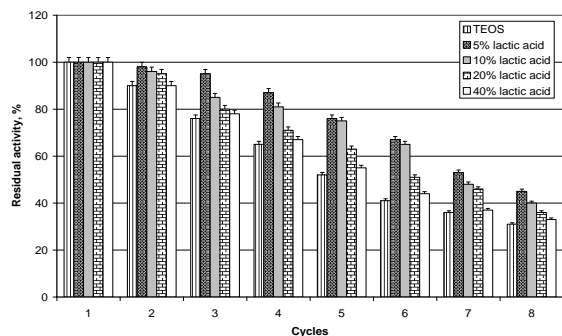
Fig. 2. AFM images and height distribution profile of hybrids containing a – 5 wt. % lactic acid; b – 20 wt. % lactic acid; c – 5 wt. % sepharose and d – 20 wt. % sepharose; e – 5 wt. % PEO and agar and f – 20 wt. % PEO and agar.

consisting of well-defined nanounits and their aggregates formed by self-organizing processes, was observed by the AFM studies. The size of nanoparticles was from 10 to 18 nm and the dimensions of their self-assembled aggregates were about 49-76 nm (Fig. 2). In the same figure the height distribution profiles of surface roughness are shown. The histograms of the surface height

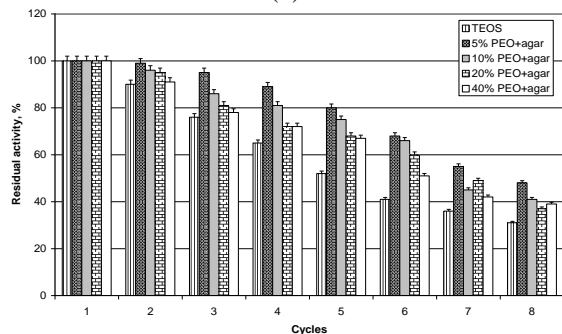
distribution profiles obtained from AFM topography images showed that all hybrids had a surface with irregularities.



(a)



(b)



(c)

Fig. 3. Comparison between the activity obtained by the immobilized cells at multiple use with matrices with different organic constituent.

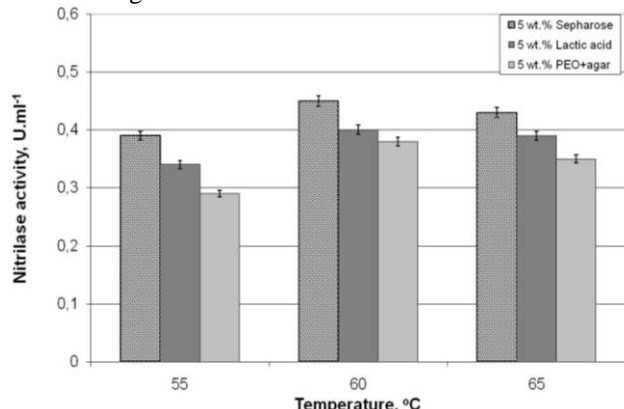
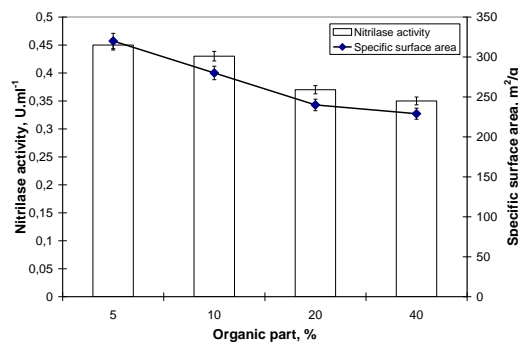
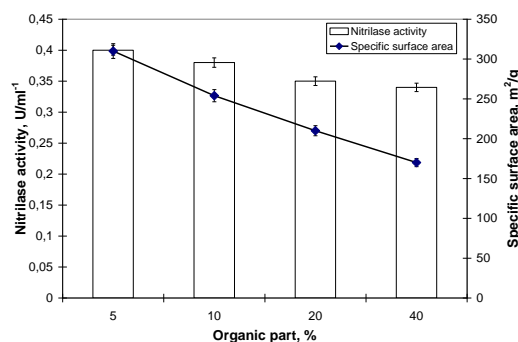


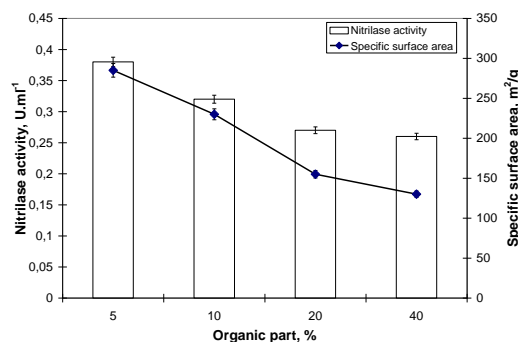
Fig. 4. Influence of temperature on the nitrilase activity of immobilized *Bacillus* sp. UG-5B strain. Error bars represent a deviation obtained from the triplicate measurements.



(a)



(b)



(c)

Fig. 5. Influence of specific surface area on the nitrilase activity of immobilized *Bacillus* sp. UG-5B strain (a-sepharose; b-lactic acid; c-PEO+agar) Error bars represent a deviation obtained from the triplicate measurements.

Thus synthesized, the hybrid materials were tested as matrices for immobilization of the suspension of cells. Different parameters influenced the nitrilase activity of the immobilized biocatalyst. Their optimization was expected to lead to an enhanced enzyme activity compared to the free cells. The optimum pH for the nitrilase activity of free cells proved to be 6.0-8.0. The pH of the matrices was adjusted to 7.0-7.2 which appeared to be most appropriate for the cells entrapped in their volume. Figure 3 shows the comparison between the activity displayed by the immobilized cells at

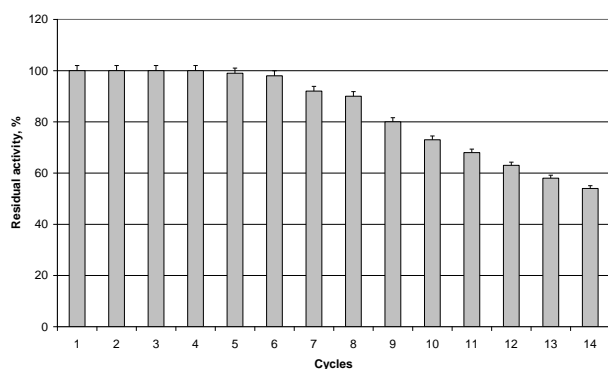


Fig. 6. Reusability of the biocatalyst (TEOS and 5 wt.% sepharose) obtained after optimization of the immobilization parameters.

multiple use when each matrix contains only SiO₂ and different percentage of organic constituent. The addition of an organic part plays a favorable role when living objects are entrapped in the gel matrix. Concerning the type of the hybrid matrix, best results for *Bacillus sp.* UG-5B were achieved when immobilization was carried out in a matrix containing 5 wt. % sepharose. This fact can be explained by the different chemical composition and structure of the organic part included.

The obtained materials with 5 wt.% organic constituent with immobilized cells were tested for their behavior under different temperatures in the range from 50°C to 65°C (Fig. 4). Highest enzyme production for the immobilized preparations was obtained when the temperature maintained during the evaluated process was 60°C. The nitrilase activity only slightly decreases when temperature is increased to 65°C (0.43 U ml⁻¹ for the matrix with sepharose, 0.39 U ml⁻¹ when lactic acid is included in the hybrid matrix and 0.35 U ml⁻¹ when PEO+agar is present as an organic part), which is due to its thermostability [13]. Involving thermostable enzymes in industrial processes gives the advantage of a fast process and least contamination [14]. The nitrilase enzyme produced by *Rhodococcus rhodochrous* was found to be fairly thermostable at 45°C [8], while the nitrilase of *Bacillus sp.* UG-5B shows highest values at 60°C. Another parameter influencing the enzyme activity of immobilized preparations is the specific surface area of the hybrid materials (Fig. 5). The larger surface area promotes higher nitrilase activity when 5 wt.% of sepharose are present in the hybrid matrix (Fig. 5a). This is in correlation with the pore size, permitting free substrate penetration. Inclusion of 40 wt.% sepharose leads to lower nitrilase yield, corresponding to the lower specific surface area. The specific surface area decreases with the increase of the organic part

content, leading to a gradual increase in enzyme activity. Reusability was tested for the immobilized bacterial cells included in the most suitable matrix for highest nitrilase activity, namely, this containing 5% sepharose (Fig. 6). In this case the half-life of enzyme activity was retained for 14 reaction cycles, each carried out with the addition of a fresh toxic substrate (benzonitrile) for degradation. The proven reusability indicates an efficient process that is possible to be carried out at the optimal conditions for operation of the immobilized system.

CONCLUSION

All hybrid materials used appeared to be appropriate carriers for the entrapped bacterial cells. The biocompatibility of the hybrid materials allows the bioactivity of cells to be retained. The obtained biocatalysts can be useful in enzymology and biotechnology and ecology, using the hydrolytic enzyme properties. Nitriles can cause harmful effects on human health, so there exists an urgent need for their removal. Immobilization of cells, producers of nitrilase can offer solution to the problems that appear with free cells, using their advantages - retention of catalytic activity, protection of cells against substrate inhibitory effects, as well as stability and increased enzyme yield, achieved by optimization of the factors, influencing the immobilization process.

REFERENCES

1. A. Kumar, D. Depan, N. Tomer, R. Singh, *Prog. Polym. Sci.*, **34**, 479 (2009).
2. S. Pandey, S. Mishra, *J. Sol-Gel Sci. Tech.* **59**, 73 (2011).
3. D. Avnir, T. Coradin, O. Lev, J. Livage, *J. Mater. Chem.*, **16**, 1013 (2006).
4. M. Peralta-Pérez, M. Martínez-Trujillo, G. Nevárez-Moorillón, R. Pérez-Bedolla, M. García-Rivero, *J. Sol-Gel Sci. & Tech.*, **57**, 6 (2011).
5. W.-Sh. Lee, I.-Ch. Chen, Ch.-H. Chang, Sh.-Sh. Yang, *Renewable Energy*, **39**, 216 (2012).
6. A. Soares, M. Murto, B. Guieysse, B. Mattiasson, *Appl. Microbiol. Biotechnol.*, **69**, 597 (2006).
7. C. Brenner, *Current Opinion in Structural Biology*, **12**, 775 (2002).
8. V. Gupta, S. Gaiind, P.K. Verma, N. Sood, A.K. Srivastava, *African J. Microbiol. Res.*, **4**, 1148 (2010).
9. R. N. Thuku, D. Brady, M. J. Benedik, B. T. Sewell, *J. Appl. Microbiol.*, **106**, 703 (2009).
10. C.-C. Wang, C.-M. Lee, Li-Jung L.-J. Chen, *J. Env. Sci. Health, Part A*, **39**, 1767 (2004).
11. L. Kabaivanova, E. Dobreva, E. Emanuilova, G. Chernev, B. Samuneva, I. Salvado, *Minerva Biotechnol.*, **18**, 23 (2006).

12. J. Fawcett, J.Scott, *J. Clin. Pathol.*, 13, 156 (1960). [14] G. Haki, S. Rakshit, *Biores. Tech.*, **389**, 17
13. L. Kabaivanova, P. Dimitrov, I. Boyadzhieva, S. Engibarov, E. Dobreva, E. Emanuilova, *World J. Microbiol. Biotechnol.*, **24**, 2383 (2008). (2009).

ПАРАМЕТРИ НА ХИБРИДНИ МАТЕРИАЛИ, ВЛИЯЕЩИ ВЪРХУ ЕНЗИМНАТА АКТИВНОСТ НА ИМОБИЛИЗИРАНИ КЛЕТКИ

Л. В. Кабаиванова¹, Г. Е. Чернев², П. В. Марков³, И. М. Миранда Салвадо⁴

¹ *Институт по микробиология, Българска академия на науките, ул. „Акад. Г. Бончев“, 26, 1113 София, България*

² *Катедра технология на силикатите, Химикотехнологичен и метарулгичен университет, бул. „Кл. Охридски“ 8, 1756 София, България*

³ *Институт по обща и неорганична химия, Българска академия на науките, ул. „Акад. Г. Бончев“, 11, 1113 София, България*

⁴ *Департамент по материално и керамично инженерство, CICECO, Университет на Авеиро, Португалия*

Получена на 29 октомври, 2012 г.; коригирана на 7 февруари, 2013 г.

(Резюме)

Хибридни материали, синтезирани по зол-гелен метод, бяха използвани като матрици за имобилизация на бактериални клетки, продуценти на ензима нитрилаза. В структурните изследвания на синтезираните хибриди бяха използвани различни методи: Инфрочервена спектроскопия (FT-IR), ВЕТ-анализ и атомно силова микроскопия (AFM). Проследено беше влиянието на структурата на тези материали върху техните свойства. Получените хибридни материали бяха успешно приложени за имобилизация на живи бактериални клетки, при което жизнеността им беше запазена и ензимните им системи запазиха своите функции в имобилизираните системи. Влиянието на различните параметри по време на процедурата на имобилизация беше оценено за оптимизация на процеса и увеличение на ензимната активност на изследвания ензим. Най-благоприятен ефект върху клетките на щам *Bacillus sp.* оказа матрицата с 5 wt.% сефароза и получената ензимна активност беше 0.45 U ml^{-1} , когато процесът се провежда при 60°C . Увеличената специфична повърхност на матрицата беше още един фактор, водещ до повишена нитрилазна активност.

Phase composition and microstructure of sodium-alumoborosilicate glasses and glass-ceramics in the system $\text{Na}_2\text{O}/\text{BaO}/\text{TiO}_2/\text{Al}_2\text{O}_3/\text{B}_2\text{O}_3/\text{SiO}_2/\text{Fe}_2\text{O}_3$

R. Harizanova^{1*}, L. Vladislavova¹, C. Bocker², C. Rüssel², I. Gugov¹

¹University of Chemical Technology and Metallurgy, 8, Kl. Ohridski Blvd., 1756 Sofia, Bulgaria

²Institut für Glaschemie "Otto-Schott-Institut", Friedrich-Schiller-Universität, Fraunhoferstr. 6, 07743 Jena, Germany

Received January 2, 2013; Revised February 2, 2013

The present work reports on the synthesis, phase formation and microstructure of glasses and glass-ceramics, obtained in the system $\text{Na}_2\text{O}/\text{TiO}_2/\text{BaO}/\text{Al}_2\text{O}_3/\text{B}_2\text{O}_3/\text{SiO}_2/\text{Fe}_2\text{O}_3$. The characteristic temperatures of the samples are determined by differential thermal analysis. X-ray diffraction is used for phase identification. Scanning electron microscopy, combined with energy dispersive X-ray analysis, is used for microstructural characterization and determination of the chemical composition of the formed crystals. All investigated compositions were amorphous. The annealing of the obtained glasses results in formation of spherical BaTiO_3 particles with sizes in the range from 100 nm to several μm .

Keywords: invert glass; barium titanate; nanocrystallisation; microstructure

1. INTRODUCTION

Barium titanate is a well-known dielectric material which possesses multiple polymorphic modifications. The tetragonal modification is stable at room temperature and is the predominantly observed one, which results in ferroelectric properties. Tetragonal barium titanate is used for the preparation of powerful capacitors and as a substitute of the magnetic RAM, e.g. as FRAM [1-5]. However, the cubic modification of BaTiO_3 which is stable at temperatures above the Curie temperature ($\sim 120^\circ\text{C}$) is also characterized by a high dielectric constant and due to the lack of ferroelectricity, by isotropic dielectric properties [1, 4, 5]. Thus, it finds application in multilayered capacitors for energy storage [1, 3, 4] and depending on its optical properties, it may be a promising candidate for UV laser preparation for optoelectronic applications [5]. Different experimental techniques are used to obtain barium titanate as bulk material [1, 2, 4, 5]. The preparation of BaTiO_3 thin films is also reported in the literature [3, 6].

The different allotropic modifications of BaTiO_3 can be stabilized at room temperature by addition of dopants of different type and concentration. The various crystallite sizes will also lead to stabilization of one or another modification of

barium titanate. This enables to control the properties of the resulting materials [2, 3]. In the literature, the addition of 3d-transition metal oxides (for example iron oxides) to systems in which BaTiO_3 crystallizes is reported [2]. Conventional barium titanate ceramics are prepared by the chemical reaction of barium carbonate and titanium oxide to barium titanate, subsequent milling and sintering [2]. Also, the preparation of barium titanate nanorods by means of a hydrothermal method is reported in [5]. These nanorods show light emission in the blue part of the visible spectrum if irradiated with UV light.

In the literature, also advanced glass melting techniques for the preparation of barium titanate and magnetite nanoparticles are reported. The materials prepared in this way are promising candidates for application in spintronics [7, 8]. Recent studies were carried out in the system $(24-y)\text{Na}_2\text{O}/y\text{Al}_2\text{O}_3/14\text{B}_2\text{O}_3/37\text{SiO}_2/25\text{Fe}_2\text{O}_3$ with $y = 8, 12, 14$ and 16 [9] while other investigations were performed on compositions derived from this system [10-12]. It was reported that primarily phase separation occurs in the prepared glasses and droplets with sizes in the range from 100 to 800 nm enriched in B_2O_3 and FeO_x are formed. Subsequently, magnetite crystals with sizes in the range from 25 to 40 nm precipitate within these droplets [12]. The materials prepared in this way may be suitable for applications as multicore magnetic nanoparticles.

* To whom all correspondence should be sent:
E-mail: ruza_harizanova@yahoo.com

This paper reports on the synthesis and characterization of glasses and glass-ceramics in the system $(23.1-x)\text{Na}_2\text{O}/23.1\text{BaO}/23\text{TiO}_2/7.6\text{B}_2\text{O}_3/17.4\text{SiO}_2/5.8\text{Fe}_2\text{O}_3/x\text{Al}_2\text{O}_3$. The reported glasses contain less than 30 mol % glass-forming oxides. The occurrence of droplet-like regions in which cubic barium titanate crystallizes is observed after annealing of samples from all glass compositions in the system.

2. EXPERIMENTAL

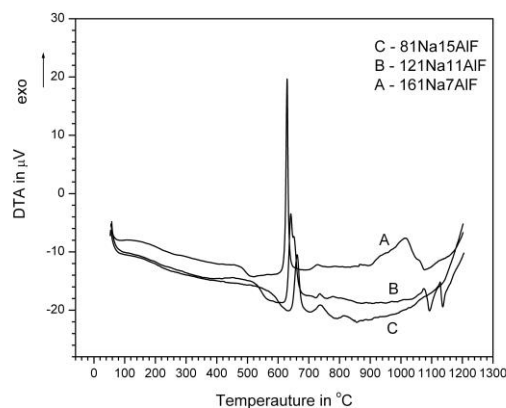
Samples with the mol % compositions $(23.1-x)\text{Na}_2\text{O}/23.1\text{BaO}/23\text{TiO}_2/7.6\text{B}_2\text{O}_3/17.4\text{SiO}_2/5.8\text{Fe}_2\text{O}_3/x\text{Al}_2\text{O}_3$, $x = 0, 3, 7, 11, 15$ (batch composition) are melted from the following reagent grade raw materials: Na_2CO_3 , BaCO_3 , TiO_2 , $\text{Al}(\text{OH})_3$, $\text{B}(\text{OH})_3$, SiO_2 and Fe_2O_3 . The glasses are melted in 60 g batches for 1 h at 1250 °C in air using Pt crucibles in a furnace with SiC heating elements. The melts are quenched on a copper block without pressing. Then, in order to increase the mechanical stability and to minimize internal stresses, the glass is transferred to a pre-heated graphite-mould and held for 15 min at 450°C in a muffle furnace. Subsequently, the furnace is switched off and the sample is allowed to cool to room temperature. Crystallization of the samples is carried out at 550°C in a muffle furnace for different times.

The phase compositions of the samples from all melted compositions are studied by X-ray diffraction (XRD), *Siemens D5000* using $\text{Cu-K}\alpha$ radiation ($\lambda = 1.5406 \text{ \AA}$) and Ni filter. The glass transition and crystallisation temperatures are determined on bulk samples by differential thermal analysis (DTA), *Perkin Elmer Diamond TG/DTA*. The microstructure and the elemental composition of the prepared glasses and subsequently, of the crystallised samples is further analysed by scanning electron microscopy (SEM) in combination with energy-dispersive (EDX) analysis, (*JSM-7001F, JEOL Ltd., Japan*). Imaging of the crystallised samples is performed on polished samples, or if this did not result in a good contrast, on samples etched for 5 s in 1% HCl solution. The topography of selected samples is studied on polished surfaces by atomic force microscopy (AFM), *Zeiss Ultra Objective, Carl Zeiss GmbH, Germany*.

3. RESULTS AND DISCUSSION

The samples show a dark brown coloration after quenching on the copper plate. Some parts of the surface are slightly crystallised and

formation of droplet-like light brown regions is observed. The bulk of all samples is, as seen at a fractured surface, glassy. The XRD patterns of the bulk specimens prove that the samples are amorphous, which indicates that the quantity of crystals is negligibly small and they are mainly observed at the surface.



The DTA profiles of the melted glasses, as shown for three of them in Fig. 1, allow to determine the glass transition and the crystallisation temperatures of the prepared materials. They further help to choose appropriate time-temperature annealing regimes in order to study the crystallisation behaviour of the samples. In Figure 1 DTA profiles for the samples with 16.1 mol% Na_2O and 7 mol% Al_2O_3 (sample A), 12.1 mol% Na_2O and 11 mol% Al_2O_3 (sample B) and 8.1 mol% Na_2O and 15 mol% Al_2O_3 (sample C) are shown. As seen in the Figure, the glass transition temperature of sample C with the smallest alkali and highest alumina concentration increases to about 580°C in comparison to samples A and B with glass transition temperatures of 480°C and 530°C, respectively. The crystallisation temperatures follow the same trend. The effect of the varied Na_2O and Al_2O_3 concentrations on the glass transition temperature has already been reported by other authors for sodium aluminosilicate glasses of various compositions [13-18]. It has been observed that with increasing the alumina concentration, the viscosity and the glass forming ability also increase and the maximum value of viscosity is achieved for a ratio $[\text{Na}_2\text{O}]/[\text{Al}_2\text{O}_3] = 1$ [11, 13-18]. A similar observation is reported in our

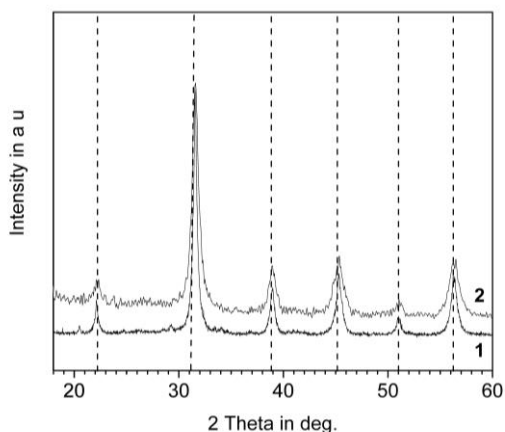


Fig. 2 XRD-patterns of samples with 23.1 mol% Na₂O and 0 mol% Al₂O₃ (1) and with 20.1 mol% Na₂O and 3 mol% Al₂O₃ (2), annealed respectively for 4h and 3h at 550°C - formation of cubic BaTiO₃; dashed line – lines of BaTiO₃.

study – the melts with equimolar alumina and sodium oxide concentrations showed a glass transition temperature about 50 K higher than that of the sample with 16.1 mol% Na₂O and 7 mol% Al₂O₃ and 100°C higher than that of the sample with 0 mol% Al₂O₃.

In order to investigate the crystallisation behaviour of the prepared glasses with the compositions (23.1-x)Na₂O/23.1BaO/23TiO₂/7.6B₂O₃/17.4SiO₂/5.8Fe₂O₃/xAl₂O₃ with x = 0, 3, 7, 11, pieces from the bulk were chosen and annealed for 3 or 4 h at 550°C, i.e. above or near T_g. The annealing times were chosen in such a way that the average crystallite size hardly changes when increasing the time of thermal treatment. Thus, the crystals precipitated in specimens with different compositions may be compared. The resulting samples are visually well-crystallized in the bulk and the XRD-patterns show only the formation of cubic BaTiO₃, (JCPDS Nr. 01-079-2263), as shown in Figure 2. The obtained BaTiO₃ phase is recognized as the cubic modification since there is no visible splitting in the characteristic peak at about 45.3° – as it should be in the case of the tetragonal BaTiO₃ modification [1, 19].

Some authors report that the change in the symmetry of barium titanate from cubic to tetragonal depends on the size of the precipitated crystals [1, 19] or even discuss the formation of a tetragonal core and a cubic shell

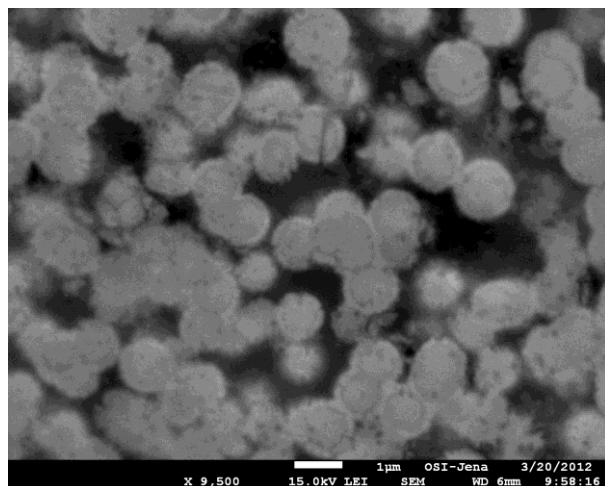


Fig. 3 SEM-micrograph of a sample with 23.1 mol% Na₂O and 0 mol% Al₂O₃ crystallised for 4h at 550°C

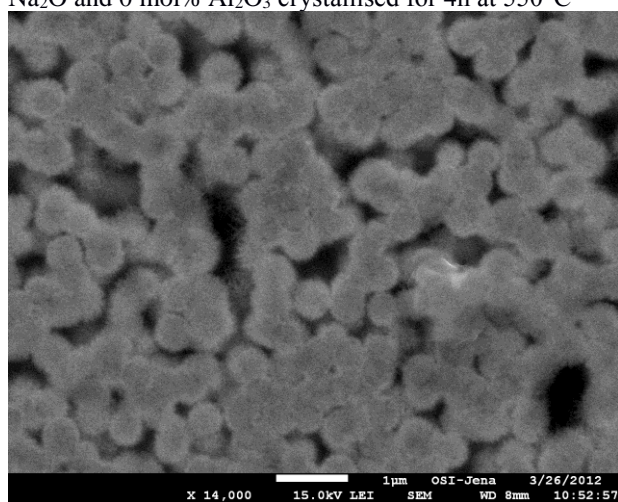


Fig. 4 SEM-micrograph of a sample with 20.1 mol% Na₂O and 3 mol% Al₂O₃ crystallised for 3h at 550°C.

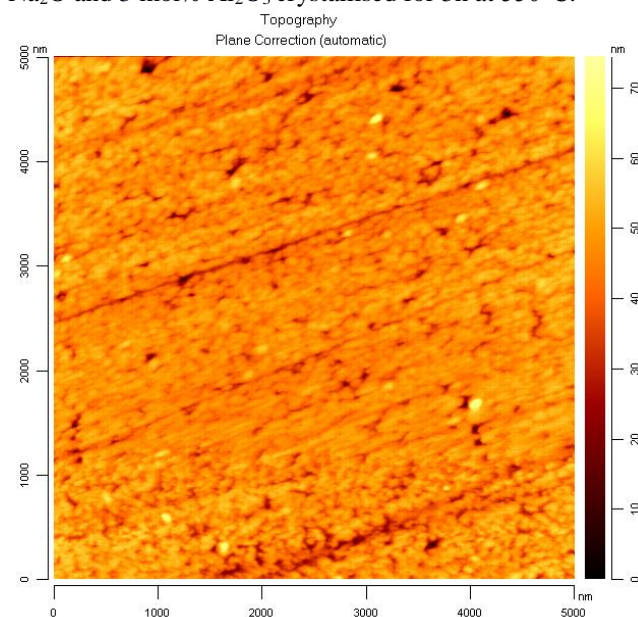


Fig. 5 AFM image (topography mode) of a sample with 16.1 mol% Na₂O and 7 mol% Al₂O₃, annealed for 3h at 550°C – average size of the spherical BaTiO₃ crystals about 150 nm.

for the growing barium titanate particle [1]. In our work, however, we did not observe up to now such a dependency and the crystallised BaTiO₃ is always cubic. Similar observations are done when imaging the microstructure of the annealed samples (see Figures 3 to 5) – only one morphological type of crystals is present. The SEM imaging of samples with different thermal history and composition suggests that for annealing times $t \geq 3$ h the mean size of the formed globular crystals only slightly changes. In Figure 3 a SEM micrograph of a sample without Al₂O₃ is shown. It is observed that spherical crystals with a mean size of about 1 μ m are formed. The same crystal morphology is already seen in other, similar as chemical composition, glass-ceramic materials [9, 12] and suggests the idea that first phase separation and subsequently crystallisation in the droplets may occur in the present set of compositions. The brighter appearance of the formed crystals serves as an evidence that they contain the heavier elements of the initial composition, e. g. Ba, Ti and probably, also some Fe. The addition of transition metal oxides as dopants, in the present study Fe and Ti, is a well-known method for changing the modification and thus, the properties of the resulting crystals. This has already been reported for other Fe- and (Ba,Fe,Ti)-containing glass systems [2,7,11]. The successful combination of two or more transition metals may result in the formation of core-shell structures composed by both, ferroelectric and ferromagnetic crystals. This will enable to combine the properties of the two phases formed, which may result in multiferroic properties and the synthesis products can find unique applications in electronics [7, 8]. Anyway, the presented XRD data, as seen in Fig. 1, support the presence of only Ba and Ti and no Fe in the crystals. The total lack of Fe in the barium titanate crystals, or its presence in concentrations too small to be detected, may be attributed to the relatively low Fe₂O₃ concentration. This is in contrast to the data from other authors, who by sintering powders obtained Fe-doped barium titanate [2]. According to these reports, however, the Fe-doped barium titanate crystals change their

symmetry from tetragonal to hexagonal. This effect occurs in parallel to the incorporation of iron and is undesired because the hexagonal phase is not ferroelectric and furthermore, in comparison to the cubic modification it possesses worse dielectric parameters.

The SEM-micrograph of a sample with 20.1 mol% Na₂O and 3 mol% Al₂O₃ (see Figure 4) shows crystals with an average size of about 500 nm. The higher magnification in Figure 4, compared to that in Figure 3, allows seeing that the separate spherical crystals are in close contact with each other, which constrains their further growth. These crystals are smaller than the ones shown in Figure 3, which represents a SEM micrograph of the composition with 0 mol% Al₂O₃. The same trend – decrease of the average size of the crystals formed with increasing alumina concentration - is also observed in the XRD patterns of Figure 2. Here the peaks of the sample with 3 mol % Al₂O₃ are wider than those with 0 mol% Al₂O₃. The latter observation might be explained by the higher glass transition temperature and hence, the higher viscosity of the glass with a higher Al₂O₃ concentration when annealed at the same temperature (550°C) as the glass without alumina.

The microstructure of the samples shown in Figures 3 and 4 proves the existence of spherical crystals with core-shell structure. Similar observations are done by other authors who report the combination of two modifications of BaTiO₃, coexisting in one core-shell crystal – tetragonal core and cubic shell [1]. In [1] they report that the size of the formed barium titanate crystals determines the allotropic modification present and that the process of crystallite growth leads to transition within one and the same particle from cubic to tetragonal barium titanate. In our investigation, however, we could not conclude if this is the reason for the formation of core-shell structure in the growing crystals and further investigation of the particles is needed in order to elucidate this problem. In general, the imaging of the samples with increasing Al₂O₃ content is difficult due to the decreasing size of the crystals. Actually, the crystal morphology in the sample with 7 mol% Al₂O₃ crystallised

for 3 h at 550°C could only be investigated by AFM – the size of the crystals was found to vary from about 100 to 150 nm, as seen in Figure 5. From Figures 3 to 5 it can be concluded that the volume concentration of crystals in the samples is high – there is almost no glassy phase remaining between the crystals. The separate particles tend to aggregate and form larger complexes which grow together – as seen in Figure 3 and already observed in other systems where the crystallisation is preceded by droplet-like phase separation [9, 12].

The observed morphology of the formed crystals, as well as the resulting size variation depending on the composition of the initial glasses, may affect the dielectric properties of the obtained barium titanate glass-ceramics and will be a subject of further investigation.

4. CONCLUSIONS

A set of invert glass compositions $(23.1-x)\text{Na}_2\text{O}/23.1\text{BaO}/23\text{TiO}_2/7.6\text{B}_2\text{O}_3/17.4\text{SiO}_2/5.8\text{Fe}_2\text{O}_3/x\text{Al}_2\text{O}_3$ is melted and subsequently quenched on a copper block, which leads to glass formation. Annealing above or near T_g results in the crystallisation of crystals of cubic BaTiO_3 gathered in spherical particles in the amorphous matrix, whose mean sizes vary from 100 nm to 1 μm for the different compositions. The X-ray diffraction studies and the SEM investigations of the spherical particles allow concluding that these are mainly enriched in barium and titanium oxide and formation of cubic BaTiO_3 occurs without the participation of Fe in the crystals. With increasing alumina and decreasing sodium oxide concentrations, the average particle sizes decrease.

Acknowledgements: This work was financially supported by contract № D02-797/28.08.2012, index: P-5-22/2012, project: BG051PO001-3.3-

05/0001 «Science-business», funded by Operational program «Development of human resources».

REFERENCES

1. J.F. Capsal, E. Dantras, L. Laffont, J. Dandurand, C. Lacabanne, *J. Non-Cryst. Solids*, **356**, 629 (2010).
2. G.P. Du, Z. J. Hu, Q. F. Han, X. M. Qin, W.J. Shi, *Journal of Alloys and Compounds*, **492**, L79 (2010).
3. T.J Jackson, I. Jones, *J. Mater. Sci.*, **44**, 5288 (2009).
4. Z. Libor, S.A. Wilson, Q. Zhang, *J Mater Sci.*, **46**, 5385 (2011).
5. R. Vijayalakshmi, V. Rajendran, *Digest Journal of Nanomaterials and Biostructures*, **5**, 511 (2010).
6. S.F. Mendes, C.M. Costa, C. Caparros, V. Sencadas, S. Lanceros-Mendez, *J. Mater. Sci.*, **47**, 1378 (2012).
7. R.P. Maiti, S. Basu, S. Bhattacharya, D. Chakravorty, *J. Non-Cryst. Solids*, **355**, 2254 (2012).
8. A.K. Zvezdin, A.S. Logginov, G.A. Meshkov, A.P. Pyatakov, *Bull. Russian Acad. Sci.: Physics*, **71**, 1561 (2007).
9. R. Harizanova, G. Völksch, C. Rüssel, *J. Mater. Sci.*, **45**, 1350 (2010).
10. W. Vogel in: *Glasschemistry*, 3 Ed. Springer-Verlag, Berlin-New York-London-Paris-Tokyo-Hong Kong-Barcelona-Budapest, 1992.
11. R. Harizanova, I. Gugov, C. Rüssel, D. Tatchev, V. S. Raghuvanshi, A. Hoell, *J. Mater. Sci.: Size Dependent Effects* **46**, 7169 (2011).
12. C. Worsch, P. Schaaf, R. Harizanova, C. Rüssel, *J. Mater. Sci.*, **47**, 5886 (2012).
13. K. El-Egili, *Phys., B* **325**, 340 (2003).
14. S. Hornschuh, B. Messerschmidt, T. Possner, U. Possner, C. Rüssel, *J. Non-Cryst. Sol.*, **347**, 121 (2004).
15. L. Hong, P. Hrma, J.D. Vienna, M. Qian, Y. Su, D.E. Smith, *J. Non-Cryst. Sol.*, **331**, 202 (2003).
16. D. Benne, C. Rüssel, M. Menzel, K. Becker, *J. Non-Cryst. Sol.*, **337**, 232 (2004).
17. H. Schirmer, R. Keding, C. Rüssel, *J. Non-Cryst. Sol.*, **336**, 37 (2004).
18. D. Benne, C. Rüssel, D. Niemer, M. Menzel, K. Becker, *J. Non-Cryst. Sol.*, **345-346**, 203 (2004).
19. S.D. Vacche, F. Oliveira, Y. Leterrier, V. Michaud, D. Damjanovic, J.E. Manson, *J. Mater. Sci.*, **47**, 4763 (2012), DOI 10.1007/s10853-012-6362-x.

ФАЗОВ СЪСТАВ И МИКРОСТРУКТУРА НА НАТРИЕВО-АЛУМОБОРОСИЛИКАТНИ СЪТЪКЛА И СЪТЪКЛОКЕРАМИКИ В СИСТЕМАТА $\text{Na}_2\text{O}/\text{BaO}/\text{TiO}_2/\text{Al}_2\text{O}_3/\text{B}_2\text{O}_3/\text{SiO}_2/\text{Fe}_2\text{O}_3$

Р. Харизанова^{1*}, Л. Владиславова¹, Кр. Бокър², Кр. Рюсел², И. Гугов¹

¹*Химикотехнологичен и металургичен университет, бул. "Кл. Охридски" № 8, 1756 София, България*

²*Ото Шот институт по химия на стъклото, Университет „Фридрих Шилер“, ул. „Фраунхофер“ № 6, 07743 Йена, Германия*

Получена на 2 януари, 2013 г.; коригирана на 2 февруари, 2013 г.

(Резюме)

Настоящата работа докладва данни за синтеза, фазообразуването и микроструктурата на стъкла и стъклокерамики, получени в системата $\text{Na}_2\text{O}/\text{TiO}_2/\text{BaO}/\text{Al}_2\text{O}_3/\text{B}_2\text{O}_3/\text{SiO}_2/\text{Fe}_2\text{O}_3$. Характеристичните температури на пробите са определени с помощта на диференциален термичен анализ. Методът на рентгеновата дифракция е използван за фазова идентификация. Сканираща електронна микроскопия, комбинирана с енергийно-дисперсивен рентгенов анализ, позволява характеризиране на микроструктурата и определяне на химичния състав на формираните кристали. Продуктите на синтеза за всички изследвани състави са аморфни. Темперирането на получените стъкла води до кристализацията на сферични BaTiO_3 частици с размери от 100 nm до няколко μm .

Membrane fusion based on the stalk model

M. Hadzhilazova^{1*}, J.-F. Ganghoffer²

¹*Institute of Biophysics and Biomedical Engineering, Bulgarian Academy of Sciences, Acad.G. Bonchev Str.,Bl. 21, 1113 Sofia, Bulgaria*

²*LEMETA – ENSEM 2, Avenue de la Foret de Haye, TSA 60604, 54518 Vandoeuvre, France*

Received March 6, 2013; Accepted April 24, 2013

It is a commonly accepted assumption that membrane fusion involves an hour-glass-shaped local contact between two monolayers of opposing membranes, an intermediate structure called a stalk. The shape of the stalk is considered as an axisymmetrical surface of revolution in 3D space, with a planar geometry in the initial configuration. The total energy of the stalk is evaluated from the assumption that the stalk has a constant mean curvature. We analyze on this basis the energetic path of evolution of the stalk from hemifusion to complete fusion, adopting the radius of the stalk, the peel-off angle at the interstices and the stalk total energy as characteristic quantities. An extension of the original model is proposed, in which any geometrical feature of the stalks can be expressed in explicit form, by considering the stalks as nodoid surfaces.

Keywords: lipid membranes, stalk model, nodoid surfaces.

INTRODUCTION

Membrane fusion plays a vital role in cell physiology and life, and for this reason has attracted the interest of many researchers, resulting in many attempts to develop representative models of this process. The ability to fuse is shared by biological membranes, consisting of phospholipid bilayers with embedded and bound membrane proteins, and by artificially formed purely lipid membranes. Normally, the membranes are mechanically stable, due to powerful hydrophobic effect [38], which drives self-assembly of the lipid molecules into bilayer and maintains the bilayer integrity. Membrane fusion requires transient structural reorganization of at least some lipids (see [1, 4, 8, 22]). Experimental evidence points to the existence of so-called hemifusion structures [3, 4, 39], which are relatively long living intermediates appearing during the early stage of fusion. Membrane hemifusion is a possible pathway [32] to the complete fusion of membranes [4]. The modeling of the lipidic fusion intermediates has more than two decades history. Although, at the early stages, several different structures have been suggested, only one of them, called fusion stalk [9,15], is currently recognized to describe adequately the transition stage of membrane fusion [4,11].

Fusion stalk is a local lipidic connection

between the proximal (contacting) monolayers of the fusing membranes. At the stage of stalk formation, the distal monolayers of the membranes are still separated, and the achieved state is referred to as hemifusion. A physical model of the fusion process, based on this hypothetical intermediate and referred to as the stalk model has been developed in a series of contributions [4, 14, 20, 24, 25] and further modified by Siegel [34, 35] and Kuzmin et al. [18]. A number of important predictions of the stalk hypothesis have been verified experimentally for fusion of protein-free lipid bilayers and for some examples of biological fusion. The hypothesis suggests that merger of the proximal monolayers of the membranes precedes merger of their distal monolayers. Indeed, the existence of a distinct hemifusion stage has been documented for different experimental systems based on protein-free bilayers [3-5,19,33] and for fusion of biological membranes [6, 12, 21, 29, 37].

Current theories associate the initiation of hemifusion with the formation of a contact zone between the membranes in which the two proximal monolayers are connected by a stalk-shaped neck. The stalk then expands and a region is formed in which the two distal monolayers form a single bilayer. In general, the energetic cost of the splay of the lipid chains in the stalk prohibits its spontaneous expansion. However, the presence of additional, external forces (e.g., pressure, surface tension gradients, electrostatic

* To whom all correspondence should be sent:
E-mail: murryh@obzor.bio21.bas.bg



Fig.1. Schematic view of the process of fusion via stalk formation.

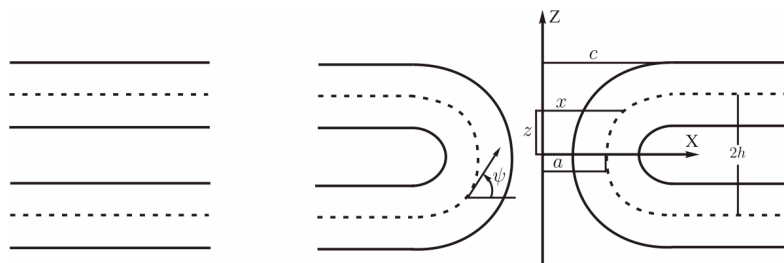


Fig. 2. Steps in membrane fusion. Solid lines represent hydrophilic surfaces, dotted lines hydrophobic surfaces (left). Geometric parameters of the stalk (right).

effects) can lead to expansion of the stalk into a hemifusion region and to the growth of this zone. Clear evidence for the existence of these two distinct prefusion stages, stalk formation and hemifusion, was found for poly(ethylene glycol)-mediated fusion of vesicles [19]. Looking at a much smaller scales than continuum models do, molecular dynamics simulations allow to study the biological processes of lipid vesicle fusion in atomic details, as reported in [13].

A few words related to energetic aspects are in order, since a few factors may influence the energy required to form intermediate structures. A potential effect of membrane lateral tension on membrane fusion was assessed by two-dimensional simulations of the contact of monolayers in [2]. In [7], an energetically feasible structure of pre-stalk intermediates has been advanced, called point-like protrusion. The role of the Gaussian curvature elastic energy of the intermediate structures on membrane fusion has been highlighted in [36]. The role of membrane edges due to tilt deformations as a mechanism for the strong reduction of the energy of fusion stalks has been analyzed in [28]. The energetics of formation of vesicle intermediates was analyzed in [23], where the authors calculate the effects of membrane curvature and osmotic stress, basing on the stalk assumption. A new structure of the fusion stalk has been presented in [17], the deformations of the two membrane monolayers not only involve bending as in [15, 25,34], but also a tilt of the hydrocarbon chains. The tilt constitutes an additional degree of freedom and allows the monolayers to relax the overall energy. This view contributes to resolve partially the energy challenge (sometimes coined

energy crisis in the relevant literature, see [17]) inherent to the fact that membrane configurations at the intermediate stages of fusion require high energy barriers.

THE STALK MODEL

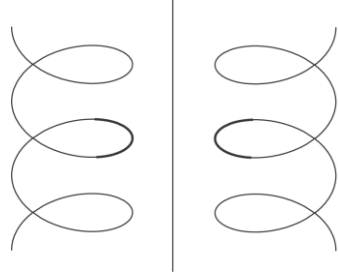
The fusion process involves the successive steps of membrane aggregation, a destabilization nucleating at a point defect inducing a highly localized rearrangement of the two bilayers, further inducing a mixing of the components of the two bilayers, resulting in either hemifusion (Fig. 1, middle) or full fusion (Fig. 1, right).

A connection between membranes involves local contacts between two phospholipid bilayers in their aqueous environment, which is difficult due to the hydrophobic nature of the interior part of the membranes (each bilayer has a trans and a cis-monolayer, Fig.2). The required connection between the two membranes in order for fusion to occur involves an hourglass-shaped local contact between two monolayers of opposing membranes, an intermediate structure called a stalk in the original model developed in [15].

The mechanical basis of the model relies on the calculation of the shape of the stalk, taken as an axisymmetrical surface of revolution in 3D space (Fig. 2), with a planar geometry in the initial configuration. The neutral surface is represented as a dotted line. There x and z are the coordinates of the contour, the parameter a is the shortest distance separating the neutral surface from the axis of revolution (the neck of the stalk), c is the distance from the axis of revolution to the point where the stalk branches become horizontal (the width of the stalk), $2h$ is

the distance separating the two neutral surfaces, and the angle between the neutral surface and the horizontal line is ψ .

The contour of the stalk surface is given from the slope ψ . The bending energy of the stalk depends on the principal and the spontaneous curvatures. Assuming that the curvature of the stalk is constant, the total energy of the stalk is calculated versus parameter a , and is found to be negative, hence promoting hemifusion (the presence of spontaneous curvature in the monolayers favors hemifusion). We analyze the path of evolution of a stalk from hemifusion to complete fusion, versus the radius of the stalk, the peel-off angle at the interstices, and the stalk total energy. The present contribution proposes an extension of the model suggested in [26], by considering explicitly a subclass of the Delaunay surfaces, the so called nodoid surfaces. Following the argumentation developed in [10] in the case of beaded nerve fibers (the surfaces



there are unduloids), we elaborate a model in which any geometrical characteristic of the stalks can be expressed in explicit form, by considering the stalks as nodoid surfaces Fig. 3.

A novel description of the shape of the stalk is next exposed.

THE MATHEMATICAL DESCRIPTION

The sum of the principal curvatures is given by the classical relation

$$c_p(x) + c_m(x) = c_{\text{stalk}} \quad (1)$$

with the two principal curvatures expressed versus the angle $\psi(x)$ as

$$c_p(x) = \frac{\sin \psi(x)}{x}, \quad c_m(x) = \cos \psi(x) \frac{d\psi}{dx}. \quad (2)$$

The slope of the at any point along the contour of the stalk surface is determined from

$$\frac{dz}{dx} = \tan \psi(x) = \frac{xc_p}{\sqrt{1 - x^2 c_p^2}}. \quad (3)$$

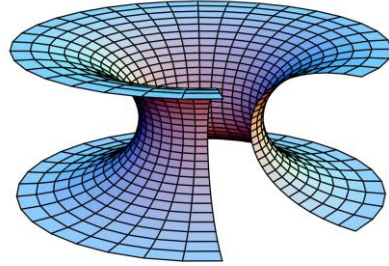


Fig. 3. The profile curves of thenodoid (left, solid parts) generating under revolution the stalk surface and a 3D-view of theopen part of the stalk (right).

Previous relations then lead after straightforward calculations to the equations

$$xc_p = \frac{1}{2}c_{\text{stalk}}x + \frac{a}{x}\left(1 - \frac{1}{2}c_{\text{stalk}}a\right) \quad (4)$$

$$\frac{dz}{dx} = \left\{ \left[\frac{1}{2}c_{\text{stalk}}x + \frac{a}{x}\left(1 - \frac{1}{2}c_{\text{stalk}}a\right) \right]^2 - 1 \right\}^{-1/2}. \quad (5)$$

Next, due to the relations we have also

$$c = \sqrt{a^2 - \frac{2a}{c_{\text{stalk}}}} \quad \text{or} \quad \frac{c}{a} = \sqrt{1 - \frac{2}{ac_{\text{stalk}}}}. \quad (6)$$

From all above it results that the contour of the stalk surface is given as the integral

$$\frac{z}{a} = \int_1^{x/a} \left\{ \left[\frac{1}{2}ac_{\text{stalk}}t + \frac{1}{t}\left(1 - \frac{1}{2}ac_{\text{stalk}}\right) \right]^2 - 1 \right\}^{-1/2} dt \quad (7)$$

and when $c_{\text{stalk}} = \mathbb{h} = \text{const}$ the stalk is called stress free. The surface specified by the equation (7) is a constant mean curvature (CMC) surface. CMC surfaces of revolution were classified long time ago by the French geometer Delaunay and were described in analytical form in [30, 31]. Differentiating $c_p(x)$ and taking into account the

expression for $c_m(x)$ one gets the equation

$$\frac{dc_p(x)}{dx} = \frac{c_m(x) - c_p(x)}{x}. \quad (8)$$

This equation and the CMC condition

$$H = \frac{c_m(x) + c_p(x)}{2} = \mathbb{h} = \text{const} \quad (9)$$

yields

$$\frac{dc_p(x)}{dx} = \frac{2(\mathbb{h} - c_p(x))}{x} \quad (10)$$

and therefore

$$c_p(x) = \mathbb{h} + \frac{\mathbb{b}}{x^2} \quad (11)$$

where \mathbb{b} is the integration constant.

By taking into account the geometrical relation

$c_p(x) = \frac{\sin \psi(x)}{x}$ one finds immediately

$$\sin \psi(x) = \mathbb{h}x + \frac{\mathbb{b}}{x} \quad (12)$$

and this is exactly the Gauss map of the surface.

From the two obvious geometrical conditions

$$\mathbb{h}a + \frac{\mathbb{b}}{a} = 1, \quad \mathbb{h}c + \frac{\mathbb{b}}{c} = 0 \quad (13)$$

it follows that

$$\mathbb{h} = \frac{a}{a^2 - c^2}, \quad \mathbb{b} = -\frac{ac^2}{a^2 - c^2}. \quad (14)$$

Finally, the integration of the slope equation

$$\frac{dz}{dx} = \tan \psi(x) \quad (15)$$

gives the profile curve

$$z = \int \tan \psi(x) dx = a \int_a^x \frac{(x^2 - c^2) dx}{\sqrt{(x^2 - a^2)(c^4 - a^2 x^2)}}. \quad (16)$$

A parameterization of the contour can be done using the elliptic functions, i.e.,

$$x(u) = \frac{c^2}{a} \operatorname{dn}(u, k), \quad k = \frac{\sqrt{c^4 - a^4}}{c^2}$$

$$z(u) = \frac{c^2}{a} E(\operatorname{am}(u, k), k) - aF(\operatorname{am}(u, k), k) \quad (17)$$

in which $F(\operatorname{am}(u, k), k)$, $E(\operatorname{am}(u, k), k)$ denote the incomplete elliptic integral of the first and second kind respectively, that depend on their argument in the first slot and the elliptic modulus in the second slot. Plots of the meridional sections of the cell fusion resulting from those expressions are shown in Fig. 3 (left) and a 3D view of the stalk is pictured on the right.

GEOMETRIC AND ENERGETIC ASPECTS

Having the explicit parameterization (17) of the profile curves it is a simple matter to write down the parametrization of the relevant part of the stalk surfaces in the form

$$\tilde{\mathbf{x}} = (x(u) \cos v, x(u) \sin v, z(u) - z(K(k))), \quad v \in (0, 2\pi). \quad (18)$$

With this at hand it is easy to find also coefficients E , F , and G of the first fundamental form of the surface (18) via the formulas

$$E = \tilde{\mathbf{x}}_u \cdot \tilde{\mathbf{x}}_u = \frac{(a^2 - c^2)^2 \operatorname{dn}^2(u, k)}{a^2}$$

$$F = \tilde{\mathbf{x}}_u \cdot \tilde{\mathbf{x}}_v = 0$$

$$G = \tilde{\mathbf{x}}_v \cdot \tilde{\mathbf{x}}_v = \frac{c^4 \operatorname{dn}^2(u, k)}{a^2}.$$

These coefficients are necessary to find out the infinitesimal element $dA = \sqrt{EG - F^2} du \wedge dv$ of the surface area

$$dA = \frac{c^2(c^2 - a^2) \operatorname{dn}^2(u, k)}{a^2} du \wedge dv, \quad u \in \left\{ \frac{K(k)}{2}, \frac{3K(k)}{2} \right\}.$$

Integrating over the whole surface of the neck one easily finds that the energy of the stalk is

given by the formula

$$W_s = \frac{1}{2} \bar{k} [(c_{\text{stalk}} - \mathbb{h})^2 - \mathbb{h}^2] A = 2\pi \bar{k} \frac{c^2(c^2 - a^2)}{a^2} E(t, k) \Big|_{K(k)/2}^{K(k)} \quad (20)$$

in which \bar{k} is the bending module and $E(K(k), k)$ and $E(K(k)/2, k)$ denote the complete elliptic integrals of the second kind.

Having the explicit parametrization (18) of the stalk one can find also its height $2h$ (see Fig. 2) by the formula

$$h = z(K(k)/2) - z(K(k)). \quad (21)$$

This allows to plot the dimensionless normalized distance h/a which depends only on a single parameter c (i.e., \mathbb{h}) and to compare it with the approximate function presented in [26]. The result is depicted as curve 1 in Fig. 4.

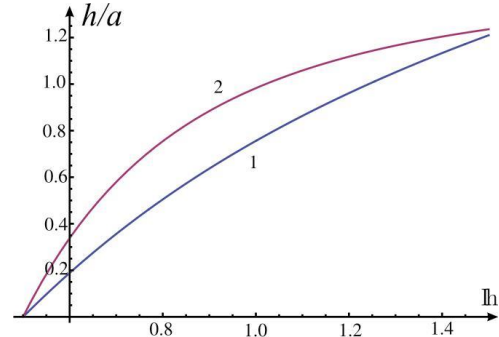


Fig. 4. The first curve is produced via the analytical result (21) and the second one is plotted by making use of the approximation formula presented in [26].

It should be noted that the resulting plot in Fig. 4 has an universal character which is applicable to any spontaneous curvature.

CONCLUSIONS

Fusion involves drastic although local changes in the initial membrane structure. The membrane configurations emerging at the intermediate stages of fusion require input of energy and, hence, represent energy barriers the membranes have to overcome on the way to the new fused state. Those energy barriers are essential determinants of the fusion rate. The free energy of fusion stalks has been calculated by different approaches.

E.g., Kuzmin et al. [18] suggested a theoretical model that includes, besides bending, a tilt of the lipid molecules. The model starts from preformed nipples that decrease the local distance of two fusing membranes and requires an extraordinary high energy to form a stalk out of two apposed, planar bilayers. The geometry of this model however is predefined.

Markin and Albanesi [26] postulated a stress

free stalk. The key point of their model is the optimization of the cross-sectional shape of the stalks neck in terms of its bending energy. Relying on numerics they did not recognize that this is a constant mean curvature surface which is the main point of the present study.

REFERENCES

1. K. Burger, *Traffic*, **1**, 605 (2000).
2. A. Chanturiya, P. Scaria, O. Kuksenok, M. Woodle, *Biophys. J.*, **82**, 3072 (2002).
3. A. Chanturiya, L. Chernomordik, J. Zimmerberg, 1997. *Proc. Natl. Acad. Sci. U.S.A.*, **94**, 14423 (1997).
4. L. Chernomordik, M. Kozlov, J. Zimmerberg, *J. Membr. Biol.*, **146**, 1 (1995).
5. L. Chernomordik, A. Chanturiya, J. Green, J. Zimmerberg, *Biophys. J.*, **69**, 922 (1995).
6. L. Chernomordik, V. Frolov, E. Leikina, P. Bronk, J. Zimmerberg, *J. Cell Biol.*, **140**, 1369 (1998).
7. A. Elfrat, L. Chernomordik, M. Kozlov, *Biophys. J.*, **92**, L61 (2007).
8. R. Epanand, *Biosci. Rep.*, **20**, 435 (2000).
9. D. Gingell, L. Ginsberg, In: *Membrane Fusion*, G. Paste and G. Nicolson (Eds), 791 (1978).
10. M. Hadzhilazova, J. F. Ganghoffer, I. Mladenov, *CRAS (Sofia)*, **66**, 103 (2010).
11. R. Jahn, T. Sudhof, *Ann. Rev. Biochem.*, **68**, 863 (1999).
12. G. Kemble, T. Danieli, J. White, *Cell*, **76**, 383 (1994).
13. V. Knecht, S. Marrink, *Biophys. J.*, **92**, 4254 (2007).
14. M. Kozlov, S. Leikin, L. Chernomordik, V. Markin, Y. Chizmadzhev, *Eur. Biophys. J.*, **17**, 121 (1989).
15. M. Kozlov, V. Markin, *Biofizika*, **28**, 242 (1983).
16. Y. Kozlovsky, L. Chernomordik, M. Kozlov, *Biophys. J.*, **83**, 2634 (2002).
17. Y. Kozlovsky, M. Kozlov, *Biophys. J.*, **82**, 882 (2002).
18. P. Kuzmin, J. Zimmerberg, Y. Chizmadzhev, F. Cohen, *Proc. Natl. Acad. Sci. U.S.A.*, **98**, 7235 (2001).
19. J. Lee, B. Lentz, *Biochemistry*, **36**, 6251 (1997).
20. S. Leikin, M. Kozlov, L. Chernomordik, V. Markin, Y. Chizmadzhev, *J. Theor. Biol.*, **129**, 411 (1987).
21. E. Leikina, L. Chernomordik, *Mol. Biol. Cell*, **11**, 2359 (2000).
22. B. Lentz, V. Malinin, M. Haque, K. Evans, *Curr. Opin. Struct. Biol.*, **10**, 607 (2000).
23. V. Malinin, B. Lentz, *Biophys. J.*, **86**, 2951 (2004).
24. V. Markin, M. Kozlov, *Biofizika*, **28**, 73 (1983).
25. V. Markin, M. Kozlov, V. Borovjagin, *Gen. Physiol. Biophys.*, **5**, 361 (1984).
26. V. Markin, J. Albanesi, *Biophys. J.*, **82**, 693 (2002).
27. V. Markin, D. Tanellian, R. Jersild, S. Ochs, *Biophysical J.*, **78**, 2852 (1999).
28. S. May, *Biophys. J.*, **83**, 2969 (2002).
29. G. Melikyan, J. White, F. Cohen, *J. Cell Biol.*, **131**, 679 (1995).
30. I. Mladenov, *Eur. Phys. J. B*, **29**, 327 (2002).
31. I. Mladenov, *CRAS (Sofia)*, **53**, 13 (2000).
32. M. Muller, K. Katsov, M. Schick, *J. Chem. Phys.*, **116**, 2342 (2002).
33. D. Pantazatos, R. MacDonald, *J. Membr. Biol.*, **170**, 2738 (1999).
34. D. Siegel, *Biophys. J.*, **76**, 291 (1999).
35. D. Siegel, *Biophys. J.*, **65**, 2124 (1993).
36. D. Siegel, *Biophys. J.*, **95**, 5200 (2008).
37. L. Song, Q. Ahkong, D. Georgescauld, J. Lucy, *Biochim. Biophys. Acta.*, **1065**, 5462 (1991).
38. C. Tanford, *The Hydrophobic Effect. Formation of Micelles and Biological Membranes*, Wiley, New York (1980).
39. J. Zimmerberg, S. Vogel, L. Chernomordik, *Ann. Rev. Biophys. Biomol. Struct.*, **22**, 433 (1993).

Acknowledgements: The first named author would like to acknowledge the support by the Bulgarian Ministry of Education, Youth and Science under the Project "Science and Business" BG051PO001/3.3-05-001 within "Human Resources Development" Operational Program of the European Social Fund.

СТЕБЛОВИ МОДЕЛ НА СЛИВАНЕ НА МЕМБРАНИ

М. Хаджилазова^{1*}, Ж.-Фр. Гангхофер²

¹ *Институт по биофизика и биомедицинско инженерство, Българска академия на науките, ул. Акад. Г. Бончев, бл.21, 1113 София, България*

² *LEMTA – ENSEM 2, ул. Форет Хайе, 54518 Вандьовър, П.К. 60604, Франция*

Постъпила на 6 март, 2013 г.; приета на 24 април, 2013 г.

(Резюме)

Съвременното схващане относно сливането на мембраните е, че при този процес формата на двете локални контактни повърхнини на участващите мембрани е подобна на формата на пясъчен часовник, която се оприличава със стебло. Формата на стеблото се разглежда като аксиално симетрична повърхнина в тримерното пространство, докато първоначалната конфигурация е с равнинна геометрия. Пълната енергия на стеблото е пресметната като следствие на предположението, че стеблото има постоянна средна кривина. На тази основа е анализирана и еволюцията на енергетичния път на стеблото от полусливане до пълно сливане, отчитайки радиалното отстояние на стеблото до оста на симетрия като функция на ъгъла който сключва тангентата с абсцисата в точките от профилната крива. Представено е разширение на съществуващия модел, в които геометричните характеристики на стеблото са представени в явна форма и отчитайки, че то има формата на нодоид, характеристиките на мембраната и заобикалящата я среда.

High vacuum phase transformation of fluorspar vapors to crystal aggregates

J. Mouhovski*, O. Vitov, V. Dimov, B. Kostova, S. Gechev

*Institute of Mineralogy and Crystallography "Acad. Ivan Kostov",
Bulgarian Academy of Sciences, Acad. Georgy Bonchev Str., bl.107, 1113 Sofia, Bulgaria*

Received April 4, 2013; Accepted April 24, 2013

Complex crystal aggregates from fluorspar are grown from vapor phase at specific P - T conditions. Quasi-equilibrium for occurring mass-transport processes, phase transformations and crystal-chemical reactions is attained in multicameral mode crucible by changing the temperature pressure imposed on molten portions of the used natural fluorite and/or by varying the gas-permeability of the channels connecting different sections in crucible interior to vacuum ambient. The sizes of the channels are reduced to provide Knudsen type diffusion thus limiting the induced vapor fluxes through them leading to super-saturation inside the peripheral crucible compartment. The grown aggregates reveal a complicated habit formed during three stages growing process provided by relevant thermodynamic and phases. The residual stresses in the aggregates are not observed whereas those in simultaneously grown boules from the non-vaporized melts in crucible cameras are clearly distinguished. The optical transmittance of the boules are considerably higher, especially in the UV, comparing to that of crystal aggregates, showing several peaks of specific light-absorption due to enhanced presence of rare-earth (RE) impurities. The aggregates manifest their nearly full reflectivity from visible to near IR region. The growth mechanisms from vapor phase by using natural fluorite with RE are explained on thermodynamic grounds that allows the processes being put under reliable control. The results are anticipated to help for developing new perspective techniques for vapor phase growth of several fluoride compounds with complex structure and composition but with wide application. Similar growth mechanisms for CaF_2 crystals are speculated being possible on the Moon in its very early period of formation.

Keywords: crystal structure, mass transfer, phase equilibrium, purification, optical medium

INTRODUCTION

The growth mechanism of calcium fluoride – as product of ore mineralization or artificially grown crystals – depends on thermodynamic and crystal-chemical conditions of the surrounding medium. Both the crystal habit and crystallographic character of crystal faces can be changed in accordance with P - T mineralization conditions and solutions chemistry. It was firmly established crystal transition from octahedral to cubic form via some more complex intermediate forms [1]. The habit of the real crystals is, as a rule, not geometrically regular that is due to irregularity in the mass-transport for supplying substance. One-directional supply has been proved to distort gradually the cubic crystal to mosaic block, rod-like or lamellar whereat the symmetry decreases, the habit becoming in some cases completely irregular.

The exact reconstruction of the existed thermodynamic and crystal-chemical conditions during the growth of CaF_2 natural or artificial crystals appears a challenging task since it helps the researchers to clarify the variety of interrelating factors that may influence considerably the crystal

alterations during ore mineralization as well as during the application of the already developed growing techniques (from solution, melt or vapor). In the present paper the accent is put on the growth of CaF_2 crystals from vapor phase as the less explored technique as compared to growth from solution and especially to growth from melt [2].

The object in study – single CaF_2 – has been won recognition as preferable in many cases optical medium for manufacturing optical elements appropriate to satisfy the fast increasing needs of large scale optics in deep ultra violet (UV), visible (Vis) and infrared (IR) spectral regions. Since the direct usage of natural fluoride for manufacturing thereof optical elements is strongly restricted due to impossibility, in practical, to be found sufficiently homogeneous large single crystals with minimum structural defect, the fluorspar has to be transformed appropriately to sintered or polycrystalline precursors that to be used as starting material. On this ground several industrial techniques have been developed for growing an artificial fluorite from melt [2] unlike the growth of CaF_2 crystals in over-saturated solutions where the small sizes, incomparably lower crystallization rate,

* To whom all correspondence should be sent:
E-mail: jmouhovski@abv.bg

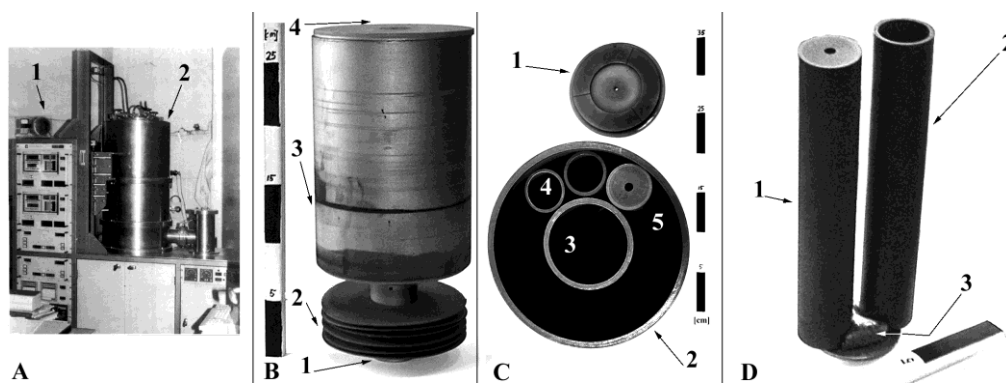


Fig. 1. A – Apparatus for crystal growing by BS method with furnace control panel assy (1) and growing chamber (2); B – multicameral graphite crucible with supporting tail-end (1), batch of separated heat-adjusting Mo-rings (2), cylindric body (3) and general cover with axially drilled channel (4); C – cross-section of multicameral crucible (2) with a central camera (3) and up to 9 peripheral inserts (4), covered with corresponding lids (1) and (5). Some of the lids can be taken away to accelerate the melt vaporization; D – view of two peripheral inserts (1) and (2), in-between the bottom section of which a fluorospar condensate is formed by a shape of segment (3).

and uncontrollable arising lattice defects have made it groundless. Nevertheless the latest very strict requirements of vacuum UV and UV-laser optics put higher challenges before the growers as concerning the purity of starting fluorospar and final product and the cost of the later. Here the Single Crystal Technology appears a promising method for increasing significantly the yield of high-sized CaF_2 crystals [3].

Without comparable industrial effect but submitting several specific scientific issues appeared the growth of CaF_2 crystals from fluorospar vapor containing some REs impurities. Such starting material was used for development of original Bridgman-Stockberger (BS) growing technique where, in multi-camera crucible with original construction, several boules were grown from melts while inhomogeneous substance was crystallized from vapor phase in supersaturated peripheral crucible compartment [4]. At that the RE content in the grown boules can be substantially reduces at the expense of enriched correspondingly to RE vapor grown substance. The technique's efficiency depends on the ability a given RE to form a stable fluoride composition, the ionized molecules of which may evaporate easily at the temperature of the molten starting fluorospar and the pressure over its surface. It was approved the process can be put under control if an appropriate P - T equilibrium was kept in all crucible cameras. These cameras represent several inner axial-symmetric inserts, loaded with starting grained purified fluorospar (or thereof made precursors), and put in a *peripheral compartment* (PC) with annular cross-section (**Fig. 1B, C**). A central compartment – “crucible core” – was also loaded with another

portion of fluorospar. One may adjust P - T conditions inside the crucible so that to provide an intensive bulk boiling in all peripheral and central melts. This way vaporized material supersaturated the free space in the PC, initiating nucleation upon its coolest bottom section to start, during the slow crucible withdrawal towards the lower (“cold”) furnace zone. Thus formed crystallite was being enriched to those REs, the fluorides of which possessed sufficiently high vapor pressure to endure effective liquid to vapor phase transformation. As a resulting production represented a relatively cheap batch of parallel boules with very high and close to each other optical characteristics that may satisfy even the contemporary, mostly strict demands of VUV- and UV-optics whereas the PC sublimate, depending on the degree of its RE's concentration, can be used for manufacturing selective light-shutters.

The present survey aims at experimental and theoretical investigation of the possible phase transformations of fluorospar vapor in the above described multi-camera crucible at large varying P - T conditions, wherein the grown crystallite would be expected to possess unique structure and properties. This suggests to be determined the triple point (t.p.) phase diagram for the used fluorospar that would allow being studied the relevant alterations in quasi-equilibrium for the proceeding mass-transport phenomena and related kinetic reactions. The longitudinal cross section view of the grown crystallite would reveal how manner the crystal habit may change according to phase transformations mode. The results are anticipated to clarify the mechanisms and regularities that govern the processes and phenomena proceeding. This may

increase the significance of growing single and mixed crystal fluoride compounds from vapor phase by modification and/or optimization of the applied technique on the base on reliable thermodynamic grounds. From geological point of view the results can promote model simulations of some mineral-genetic processes grounded on HV low-gravity emissions that could be thought being existed on the Moon or other small sized space objects where similar conditions could whenever being existed.

MATERIAL, METHODS AND APPARATUS

The starting material – grained fluor spar – contained several tens ppm in total RE elements where cerium was the prevalent one [5].

The growing experiments were performed using BS apparatus (**Fig. 1a**), the furnace unit of which allows a precise control over the thermal field configuration.

Conditions for condensation or sublimation of fluorite vapors were created by super-saturating the free space in the PC of the above described multi-camera mode crucible made by low porous, high purity graphite. The crucible cameras were loaded by weighed out portions of fluor spar, mixed carefully with 2.4 wt.% PbF_2 that acted as scavenger during the heating stage, thus providing a removal – by chemical reactions – of the mostly oxygen-containing contaminants [6]. The free spaces in crucible cameras were connected to PC free space by parallel system of channels, drilled axially in corresponding cameras' lids. The gas-permeability of the channels, depending on their diameter and length, can determine as prevalent one of the three possible mass-transport mechanisms: Knudsen diffusion, normal diffusion or viscous flow. An axial channel in the outer cover of the crucible connected its interior to the vacuum chamber ambient. The partial and/or total effective gas-conductivities of such designed system of channels determine the established pressures inside the cameras and the PC at a given T -head imposed on the loaded crucible. The methodology consisted in providing an intensive vaporization of different in mass%, but significant partitions from the molten portions in the cameras at controlled P - T conditions, which led to super-saturation by fluor spar vapors of the free space inside the PC, with following therein crystallization of condensed and/or sublimated substance on the cooler surface of the flat bottom in-between the inserts, during the slow crucible withdrawal towards the cold furnace zone. Essentially, the experiments were

implemented as combined simultaneous crystal growing from melt (inside the cameras) and from vapor – in the PC.

The vaporized quantities were calculated as the differences between the initial and final gross weights in the loaded inserts. An average time-duration of the process was taken to estimate the vapor fluxes throughout the lids' channels.

The T -head upon the molten portions was altered to vary differently: up to 34 K (“low” head), from 35 to 160 K – “intermediate” head and above 160 K – “high” head. This way a sequence of physical-chemical and/or crystal-chemical processes was initiated leading to shift in desorption/adsorption equilibrium, evaporation/vaporization by melt boiling, condensation, ionic replacements into fluorite lattice, melt and vapor crystallization (sublimation).

Longitudinally processed probes of the crystallized material were investigated by optical microscope in reflected and transmitted light, electron microscope and electron-transmission microscope. The used transmission electron microscope (TEM) Phillips EM 420 worked with accelerating voltage of 100 kV. The needed specimens were prepared by the method of wet suspending after grinding in alcohol and deposition on a perforated carbon film with a thickness below 0.5 nm, mounted onto 3 mm diameter copper grid disks.

The spectral distribution of the optical transmission t was measured at room temperature on 2.0 ± 0.15 mm-thick bi-side polished parallel plates within an accuracy of ± 0.3 nm in the spectral range 195 – 800 nm using a Varian's UV-VIS spectrophotometer Cary 100. The absorption coefficient, α , was calculated via Beer-Lamber's formula $\alpha = d^{-1} \ln (1/t)$ with d being the sample thickness. These samples were tested as well for internal stresses in polariscope/polarimeter PKS-250 U.4.1.

The total internal reflection of fine grinding probes was measured by using Evolution 300 UV-VIS Spectrometer of THERMA.

RESULTS AND DISCUSSION

The condensation/sublimation of fluorite vapors was found to start on segmental areas between the particular inserts (**Fig. 1D and Fig. 2a**). At larger resolution it is seen each one segment was built up forming a basis representing pseudo-grained fluorite aggregate consisting in skeleton CaF_2 small crystals whereupon one may think being condensed and crystallized fluorite drops (**Fig. 2b**).

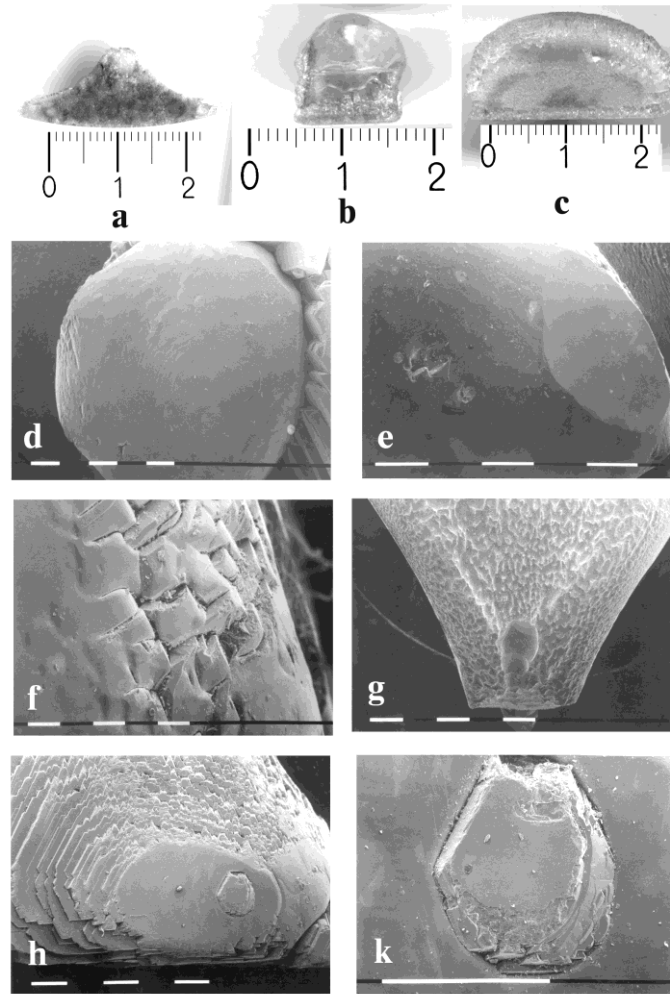


Fig. 2. Optical microscope pictures of crystallized material in the PC of multicameral crucible imposed 7 hours in HV at constant T -head, followed by 28 hours lasting crucible withdrawal with speed of 4 mm per hour in optimized furnace unit of BS apparatus. **a** – condensed fluorspar vapors with segmental shape; **b** - condensed and crystallized fluorite drops; **c** – selectively grown plate-like and acicular fluorite crystals; **d** – fluorite drops, surrounded by deeper globules, connected by fine particles of graphite and fluorite; **e, f** – different faceting of crystal faces for the condensed drops; **g** – equal in sizes pits on places found close to inserts’ external surface; **h** – a stem-like single crystal with hexagonal cross-section, incorporated into a fluorite drop; **k** – scale up fragment of picture h.

On the surface of thus formed basis, numbers of plate-like and acicular crystals were grown selectively (**Fig. 2c**).

The basis with height of ≈ 4 mm was shown in **Fig. 2d** being built in light corns, surrounded by deeper globules with diameter of ≈ 1 mm connected by fine particles of graphite and fluorite. The drops, sized between 4 and 10 mm, turned out clear, without any inclusions and defects. The smaller ones were found close to ideal sphere while the bigger ones represented oblate spheroids. The basic-drops boundary was sharply manifested as the wetting angle between the sharp surface basic and the drops varied from 20 to 60 degrees of circle (measured from the SEM photos). This suggests a large surface tension for condensing drops. Their

faceting occurred either with [111] crystal faces or with numbers of [110] or [100] rough teeth-like edges (**Fig. 2e, f**). In some cases these details were rounded due, more likely, to re-melting the crystallized substance and/or sublimation phenomena that was identified on **Fig. 2g** where several equal in sizes pits were seen to appear on the places found close to inserts’ external surface. A case was also observed where a plane was faceting a drop (**Fig. 2e**) that can consider an indication for slower crystal growth on (111)-direction as comparing (100) and (110) directions, owing to mass-redistribution from drop’s surface of the observed plane zone to the rest part of the aggregate. In other case there was observed a stem-like single crystal with hexagonal cross-section

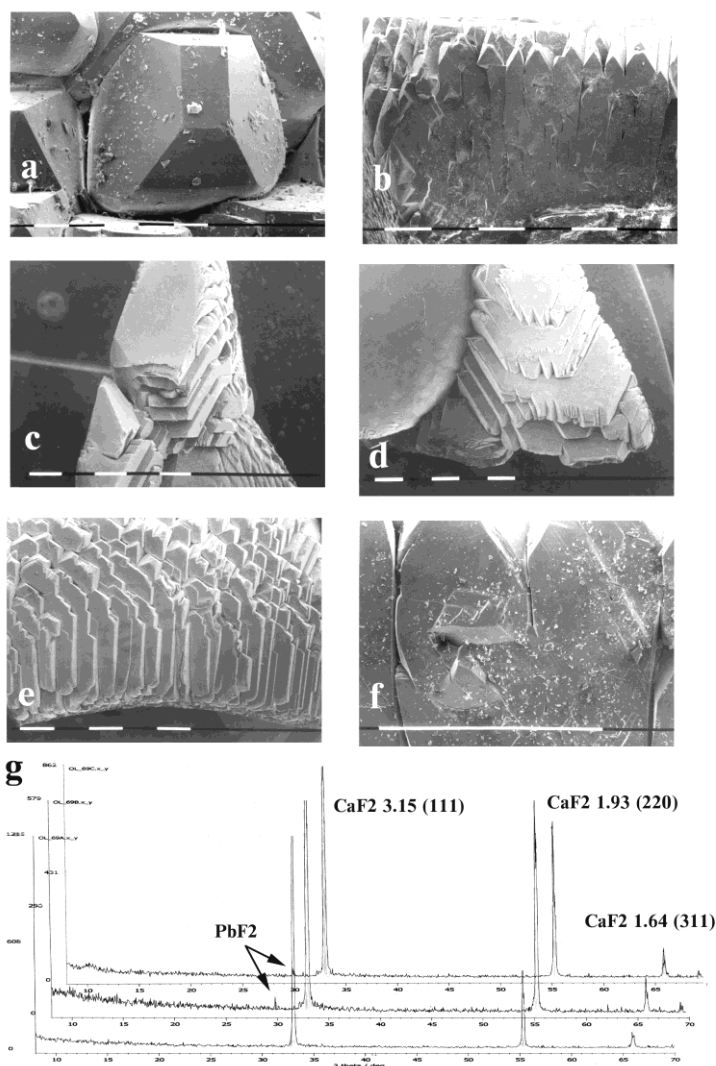


Fig. 3. Longitudinal cross-sectional view in optical microscope of probes taken from the material crystallized in PC: **a**, **b** – stem- and plate-like crystals, crystallized on (100)- and (110)-directions with rectangular and square cross-sections; **c**, **d**, **e** – crystal aggregates – packages of hexagonal plates with acute teeth-like tips; **f** – splitting and secondary selection for growing crystals; **undermost** – X-ray diagrams of three distinguished zones in the grown aggregates.

grown on (111)-direction that was incorporated into a fluorite drop (**Fig. 2h**) where partial re-melting of crystal faces can explain the scale up view of the picture (**Fig. 2k**). At this junction one may suppose the observed hexagonal single crystal has been grown before the condensation and crystallization of the surrounding drop to proceed.

Going further upwards the studied sample aggregate it is seen that from fluorite drops have been grown numbers of equal in sizes and with equal orientation needle- and plate-like crystals. Here some speculative suggestions as regards the nucleation mechanism can be done. In the case under consideration – as contrasted with the crystallization proceeding via (111)-faceting in the condensed drop – the crystallization of the stem- and plate-like crystals was occurred on (100)- and

(110)-directions with clearly seen rectangular and square cross-section (**Fig. 3a, b**).

The orientation of these needle- and plate-like crystals should inherit partially the drop's matrix that bore a specific surface of the aggregates – packages of hexagonal plates with acute teeth-like tips (**Fig 3c, d, e**). It can be supposed a strong competition to proceed between thus growing single crystals in supersaturated by fluorspar vapor ambient. Owing to that, the growth of crystals, being they even insignificantly disoriented outside the general (110) and (100)-directions, would be totally suppressed. Thence specific rounded off cavities arise between the needle- and plate-like single crystals in the region of their expansion. Considerable effect gained as well the structural defects that caused splitting and secondary selection for growing crystals (**Fig. 3f**).

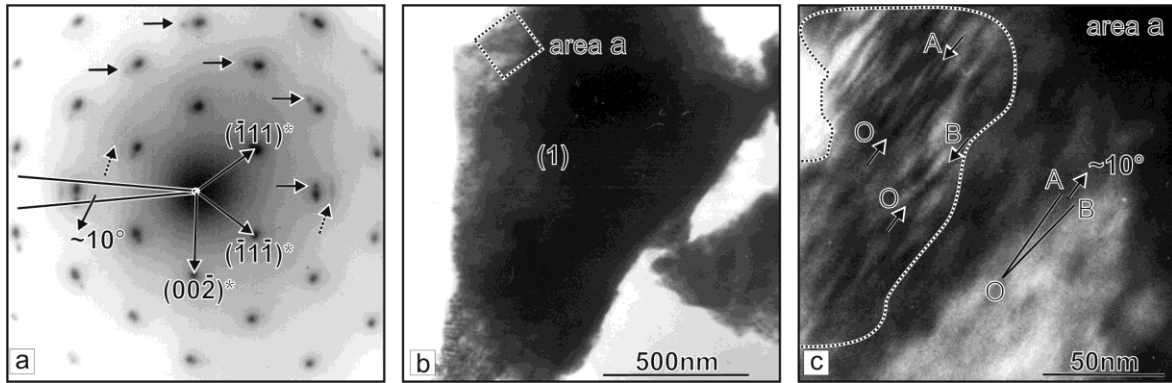


Fig. 4. TEM analysis of probes taken from crystal section shaped during the second stage of growing. **a** – SAEDI along [110] direction of area **a** from crystal (1) shown at (b); **b** – Microcrystal (1) oriented at (110) plane; **c** – above eight as much higher magnification of area **a** from the crystal (1).

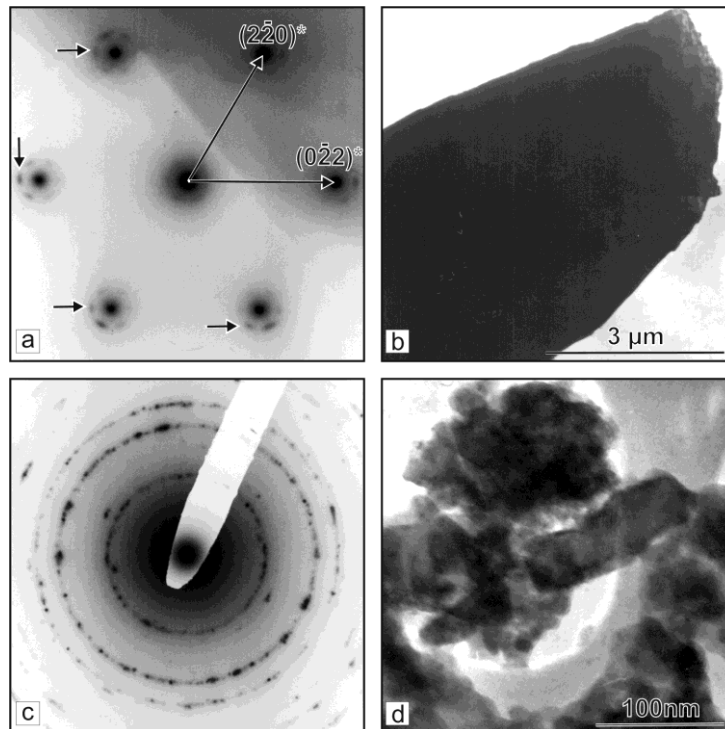


Fig. 5. TEM analysis of probes taken from crystal section grown during the third stage of the process: **a** – SAEDI along [111] direction of round area from crystal shown at (b); **b** – micro-crystal oriented at (111) plane; **c** – polycrystal SAEDI of round area from crystal shown at (d) **d** – microcrystals with grain-shaped structure.

By X-rays phase analysis were distinguished three zones of grown fluorite aggregates, and their stoichiometry were found to correspond of pure CaF_2 without any X-raying peculiarities (**Fig. 3-undermost**).

The electron diffraction analysis performed by TEM manifested the growth of needle- and plate-like crystals on definite fluorite drop should be accompanied by its (111)-epitaxy related to (110)- and (100)-epitaxy for corresponding basic forms. The surface atomic layer should be modulated due to establishing radius for drop's rounding that would cause splitting of the crystal lattice for growing on the drop crystals. These processes were identified on the electron-diffraction pictures as

enlargement and splitting of the index reflection spots.

Three samples thought relevant to different growth stages were investigated by TEM analysis. In the sample corresponding to the *first growth* stage (primary vapour phase crystallization) the $\mu\text{-sized}$ crystals were observed (**Fig. 4b**). The obtained selected area electron diffraction image (SAEDI) showed that the different particles actually are single-crystals. The point maximums are arc-like splitted and the arcs (indicate with arrow) are curved at round 10° (**Fig. 4a**). After multiple magnifications of the particles (**Fig. 4c**), the diffraction contrast visualized nano-sized defect

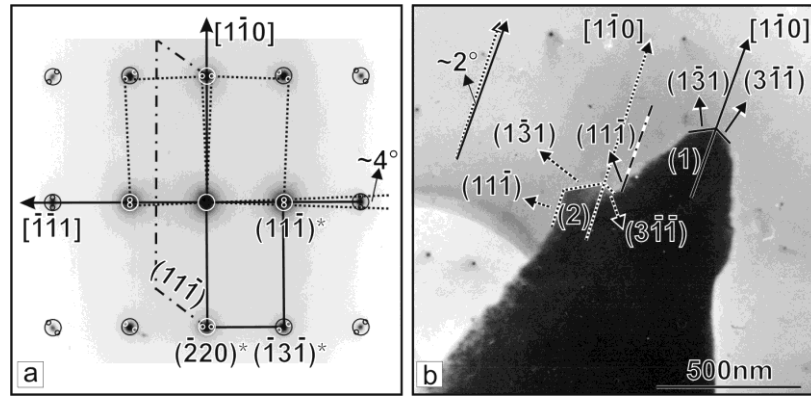


Fig. 6. TEM analysis of probes taken from crystal section grown during the first stage of the process: **a** – SAEDI along [112] direction of area **a** from crystal (1) shown at (b); **b** – micro-crystal (1) oriented at (112) plane.

areas disoriented up to 10°, which coincide with the arc-like splitting of diffraction maximums.

In the sample from the *second growth stage* it was observed a drop-like crystal, round 1 cm in diameter, built from nm to μm separate mono-crystals (**Fig. 5b, d**). SAEDI showed the existence of satellite (indicate with arrow) reflexes, the disposition of which approved a perfect structure of mono-crystals (**Fig. 5a**). The mono-crystals are situated accidentally each by other and formed poly-crystal SAEDI where no proofs for texturization exist (**Fig. 5c, d**).

The sample from the *third growth stage* is present from micro-crystals, grown on the crop-like crystal. **Fig. 6a** shows the SAEDI from [112] direction, resultant from the micro-crystal on **Fig. 6b**.

It is seen that two satellite point maximums are situated at both sides of each main maximum at angle round 2°. The particle morphology shows mono-crystal (marked on **Fig. 6b**. as 1) with [110] growth direction, development of the (131) and (311) crystal faces. One can observe and the second one crystal (marked on **Fig. 6b** as 2 and with dotted lines), fused with the first one on (111) crystal face, and having the same growth direction, development of the same crystal faces. Round 2° fusion angle was measured between the two crystals, which coincides with the angle between the satellite point maximums.

The analyzed view of SEM-microscopy pictures allowed to be reconstructed the growth itself. It was started with slightly disoriented each other nano-crystals joined in micro-crystals, which were differently oriented to the matrix and created a thin layer. After the thin layer was grown the drop-like poly-crystal aggregate was built up from perfect mono-crystals different in sizes. Over them grew up small-angle fused mono-crystals due to the almost spherical matrix. Spectrophotometric analysis (**Fig.**

7) was performed using 4 samples, two of which (sample 1 and 2) were taken from boules grown into different crucible inserts whereas the other two (sample 3 and 4) – from crystallized material after condensation/sublimation of fluorspar vapor in the peripheral crucible compartment during the same growth run. It is seen the spectra of samples 3 and 4, grown from the vapor phase, contain two clear bands which, according to literature [7-10], can be attributed to absorption near 198 and 306 nm due to 4*f* – 5*d* electron transitions in Ce³⁺. The peaks positions for both crystals were found being slightly shifted at 197.3 nm and 302.5 nm, respectively.

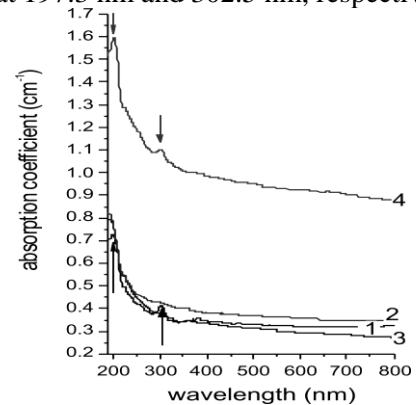


Fig. 7. Optical absorption coefficient spectra of CaF₂ single crystals grown in different crucible compartments from melt (samples 1 and 2) and from vapor phase (samples 3 and 4).

One may suppose that fact is being a result of Sr replacement for Ca into fluorite lattice, the presence of which in the starting raw material was identified by independent AAS analysis to vary within 0.03 and 0.05 wt % [11]. Thence, in accordance with previously published data [12], a conclusion was made the investigated samples can be considered as a mixed Ca_{1-x}Sr_xF₂ system with a very small *x*-proportion where part of Sr bi-valence ions have been replaced by cluster formations of Ce³⁺ ions compensated by F⁻-interstitial. The efficiency of such replacement has been studied being high for

single alkali-earth host crystals [8] as well as for mixed calcium strontium fluoride system [11].

The spectra of samples 1 and 2 (grown from non-vaporized melts in crucible inserts) did not reveal a presence of any absorption bands that suggests, in practice, all Ce ppm-amount has been transmitted from liquid to vapor phase and crystallized thereof aggregates. The absorption coefficient spectra for samples Nos. 1, 2 and 3 are close to each other along the whole visible spectral range, from 400 to 800 nm, manifesting a gradual decrease therein, covered relatively narrow region ($0.4 - 0.3 \text{ cm}^{-1}$). The steeper slope of curve 3, similar to that of curve 4, manifests a better microstructure for both samples grown from vapor phase, despite the curve 4 was located much higher compared to the other three curves, indicating a presence of light-scattering centers, caused by very fine graphite inclusions randomly dispersed in this sample, established by SEM microprobe analysis. At the same time, the performed comparative polarimetry of the investigated four samples showed an absence of residual stresses (deep purple coloration) of samples 3 and 4, in contrast to samples 1 and 2 wherein the deep purple was surrounded by narrow strips of red (22 nm/cm) and blue (108 nm/cm) colors. This result can be explained by external pressure whereupon the growing boules have been undergone from the wall of the inserts while similar effect should not appear in the PC at the places where the crystals were grown free of such pressure.

The view and optical properties of crystal aggregates grown in the PC lead to conclusion of their 3-stage formation. Thermodynamically such

suggestion can be supported accepting relevant alteration in P - T conditions according to triple point phase equilibrium: $\text{CaF}_{2\beta\text{cr}} - \text{CaF}_{2\text{melt}} - \text{CaF}_{2\text{vap}}$ established inside the PC. Taking \ln -form for P -phase equilibrium:

$$\ln P(\text{CaF}_{2\beta\text{cr}}) = \ln P(\text{CaF}_{2\text{melt}}) \quad (1)$$

where the vapor pressure – T relationships for tetragonal β - CaF_2 crystal phase and liquid CaF_2 are expressed by [13]:

$$\text{CaF}_{2\beta\text{cr}}: \ln P(\text{atm}) = -53480/T - 0.525 \ln T + 56.08 \quad (2)$$

$$\text{CaF}_{2\text{melt}}: \ln P(\text{atm}) = -50200/T - 4.525 \ln T + 53.96 \quad (3)$$

one can easily calculated the lowest possible t.p. being at $T = 1689 \text{ K}$ ($1416 \text{ }^\circ\text{C}$) and $P = 8.35 \cdot 10^{-5}$ bars or 0.0635 torr. At such P - T conditions established in the peripheral crucible compartment, vapor to crystal phase transition (sublimation) should start on places where $T < 1689 \text{ K}$. At the same time, the maintained low total vapor pressure inside the crucible inserts/central camera provides a mode of bulk boiling into the melts that initiate an intensive vaporization, exceeding considerably the surface evaporation. Besides, the cooling of the lower section of overheated crucible below 1689 K will start in a very short time after it has been moved towards the lower (“cold”) furnace zone.

As higher temperature head has been imposed on fluorspar melts in the inserts, that is, when overheating T has been set up above 1689 K, the sublimation/bulk boiling processes would occur at relevant higher super-saturation pressure $P_{\text{tub}} > 0.0635$ torr following the $P - T$ phase diagram on **Fig. 8a**. Supplement control can be implemented efficiently by appropriate alteration of the effective

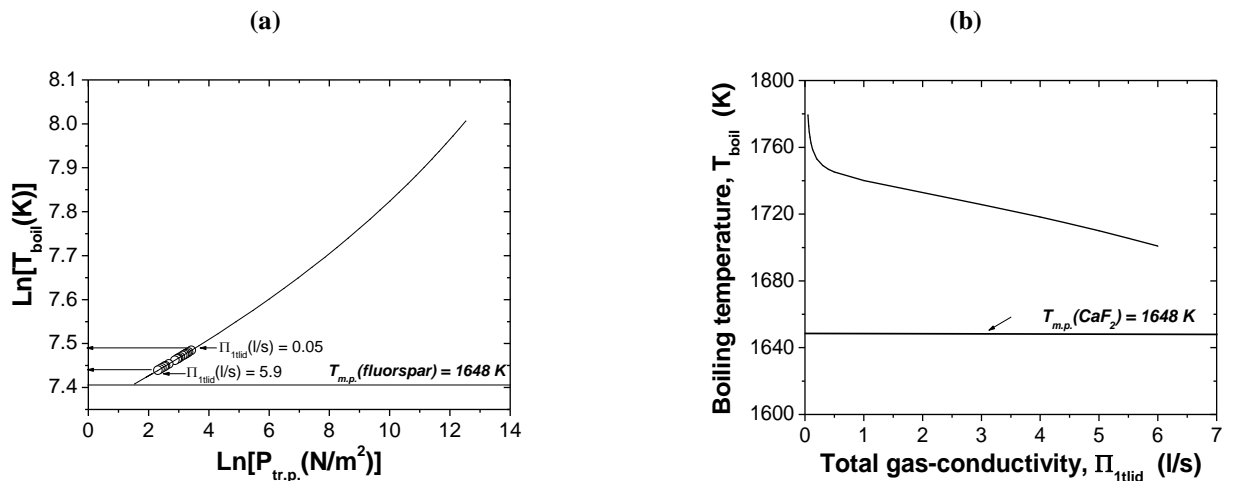


Fig. 8. a – \ln -dependence of boiling temperature on equilibrium pressure inside the different crucible cameras (inserts). **b** – Boiling temperature of CaF_2 melts in crucible inserts versus total gas-conductivity in corresponding lids’ channels.

total gas-conductivity for the system of inner parallel lids' channels and the channel in the general crucible cover (**Fig. 8b**).

For each one P - T combination conditioned being below the equilibrium curve (**Fig. 8a**) the sublimation and bulk boiling will be totally suppressed being replaced by vapor to liquid phase transition (condensation). This will occur when the vacuum system succeeds to maintain a residual pressure inside the crucible below the found lowest value of 0.0635 torr in the t.p. phase diagram. Here the vacuum system influence can be kept under control by altering appropriately the channel gas-permeability of the outer crucible cover so that being provided Knudsen diffusion in it as the slowest possible mass-transport mechanism independent on the mean pressure into the channel. The condensate will start to crystallize upwards on the places, the temperature of which was dropped below the fluor spar m.p. T , that is, near to the bottom of the crucible during its penetration into the cold furnace zone Z2. On this thermodynamic ground, the three stages of aggregates' formation can find a reasonable explanation.

The first stage should cover the initial time interval of crucible movement towards Z2 when P - T conditions in the PC have been adjusted – by appropriate chosen T -pressure and/or channels' gas-conductivities – being stayed higher than P - T phase equilibrium curve shown in **Fig. 8a**. Such thermodynamic conditions mean super-saturation by fluor spar vapor of the free space in this compartment. It occurs when the general channel gas-permeability is being chosen sufficiently low to determined Knudsen diffusion for gaseous/vapor molecules and ions along the channel, whereat its mass-transport resistance restricts the vapor flux towards the vacuum chamber. Such conditions are favorable for appearance of numbers of nucleation centers on definite spots of the inner flatten surface of crucible bottom (bounded by relevant catenaries pertaining to the round solid grounds of the inserts) in conjunction with its microstructure. These centers lead to spontaneous growth of the observed crystallites and very small globules. In fact the established vapor pressure in the compartment depends on both, the effective total gas-conductivity of the system of inner lids' channels and the channel of the general crucible cover. Thus the thermodynamic conditions in the PC may be adjusted precisely choosing appropriate gas-permeability's combinations.

Since the sublimation growth rate upwards is lower as compared to the speed of crucible

withdrawal throughout the adiabatic furnace zone, characterizing itself by a steep negative vertical T -gradient, the mean temperature in the compartment start to decrease, as the T -fall will be faster nearby the sublimating on the ground aggregates. Simultaneously, the level of super-saturation pressure drops down in accordance with strong T -dependence ($\approx T^{2.3}$ [5]) of the attenuating bulk boiling mechanism into the melts. As a result the probability for condensation and following growth of fluorite drops upon the already grown globules/crystallites will rise up sharply (stage 2) what really occurs as it is seen on the pictures in **Fig. 2** and **Fig. 3**.

The last (third) stage supposes the super-saturation to increases again over the equilibrium owing to accelerating growth in the condensed drops whereat the temperature of their tip surface tends to increase rapidly towards the corresponding phase equilibrium value. As a result of that needles and plates start to grow up upon the drops. As intensively these forms are growing as larger the liberated specific heat of crystallization becomes that leads to supplementary re-heating the aggregates with great probability for their partial re-melting. This explains the observed microscopic pictures on **Fig. 2h, k**.

Speculating with these results, one could suppose similar mechanism to induce growth of huge number of various fluorite crystal aggregates at specific Moon's conditions (HV, low gravity, high- T) when, million years ago, large areas of its surface has been occupied by basaltic likes. These likes could think being a source of intensive evaporation of fluorite at low gravity and absence of atmosphere. This mineral may suggest being present in the wombs of the Moon in the very early time of its formation as Earth's satellite. Further, one can suppose the evaporated in the space substance to fall dawn slowly on the surface due to gravity force, whereon to condense and crystallize and/or sublimate on mostly cool poles' regions of the Moon. The very high brightness of 10.0 (and correspondingly estimated albedo) that has been established for certain regions on the Moon (for example the central peaks of Aristarchus [14,15]) means reflectivity close to 100% within a large spectral region. Similar reflectivity spectra are found for investigated CaF_2 aggregates (**Fig. 9**).

As seen the corrected baseline shows 100% relative reflectance, that is, zero absorbance within Vis – near IR. Maximum absorbance is observed in UV region manifested by a slight peak at 265 nm. The similarity for reflectivity spectra pertaining to

aggregates' crystals in study and some Moon's regions is a ground for providing further exploration. This way one could approve or reject the proposed challenging hypothesis for existing nowadays regions on the Moon where to be found any crystalline fluorite.

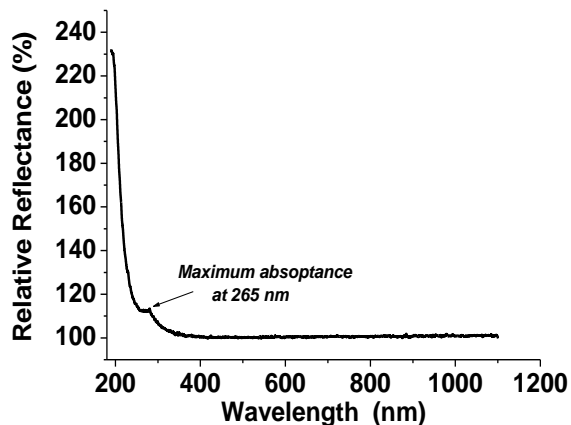


Fig. 9. Reflectance spectrum of CaF_2 powder ground from the aggregates grown in PC of the crucible. The baseline was corrected to spectrum of reference sample: Pretralon – PTFE with reflection of 99% in 400–1400 nm region and >95% – in 200–250 nm region.

CONCLUSIONS

The CaF_2 vapor growth mechanism may be altered controllably to produce complex crystal aggregates depending on established P - T quasi-equilibrium in evacuating permanently space. This is attained by appropriate alteration of temperature head where to are imposed several molten portions of fluorspar in multi-camera crucible accordingly the sizes (gas-permeability) of the channels connecting different section in crucible interior and ambient. Sufficiently small sizes of the channels provide Knudsen type diffusion that determines the slowest possible rate for proceeding mass-transport processes in vapor/gaseous phase that leads to fast super-saturation by CaF_2 vapor the free space in the crucible, the movement of which towards to cooler furnace zone causes relevant alteration in P - T phase equilibrium. The complicated habit of grown aggregates is formed during three consecutively proceeding growing stages in accordance with the induced thermodynamic alterations providing direct vapor to solid phase transformation (sublimation) or indirect one – via vapor condensation and following crystallization. The sublimated crystals appear free of any residual stresses whereas simultaneously grown boules from non-vaporized melts in crucible cameras show stresses' distribution characteristic of the external pressure imposed from cameras' wall on growing crystal. The optical transmission spectrum t of the

boules is considerably better, especially in the UV, comparing to crystal aggregates containing randomly dispersed graphite inclusions, the t -spectra of which aggregates show several peaks of light-absorption specific for calcium strontium solid solution system. The aggregates manifest as well nearly full reflectivity from Vis to near IR region.

The clarification of the growth mechanism of CaF_2 from vapor phase by using natural fluorite as starting material and how it could be efficiently controlled gives opportunity for optimization of the existing but as well for developing new more efficient techniques on the base of effective phase transformation control so that to be produced low cost crystals with improved characteristics at the expense of deep RE-purification of the starting material. These techniques are supposed being appropriate for growing several mixed fluoride crystal systems with unique properties.

The results can be used for modeling fluorite mineralization from vapor phase in HV conditions where the crystal habit is being widely varied. Such models are ground for hypothesizing similar crystals formations could be found on the Moon in differentiated as isolated mineral fluorite deposits.

REFERENCES

1. N.P. Yushkin, N.V. Volkova, G.A. Markova, *Opticheskii Fljuorit*, Nauka, Moskwa, 1983, p. 20 (in Russian).
2. J.T. Mouhovski, *Prog. Cryst. Growth Charact. Mater.*, **53**, 79 (2007).
3. K.A. Pandelisev, in: The 2nd Intern Symp on 157 Lithography, Dana Point, CA, USA, 14-17 May 2001.
4. J.T. Mouhovski, V.Tz. Penev, R.B. Kuneva, *Cryst. Res. Technol.*, **31**, No. 6, 727 (1996).
5. I.T. Mouhovski, in: *Optical fluorides: purification and crystal growing, applicability and perspectives*, Akad. Izd. "M. Drinov", Sofia, 2013, p. 145.
6. J.T. Mouhovski, V.B. Genov, L. Pirgov, V.Tz. Penev, *Mater. Res. Innovations*, **3**, 138 (1999).
7. A.A. Kaplyansky, V.N. Medvedev, P.P. Feofilov, *Opt. Spectrosc.*, **14**, 664 (1963) (in Russian).
8. E. Loh, *Phys. Rev.*, **154**, 270 (1967).
9. E. Loh, *Phys. Rev.*, **147**, 332 (1966).
10. D.S. McClure, Ch. Pedrini, *Phys. Rev. B*, **32**, 8465 (1985).
11. I. T. Muhovski, in: *Izrastvane na optitzeski kristali ot CaF_2* , NACID, CNTB, Sofia, 2006 (in Bulgarian).
12. B. Kostova, J. Mouhovski, O. Petrov, L. Dimitrov, L. Konstantinov, *Mater. Chem. Phys.*, **113**, 260 (2009).
13. E. Gmelin, in: *Handbuch der anorganischen Chemie*, Weinheim/Bergstr. Verlag Chemie, GMBH., 1976, 8 Auflage, Teil C3, Vol. 39, p. 78.
14. [http://en.wikipedia.org/wiki/Aristarchus_\(crater\)](http://en.wikipedia.org/wiki/Aristarchus_(crater)).
15. <http://www.youtube.com/watch?v=aqpdN5isp8Y>.

ВИСОКОВАКУУМНИ ФАЗОВИ ПРЕВРЪЩАНИЯ НА ФЛУОРИТОВИ ПАРИ В КРИСТАЛНИ АГРЕГАТИ

Й. Муховски*, О. Витов, В. Димов, Б. Костова, С. Гечев

*Институт по минералогия и кристалография "Акад. Иван Костов", Българската академия на науките,
ул. „Акад. Георги Бончев, бл.107, 1113 София, България*

Постъпила на 4 април, 2013 г.; приета на 24 април, 2013 г.

(Резюме)

Комплексни кристални флуоритови агрегати са израсли от парна фаза при специфични $P - T$ условия. Квази-равновесието за протичащите масопреносни процеси, фазовите превръщания и кристално-химичните реакции е постигнато в многокамерен тип тигел чрез промяна на температурния натиск, приложен върху разтопени порции от естествен флуорит и/или чрез подходящо вариране на газопропускливостта на каналите, свързващи различни секции от вътрешността на тигела с околната вакуумна среда. Размерите на каналите са намалени, така че да обезпечат Кнудсенов тип дифузия, ограничавайки по този начин скоростта на паропренасянето през тях, водещо до свръхнасищане на периферното отделение на тигела. Израслите агрегати разкриват сложен хабитус, образуван по време на триетапния процес на израстване и обезпечен от отговорните за това термодинамика и фази. В агрегатите не се наблюдават остатъчни напрежения, докато такива се разграничават ясно в були, едновременно израсли с тях от неизпарената част на стопилките в камерите на тигела. Оптичната пропускливост на булите е значително по-висока от тази, измерена за кристалните агрегати, особено в ултравиолетовия спектрален диапазон, разкривайки няколко ивици на специфична светлинна абсорбция, дължащи се на увеличено присъствие на редкоземни (РЗ) примесни центрове в кристалната решетка. Агрегатите разкриват тяхната практически пълна отражателна способност от видимата до близката инфрачервена спектрални области. Механизмите за растеж от газова фаза при използване на природен флуорит с РЗ примеси са обяснени въз основа на термодинамични съображения, което позволява надежден контрол върху процесите. Предполага се, че резултатите ще спомогнат за разработването на нови перспективни техники на кристален растеж от парна фаза на някои флуорни съединения със сложна структура и състав, но с широко приложение. Може да се допусне, че подобни механизми на растеж на CaF_2 кристали са съществували през началния период от формирането на Луната.

Nano silica phosphoric acid as an efficient catalyst for one-pot synthesis of 2,4,5-trisubstituted imidazoles under solvent free condition

A. Bamoniri^{*1}, B.F. Mirjalili², S. Nazemian¹, N.Y. Mahabadi¹

¹Department of Organic Chemistry, Faculty of Chemistry, University of Kashan, Kashan, I.R. Iran

²Department of Chemistry, College of Science, Yazd University, Yazd, PO Box 8915813149, I.R. Iran

Received January 7, 2013; accepted March 27, 2013

Nano silica phosphoric acid has been found to be an extremely efficient catalyst for the preparation of 2,4,5-trisubstituted imidazoles via three-component reactions of benzil, aldehydes and ammonium acetate under solvent free conditions. This process is simple and environmental benign in good to excellent yields. Furthermore, the catalyst can be recovered conveniently and reused for at least three times with a gradual decline in activity.

Keywords: 2,4,5-trisubstituted imidazole, nano-silica phosphoric acid, benzil, solvent-free conditions, heterogeneous catalyst.

INTRODUCTION

Compounds with an imidazole moiety have many pharmacological properties and play important roles in biochemical processes [1] Many of the substituted imidazoles are known as inhibitors of fungicides and herbicides, plant growth regulators and therapeutic agents [2] Recent advances in green chemistry and organometallic chemistry have extended the boundary of imidazoles to the synthesis and application of a large class of imidazoles as ionic liquids and imidazole related N-heterocyclic carbenes [3]. The best reported route for synthesis of 2,4,5-trisubstituted imidazoles is presented by condensation of benzil, aldehydes and ammonium acetate in the presence of an acidic catalyst.

Recently some catalysts such as L-Proline [4], montmorillonite K10 [5], zeolite [5], nano sulfated zirconia [5], [EMIM]OAc [6], Zr(acac)₄ [7], [HeMIM]BF₄ [8], HOAc [9], tetra-butyl ammonium bromide (TBAB) [10], polymer-supported zinc chloride [11] and potassium dihydrogen phosphate [12] have been applied for the above mentioned route.

Some of the reported protocols have disadvantages such as harsh reaction conditions, poor yields, prolonged reaction times, use of hazardous and often expensive acid catalysts. Moreover, the synthesis of these heterocycle compounds has been usually carried out in polar solvents such as ethanol, methanol, acetic acid, DMF and DMSO leading to uncomfortable

isolation and recovery procedures. These processes also have generated wastes containing catalysts and solvents, which must be recovered, treated and disposed off. During the course of our studies towards the development of new protocols to the synthesis of organic compounds, we wish to report a simple and efficient method for the synthesis of 2,4,5-triaryl substituted imidazoles in the presence of nano-silica phosphoric acid (nano-SPA) under solvent free conditions.

EXPERIMENTAL

Material and methods

Chemicals were purchased from Sigma–Aldrich and Merck chemical companies and were used without any purification. All products were characterized by their FT-IR, ¹H-NMR and comparison of their physical properties with those reported in the literature. FT-IR spectra were recorded on a Bruker, Equinox 55 spectrometer. In all cases, the ¹H-NMR spectra were recorded on a Bruker DRX-400 Avance instrument. Nano-SPA was synthesized according to SPA procedure [22]. The SEM photograph of nano particles was determined with VEGA/TESCAN scanning electron microscope. The TEM photograph was determined by Leo 912AB OMEGA microscope.

General procedure for the synthesis of 2,4,5-trisubstituted imidazoles

Benzil (4 mmol), aldehyde (4 mmol), ammonium acetate (8 mmol) and nano-SPA (0.04 g) was heated with stirring at 140 °C for 3 h (Table 2). The progress of the reaction was followed by TLC on silica gel polygram SIL G /UV 254 plates.

* To whom all correspondence should be sent:
E-mail: bamoniri@kashanu.ac.ir

After completion of the reaction, the mixture was cooled to room temperature. CHCl_3 was added to the mixture and filtered to remove the catalyst. After evaporation of the solvent, an oily residue or an impure solid was obtained. By adding ethanol and water to the residue, a milky to yellow solid was obtained. The solid was then crystallized from ethanol. All products are known and were identified by comparison of their physical and spectral data with those of authentic samples.

RESULTS AND DISCUSSION

Nano silica phosphoric acid (nano-SPA) as an efficient and reusable catalyst was prepared by reaction of nano-silica chloride with dry phosphoric acid. Nano silica chloride was prepared by reaction of commercial nano silicagel with thionyl chloride in reflux condition. The particle size of nano-SPA was measured by SEM and TEM photography (Figure1). As it is shown in SEM and TEM photographs, the scale of nano-SPA particles are smaller than 100 nm.

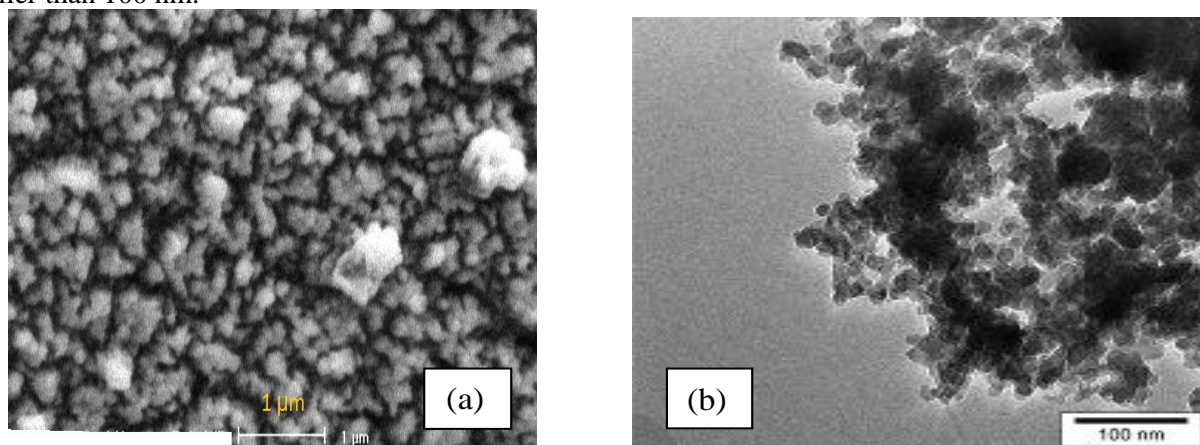
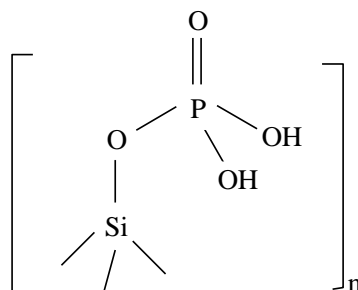


Fig. 1. SEM (a) and TEM (b) photographs of nano SPA.



Scheme 1. A proposed structure for nano-SPA.

The acidic capacity of nano-SPA was presented $10.32 \text{ mmol. g}^{-1}$. It was determined *via* titration of 0.2 g of nano-SPA with standard solution of NaOH . The FT-IR (ATR) spectra of silica chloride, nano-SPA and $\text{H}_3\text{PO}_4 \cdot \text{SiO}_2$ were shown in Figure 2. In all ATR spectra, the Si-O-H and Si-O-Si stretching bands are appeared in the range of 900 to 1100 cm^{-1} . In silica chloride spectrum, the Si-Cl stretching band is appeared in 700 cm^{-1} . In ATR spectra of nano-SPA and $\text{H}_3\text{PO}_4 \cdot \text{SiO}_2$, the P-O-H, P=O, P-O stretching bands are appeared in 910 - 1040 , 1637 and 2400 - 2800 cm^{-1} respectively. According to above data, we have suggested the structure for nano-SPA with PO_3H_2 on silica gel (Scheme 1).

The X-ray diffraction (XRD) patterns of nano- SiO_2 and nano-SPA are shown in Figure 3. Nano- SiO_2 XRD pattern has a strong peak in 2θ value of 21.8024° and FWHM equal to 1.771 and nano-SPA XRD pattern has a strong broad peak in 21.718 and FWHM equal to 2.3616 .

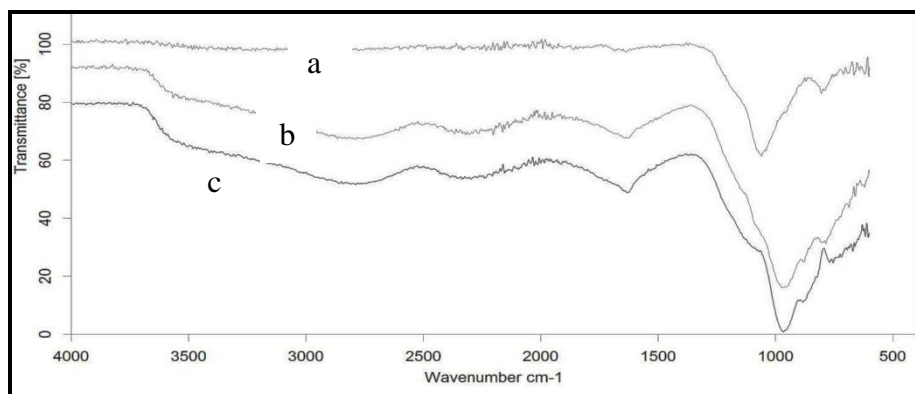


Fig. 2. ATR of (a) silica chloride, (b) nano-SPA and c) H₃PO₄.SiO₂.

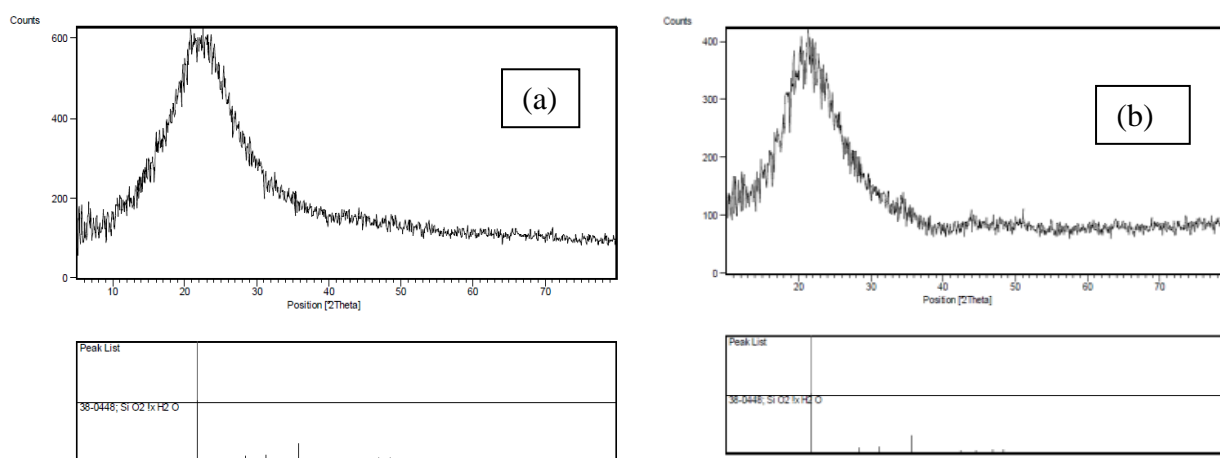
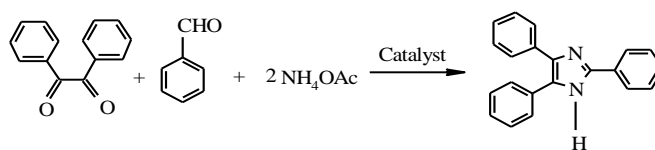


Fig. 3. X-ray diffraction (XRD) pattern of a) nano SiO₂ and b) nano-SPA

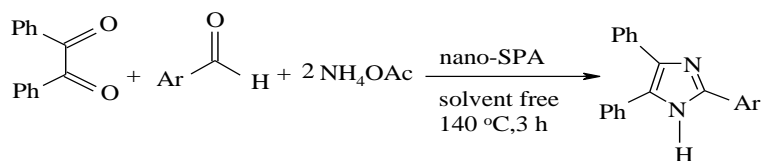
To find the optimum condition for the synthesis of 2,4,5-trisubstituted imidazoles in the presence of solid acid, we have synthesized 2, 4, 5-triphenyl imidazole in the presence of SPA and nano-SPA under various conditions (Table 1).

Reactions at different temperatures and various molar ratios of substrates in the presence of SPA and nano-SPA revealed that the best condition was presented as solvent-free at 140 °C and a ratio of aldehyde (mmol): benzil (mmol): ammonium acetate (mmol): nano-SPA (g) equal to 1:1:2:0.01. The reusability of the nano-SPA catalyst was also

examined for three times. After each run, the product was filtered, the solvent was evaporated and the catalyst was washed with CHCl₃ and reused. Treatment with CHCl₃ removes tars more efficiently from the catalyst surface (table 1, entries 14 and 15). The catalyst was reusable, although a gradual decline in activity was observed. Therefore, various aldehydes were used as substrates for the synthesis of 2,4,5-tri-substituted imidazoles at 140°C under solvent-free condition (Scheme 1 and Table 2).

Table 1. Synthesis of 2,4,5-triphenyl imidazole using SPA or nano-SPA under different conditions^a^aThe molar ratio of benzaldehyde: benzil: ammonium acetate is equal to 1:1:2

Entry	Catalyst, (g)	Solvent	Condition	Time, (h)	Yield, (%)	Ref.
1	SPA (0.05)	-	120 °C	3	60	-
2	SPA (0.06)	-	120°C	3	50	-
3	SPA (0.06)	-	140°C	3	92	-
4	SPA (0.06)	DMSO	110°C	3	86	-
5	SPA (0.06)	CH ₂ Cl ₂	45 °C	24	20	-
6	SPA (0.06)	<i>n</i> -Hexane	50 °C	24	50	-
7	SPA (0.06)	EtOH	75°C	6	48	-
8	SPA (0.06)	HOAc	80°C	24	50	-
9	SPA (0.06)	MeOH	65 °C	6	46	-
10	SPA (0.06)	Isopropanol	82°C	6	45	-
11	SPA (0.06)	-	Ball mill	30 (min)	60	-
12	SPA (0.06)	Ethyl acetate	Ultrasound	30 (min)	70	-
13	nano-SPA (0.01)	-	140 °C	3	95	-
14	nano-SPA (0.01), 2nd run	-	140 °C	4	65	-
15	nano-SPA (0.01), 3rd run	-	140 °C	4	50	-
16	L-Proline	MeOH	60°C	9	90	[4]
17	Zeolite	EtOH	reflux	60 (min)	80	[5]
18	K10	EtOH	reflux	90 (min)	70	[5]
19	Nano –sulfated zirconia	EtOH	reflux	45 (min)	87	[5]
20	[EMIM]OAc	EtOH	Utlasound/r.t.	45 (min)	87	[6]
21	Zr(acac) ₄	EtOH	Utlasound/r.t.	25 (min)	94	[7]
22	Zr(acac) ₄	EtOH	reflux	2.5	90	[7]
23	[HeMIM]BF ₄	-	MW	2 (min)	93	[8]
24	-	HOAc	MW	5 (min)	98	[9]
25	TBAB	Isopropanol	82°C	20 (min)	95	[10]
26	Polymer-ZnCl ₂	EtOH	reflux	4	96	[11]
27	KH ₂ PO ₄	EtOH	reflux	40 (min)	93	[12]
28	SSA	-	130 °C	50 (min)	83	[14]
29	SSA	-	mw	10 (min)	85	[14]
30	I ₂	EtOH	75°C	15 (min)	99	[15]
31	[Hbim]BF ₄	-	100°C	25 (min)	93	[16]
32	InCl ₃ .3H ₂ O	MeOH	r.t	12	73	[17]
33	-	PEG-400	110°C	1/5	88	[18]
34	Yb(OTf) ₃	HOAc	70°C	2	92	[19]

Table 2. Synthesis of 2,4,5-trisubstituted imidazoles in the presence of nano-SPA at 140 °C and solvent free condition in 3 hours.^a^aThe molar ratio of aldehyde: benzil: ammonium acetate is equal to 1:1:2

Entry	Ar	Yield, (%) ^b	M.P., °C (lit.)	Ref.
1	C ₆ H ₅	90	274(274-275)	[6]
2	4-CH ₃ C ₆ H ₄	87	236(227-229)	[14]
3	4-NO ₂ C ₆ H ₄	78	240(239-242)	[6]
4	4-ClC ₆ H ₄	85	261(260-262)	[5]
5	2-OMeC ₆ H ₄	93	210(210-211)	[4]
6	4-OMeC ₆ H ₄	94	230 (230–231)	[7]
7	2-ClC ₆ H ₄	80	186(188)	[16]
8	2,4-DiClC ₆ H ₃	88	175(174-175)	[7]
9	4-BrC ₆ H ₄	80	254(254-256)	[5]
10	2-NO ₂ C ₆ H ₄	88	230 (230–231)	[4]
11	3-NO ₂ C ₆ H ₄	89	>300 (>300)[[18]
12	4-OH C ₆ H ₄	90	267 (265–267)	[18]
13	2-BrC ₆ H ₄	80	201 (201-202)	[6]

CONCLUSION

In this article, we have synthesized nano silica phosphoric acid and studied its structure with FT-IR, XRD, SEM and TEM. A simple method for the synthesis of 2,4,5-trisubstituted imidazoles using nano-silica phosphoric acid as a reusable, eco-friendly, inexpensive and efficient catalyst was demonstrated. Short reaction times, high yields, simplicity of operation and easy work-up are some advantages of this method.

Acknowledgment: The authors are grateful to University of Kashan for supporting this work by Grant No (159189/7).

REFERENCES

- J. G. Lambardino, E. H. Wiseman, *J. Med. Chem.*, **17**, 1182 (1974).
- T. Maier, R. Schmierer, K. Bauer, H. Bieringer, H. Buerstell, B. Sachse, US Patent 820335, 1989; *Chem. Abstr.*, **111**, 19494 (1989).
- T. Welton, *Chem. Rev.*, **99**, 2071 (1999).
- S. Samai, G. C. Nandi, P. Singh, M. S. Singh, *Tetrahedron*, **65**, 10155 (2009).
- A. Teimouri, A. Najafi Chermahini, *J. Mol. Catal. A-Chem.*, **346**, 39 (2011).
- H. Zang, Q. Su, Y. Mo, B. W. Cheng, S. Jun, *Ultrason. Sonochem.*, **17**, 749 (2010).
- A.R. Khosropour, *Ultrason. Sonochem.*, **15**, 659 (2008).
- M. Xia, Y. Lu, *J. Mol. Catal. A:Chem.*, **265**, 205 (2007).
- S. E. Wolkenberg, D. D. Wisnoski, H. William Leister, Y. Wang, *Org. Lett.*, **6**, 1453 (2004).
- M. V. Chary, N. C. Keerthysri, S. V. N. Vupallapati, N. Lingaiah, S. Kantevari, *Catal. Commun.*, **9**, 2013 (2008).
- L. Wang, C. Cai, *Monatsh. Chem.*, **140**, 541 (2009).
- R. S. Joshi, P. G. Mandhane, M. U. Shaikh, R. P. Kale, C. H. Gill, *Chinese. Chem. Lett.*, **21**, 429 (2010).
- M.A. Zolfigol, F. Shirini, K. Zamani, E. Ghofrani, S. Ebrahimi, *Phosphorus, Sulfur, Silicon Relat. Elem.*, **179**, 2177 (2004).
- A. Shaabani, A. Rahmati, E. Farhangi, Z. Badri, *Catal. Commun.*, **8**, 1149 (2007).
- M. Kidwai, P. Mothsra, V. Bansal, R. K. Somvanshi, A. S. Ethayathulla, S. Dey, T.P. Singh, *J. Mol. Catal. A:Chem.*, **265**, 177 (2007).
- S. A. Siddiqui, U. C. Narkhede, S. S. Palimkar, T. Daniel, R. J. Lahoti, K. V. Srinivasan, *Tetrahedron*, **61**, 3539 (2005).
- S. D. Sharma, P. Hazarika, D. Konwar, *Tetrahedron Lett.*, **49**, 2216 (2008).
- X. C. Wang, H. P. Gong, Z. J. Quan, L. Li, H. L. Ye, *Chinese Chem. Lett.*, **20**, 44 (2009).
- L. Min, Y. H. Wang, H. Tian, Y. F. Yao, J. H. Shao, B. Liu, *J. Fluorine Chem.*, **127**, 1570 (2006).

НАНО-СИЛИЦИЕВО-ФОСФОРНА КИСЕЛИНА КАТО ЕФЕКТИВЕН КАТАЛИЗАТОР
ПРИ ЕДНОСТЕПЕННАТА СИНТЕЗА НА 2,4,5-ТРИ-ЗАМЕСТЕНИ ИМИДАЗОЛИ В
ОТСЪСТВИЕ НА РАЗТВОРИТЕЛ

А. Бамонири^{*1}, Б.Ф. Мирджалили², С. Наземиан¹, Н.Я. Махабади¹

¹Департамент по органична химия, Химически факултет, Университет в Кашан, Кашан, Иран

²Департамент по химия, Колеж за наука, Университет в Язд, Язд, P.O. Box 8915813149, Иран

Постъпила на 7 януари, 2013 г.; приета на 27 март, 2013 г.

(Резюме)

Установено е, че нано-силициево-фосфорната киселина е изключително ефективен катализатор за получаването на 2,4,5-тризаместени имидазоли чрез три-компонентна реакция на бензил, алдехиди и амониеш ацетат в отсъствие на разтворител. Процесът е прост и съвместим с опазването на околната среда, като дава високи добиви. Освен това катализаторът лесно се регенерира и може да се използва трикратно с постепенно спадане на активността му.

Design, synthesis and pharmacological screening of some [3-benzoyl-5-(4-substituted)-2, 3-dihydro-1,3,4-oxadiazol-2-yl] and [5-(4-substituted)-4H-1, 2, 4-triazol-3-yl] derivatives

N.S. Dighe^{*1}, R.B. Saudagar², D.A. Jain³

¹Department of Pharmaceutical Chemistry, Pravara Rural College of Pharmacy, Loni, MS, India-413736.

²Department of Pharmaceutical Chemistry, R.G.Sapkal College of Pharmacy, Nashik, M.S. India.

³Department Of Pharmaceutical Sciences and Research, Bhagwant University, Ajmer, Rajasthan, India

Received September 28, 2012; Revised April 15, 2013

A novel series of some substituted [3-benzoyl-5-(4-substituted)-2,3-dihydro-1,3,4-oxadiazol-2-yl] and [5-(4-substituted)-4h-1,2,4-triazol-3-yl] derivatives were prepared from benzoic acid hydrazones with the aim to get better antibacterial activity, antifungal activity, antitubercular and anti-inflammatory activity. Chemical structures of synthesized compounds were supported by means of IR, ¹H NMR and mass spectroscopy. Title compounds were evaluated for antibacterial activity, antifungal activity, antitubercular and anti-inflammatory activities. QSAR for the title compounds had been performed using TSAR 3.3 software and results were found satisfactory. Among the synthesized compounds some compounds found to possess all these activities

Key-words: QSAR, antibacterial, antifungal, antitubercular, anti-inflammatory activity.

INTRODUCTION

As the currently marketed drugs like isoniazide offer resistance against tubercle bacilli there is need to develop newer chemical entities which offer least resistance with suitable molecular modifications such as conversion into corresponding aryl Oxadiazoles, 1,2,4-triazole derivatives. This found fruitful in relieving these problems associated with currently marketed antitubercular drugs. Microbial infections have become more dreadful and dangerous so the search of new antibiotics and antibacterial is a continuous process in drug discovery. The 1,3,4-oxadiazole and 1,2,4-triazoles had been reported for various biological activities like antimicrobial activity [1], antitubercular activity[2], anticancer activity[3], anti-inflammatory activity[4], MAO inhibitors [5], analgesic activity [6], glycogen synthase kinase-3 β inhibitors [7] etc. With reference to above reported medicinal utilities of 5-aryl-1,3,4- Oxadiazoles and 1,2,4-triazole derivatives promote to synthesize new potential 5-aryl-1,3,4- Oxadiazoles and 1,2,4-triazole derivatives and evaluate its possible pharmacological activities like antifungal, antibacterial, anti-HIV, anticancer, antitubercular, antiviral etc. Based on these observations it was planned to synthesize some 5-aryl-1, 3, 4-

oxadiazole and 1, 2, 4-triazole derivatives and screened for antimicrobial, antitubercular and anti-inflammatory activities.

EXPERIMENTAL

Materials&Methods

Melting points were determined in open capillary method and are uncorrected. The ¹H-NMR spectra were recorded on sophisticated multinuclear FT-NMR Spec-trometer model Advance-II (Bruker) using dimethylsulfoxide-*d*₆ as solvent and tetramethylsilane as internal standard. IR spectra were recorded on Thermo Nicolet IR 200 spectrophotometer using KBr disc method. Biological activity (anti-inflammatory activity) values are reported as inhibitory activity on Carrageenan induced rat paw edema (% inhibition at 2 hr). Pharmacological screening values therein were converted into Log (% Inh) were used for multiple correlation analysis with descriptors generated using TSAR 3.3 software.

QSAR Methodology

All molecules were drawn in Chem draw ultra 8.0 module in Chemoffice 2004 software and imported into TSAR software. Charges were derived using Charge 2-Derive charges option and optimized by using Cosmic-optimize 3 D option in the structure menu of the project table. Substituents

* To whom all correspondence should be sent:
E-mail: nachiket1111@rediffmail.com

were defined and descriptors were calculated for whole molecule as well as for the Substituents. Several equations were generated correlating both Log (% Inh) with physicochemical parameters (descriptors) by multiple linear regression analysis (MLR) method. Data was standardized by range and leave one out method was used for cross validation. Models were excluded if correlation was exceeding 0.9 for more rigorous analysis. Correlation matrix was generated to find any Interrelation between the descriptors. Interrelation between the descriptors in the final equation is less than 0.2. [8]

Antimicrobial screening Antibacterial activity

The newly prepared compounds were screened for their antibacterial activity against *Escherichia coli* (MTCC 443), *Bacillus subtilis* (ATCC12228) and *Staphylococcus aureus* (ATCC25923) bacterial strains by disc diffusion method. In all the determinations tests were performed in triplicate and the results were taken as a mean of three determinations. Levofloxacin was used as a standard drug [9].

Anti fungal activity

The newly prepared compounds were screened for their antifungal activity against *C. albicans* and *A. niger* in DMSO by agar diffusion method. In all the determinations tests were performed in triplicate and the results were taken as a mean of three determinations. Amphotericin B was used as a standard drug.

Anti-tubercular activity

The antitubercular screening was carried out by Middle brook 7H9 agar medium against H₃₇Rv. Strain. Middle brook 7H9 agar medium containing different derivatives, standard drug as well as control, Middle brook 7H9 agar medium was

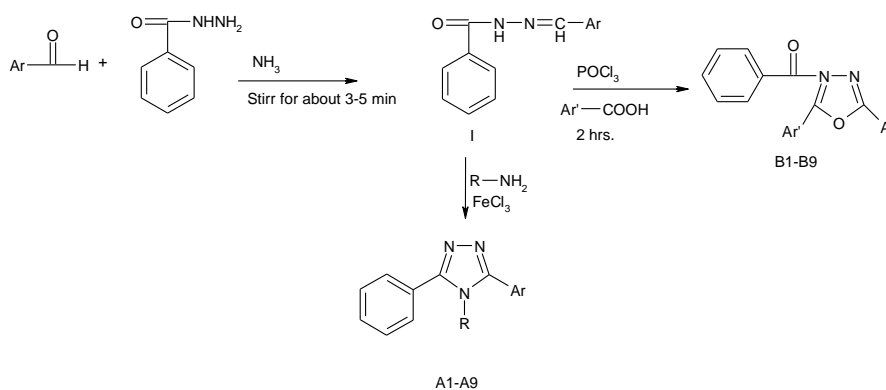
inoculated with *Mycobacterium tuberculosis* of H₃₇Rv Strain. The inoculated bottles were incubated for 37°C for 4 weeks. At the end of 4 weeks they were checked for growth. [10]

Anti-inflammatory activity

Carrageenan Induced hind Paw Edema: Anti-inflammatory activity was determined by Carrageenan Induced Rat hind Paw method of winter et al. wistar rats (120-150 g) was used for the experiment. The conventional laboratory diet was fed with adequate supply of drinking water. The animals were randomly selected, marked to permit individual identification and kept in polypropylene cages for one week prior to dosing to allow acclimatization of them to laboratory conditions. The drugs were prepared as a suspension by triturating with water and 0.5% sodium CMC. The standard group received 50mg/kg body weight of Ibuprofen, test group received 200mg/kg body weight of synthesized compounds and the control group received 1% w/v of CMC. [11]

Synthesis of [3-benzoyl-5-(4-substituted)-2, 3-dihydro-1, 3, 4-oxadiazol-2-yl] (A₁-A₉)

To a mixture of 0.01 mole of **I** and 0.01 mole of benzoic acid was added 10 mole of Phosphorus oxychloride at temp. of -5°C. The reaction mixture refluxed at 100 °C for 2 hrs. The reaction mixture was cooled to room temperature, the excess of POCl₃ was concentrated through high vacuum, the residue was quenched with ice and the solid separated was filtered and dried through pump to afford corresponding aryl Oxadiazole (**A1**). Similarly **1b-3c** was prepared using **2** and **3** along with Para Amino Benzoic acid and Para amino Salicylic acid respectively [12].



Scheme

Comp. Code	Ar	R	Comp. code	Ar'
A1			B ₁	
A2			B ₂	
A3			B ₃	
A4			B ₄	
A5			B ₅	
A6			B ₆	
A7			B ₇	
A8			B ₈	
A9			B ₉	

Synthesis of [5-(4-substituted)-4H-1, 2, 4-triazol-3-yl] (B₁-B₉)

Mixture of 0.01 mole of I₁, FeCl₃.6H₂O (0.02 mole)&0.01 mole of INH /Pyrazinamide/ Benzamide was ground by pestle & mortar at room temp. After complete conversion as indicated by TLC. The reaction mixture was digested with water. The resultant solid was filtered, washed with water. The crude material is purified by recrystallization from methanol to afford corresponding triazoles (B₁-B₃). Similarly B₄-B₉ was prepared using I₂ and I₃ respectively [13].

Spectral data

A₁: IR (KBr) cm⁻¹: 3310.43 (-CH=CH str.), 3213.45 (-NH str.), 3010.23 (Ar-CH str.), 1682.11 (-C=O str.), 1525.32 (-C=N str), 1245.36 (-C-N str). **¹H NMR:** 7.6-7.8 (4H pyridine), 6.8-7.0 (2H -CH=CH), 6.8-7.2 (10H phenyl), 4.0 (1H -NH), **m/e(100%):** 367.14

A₂: IR (KBr) cm⁻¹: 3310.43 (-CH=CH str.), 3010.23 (Ar-CH str.), 1682.11 (-C=O str.), 1525.32 (-C=N str), 1245.36 (-C-N str). **¹H NMR:** 8.1-8.6 (3H pyrazine), 6.8-7.0 (2H -CH=CH), 6.8-7.2 (10H phenyl), **m/e(100%):** 353.13

A₃: IR (KBr) cm⁻¹: 3310.43 (-CH=CH str.), 3213.45 (-NH str.), 3010.23 (Ar-CH str.), 1682.11 (-C=O str.), 1525.32 (-C=N str), 1245.36 (-C-N str). **¹H NMR:** 6.8-7.0 (2H -CH=CH), 6.8-7.2 (15H phenyl), **m/e(100%):** 366.15

A₄: IR (KBr) cm⁻¹: 3213.45 (-NH str.), 3010.23 (Ar-CH str.), 1682.11 (-C=O str.), 1525.32 (-C=N str), 1245.36 (-C-N str). **¹H NMR:** 7.6-7.8 (4H pyridine), 6.8-7.2 (9H phenyl), 4.0 (1H NH), 0.8-1.2 (3H -OCH₃), **m/e(100%):** 371.14

A₅: IR (KBr) cm⁻¹: 3010.23 (Ar-CH str.), 1682.11 (-C=O str.), 1525.32 (-C=N str), 1245.36 (-C-N str). **¹H NMR:** 8.1-8.6 (3H pyrazine), 6.8-7.2 (9H phenyl), 0.8-1.2 (3H -OCH₃), **m/e(100%):** 357.12

A₆: IR (KBr) cm⁻¹: 3213.45 (-NH str.), 3010.23 (Ar-CH str.), 1682.11 (-C=O str), 1525.32 (-C=N str), 1245.36 (-C-N str). **¹H NMR:** 6.8-7.2 (15 H phenyl), 0.8-1.2 (3H -OCH₃), **m/e(100%):** 355.13

A₇: IR (KBr) cm⁻¹: 3213.45 (-NH str.), 3010.23 (Ar-CH str.), 1682.11 (-C=O str.), 1525.32 (-C=N str), 1245.36 (-C-N str), 1016.11 (-C-O-C str.). **¹H NMR:** 7.6-7.8 (4H pyridine), 6.8-7.2 (5H phenyl), 5.4-5.8 (3H furyl), 4.0 (1H NH), **m/e(100%):** 331.11

A₈: IR (KBr) cm⁻¹: 3010.23 (Ar-CH str.), 1682.11 (-C=O str.), 1525.32 (-C=N str), 1245.36 (-C-N str), 1016.11 (-C-O-C str.). **¹H NMR:** 8.1-8.6 (3H pyrazine), 6.8-7.2 (5H phenyl), 5.4-5.8 (3H furyl), **m/e(100%):** 317.09

A₉: IR (KBr) cm⁻¹: 3213.45 (-NH str.), 3010.23 (Ar-CH str.), 1682.11 (-C=O str.), 1525.32 (-C=N str), 1245.36 (-C-N str), 1016.11 (-C-O-C str.). **¹H NMR:** 6.8-7.2 (10H phenyl), 5.4-5.8 (3H furyl), **m/e(100%):** 315.10

B₁: IR (KBr) cm⁻¹: 3310.23 (-CH=CH str.), 3010.23 (Ar-CH str.), 1689.78 (-C=O str), 1525.32 (-C=N str), 1245.36 (-C-N str), 1016.38 cm⁻¹(-C-O-C str), **¹H NMR:** 6.8-7.2 (15 H phenyl), 6.0-6.4 (2H -CH=CH), 5.8 (1H 1,3,4-Oxadiazolyl), **m/e(100%):** 354.14

B₂: IR (KBr) cm⁻¹: 3310.23 (-CH=CH str.), 3208.12 (-NH₂ str.), 3010.23 (Ar-CH str.), 1689.78 (-C=O str), 1525.32 (-C=N str), 1245.36 (-C-N str), 1016.38 cm⁻¹(-C-O-C str), **¹H NMR:** 8.2-8.6 (3H pyrazine), 6.8-7.2 (14H phenyl), 6.0-6.4 (2H -CH=CH), 5.8 (1H 1,3,4-Oxadiazolyl), 4.8-5.2 (2H -NH₂), **m/e(100%):** 369.15

B₃: IR (KBr) cm⁻¹: 3310.23 (-CH=CH str.), 3208.12 (-NH₂ str.), 3210.45 (-OH str.), 3010.23 (Ar-CH str.), 1689.78 (-C=O str), 1525.32 (-C=N str), 1245.36 (-C-N str), 1016.38 cm⁻¹(-C-O-C str), **¹H NMR:** 6.8-7.2 (13H phenyl), 6.0-6.4 (2H -CH=CH), 5.8 (1H 1,3,4-Oxadiazolyl), 5.0 (1H -OH), 4.2 (2H -NH₂), **m/e(100%):** 385.14

B₄: IR (KBr) cm⁻¹: 3010.23 (Ar-CH str.), 2810.23 (-CH₃ str.), 1689.78 (-C=O str), 1525.32 (-C=N str), 1245.36 (-C-N str), 1016.38 cm⁻¹(-C-O-C str), **¹H NMR:** 6.8-7.2 (14 H phenyl), 6.0-6.4 (2H -CH=CH), 5.8 (1H 1,3,4-Oxadiazolyl), 0.8-1.2 (3H -CH₃), **m/e(100%):** 360.15

B₅: IR (KBr) cm⁻¹: 3210.45 (-NH₂ str.), 3010.23 (Ar-CH str.), 1689.78 (-C=O str), 1525.32 (-C=N str), 1245.36 (-C-N str), 1016.38 cm⁻¹(-C-O-C str), **¹H NMR:** 6.8-7.2 (13 H phenyl), 5.8 (1H 1,3,4-Oxadiazolyl), 4.8-5.2 (2H -NH₂), 0.8-1.2 (3H -CH₃), **m/e(100%):** 375.16

B₆: IR (KBr) cm⁻¹: 3210.45 (-OH str.), 3208.13 (-NH₂ str.), 3010.23 (Ar-CH str.), 1689.78 (-C=O str), 1525.32 (-C=N str), 1245.36 (-C-N str), 1016.38 cm⁻¹(-C-O-C str), **¹H NMR:** 6.8-7.2 (12 H phenyl), 5.8 (1H 1,3,4-Oxadiazolyl), 5.0 (1H -OH), 4.2 (2H -NH₂), 0.8-1.2 (3H -CH₃), **m/e(100%):** 391.15

B₇: IR (KBr) cm⁻¹: 3010.23 (Ar-CH str.), 1689.78 (-C=O str), 1525.32 (-C=N str), 1245.36 (-C-N str), 1016.38 cm⁻¹(-C-O-C str), **¹H NMR:** 6.8-7.2 (10 H phenyl), 6.2-6.6 (3H furyl), 5.8 (1H 1,3,4-Oxadiazolyl), **m/e(100%):** 320.12

B₈: IR (KBr) cm⁻¹: 3210.23 (-NH₂ str.), 3010.23 (Ar-CH str.), 1689.78 (-C=O str), 1525.32 (-C=N str), 1245.36 (-C-N str), 1016.38 cm⁻¹(-C-O-C str), **¹H NMR:** 6.8-7.2 (9H phenyl), 6.2-6.6 (3H furyl),

5.8 (1H 1,3,4-Oxadiazolyl), 408-5.2 (2H -NH₂), (-C=N str), 1245.36 (-C-N str), 1016.38 cm⁻¹(-C-O-C str), ¹H NMR: 6.8-7.2 (8 H phenyl), 5.8 (1H 1,3,4-Oxadiazolyl), 5.0 (1H -OH), 4.2 (2H -NH₂), m/e(100%): 335.13
B₉: 3210.45 (-OH str.), 3208.13 (-NH₂ str.), 3010.23 (Ar-CH str.), 1689.78 (-C=O str), 1525.32 m/e(100%): 351.12

Table 1. Analytical & physicochemical data of the synthesized compounds (A₁-A₉ & B₁-B₉)

Comp.	Mol. Formula	Mol. Wt.	M.P. °C	Yield %	Elemental analyses		
					Calcd. (found)		
					C	H	N
A ₁	C ₂₂ H ₁₇ N ₅ O	367.40	196-198	75.64	71.92	4.66	19.06
A ₂	C ₂₁ H ₁₅ N ₅ O	353.38	240-242	74.67	71.38	4.28	19.82
A ₃	C ₂₃ H ₁₈ N ₄ O	366.42	231-233	68.24	75.39	4.95	15.29
A ₄	C ₂₁ H ₁₇ N ₅ O ₂	371.39	225-257	77.06	67.91	4.61	18.86
A ₅	C ₂₀ H ₁₅ N ₅ O ₂	357.37	250-252	66.95	6.22	4.23	19.60
A ₆	C ₂₂ H ₁₇ N ₃ O ₂	355.39	272-275	72.23	74.35	4.82	11.82
A ₇	C ₁₈ H ₁₃ N ₅ O ₂	331.33	188-190	64.99	65.25	3.95	21.14
A ₈	C ₁₇ H ₁₁ N ₅ O ₂	37.30	210-212	68.82	64.35	3.49	22.07
A ₉	C ₁₉ H ₁₃ N ₃ O ₂	315.33	228-230	75.68	72.37	4.16	13.33
B ₁	C ₂₃ H ₁₈ N ₂ O ₂	354.40	250-253	79.85	77.95	5.12	7.90
B ₂	C ₂₃ H ₁₉ N ₃ O ₂	369.42	230-233	80.12	74.78	5.18	11.37
B ₃	C ₂₃ H ₁₉ N ₃ O ₃	385.42	210-212	72.15	71.67	4.97	10.90
B ₄	C ₂₂ H ₁₂₀ N ₂ O ₃	360.41	184-186	67.94	73.32	5.59	7.77
B ₅	C ₂₂ H ₂₁ N ₃ O ₃	375.42	230-232	64.72	70.38	4.64	11.19
B ₆	C ₂₂ H ₂₁ N ₃ O ₄	391.42	263-265	71.67	67.51	5.41	10.17
B ₇	C ₁₉ H ₁₆ N ₂ O ₃	320.34	210-212	70.96	71.24	5.03	8.74
B ₈	C ₁₉ H ₁₇ N ₃ O ₃	335.36	233-235	71.67	68.05	5.11	12.53
B ₉	C ₁₉ H ₁₇ N ₃ O ₄	351.36	273-275	71.72	64.95	4.88	11.96

Table 2. Antibacterial and antifungal activity of synthesized compounds (A₁-A₉ & B₁-B₉)

Compd.	Zone of inhibition at 200µcg/mL (in mm.)				
	<i>E. coli</i>	<i>B. subtilis</i>	<i>S. aureus</i>	<i>A. niger</i>	<i>C. albicans</i>
A ₁	24	25	26	15	22
A ₂	20	23	25	16	21
A ₃	20	24	25	19	22
A ₄	25	26	23	20	21
A ₅	24	23	26	21	22
A ₆	20	22	24	18	23
A ₇	21	23	22	20	21
A ₈	22	24	25	20	22
A ₉	23	22	20	18	22
B ₁	24	26	23	19	21
B ₂	25	23	24	21	23
B ₃	26	22	24	20	22
B ₄	24	25	26	21	23
B ₅	23	25	26	20	22
B ₆	26	23	26	20	21
B ₇	26	23	25	19	21
B ₈	25	24	26	20	21
B ₉	25	26	26	21	20
Levofloxacin	26	25	26	-	-
Amphotericin B	-	-	-	22	23

Table 3. Antitubercular activity of the synthesized compounds (A₁-A₉ & B₁-B₉).

Compound	25 µg/mL	50 µg/mL	100 µg/mL
A ₁	R	S	S
A ₂	R	R	S
A ₃	R	R	R
A ₄	R	S	S
A ₅	R	R	S
A ₆	R	R	R
A ₇	R	S	S
A ₈	R	R	S
A ₉	R	R	R
B ₁	R	S	S
B ₂	R	R	S
B ₃	R	R	R
B ₄	R	S	S
B ₅	R	R	S
B ₆	R	R	R
B ₇	R	S	S
B ₈	R	R	S
B ₉	R	R	R
Streptomycin	S	S	S

Table 4. Anti-inflammatory activity of synthesized compounds (A₁-A₉ & B₁-B₉)

Treatment	Mean increase in paw volume (ml)±SEM									
	Time in minute									
	0	% inhibition	30	% inhibition	60	% inhibition	90	% inhibition	120	% inhibition
Carrageenen (Control)	0.24±0.01		0.48±0.03		0.78±0.09		0.85±0.12		0.89±0.14	
Ibuprofen	0.24±0.03	0	0.31±0.07	35.41	0.30±0.07	61.53	0.27±0.06	68.23	0.26±0.13	70.78
A ₁	0.24±0.01	0	0.34±0.03	29.16	0.35±0.01	55.12	0.33±0.01	61.17	0.30±0.01	66.29
A ₂	0.24±0.02	0	0.33±0.03	31.25	0.32±0.01	58.97	0.30±0.01	64.70	0.28±0.02	68.53
A ₃	0.23±0.01	4.16	0.34±0.01	29.16	0.38±0.01	51.28	0.38±0.02	55.29	0.32±0.02	64.04
A ₄	0.24±0.02	0	0.33±0.01	31.25	0.33±0.02	57.69	0.31±0.02	63.52	0.29±0.01	67.41
A ₅	0.23±0.01	4.16	0.32±0.01	33.33	0.34±0.01	56.41	0.32±0.01	62.35	0.30±0.02	66.29
A ₆	0.24±0.02	0	0.35±0.01	27.08	0.39±0.02	50	0.38±0.01	55.29	0.32±0.03	64.04
A ₇	0.23±0.02	4.16	0.33±0.01	31.25	0.35±0.02	55.12	0.34±0.02	60	0.30±0.01	66.29
A ₈	0.24±0.02	0	0.33±0.02	31.25	0.35±0.03	55.12	0.31±0.02	63.52	0.30±0.02	66.29
A ₉	0.23±0.03	4.16	0.33±0.02	31.25	0.34±0.01	56.41	0.32±0.02	62.35	0.30±0.02	66.29
B ₁	0.24±0.01	0	0.32±0.02	33.33	0.34±0.02	56.41	0.33±0.01	61.17	0.29±0.01	67.41
B ₂	0.24±0.02	0	0.34±0.03	29.16	0.34±0.03	56.41	0.35±0.01	58.82	0.31±0.02	65.16
B ₃	0.23±0.03	4.16	0.33±0.04	31.25	0.35±0.01	55.12	0.33±0.02	61.17	0.30±0.03	66.29
B ₄	0.24±0.01	0	0.36±0.01	25.00	0.35±0.02	55.12	0.35±0.02	58.82	0.33±0.02	62.92
B ₅	0.24±0.01	0	0.34±0.01	29.16	0.36±0.01	53.84	0.35±0.02	58.82	0.31±0.01	65.16
B ₆	0.24±0.01	0	0.34±0.02	29.16	0.35±0.02	55.12	0.35±0.01	58.82	0.33±0.02	62.92
B ₇	0.23±0.01	4.16	0.33±0.02	31.25	0.34±0.02	56.41	0.32±0.02	62.35	0.30±0.01	66.29
B ₈	0.24±0.02	0	0.34±0.03	29.16	0.36±0.03	53.84	0.36±0.03	57.64	0.32±0.03	64.04
B ₉	0.24±0.02	0	0.34±0.02	29.16	0.37±0.02	52.56	0.36±0.03	57.64	0.33±0.02	62.92

Table 5. Structures and Log (% Inh) of A₁-A₉ and B₁-B₉.

Sr. No.	Comp. Name	Structure	% Inh	Log (% Inh)
1.	A ₁		66.29	1.821448
2.	A ₂		68.53	1.835881
3.	A ₃		64.04	1.806451
4.	A ₄		67.41	1.828724
5.	A ₅		66.29	1.821448
6.	A ₆		64.04	1.806451
7.	A ₇		66.29	1.821448
8.	A ₈		66.29	1.821448
9.	A ₉		66.29	1.821448
10.	B ₁		67.41	1.828724

11.	B₂		65.16	1.813981
12	B₃		66.29	1.821448
13	B₄		62.92	1.798789
14	B₅		65.16	1.813981
15	B₆		62.92	1.798789
16	B₇		66.29	1.821448
17	B₈		64.04	1.806451
18	B₉		62.92	1.798789

Table 6. Equations generated between log (% Inh) and descriptors.

Sr. No.	Equation	N	S	R	r ²	r ² _{cv}	F
Series (A ₁ -A ₉ and B ₁ -B ₉)	Y = -0.199 * X ₃ - 0.229 * X ₁ - 1.553 * X ₂ - 12.575	18	0.361	0.838	0.702	0.538	14.17

Where

Y = Log (% Inh)

X₁: ClogP -

X₂ = VAMP HOMO (Whole Molecule)

X₃ = Dipole Moment Z Component (Whole Molecule)

X₄ = Inertia Moment 2 Length (Whole Molecule)

Significance of the terms:

N= No. of Molecules

s = standard error --- less is better

r = correlation coefficient – higher is better > 0.7,

r²_{cv} = cross validated r² - higher is better > 0.5,

F Value = higher is better

Observed and predicted data and graphs are presented in Table 6 and Fig 1.

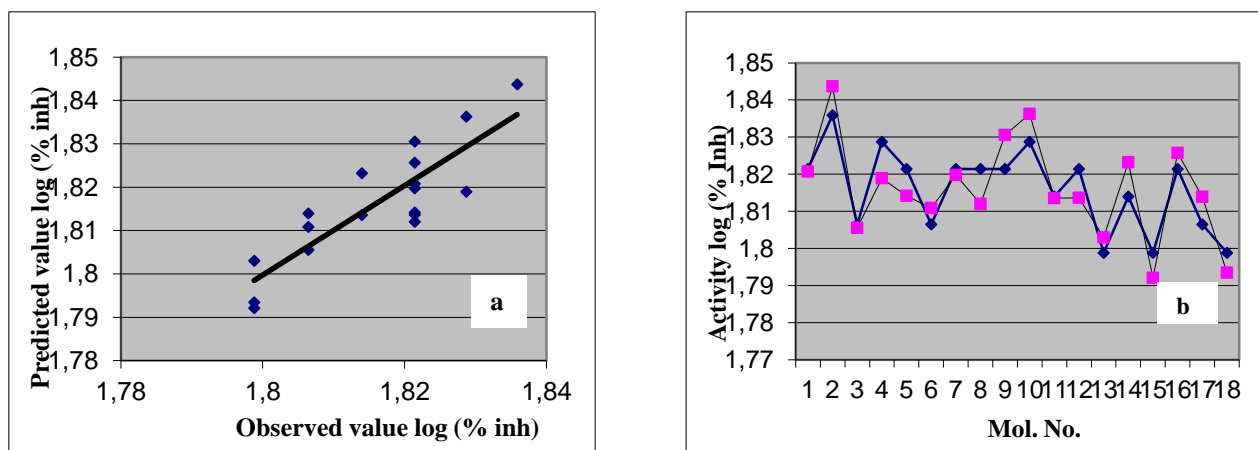


Fig 1. (a) Correlation graph; (b) Histogram of observed and predicted log (% Inh) data for 18 compounds

Table 7. Observed and predicted log (% Inh) value data for 18 compounds

Comp. No.	Observed Value	Predicted Value	Residual Value	Residual Variance
A ₁	1.821448	1.820758	0.00069	0.0043
A ₂	1.835881	1.843681	-0.0078	0.0027
A ₃	1.806451	1.805551	0.0009	0.0090
A ₄	1.828724	1.818924	0.0098	0.0009
A ₅	1.821448	1.814184	0.007264	0.0049
A ₆	1.806451	1.810851	-0.0044	0.0070
A ₇	1.821448	1.819752	0.001696	0.0044
A ₈	1.821448	1.812048	0.0094	0.0060
A ₉	1.821448	1.830548	-0.0091	0.0313
B ₁	1.828724	1.836242	-0.00752	0.0019
B ₂	1.813981	1.813581	0.0004	0.0035
B ₃	1.821448	1.813648	0.0078	0.0006
B ₄	1.798789	1.802989	-0.0042	0.0403
B ₅	1.813981	1.823181	-0.0092	0.0122
B ₆	1.798789	1.7921	0.006689	0.0273
B ₇	1.821448	1.825678	-0.00423	0.0135
B ₈	1.806451	1.813899	-0.00745	0.0049
B ₉	1.798789	1.79345	0.005339	0.0324

DISCUSSION

Statistical evaluation of the equations is in accepted range. The correlation coefficient is high with less standard error. The residual value and residual variance for each series also is less indicating good predictive power of models. From equation it is observed that two electronic parameters Dipole Moment Z Component (Whole Molecule) and VAMP HOMO (Whole Molecule) as well as one steric parameter Inertia Moment 2 Length (Whole Molecule) contribute (-0.227, -1.469 and -0.414 respectively) negatively for the activity so electron withdrawing and less bulky groups may enhance the activity (% Inh).

The synthesized derivatives were screened for anti-bacterial activity using DMF as a solvent against the organisms *S. aureus*, *B. subtilis* and *E. coli*, and antifungal activity using *C. albicans* and

A. niger by disc diffusion method on nutrient agar media. The standard drug used was Levofloxacin and Amphotericin B for antibacterial and antifungal activity respectively.

Antibacterial activity

The compounds A₁, A₂, A₃, A₅, A₈, B₄, B₅, B₆, B₇, B₈, B₉ has excellent Antibacterial activity against *S. aureus*, the compounds A₁, B₄, B₅ have shown Antibacterial activity against *B. subtilis*, while A₄, B₂, B₃, B₆, B₇, B₈, B₉ shows Antibacterial activity against *E. coli*, when compared with standard Levofloxacin.

Antifungal activity

The compounds A₅, B₂, B₄, B₉ has excellent antifungal activity against *Aspergillus niger* (NCIM

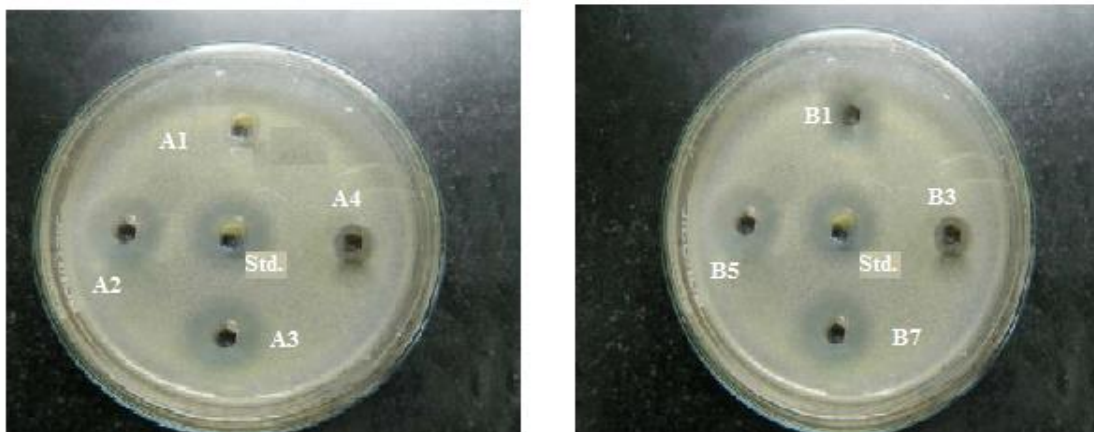


Fig. 2. Anti-bacterial activity of synthesized compounds

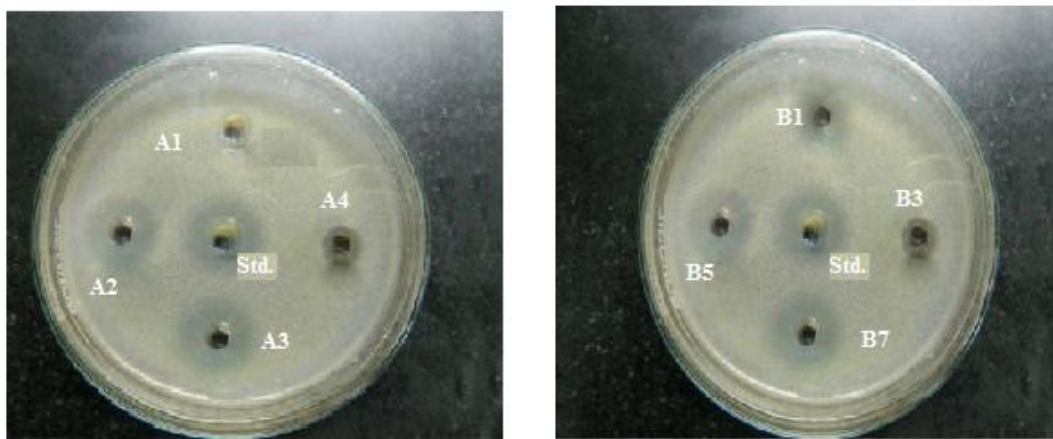


Fig. 3. Antifungal activity of synthesized compounds.

596), while the compounds A₁, A₃, A₅, A₆, A₈, A₉, B₂, B₃, B₄, have shown Antifungal activity against *Candida albicans* (NCIM 3102) when compared with standard Amphotericin B.

Antitubercular activity

All the compounds were screened for antitubercular activity by Middle brook 7H9 agar medium as described by Elmer WK et al. against H₃₇Rv strain. Compounds **A₁**, **A₄**, **A₇**, **B₂**, **B₄**, and **B₇** has shown promising antitubercular activity.

Anti-Inflammatory activity

All the compounds were evaluated for Anti-inflammatory activity by Carrageenan Induced Rat hind Paw method. The synthesized compounds **A₂**, **A₄**, **A₅**, **A₆**, **A₈**, **B₁**, **B₃**, **B₇**, and **B₈** showed better anti-inflammatory activity found comparable with standard drug Ibuprofen (70.78% inhibition) at the same dose (100 µg/kg).

REFERENCES

- 1.M.M. Burbuliene, *Il Farmaco*, **59**, 767 (2004).
- 2.B.Chandrakantha, P.Shetty, V.Nambiyar, *Synthesis, Eur.J. Medic. Chem.*, **44**, 1 (2009).
- 3.V.V. Dabholkar, N.V., *Int. J.Chem. Environ. Pharm. Res.*, **2**, 1 (2011).
- 4.V. Jakubkiene, *Il Farmaco*, **58**, 323 (2003).
- 5.B. Jayashankar, *Eur.J. Medic. Chem.*, **44**, 3898 (2009).
- 6.Zhong Li, Xuhong Qian, *Bioorgan.&Medic.Chem.*, **16**, 7565 (2008).
- 7.L. Benmekhbi, M. Bencharif, L. Bencharif, S. Mosbah, *Int. J. Electrochem. Sci.*, **6**, 1991(2011).
- 8.K.Mogilaiah, K.Vidya, T. Kumara, *Ind. J. Chem.*, **48B**, 599 (2009).
- 9.E. Palaska, *Il Farmaco*, **57**, 539 (2002).
- 10.A. Palomer, J.J. Pérez, S. Navea, O. Llorens, J. Pascual, L. García, D. Mauleón, *J. Med. Chem.*, **43** 2280 (2000).
- 11.M. Saitoh, J. Kunitomo, *Bioorgan.&Medic.Chem.*, **17**, 2017 (2009).
- 12.Baoan Song, *Bioorgan.&Medic.Chem. Lett.*, **16**, 5036 (2006).
- 13.M. Srivastava, D. Singh, A.S. Kushwah, P.D. Gokulan, *J. Current Pharm. Res.*, **4**, 20 (2010).

ДИЗАЙН, СИНТЕЗА И ФАРМАКОЛОГИЧЕН СКРИЙНИНГ НА НЯКОИ [3-БЕНЗОИЛ-5-(4-ЗАМЕСТЕНИ)-2, 3-ДИХИДРО-1,3,4-ОКСАДИАЗОЛ-2-ИЛ] И [5-(4-ЗАМЕСТЕНИ)-4H-1, 2, 4-ТРИАЗОЛ-3-ИЛ] ПРОИЗВОДНИ

Н.С. Дигхе*¹, Р.Б. Саудагар², Д.А. Джейн³

¹Департамент по фармацевтична химия, Селскостопански колеж по фармация Правара, Лони, Индия.

²Департамент по фармацевтична химия, Колеж по фармация Р.Г. Саптал, Нашик, Индия

³департамент по фармацевтични науки и изследвания, Университет Бхагвант, Аджмер, Раджастан, Индия

Постъпила на 28 септември, 2012 г.; коригирана на 15 април, 2013 г.

(Резюме)

Синтезирана е нова серия от някои заместени [3-бензоил-5-(4-заместени)-2, 3-дихидро-1,3,4-оксадиазол-2-ил] и [5-(4-заместени)-4H-1, 2, 4-триазол-3-ил] производни. Целта е постигането на по-добра антибактериална, противогъбична, противотуберкуозна и противовъзпалителна активност. Химичната структура на синтезираните съединения е потвърдена от IR, ¹H NMR и мас-спектроскопия. Съединенията са оценени за антибактериална, противогъбична, противотуберкуозна и противовъзпалителна активност. Получения са задоволителни резултати за сравнението по метода QSAR с използването на софтуер TSAR 3.3. Някои от съединенията проявяват всички изброени активности.

Synthesis, spectral characterization and theoretical investigation of some new mercury four coordinated complexes

M. Montazerzohori*¹, H. Tavakol², S. Kheiri¹, S. A. Musavi¹, S. Joohari³

¹Department of Chemistry, Yasouj University, Yasouj 75918-74831, Iran

²Department of Chemistry, Isfahan University of Technology, Isfahan, Iran

³Department of Basic Science, Yasouj Branch, Islamic Azad University, Yasouj, Iran

Received October 29, 2012; Revised April 9, 2013

Some new mercury complexes of a bidentate Schiff base ligand with two nitrogen atoms as donor sites have been prepared and characterized by spectroscopic and analytical studies such as IR, UV-Vis, ¹H NMR and ¹³C NMR, elemental analysis and molar conductivity. The IR spectrum of ligand showed the characteristic asymmetric and symmetric vibrations of iminic groups at 1624 and 1620 cm⁻¹ respectively that were unified and shifted by 6-8 cm⁻¹ to lower energies. The iminic proton signals of ligand were appeared as two doublets at 7.87 and 7.77 ppm that were downfielded to 7.92-8.91 ppm after coordination to mercury ion in the complexes. The analytical data confirmed 1:1 ratio for ligand to metal salt in all complexes. The structural optimization of ligand and complexes was performed at the UB3LYP/LANL2MB/ level of theory and then some important structural (Bond length(Å), Bond angle(°) and Torsion angle(°)) and theoretical energetic(HF-Energy, ZPE, ΔE, ΔG, ΔE_{electronic} and ΔH) data were derived. The bond lengths(Å) of Hg-N(1) and Hg-N(2) were decreased from mercury chloride to mercury thiocyanate complex and then decreased in mercury azide complex. The bond angle (°) of N(1)-Hg-N(2) in the complexes was smoothly increased from mercury chloride to mercury thiocyanate complex and then decreased in mercury azide complex. The opposite of this trend was evaluated for X(1)-Hg-X(2). Accordingly pseudo-tetrahedral geometry was suggested for all complexes. Therefore the general formula for Hg(II) complexes is MLX₂ that in which X= Cl⁻, Br⁻, I⁻, SCN⁻ and N₃⁻.

Key-words: Schiff base; Theoretical; Optimization; Spectroscopic; Mercury.

INTRODUCTION

Schiff bases as an important class of chelating ligands have played an important role in the development of coordination chemistry because of formation of various stable complexes with the most transition metal ions [1–7]. Synthesis of new Schiff bases and their metal complexes are still the aim of many recent investigations due to the wide applications of Schiff bases ligands and their complexes in the biological and chemical fields [6–10]. DNA cleavage activity [11], biomimetic enzyme models [12–14], tumor growth inhibitors, as antiviral, antifungal and antibacterial agents in biological fields [15–18] and ability to reversibly binding oxygen [19], their usage as catalysis [20–23], liquid crystal [24, 25], pigments and dyes and polymer stabilizers [26] in chemical fields are the most important applications of Schiff bases. Also, Schiff-bases with donors (N, O, S and etc.) have structural similarities with neutral biological systems and due to the presence of imine groups are

utilized in explanation of the mechanism of transformation and racemization reaction in biological system [27–29].

In the course of our studies on transition metal Schiff base complexes [30–35], we report synthesis and characterization a series of HgLX₂ in which X= Cl⁻, Br⁻, I⁻, SCN⁻ and N₃⁻ with N, N'-bis((E)3-phenylallylidene)-4-methyl-1,2-phenyldiamine (L) as a new bidentate ligand. The structural features of the Schiff base and their metal complexes have been studied by various spectral and analytical. Furthermore, the structural optimization of ligand and complexes was performed at the UB3LYP/LANL2MB/ level of theory and then some important structural and theoretical energetic data were derived.

EXPERIMENTAL

Materials and methods

Cinnamaldehyde, 4-methyl-1,2-phenyldiamine, mercury(II) halides and other chemicals were purchased from either Aldrich, Merck or BDH Chemicals. All of the chemicals used were analytical grade. Solvents such as methanol and dichloromethane were purified and dried before the

* To whom all correspondence should be sent:
E-mail: mmzohori@mail.yu.ac.ir

use according to the standard methods. FT-IR spectra as KBr pellets were recorded on a JASCO FT/IR-680 spectrometer in the 4000–400 cm^{-1} range. Electronic spectra were recorded in DMSO and chloroform solutions on a JASCO-V570 model spectrometer with quartz cells of 0.5cm path length. ^1H and ^{13}C NMR spectra were obtained using a Bruker DPX FT-NMR spectrometer at 500MHz with the samples dissolved in DMSO- d_6 mixture using TMS as internal standard. Carbon, hydrogen and nitrogen of dried samples were performed using elemental analyzer. The melting points ($^\circ\text{C}$) of the complexes were recorded on BI Barnstead melting point instrument. Conductivity measurements of the ligand and their complexes were made on freshly prepared 10^{-3} M solutions in DMSO and/or chloroform at room temperature with a Metrohm 712 conductometer with a dip-type conductivity cell made of platinum black. Theoretical optimization of the Schiff-base ligand and its complexes were carried out at the UB3LYP/LANL2MB/level of theory.

Preparation of N, N'-bis((E)3-phenylallylidene)-4-methyl-1,2-phenyldiamin (L)

N, N'-bis((E)3-phenylallylidene)-4-methyl-1,2-phenyldiamin (L) as a bidentate Schiff base was synthesized by condensation reaction between 4-methyl-1,2-phenyldiamine (5 mmol, 0.611 g) and trans-cinnamaldehyde (10 mmol, 1.321 g) in 40 mL diethyl ether as solvent under ice bath with rigorous stirring for 5-6 h. After completion of the reaction, the solvent was reduced under vacuum to give the Schiff base as very viscous oil. For more purification, the oil was washed twice with n-hexane and dried under vacuum.

IR(KBr, cm^{-1}): 3376(m), 3051(w), 3024(w), 2916(w), 2848(w), 1624(s), 1600(s), 1582(s), 1507(s), 1448(s), 1382(w), 1302(m), 1150(w), 998(m), 848(w), 802(m), 751(s), 690(s). UV-Vis [(CHCl₃), $\lambda(\text{nm})$ ($\epsilon, \text{M}^{-1}\text{cm}^{-1}$): 296(37173) and 376(13002). ^1H -NMR spectra (in DMSO- d_6)(ppm): 7.87(d, 1H, J= 7.15 Hz), 7.77(d, 1H, J= 6.52 Hz), 7.66-7.42(m, 6H), 7.24(m, 5H), 7.04(d, 2H, J= 8.30 Hz), 7.00(bd, 2H, J= 8.20 Hz), 6.91(d, 2H, J= 8.45 Hz), 2.43(s, 3H).

Preparation of mercury complexes

A solution of ligand (1 mmol, 0.350 g) in 10 mL methanol was added drop wise to a methanolic solution (20 mL) of HgX_2 salts, in which X= chloride, bromide, iodide, thiocyanate and azide (mercury thiocyanate and azide were prepared similar to previous report[31]), under severe stirring

under room temperature conditions. The complexes were obtained after 2-3 h as colored precipitates that were filtered and washed with ethanol for more purification. Then complexes were dried at 80-100 $^\circ\text{C}$ under vacuum and were kept in a desiccator over silica-gel.

HgLCl₂:

IR(KBr), cm^{-1} : 3434(m), 3055(w), 3026(w), 2919(w), 2854(w), 1618(vs), 1575(vs), 1564(vs), 1492(m), 1448(m), 1368(m), 1168(s), 992(m), 857(w), 807(m), 748(s), 686(s), 458(w). UV-Vis[(CHCl₃), $\lambda(\text{nm})$ ($\epsilon, \text{M}^{-1}\text{cm}^{-1}$): 326(44496) and 376(33708). ^1H -NMR spectra (in DMSO- d_6)(ppm): 8.77(bs, 2H), 7.68(bs, 4H), 7.58(bs, 3H), 7.42(bs, 6H), 7.24(m, 4H), 2.35(s, 3H). ^{13}C -NMR spectra (in DMSO- d_6)(ppm): 164.30, 163.56, 148.52, 148.12, 140.98, 138.75, 138.52, 134.88, 134.82, 130.68, 130.63, 129.20, 129.08, 129.00, 128.04, 127.99, 126.70, 119.72, 119.08, 20.73.

HgLBr₂:

IR(KBr), cm^{-1} : 3445(m), 3054(w), 3026(w), 2919(w), 2852(w), 1618(vs), 1575(vs), 1562(vs), 1492(m), 1348(m), 1366(w), 1167(s), 990(m), 856(w), 748(s), 686(s), 458(w). UV-Vis[(CHCl₃), $\lambda(\text{nm})$ ($\epsilon, \text{M}^{-1}\text{cm}^{-1}$): 327(39674) and 377(29963). ^1H -NMR spectra (in DMSO- d_6)(ppm): 8.85(s, 1H), 8.84(s, 1H), 7.67(d, 4H), 7.62(m, 4H), 7.43(m, 6H), 7.34(d, 1H, J= 7.90 Hz), 7.14(d, 2H, J= 14.10 Hz), 2.36(s, 3H). ^{13}C -NMR spectra (in DMSO- d_6)(ppm): 164.46, 163.68, 149.02, 148.60, 140.84, 138.80, 138.62, 134.77, 134.72, 130.83, 130.77, 129.45, 129.14, 128.99, 128.91, 128.64, 126.36, 119.74, 119.12, 20.76.

HgLI₂:

IR(KBr), cm^{-1} : 3466(m), 3053(w), 3024(w), 2920(w), 2856(w), 1616(vs), 1575(vs), 1561(vs), 1491(m), 1448(m), 1364(w), 1168(s), 985(s), 861(w), 806(m), 748(vs), 686(s), 458(w). UV-Vis[(CHCl₃), $\lambda(\text{nm})$ ($\epsilon, \text{M}^{-1}\text{cm}^{-1}$): 326(32623) and 376(23042). ^1H -NMR spectra (in DMSO- d_6)(ppm): 7.92(d, 1H, J= 16.50 Hz), 7.89(d, 1H, J= 19.60 Hz), 7.73(bs, 6H), 7.51(m, 4H), 7.29(m, 5H), 7.27(d, 2H, J= 16.05 Hz), 3.17(s, 3H).

HgL(SCN)₂:

IR(KBr), cm^{-1} : 3481(m), 3056(w), 3025(w), 2922(w), 2853(w), 2118(vs), 1617(vs), 1575(vs), 1562(vs), 1493(m), 1448(m), 1368(m), 1169(s), 993(m), 853(w), 750(s), 685(m), 462(w). UV-Vis[(DMSO), $\lambda(\text{nm})$ ($\epsilon, \text{M}^{-1}\text{cm}^{-1}$): 333(41070) and 379(32160). ^1H -NMR spectra (in DMSO- d_6)(ppm): 8.91(bs, 2H), 7.63(m, 6H), 7.44(m, 5H), 7.19(m, 4H), 6.75(m, 1H), 6.53(m, 1H), 2.37(s, 3H). ^{13}C -NMR spectra (in DMSO- d_6)(ppm): 164.72, 163.96, 149.30, 148.91, 141.00, 138.80, 138.71, 134.77,

134.72, 130.76, 130.70, 129.38, 129.02, 128.24, 128.20, 127.86, 127.44, 126.39, 119.86, 119.24, 20.68.

$HgL(N_3)_2$:

IR(KBr), cm^{-1} : 3453(m), 3055(w), 2926(w), 2853(w), 2035(vs), 1616(m), 1575(m), 1490(w), 1448(m), 1367(w), 1166(m), 995(m), 858(w), 752(m), 685(m), 458(w). UV-Vis[($CHCl_3$), λ (nm) ($\epsilon, M^{-1}cm^{-1}$): 323(33768) and 377(24461). 1H -NMR spectra (in $DMSO-d_6$)(ppm): 8.55(bs, 2H), 7.78(m, 2H), 7.66(m, 4H), 7.41(m, 8H), 7.20(m, 2H), 6.99(s, 1H), 2.33(s, 3H).

RESULTS AND DISCUSSION

Physical data

The Schiff base ligand, N, N'-bis((E)3-phenylallylidene)-4-methyl-1,2-phenylenediamine (L) was prepared by condensation of trans-cinnamaldehyde and 4-methyl-1,2-phenylenediamine in a 2:1 molar ratio. Some Schiff base complexes of mercury(II) were synthesized successfully with this ligand and the structure of ligand and its complexes was confirmed by the data obtained from elemental analysis, IR, UV-Vis and 1H and ^{13}C NMR spectra. Elemental analyses and other physical properties of the ligand and its complexes are summarized in table 1. The results of the elemental analyses are in a good agreement with the proposed formula. The molar conductivity of ligand and all mercury complexes have been recorded in the solutions of chloroform (10^{-3} M) except for $HgL(N_3)_2$ that measured in DMSO at room temperature. The range of molar conductivity (0.44 - 15.840 $cm^2 \Omega^{-1}M^{-1}$) exhibit all complexes are naturally non-electrolytes [36].

IR spectra

The most important infra-red frequencies of the Schiff base ligand (L) and its complexes are listed in table 2. In the spectrum of ligand, appearance of the strong bands at 1624 and 1620 cm^{-1} that are assigned to the asymmetric and symmetric stretching modes of the azomethine groups, $\nu(C=N)$, indicating that the condensation has been occurred successfully. In the spectra of all complexes this peak shifted about 6 - 8 cm^{-1} to the lower energies [37, 38]. The lowering in frequency of vibration of the azomethine (C=N) bond in the complexes spectra is an evidence that the Schiff base has been bonded to the mercury ion. In the

spectrum of ligand, the absorption bands assigned to aromatic, aliphatic and iminic CH were appeared at 3051 and 3024 , 2916 and 2848 cm^{-1} , respectively. For all complexes, these bands have smoothly shifted to the higher frequencies. The stretching frequency in the spectrum of ligand at 1582 cm^{-1} is assigned to the olefinic moieties [39], $\nu(C=C)$, that shifted to the lower frequency after coordination of ligand to the metal ion. The most important absorption bands in the spectra of complexes that are observed as weak peaks at the region 446 - 474 cm^{-1} maybe assigned to stretching frequency of M-N [40]. In the IR spectrum of $HgL(SCN)_2$, the strong absorption peak at 2118 cm^{-1} is assigned to coordination of $-SCN(S-$ coordinated) to the mercury ion while the peak at 2035 cm^{-1} in the spectrum of $HgL(N_3)_2$ is attributed to coordination of the N_3^- to metal ion [41, 42].

Electronic Spectra

The spectral data including the λ_{max} are shown in table 2. Electronic spectra of the ligand and its complexes were measured in $CHCl_3$ except for $HgL(N_3)_2$ that was recorded in DMSO at room temperature. In the spectrum of ligand two absorption bands are appeared. One of them is due to $\pi-\pi^*$ electron transfer of aromatic rings that is appeared at 296 nm and the other one at 376 nm is attributed to $\pi-\pi^*$ transition of the azomethine group which is mainly localized within the imine chromophore. In the electronic spectra of the complexes, the absorption band of aromatic rings shifted to the higher wavelengths. Observation of electronic spectra of complexes exhibited that the iminic band for entries 3, 5 and 6 shifted a few nanometers to higher wavelengths and for entries 2 and 4, this band had not shift. Each two transition bands are found to have more intensity after coordination of ligand to metal ion. For the complexes of IIB transition metals, the $d-d$ transition bands are not expected due to d^{10} electron configuration. In these types of complexes, the most important bands are charge transfer (L-M) transition. In the electronic spectra of titled complexes, the bands of charge transfer (L-M) transition were not observed that may be because of overlapping of it with $\pi-\pi^*$ transition of the ligand [43]. According to our previous report on this type of ligands, the suggested structure for the complexes is pseudo-tetrahedral [30, 31, 44] as drawn in fig. 1.

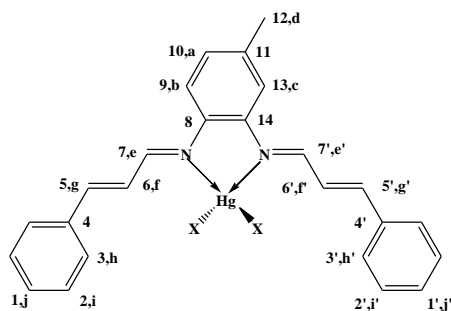


Fig. 1. Suggested structure for the complexes with general formula $HgLX_2$ wherein $X = Cl^-, Br^-, I^-, SCN^-, N_3^-$.

Table 1. Synthetic, analytical and conductivity data for the ligand and its complexes.

Compound	Color	M.p.(°C)	Yield (%)	Found (Calcd.) (%)			ΛM ($cm^2 \Omega^{-1} M^{-1}$)	
				C	N	H		
1	Ligand	Light yellow	Viscose oil	81	85.38 (85.68)	8.19(7.99)	6.13(6.33)	0.313
2	Hg Cl_2	Brown	183(dec.)	71	48.48(48.28)	4.38(4.50)	3.46(3.57)	0.440
3	Hg Br_2	Orange	172(dec.)	70	42.34(42.24)	4.04(4.94)	3.22(3.12)	3.297
4	Hg L_2	Brown	172(dec.)	88	37.52(37.31)	3.39(3.48)	2.86(2.76)	1.399
5	Hg $L(SCN)_2$	Brown	161(dec.)	70	-	-	-	0.912
6	Hg $L(N_3)_2$	Brown	169(dec.)	72	-	-	-	15.840

Table 2. Infra-red (cm^{-1}) and UV-Vis (nm) spectral data of the Schiff-base ligand and its complexes.

Compounds	$\nu CH_{arom.}$	$\nu CH_{aliph.}$	$\nu CH_{i, min}$	$\nu C=N$	$\nu C=C$	$\nu CH_{arom(oop)}$	$\nu C-C_{arom(oop)}$	$\nu M-N$	$-SCN^- / -N_3^-$	λ_{max}	
1	Ligand	3051, 3024	2916	2848	1624	1582	751	690	-	-	296, 376
2	Hg Cl_2	3055, 3026	2919	2854	1618	1575	748	686	458	-	326, 376
3	Hg Br_2	3054, 3026	2919	2852	1618	1575	748	686	458	-	327, 379
4	Hg L_2	3053, 3024	2920	2856	1616	1575	748	686	458	-	326, 376
5	Hg $L(SCN)_2$	3056, 3025	2922	2853	1617	1575	750	685	462	2118	333, 379
6	Hg $L(N_3)_2$	3055	2926	2853	1616	1575	752	685	458	2035	323, 379

1H and ^{13}C NMR spectra

The 1H and ^{13}C NMR spectra of ligand and its complexes were recorded in deuterated dimethylsulfoxide (DMSO- d_6) at 500 MHz. The results obtained from the studies of 1H and ^{13}C NMR spectra exhibit that the data are in agreement with pseudo-tetrahedral structure that is proposed for complexes (fig 1.). According to 1H NMR spectrum of ligand, the signal of methylene protons ($3H_d$) appeared at 2.43 ppm as a singlet. This signal shifted to up fields after coordination of ligand to mercury ion except in entry 4 that shifted to 3.17 ppm. Because of unsymmetrical structure of ligand, the signals of iminic protons have different chemical shifts and showed as individual doublet signal at 7.87 ppm for $1H_e$ and 7.77 ppm for $1H_{e'}$ due to coupling with $1H_f$ and $1H_{f'}$ respectively that shifted to weaker fields in the 1H NMR spectra of all complexes in relative to free ligand. After

coordination of ligand to metal ion, the shapes of the iminic protons peaks have been changed in some cases. For example, these signals in the entries 2, 5 and 6 overlapped together and were shown as broad singlet. The changes in the locations and shapes of iminic protons resonance signals are other evidences to confirm the synthesis of Schiff base complexes. In the spectrum of ligand, the signals of $4H_{h, h', j}$ and j' and $3H_{i, i'}$ and c are appeared as multiplet signals at 7.42-7.66 and 7.24 ppm respectively. The resonance of $1H_a$ and $1H_b$ were observed at 7.04 ppm as a broad doublet signals that were shifted to down field after complexation in the complexes. In the spectrum of ligand, the signal of olefinic protons $1H_f$ and $1H_{f'}$ appeared at 7.00 ppm as a broad doublet that had a red shift in the spectra of all complexes. $1H_g$ and $1H_{g'}$ exhibited a doublet signal at 6.91 ppm due to coupling with $1H_f$ and $1H_{f'}$ respectively. In the spectra of all complexes, this signal shifted to down

fields except for complex of entry 5 that shifted to up fields as two individual multiplet signals. The ^{13}C NMR spectra of the complexes showed two different signals for iminic carbons that appeared at 164.30-164.72 ppm for C_7' and at 163.56-164.96 ppm for C_7 . The signals of carbon atoms adjacent to the donor nitrogen atoms, C_{14} and C_8 were appeared in weaker fields at the region 148.52-149.30 ppm and 148.12-148.91 ppm respectively. Also the resonances of methyl carbon atoms (C_{12}) were observed at the range of 20.68-20.76 ppm. In the ^{13}C NMR spectrum of $\text{HgL}(\text{SCN})_2$, the resonance at 129.38 ppm may be assigned to carbons of SCN^- moiety. The other signals are appeared as it has listed in the experimental section. FT-IR, UV-visible, ^1H -NMR and ^{13}C -NMR spectra of HgLCl_2 are depicted in figure 2 as typical spectra.

Optimization of structures

The structure of ligand and its mercury complexes was optimized theoretically at the level of UB3LYP/LANL2MB. The optimized structures of ligand, HgLBr_2 and $\text{HgL}(\text{N}_3)_2$ are shown in Figure 3. The results predict the pseudo-tetrahedral

geometry for all complexes. Some energetic and structural parameters are summarized at table 3 and 4. HF energy, zero point energy, total energy, Gibbs free energy, enthalpy, electronic energy and corrected ones were evaluated in the ranges of -1062.10 –(-1428.90), 0423-0.446, -1061.696(-1428.461), -1061.739(-1428.518), -1061.655(-1428.410) respectively as seen in table 1. As shown in table 4, the imine bonds of free ligand are shortened after coordination to mercury ion due to probable π -back bonding from mercury ion to π^* of $\text{C}=\text{N}$ bond of ligand. M-N(1) and M-N(2) bonds are shortened from mercury chloride to mercury thiocyanate complex and then lengthened at azide complex. The angle of N(2)-Hg-N(1) is increased from mercury chloride(72.446°) to mercury thiocyanate complex(73.598°) and then decreased at azide complex(68.335°). The angle of X(1)-M-X(2) show a reverse trend with respect to N(2)-Hg-N(1) so that is decreased from mercury chloride(129.603°) to mercury thiocyanate complex(125.858°) and then increased at azide complex(169.605°). The torsion angles around the

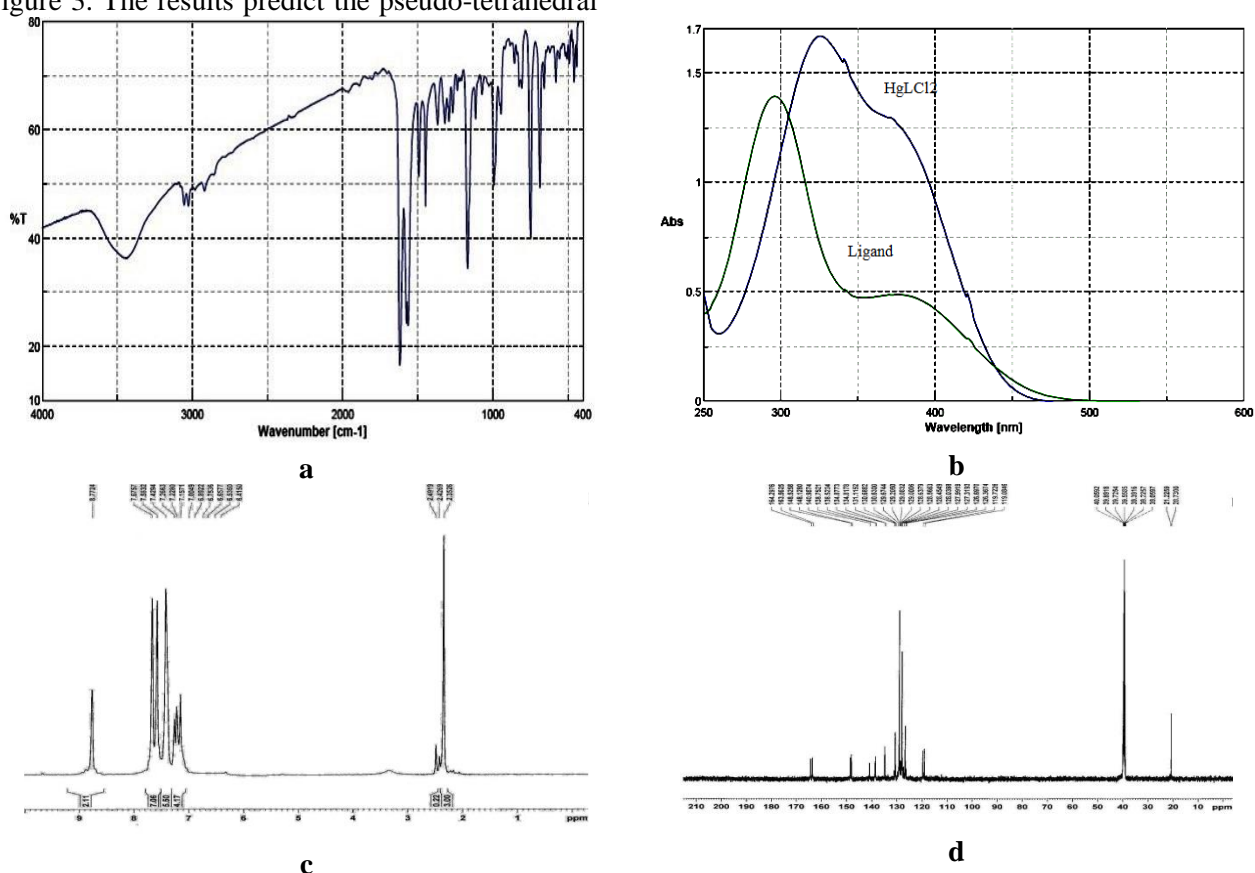
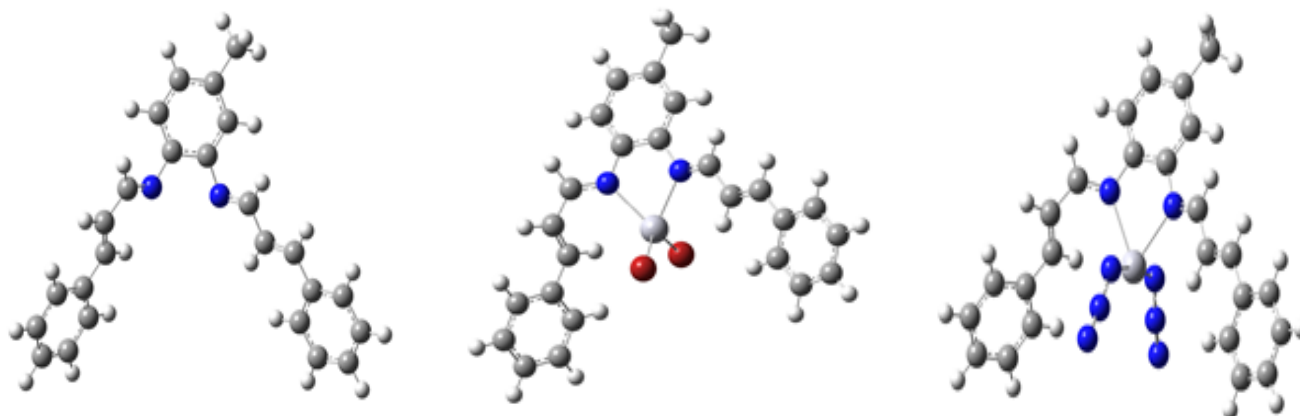


Fig. 2. The FT-IR(a) UV-visible(b), ^1H -NMR(c) and ^{13}C -NMR(d) spectra of HgLCl_2



Ligand

HgLBr₂

HgL(N₃)₂

Fig. 3. Optimized structure of ligand and two complexes

Table 3. Some energetic parameters derived for optimized structure of complexes.

Compound	HF Energy	ZPE	corrected ZPE	corrected total ΔE	ΔG	Corrected ΔG	Total $\Delta E_{\text{elect.}}$	ΔH	corrected ΔH
ligand	-1062.10	0.423	0.406	-1061.696	-1061.739	-1061.755	-1061.656	-1061.655	-1061.671
HgCl ₂	-1134.90	0.426	0.409	-1134.490	-1134.545	-1134.561	-1134.443	-1134.442	-1134.458
HgBr ₂	-1131.35	0.426	0.409	-1130.940	-1130.996	-1131.012	-1130.894	-1130.893	-1130.909
HgI ₂	-1127.80	0.425	0.409	-1127.388	-1127.443	-1127.459	-1127.342	-1127.341	-1127.357
HgL(SCN) ₂	-1308.40	0.444	0.426	-1307.969	-1308.026	-1308.042	-1307.919	-1307.918	-1307.935
HgL(N ₃) ₂	-1428.90	0.446	0.429	-1428.461	-1428.518	-1428.535	-1428.410	-1428.410	-1428.427

Table 4. Selected bond distances, bond angles and torsion angles of optimized structures.

Selected data	L	HgCl ₂	HgBr ₂	HgI ₂	HgL(SCN) ₂	HgL(N ₃) ₂
<u>Bond length(Å)</u>						
Hg-N(1)	-	2.377	2.373	2.370	2.355	2.510
Hg-N(2)	-	2.375	2.373	2.368	2.369	2.504
Hg-X(1)	-	2.622	2.786	2.985	2.754	2.265
Hg-X(2)	-	2.620	2.787	2.987	2.759	2.262
C(7)=N(1)	1.331	1.339	1.339	1.340	1.340	1.336
C(7')=N(2)	1.330	1.338	1.338	1.340	1.342	1.336
<u>Bond angle(°)</u>						
N(2)-Hg-N(1)	-	72.446	72.695	72.989	73.598	68.335
N(2)-Hg-X	-	106.889	112.268	112.05	111.394	92.636
N(2)-Hg-Y	-	105.411	109.876	111.63	112.989	96.022
N(1)-Hg-X(1)	-	113.928	106.908	108.30	114.820	92.936
N(1)-Hg-X(2)	-	114.292	112.138	110.51	106.242	95.595
X(1)-M-X(2)	-	129.603	128.942	127.88	125.858	169.605
<u>Torsion angle(°)</u>						
N(1)-C(8)-C(14)-N(2)	0.089	-1.700	-1.281	-0.801	-2.079	-1.708
N(1)-C(7)-C(6)-C(5)	-1.015	-27.649	-26.509	-25.775	-26.838	25.321
N(2)-C(7')-C(6')-C(5')	-179.181	-179.625	-178.869	-2.423	177.861	179.032
C(6)-C(5)-C(4)-C(3)	179.63	-179.812	-179.422	-179.83	169.894	177.325
C(6')-C(5')-C(4')-C(3')	-0.429	174.951	-4.114	-2.948	-5.738	-1.431

C(8)-C(14), C(7)-C(6), C(7')-C(6'), C(5)-C(4) and C(5')-C(4') based on numbering in the figure 1, were extracted from optimized structures and tabulated in table 4. As seen in table 4, torsional angles suggest the non-planer structure of ligand in all compounds. Two azomethine nitrogens are not in a plane and have an angle in the range of 0.089°-(-2.079)° with respect to each other. The imine and olefin bonds have torsional angles of -27.649° to -1.015° and -178.869° to 179.032° in both sides of ligand structure of complexes. The left and right phenyl rings of aldehyde section of ligand have torsional angles of -179.83° to 179.63° and -5.738° to 174.951° respectively with respect to the conjugated olefin bonds in the ligand and its complexes.

CONCLUSION

In this work, we reported the synthesis of some new mercury complexes of a bidentate Schiff base ligand. These compounds were characterized by spectroscopic and analytical studies such as IR, UV-Vis, ¹H NMR and ¹³C NMR, elemental analysis and molar conductivity. The general formula of MLX₂ was proposed for Hg(II) complexes in which X is Cl⁻, Br⁻, I⁻, SCN⁻ and N₃⁻. Furthermore, the structural ligand and complexes were optimized at the UB3LYP/LANL2MB/ level of theory and then some important structural (Bond length(Å), Bond angle(°) and Torsion angle(°)) and theoretical energetic(HF-Energy, ZPE, ΔE, ΔG, ΔE_{electronic} and ΔH) data were derived. Consequently, the pseudo-tetrahedral geometry was suggested for all mercury complexes.

Acknowledgment: Partial support of this work by Yasouj University is acknowledged.

REFERENCES

1. C. Sousa, C. Freire, B. de Castro, *Molecules*, **8**, 894 (2003).
2. V.K. Singh, R. Sinha, R. Kant, B.K. Sinha, *Asian J. Chem.*, **10**, 532 (1998).
3. L.T. Yildirm, O. Atakol, *Cryst. Res. Technol.*, **37**, 1352 (2002).
4. A. Pui, *Croat. Chem. Acta*, **75**, 165 (2002).
5. A. D. Garnovski, A.L. Nivorozhkin, V.I. Minkin, *Coord. Chem. Rev.*, **126**, 1 (1993).
6. H. Keypour, N. Rahpeyma, P. Arzhang, M. Rezaeivala, Y. Elerman, O. Buyukgungor, L. Valencia, *Polyhedron*, **29**, 1144 (2010).
7. A.A. El-Sherif, T.M.A. Eldebss, *Spectrochim. Acta A*, **79**, 1803 (2011).

8. M. Lanznaster, A. Neves, A.J. Bortoluzzi, A.M.C. Assumpcao, I. Vencato, S.P. Machado, S.M. Drechsel, *Inorg Chem.*, **45**, 1005 (2006).
9. T. Ueno, T. Koshiyama, M. Ohashi, K. Kondo, M. Kono, A. Suzuki, T. Yamane, Y. Watanabe, *J. Am. Chem. Soc.*, **127**, 6556 (2005).
10. T. Ueno, T. Koshiyama, S. Abe, N. Yokoi, M. Ohashi, H. Nakajima, Y. Watanabe, *J. Organomet. Chem.*, **692**, 142 (2007).
11. N. Shahabadi, S. Kashanian, F. Darabi, *Eur. J. Med. Chem.*, **45**, 4239 (2010).
12. S.R. Collinson, D.E. Fenton, *Coord. Chem. Rev.*, **148**, 19 (1996).
13. [13] M.L.P. Santos, I.A. Bagatin, E.M. Pereira, A.M.C. Ferreira, *J. Chem. Soc., Dalton Trans.*, 838(2001).
14. H.S. He, D.T. Puerta, S.M. Cohen, K.R. Rodgers, *Inorg. Chem.*, **44**, 7431 (2005).
15. M. Wang, L.F. Wang, Y.Z. Li, Q.X. Li, Z.D. Xu, D.Q. Qu, *Transition Met. Chem.*, **26**, 307 (2001).
16. N.N. Gulerman, S. Rollas, H. Erdeniz, M. Kiraj, *J. Pharm. Sci.*, **26**, 1 (2001).
17. P. Tarasconi, S. Capacchi, G. Pelosi, M. Corina, R. Albertini, A. Bonati, P.P. Dall'Aglio, P. Lunghi, S. Pinelli, *Bioorg. Med. Chem.*, **8**, 154 (2000).
18. R.R. Mohamed, A.M. Fekry, *Int. J. Electrochem. Sci.*, **6**, 2488 (2011).
19. S. Park, V.K. Mathur, R.P. Planap, *Polyhedron*, **17**, 325 (1998).
20. K.C. Gupta, A.K. Sutar, *Coord. Chem. Rev.*, **252**, 1420 (2008).
21. N.S. Venkataramanan, G. Kuppuraj, S. Rajagopal, *Coord. Chem. Rev.*, **249**, 1249 (2005).
22. T. Katsuki, *Coord. Chem. Rev.*, **140**, 189 (1995).
23. M. Montazerzohori, M.H. Habibi, L. Zamani-Fradonbe, S.A.R. Musavi, *Arkivoc*, **xi**, 238 (2008).
24. F. Yuksel, D. Atilla, V. Ahsen, *Polyhedron*, **26**, 4551 (2007).
25. B.Y. Zhang, F.B. Meng, M. Tian, W.Q. Xiao, *Teact. Funct. Polymer*, **66**, 551 (2005).
26. D. N. Dhar, C.L. Taploo, *J. Sci. Ind. Res.*, **41**, 501 (1982).
27. E. Keskioglu, A.B. Gunduzalp, S. Cete, F. Hamurcu, B. Erk, *Spectrochim. Acta A*, **70**, 634 (2008).
28. J.Z. Wu, L. Yuan, *J. Inorg. Biochem.*, **98**, 41 (2004).
29. K.P. Balasubramanian, K. Parameswari, V. Chinnusamy, R. Prabhakaran, K. Natarajan, *Spectrochim. Acta A*, **65**, 678 (2006).
30. M.H. Habibi, M. Montazerzohori, A. Lalegani, R.W. Harington, W. Clegg, *Anal. Sci. X-ray Struct. Anal. Online*, **23**, X49 (2007).
31. M. Montazerzohori, S.A. Musavi, *J. Coord. Chem.*, **61**, 3934 (2008).
32. S. Joohari, M. Montazerzohori, S.A. Musavi, *Asian J. Chem.*, **21**, 3755 (2009).
33. M. Montazerzohori, S. Joohari, V. Nouroozi, S. Hashemi, Z. Kazemi, S.A. Musavi, *Indian J. Sci. Technol.*, **4**, 373 (2011).

34. M. Montazerzohori, S. Joohari, S.A. Musavi, *Spectrochim. Acta A*, **73**, 231 (2009).
35. M. Montazerzohori, V. Nouroozi, S. Hashemi, Z. Kazemi, S. Joohari, S.A. Musavi, *Asian J. Chem.*, **23** 5399 (2011).
36. A. Golcu, M. Tumer, H. Demirelli, R.A. Wheatley, *Inorg. Chim. Acta*, **358**, 1785 (2005).
37. A.A. Adel, A. A. Emara, O. Saleh, M. Adly, *Spectrochim. Acta A*, **68**, 592 (2007).
38. M.T.H. Tarafder, T. Jin, K.A. Crouse, A.M. Ali, B.M. Yamin, H.K. Fun, *Polyhedron*, **21**, 2547 (2002).
39. I. Picon-Ferrer, F. Hueso-Ureoa, N.A. Illan-Cabeza, S.B. Jiménez-Pulido, J.M. Martínez-Martos, M.J. Ramirez-Exposito, M.N. Moreno-Carretero, *J. Inorg. Biochem.*, 103, 94 (2009).
40. M. Sonmez, M. Sekerci, *Synth. React. Inorg. Met.-Org. Chem.*, **34**, 489 (2004).
41. C. Zhang, G. Tian, B. Liu, *Transition Met. Chem.*, **25**, 377 (2000).
42. S. Sen, P. Talukder, G. Rosair, S. Mitra, *Struct. Chem.*, **16**, 605 (2005).
43. S. Dehghanpour, A.H. Mahmoudkhani, A.M. Amirnasr, *Struc. Chem.*, **17**, 255 (2006).
44. M.H. Habibi, M. Montazerzohori, A. Lalegani, R.W. Harington, W. Clegg, *Anal. Sci.: X-ray Struct. Anal. Online*, **23**, X51 (2007).

СИНТЕЗА, СПЕКТРАЛНО ОХАРАКТЕРИЗИРАНЕ И ТЕОРЕТИЧНО ИЗСЛЕДВАНЕ ЗА НЯКОИ ЖИВАЧНИ КОМПЛЕКСИ С КООРДИНАЦИОННО ЧИСЛО ЧЕТИРИ

М. Монтезрозохори^{*1}, Х. Тавакол², С. Хеири¹, С.А. Мусави¹, С.Джухари³

¹Департамент по химия, Университет в Ясудж, Ясудж, Иран

²Департамент по химия, Университет в Исфахан, Исфахан, Иран

³Департамент по фундаментални науки, Клон Ясудж, Ислямски унишверситет Азад, Ясудж, Иран

Постъпила на 29 октомври, 2012 г.; коригирана на 9 април, 2013 г.

(Резюме)

Получени са нови комплекси на живака с лиганди от бидентатни Шифови бази с два азотни атома като донори охарактеризирани чрез спектроскопични и аналитични методи, като IR, UV-Vis, ¹H NMR и ¹³C NMR, елементен анализ и моларна проводимост. IR-спектрите на лигандите показват характеристични на асиметрични и симетрични вибрации на имино-групите при съответно 1624 и 1620 cm⁻¹, които се изравняват и отместват с 6-8 cm⁻¹ към по-ниски енергии. Иминните протонни сигнали на лигандите се появяват като два дублета при 7.87 и 7.77 ppm, които се понижават до 7.92-8.91 ppm след координиране към живачните йони в тези комплекси. Данните от анализите, потвърдени при отношение 1:1 за лигандите към металната сол във всички комплекси. Структурната оптимизация на лигандите и комплексите е представена при нивото UB3LYP/LANL2MB на теорията и са получени някои важни структурни данни (дължина на връзката (Å), ъгъл на връзката (°) and ъгъл на усукване (°)) и на енергетични характеристики (HF-енергия, ZPE, ΔE, ΔG, ΔE_{електронна} и ΔH). Дължините на връзката (Å) Hg-N(1) и Hg-N(2) намаляват от комплексите меркури-хлорид към меркури-тиоцианат и до комплекса меркури-азид. Ъгълът на връзката (°) от N(1)-Hg-N(2) в комплексите плавно намалява от комплексите меркури-хлорид към меркури-тиоцианат и до комплекса меркури-азид. Обратната тенденция се забелязва за X(1)-Hg-X(2). Псевдо-тетраедрична геометрия се предлага за всички комплекси. Обща формула за Hg(II)-комплексите е MLX₂ където X= Cl⁻, Br⁻, I⁻, SCN⁻ and N₃⁻.

Phase equilibrium modeling for binary systems containing CO₂ using artificial neural networks

S. Atashrouz*, H. Mirshekar

Department of Chemical Engineering, Amirkabir University of Technology (Tehran Polytechnic), Mahshahr Campus, Mahshahr, P.O. Box 415, Iran.

Received January 7, 2013; Revised May 28, 2013

In this study, two mathematical models based on the Feed-Forward Back Propagation Artificial Neural Network (FFBP-ANN) are employed for the prediction of CO₂ mole fraction in liquid (x_1) and vapor (y_1) phases in the Vapor Liquid Equilibrium (VLE) for fifty-six CO₂-containing binary mixtures. 2104 data sets from the open literature have been used to construct the models. Furthermore, some new experimental data (not applied in ANN training) have been used to examine the reliability of the model. Predictions using ANN were compared with available literature data and the results confirm that there is a reasonable conformity between the predicted values and the experimental data. The average absolute deviation percent (AAD (%)) for ANN model I (x_1 prediction) and ANN model II (y_1 prediction) are 1.572 and 0.848 respectively. The study shows that the neural network model is a good alternative method for the estimation of phase equilibrium properties for this type of mixtures.

Key words: vapor liquid equilibria; carbon dioxide; modeling; artificial neural network, supercritical fluid extraction, refrigerant

INTRODUCTION

Prediction of vapor liquid equilibrium data is a necessary need in chemical engineering processes. Carbon dioxide (CO₂) is an important component in binary mixtures and estimation of VLE data for binary mixtures containing CO₂ is necessary in different processes such as supercritical extraction, refrigeration, absorption and more recently, in the development of new and improved methods for carbon capture and storage [1]. Supercritical fluid extraction processes for selectively recovering high purity active principles from biological substrates is a technology of interest to the food, cosmetics and pharmaceutical industries. Extraction using supercritical fluids is now being used in the industry because it is non-flammable, non-toxic and it is available in a highly purified form at low cost and it can be employed at near-environmental temperatures [2–4]. However, the design of this type of processes requires the knowledge of phase equilibrium diagrams over a vast range of temperatures and pressures [5]. From this point of view, knowledge of the phase behavior of systems containing carbon dioxide is of growing importance due to the increased use of supercritical CO₂ as an

environmentally benign solvent alternative to volatile organics in chemical processes [1]. Another application of carbon dioxide is recently in binary systems that have been utilized for crystallization, purification of solids and reaction media. CO₂ and methanol binary mixture is an example of this type of systems [6]. Also binary mixtures containing CO₂ and refrigerant mixtures are recently of great importance. For nearly 60 years, chlorofluorocarbons (CFCs) have been widely used as solvents, foam-blowing agents, aerosols and especially refrigerants due to their stability, non-toxicity, non-flammability, good thermodynamic properties and so on. However, they also have a harmful effect on the earth's protective ozone layer. So, they have been regulated internationally by Montreal Protocol since 1989. Much effort has been made to find the suitable replacement for CFCs. Initial CFC alternatives included some hydro chlorofluorocarbons (HCFCs) but they will be also phased out internationally because their ozone depletion potentials (ODPs) and global warming potentials (GWPs) are significant though less than those of CFCs. Hydrofluorocarbons (HFCs) synthetic refrigerants which have zero ODPs were proposed as promising replacements for CFCs and HCFCs. HFC-134a (1,1,1,2-tetrafluoroethane; CF₃CH₂F) is an environmentally acceptable refrigerant, which

* To whom all correspondence should be sent:
E-mail: s.atashrouz@gmail.com

has replaced the ozone-depleting dichlorodifluoromethane (CFC-12) in a wide range of applications especially in automotive air-conditioning and domestic refrigeration [7]. In order to develop refrigeration processes estimation of VLE data for binary mixtures containing CO₂ and HFCs has a great importance. Furthermore for the new total flooding clean agents that were being developed to replace certain Halon fire extinguishing agents, the discharge time required to achieve 95% of the minimum design concentration shall not exceed 10 s and the expellant gas is needed for their lack of vapor pressure. Generally, Nitrogen is used as an expellant gas because it does not be liquefied at high pressure, but carbon dioxide has some merits to nitrogen such as price, storage area and supplementary extinguishing effect for R123 and R124 as fire extinguishing agents [8]. In another environmentally view, the emission of carbon dioxide has been identified as the main contributor to global warming and climate change. The challenge for modern industry is to find cost effective solutions that will reduce the release of CO₂ into the atmosphere. Reduction of CO₂ emissions can be achieved by a variety of means. A physical absorption process is one of the most important possibilities. The advantage of this method is that it requires relatively little energy. Diisopropylether, an excellent solvent, is expected to absorb CO₂ [9]. So in this point of view, knowledge of VLE data for binary mixtures that has a solvent for absorption of CO₂ is important. In another application the high-pressure phase equilibrium information of mixtures composed of CO₂ and alcohols is of particular importance and has been actively studied for various utilities. For example, the phase equilibrium behaviors of low-molecular weight alcohols such as methanol and ethanol in CO₂ are essential for the effective evaluation of cosolvents to CO₂-based supercritical solvents. Also the phase equilibrium information of high molecular weight alcohols such as 2-ethoxyethanol with CO₂ is valuably used to processes in the food and cosmetic industries [10].

Information about the phase behavior of fluid mixtures can be obtained from direct measurement of phase equilibrium data or by the use of equation of state based thermodynamic models. Direct measurement of precise experimental data is often difficult and expensive, while in the second method Several conventional thermodynamic models such as equations of state (EoS) are used for estimating the VLE [11]. A thermodynamic model provides the necessary relationships between thermodynamic properties and can be used in combination with

fundamental relations to generate all the properties required to perform phase equilibrium calculations. The most common thermodynamic models are equations of state and among them cubic equations of state are the most popular. Although thermodynamic models have been derived from strong theoretical principles these methods include a large number of equation of states and excess Gibbs free energy models. that are tedious and involve a certain amount of empiricism to determine mixture constants, through fitting experimental data and using various arbitrary mixing rules, making difficult the selection of the appropriate model for a particular case [12].

On the other hand artificial neural networks(ANN), which can be viewed as an universal approximation tool with an inherent ability to extract from experimental data the highly non-linear and complex relationships between the variables of the problem handled, have gained broad attention within process engineering as a robust and efficient computational tool [12]. Recently, ANN has found extensive application in the field of thermodynamics and transport properties such as the estimation of VLE, viscosity, density, vapor pressure, compressibility factor and thermal conductivity and etc [13–18].

In this research, two comprehensive models based on multi-layer FFBP-ANN were developed to estimate VLE data for fifty-six binary mixtures containing CO₂, the importance of which was mentioned above. Model I and model II predict CO₂ mole fractions in the liquid (x_1) and vapor (y_1) phases respectively. The mixtures include 1-butanol, 1-heptanol, 1-hexanol, 1-octanol, 1-pentanol, 1-propanol, 2-butanol, 2-ethoxyethanol, 2-methoxyethanol, 2-methyl-1-propanol, 2-pentanol, 2-propanol, 3-methyl-1-butanol, 3-methyl-2-butanol, 3-pentanol, acetic acid, α -pinene, benzene, chloroform, cyclohexanol, cyclohexanone, cyclopentanol, decanal, DHAEE, DIPE, ethyl butyrate, EPAEE, ethanol, fenchone, H₂, limonene, methanol, methyl acetate, methyl linoleate, methyl oleate, methyl propionate, m-xylene, n-hexane, dimethylformamide, n-octacosane, n-octane, o-xylene, propylene carbonate, perfluorohexane, propane, p-xylene, R32, R116, R123, R134a, R152a, R610, styrene, tertpentanol, tetrahydrofuran and water. The developed models were trained and evaluated by using the experimental data for binary mixtures reported by [1–3], [5–9], [19–50] and properties for fifty-six pure components reported by [19], [20], [51]. The experimental data were divided into three groups in the random manner for the

development of the ANN models. One part of the experimental data (60%) was used to train the networks and the rest was used to evaluate the performance of the networks for the test (20%) and validation (20%) of the model. Finally, for the model validation, the prediction of the ANN models was compared with the experimental data.

Applications of ANN for the prediction of VLE

Applications of ANN for the prediction of VLE have been reported in a number of papers. Application of ANNs to predict VLE was first conducted by Petersen et al. [52]. They have developed an ANN with aim of estimating activity coefficient based on group contribution methods. After that ANN has been used to estimate bubble point conditions of the benzene-toluene binary mixture by Guimaraes and McGreavy [53]. Sharma et al. [54] have reported the use of ANN models to predict the liquid and vapor phase compositions for VLE calculation of methane-ethane and ammonia-water binary mixtures. Urata et al. [55] have developed a new way for prediction of VLE using ANN in three steps. In the first step, the sign of logarithm of activity coefficient (γ) is estimated for each binary system using ANN. In the second step, two sets of relation between liquid mole fraction and $\ln(\gamma)$ are constructed. And finally in the third step, vapor-liquid composition and equilibrium temperature are calculated using the estimated activity coefficient. The researches that were mentioned above have used multilayer perceptron (MLP) network for VLE calculation but Ganguly [56] has developed ANN with radial basis function (RBF) network to predict VLE of binary and ternary systems. Piowtrowski et al. [57] have used a feed forward multilayer neural network to simulate complex VLE in an industrial process of urea synthesis from ammonia and carbon dioxide. Bilgin [58] employed a FFBP neural network to estimate the isobaric VLE data for the methylcyclohexane-toluene and isopropanol-methyl isobutyl ketone binary mixtures. Mohanty [59] has used multilayer perceptron ANN to predict liquid and vapor phase compositions for CO₂- ethylcaprate, CO₂- ethylcaproate and CO₂- ethylcaprylate binaries. Also Mohanty [60] in another paper has reported the use of ANN to estimate the bubble pressure and the vapor phase composition of the CO₂-difluoromethane with this aim that difluoromethane was an attractive alternative to chlorofluorocarbons (CFCs) and hydro chlorofluorocarbons (HCFCs). Karimi and Yousefi [11] have developed four ANNs for estimating VLE data for four binary refrigerant

mixtures. Yamamoto and Tochigi [61] have used a reconstruction-learning neural network to estimating margules parameters and then they used of the margules parameters to estimate VLE for binary mixtures mentioned in their work. Ghanadzadeh and Ahmadifar [62] have used ANN for prediction of boiling temperature of two binary alcohol mixtures. Si-Mousa et al. [12] have used ANN to correlate VLE of CO₂- esters mixtures in high pressure condition. Faúndez et al. [13] have applied an ANN for Phase equilibrium modeling in ethanol- congener mixtures in the alcoholic beverage production. Also Faúndez et al. [63] have employed ANN to estimate water- congener mixtures found in alcoholic beverages. Zarenezhad and Aminian [64] have developed a feed forward neural network model with four hidden layers to predict the vapor-liquid equilibrium of seven binary mixtures of CO₂-alkanols. Abedini et al. [4] have used ANN to estimate VLE data of six CO₂- alcohol systems include CO₂- methanol, CO₂- ethanol, CO₂- 1-butanol, CO₂- 2-butanol, CO₂-1-pentanol and CO₂-2-pentanol.

As it is mentioned, information about phase behavior for binary mixtures containing CO₂ has a great importance in different processes. The previous works do not develop a widespread model, as an example, they only develop models containing CO₂ and alcohols or esters. This type of modeling is not a model which corresponds to different binary systems and is limited to especially binary mixtures, with the same chemical groups. The present work, with the aim of developing a comprehensive model, corresponds to different binary systems and has not been presented in the literature.

Artificial Neural Network

Neural networks consist of arrays of simple active units linked by weighted connections. ANN consists of multiple layers of neurons arranged in such a way that each neuron in one layer is connected with each neuron in the next layer. The network used in this study is a multi-layer feed forward neural network with a learning scheme of the Back-Propagation (BP) of errors and the *Levenberg-Marquardt* algorithm for the adjustment of the connecting weights. Neurons are the fundamental processing element of an ANN, which are arranged in layers that make up the global architecture[11].

The main advantage of using ANNs to predict the VLE data lies in their ability to learn the relationship between the complex VLE data for different binary mixtures. The ANN input is the first layer in the network through which the information is supplied.

The number of neurons in the input layer depends on the network input parameters. Hidden layers connect the input and output layers. Hidden layers enrich the network for learning the relation between input and output data. In theory, ANN with only one hidden layer and enough neurons in the hidden layer, has the ability to learn any relation between the input and output data. Transfer function is the mathematic function that determines the relation between neuron output and the network. In other words, transfer function indicates the degree of nonlinearity in the network. Practically, in the feed forward BP-ANN model some limited functions are used as transfer functions[65]. Normally, the transfer functions of all neurons in the hidden layers are similar. Also, for all neurons in the output layer, the same transfer function is used. For the prediction of phenomena, logistic transfer function is the most conventional transfer function that is used in the hidden layers, because it is very easy to differentiate the sigmoid transfer function for using in the BP algorithm [66–68]. The sigmoid transfer function is as follows:

$$O_{pj}(net) = \frac{1}{1 + e^{-net}} \quad (1-a)$$

$$net = \sum_{i=0}^{n-1} w_i x_i \quad (1-b)$$

Which "n" in Eq. (1) is the number of inputs to the neuron. "w_i" is the weight coefficient corresponding to the input "x_i" and "O_{pj}" is the output corresponding to the "j" neuron. For completion of this section, we illustrate the learning BP algorithm.

ANN Training Algorithm

The Back-Propagation Algorithm is one of Least Mean Square methods, which is normally used in engineering. In a multilayer perceptron, each neuron of a layer is linked to all neurons of the previous layer. Fig. 1 shows a perceptron with a hidden layer. Each layer output acts as the input to the next neurons.

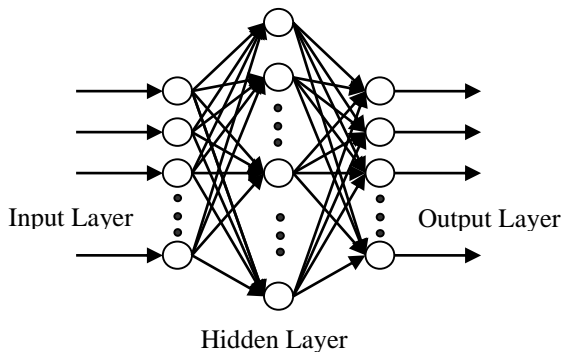


Fig. 1. Perceptron structure with a hidden layer

In order to train Multilayer Feed Forward Neural Network, Back-Propagation Law is used. In the first stage, all weights and biases are selected according to small random numbers. In the second stage, input vector $X_p = x_0, x_1, \dots, x_{n-1}$ and the target exit $T_p = t_0, t_1, \dots, t_{m-1}$ are given to the network, where the subscripts n and m are the numbers of input and output vector, respectively. In the third stage, the following quantitative values are calculated and transferred to the subsequent layer until it eventually reaches the exit layer [69].

$$O_{pj} = f[\sum_{i=0}^{n-1} w_i x_i] \quad (2)$$

The fourth stage begins from the exit layer, during which the weight coefficients are corrected.

$$w_{ij}(t + 1) = w_{ij}(t) + \eta \delta_{pj} O_{pj} \quad (3)$$

Where "W_{ij}(t)" stands for the weight coefficients from node "i" to node "j" in time "t", "η" is the rate coefficient, "δ_{pj}" refers to the corresponding error of input pattern "P" to the node "j" and "O_{pj}" is the output corresponding to the "j" neuron. "δ_{pj}" is calculated by the following equations for exit layer and hidden layer, respectively:

$$\delta_{pj} = O_{pj}(1 - O_{pj})(t_{pj} - O_{pj}) \quad (4)$$

$$\delta_{pj} = O_{pj}(1 - O_{pj}) \sum_k \delta_{pk} w_{jk} \quad (5)$$

Here, the \sum acts for k nodes on the subsequent layer after the node "j" [69]. In the learning process, there are several parameters that have influence on the ANN training. These parameters are the number of iterations, number of hidden layers and the number of hidden neurons. To find the best architecture of the model, best set of the aforementioned parameters based on minimizing the network output error should be chosen [70].

EXPERIMENTAL DATA

The first step in an ANN modeling is compiling the database to train the network and to evaluate network ability for generalization. In the present study, the experimental VLE data for fifty-six mixtures reported by [1–3], [5–9], [19–50] have been used for training and validation of the ANN models. The pure component properties (normal boiling point (T_b), critical temperature (T_c), critical pressure (P_c) and acentric factor (ω)) of the fifty-

six Pure component used in this work were collected from different literature [19], [20], [51] and the collection was listed in Appendix I. also the range of T, P, x₁ and y₁ is reported in Appendix II.

Development of the ANN Model

In estimating VLE by using ANN, most of the previous works predict two VLE parameters, and all of them use only one ANN model for predicting these two VLE parameters. The use of only one ANN for the prediction of two VLE parameters leads to the complexity of the network and also reduces the network accuracy. This is because of the order of standard deviation for the output parameters.

Standard deviation (STD) for a number of data sets defines as:

$$STD = \frac{1}{n} \sum_{i=1}^n (x_i - \bar{x})^2 \quad (6)$$

Where

$$\bar{x} = \frac{1}{n} \sum_{i=1}^n x_i \quad (7)$$

In Eq. (6) and Eq. (7) "n" is the number of data point and " \bar{x} " is the average of data sets.

When the order of standard deviation of an output parameter is higher than the other, the error of the higher standard deviation output, affects the other output parameter and this problem reduces accuracy of ANN model.

To investigate this influence, with the aim of calculating x₁ and y₁, three models were considered:

Model I (x₁ prediction), model II (y₁ prediction) and the model III (x₁ and y₁ prediction). The inputs of the all models are P, T, T_c, P_c, ω . The standard deviation of y₁ and x₁ is 0.1794 and 0.2751 respectively. Model I and model II with 339 and 310 parameters respectively and model III with different structure has been developed and the results were shown in Table 1. As shown model I that predicts only x₁ has more accuracy in comparison with other structures of model III. The accuracy of this model is better than even the ANN structures with more parameters in model III. Also in regard to model II the accuracy of this model is better in predicting of y₁ than the entire model III structures. So according to Table 1 for VLE modeling by ANN for have more accuracy we should develop two separate ANN for every VLE parameter

Two ANN models were considered for the prediction of CO₂ mole fraction in the vapor and liquid phases. In order to describe the phase behavior of the fifty-six CO₂ (1) - component (2) binaries by two ANN models, eight variables have been selected in this work: four intensive state variables (equilibrium temperature, equilibrium pressure and equilibrium CO₂ mole fractions in the liquid and vapor phases) and four pure component properties of the components (normal boiling point, critical temperature, critical pressure and acentric factor). The choice of the input and output variables was based on the phase rule. Therefore, the equilibrium temperature and pressure, together with the pure

Table 1. AAD (%) for model I, model II and different structure of model III.

Number of ANN parameters	AAD (%)	
	x ₁	y ₁
339 ^a	1.572	-
310 ^b	-	0.848
101	4.781	2.425
182	3.674	2.283
275	2.556	1.580
321	2.405	1.601
460	2.109	1.373
671	2.033	1.270
839	2.069	1.248
911	1.776	1.319
959	2.014	1.416
1103	2.092	1.313
1962	1.658	1.087
4438	2.085	1.253

^amodel I: predicting only x₁

^bmodel II: predicting only y₁

Table 2. Architecture of the optimized ANN models.

Network Type	Training Algorithm	Hidden layer 1		Hidden layer 2		Output layer	
		No. of neurons	Activation function	No. of neurons	Activation function	No. of neurons	Activation function
FFBP-ANN ^a	BRBP using Levenberg-Marquardt optimization ^b	Model I: 14 Model II: 15	<i>tansig</i> MATLAB function	Model I: 15 Model II: 12	<i>tansig</i> MATLAB function	1	Linear (<i>purelin</i> MATLAB function)

^a*newff* MATLAB function.

^b*trainbr* MATLAB function.

component properties have been selected as input variables and the CO₂ mole fraction in the liquid and vapor phases as output variables. A simple scheme of inputs and output to the developed ANN models was shown in Fig. 2.

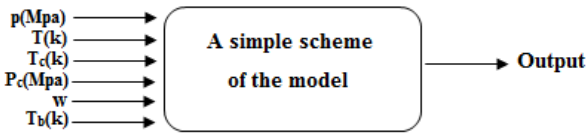


Fig. 2. A simple scheme of inputs and output to the models, output for the model I and model II are x_1 and y_1 respectively

In the training phase, the number of neurons in the hidden layers was important for the network optimization. However, decision on the number of hidden layers neurons is difficult because it depends on the specific problem being solved using ANN. With too few neurons, the network may not be powerful enough for a given learning task. With a large number of neurons, the ANN may memorize the input training data very well so that the network tends to perform poorly on new test data and is called “over-fitting”. To prevent the over-fitting issue, we should evaluate average absolute deviation percent (AAD (%)) for train set, validation set and test set and they must be in the same order of magnitude. Average absolute deviation percent (AAD (%)) was calculated from the following relation:

$$AAD (\%) = \frac{100}{n} \sum_{i=1}^n |y_i^{Exp} - y_i^{Calc}| \quad (8)$$

Where “ n ” is the number of data point, “ Exp ” and “ $Calc$ ” superscripts stand for the experimental and calculated CO₂ mole fraction respectively.

ANN modeling for the VLE of fifty-six CO₂ (1)-component (2) binaries was carried out in MATLAB ver. 7.9.0 program. Initially, the program starts with the default FFBP-ANN type (*newff* MATLAB function), the *Levenberg-Marquardt BP* training algorithm (*trainlm* MATLAB training function) and one hidden layer. Once the topology is specified the starting and ending number(s) of neurons in the hidden layer(s) have to be specified.

The number of neurons in hidden layer(s) is then modified by adding neurons one at a time. The procedure begins with the logarithmic sigmoid activation function and then the hyperbolic tangent sigmoid activation function for the hidden layers and the linear activation function for the output layer. The results of different runs of the program show that the Bayesian Regularization Back Propagation (BRBP), using *Levenberg-Marquardt* optimization models, train more successfully than models using attenuated training. Table 2 shows the structure of the optimized ANN models.

RESULTS AND DISCUSSION

Using the random selection method, 60% of all data were assigned to the training set, 20% of all data were assigned to the validation set and the rest of the data were used as the test set. In the training process, different hidden layers and neurons were tried and finally the optimized ANN obtained for this study were two networks with two hidden layers containing 14 neurons in layer 1 and 15 neurons in layer 2 for model I and two hidden layers containing 15 neurons in layer 1 and 12 neurons in layer 2 for model II. In an optimized ANN, the AAD (%) for the train, validation and test data sets are in the same order of magnitude. AAD (%) and also, network performance, sum of squares error (SSE) for the train, validation and test sets of data were listed in Table 3.

Table 3. SSE and AAD (%) for the models.

Model	SSE	AAD (%) train	AAD (%) test	AAD (%) validation
I	0.38097	1.603	1.497	1.572
II	0.26887	0.864	0.751	0.896

The ability of the models for the prediction of CO₂ mole fraction in the vapor and liquid phases are shown in the Fig. 3 and Fig. 4. Where “ R ” is correlation coefficient and defined by:

$$R = Correl(x, y) = \frac{\sum_{i=1}^n (x-\bar{x})(y-\bar{y})}{\sqrt{\sum_{i=1}^n (x-\bar{x})^2 \sum_{i=1}^n (y-\bar{y})^2}} \quad (9)$$

Where "n" is the number of data point, "x" and "y" are target and output parameters respectively and " \bar{x} " and " \bar{y} " are the average of the target and output.

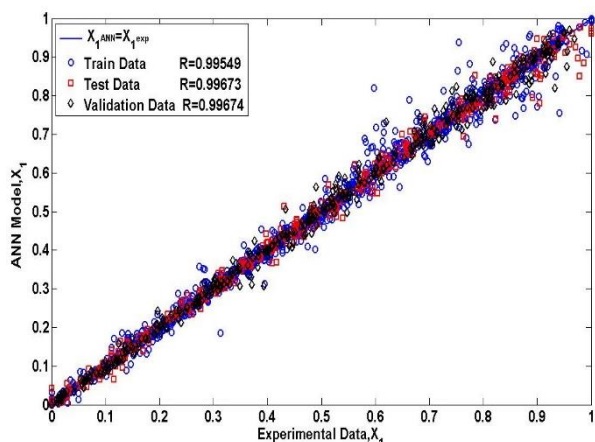


Fig. 3. Comparison of the experimental and modeling results for the mole fraction in liquid phase of CO₂ in fifty-six binary mixtures by ANN model I.

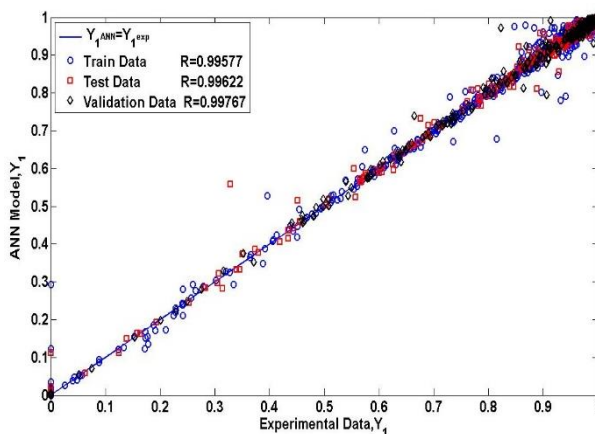


Fig. 4. Comparison of the experimental and modeling results for the mole fraction in vapor phase of CO₂ in fifty-six binary mixtures by ANN model II.

As shown, good agreement for the prediction of ANN model and the experimental data are observed. So the ANN models can be reliably used to estimate x_1 and y_1 for CO₂- binary systems within the ranges of parameters considered in this work.

Figs. 5 to 9 show the y_1 - x_1 curves for the five CO₂-containing binary mixtures including 1-butanol, propane, R610, perflourohexane and 1-propanol and also Figs. 10 to 14 show the p - x_1 y_1 curves for five CO₂-containing binary mixtures including 2-butanol, 2-methoxyethanol, H₂, R123, R152a at different temperatures. The lines are the results of ANN models. They include a comparison between experimental data and ANN results. As shown, the Figures show good agreement between experimental data and the prediction of the ANN models. By comparing the behavior of Fig. 12 with that of other p - x_1 y_1 Figures, it can be seen that

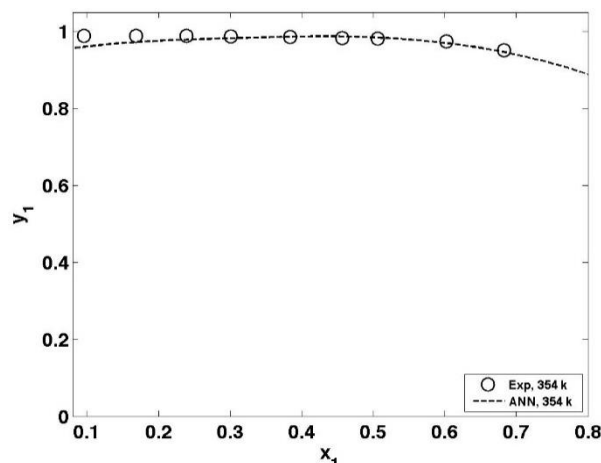


Fig. 5. y_1 - x_1 curve for the CO₂ (1) – 1-butanol (2) binary mixture at 354 k.

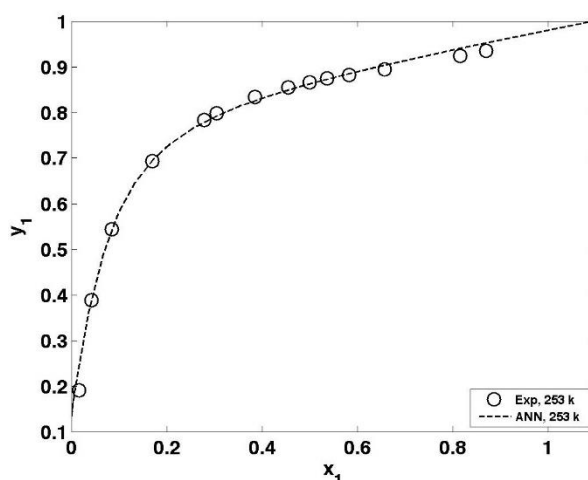


Fig. 6. y_1 - x_1 curve for the CO₂ (1)–Propane (2) binary mixture at 253 k.

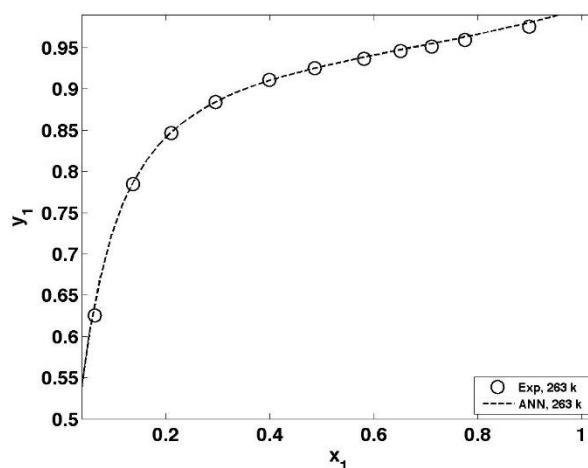


Fig. 7. y_1 - x_1 curve for the CO₂ (1) – R610 (2) binary mixture at 263 k.

treatment of H₂-CO₂ system is completely different from others, while the ANN models with a good reliability predict this treatment and this shows that ANN models are strong models to predict VLE data even with completely different treatment.

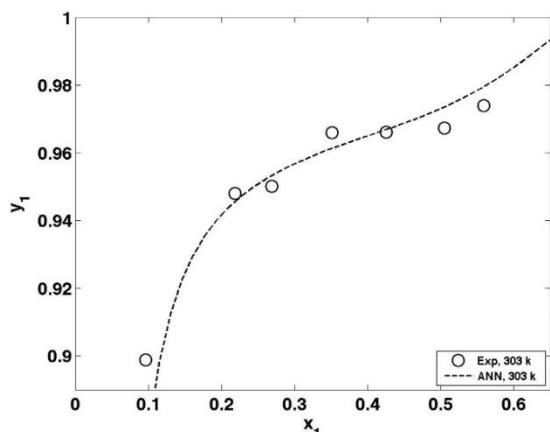


Fig. 8. y_1 - x_1 curve for the CO₂ (1) – Perfluorohexane (2) binary mixture at 303 k.

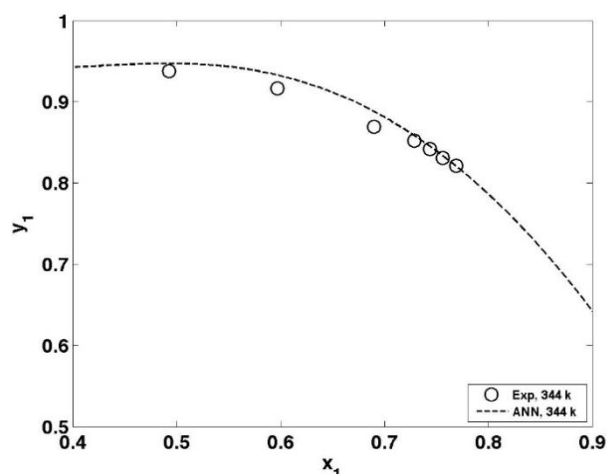


Fig. 9. y_1 - x_1 curve for the CO₂ (1) – 1-propanol (2) binary mixture at 344 k.

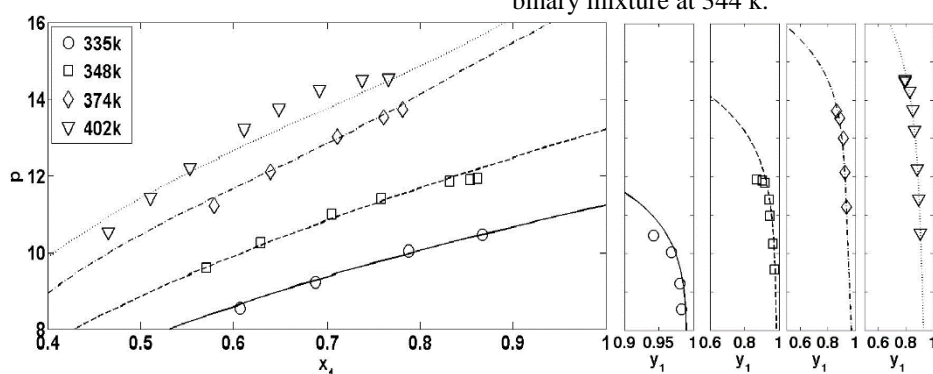


Fig. 10. p - x_1 - y_1 curve for the CO₂ (1) – 2-butanol (2) binary mixture at different temperatures.

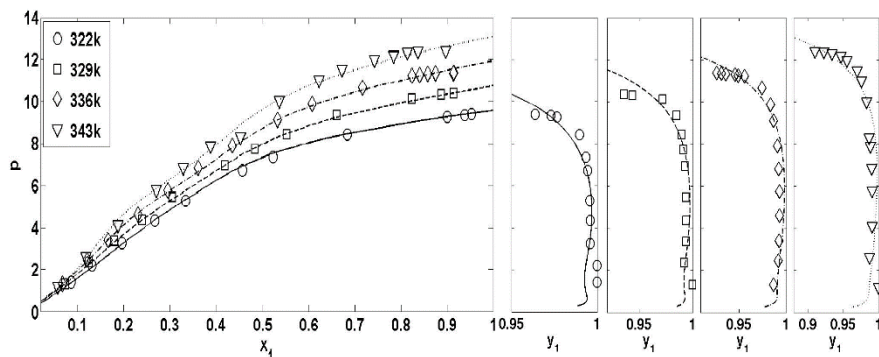


Fig. 11. p - x_1 - y_1 curve for the CO₂ (1) – 2-methoxyethanol (2) binary mixture at different temperatures.

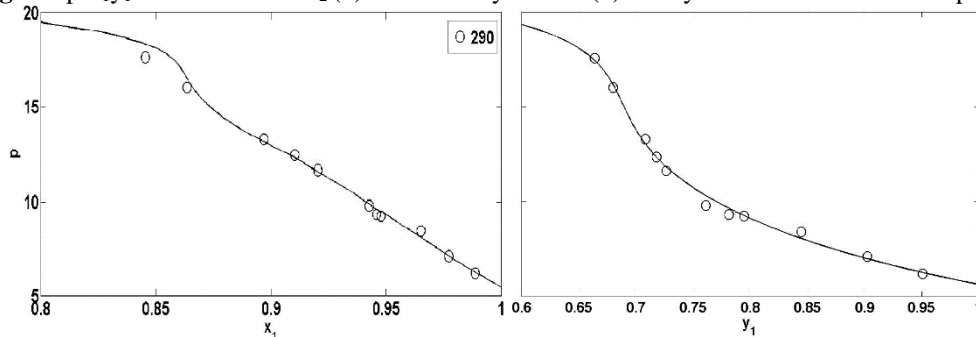


Fig. 12. p - x_1 - y_1 curve for the CO₂ (1) – H₂ (2) binary mixture at 290 k.

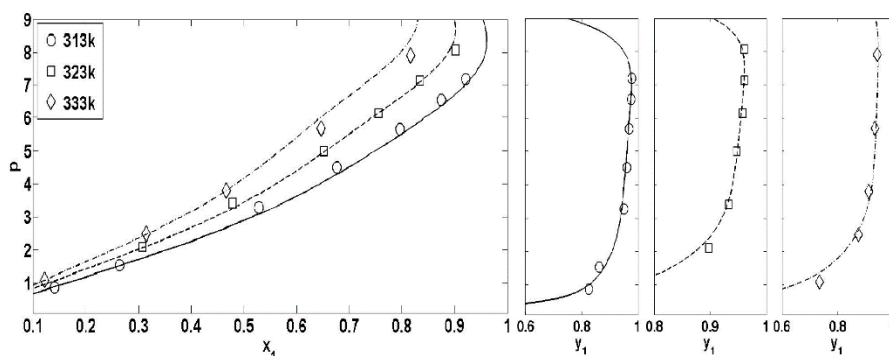


Fig. 13. p - x_1y_1 curve for the CO₂ (1) – R123 (2) binary mixture at different temperatures.

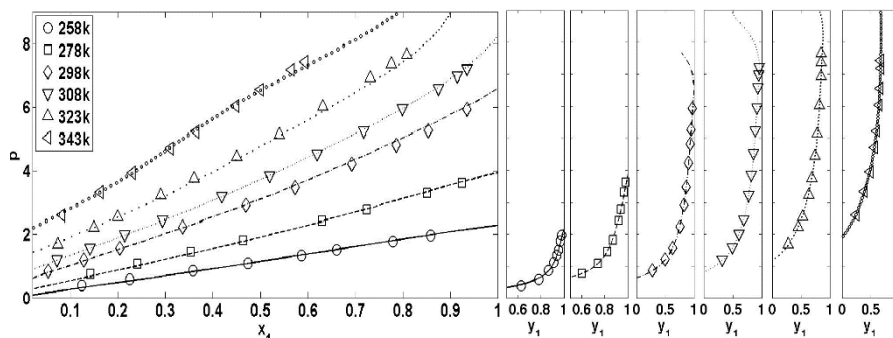


Fig. 14. p - x_1y_1 curve for the CO₂ (1) – R152a (2) binary mixture at different temperatures.

CONCLUSIONS

In this work, two comprehensive FFBP-ANN models were developed for the prediction of x_1 and y_1 data for fifty-six CO₂-containing binary mixtures at different temperature range. It was shown that good agreement between the model predictions and the experimental data was achieved.

The study and its results allow us to obtain these conclusions:

1. It was shown that in prediction of two VLE parameters by use of ANN for reducing the errors and increases the accuracy of ANN, two separate ANN for every parameter should be used.

2. The advantage of the ANN model is its applicability for the all fifty-six CO₂-containing binary mixtures in just two models, while the thermodynamic models are used for an especially binary mixture.

3. Use of ANN models for prediction of VLE data is less cumbersome way in comparison with thermodynamic models, especially in cases with no information about appropriate thermodynamic model.

4. The AAD (%) for the model I and model II were obtained 1.572 and 0.848 respectively. Therefore, the ANN model can be reliably used to estimate x_1 and y_1 for CO₂- binary systems within the ranges of parameters considered in this work.

Acknowledgements: The authors gratefully acknowledge to amir abbas pouladi for his help in this work.

REFERENCES

1. K. Tochigi, T. Namae, T. Suga, H. Matsuda, K. Kurihara, M. C. Ramos, C. McCabe, *J. Supercrit. Fluid*, **55**, 682, (2010).
2. A. Bejarano, J. E. Gutiérrez, K. a. Araus, J. C. de la Fuente, *J. Chem. Thermodyn.*, **43**, 759, (2011).
3. J.E. Gutiérrez, A. Bejarano, J.C.D.L. Fuente, *J. Chem. Thermodyn.*, **42**, 591, (2010).
4. R. Abedini, I. Zanganeh, M. Mohagheghian, *J. Phase Equilib. Diff.*, **32**, 105, (2011).
5. G. Silva-Oliver, L.A. Galicia-Luna, *Fluid Phase Equilib.*, **182**, 145, (2001).
6. K. Bezaehtak, G.B. Combes, F. Dehghani, N. R. Foster, D. L. Tomasko, *J. Chem. Eng. Data*, **47**, 161, (2002).
7. J.S. Lim, J.M. Jin, K.P. Yoo, *J. Supercrit. Fluid*, **44**, 279, (2008).
8. K. Jeong, J. Im, G. Lee, Y.J. Lee, H. Kim, *Fluid Phase Equilib.*, **251**, 63, (2007).
9. C. Zhu, X. Wu, D. Zheng, W. He, S. Jing, *Fluid Phase Equilib.*, **264**, 259, (2008).
10. I.P. Koronaki, E. Rogdakis, T. Kakatsiou, *Energ. Convers. Manage.*, **60**, 152, (2012).
11. H. Karimi, F. Yousefi, *Chinese J. Chem. Eng.*, **15**, 765, (2007).
12. C. Si-Moussa, S. Hanini, R. Derriche, M. Bouhedda, A. Bouzidi, *Braz. J. Chem. Eng.*, **25**, 183, (2008).
13. C.A. Faúndez, F.A. Quiero, J.O. Valderrama, *Fluid Phase Equilib.*, **292**, 29, (2010).
14. M. Safamirzaei, H. Modarress, Mohsen-Nia, *Fluid Phase Equilib.*, **289**, 32, (2010).
15. F. Eslamimanesh, A. Gharagheizi, A.H. Mohammadi, D. Richon, *Chem. Eng. Sci.*, **66**, 3039, (2011).

16. A. Sencan, I.I. Köse, R. Selbas, *Energ. Convers. Manage.*, **52**, 958, (2011).
17. A. Sozen, E. Arcaklioglu, T. Menlik, *Expert Syst. Appl.*, **37**, 1158, (2010).
18. Y. Bakhbaki, *Expert Syst. Appl.*, **38**, 11355, (2011).
19. C. Ming J. Chang, M. Shian Lee, B. chin Li, P.yen Chen, *Fluid Phase Equilibr.*, **233**, 56, (2005).
20. M. Akgu, N. A. Akgu, S. Dinc, *J. Supercrit. Fluid*, **15**, 117, (1999).
21. G. Silva-Oliver, L.A. Galicia-Luna, *Fluid Phase Equilibr.*, **199**, 213, (2002).
22. Ž. Knez, M. Škerget, L. Ilić, C. Lütge, *J. Supercrit. Fluid*, **43**, 383, (2008).
23. O. Elizalde-Solis, L.A. Galicia-Luna, S. I. Sandler, J. G. Sampayo-Hernández, *Fluid Phase Equilibr.*, **210**, 215, (2003).
24. W.H. Hwu, J.S. Cheng, K.W. Cheng, Y.P. Chen, *J. Supercrit. Fluid*, **28**, 1, (2004).
25. O. Elizalde-Solis, L.A. Galicia-Luna, L.E. Camacho-Camacho, *Fluid Phase Equilibr.*, **259**, 23, (2007).
26. T. Hiaki, H. Miyagi, T. Tsuji, M. Hongo, *J. Supercrit. Fluid*, **13**, 23, (1998).
27. S. N. Joung, C. W. Yoo, H. Y. Shin, S. Y. Kim, K. P. Yoo, C. S. Lee, W. S. Huh, *Fluid Phase Equilibr.*, **185**, 219, (2001).
28. W. Lin, H. Xiaosong, Z. Lan, C. Kaixun, *Chinese J. Chem. Eng.*, **17**, 642, (2009).
29. H. S. Lee, H. Lee, *Fluid Phase Equilibr.*, **150**, 695, (1998).
30. A. Bamberger, G. Sieder, G. Maurer, *J. Supercrit. Fluid*, **17**, 97, (2000).
31. K. Ohgaki and T. Katayama, *J. Chem. Eng. Data*, **21**, 53, (1976).
32. A. M. Scurto, C. M. Lubbers, G. Xu, J. F. Brennecke, *Fluid Phase Equilibr.*, **190**, 135, (2001).
33. S. Laugier, D. Richon, *J. Chem. Eng. Data*, **42**, 155, (1997).
34. P. Naidoo, J. D. Raal, D. Ramjugernath, *J. Chem. Eng. Data*, **55**, 196, (2010).
35. M. V. da Silva, D. Barbosa, P. O. Ferreira, *J. Chem. Eng. Data*, **47**, 1171, (2002).
36. L. Hongling, Z. Rongjiao, X. Wei, L. Yanfen, S. Yongju, T. Yiling, *J. Chem. Eng. Data*, **56**, 1148, (2011).
37. F. Gironi, M. Maschietti, *J. Supercrit. Fluid*, **70**, 8, (2012).
38. S. Schwinghammer, M. Siebenhofer, R. Marr, *J. Supercrit. Fluid*, **38**, 1, (2006).
39. L. Hongling, Z. Rongjiao, X. Wei, X. Hongfei, D. Zeliang, T. Yiling, *J. Chem. Eng. Data*, **54**, 1510, (2009).
40. C. Duran-Valencia, A. Valtz, L.A. Galicia-Luna, D. Richon, *J. Chem. Eng. Data*, **46**, 1589, (2001).
41. S.H. Huang, H.M. Lin, K.C. Chao, *J. Chem. Eng. Data*, **33**, 143, (1988).
42. J.H. Kim, M.S. Kim, *Fluid Phase Equilibr.*, **238**, 13, (2005).
43. F. Rivollet, A. Chapoy, C. Coquelet, D. Richon, *Fluid Phase Equilibr.*, **218**, 95, (2004).
44. A. Valtz, C. Coquelet, D. Richon, *Fluid Phase Equilibr.*, **258**, 179, (2007).
45. C. Duran-Valencia, G. Pointurier, A. Valtz, P. Guilbot, D. Richon, *J. Chem. Eng. Data*, **47**, 59, (2002).
46. H. Madani, A. Valtz, C. Coquelet, A. H. Meniai, D. Richon, *J. Chem. Thermodyn.*, **40**, 1490, (2008).
47. A. Valtz, X. Courtial, E. Johansson, C. Coquelet, D. Ramjugernath, *Fluid Phase Equilibr.*, **304**, 44, (2011).
48. M. Akgün, D. Emel, N. Baran, N.A. Akgün, S. Deniz, S. Dinçer, *J. Supercrit. Fluid*, **31**, 27, (2004).
49. W. Lin, L. Jian-cheng, Y. Hao, C. Kai-xun, *Chem. Res. Chinese U.*, **27**, 678, (2011).
50. D. Kodama, T. Yagihashi, T. Hosoya, M. Kato, *Fluid Phase Equilibr.*, **297**, 168, (2010).
51. Aspen Hysys 2006 Software- aspenONE.
52. P. Petersen, R. Fredenslund, A. Rasmussen, *Comput. Chem. Eng.*, **18**, 63, (1994).
53. C. Guimaraes, P.R.B. McGreavy, *Comput. Chem. Eng.*, **19**, 741, (1995).
54. R. Sharma, D. Singhal, R. Ghosh, A. Dwivedi, *Comput. Chem. Eng.*, **23**, 385, (1999).
55. S. Urata, A. Takada, J. Murata, T. Hiaki, A. Sekiya, *Fluid Phase Equilibr.*, **199**, 63, (2002).
56. S. Ganguly, *Comput. Chem. Eng.*, **27**, 1445, (2003).
57. K. Piotrowski, J. Piotrowski, J. Schlesinger, *Chem. Eng. Process.*, **42**, 285, (2003).
58. M. Bilgin, *J. Serb. Chem. Soc.*, **69**, 669, (2004).
59. S. Mohanty, *Fluid Phase Equilibr.*, **235**, 92, (2005).
60. S. Mohanty, *Int. J. Refrig.*, **29**, 243, (2006).
61. H. Yamamoto, K. Tochigi, *Fluid Phase Equilibr.*, **257**, 169, (2007).
62. H. Ghanadzadeh, H. Ahmadifar, *J. Chem. Thermodyn.*, **40**, 1152, (2008).
63. C.A. Faúndez, F.A. Quiero, J. O. Valderrama, *Chem. Eng. Commun.*, **198**, 102, (2011).
64. B. Zarenezhad and A. Aminian, *Korean J. Chem. Eng.*, **28**, 1286, (2011).
65. G. Zhang, B. E. Patuwo, M. Y. Hu, *Int. J. Forecasting*, **14**, 35, (1998).
66. H.J. Manohar, R. Saravanan, S. Renganarayanan, *Energ. Convers. Manage.*, **47**, 2202, (2006).
67. A. Malallah, I.S. Nashawi, *J. Petrol. Sci. Eng.*, **49**, 193, (2005).
68. M. Chakraborty, C. Bhattacharya, S. Dutta, *J. Membrane Sci.*, **220**, 155, (2003).
69. R. Beale, T. Jackson, *Neural Computing: An Introduction, Institute of Physics Publishing, London*, 1998.
70. A.R. Moghadassi, M.R. Nikkolgh, S.M. Hosseini, F. Parvizian, A. Sanaeirad, *Arpn-Jeas*, **6**, 100, (2011).

Appendix I. Physical properties for components used in this work ^a

Name	T _b (k)	T _c (k)	P _c (Mpa)	Acentricity
1-Butanol	390.90	563.10	4.42	0.5930
1-heptanol	449.80	632.00	3.16	0.5600
1-hexanol	430.20	611.00	3.47	0.5600
1-octanol	468.30	652.50	2.86	0.5870
1-pentanol	411.10	588.20	3.91	0.5790
1-Propanol	370.30	536.80	5.17	0.6230
2-butanol	372.70	536.10	4.17	0.5770
2-ethoxyethanol	408.15	567.00	4.23	0.7591
2-methoxyethanol	397.55	562.00	5.01	0.7311
2-methyl-1-propanol	381.00	547.80	4.20	0.5920
2-pentanol	392.15	552.00	3.87	0.6746
2-propanol	355.40	508.30	4.76	0.6650
3-methyl-1-butanol	405.20	579.40	3.92	0.5558
3-methyl-2-butanol	384.65	572.00	3.96	0.3510
3-pentanol	388.45	547.00	3.87	0.6748
Acetic acid	391.10	592.70	5.77	0.4470
a-pinene	429.29	632.00	2.76	0.2862
Benzene	353.24	562.10	4.92	0.2150
Chloroform	334.30	536.40	5.37	0.2180
Cyclohexanol	434.30	625.00	3.75	0.5280
Cyclohexanone	428.80	627.00	3.90	0.4480
Cyclopentanol	413.95	577.58	4.39	0.7738
Decanal	488.15	657.00	2.15	0.6416
DHAEE ^b	655.63	803.10	1.14	1.0797
DIPE	341.70	500.30	2.88	0.3310
Ethyl Butyrate	394.70	567.00	3.06	0.4610
EPAEE ^b	640.81	792.66	1.22	1.0102
Ethanol	351.40	513.90	6.15	0.6444
fenchone ^c	466.00	685.19	2.98	0.3335
H ₂	20.55	33.44	1.32	-0.1201
limonene ^c	449.00	659.48	2.75	0.3232
Methanol	337.80	512.60	7.38	0.5570
methyl acetate	330.40	506.80	4.69	0.3260
methyl linoleate	551.32	749.58	2.11	0.5699
methyl oleate	617.00	764.00	1.28	1.0490
methyl propionate	352.80	530.60	4.00	0.3500
m-xylene	412.27	617.05	3.54	0.3260
n-hexane	341.88	507.90	3.03	0.3007
N,N-dimethylformamide	426.15	647.00	4.42	0.3755
n-octacosane	704.76	832.00	0.85	1.2375
n-octane	398.82	568.60	2.50	0.4018
o-xylene	417.58	630.37	3.73	0.3023
propylene carbonate	515.05	778.25	5.40	0.6325
Perfluorohexane	329.80	448.80	1.66	0.5140
Propane	231.05	369.90	4.26	0.1524
P-xylene	411.51	616.26	3.51	0.3259
R32	221.50	351.60	5.82	0.2710
R-116	194.90	293.00	3.06	0.2451
R123	300.76	458.15	3.79	0.2931
R134a	246.93	374.15	4.06	0.3256
R152a	248.16	387.04	4.44	0.2557
R610	271.20	386.40	2.32	0.3740
styrene	418.31	636.00	3.84	0.2971
tertpentanol	375.50	545.00	3.95	0.4831
Tetrahydrofuran	337.00	540.10	5.19	0.2169
water	373.15	647.30	22.12	0.3440

^a Taken from Ref. [51]. ^b Taken from Ref. [19]. ^c Taken from Ref. [20].

Appendix II. Range of data used for developing of the ANN models.

Systems: CO ₂ (1) +	T/K	ΔP /Mpa	Δx_1	Δy_1
1-butanol	354,398,430,324,333,355,392,426,313	2.067-16.939	0.074-0.9031	0.7976-0.9959
1-heptanol	374,411,431	4.038-21.391	0.2173-0.87	0.8932-0.9978
1-hexanol	324,353,397,403,431,432	2.268-20.128	0.035-0.9008	0.801-0.9974
1-octanol	328	4-15	0.2406-0.7772	0.9435-0.9997
1-pentanol	313,323,333	1.81-11.72	0.091-0.76	0.968-0.998
1-propanol	344,373,397,426,313,323,333	2.15-15.769	0.095-0.835	0.54-0.993
2-butanol	335,348,374,402,431,313	4.03-14.536	0.2906-0.8965	0.7082-0.9946
2-ethoxyethanol	323,330,337,344	1.29-12.37	0.0788-0.969	0.9052-0.9999
2-methoxyethanol	322,329,336,343	1.19-12.4	0.0576-0.9535	0.9105-0.9999
2-methyl-1-propanol	313,323,333,313,323,333,343,353	2.11-14.04	0.094-0.9328	0.9294-0.9961
2-pentanol	313,313,323,333	1-10.587	0.025-0.985	0.9645-0.997
2-propanol	334,344,353,378,398,413,432,443	2.03-13.788	0.06-0.888	0.443-0.975
3-methyl-1-butanol	313,323,333	2.08-10.68	0.111-0.895	0.97-0.994
3-methyl-2-butanol	313,323,333	2.147-10.249	0.105-0.9055	0.9681-0.9956
3-pentanol	313,323,333	1.942-10.207	0.0957-0.9072	0.9678-0.9942
acetic acid	313,333,353	1.1-11.1	0.0964-0.7098	0.948-0.9952
a-pinene	313,323,333	7.15-10.93	0.478-0.908	0.983-0.9983
benzene	298,313	0.89383-7.7504	0.1063-0.9327	0.9754-0.9959
Chloform	303,313,323,333	0.032416-9.9689	0-1	0-1
cyclohexanol	433,473	3.55-21.5	0.089-0.602	0.84-0.947
Cyclohexanone	433,453	3.03-21.52	0.103-0.736	0.843-0.962
cyclopentanol	373,403	0.914-11.838	0.0177-0.3942	0.9264-0.9891
decanal	288,303,313	1.68-8.22	0.28-0.96	0.989-0.998
DHAE	313,333	4.24-23.54	0.5325-0.9443	0.9822-0.9999
diisopropyl ether	265,273,293,313,333	0.547-2.554	0.1127-0.7589	0.9269-0.9998
EB	313,333,353,373	2-12	0.18-0.9495	0.8153-0.9978
EPAAE	313,333	2.86-20.79	0.2842-0.9402	0.979-0.9999
ethanol	313,333,353,313,313,322,333,338,344	0.57-13.9	0.0269-0.9668	0.8068-0.9948
Fenchone	313,323,333	7.04-11.2	0.606-0.92	0.9808-0.9997
H ₂	278,290	4.805-19.253	0.8455-0.9912	0.4945-0.9575
limonene	313,323,333,323,343	7.04-13.5	0.429-0.93156	0.96053-0.9996
methanol	313,278,288,298,308,313,320,330,335,342,303	0.573-12.39	0.0247-0.935	0.0977-0.9982
methyl acetate	308,318,328	0.7-9	0.128-0.9802	0.892-0.9978
methyl linoleate	313,333	2.86-18.03	0.5217-0.9509	0.9806-0.9999
methyl oleate	313,333	2.86-18.03	0.4876-0.943	0.9812-0.9999
methyl propionate	313,333,353,373	1-12	0.3125-0.9058	0.3282-0.9887
m-xylene	313,333,353	0.7-10.37	0.04-0.6971	0.951-0.9754
n-hexane	298,313	0.44372-7.6578	0.0495-0.924	0.9253-0.9904
dimethylformamide	293,313,338	0.43-11.05	0.0345-0.8823	0.9874-0.9998
n-octacosane	573	0.99405-5.0574	0.0596-0.27	0.9957-0.9983
n-octane	313	0.52-3.522	0.0588-0.3905	0.9966-0.9979
o-xylene	313,333,353	0.79-14.86	0.0536-0.8345	0.8469-0.9756
PC	313,333,353,373	1-13	0.081-0.7279	0.952-0.9968
perfluorohexane	303,313,323	0.479-3.454	0.0911-0.5588	0.8467-0.9806
propane	253,263,273,283,293,303,313,323	0.2442-7.2062	0-1	0-1
P-xylene	313,333,353	0.61-12.37	0.04-0.8377	0.8228-0.9748
R32	283,293,303,305,313,323,333,343	1.106-7.464	0-1	0-1
R116	253,273,283,291,294,296	1.051-6.448	0-1	0-1
R123	313,323,333	0.873-8.074	0.1219-0.9209	0.7352-0.9788
R134a	252, 272, 292, 323,328,329,333,338,339,354	0.131-7.369	0-0.867	0-0.983
R152a	258,278,298,308,323,343	0.144-7.6482	0-1	0-1
R610	263,283,303,308,323,338,352	0.1823-6.8628	0.0218-0.9473	0.2418-0.983
styrene	333,338,343,348	6-13.42	0.428-0.932	0.895-0.998
tertpentanol	313,323,333,345	4.56-11.44	0.2409-0.9236	0.9253-0.9977
tetrahydrofuran	313,333,353,298,313	0.47-10.29	0.0687-0.983	0.9347-0.998
water	323,333,353	4.05-14.11	0.008-0.0217	0.9857-0.9966

МОДЕЛИРАНЕ ЧРЕЗ ИЗКУСТВЕНИ НЕВРОННИ МРЕЖИ НА БИНАРНИ СИСТЕМИ, СЪДЪРЖАЩИ ВЪГЛЕРОДЕН ДИОКСИД

С.Аташруз*, Х. Мишекар

Департамент по инженерна химия, Технологичен университет Амиркабир (Политехнически университет в Техеран), Кампус Махшахр, Махшахр, Иран.

Постъпила на 7 януари, 2013 г.; коригирана на 28 май, 2013 г.

Използвани се два математични модела, базирани на FFBP-ANN-невронни мрежи за предсказването на молните части на CO₂ в течна (x_1) и парова (y_1) фаза при равновесието течност-пари (VLE) за петдесет и шест бинарни смеси, съдържащи CO₂. За съставяне на моделите са използвани 2104 групи от данни, намерени в литературата. За тестването на моделите са използвани експериментални данни, неприлагани при ANN-тренирането. Предсказаните резултати, получени чрез невронните мрежи са сравнени с достъпни литературни данни и е намерено резонно съгласие с тях. Средните абсолютни отклонения, получени с модела ANN-I за молните части x_1 и с модела ANN-II за молните части y_1 са съответно 1.572 % и 0.848 %. Изследването показва, че моделирането с невронни мрежи е добър алтернативен метод за оценяването на фазовите равновесия за този тип системи.

The effect of temperature on rate of bacterial oxidation of Fe(II)

D. Tekin^{1*}, S. Yörük¹, Y.K. Bayhan²

¹ Faculty of Engineering, Department of Environmental Engineering, Atatürk University, 25240 Erzurum, Turkey

² Faculty of Engineering, Department of Chemical Engineering, Atatürk University, 25240 Erzurum, Turkey

Received February 7, 2013; Accepted March 26, 2013

In this study, the effect of temperature on the rate of bacterial oxidation of Fe (II) at different microbial concentrations has been investigated. Reactions were carried out by using r4A1FC2B3 strain of *Acidithiobacillus ferrooxidans* at 15, 25 and 35 °C and maximum bacterial activity, thus maximum oxidation rate, was reached at 35 °C. At this temperature, the lag phase, the adaptation period of the bacteria, was very short and oxidation started immediately. The average bacteria count determined by microscopic method was 2.321×10^6 cells/mL.

Key words: Fe (II), bacterial oxidation, *Acidithiobacillus ferrooxidans*, effect of temperature

INTRODUCTION

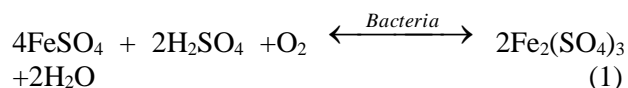
The bioleaching involves the extraction of metallic compounds from ores and concentrates by using the catalyst effects of microorganisms under normal pressure and between 5-90 °C. It is a simple, efficient and environmentally friendly method to process ores and has been successfully applied in the industrial scale for the recovery of copper, gold and uranium over 25 years. The process utilizes water, air, and microorganisms which all can easily be found from the environment [1,2].

Belonging to the chemotrophic organisms, *Acidithiobacillus ferrooxidans* are the most used bacteria in the bioleaching process. The organism is rod shaped, non-spored, a gram-negative, self spontaneous, single pole whipped. It uses carbon dioxide as the carbon source and ammonium as nitrogen source [3-5]. Espejo et al.[6] studied the oxidation of Fe(II) and elemental sulfur by both, adsorbed and non-adsorbed *A. ferrooxidans* on solid surface. Nestor et al.[7] investigated the leaching mechanisms of refractory gold minerals by *A. ferrooxidans*. Mason and Rice [8], following an adaptation process, studied the leaching of iron and nickel from Ni-Fe(II)-FeS and Cu-Ni-Fe concentrates by using *A. Ferrooxidans*.

Sand et.al.[9] studied the bacterial leaching of metal sulfides by different bacteria and observed diverse effects of different bacteria on leaching and the generation of sulfuric acid and Fe(III) ions by bacteria such as *Acidithiobacillus ferrooxidans*, *Leptospirillum ferrooxidans* and *Sulfolobus/*

Acidionus. Ojumu et al. [10] presented a review on published studies and related rate equations for microbial ferrous-iron oxidation. They reported a broad range of kinetics models and large discrepancies on kinetics constants. They also indicated the lack of data on the effects of some factors such as pH and temperature on biooxidation.

As the case for chemical reactions, biological reactions are also temperature dependent. However, unlike chemical reactions, the rate of biological reactions starts decreasing over a certain temperature and it is important to determine optimum reaction temperature where the rate is maximum. Bosecker [11] found out that, with the *Acidithiobacillus ferrooxidans* the rate of oxidation of Fe(II) was lower temperatures. In lower temperatures, there is a reduction in the extraction of metals. However, at higher temperatures thermophilic bacteria can be used for leaching. The bacterial oxidation of ferrous iron is based on the reaction:



EXPERIMENTAL

Bacteria and Medium

The bacteria *Acidithiobacillus ferrooxidans* which are non-spore cells growing under aerobic conditions were obtained from acid mine drainages. The bacteria, also used by Kocadağistan [12], were the type r4A1FC2B3 modified by the use of 9K33 growth medium of 9K by Silverman and Lundgren [13]. The medium was sterilized by autoclaving,

* To whom all correspondence should be sent:
E-mail: deryatekin@atauni.edu.tr

where the basal salt and iron solution being autoclaved separately and combined when cool. In order to reduce the precipitation of ferric iron, 10 N H₂SO₄ was added to the iron solution. Cultures of *r4A1FC2B3* were incubated in 500-mL Erlenmeyer flasks each containing 200 mL of 9K medium and 10% (v/v) inoculum at a constant temperature of 30°C on a rotary shaker at 200 rpm.

Preparation of Cell Suspension

Cultures of *r4A1FC2B3* grown under the conditions already described were used to prepare the cell suspension. Bacteria were harvested toward the end of their exponential phase of growth (36–48 h after inoculation). In order to remove the insoluble ferric iron compounds, the cultures were filtered. Cells were washed twice with 10 mL of a solution of sulfuric acid (pH 2.0) to remove the remaining ferric iron. The cell pellet was finally suspended in 6 mL of a sulfuric acid solution of pH 2.0. In order to make cell suspensions of different concentrations, different volumes of *r4A1FC2B3* culture were used. Before using a cell suspension in initial-rate experiments, its bacterial concentration was determined.

Bacterial oxidation experiments

Bacterial oxidation experiments of Fe(II) were carried out in a shaker of the type ROSI 1000 Thermolyne Orbital Shaking Incubator. During the experiments, several samples at certain intervals were taken for Fe(II) and Fe(III) analyses. For Fe(II) analyses, Shimadzu UV160A spectrophotometer was used. Fe(III) analyses were completed by titration using EDTA solution with sulfosalisilic acid indicator.

RESULTS AND DISCUSSION

The growth of bacteria was followed by microscopic method proposed by Gürgün and Halkman [14]. The average count of bacteria was found to be $2,321 \times 10^6$.

Since in the isolation experiments of the *r4A1FC2B3* bacteria strain, the bacteria was adapted to 15, 25 and 35 Celsius degrees, the effect of temperature on the bacterial oxidation of Fe(II) is investigated with experiments at these temperatures. All experiments were made using the pH value of 2 and repeated for each bacterial concentration. In each experiment Fe(II) and Fe(III) analysis were made at different times and the results obtained are shown at Figure 1-4. As seen from the Figures, maximum oxidation was obtained at 35°C. This was in agreement with others, that the maximum temperature for bacteria to grow is pH

dependent, and found to be 45°C over the pH range of 2.5 to 3.5 and 35°C at a pH of 1.5 [15,16], where maximum temperature for bacteria to grow is pH dependent and a lower optimum temperature with decreasing pH was expressed [16].

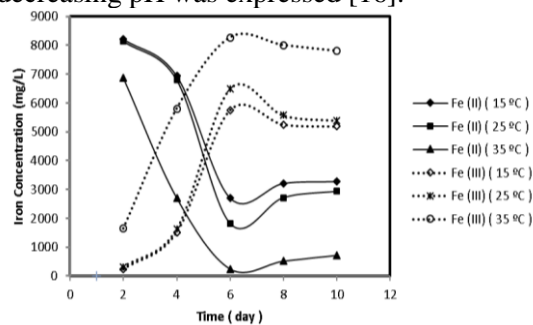


Fig. 1. Concentrations of Fe(II) and Fe(III) vs. time, for different temperatures (For initial bacteria conc. $0,5 \times 10^5$ cells/ml)

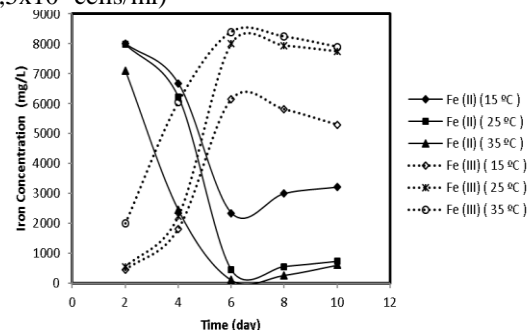


Fig. 2. Concentrations of Fe(II) and Fe(III) vs. time, for different temperatures (For initial bacteria conc. 1×10^5 cells/ml)

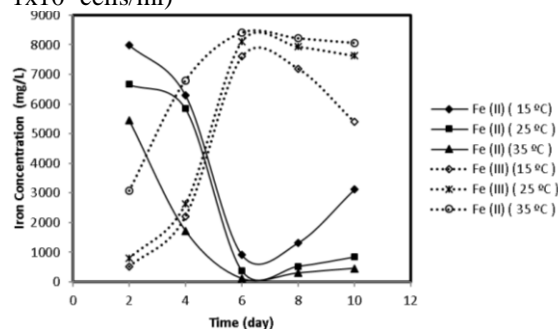


Fig. 3. Concentrations of Fe(II) and Fe(III) vs. time, for different temperatures (For initial bacteria conc. $1,5 \times 10^5$ cells/ml)

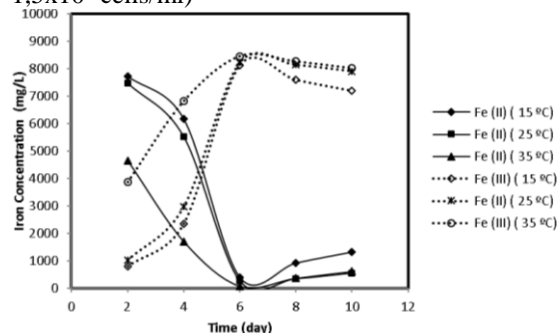


Fig. 4. Concentrations of Fe(II) and Fe(III) vs. time, for different temperatures (For initial bacteria conc. 2×10^5 cells/ml)

CONCLUSIONS

From the Figures 1-4 obtained for the bacterial oxidations of Fe(II) at 15 °C, 25 °C and 35 °C, the following conclusions may be drawn.

Highest conversion of Fe(II) was reached at the end of the 6th day. For the experiments carried out at 15 °C by adding 0.5 mL bacteria initially, concentration of Fe(II) was 8,210 mg/L at the end of the 2nd day which dropped to 2,706 mg/L at the end of 6th day. However, the corresponding concentration values of Fe(II) at 25°C were 8,150 mg/L and 1,820 mg/L, whereas for 35°C, Fe(II) concentrations were 6875 mg/L and 516 mg/L at the end of 2nd and 6th day, respectively.

When 1 ml of bacteria is added initially, these values of Fe(II) dropped from 8,009 mg/L to 2,350 mg/L for 15°C, from 7,993 mg/L to 446 mg/L for 25°C and from 7,100 mg/L to 116 mg/L for 35°C. For an initial bacteria concentration of 1.5 ml, the Fe(II) concentrations at the end of 2nd and 6th day were 7,991 mg/L and 912 mg/L for 15°C, 7,660 mg/L and 374 mg/L for 25°C, 5,449 mg/L and 106 mg/L for 35°C. If the initial concentration of bacteria increases to 2 mL, corresponding Fe(II) concentrations of 7,726 mg/L and 392 mg/L for 15°C, 7,465 mg/L and 265 mg/L for 25°C and 4,649 mg/L and 66 mg/L for 35°C were obtained.

REFERENCES

1. B.P. Gilbertson, *Mineral Processing and Extractive Metallurgy*, **109**, 61 (2000).
2. H. Brandl, Microbial leaching of metals. In: Rehm H.J. (ed.), *Biotechnology*, Wiley-VCH, Weinheim, 2001, p. 191.
3. J.A. Brierly, C.L. Brierly, *Can. J. Microbiol.*, **19**, 183 (1973).
4. A. Sandström, S. Petersson, *Hydrometallurgy*, **46**, 181 (1997).
5. M.E. Clark, J.D. Batty, C.B. Van Buuren, D.W. Dew, M.A. Eamon, *Hydrometallurgy*, **83**, 3 (2006).
6. R.T. Espejo, B. Escobar, E. Jedlicki, P. Uribe, R. Badilla-Ohlbaum, *Applied and Environmental Microbiology*, **54**, 1694 (1988).
7. D. Nestor, U. Valdivia, P.A. Chaves, *Int. J. Miner. Process.*, **62**, 187 (2001).
8. L.J. Mason, N.M. Rice, *Minerals Engineering*, **15**, 795(2002).
9. W. Sand, T. Gehrke, P.G. Jozsa, A. Schippers, *Hydrometallurgy*, **59**, 159 (2001).
10. T.V. Ojumu, J. Petersen, G.E. Searby, G.S. Hansford, *Hydrometallurgy*, **83**, 21 (2006).
11. K. Bosecker, *FEMS Microbiology Reviews*, **20**, 591(1997).
12. E. Kocadağistan, Biorecovery of copper ore from Cayeli(Turkey), Ph Thesis, Ataturk University, Erzurum, 2007.
13. M.P. Silverman, D.G. Lundgren, *J. Bacteriol.* **77**, 642 (1959).
14. V. Gürgün, K. Halkman, Gıda teknolojisi dergisi, 7 Ankara, 1990.
15. M. Nemati, S.T.L. Harrison, *Journal of Chemical Technology and Biotechnology*, **75**, 526 (2000).
16. L. Ahonen, O.H. Tuovinen, *Appl. Environ. Microbiol.* **55**, 312 (1989).

ВЛИЯНИЕ НА ТЕМПЕРАТУРАТА ВЪРХУ СКОРОСТТА НА БАКТЕРИАЛНО ОКИСЛЕНИЕ НА Fe(II)

Д. Текин*, С. Йорюк¹, Й.К. Байхан

¹ Департамент по екологично инженерство, Факултет по инженерство, Университет Ататюрк, Ерзорум, Турция

² Департамент по химично инженерство, Факултет по инженерство, Университет Ататюрк, Ерзорум, Турция

Постъпила на 7 февруари, 2013 г.; приета на 26 март, 2013 г.

Ш настоящата работа се изследва скоростта на бактериално окисление на Fe (II) при различни концентрации на микроорганизми. Реакциите са извършени с шам r4A1FC2B3 на *Acidithiobacillus ferrooxidans* при 15, 25 и 35°C. Максимална микробна активност и съответно скорост на окисление са постигнати при 35 °C. При тази температура лаг-фазата (периодът за адаптиране) на бактериите е много кратък и окислението започва незабавно. Средният брой на бактериите е 2.321×10^6 клетки/мл.

Hydrodesulfurization of thiophene on the CoMo/Al₂O₃ catalyst modified by coking pretreatment

Bl. V. Itoua^{1, 2*}, C. Vladov¹, P. Ongoka², L. Petrov³

¹ Institute of Catalysis, Bulgarian Academy of sciences, Sofia 1113, Bulgaria

² Ecole Normale Supérieure BP 237, Université Marien Ngouabi, Brazzaville- Congo ;

³ SABIC Chair of Catalysis, Chemical and Materials Engineering Department, Faculty of Engineering, King Abdulaziz University, Jeddah, Kingdom of Saudi Arabia

Received: March 13, 2013; revised: September 21, 2013

The activity of a commercial CoMo/Al₂O₃ catalyst was examined in the reaction of thiophene hydrodesulphurization. The catalytic measurements were performed in a gradientless flow circulating system at atmospheric pressure. It was found that preliminary coking of the catalyst lead to a considerable decrease of its hydrodesulphurization activity while the selectivity to butane increases. It is also found that the catalyst coking pretreatment reduces its surface, and the formation of monolayer coke and dendrites is observed. It's possible at special conditions of catalyst coking, to increase the selectivity and therefore output of some products in the reaction.

Keywords: activity; Cobalt-molybdenum/alumina; catalyst; coking pretreatment; thiophene hydrodesulphurization

INTRODUCTION

The main reasons for the deactivation of Co-Mo/Al₂O₃ catalysts are the coke formation, the adsorption of the nitrogen containing compounds and heavy metals on their surface [1]. A broad area in the literature is also devoted to the question of the influence of coke on the physico-chemical properties of the heterogeneous catalytic systems including Co-Mo catalysts [2]. During the formation of coke part of the active centers of catalysts are blocked and their activities decreases. The study of the mechanism of the formation of coke becomes complicated owing to the fact that, the precursors of coke can be reagents, intermediates and the products of the reaction. The effect of coke on the selectivity of these catalysts is not well elucidated and carbonaceous deposit influence differently sites on the catalytic surface [3]. In some cases it can be shown that the reduction of the general activity of the catalyst is beneficial to its selectivity. The coking pretreatment of catalyst is one of method to study the influence of coke formation on their physico-chemical properties. Such pretreatment of heterogeneous catalysts use various types of coking agent like anthracene, naphthalene and cyclohexene [4], phenanthrene [5], toluene [6], butene [7],

butadiene [8], propene and toluene [9], acetylene [10]. The present work studies the effect of coking on the catalytic properties of CoMo/Al₂O₃ hydrotreating catalysts, using toluene as a coking agent.

EXPERIMENTAL

Catalyst

An alumina supported cobalt-molybdenum industrial catalyst 5AKM, (Russian product) was used for all the experiments. The composition of active parts of catalyst in wt.% is CoO 4 % , MoO₃ 13 % , Fe₂O₃ 0,13 %.

Catalytic activity measurements

The catalytic activity was measured at atmospheric pressure in a metal flow-circulating gradientless system connected directly to a gas chromatograph by means of a 6-way valve. The circulating contour was kept at a constant temperature of 110°C [15]. Thiophene hydrodesulphurization was used as a model reaction. All runs were carried out in the 200 – 425 °C range with excess hydrogen. The hydrogen–thiophene volumetric ratio at the reactor inlet was 30:1. The thiophene Gas Hourly Space Velocity (GHSV) was 33.5 h⁻¹. The temperature in the reactor was maintained within ± 1.0°C accuracy. Product selectivities were estimated as a ratio between the

* To whom all correspondence should be sent:
E-mail: itoua_63@yahoo.fr

reaction rate of production of the corresponding product and the sum of the reaction rates of all products.

Experimental confirmation that the reaction proceeded in the kinetic region was obtained by carrying out experiments with differently sized catalyst grains and by calculating Weisz's criterion [16] which was less than 1.

The reactor was loaded with 1 g of catalyst of 0.1 mm size. Thiophene was introduced into the reactor with a Gilson 302 pump. Hydrogen was admitted within 1% accuracy using a Matheson electronic mass flow controller.

The catalyst activation of samples were treated in a routine way prior to the activity measurements. The procedure involved drying for 1 h at 120°C in a flow of purified hydrogen at rate of 60 ml.h⁻¹. After that the temperature was slowly raised to 400° C and the catalyst is reduced at the same temperature for 2 h. Catalyst sulphidisation was performed at 400° C for 2 h using a hydrogen-hydrogen sulfide gas mixture (9:1) at a flow rate of 70 ml.h⁻¹.

After activation the hydrogen sulfide flow was stopped and the temperature was lowered to the operating range for 1 h. After this preliminary operation the activity measurements were started.

Coking pretreatment of catalyst

Different tests were providing preliminary to find optimal conditions of coking. Various liquid toluene flows (1.2, 2.4 and 3.6 ml.h⁻¹) were used at different coking times (2, 3, 4 and 20h). Regarding the requirements of the equipment and the proceeding conditions of HDS reaction, the optimal toluene flow selected for precoking was 1.2 ml.h⁻¹.

Coking was carried out in the same reactor after the activation of catalyst. The coking agent used was toluene. The conditions of catalyst coking are as follows: reaction temperature = 450°C; feed rate of toluene = 1, 2 ml.h⁻¹. The process proceeds in a flow of Ar at a flow rate of 1700 ml.h⁻¹. Before introducing toluene, the catalyst is flushed with Argon for 15 min.

Analytical methods

The reaction products were analyzed using online gas chromatograph (Tsvet 104) equipped with a thermal conductivity detector and six ports sampling valve. Reaction products were separated using two columns one for the analysis of thiophene at a column temperature of 110°C (2 m long column packed with 10% Carbowax 1500 on Chromosorb W) The second column (8 m long, packed with 20% oxidipropionitrile on Diatomite C) was used to analyze hydrogen sulphide and C4 hydrocarbons, at

15 °C. Hydrogen was used as a carrier gas at a rate of 40 ml min⁻¹ [17].

Electron spin resonance (ESR) spectra were recorded on a Bruker 200 D instrument at room temperature in the 0-5000 G range. All the spectra were acquired under similar conditions.

RESULTS AND DISCUSSION

For quantitative measurement of deposited coke ESR technique were used. Figure 1 shows the Electron Spin Resonance (ESR) spectra of the standard activated carbon and of the coke in the catalyst (curves 1 and 2).



Fig. 1. ESR signal of standard activated carbon and of coke on the catalyst

Figure 2 presents the number of paramagnetic particles formed versus coking time. The curve has three different regions. The initial coking process starts slowly and after 1.5 h it is accelerated substantially until 5th h. Up to 5 h the curve grows as a straight line to 20h. The explanation of this behavior of the catalyst is following. In the first two hours a few coking centers are formed on the catalyst surface of the fresh catalyst. After reaching some critical value of the formed coking centers period a fast deposition of coke on those centers proceeds in the second period. In the third period formation of new coking centers on the less active catalyst centers followed by deposition of additional coke on them is evident.

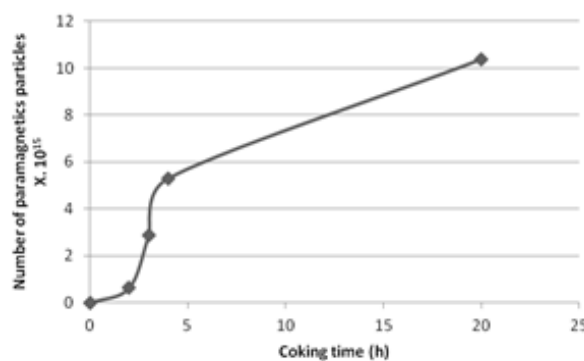


Fig. 2. Number of paramagnetic particles formed versus coking time

Figure 3 presents the dependence of the rate of thiophene decomposition at 350°C on the number of

paramagnetic particles formed on the catalyst surface at different coking time. The reduction in the activity of the catalyst is almost proportional to the increase in the number of paramagnetic particles. This dependence has also three divisions, which correspond to divisions in the curve on Figure 2. In the first period of time a linear fast decrease of the reaction rate is observed because most active catalyst active centers are blocked. In the second period reaction rate is constant which means that the coke is deposited on initially formed coking centers. After multi layers coke deposit was formed in the third period steady decrease of reaction rate was observed due to constant rate of blocking the less active surface active centers.

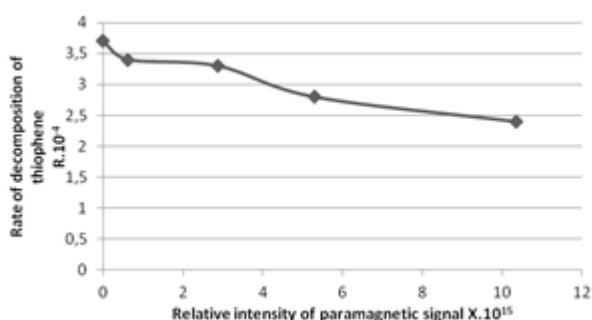


Fig. 3. Dependence of the rate of decomposition of thiophene with the relative intensity of paramagnetic signal (relative quantity of coke)

Figure 4, shows the dependence of the rate of decomposition of thiophene on temperature for fresh and coked catalyst for 3 h with $2,87 \cdot 10^{15}$ paramagnetic particles deposited. For the two samples the dependence has the same character. This clearly indicates that the mechanism of the process does not change after the coking of catalyst. With the increase in temperature, the rate of decomposition of thiophene increases. For all temperatures studied, fresh catalyst's activity is 15 % higher than the coked sample.

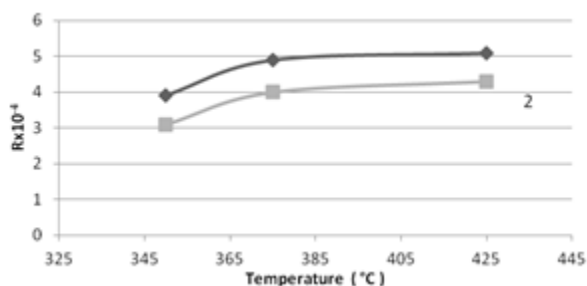


Fig. 4. Dependence of the rate of decomposition of thiophene with temperature of reaction. 1 - fresh catalyst, 2 - coked catalyst for 3 hours

To have an idea about the way in which deposited coke is located on the surface of the catalyst, we have measured its specific surface at different period of coking. Figure 5 presents the dependence of the surface area of the catalyst from quantity of coke deposited defined by the intensity of the signal $g=2.004$.

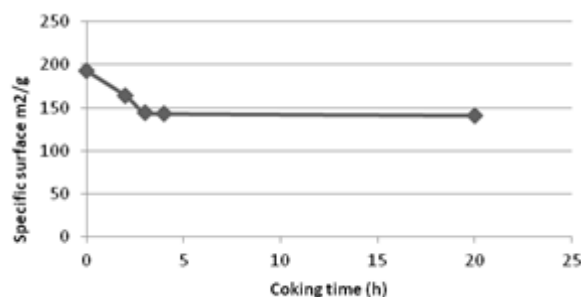


Fig. 5: Surface area of the catalysts coked at different time

It is seen that specific surface area decreases quickly at the beginning of coking process until approximately the third hour corresponding to $2,87 \cdot 10^{15}$ paramagnetic particles. With the increase in the quantity of coke after 20 h of coking, there is very small changes of the surface area of the catalyst, nevertheless there is an increased in the quantity of coke deposited on its surface. The results presented on figure 2 confirms the suggestion of monolayer-multilayer growth of coke on the catalyst surface [11]. The rate of thiophene decomposition is reduced by coke deactivation. On figure 5 the specific surface is practically unchanged up to 5 h. Probably multilayer coke is formed and not occupied all catalyst surface [12]. The influence of this coke is not sensitive on the specific surface.

Table 1 shows the selectivity of each product in the reaction at various temperatures for catalyst coked for 3h and for fresh sample. It can be seen that, at the same temperature the butane selectivity of coked catalyst is higher than that of the fresh sample. With the increasing of temperature the butane selectivity of both samples grows, however at the same degree of thiophene conversion carried at low temperature, the butane selectivity of the coked sample is higher than that of the fresh sample. The higher butane selectivity of coked catalyst compared to that of the fresh sample shows that, under the conditions of our tests, coking has little influence on the hydrogenation sites. This behavior can be explained by the observations reported in [13, 14]. The formation of coke on the catalyst surface not concerns all its surface. Part of catalyst sites preserve its activity.

Table 1. Selectivities on the different hydrocarbon reaction products during the HDS of thiophene decomposition on catalyst coked for 3h and for fresh catalyst

Catalyst	T °C	Butane	1-butene	Trans- 2- butene	Cis-2- butene
Fresh	350	0,31	0,12	0,32	0,2
Coked		0,43	0,08	0,29	0,18
Fresh	375	0,33	0,17	0,3	0,2
Coked		0,55	0,08	0,2	0,14
Fresh	425	0,42	0,15	0,25	0,17
Coked		0,71	0,05	0,12	0,09

Other studies show that the formation of coke on the surface of Co-Mo/Al₂O₃ catalysts does not influence the process of adsorption and desorption of the reagents and the products on the virgin surface of catalyst [14]. Our results confirms the existence of several types of active centers, which are influenced by the formation of coke obtained during the reaction of hydrogenation.

The selectivity of butylene-1 of coked catalyst is smaller than that of fresh catalyst at the same temperature of reaction. That is in line with the observation of high hydrogenation rate on coked catalysts. With the increase of the temperature, the selectivity of the fresh sample increases whereas that of the coked sample decreases. The higher butene-1 selectivity of fresh catalyst can be explained by the high temperature dependence of the activity of the active sites of hydrodesulfurization on temperature compared to those of hydrogenation and isomerization active sites. The low butylene-1 selectivity of coked catalyst shows that, after coking the rate of butane-1 rate formation is significantly reduced due to decrease of rate of decomposition of thiophene compared to that of hydrogenation and isomerization reactions.

After coking, the cis-2-butylene and trans-2-butylene selectivities decrease which shows that, coking led also to partial deactivation of the isomerization centers. The selectivities of these products decrease with the increase in the temperature, which is a proof that the rate of conversion of butylene-1 into butane increases more quickly than its isomerization to cis-2-butylene and trans-2-butylene.

CONCLUSION

On the basis of the results obtained, following conclusions can be made:

There are three periods of coking of hydrodesulfurization CoMo/Al₂O₃ catalyst in which catalyst deactivation is proceeding by different mechanisms.

Most of deposited coke forms multi-layer coke coverage of the surface, mainly during second and third period of coking.

The three types of active centers: hydrodesulphurization, hydrogenation and isomerization, are deactivated in different way during catalyst coking. The centers of hydrodesulphurization and isomerization are not very sensitive to coke while the centers of hydrogenation are more sensitive. That gives the possibility, by a partial deactivation of the catalyst to influence on its selectivity and respectively on the output of the various products of the reaction.

REFERENCES

- 1 D. Song, S. Jeong, F.E. Massoth, *Catal.Today*, **37**, 267 (1997)
- 2 J.H. Koh, J.J. Lee, H. Kim, A. Cho, S.H. Moon, *Appl. Catal. B: Environmental*, **86**, 176 (2009)
- 3 S. Hatanaka, M. Yamada, O. Sadakane, *Ind. Eng. Chem. Res.*, **37**, 1748 (1998)
- 4 S.-K. Song, S.-K. Ihm, *Korean J. Chem. Eng.*, **20**, 284 (2003)
- 5 A.W. Scaroni, R.G. Jenkins, P.L. Walker, Jr., *Appl. Catal.*, **14**, 173 (1985)
- 6 Magnoux P., Canaff. C Machado F., Guisnet M., *J. Catal.* **134**, 286- (1992)
- 7 R.T.K. Baker, M.A. Barber, P.S. Harris, *J. Catal.* **26**, 51 (1972)
- 8 J.A. Pena, A. Monzon, J. Santamaria, *J. Catal.* **142**, 59 (1993)
- 9 A. Orteaga, J.L.G. Fierro, P. Grange, B. Delmon, *Appl. Catal.*, **34**, 89 (1987)
- 10 R.T.K. Baker, R.J. Waite, *J. Catal.* **37**, 101 (1975)
- 11 I. S. Nam, J. R Kitrell, *Ind. Eng. Chem. Res. Dev.*, **23**, 237 (1984)
- 12 J. V. Sanders , J. A. Spink and S.S. Pollack , *Appl. Catal.*, **5**, 65 (1983)
- 13 K. J. Klingsman, H. H. Lee, *AIChE J.*, **32**, 309 (1986)
- 14 R. Ramachandran , F. E. Massoth , *Chem. Eng. Commun.*, **18**, 239 (1982)
- 15 L. Petrov, Ch. Vladov, D. Shopov, *Bull. Soc. Belg.*, **96**, 643 (1987)
- 16 P. Weisz, *Z. Phys. Chem.*, **II**, 1 (1957)
- 17 L. Petrov, Ch. Vladov, D. Shopov in: D. Shopov, A. Andreev, A. Palazov, L. Petrov (Editors), Proc. 4th Int. Symp. Heterogeneous Catal., Varna, 1979, Part II. Publishing House of Bulgarian Academy of Sciences, Sofia, 1973, p.303 (in Russian).

ХИДРООЧИСТКА НА ТИОФЕН ВЪРХУ CoMo/Al₂O₃ КАТАЛИЗАТОР, МОДИФИЦИРАН ЧРЕЗ ПРЕДВАРИТЕЛНА КОКСУВАЩА ОБРАБОТКА

Бл. В. Итуа^{1,2}, Ч. Владов¹, П. Онгока², Л. Петров³

¹ *Институт по катализ, Българска академия на науките, София 1113, България*

² *Висше училище ВР 237, Университет Мариен Нгуаби, Бразавил, Конго;*

³ *Департамент по химично и материално инженерство, Факултет по инженерство, Университет крал Абдулазиз, Джеда, Кралство Саудитска Арабия*

Постъпила на 13 март, 2013 г.; преработена на 21 септември, 2013 г.

(Резюме)

Активността на търговски CoMo/Al₂O₃ катализатор бе изследвана в реакцията на хидроочистка на тиофен. Каталитичните измервания се извършваха в циркулираща безградиентна система при атмосферно налягане. Установено бе, че предварително коксуване на катализатора води до значително намаляване на активността му, докато селективността по отношение на бутана се увеличава. Установено бе също така, че предварителното третиране на катализатора чрез коксуване намалява неговата повърхност и се наблюдава образуването на монослой от кокс и дендрити. Възможно е при специални условия на коксуване на катализатора да увеличи селективността и следователно добива на някои продукти на реакцията.

Synthesis and evaluation of some substituted pyrazole derivatives of biological interest

S.R. Pattan^{1*}, P.V. Patel¹, G.S. Athare¹, A.B. Jagnar¹, S.A. Nirmal³, J.S.Pattan²

¹Department of Pharmaceutical Chemistry, Pravara Rural College of Pharmacy, Loni, MS, India-413736.

²Dept of Biotechnology-PVP Arts, Science, Commerce College, Loni-MS, India-413713

³Department of Pharmacognosy, Pravara Rural College of Pharmacy, Loni, MS, India-413736

Received November 7, 2012; Revised February 27, 2013

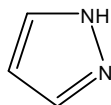
Pyrazole and their derivatives are found to have profound biological activity. In the present work some novel substituted pyrazole derivatives were synthesized. Pyrazole are synthesized by treating ethyl bis [methylthio] -2-cyanoacrylate with hydrazide derivatives. The derivatives of pyrazole were prepared by Schiff base reaction. All the synthesized compounds were characterized by IR, ¹H-NMR and Elemental Analysis. All the newly synthesized derivatives were evaluated for antimicrobial activity on different micro-organisms (*E.coli*, *S. aureus*, *A.niger*, *C. albicans*) at the concentration of 200 µg/mL by using cup-plate agar diffusion method. The activity was measured in terms of zone of inhibition and compared with standard drug ciprofloxacin for antibacterial and griseofulvin for antifungal activity. These compounds were also evaluated for antitubercular activity (*M. tuberculli*) at 25, 50 and 100 µg/mL concentrations. All the compounds were screened for *in-vitro* anti-inflammatory activity at different concentration like 200 µg/ml, and 300 µg/ml, by inhibition of protein denaturation method. Ibuprofen was used as standard drug. Potent compounds were screened for *in vivo* anti-inflammatory activity in albino rats at 200 µg/ml concentration to confirm the results.

Keywords: Pyrazoles; Antibacterial; Antitubercular and Anti-inflammatory.

1. INTRODUCTION

Pyrazoles

Pyrazoles refers to the class of heterocyclic compounds characterized by 5 – membered aromatic ring structure composed of three carbon atoms and two nitrogen atoms in adjacent positions, of two nitrogen atoms one basic nitrogen and neutral nitrogen, the aromatic nature arises from the four electrons and the unshared pair of electrons on the –NH nitrogen.



pyrazole

Pyrazole derivatives have a long history of application in agrochemicals as herbicides and insecticides and in pharmaceutical industry as antipyretic and anti-inflammatory. Antipyrine is the one of the earliest synthetic drugs and is named after its antipyretic properties. Butazolidine, another pyrazolone is a powerful anti-inflammatory drug used in rheumatic conditions. Many pyrazole derivatives are associated with anti-fungal, anti-

diabetic and anti-inflammatory properties. The success of pyrazole COX-2 inhibitor has further highlighted the importance of this heterocycle in medicinal chemistry.

Pyrazole derivatives have been reported to show a broad spectrum of biological activity including antimicrobial [29-44], anti-inflammatory [45-54], antituberculosis [55, 56], antiviral [57, 58], hypoglycemic [59, 60], anti-tumor [20-25], antihypertensive [26-28]. Due to its wide range of biological activity, pyrazoles have received a considerable interest in the field of drug discovery and therefore pyrazole ring constitutes a relevant synthetic target in pharmaceutical industry. In fact, such a heterocyclic moiety represents the core structure of a number of drugs.

RESULTS AND DISCUSSION

The twelve Pyrazole derivatives have been synthesized during the course of research work.

The synthesized compounds were subjected to various antibacterial, antifungal and antitubercular and anti-inflammatory screening by the standard methods.

• **Antibacterial activity:** All the compounds were screened for antibacterial activity at 200 µg/ml concentration. However the compounds **A₂**,

* To whom all correspondence should be sent:
E-mail: shashipattan@yahoo.com

A₃, B₂, C₂ and C₃ have shown maximum antibacterial activity, while the remaining compounds have also shown moderate antibacterial activity, when compared with standard drug **Ciprofloxacin** against *Staphylococcus aureus* (Gram positive) and *Escherichia coli* (Gram negative).

- **Antifungal activity:** All the compounds were screened for antifungal activity. However Compound A₂, B₂, B₃, C₂ and C₃ have showed maximum activity, while the remaining compounds have also shown moderate Antifungal activity, when compared with standard **Griseofulvin** against *Aspergillus niger* & *Candida albicans*.

- **Antitubercular activity:** All the compounds were screened for antitubercular activity by Middle brook 7H9 agar medium as described by Elmer WK et al. against H₃₇Rv Strain. However Compounds A₄, B₁, B₂, B₃ and B₄ have shown promising antitubercular activity against *Mycobacterium tuberculosis* of H₃₇Rv Strain. **Streptomycin** was use as std. drug.

- **Anti-inflammatory activity:** All the compounds were screened for *in-vitro* anti-inflammatory activity at different concentration like 200 µg/ml, and 300 µg/ml, by inhibition of protein denaturation method. Compounds A₂, A₃, B₂, B₃, C₃ and C₄ have shown promising anti-inflammatory activity. **Ibuprofen** was used as standard drug. The Compounds A₁, A₂, B₃, B₄, C₂ and C₃ were screened for the *in vivo* anti-inflammatory activity at 200 µg/ml concentration. Compound A₂, B₃, B₄, C₂ and C₃ shows good anti-inflammatory activity.

Regarding the above result, it is suggested that compounds substituted with electron-releasing groups (-OCH₃, -OH) increase the antimicrobial activity and anti-inflammatory activity.

The proposed work has given out many active antibacterial, antifungal, antitubercular and anti-inflammatory agents. Some of the compounds have showed moderate activities. These compounds with suitable modification can be explored better for their therapeutic activities in the future.

The experimental work comprises of scheme (procedures) [55,56,57,58,59]

1. Synthesis of ethyl bis(methylthio)- 2 cyanoacrylate.

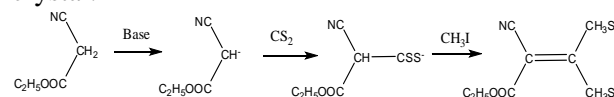
2. General procedure for synthesis of ethyl 5-amino-3-(methylthio)-1-substituted-1H-pyrazole-4-carboxylate

3. General procedure for synthesis of 1-substituted-5-amino-4-[(hydrazinooxy)carbonyl]-1H-pyrazole.

4. General Procedure for synthesis of 2-[[5-amino-1-substituted-3-(methylthio)-1H-pyrazole-4-yl]carbonyl]-5-methyl-2,4-dihydro-3H-pyrazole-3-one.(V)

5. General procedure for synthesis of derivative of pyrazole.

Step 1: Synthesis of ethyl bis(methylthio)- 2 cyanoacrylate(I): Pulverized potassium hydroxide (0.2mol) was suspended in dioxane (100mL) and a solution of ethylcyanoacetate (0.1mol) and carbon disulphide(0.1mol) in dioxane(50mL) was added with stirring and cooling to maintain temperature of 15-20°C. After stirring for 20 min, the solution was diluted with 250 ml ether. The yellow precipitate was filtered, washed with dioxane-ether and dried in vacuo over NaOH and P₂O₅. A solution of dithiolates (2mM) and methyl iodide (4mM) in abs. ethanol was kept at 0°C for 2 days. The ethanol was removed by evaporation in vacuo and water added to the residue. The insoluble solid was filtered and dried on recrystallised ether to yield colorless crystal.



Step 2: General procedure for synthesis of ethyl 5-amino-3-(methylthio)-1-substituted-1H-pyrazole-4-carboxylate (III): A hydrazide derivative (100 mM) and ketene dithioacetal derivative (150 mM) in methanol (70 mL) was heated under reflux till completion of reaction. The reaction was monitored by thin layer chromatography using mixture of chloroform and methanol (8:2) as eluent. The reaction mass was cooled to 0-5° C to crystallize the product. On filtration and washing with chilled methanol it afforded pyrazole derivatives

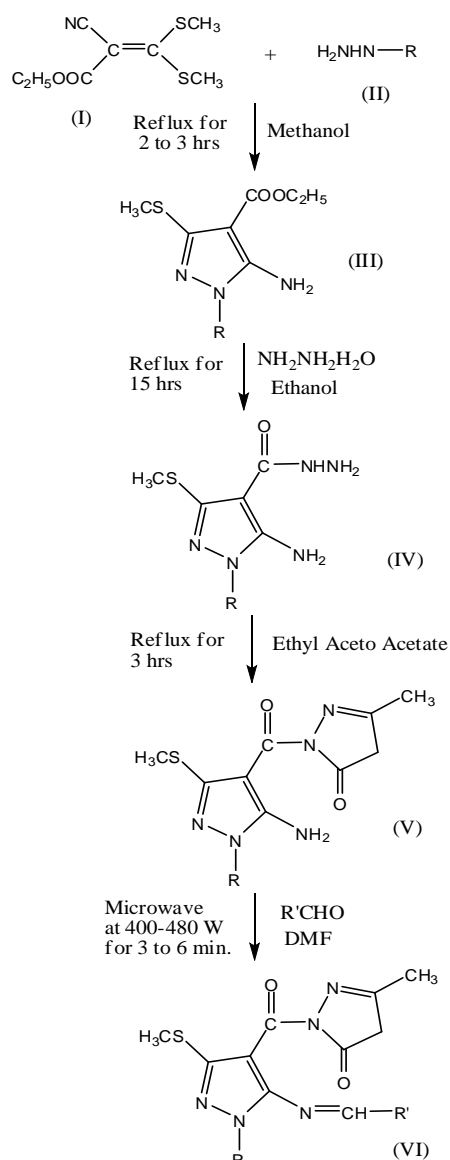
Step 3: General procedure for synthesis of 1-substituted-5-amino-4-[(hydrazinooxy)carbonyl]-1H-pyrazole(IV): A mixture of 0.01 mole of com.(III) and 0.2 mole (10mL) of Hydrazine hydrate were taken in 250 mL round bottom flask attached to a refluxed condenser and refluxed with 50 ml of 95% ethanol for 15 hrs. The resultant mixture was concentrated in 250 ml beaker. It was cooled at room temperature and kept in refrigerator for 2 hrs. The solid mass thus separated out was filtered, dried and purified by recrystallization from ethanol.

Step 4: General Procedure for synthesis of 2-[[5-amino-1-substituted-3(methylthio)-1H-pyrazole-4-yl]carbonyl]-5-methyl-2,4-dihydro-3H-pyrazole-3-one.(V): A mixture of the hydrazide (IV) (10 mM) and ethyl acetoacetate (10 mM) in

absolute ethanol was heated at reflux for 3 h. The reaction mixture was cooled and the formed precipitate was filtered off, dried and recrystallized from acetic acid.

Step 5: General procedure for Microwave Assisted synthesis of derivative of pyrazole(VI): A mixture of 2 mM of aldehyde and 2 mM of different aryl or alkyl amines (V) was taken and triturated in a mortar pestle. Then above mixture was transferred to a vessel which was then kept in microwave for synthesis. 4 to 5 mL of DMF was also added to mixture before putting it in microwave. Microwave was run at 400-480 W for 3 to 6 min for depending on reaction mixtures. Reaction completion was monitored continuously after each run by TLC. Then product was washed with ethanol, solvent was evaporated, dried and recrystallized with ethanol.

Scheme:



SPECTRAL DATA

Infra Red / ¹H-NMR spectral study of the synthesized compounds. (A₁-C₄)

A₁

IR Bands (cm⁻¹): 2997, 1712, 1630, 1602, 1112, 668

Types of Vibrations: C-H, C=O, C=N, C=C, C-N, C-S-C

δ Values in ppm: 8.76-9.34, 7.52-7.83, 1.94-2.53

No. Of Protons: 3H of Pyrazine, 6 H of Aryl, 2 H of Methyl.

A₂

IR Bands (cm⁻¹): 2992, 1710, 1645, 1610, 1142, 1086, 686.

Types of Vibrations: C-H, C=O, C=N, C=C, C-N, C-O, C-S-C.

δ Values in ppm: 8.76-9.34, 7.62-7.84, 2.53.

No. Of Protons: 3H of Pyrazine, 4 H of Aryl, 1 H of Methyl.

A₃

IR Bands (cm⁻¹): 3398, 2988, 1698, 1634, 1592, 1286, 1046, 694

Types of Vibrations: 10.9, 8.7-8.6, 8.0, 7.65-7.03, 2.8, 2.5, 1.8

δ Values in ppm: 8.76-9.34, 7.62-7.84, 2.8.

No. Of Protons: 3H of Pyrazine, 4 H of Aryl, 3 H of Methyl.

A₄

IR Bands (cm⁻¹): 2998, 1702, 1653, 1612, 1574, 1086, 674

Types of Vibrations: C-H, C=O, C=N, C=C, C=C, C-N, C-S-C

δ Values in ppm: 8.76-9.34, 7.33-7.60, 1.94-2.53.

No. Of Protons: 3H of Pyrazine, 5 H of Benzene, 2 H of Methyl.

B₁

IR Bands (cm⁻¹): 1699, 1634, 1597, 1080, 683

Types of Vibrations: C-H, C=O, C=N, C=C, C-N, C-S-C

δ Values in ppm: 7.92-, 7.33-7.60, 1.94-2.53.

No. Of Protons: 4 H of 4-Pyridine, 6 H of Aryl, 2 H of Methyl.

B₃

IR Bands (cm⁻¹): 3400, 2994, 1689, 1622, 1586, 1124, 1078, 697

Types of Vibrations: O-H, C-H, C=O, C=N, C=C, C-N, C-O, C-S-C

δ Values in ppm: 7.92-8.89, 7.08-8.59, 1.94-2.53.

No. Of Protons: 4 H of 4-Pyridine, 5 H of Aryl, 2 H of 2 Methyl.

B₄

IR Bands (cm⁻¹): 2997, 1762, 1699, 1621, 1015, 681

Types of Vibrations: C-H, C=O, C=N, C=C, C-N, C-S-C.

δ Values in ppm: 7.92-8.84, 7.33-8.60, 1.94-2.53.

No. Of Protons: 4 H of 4-Pyridine, 5 H of 1-Benzene, 2 H of 2 Methyl.

C₁

IR Bands (cm⁻¹): 3016, 1709, 1642, 1602, 1087, 690

Types of Vibrations: C-H, C=O, C=N, C=C, C-N, C-S-C

δ Values in ppm: 7.92-8.84, 7.33-8.60, 1.94-2.53.

No. Of Protons: 5 H of Benzene, 5 H of Aryl, 2 H of Methyl.

C₂

IR Bands (cm⁻¹): 3021, 1702, 1641, 1578, 1210, 1043, 673

Types of Vibrations: C-H, C=O, C=N, C=C, C-N, C-O, C-S-C

δ Values in ppm: 1.6-4.22, 6.8-8.59, 7.45-8.04

No. Of Protons: 5 H of 1-Benzene, 5 H of Aryl, 2 H of Methyl

C₃

IR Bands (cm⁻¹): 3024, 1731, 651, 1597, 1253, 1104, 686

Types of Vibrations: C-H, C=O, C=N, C=C, C-N, C-O, C-S-C

δ Values in ppm: 7.02-8.59, 7.45-8.04, 1.94-2.53

No. Of Protons: 5 H of 1-Benzene, 4 H of Aryl, 2 H of Methyl

C₄

IR Bands (cm⁻¹): 3026, 1714, 1640, 1600, 1131, 692

Types of Vibrations: C-H, C=O, C=N, C=C, C-N, C-S-C

δ Values in ppm: 7.33-8.04, 5.5-6.6, 1.94-2.53

No. Of Protons: 10 H of 1-Benzene, 2 H of methylene, 2 H of Methyl

INSTRUMENTAL DETAILS

Infrared Spectra

The peaks in IR Spectrum gave an idea about the probable structure of the compound. IR region ranges between 4000-650 cm⁻¹. The derivatives including intermediates were recorded on Jasco FT/IR 4100, which showed different vibration levels of molecules by using potassium bromide (KBr) pellet technique.

¹H-NMR Spectra

NMR Spectroscopy enables us to record differences in magnetic properties of the various magnetic nuclei present and to deduce in the large measure about the position of these nuclei within the molecule. We can deduce how many different kinds of environment are there in the molecules and also which atoms are present in neighboring groups. The proton NMR spectra, enables us to know different chemical and magnetic environments corresponding to protons in molecules.

¹H-NMR of the title compounds were recorded on sophisticated multinuclear FT NMR Spectrometer model Avance-II (Bruker), DMSO-d₆ as internal standards. The instrument is equipped with a Gyromagnet of field strength 9.4T. Its ¹H frequency is 400 MHz. The chemical shift data were expressed as δ-values related to TMS.

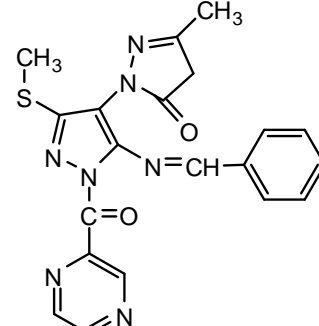
C H N Analysis

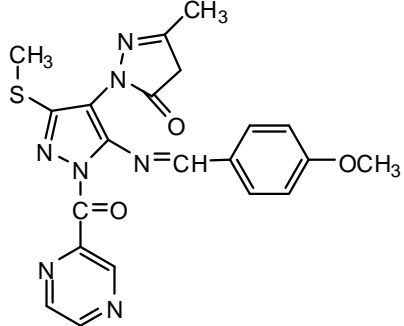
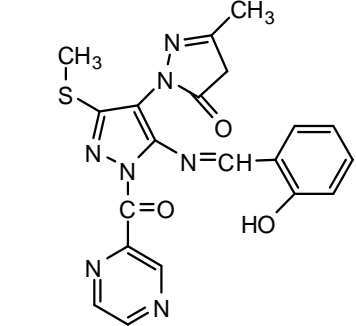
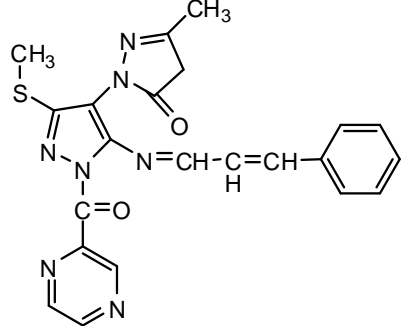
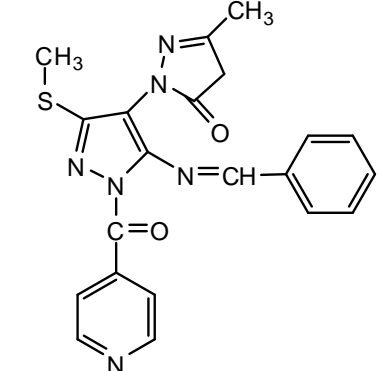
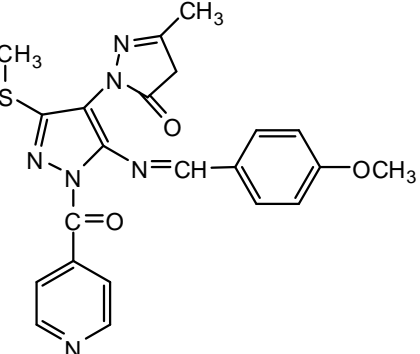
The permiscible limit for C H N analysis were performed on Thermo finnigan. Model: FLASH EA 1112 series.

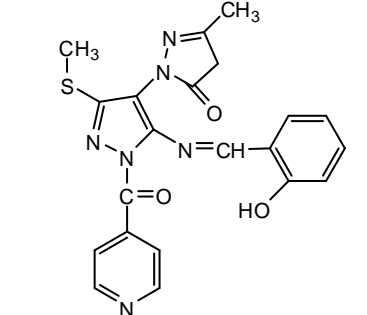
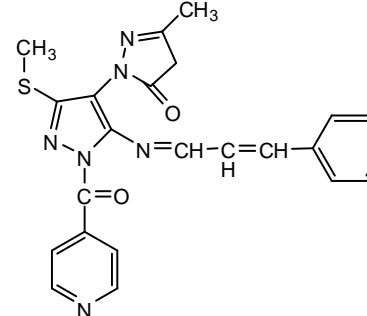
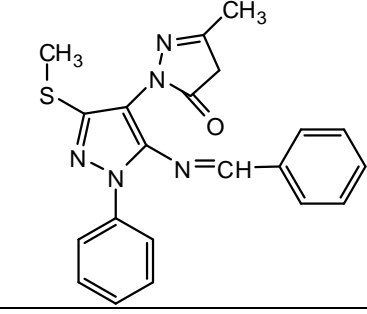
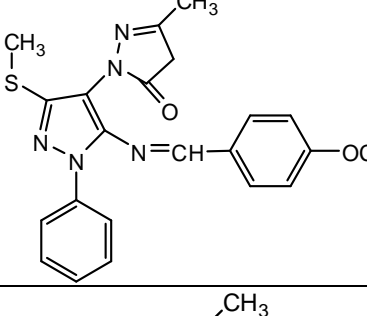
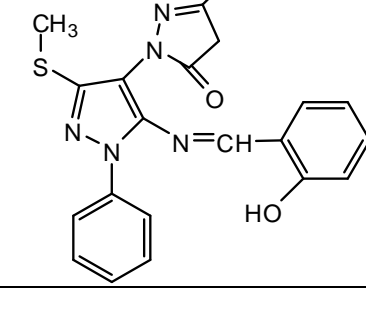
Microwave Synthesis

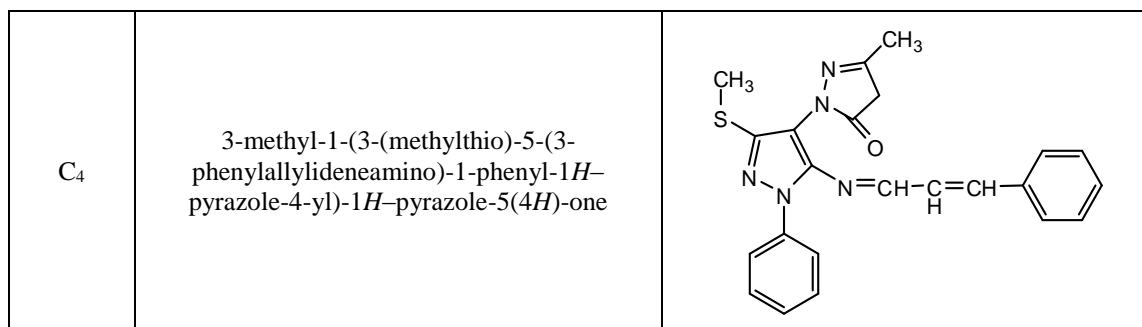
Microwave synthesis were performed on instrument of LG company, Model no.:MH-6349 EB.

Table of derivatives. List of synthesized compounds with their IUPAC names.

<p>A₁</p>	<p>1-(5-(benzylideneamino)-3-(methylthio)-1-(pyrazine-2-carbonyl)-1H-pyrazole-4-yl)-3-methyl-1H-pyrazole-5(4H)-one</p>	
----------------------	------------------------------------------------------------------------------------------------------------------------	--------------------------------------------------------------------------------------

A ₂	1-(5-(4-methoxybenzylideneamino)-3-(methylthio)-1-(pyrazine-2-carbonyl)-1H-pyrazole-4-yl)-3-methyl-1H-pyrazole-5(4H)-one	
A ₃	1-(5-(2-hydroxybenzylideneamino)-3-(methylthio)-1-(pyrazine-2-carbonyl)-1H-pyrazole-4-yl)-3-methyl-1H-pyrazole-5(4H)-one	
A ₄	3-methyl-1-(3-(methylthio)-5-(3-phenylallylideneamino)-1-(pyrazine-2-carbonyl)-1H-pyrazole-4-yl)-1H-pyrazole-5(4H)-one	
B ₁	1-(5-(benzylideneamino)-1-isonicotinoyl-3-(methylthio)-1H-pyrazole-4-yl)-3-methyl-1H-pyrazole-5(4H)-one	
B ₂	1-(1-isonicotinoyl-5-(4-methoxybenzylideneamino)-3-(methylthio)-1H-pyrazole-4-yl)-3-methyl-1H-pyrazole-5(4H)-one	

<p>B₃</p>	<p>1-(5-(2-hydroxybenzylideneamino)-1-isonicotinoyl-3-(methylthio)-1H-pyrazole-4-yl)-3-methyl-1H-pyrazole-5(4H)-one</p>	
<p>B₄</p>	<p>1-(1-isonicotinoyl-3-(methylthio)-5-(3-phenylallylideneamino)-1H-pyrazole-4-yl)-3-methyl-1H-pyrazole-5(4H)-one</p>	
<p>C₁</p>	<p>1-(5-(benzylideneamino)-3-(methylthio)-1-phenyl-1H-pyrazole-4-yl)-3-methyl-1H-pyrazole-5(4H)-one</p>	
<p>C₂</p>	<p>1-(5-(4-methoxybenzylideneamino)-3-(methylthio)-1-phenyl-1H-pyrazole-4-yl)-3-methyl-1H-pyrazole-5(4H)-one</p>	
<p>C₃</p>	<p>1-(5-(2-hydroxybenzylideneamino)-3-(methylthio)-1-phenyl-1H-pyrazole-4-yl)-3-methyl-1H-pyrazole-5(4H)-one</p>	

**Table.** Analytical data of synthesized compounds

Comp.	Mol. Formula	Mol. Wt.	M.P °C	Rf Value	Yield %	Elemental analyses		
						Calcd. (Found)		
						C	H	N
A ₁	C ₂₀ H ₁₇ N ₇ O ₂ S	419.46	140-142	0.74	71	57.27 (57.22)	4.09 (4.20)	23.37 (23.34)
A ₂	C ₂₁ H ₁₉ N ₇ O ₃ S	449.49	143-145	0.70	67	56.11 (56.15)	4.26 (4.30)	21.81 (21.84)
A ₃	C ₂₀ H ₁₇ N ₇ O ₃ S	435.46	152-154	0.67	63	55.16 (55.11)	3.93 (3.90)	22.52 (22.49)
A ₄	C ₂₂ H ₁₉ N ₇ O ₂ S	445.50	194-196	0.72	79	59.31 (59.42)	4.30 (4.02)	22.01 (22.10)
B ₁	C ₂₁ H ₁ N ₆ O ₂ S	418.47	178-180	0.76	58	60.27 (60.31)	4.34 (4.30)	20.08 (20.06)
B ₂	C ₂₂ H ₂₀ N ₆ O ₃ S	448.50	145-147	0.75	56	58.92 (58.89)	4.49 (4.54)	18.74 (18.78)
B ₃	C ₂₁ H ₁₈ N ₆ O ₃ S	434.47	146-148	0.71	65	58.05 (58.03)	4.18 (4.24)	19.34 (19.33)
B ₄	C ₂₃ H ₂₀ N ₆ O ₂ S	444.51	186-188	0.68	70	62.15 (62.10)	4.54 (4.55)	18.91 (18.90)
C ₁	C ₂₁ H ₁₉ N ₅ OS	389.47	126-128	0.76	63	64.47 (64.45)	4.92 (4.89)	17.98 (17.94)
C ₂	C ₂₂ H ₂₁ N ₅ O ₂ S	419.50	139-141	0.68	64	62.99 (62.78)	5.05 (5.31)	16.69 (16.58)
C ₃	C ₂₁ H ₁₉ N ₅ O ₂ S	405.47	146-148	0.65	68	62.21 (62.22)	4.72 (4.73)	17.21 (17.18)
C ₄	C ₂₃ H ₂₁ N ₅ OS	415.51	165-167	0.72	72	66.48 (66.44)	5.09 (5.05)	16.85 (16.86)

TLC Solvents: Methanol:Benzen (1:9)

PHARMACOLOGICAL AND MICROBIOLOGICAL SCREENING

Anti-bacterial and Anti-fungal activity of synthesized compounds:

Compd.	Zone of inhibition at 200µcg/mL (in mm.)			
	<i>E. coli</i>	<i>S. aureus</i>	<i>A. niger</i>	<i>C. albicans</i>
	ATCC 25922	ATCC 25923	NCIM 596	NCIM 3102
A ₁	16	14	12	16
A ₂	18	23	21	23
A ₃	21	24	21	18
A ₄	15	16	14	18
B ₁	12	14	16	14
B ₂	18	22	24	25
B ₃	16	19	23	24
B ₄	18	17	14	22
C ₁	13	14	12	20
C ₂	18	21	22	24
C ₃	22	24	20	26
C ₄	18	12	17	13
Ciprofloxacin	28	26	-	-
Griseofulvin	-	-	28	25

Compounds **A₂**, **A₃**, **B₂**, **C₂** and **C₃** have shown promising antibacterial activity against **Std. Ciprofloxacin**. Compounds **A₂**, **B₂**, **B₃**, **C₂** and **C₃** have exhibited excellent antifungal activities against **Std. Griseofulvin**.

Anti-tubercular activity of the synthesized compounds:

Compound code	25 µg /mL	50 µg /mL	100 µg /mL
A ₁	R	R	S
A ₂	R	R	R
A ₃	R	R	S
A ₄	R	S	S
B ₁	R	S	S
B ₂	R	S	S
B ₃	R	S	S
B ₄	R	S	S
C ₁	R	R	R
C ₂	R	R	R
C ₃	R	R	R
C ₄	R	R	R
Streptomycin	S	S	S

R- Resistance; S- Sensitive

Compounds **A₄**, **B₁**, **B₂**, **B₃** and **B₄** have shown promising antitubercular activity at both the concentration 50 and 100 µg /mL. H₃₇ Rv strain was used as standard tubercular organism.

Streptomycin was used as standard drug. However, Streptomycin has shown antitubercular activity at 25 µg /mL.

In-vitro Anti-inflammatory activity of the synthesized compounds:

Compound	Absorbance Value (Mean + SE)		Inhibition of Denaturation (in %)	
	200 µg/mL	300 µg/mL	200 µg/mL	300 µg/mL
Control	0.095	0.095	-	-
Ibuprofen	0.180	0.195	89.4%	105.2%
A ₁	0.142	0.152	49.47%	60.00%
A ₂	0.162	0.173	70.52%	82.10%
A ₃	0.156	0.169	64.21%	77.89%
A ₄	0.130	0.143	36.84%	50.52%
B ₁	0.134	0.141	41.05%	48.42%
B ₂	0.146	0.157	53.68%	65.26%
B ₃	0.155	0.167	63.15%	75.78%
B ₄	0.135	0.146	42.10%	53.68%
C ₁	0.130	0.139	36.84%	46.31%
C ₂	0.141	0.152	48.42%	60.00%
C ₃	0.160	0.174	68.42%	83.15%
C ₄	0.142	0.158	49.47%	66.31%

The percentage inhibition of denaturation was calculated by using following formula:

$$\% \text{ of Inhibition} = 100 \times [V_t / V_c - 1]$$

Where, V_t = Mean absorbance of test sample.
V_c = Mean absorbance of control.

In-vivo Anti-inflammatory activity of the synthesized compounds

Compound	Increase paw volume			% Decrease paw volume after 3 hour
	1 hour	2 hour	3 hour	
Control	0.37(±0.02)	0.39(±0.008)	0.45(±0.03)	
Diclofenac sodium	0.10(±0.03) ***	0.10(±0.05) ***	0.12(±0.011) ***	73.33
A₁	0.12(±0.007) ***	0.23(±0.03) **	0.26(±0.02) **	42.22
A₂	0.08(±0.02) ***	0.09(±0.05) ***	0.13(±0.009) ***	71.22
B₃	0.08(±0.009) ***	0.12(±0.05) ***	0.17(±0.011) ***	62.23
B₄	0.10(±0.06) ***	0.13(±0.009) ***	0.16(±0.02) ***	64.45
C₂	0.07(±0.04) ***	0.09(±0.05) ***	0.14(±0.009) ***	68.89
C₃	0.11(±0.03) ***	0.14(±0.07) ***	0.16(±0.012) ***	64.45

The results are expressed as mean ± SEM (n =6). Significance was calculated by using one-way ANOVA with Dunnett's t- test. The difference in results was considered significant when p<0.05. *p<0.05 vs control at 200 mg/kg b.w; **p<0.01 vs control at 200 mg/kg b.w; ***p< 0.001 vs control at 200 mg/kg b.w.

Acknowledgement: The authors wish to express their sincere thanks to Hon. Padmabhushan Shri. Balasaheb Vikhe Patil, Ex-Minister, Govt. of India and Shri Adv. Rajendra Vikhe Patil, Managing Trustee, Prof. D.R. Karnure Technical adviser Pravara Rural Education Society, Loni, for their constant encouragement and support.

REFERENCES

- 1.L. Thomas, D.A. Williams, V.F. Roche, W.S. Zito. Foyes Principle of Medicinal Chemistry. 6thed. Newyork: Lippincott publishers; 1998.
- 2.K.D.Tripathi, Essentials of Medical Pharmacology. 5th ed. India: J P Brothers Medical publishers; 2003.
- 3.J.A.Maertens, *Clin. Microbial Infect.*, **10**, 1 (2004).
- 4.R.K. Bansal. Hetrocyclic chemistry. 4thed.: New age International Publishers; 2007.
- 5.<http://www.wikipedia.com/pyrazoles>.
- 6.Cotton, Kumar, Robbins. Pathoioic Basis of Disease. 5th edition Philadelphia; p.51.
- 7.H. Harsh Mohan, Ed. In Textbook of Pathology. 4thEdn, Jaypee Brothers, Medical Publishers (P) Ltd New Delhi; 2000: p.114-119.
- 8.B. Walzog, P.G. Gouhteng, *News Physiol. Sci.* **5**, 107 (2000).
- 9.Katzung, Pharmacology. The Eicosanoids: Prostaglandins, Thromboxanes, Leukotrienes, & Related compound; p.436
- 10.H. Mohan, Ed. In text book of Pathology. 2ndEdn, Jaypee Brothers, Medical Publishers (P) Ltd, New Delhi; 1995: p. 92.
- 11.U. Wiedermann et al.,*Scand. J. Immunol.* **44**, 578 (1996).
- 12.J.Y. Wang, P.R. Hsueh, I.S. Jan et al., *Thorax*, **61**, 903 (2006).
- 13.H.L. David, *Appl. Microbiol.*, **20**, 810 (1970).
- 14."A controlled trial of 6 months' chemotherapy in pulmonary tuberculosis. Final report: results during the 36 months after the end of chemotherapy and beyond. British Thoracic Society". *British Journal of Diseases of the Chest*, **78** (4): 330–6.
- 15.M.D. Iseman, *The International Journal of Tuberculosis and Lung Disease*,**2** (11): 867.(1998).
- 16.T.R. Sterling, H.P. Lehmann, T.R. Frieden, *BMJ* **326** (7389): 574(2003)..
- 17.K. D. Tripathi, Essentials of Medical Pharmacology, Jaypee Brothers Medical Publishers Ltd. New Delhi, 5th edition; 2004, 698-708.
- 18.Goodman Gilman, The Pharmacological Basis of Therapeutics, McGraw Hill Medical Publishing Division 10thediton; 2001, 1284.
- 19.M. Gupta, S. Paul, R. Gupta., *Acta Chim. Slov* 2009; 56: 749–64.
- 20.P.-Ch. Lv., H.-L. Zhu, H.-Q. Li, J. Sun, Y. Zhou., *Bioorg. Med. Chem.*, **18**: 4606 (2010)
- 21.M. S., Christodoulou, L. Sandra, K. M. Kasiotis, S. A. Harotounian, *Bioorg. Med. Chem.*, **18**, 4338 (2010)
- 22.R. Lin, G. Chiu, Y. Yu, P. J. Connolly, S. Li, Y. Lu, M. Adams, A. R. Fuentes-Pesquera, S. L. Emanuel, L. M. Greenberger, *Bioorg. Med. Chem. Lett*, **17**, 4557 (2007)
- 23.Y. Zhang, L. Zhang, L. Liu, J. Guo, D. Wua, G. Xu, *Inorganica Chimica Acta* **363**, 289 (2010)
- 24.D. Jia, *Inorganica Chimica Acta* **363**, 289(2010)
- 25.H. R. Brunner, K. Eichenbergen, *et.al; Expermentia*, **22**, 208 (1966)
- 26.L. Kuczynski, A. E. Morzik, W. Banasszki, K. Poreba, *Pol J Pharmacol Pharm*, **31**(3), 217 (1979)
- 27.A. Ikno, Y. Terno, H. Yoshiyaru, S. Katsunori, S. Hatsno, K. Masaru, U. Osamu, U. Mitahiko, *Chem Pharm Bull*; **35**(8): 3235(1987), CA. 110: 95080c, (1989)
- 28.M. Bonesi, M. R. Loizzo, G. A. Statti, S. Michel, F. Tillequin, Menichini, *Bioorg. Med. Chem. Lett*, **20**, 1990 (2010)
- 29.V.K. Ahluwalia, B. Mittal, *Indian J. Chemistry*, **8**,17. (1989)
- 30.R.B. Palkar, H.E. Master, *Indian J. Heterocyclic Chemistry*, **8**,17 (1997)
- 31.Udupi R.H., S. Narayan Rao, A.R. Bhat, *Ind. J. Het. Chem.*, **7**; 217(1998)
- 32.V.B.; Halnor, N.S. Joshi, B.K.Karale, C.H. Gill, *Ind. J. Het. Chem.*, **14**, 371 (2005)
- 33.S. Bondock, W. Fadaly, M. A. Metwally, *Eur. J. Med. Chem.*, **45**, 3692 (2010)
- 34.S. Radi, S. Salhi, A. Radi, *Letters in Drug Design & Discovery*, **7**, 27 (2010)
- 35.S. K. Sahu, M. Banerjee, A. Samantray, C. Behera, M.A. Azam, *Tropical J. Pharm. Research*, **7**(2): 961 (2008)
- 36.R. Sridhar, P. J. Perumal, S. Etti, G. Shanmugam, M. N. Ponnuswamy, V. R. Prabavathy, N. Mathivanan, *Bioorg. Med. Chem. Lett*, **14**: 6035 (2004)
- 37.N. RaoJyothi, K.V. Sujith, B. Kalluraya, *Saudi Chem. Soc*, **12**(3), 347 (2008)
- 38.N. SatheeshaRai, BalakrishnaKalluraya. *Indian J Chem*, **46B**, 375 (2007)
- 39.N.D. Argade, B. K. Kalrale, C.H. Gill, *E-Journal Chemistry*, **5** (1): 120 (2008)
- 40.P.T. Chovatia, J.D. Akabari, P.K. Kachhadia, P.D. Zalavadia, H.S. Joshi, *J. Serb. Chem. Soc*, 71(7): 713 (2007)
- 41.M. Kuntal, K.Yadvendra, *Bioorganic & Medicinal Chemistry Letters*, **19**, 2688 (2009)
- 42.M. S. Karthikeyan, B.S.Holla, N.S.Kumari, *Eur. J. Med.Chem.*, **42**, 30 (2007)
- 43.R. VenkatRagavan, V. Vijayakumar, N. SuchethaKumari, *Eur. J. Med.Chem.*, **45**,1173 (2010)
- 44.G. Menozzi, L. Merello, P. Fossa, S.Schenone, A. Ranise, L. Mosti et al. *Bioorganic & Medicinal Chemistry*, **12**, 5465 (2004)
- 45.B. Coli, Silverstrini *et al; Ep Med. Pathol*, **6**, 68. (1967)
- 46.S. Sarangan, S.T.Somashekhara, *J. Ind. Chem. Soc*, **53**, 426, (1976)
- 47.M.Abdul-Aziz, O. M. Aly, *Eur. J. Med. Chem.*, **44**, 3068 (2009)
- 48.F. F. Barsoum, A. S. Girgis, , *Eur. J. Med. Chem.* , **44**, 2172 (2009) AlkaChauhan et al /Int.J. ChemTech Res.2011,3(1)
- 49.A. A. Bekhit, H. M. A. Ashour, Y. S. A. Ghany, A. El-Din, A. Bekhit, A. Baraka, *Eur J. Med. Chem.*, **43**, 456 (2008)
- 50.A. Bргуete, E. Pontiki, D. Hadjipavlou-Litina, R. Villar, E. Vicente, B. Solano, S. Ancizu, S. Perez-

- Silanes, I. Aldanaa, A. Monge, *Bioorg. Med. Chem. Lett.*, **17**, 6439 (2007)
51. N. Gokhan-Kelekc, S. Yabanoglu, E. Kupeli, U. Salgin, O. Ozgen, G. Ucar, E. Yesilada, E. Kendi, Y. Yesiladaf, A. AltanBilgin, *Bioorg. Med. Chem.*, **15**, 5775 (2007)
52. S. M. Sakya, H.Cheng, K. M. L. DeMello, A. Shavnya, M. L. Minich, B. Rast, J. Dutra, Ch. Li, R. J. Rafka, D. A. Koss, J. Li, B.H. Jaynes, C. B. Ziegler, D. W. Mann, C. F. Petras, S. B. Seibel, A. M. Silvia, D. M. George, A. Hickman, M. L. Haven, M.P. Lynch., *Bioorganic & Med. Chem. Letters*, **16**, 1202 (2006)
53. M. Ezawa, D.S. Garvey, D.R. Janero, S.P. Khanapure, L.G. Letts, *Let. Drug Design & Discovery*, **2**, 40 (2005)
54. L. Gomez, M. D. Hack, K. McClure, C. Sehon, L. Huang, M. Morton et al. *Bio-org & Med Chem Letters*, **17**, 6493 (2007)
55. K.A. Jensen, L. Henrikesen, *Acta. Chem. Scand.*, **22**, 1170 (1968)
56. Singaravelmohan, SarkkariAnanthan , *IJSPR*, **1**(9), 391 (2010)
57. Sh. R. Pattan, P. A. Rabara, J. S. Pattan, A. A. Bukitagar, V. S. Wakale, D. S. Musmade, *Indian Journal of Chemistry*, **48 B**, 1453 (2009)
58. G. A. Idrees, O. M. Aly, A. A. G. El-Din, Abu-Rahma, M.F. Radwan, *Eur. J. Med. Chem.*, **44**, 3973 (2009)
59. P. Kamaria, N. Kawathekar, P. Chaturvedi; *E-Journal of Chemistry*, **8**(1), 305 ()
60. Smith, D L., forist, A A., et al; *J. Med. Chem*, **8**: 350 (1965)

СИНТЕЗА И ОХАРАКТЕРИЗИРАНЕ НА НЯКОИ ЗАМЕСТЕНИ ПРОИЗВОДНИ НА ПИРАЗОЛА С БИОЛОГИЧНО ПРИЛОЖЕНИЕ

С.Р. Патан^{1*}, П.В. Пател¹, Г.С. Атхар¹, А.Б. Джангар¹, С.А. Патан³, Дж.С. Патан²

¹Департамент по фармацевтична химия, Селскостопански колеж по фармация „Правара“, Лони, Индия

²Департамент по биотехнология, Колеж по изкуства, наука и търговия RVP, Лони, Индия

³Департамент по фармакогнозия, Колеж по изкуства, наука и търговия RVP, Лони, Индия

Постъпила на 7 ноември, 2012 г.; коригирана на 27 февруари, 2013 г.

(Резюме)

Пиразолът и неговите производни имат голяма биологична активност. В настоящата работа са синтезирани нови заместени производни на пиразола. Те са синтезирани чрез третирането на етил бис-[метилтио] -2-цианоакрилатс производни на хидразида. Производните на пиразола са получени чрез реакция с Шифови бази. Всички получени съединения са охарактеризирани с IR, ¹H-NMR и елементен анализ. Всички новосинтезирани съединения са изпитани за антимикробна активност върху различни микроорганизми (*E.coli*, *S. aureus*, *A.niger*, *C. albicans*) при концентрации 200 µg/mL чрез дифузия в агар в стъкла на Петри. Активността е определяна чрез зоните на инхибиране и сравнена с действието на стандартното лекарство ципрофлоксацин за антимикробна и с гризеофулвин за антигъбична активност. Изпитаните съединения са тествани и за антитуберкулозна активност спрямо *M. tuberculli* при концентрации от 25, 50 и 100 µg/mL, а за *in-vitro* противовъзпалителна активност – при концентрации 200 µg/ml и 300 µg/ml по метода на денатурирането на протеини. Като стандартно лекарство е използван ибупрофен. Съединенията са изпитани за *in vivo* противовъзпалителна активност спрямо бели мишки при 200 µg/ml за потвърждение на резултатите.

Synthesis and structure of some novel dicoumarinamines

B. Mikhova,¹ V. Janevska,² B. Stamboliyska,¹ G. Draeger,³ E. Popovski^{2,*}

¹ Institute of Organic Chemistry with Centre of Phytochemistry, Bulgarian Academy of Sciences, Acad. G. Bonchev Str., Build. 9, 1113 Sofia, Bulgaria

² Institute of Chemistry, Faculty of Natural Sciences and Mathematics, Ss. Cyril and Methodius University, Arhimedova 5, 1000 Skopje, P.O. Box 162, Macedonia

³ Institute of Organic Chemistry, Leibniz Universität Hannover, D-30167, Hannover, Germany

Received January 23, 2013; Revised March 30, 2013

The present paper reports the synthesis and characterization of novel dicoumarinamines (7) as potential bioisostere compounds of dicoumarols (4). 3,3'-Methylenebis(4-amino-2H-chromen-2-one) (7a) was obtained in high yield in a reaction of 4-aminocoumarine (5) with aqueous formaldehyde. Best results in reactions of 5 with aldehydes 6 (b-h) were obtained when reactions were performed in acidified ethanol as a solvent. The structure and relative stability of the possible rotamers were studied by DFT methods at B3LYP/6-31+G** level with regard to their potential biological activity.

Key words: aminocoumarins, bioisostere, dicoumarols, anticoagulant, DFT.

1. INTRODUCTION

Currently, the chemistry and bioactivity of coumarins are of remarkable interest to medicinal chemists. Large number of compounds with coumarin scaffold are known to possess a wide range of pharmacological properties including antibacterial [1-2], antifungal [3-4], antioxidant [5-6], anticancer [7-8], antituberculosis [9-10], anti-HIV [11-12], antimalarial [13-14], anti-inflammatory [15], anti-allergic [16], and many other activities.

Probably, the most well-known bioactive coumarins are anticoagulants. Over six decades, warfarin (1) is the mainly prescribed oral anticoagulant drug. In last 20 years, related compounds, such as phenprocoumon (2) and acenocoumarol (3) are used as oral anticoagulation therapy worldwide (Figure 1). Nowadays, new or modified coumarins with same pharmacological activity are still in the focus of many research groups [17-20]. All these compounds are analogues and inspired of dicoumarol (4a) as a prototype. Anticoagulant activity of 4a is known for nearly one century and even before discovering of its structure in 1940. Dicoumarols (4) and similar [21] compounds nevertheless attract intense interest because of their activity (Figure 1) [22-26].

The different substituents in the coumarin derivatives have considerable influence on their biological activity. So, the identification of crucial structural characteristic is essential for the

development of new analogues with improved efficacy and lower side-effects. The design and synthesis of new derivatives with high specific activity for known and other pharmacological targets is a nowadays challenge. The present paper reports the synthesis and characterization of novel dicoumarinamines (7) as potential bioisosteric compounds of 4. Also, density functional theory (DFT) was employed to interpret the observed NMR spectra of the studied species. These results were used to investigate the preferred conformation of the compounds and the molecular properties with regard to their potential biological activity

EXPERIMENTAL

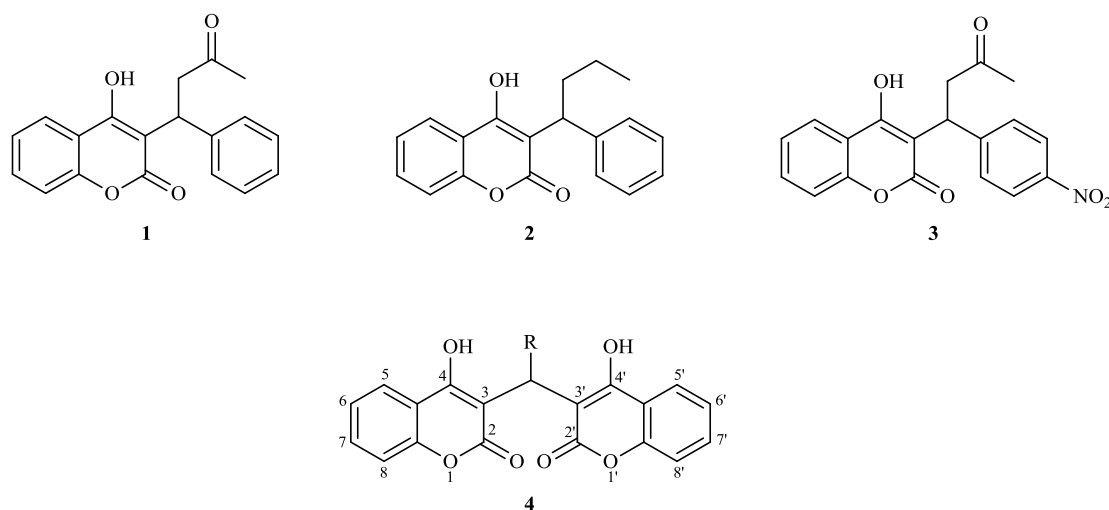
Aldehydes 6 were purchased commercially and used without further purification.

Melting points were determined on a Reichert hot-stage apparatus.

The FTIR spectra (4000-400 cm⁻¹) were recorded at ambient temperature with 16 scans on Perkin-Elmer System 2000 with the resolution of 4 cm⁻¹ using KBr pellets. The data for strong (s) and very strong (vs) bands are given.

The NMR spectra were run on a Bruker 250 DRX Spectrometer using standard Bruker Topspin software. DMSO-d₆ was used as a solvent and the chemical shifts were referenced to the residual solvent signal (2.5 ppm for ¹H and 39.5 ppm for ¹³C spectra). The signals were assigned with the aid of 1D and 2D ¹H, ¹³C, DEPT, COSY, HMQC and HMBC spectra. The digital resolution of the 1D-spectra was 0.12 Hz/Pt for ¹H and 1.4 Hz/Pt for ¹³C.

* To whom all correspondence should be sent:
E-mail: popovski.emil@gmail.com



R = H (for **4a**), alkyl, aryl, heterocyclic

Fig. 1. Structures of well-known anticoagulants

The HR-ESI mass spectra were recorded on a QToF premiere conjugated with HPLC system.

The quantum chemical calculations were performed using the Gaussian 09 program package [27] running on MADARA grid. The geometries of possible conformational isomers of compound 7h were fully optimized using density functional theory (DFT). We employed B3LYP functional and standard 6-311+G** basis set. The stationary points found on the molecular potential energy hypersurfaces were characterized using standard analytical harmonic vibrational analyses.

4-Amino-2H-chromen-2-one (**5**) is not commercially available and it was synthesized as described previously [28].

3,3'-Methylenebis(4-amino-2H-chromen-2-one) (**7a**, C₁₉H₁₄N₂O₄).

To an aqueous (37%) formaldehyde solution (50 cm³), well powdered **5** (1.012 g; 6.28 mmol) was added. The reaction mixture was stirred and heated up to 60 °C. After 2 h, the dense mixture was left to cool at room temperature. The crystals of the product **7a** were collected by simple vacuum filtration. The typical yield of crude product was about 80%. For additional 10%, filtrate was cooled in ice bath. The purification was performed by dissolving the product in DMSO and precipitation with ethanol. Dirty white crystals, Mp: >300 °C (decomp.); FTIR(KBr)/cm⁻¹: 3391(s), 3213(s), 1669(s), 1645(vs), 1614(vs), 1600(vs), 1551(s), 748 (s); ¹H-NMR (250.13 MHz; DMSO-d₆) δ: 8.04 (br d, 2H, ³J = 8.0 Hz, H-5), 7.83 (br s, 4H, NH₂), 7.62 (td, 2H, ³J = 8.0 Hz, ⁴J = 2.0 Hz, H-7), 7.35 (overl, 4H, H-6, H-8), 3.65 (s, 2H, CH₂); ¹³C-NMR (62.8 MHz; DMSO-d₆) δ: 164.8 (C2), 93.6 (C3), 153.5 (C4), 114.4 (C4a), 123.1 (C5), 124.0 (C6), 132.2

(C7), 116.9 (C8), 152.0 (C8a), 21.1 (CH₂); ESI TOF-MS (positive ions) (m/z): calcd. for [M+H]⁺: 335.1032; found: 335.1034.

3,3'-Ethylidenebis(4-amino-2H-chromen-2-one)(**7b**, C₂₀H₁₆N₂O₄).

To ethanol (40 cm³), acetaldehyde (**6b**) (0.9 cm³; 16.10 mmol), well powdered **5** (1.997 g; 12.39 mmol) and 8 drops of "HCl" were added. Reaction mixture was refluxed for 2 h. After cooling, water was added (drop by drop) to precipitate the product. The typical yield of the crude product was about 90%. The purification was performed by dissolving the product in ethanol and precipitation with water. Pale ocher crystals, Mp: 202 °C (decomp.); FTIR(KBr)/cm⁻¹: 3370(s), 3221(s), 1648(vs), 1610(vs), 1546(vs), 754(s); ¹H-NMR (250.13 MHz; DMSO-d₆) δ: 8.03 (br d, 2H, ³J = 8.0 Hz, H-5), 7.79 (br s, 4H, NH₂), 7.62 (td, 2H, ³J = 8.0 Hz, ⁴J = 2.0 Hz, H-7), 7.35 (overl, 4H, H-6, H-8), 4.58 (q, 1H, ³J = 7.5 Hz, CH), 1.66 (d, 3H, ³J = 7.5 Hz, CH₃); ¹³C-NMR (62.8 MHz; DMSO-d₆) δ: 164.2 (C2), 97.1 (C3), 153.2 (C4), 114.7 (C4a), 123.1 (C5), 124.0 (C6), 132.2 (C7), 116.8 (C8), 152.0 (C8a), 27.8 (CH), 15.6 (CH₃); ESI TOF-MS (m/z): calcd. for [M+Na]⁺: 371.1008; found: 371.1007.

3,3'-Propylidenebis(4-amino-2H-chromen-2-one)(**7c**, C₂₂H₂₀N₂O₄).

To ethanol (40 cm³), butyraldehyde (**6c**) (1.4 cm³; 15.53 mmol), well powdered **5** (2.007 g; 12.45 mmol) and 8 drops of "HCl" were added. Reaction mixture was refluxed for 1 h. After cooling, the crystals of the product were collected by simple vacuum filtration. The typical yield of the crude product was about 80%. The purification was performed by recrystallization from ethanol. Colorless crystals, Mp: 262-264 °C; FTIR(KBr)/cm⁻¹

¹: 3389(s), 3212(s), 1630(vs), 1609(vs), 1546(vs), 1435(s), 756(s); ¹H-NMR (250.13 MHz; DMSO-d₆) δ: 8.02 (br d, 2H, ³J = 8.0 Hz, H-5), 7.80 (br s, 4H, NH₂), 7.53 (td, 2H, ³J = 8.0 Hz, ⁴J = 2.0 Hz, H-7), 7.25 (overl, 4H, H-6, H-8), 4.40 (br t, 1H, ³J = 7.5 Hz, CH), 2.20 (m, 2H, CH₂-a), 1.22 (m, 2H, CH₂-b), 0.85 (t, 3H, ³J = 7.5 Hz, CH₃); ¹³C-NMR (62.8 MHz; DMSO-d₆) δ: 164.4 (C2), 96.1 (C3), 153.8 (C4), 114.6 (C4a), 123.0 (C5), 123.8 (C6), 132.0 (C7), 116.6 (C8), 151.9 (C8a), 33.3 (CH), 31.0 (CH₂a), 21.4(CH₂b), 13.9 (CH₃); ESI TOF-MS (m/z): calcd. for [M+H]⁺: 377.1501 found: 377.1500.

3,3'-Furfurylidenebis(4-amino-2H-chromen-2-one)(7d, C₂₃H₁₆N₂O₅).

To ethanol (40 cm³), furfural (6c) (1.2 cm³; 14.49 mmol), well powdered 5 (1.857 g; 11.52 mmol) and 8 drops of "HCl" were added. Reaction mixture was refluxed for 90 min. After cooling, the crystals of the product were collected by simple vacuum filtration. The typical yield of the crude product was about 80%. The purification was performed by dissolving the product in DMSO and precipitation with ethanol with several drops of water. Ocher crystals, Mp: 300-301 °C; FTIR(KBr)/cm⁻¹: 3452(s), 3358(s), 3221(s), 1645(vs), 1626(vs), 1608(vs), 1598(vs), 1548(vs), 1533(s), 1438(s), 756(s); ¹H-NMR (250.13 MHz; DMSO-d₆) δ: 8.08 (br d, 2H, ³J = 7.5 Hz, H-5), 7.81 (br s, 4H, NH₂), 7.65 (td, 2H, ³J = 8.0 Hz, ⁴J = 2.0 Hz, H-7), 7.50 (br s, 1H, H-4'), 7.40 (overl, 4H, H-6, H-8), 6.33 (dd, 1H, ³J = 3.0, 2.0 Hz, H-4'), 6.02 (br s, 1H, H-3'), 5.77 (s, 1H, CH); ¹³C-NMR (62.8 MHz; DMSO-d₆) δ: 163.6 (C2), 93.6 (C3), 153.6 (C4), 114.4 (C4a), 123.2 (C5), 123.9 (C6), 132.4 (C7), 116.8 (C8), 153.6 (C8a), 33.2 (CH), 151.6 (C1-furanyl), 105.6 (C2-furanyl), 110.2 (C3-furanyl), 141.6 (C4-furanyl); ESI TOF-MS (m/z): calcd. for [M+H]⁺: 401.1137; found: 401.1140.

3,3'-Benzilidenebis(4-amino-2H-chromen-2-one) (7e, C₂₅H₁₈N₂O₄).

Synthesis and purification as 7d. The typical yield was about 85%. Colorless crystals, Mp: 328-330 °C (decomp.); FTIR(KBr)/cm⁻¹: 3375(s), 3207(s), 1667(s), 1638(vs), 1622(vs), 1609(vs), 1593(vs), 1543(vs), 1520(s), 1436(s), 752(s); ¹H-NMR(250.13 MHz; DMSO-d₆) δ: 8.07 (d, 2H, ³J = 7.5 Hz, H-5), 7.78 (br s, 4H, NH₂), 7.65 (td, 2H, ³J = 8.0 Hz, ⁴J = 2.0 Hz, H-7), 7.40 (overl, 4H, H-6, H-8), 7.20 (overl, 2H, H-m), 7.10 (overl, 3H, H-o, H-p) 5.92 (s, 1H, CH); ¹³C-NMR(62.8 MHz; DMSO-d₆) δ: 164.0 (C2), 94.5 (C3), 154.1 (C4), 114.5 (C4a), 123.2 (C5), 123.8 (C6), 132.2 (C7), 116.7 (C8), 152.1 (C8a), 37.4 (CH), 138.0 (Ci), 126.5 (Co),

128.0 (Cm), 125.4 (Cp). ESI TOF-MS (m/z): calcd. for [M+H]⁺: 411.1345; found: 411.1336.

3,3'-(4-Chlorobenzilidene)bis(4-amino-2H-chromen-2-one)(7f, C₂₅H₁₇ClN₂O₄).

Synthesis and purification as 7d. The typical yield was about 90%. Colorless crystals, Mp: 315-317 °C; FTIR(KBr)/cm⁻¹: 3403(s), 3216(s), 1637(vs), 1627(vs), 1611(vs), 1545(s), 1437(s), 758(s); ¹H-NMR(250.13 MHz; DMSO-d₆) δ: 8.08 (br d, 2H, ³J = 7.5 Hz, H-5), 7.80 (br s, 4H, NH₂), 7.65 (td, 2H, ³J = 8.0 Hz, ⁴J = 2.0 Hz, H-7), 7.40 (overl, 4H, H-6, H-8), 7.29 (d, 2H, ³J = 8.0 Hz, H-m), 7.12 (d, 2H, ³J = 8.0, H-o) 5.89 (s, 1H, CH); ¹³C-NMR(62.8 MHz; DMSO-d₆) δ: 163.9 (C2), 94.1 (C3), 154.2 (C4), 114.4 (C4a), 123.2 (C5), 123.9 (C6), 132.4 (C7), 116.7 (C8), 152.1 (C8a), 37.0 (CH), 137.2 (Ci), 128.5 (Co), 127.9 (Cm), 130.0 (Cp). ESI TOF-MS (m/z): calcd. for [M+Na]⁺: 467.0775; found: 467.0777.

3,3'-(4-Nitrobenzilidene)bis(4-amino-2H-chromen-2-one)(7g, C₂₅H₁₇N₃O₆).

Synthesis and purification as 7d. The typical yield was about 80%. Dirty white crystals, Mp: >235 °C decomp.; FTIR(KBr)/cm⁻¹: 3441(s), 3354(s), 3207(s), 1634(vs), 1609(vs), 1547(s), 1528(vs), 1439(s), 1350(s), 758(s); ¹H-NMR (250.13 MHz; DMSO-d₆) δ: 8.12 (d, 2H, ³J = 7.5 Hz, H-o), 8.11 (br d, 2H, ³J = 7.5 Hz, H-5), 7.84 (br s, 4H, NH₂), 7.65 (td, 2H, ³J = 8.0 Hz, ⁴J = 2.0 Hz, H-7), 7.40 (overl, 4H, H-6, H-8), 7.40 (d, 1H, ³J = 8.5, H-m) 6.04 (s, 1H, CH); ¹³C-NMR (62.8 MHz; CDCl₃, DMSO-d₆) δ: 164.0 (C2), 93.5 (C3), 154.4 (C4), 114.4 (C4a), 123.3 (C5), 124.0 (C6), 132.5 (C7), 116.7 (C8), 152.1 (C8a), 37.3 (CH), 141.3 (Ci), 129.6 (Co), 116.7 (Cm), 148.0 (Cp); ESI TOF-MS (m/z): calcd. for [M+Na]⁺: 478.1015; found: 478.1022.

3,3'-(4-Methoxybenzilidene)bis(4-amino-2H-chromen-2-one) (7h, C₂₆H₂₀N₂O₅).

Synthesis and purification as 7d. The typical yield was about 80%. Colorless crystals, Mp: 278-280 °C; FTIR(KBr)/cm⁻¹: 3435(s), 3382(s), 3220(s), 1644(vs), 1624(vs), 1607(vs), 1593(vs), 1546(vs), 1509(s), 1434(s), 753(s); ¹H-NMR(250.13 MHz; DMSO-d₆) δ: 8.08 (br d, 2H, ³J = 7.5 Hz, H-5), 7.78 (br s, 4H, NH₂), 7.63 (td, 2H, ³J = 8.0 Hz, ⁴J = 1.2 Hz, H-7), 7.56 (d, 2H, ³J = 8.0, H-o), 7.40 (overl, 4H, H-6, H-8), 6.81 (d, 2H, ³J = 8.0, H-m), 5.87 (s, 1H, CH), 3.71 (s, 3H, CH₃); ¹H-NMR(250 MHz; CDCl₃) δ: 7.61 (br d, 2H, ³J = 8.0 Hz, H-5), 7.56 (td, 2H, ³J = 8.0 Hz, ⁴J = 1.2 Hz, H-7), 7.30 (overl, 4H, H-6, H-8), 7.13 (d, 2H, ³J = 8.0, H-o), 7.00 (br s, 4H, NH₂), 6.78 (d, 2H, ³J = 8.0, H-m), 6.13 (s, 1H, CH), 3.74 (s, 3H, CH₃); ¹³C-NMR(62.8 MHz; DMSO-d₆) δ:

163.9 (C2), 94.7 (C3), 154.0 (C4), 114.5 (C4a), 123.2 (C5), 123.5 (C6), 132.2 (C7), 116.7 (C8), 152.1 (C8a), 36.7 (CH), 129.7 (Ci), 127.5 (Co), 113.4 (Cm), 157.8 (Cp), 54.9 (OCH₃); ¹³C-NMR(62.8 MHz; CDCl₃) δ: 165.3 (br, C2), 96.9 (br, C3), 153.9 (br, C4), 114.6 (C4a), 121.5 (C5), 123.9 (C6), 132.0 (C7), 117.5 (C8), 152.7 (C8a), 37.2 (CH), 129.7 (Ci), 127.8 (Co), 113.6 (Cm), 157.2 (Cp), 55.2 (OCH₃); ESI TOF-MS (m/z): calcd. for [M+Na]⁺: 463.1270; found: 463.1275.

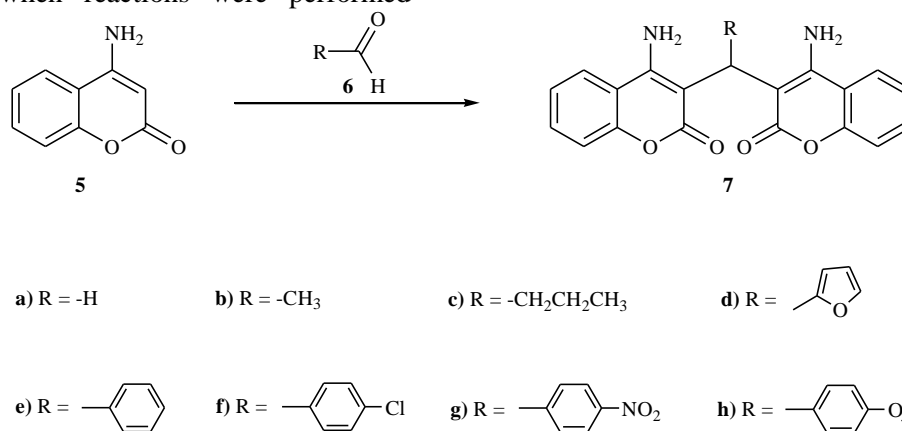
RESULTS AND DISCUSSION

Not many reactions in which 4-aminocoumarin (**5**) is involved have been studied so far, although some of its derivatives possess biological activity [29-31]. In our previous work we had shown that the C-N bond distance at **5** indicates a considerable degree of double bond character [28]. The conjugation of NH₂ with coumarine moiety is most probably the reason for very low nucleophilicity of the nitrogen atom in molecule. Knowing this, we were almost sure that aldehydes in reaction of **5** would not give nucleophilic addition product or Mannich reaction products. As we predicted, reactions of **5** with some aliphatic and aromatic aldehydes (**6**) led to corresponding dicoumarinamines (**7**) as products (Reaction Scheme 1).

Compound **5** is not soluble in water at room temperature, but soluble in aqueous solution of formaldehyde (**6a**) from where (after several minutes) crystals of dicoumaroamine **7a** were formed. Higher yield was obtained when reaction mixture was heated up to 60 °C. Reactions with other aldehydes **6** can be performed in aqueous mixture acidified with HCl, especially with alkyl aldehydes **6b** and **6c**. However, the best results were obtained when reactions were performed

refluxing acidified mixture of **5** and **6** in ethanol as a solvent.

It has been shown that the dicoumarol derivatives substituted at the bridge carbon exhibit a double hindered rotation around the bonds connecting this carbon. The restricted rotation is due to intramolecular hydrogen bonds [32-33]. The presence of hydrogen bonded structure for dicoumarols was confirmed with DFT, AIM [34] and X-ray studies [35]. The formation of these intramolecular hydrogen bonds may hold the structures in a suitable configuration for binding to an enzyme and hence may be an important factor for the biological activity. That is why we considered that is interesting to gain information on a similar process for diaminocoumarines. The most of the investigated compounds were insoluble in CDCl₃. Their NMR spectra were measured in DMSO-d₆. It is known that the intramolecular hydrogen bond is broken by the molecules of the solvent DMSO by competitive intermolecular bonding. From all investigated compounds only **7h** was dissolvable in CDCl₃ to obtain spectra in a solvent permitting formation of intermolecular hydrogen bonds. The comparison of the ¹H spectra in DMSO-d₆ and CDCl₃ showed differences in the chemical shifts, mostly of H-5 (0.46 ppm), CH (-0.26 ppm) and H-*o* (0.43 ppm), indicating different conformational behavior. The ¹H spectrum didn't exhibit doubling or broadening of signals but the signals for C-2, C-3 and C-4 in the ¹³C spectrum were broad indicating a dynamic process. Due to the low concentration, variable temperature measurements were not possible. B3LYP/6-311+G(d,p) calculations showed presence of only two stable rotamers C1 and C2 (Figure 2) with an energy difference ΔE = 9.8 kcal/mol.



Reaction Scheme 1.

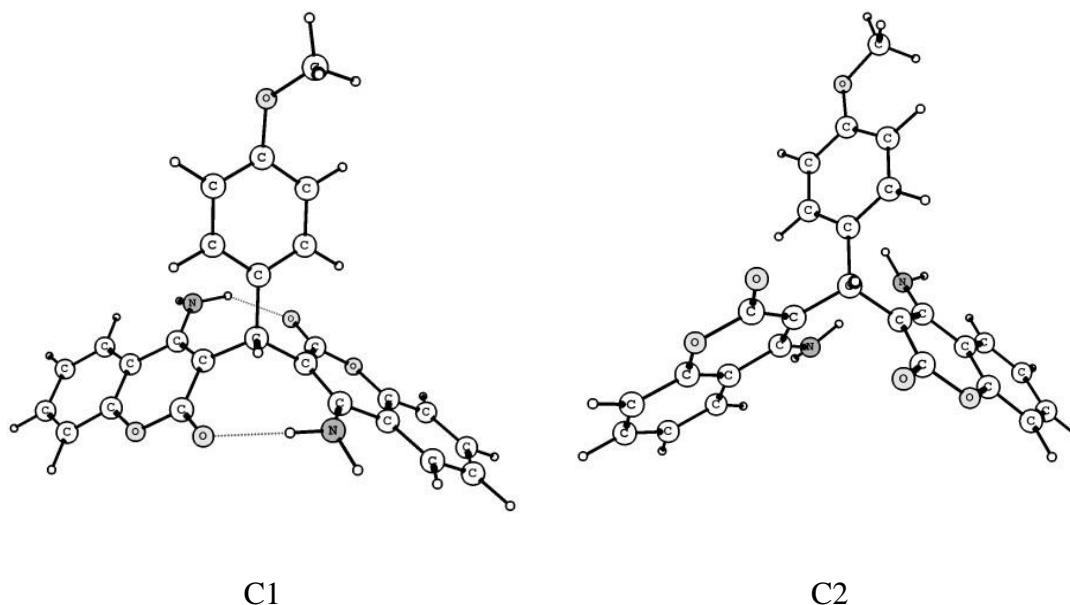


Fig. 2. Structures of the rotamers of **7h** molecule optimized by B3LYP/6-311+G** calculations.

The preferred rotamer (C1) is stabilized with an intramolecular hydrogen bond in analogy to the dicoumarols. The other is sterically favored. The hydrogen bonding $\text{NH}_2 \cdots \text{O}=\text{C}$ is less strong compared to the $\text{OH} \cdots \text{O}=\text{C}$ and the gain of steric energy could stabilize a rotamer without hydrogen bonding.

As a conclusion, 4-aminocoumarine reacts with aldehydes leading to the corresponding dicoumarinamines as products. In this way, eight compounds have been prepared and characterized for the first time. The preferred rotamer of the compound **7h** is stabilized with an intramolecular hydrogen bond in analogy to the dicoumarols. The novel dicoumarinamines might be potential bioisostere compounds of dicoumarols.

Acknowledgement: This work was supported by the Macedonian Ministry of Education and Science (Contract 03-1586) and Bulgarian National Science Fund (Contract BM-02/07)

REFERENCES

1. M. Mladenović, N. Vuković, S. Sukdolak, S. Solujić, *Molecules*, **15**, 4294 (2010).
2. A. Jakhar, J.K. Makrandi, *Indian J. Chem.*, **51**(B), 291 (2012).
3. A.A. Al-Amiery, A.A.H. Kadhum, A.B. Mohamad, *Molecules*, **17**, 5713 (2012).
4. V.M. Navarro-García, G. Rojas, M. Avilés, M. Fuentes, G. Zepeda, *Mycoses*, **54**(5), e569 (2011).
5. A.A.H. Kadhum, A.A. Al-Amiery, A.Y. Musa, A.B. Mohamad, *Int. J. Mol. Sci.*, **12**, 5747 (2011).
6. S. Čavar, F. Kovač, M. Maksimović, *Food Chem.*, **133**, 930 (2012).
7. R. Patel, N. Patel, Anti cancer activity of synthetic coumarin derivatives on Hep2 cells: Anti Cancer mechanism of Coumarin derivatives through Microtubule inhibition. LAP Lambert Academic Publishing GmbH & Co. KG: Saarbrücken, **2011**.
8. Y.M. Ma, Y.B. Zhou, C.M. Xie, D.M. Chen, J. Li, *Acta Pharmacol. Sin.*, **33**(3), 407 (2012).
9. A. Gursoy, N. Karali, *Turk. J. Chem.*, **27**, 545 (2003).
10. R.V. Patel, P. Kumari, D.P. Rajani, K. H. Chikhaliya, *Med. Chem. Res.* (Abstract from Doi: 10.1007/s00044-012-0026-x).
11. S. Stanchev, F. Jensen, A. Hinkov, V. Atanasov, P. Genova-Kalou, R. Argirova, I. Manolov, *ISRN Pharmaceutics*, Doi:10.5402/2011/137637 (2011).
12. E.B.B. Ong, N. Watanabe, A. Saito, Y. Futamura, K.H.A. El Galil, A. Koito, N. Najimudin, H. Osada, *J. Biol. Chem.*, **286**(16), 14049 (2011).
13. J.K. Adesanwo, O. Ekundayo, F.O. Shode, V.C.O. Njar, A.J.J. Van den Berge, A.T. Oludahunsi, *Niger. J. Nat. Prod. Med.*, **8**, 69, (2004).
14. R. Argotte-Ramos, G. Ramírez-Avila, C. Rodríguez-Gutiérrez Mdel, M. Ovilla-Muñoz, H. Lanz-Mendoza, M.H. Rodríguez, M. Gonzalez-Cortazar, L. Alvarez, *J. Nat. Prod.*, **69**(10), 1442 (2006).
15. Y.A. Selim, N.H. Ouf, *Org. Med. Chem. Lett.*, Doi:10.1186/2191-2858-2-1, (2012).
16. A.E. Nugroho, S. Riyanto, M.A. Sukari, K. Maeyama, *Int. J. Phytomed.*, **3**, 84, (2011).
17. M. Gebauer, *Bioorgan. Med. Chem.*, **15**(6), 2414 (2007).
18. O.M. Abdelhafez, K.M. Amin, R.Z. Batran, T.J. Maher, S.A. Nada, S. Sethumadhavan, *Bioorgan. Med. Chem.*, **18**(10), 3371 (2010).
19. J.-C. Jung, S. Oh, *Molecules*, **17**(1), 240 (2012).
20. J.-C. Jung, E. Lim, Y. Lee, D. Min, J. Ricci, O.-S. Park, M. Jung, *Molecules*, **17**(2), 2091 (2012).

21. H.Y. Zhou, J.L. Hong, P. Shu, Y.J. Ni, M.J. Qin, *Fitoterapia*, **80**(5), 283 (2009).
22. H. Madari, D. Panda, L. Wilson, R.S. Jacobs, *Cancer. Res.*, **63**(6), 1214 (2003).
23. A. Hernández, G. López-Lluch, J.A. Bernal, P. Navas, J.A. Pintor-Toro, *Mol. Cancer. Ther.*, **7**(3), 474 (2008).
24. B. Buranrat, A. Prawan, U. Kukongviriyapan, S. Kongpetch, V. Kukongviriyapan, *World J. Gastroenterol.*, **16**(19), 2362 (2010).
25. S.M. Qadri, Y. Kucherenko, C. Zelenak, K. Jilani, E. Lang, F. Lang, *Cell. Physiol. Biochem.*, **28**, 857 (2011).
26. D. Završnik, S. Muratović, D. Makuc, J. Plavec, M. Cetina, A. Nagl, E.D. Clercq, J. Balzarini, M. Mintas, *Molecules*, **16**(7), 6023 (2011).
27. M. J. Frisch, G. W. Trucks, H. B. Schlegel, G. E. Scuseria, M. A. Robb, J. R. Cheeseman, V. G. Zakrzewski, J. A. Montgomery, Jr., R. E. Stratmann, J. C. Burant, S. Dapprich, J. M. Millam, A. D. Daniels, K. N. Kudin, M. C. Strain, O. Farkas, J. Tomasi, V. Barone, M. Cossi, R. Cammi, B. Mennucci, C. Pomelli, C. Adamo, S. Clifford, J. Ochterski, G. A. Petersson, P. Y. Ayala, Q. Cui, K. Morokuma, D. K. Malick, A. D. Rabuck, K. Raghavachari, J. B. Foresman, J. Cioslowski, J. V. Ortiz, A. G. Baboul, B. B. Stefanov, G. Liu, A. Liashenko, P. Piskorz, I. Komaromi, R. Gomperts, R. L. Martin, D. J. Fox, T. Keith, M. A. Al-Laham, C. Y. Peng, A. Nanayakkara, C. Gonzalez, M. Challacombe, P. M. W. Gill, B. G. Johnson, W. Chen, M. W. Wong, J. L. Andres, M. Head-Gordon, E. S. Replogle and J. A. Pople, Gaussian 98, Revision A.7, Gaussian, Inc., Pittsburgh PA, 1998.
28. B. Stamboliyska, V. Janevska, B. Shivachev, R. P. Nikolova, G. Stojkovic, B. Mikhova, E. Popovski, *ARKIVOC*, (x), 62 (2010).
29. M. Di Braccio, G. Grossi, G. Roma, C. Marzano, F. Baccichetti, M. Simonato, F. Bordin, *Farmaco*, **58**(11), 1083 (2003).
30. G. Roma, M. Di Braccio, A. Carrieri, G. Grossi, G. Leoncini, M.G. Signorello, A. Carotti, *Biorg. Med. Chem.*, **11**, 123 (2003).
31. A.M.M. El-Saghier, M.B. Naili, B.Kh. Rammash, N.A. Saleh, K.M. Kreddanc, *ARKIVOC*, (xvi), 83 (2007).
32. R. Labbe-Bois, C. Laruelle, J. Godfroid, *J. Med. Chem.*, **18**, 85 (1975).
33. C. Laruelle, J-J. Godfroid, *Can. J. Chem.*, **54**(5), 813 (1976).
34. N. Trendafilova, G. Bauer, Ts. Mihaylov, *Chem. Phys.*, **302**, 95 (2004).
35. E. J. Valente, D. S. Eggleston, *Acta Cryst. C*, **45**, 785 (1989).

СИНТЕЗА И СТРУКТУРА НА НЯКОИ НОВИ ДИКУМАРИН-АМИНИ

Б. Михова¹, В. Яневска², Б. Стамболийска¹, Г. Дрегер³, Е. Поповски^{2,*}

¹ *Институт по органична химия с Център по фитохимия, Българска академия на науките, 1113 София*

² *Институт по химия, Факултет по естествени науки и математика, Университет „Св.св. Кирил и Методий“, Скопие, Македония*

³ *Институт по органична химия, Университет „Лайбниц“ в Хановер, Хановер, Германия*

Постъпила на 23 януари, 2013 г.; коригирана 30 март, 2013 г.

(Резюме)

В настоящата работа се съобщава за синтезата и охарактеризирането на нови дикумарин-амини (7) като потенциално био-изостерни съединения на дикумаролите (4). 3,3'-метилен-бис(4-амино-2H-хромен-2-он) (7a) е получен с висок добив в реакцията на 4-аминокумарин (5) с формалдехид във вода. Най-добри резултати на реакцията на 5 с алдехиди 6 (b-h) са постигнати когато реакцията се извършва в подкислен етанол като разтворител. Структурата и относителната стабилност на възможните ротамери са изследвани с DFT-метода на ниво B3LYP/6-31+G** с оглед тяхната биологична активност.

Comparative Studies on Russell-Saunders Atomic Term Symbols (Terms) for Equivalent Electrons of nf^4 and nf^{10} Configurations

P. L. Meena^{1*}, N. Kumar¹, A. S. Meena¹, K. S. Meena²

¹Department of Chemistry, M. L. S. University, Udaipur, Rajasthan-313001, India

²Department of Chemistry, M. L. V. Govt. College, Bhilwara, Rajasthan-311001, India

Received October 29, 2012; Revised April 9, 2013

There are two coupling schemes for obtaining Russell Saunders atomic term symbols (terms) for the equivalent electrons, one is Russell-Saunders (L-S) coupling scheme and another is spin-orbit (j-j) coupling scheme. The Russell Saunders atomic term symbol provide the information about spectral and magnetic properties of an atom. For this work computation is done to calculate all the possible microstates and atomic terms for equivalent electrons of nf^4 and nf^{10} configurations and a comparative study is carried out between the Russell Saunders atomic terms of nf^4 and nf^{10} configurations. The possible microstates counted for these configurations are 1001 and the terms obtained from these states are 47, these terms are quintets (5), triplets (22) and singlet's (20) and the predicted ground state term for both the configurations is quintet I (⁵I). The ground states for nf^4 and nf^{10} configuration are ⁵I₄ and ⁵I₈ respectively.

Key-words: Term symbol, Russell-Saunders term, Microstate, Singlet, Triplet and Quintet.

INTRODUCTION

The Russell –Saunders (L-S) coupling scheme first proposed by Henry Russell and Frederick Saunders in 1923 [1] and originally used for electrons in partially filled shells of elements with lower atomic number but for the elements with greater atomic number spin-orbit coupling becomes more significant because higher nuclear charge [2-4]. However, for heavier transition elements and rare earth elements it is still convenient to use Russell-Saunders scheme [5]. The vector model for terms which was developed before the quantum mechanical treatment was successfully used to interpret the complex spectra of systems with valence electrons in different sub shells [6]. The current nomenclature for the various energy levels (^{2S+1}L) is based on the Russell–Saunders coupling which leads to the three vectors \vec{S} , \vec{L} and \vec{J} . \vec{L} is the vectorial sum of the orbital angular momentum vectors of the valence electrons, \vec{S} is the vectorial sum of the spin angular momentum vectors of the valence electrons and \vec{J} is the vectorial sum of \vec{L} and \vec{S} . L and S coupled together to give a state of definite J [7] and the allowed values of J range from L+ S to |L-S|. The each term split into (2J+1) terms differing in energy by an amount proportional

to the applied field strength (Zeeman effect) and states are characterized by a quantum number M_J which have allowed values of J, J-1..., -J +1, -J [8]. It follows that if $L \geq S$ the J can take 2S+1 values, but if $L < S$ it can take 2L+1 values, when $L=0$ J can take only one value. The values of J may be either 1+1/2 or 1-1/2 but 1-1/2 is of lower energy state since in 1-1/2 state the orbital and spin are opposed [9, 10] By knowing the allowed values of L, S and J one can define the energy levels for the valence electrons [11].

A Russell-Saunders atomic term is applied for energy associated with the state of an atom involved in a transition and term symbols are abbreviated description of the energy levels in a multi electron atom. The degenerated state is broken up into two or more states due to electronic repulsion when the ion or atom is introduced into a lattice [12]. The equivalent electrons are those which have same values of l such as np^2 , nd^4 , nf^2 or nf^5 configuration. The formulation of hole can be used for the sub shell that is more than half full and the equivalent electrons for a pair of atoms with n^m and n^{l-x-n} ($x=6, 10$ or 14) configurations give rise identical Russell Saunders atomic term symbols [13]. Therefore, the equivalent electrons of nf^4 and nf^{10} configurations give identical terms. The numbers of microstates for the incomplete sub shell increase with increase in the number of electrons in orbital of the sub shell but in the nonequivalent electronic system the number of microstates are

* To whom all correspondence should be sent:
E-mail: parmashwar1978@gmail.com

much greater than the similar equivalent electronic system [14]. In the Russell Saunders coupling a term is specified by $(2S+1)L_J$ [2, 3, 7, 10] where $2S + 1$ the multiplicity or spin multiplicity of a term. The number of states deriving from a given term is simply $(2S+1) \times (2L+1)$ and the stability order and ground state term can be predicted by applying Hund's rule [5, 10-15].

The problem with equivalent d or f electrons or nonequivalent electrons is finding the microstates, which are 252 for nd^5 , 364 for nf^3 , 1001 for nf^4 , 2002 for nf^5 , 3003 for nf^6 and 3442 for nf^7 for equivalent electrons and for nonequivalent electrons 910 for f^2d^1 , 3640 for f^3d^1 and 10010 for f^4d^1 . Methods have been introduced to help generate the states [16, 17] and used for cases up to nd^5 for equivalent electrons. The Russell Saunders terms have been determined for equivalent electrons of nf^3 and nf^{11} configuration [18, 19] and for nonequivalent electrons of f^2d^1 configuration using R-S coupling scheme [20].

METHODOLOGY

Counting Total number of Microstates for nf^4 and nf^{10} configurations

The total number of microstates for any configuration can be counted using by following expression [21].

$$\text{Number of ways of filling electrons } N = \frac{2(2l+1)!}{x!(2(2l+1)! - x!)} \text{ or } \frac{n!}{x!(n! - x!)} \quad (1)$$

$n = 2(2l+1)$ or double of the total number of orbital's, $x =$ Total number of electrons in sub shell. So, for nf^4 configuration $n = 2(2l+1) = 14$ and $x = 4$ and for nf^{10} configuration $n = 2(2l+1) = 14$ and $x = 10$.

$$\text{For } nf^4 \text{ configuration } N = \frac{14!}{4!(14! - 4!)} \text{ and for}$$

$$nf^{10} \text{ configuration } N = \frac{14!}{10!(14! - 4!)}$$

$$N = \frac{14 \times 13 \times 12 \times 11 \times 10 \times 9 \times 8 \times 7 \times 6 \times 5 \times 4 \times 3 \times 2 \times 1}{4 \times 3 \times 2 \times 1 \times 10 \times 9 \times 8 \times 7 \times 6 \times 5 \times 4 \times 3 \times 2 \times 1}$$

Therefore, $N = 1001$ Microstates for nf^4

$$N = \frac{14 \times 13 \times 12 \times 11 \times 10 \times 9 \times 8 \times 7 \times 6 \times 5 \times 4 \times 3 \times 2 \times 1}{4 \times 3 \times 2 \times 1 \times 10 \times 9 \times 8 \times 7 \times 6 \times 5 \times 4 \times 3 \times 2 \times 1}$$

Therefore, $N = 1001$ Microstates for nf^{10}

Counting the values for Total Orbital Angular Momentum Quantum Number (L), Total Spin Angular Momentum Quantum Number (S), M_L , M_S and J

Therefore, L values for nf^4 and nf^{10} configurations are 0,1,2,3,4,5,6,7,8,9 and 10 and the

atomic terms codes for these L values are S, P, D, F, G, H, I, K, L, M and N.

The length of total orbital angular momentum vector \vec{L} is $|\vec{L}| = \sqrt{L(L+1)} \hbar$. (3)

Therefore, $|\vec{L}|$ are $\sqrt{110} \hbar$, $\sqrt{90} \hbar$, $\sqrt{72} \hbar$, $\sqrt{56} \hbar$, $\sqrt{42} \hbar$, $\sqrt{30} \hbar$, $\sqrt{20} \hbar$, $\sqrt{12} \hbar$, $\sqrt{6} \hbar$, $\sqrt{2} \hbar$ and 0.

$$\vec{S} = (s_1+s_2), (s_1+s_2-1) \dots, |(s_1-s_2)|. \quad (4)$$

Therefore, \vec{S} vectors are for nf^4 and nf^{10} configurations are 2, 1 or 0.

Therefore, \vec{S} vector length is $|\vec{S}| = \sqrt{S(S+1)} \hbar$. (5)

Therefore, for nf^4 and nf^{10} configurations of \vec{S} vectors are $\sqrt{6} \hbar$, $\sqrt{2} \hbar$ and zero.

The component of the total angular momentum along a given axis is $M_L = 2L + 1$ (6)

Here $L=10$ (maximum value of L for nf^4 and nf^{10} configurations), Therefore, $M_L = 2 \times 10 + 1 = 21$ values that ranging from +10 to -10.

The spin state for a given S value is

$$M_S = (2S+1) \quad (7)$$

Here $S=2$ (maximum value of S for nf^4 and nf^{10} configurations), Therefore, $M_S = 2 \times 2 + 1 = 5$ values that ranging from +2 to -2.

Therefore, J values for 3M term are 10, 9 and 8 and other terms illustrated in table 5 Magnitude of vector sum of L and S or magnitude of J is $\sqrt{J(J+1)} \hbar$ (8)

The vectorial sums for L and S for some terms are illustrated in figure 1.

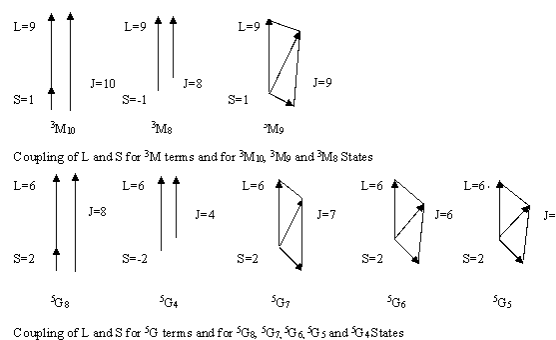


Figure 1: L-S coupling for J values for different terms and states

The Fundamental Tables for Russell Saunders Coupling Scheme

The fundamental table for equivalent electrons for nf^4 configuration (table 1) and for nf^{10} (table 2) configuration for Russell Saunders coupling scheme representing possible spin states that allowed by the Pauli Principle with the microstates. These tables include total number of microstates with spin states. The fundamental table 3

Table 1: The fundamental table for equivalent electrons of nf^4 configuration used in Russell Saunders coupling scheme representing possible spin states that allowed by the Pauli Principle with microstates.

S.N.	Possible spin states for nf^4 electrons				Total spin	Total microstates
1	↑	↑	↑	↑	+2	35
2	↑	↑	↑	↓	+1	140
3	↑	↑	↓	↓	0	210
4	↑	↓	↓	↓	-1	140
5	↓	↓	↓	↓	-2	35
6	↑↓	↑	↑		+1	105
7	↑↓	↑	↓		0	210
8	↑↓	↓	↓		-1	105
9	↑↓	↑↓			0	21

Total number of microstates for nf^4 configuration -1001

Table 2: The fundamental table for equivalent electrons of nf^{10} configuration used in Russell Saunders coupling scheme representing possible spin states that allowed by the Pauli Principle with microstates.

S.N.	Possible spin states for nf^{10} electrons						Total spin	Total microstates
1	↑↓	↑↓	↑↓	↑	↑	↑	+2	35
2	↑↓	↑↓	↑↓	↑	↑	↓	+1	140
3	↑↓	↑↓	↑↓	↑	↑	↓	0	210
4	↑↓	↑↓	↑↓	↑	↓	↓	-1	140
5	↑↓	↑↓	↑↓	↓	↓	↓	-2	35
6	↑↓	↑↓	↑↓	↑	↑		+1	105
7	↑↓	↑↓	↑↓	↑	↓		0	210
8	↑↓	↑↓	↑↓	↓	↓		-1	105
9	↑↓	↑↓	↑↓	↑↓			0	21

Total number of microstates for nf^{10} configuration - 1001

Table 3: The fundamental table representing total microstate numbers according to M_L and M_S valufor equivalent electrons of nf^4 and nf^{10} configurations.

$M_S \rightarrow$	+2	+1	0	-1	-2	Total
10			1			1
9		1	2	1		4
8		2	5	2		9
7		4	8	4		16
6	1	7	14	7	1	30
5	1	11	20	11	1	44
4	2	15	28	15	2	62
3	3	20	34	20	3	80
2	4	23	41	23	4	95
1	4	26	44	26	4	104
$\uparrow M_L$	5	27	47	27	5	111
-1	4	26	44	26	4	104
-2	4	23	41	23	4	95
-3	3	20	34	20	3	80
-4	2	15	28	15	2	62
-5	1	11	20	11	1	44
-6	1	7	14	7	1	30
-7		4	8	4		16
-8		2	5	2		9
-9		1	2	1		4
-10			1			1
Total	35	245	441	245	35	1001

representing microstate numbers according to M_L and M_S values for equivalent electrons for nf^4 and nf^{10} configurations and table 4 representing microstate array M_L versus $2S+1$ in a statistical way for both the configurations

Resolving the Microstate Chart into Appropriate Atomic States and Drawing Sub Tables for Each Terms

An atomic state forms an array of microstate consisting $2S+1$ columns and $2L+1$ rows. Thus, for a 3N state requires two columns or (21×3) array, 3M state requires (19×3) array and 5L state requires (15×5) array¹⁰. By removing each state from the microstate table a microstate sub table for each Russell Saunders term can be drawn. This treatment on microstates for both nf^4 and nf^{10} configurations give 5I , 5G , 5F , 5D , 5S , 3M , 3L , $^3K(2)$, $^3I(2)$, $^3H(4)$, $^3G(3)$, $^3F(4)$, $^3D(2)$, $^3P(3)$, 1N , $^1L(2)$, 1K , $^1I(3)$, $^1H(2)$, $^1G(4)$, 1F , $^1D(4)$ and $^1S(2)$ atomic terms. The microstates of electrons remain conserved in atomic terms, therefore, it is verified by obtaining the microstates from the atomic terms and it is given in table 5.

Stability and splitting pattern of Russell- Saunders Atomic Terms

The splitting pattern and stability order of Russell- Saunders atomic terms for equivalent or non-equivalent electrons for a particular configuration can be predicted by applying Hund's rule. For the nf^4 and nf^{10} configuration it is illustrated in (figure1) and this splitting pattern give different ground states for nf^4 and nf^{10} configurations, since one (nf^4) has less than half fill orbital configuration and another (nf^{10}) has more than half fill orbital configuration.

RESULT AND DISCUSSION

There are the three types of Russell Saunders atomic terms obtained from the microstates for equivalent electrons of nf^4 and nf^{10} configurations that are quintets (5), triplets (22) and singlet's (20). These terms are 5I , 5G , 5F , 5D , 5S , 3M , 3L , $^3K(2$ -Terms), $^3I(2$ -Terms), $^3H(4$ -Terms), $^3G(3$ -Terms), $^3F(4$ -Terms), $^3D(2$ -Terms), $^3P(3$ -Terms), 1N , $^1L(2$ -Terms), 1K , $^1I(3$ -Terms), $^1H(2$ -Terms), $^1G(4$ -Terms), 1F , $^1D(4$ -Terms) and $^1S(2$ -Terms). The ground state term for both the configurations obtained is Quintet I (5I).

CONCLUSION

It is concluded that the equivalent electrons of nf^4 and nf^{10} configurations can be arranged in 1001

$M_S \rightarrow$	+2	+1	0	-1	-2	Total
10						1
9						4
8						9
7						16
6						30
5						44
4						62
3						80
2						95
1						104
$\uparrow M_L 0$						111
-1						104
-2						95
-3						80
-4						62
-5						44
-6						30
-7						16
-8						9
-9						4
-10						1
Total	35	245	441	245	35	1001

Table 4: The fundamental table representing microstate array M_L v/s $2S+1$ in a statistical way for equivalent electrons of nf^4 and nf^{10} configurations.

S.N.	Term symbol	Total values of J	Several Possible Terms	Array	Micro States
1	1N	J=1	$^1N_{10}$	21x1	21
2	3M	J=3	$^3M_{10}, ^3M_9, ^3M_8$	19x3	57
	3L	J=3	$^3L_9, ^3L_8, ^3L_7$	17x3	51
3	$^1L(2)$	J=1	1L_8	(17x1)2	34
4	$^3K(2)$	J=3	$^3K_8, ^3K_7, ^3K_6$	(15x3)2	90
	1K	J=1	1K_7	15x1	15
	5I	J=5	$^5I_8, ^5I_7, ^5I_6, ^5I_5, ^5I_4$	13x5	65
5	$^3I(2)$	J=3	$^3I_7, ^3I_6, ^3I_5$	(13x3)2	78
	$^1I(3)$	J=1	1I_6	(13x1)	39
6	$^3H(4)$	J=3	$^3H_6, ^3H_5, ^3H_4$	(11x3)4	132
	$^1H(2)$	J=1	1H_5	(11x1)2	22
	5G	J=5	$^5G_6, ^5G_5, ^5G_4, ^5G_3, ^5G_2$	9x5	45
7	$^3G(3)$	J=3	$^3G_5, ^3G_4, ^3G_3$	(9x3)3	81
	$^1G(4)$	J=1	1G_4	(9x1)4	36
	5F	J=5	$^5F_5, ^5F_4, ^5F_3, ^5F_2, ^5F_1$	7x5	35
8	$^3F(4)$	J=3	$^3F_4, ^3F_3, ^3F_2$	(7x3)4	84
	1F	J=1	1F_3	7x1	7
	5D	J=5	$^5D_4, ^5D_3, ^5D_2, ^5D_1, ^5D_0$	5x5	25
9	$^3D(2)$	J=3	$^3D_3, ^3D_2, ^3D_1$	(5x3)2	30
	$^1D(4)$	J=1	1D_2	(5x1)4	20
10	$^3P(3)$	J=3	$^3P_2, ^3P_1, ^3P_0$	(3x3)3	27
	5S	J=1	5S_2	1x5	5
11	$^1S(2)$	J=1	1S_0	(1x1)2	2
Total number of microstates for nf^4 and nf^{10} configuration-1001					

Table 5: Conservation of state or levels a cross verification of terms and microstates for equivalent the electrons of nf^4 and nf^{10} configurations.

energy states or levels that have different values of s (spin quantum numbers) and l (angular quantum numbers) and 47 Russell-Saunders atomic spectroscopic terms symbols (terms) obtained from

these states by R-S coupling treatment. Theoretical stability order of these Russell-Saunders atomic terms according to Hund's rule is

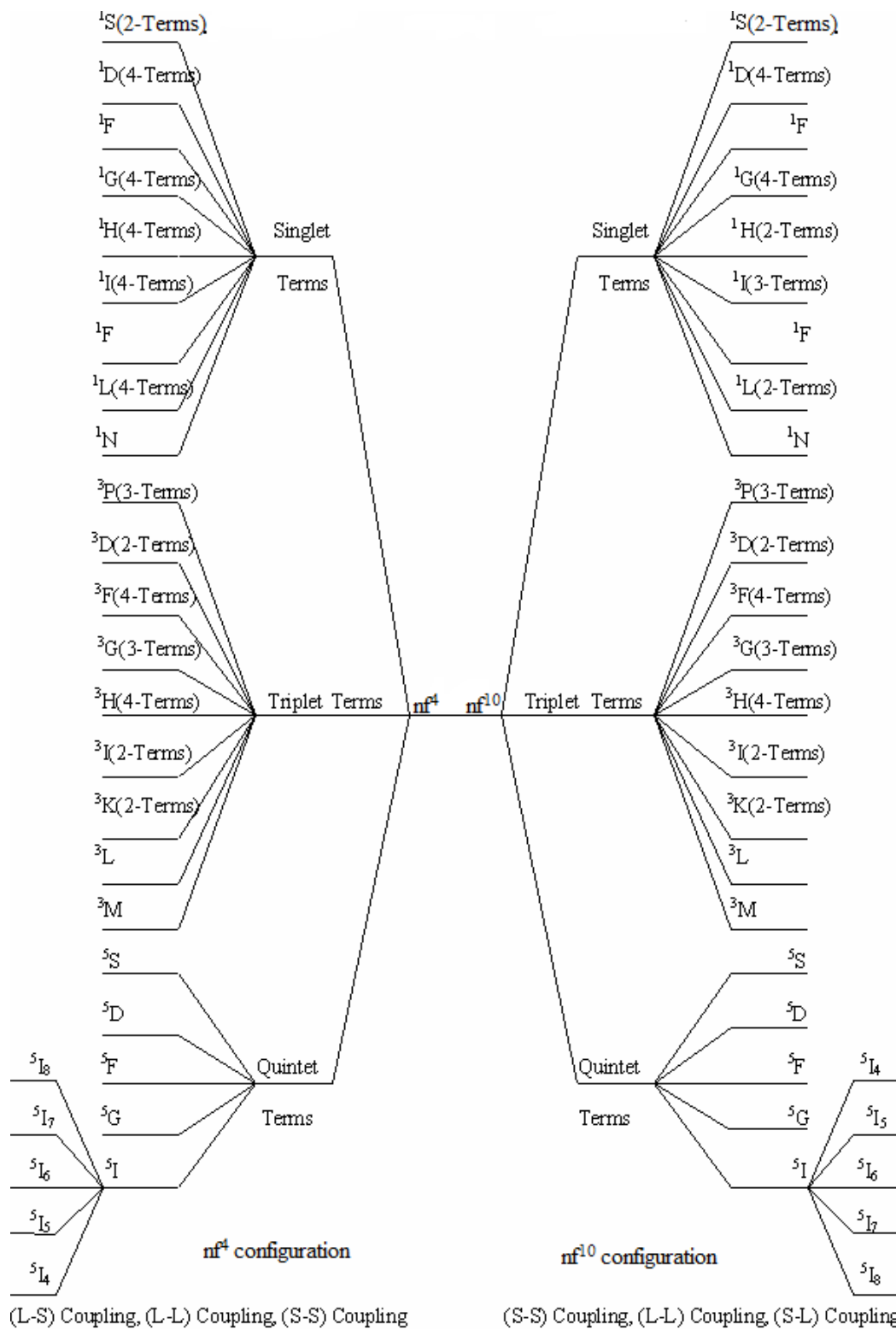


Fig. 2: The stability order and splitting pattern of Russell- Saunders atomic terms for equivalent the electrons for nf^4 and nf^{10} configurations.

$^5I_8 > ^5G > ^5F > ^5D > ^5S > ^3M > ^3L > ^3K(2) > ^3I(2) > ^3H(4) > ^3G(3) > ^3F(4) > ^3D(2) > ^3P(3) > ^1N > ^1L(2) > ^1K > ^1I(3) > ^1H(2) > ^1G(4) > ^1F > ^1D(4) > ^1S(2)$ and the stability order of ground state terms for nf^4 configuration is $^5I_8 < ^5I_7 < ^5I_6 < ^5I_5 < ^5I_4$ and for nf^{10} is $^5I_8 > ^5I_7 > ^5I_6 > ^5I_5 > ^5I_4$. This study illustrates that equivalent electrons for nf^4 and

nf^{10} configurations give same type of atomic terms and same number microstates but the ground states for both configurations are different, since nf^4 configuration has less than half fill orbital configuration while nf^{10} configuration has more than half fill orbital configuration. Therefore, the

ground state for nf^4 configuration is quintet I four (5I_4) and for nf^{10} configuration is quintet I eight (5I_8).

Acknowledgment: Authors are thankful to the members of Department of Chemistry, M. L. V. Govt. College, Bhilwara and Department of Chemistry, M. L. S. University, Udaipur, Rajasthan for helping and encouraging.

REFERENCES

1. G. K. Sweetnam, *The Command of Light*, Google books, p. 182.
2. J. L. Robert, W. J. Jones and T. Timberlake, *Astrophysics J.*, 61, 38 (1925).
3. E. Y. Wopg, *J. Chemical Phys.*, 38, 976 (1963).
4. B. P. Lever, *J. Chem. Ed.*, 45, 711-712 (1968).
5. P. R. Puri, L. R. Sharma, M. S. Pathania, "*Principle of Physical Chemistry*", Vishal Publishing Company, New Delhi, p. 104 & 107 (2008).
6. Z. Lande, *Z. Phys*, 5, 231, (1921).
7. E. M. R. Kiremire, *J. Chem. Ed.*, 64, 951-953 (1987).
8. H. N. Russell, F. A. Saunders, *Astrophysics, J.*, 61, 38, (1925).
9. B. E. Douglas, D. H. McDaniel and J. Alexander, "*Concepts of Model of Inorganic Chemistry*", 3rd Ed., Oxford and IBH Publishing Company, New Delhi, p.32-39 (1970).
10. D. H. McDaniel, *J. Chem. Ed.*, 54 (3), 147 (1977).
11. J. A. Olson, *Int. J. Quantum Chemistry*, 111, 2844-2850 (2011).
12. H. Bethe, *Amm. Physik*, 3, 121 (1929).
13. J. D. Lee, "*Concise Inorganic Chemistry*", Chapman and Hall, London, p. 947 (1996).
14. J. M. Hollas, "*Modern Spectroscopy*", Wiley India Pvt. Ltd., p.202-209 (2010).
15. D. F. Shriver and P.W. Atkins, "*Inorganic Chemistry*", Oxford University Press New York, p. 441-442 (2002).
16. K. E. Hyde, *J. Chem. Ed.*, 52, 87 (1975).
17. J. J. Vincente, *J. Chem. Ed.*, 50, 560-561 (1983).
18. P. L. Meena, P. K. Jain, N. Kumar and K. S. Meena, *Int. J. Chem. Sci.*, 9(3), 1364-1372 (2011).
19. P. L. Meena, P. K. Jain, N. Kumar and K. S. Meena, *Acta Chim. Pharm. Indica*, 2(1), 32-45 (2012).
20. P. L. Meena, P. K. Jain, N. Kumar and K. S. Meena., *Asian Journal of Chemistry*: 24(12), 5677-5679 (2012).
21. E. U. Condon and G. H. Shortly, "*The theory of atomic spectra*", Cambridge University press, London (1963).

Supplementary Data

The fundamental sub tables for each Russell Saunders atomic terms for equivalent electrons of nf^4 and nf^{10} configurations.

M_s	0
10	
9	
8	
7	
6	
5	
4	
3	
2	
1	
M_L0	
-1	
-2	
-3	
-4	
-5	
-6	
-7	
-8	
-9	
-10	
21	

$L=10, S=0, 2S+1=1, \text{Microstates}=21, \text{Term}={}^1N$

M_s	+1	0	-1
9			
8			
7			
6			
5			
4			
3			
2			
1			
M_L0			
-1			
-2			
-3			
-4			
-5			
-6			
-7			
-8			
-9			
19		19	

$L=9, S=1, 2S+1=3, \text{Microstates}=57, \text{Term}={}^3M$

M_s	+1	0	-1
8			
7			
6			
5			
4			
3			
2			
1			
$M_L 0$			
-1			
-2			
-3			
-4			
-5			
-6			
-7			
-8			
	17	17	17

L=8, S=1, 2S+1=3, Microstates=51, Term= 3L

M_s	0
8	
7	
6	
5	
4	
3	
2	
1	
$M_L 0$	
-1	
-2	
-3	
-4	
-5	
-6	
-7	
-8	
	34

L=8 S=0, 2S+1=1, Microstates=34, Term= 1L (2-Terms)

M_s	+1	0	-1
7			
6			
5			
4			
3			
2			
1			
$M_L 0$			
-1			
-2			
-3			
-4			
-5			
-6			
-7			
	30	30	30

L=7, S=1, 2S+1=3, Microstates=90, Term= 3K (2-Terms)

M_s	0
7	
6	
5	
4	
3	
2	
1	
$M_L 0$	
-1	
-2	
-3	
-4	
-5	
-6	
-7	
	15

L=7, S=0, 2S+1=1, Microstates=15, Term= 1K

M_s	+2	+1	+0	-1	-2
6					
5					
4					
3					
2					
1					
$M_L 0$					
-1					
-2					
-3					
-4					
-5					
-6					
	13	13	13	13	13

L=6, S=2, 2S+1=5, Microstates=65, Term= 5I

M_s	+1	+0	-1
6			
5			
4			
3			
2			
1			
$M_L 0$			
-1			
-2			
-3			
-4			
-5			
-6			
	26	26	26

L=6, S=1, 2S+1=3, Microstates=78, Term= 3I (2-Terms)

M_S	+0
6	
5	
4	
3	
2	
1	
$M_L 0$	
-1	
-2	
-3	
-4	
-5	
-6	
39	

L=6, S=0, 2S+1=1, Microstates=39, Term= 1I (3-Terms)

M_S	+1	0	-1
5			
4			
3			
2			
1			
$M_L 0$			
-1			
-2			
-3			
-4			
-5			
	44	44	44

L=5, S=1, 2S+1=3, Microstates=132, Term= 3H (4-Terms)

M_S	0
5	
4	
3	
2	
1	
$M_L 0$	
-1	
-2	
-3	
-4	
-5	
22	

L=5, S=0, 2S+1=1, Microstates=22, Term= 1H (2-Terms)

M_S	+2	+1	0	-1	-2
4					
3					
2					
1					
$M_L 0$					
-1					
-2					
-3					
-4					
	9	9	9	9	9

L=4, S=2, 2S+1=5, Microstates=45, Term= 5G

M_S	+1	0	-1
4			
3			
2			
1			
$M_L 0$			
-1			
-2			
-3			
-4			
	27	27	27

L=4, S=1, 2S+1=3, Microstates=81, Term= 3G (3-Terms)

M_S	+1
4	
3	
2	
1	
$M_L 0$	
-1	
-2	
-3	
-4	
36	

L=4, S=0, 2S+1=1, Microstates=36, Term= 1G (4-Terms)

M_S	+2	+1	0	-1	-2
3					
2					
1					
$M_L 0$					
-1					
-2					
-3					
	7	7	7	7	7

L=3, S=2, 2S+1=5, Microstates=35, Term= 5F

M_S	+1	0	-1
3			
2			
1			
$M_L 0$			
-1			
-2			
-3			
	28	28	28

L=3, S=1, 2S+1=3, Microstates=84, Term= 3F (4-Terms)

M_S	0
3	
2	
1	
$M_L 0$	
-1	
-2	
-3	
7	

L=3, S=0, 2S+1=1, Microstates=7, Term= 1F

M_S	+2	+1	0	-1	-2
2					
1					
$M_L 0$					
-1					
-2					
	5	5	5	5	5

$L=2, S=2, 2S+1=5, \text{Microstates}=25, \text{Term}={}^5D$

M_S	+1	0	-1
2			
1			
$M_L 0$			
-1			
-2			
	10	10	10

$L=2, S=1, 2S+1=3, \text{Microstates}=30, \text{Term}={}^3D (2\text{-Terms})$

M_S	0
$M_L 0$	
	2

$L=0, S=0, 2S+1=1, \text{Microstates}=2, \text{Term}={}^1S (2\text{-Terms})$

M_S	0
2	
1	
$M_L 0$	
-1	
-2	
	20

$L=2, S=0, 2S+1=1, \text{Microstates}=20, \text{Term}={}^1D (4\text{-Terms})$

M_S	+1	0	-1
1			
$M_L 0$			
-1			
	9	9	9

$L=1, S=1, 2S+1=3, \text{Microstates}=27, \text{Term}={}^3P (3\text{-Terms})$

M_S	+2	+1	0	-1	-2
$M_L 0$					
	1	1	1	1	1

$L=0, S=2, 2S+1=5, \text{Microstates}=5, \text{Term}={}^5S$

СРАВНИТЕЛНИ ИЗСЛЕДВАНИЯ НА АТОМНИТЕ ТЕРМОВИ СИМВОЛИ (ТЕРМОВЕ) НА RUSSELL-SAUNDERS ЗА ЕЛЕКТРОНИ ОТ nf^4 И nf^{10} -КОНФИГУРАЦИИ

П.Л. Меена^{1*}, Н. Кумар¹, А.С. Меена¹, К.С. Меена²

¹Департамент по химия, Университет М.Л.С., Удайпур, Раджастан, Индия

²Департамент по химия, Правителствен колеж М.Л.В., Бхилвара, Раджастан, Индия

Постъпила на 29 октомври, 2012 г.; коригирана на 9 април, 2013 г.

(Резюме)

Съществуват две спрегнати схеми за определянето на атомните термови символи (термове) на Russell-Saunders за еквивалентните електрони – схемата Russell-Saunders (L-S) и спин-орбиталната (j-j) схема. Атомните термови символи по Russell-Saunders дават информация за спектралните и магнитните свойства на атомите. В тази работа за извършени изчисления на всички възможни микро-състояния и атомни термове за електронните конфигурации nf^4 и nf^{10} , както и между атомните термове на Russell-Saunders на nf^4 и nf^{10} конфигурации. Възможните микро-състояния за тези конфигурации са 1001, а получените термове за тези състояния са 47, като тези термове са квинтети (5), триплети (22) и синглети (20). Термът на предсказаното основно състояние за двете конфигурации е квинтет I (5I). Основните състояния на nf^4 и nf^{10} конфигурациите са съответно 5I_4 и 5I_8 .

Metal recovery of solid metallurgical wastes. Galvanostatic electroextraction of copper from sulphate electrolytes containing Zn^{2+} and Fe^{2+} ions

G.A. Hodjaoglu, I.S. Ivanov

Institute of Physical Chemistry, Bulgarian Academy of Sciences, Acad. G. Bonchev Str., bl.11, 1113 Sofia, Bulgaria.

Received August 2, 2012; Accepted September 26, 2012

The electroextraction of copper from acidic (130 g/L H_2SO_4) sulphate electrolytes in the presence of zinc or ferrous ions was studied by means of galvanostatic methods. The coatings, deposited from electrolytes containing 1 g/L Cu^{2+} and 50 g/L Zn^{2+} , are composed predominantly of Zn (80-90%). The coatings are black and powdery. Pure Cu coatings are produced at 1 A/dm² in electrolytes containing 10 g/L Cu^{2+} and 50 g/L Zn^{2+} . The deposits are light red, smooth and semi-bright. Current efficiency of Cu deposition at 2 A/dm² from electrolytes containing 10 g/L Cu^{2+} abruptly declines with the increase in Fe^{2+} concentration. It is higher than 90% and is practically independent of Fe^{2+} concentration during deposition from electrolytes containing 50 g/L Cu^{2+} . The coatings obtained from electrolytes containing 10 g/L Cu^{2+} in the presence of Fe^{2+} ions are dark red, rough and math and those obtained from electrolytes containing 50 g/L Cu^{2+} are light red, smooth and bright. The results of the microprobe analysis indicate that in both cases the coatings are of pure copper.

Keywords: copper; zinc; iron; electrodeposition; electroextraction

INTRODUCTION

After a number of pyro- or hydrometallurgical ore treatments, large amounts of wastes with high metal content remain (Table 1).

There are numerous papers dedicated to the recovery of metals by electrolysis from scrap metal pickling wastewater [10], gold plant waste streams [11], spent copper-cyanide electroplating electrolytes [12], and stripping solutions in the manufacture of printed circuit boards [13]. Copper electrodeposition onto porous, fluidized and spouted bed electrodes and the treatment of copper-containing waste streams is studied by J. W. Evans *et al.* [14]. A study of Fe removal from Cu leachate by limestone precipitation followed by direct electrowinning of Cu has been conducted by B. Zhang [15]. The recovery of Cu from printed circuit board scraps, containing (in wt. %): Cu (24.3-30.2), Fe (0.08-0.18) and Sn (2.5 - 4.9) by mechanical processing and electrometallurgy is demonstrated by H. M. Veit *et al.* [16]. The recovery of Cu and Sn from waste stripping solutions containing 2–40 g/L Cu and 150 g/L SnO_2 is studied by S. Roy and R. Buckle [17]. M. Aghazadeh *et al.* [18] developed the fundamentals of a method for the direct recovery of Cu from brass (Cu–30 wt.% Zn) scrap based on simultaneous electrolytic dissolution of

the scrap at the anode and electrodeposition of Cu at the cathode in an acidified sulfate electrolyte. L. Petkov and B. Spasov [19] found out that electrolytic Cu extraction from dilute H_2SO_4 solutions on a pulsating cathode permits complete Cu extraction from these solutions. L. Petkov and I. Dardanova [20] established that electrolysis from dilute H_2SO_4 solutions by a fluidized bed cathode reduces the Cu content from 1 g/L to 0.2-0.5 mg/L.

These methods, however, are inapplicable to the extraction of metals from solid wastes like powders, cakes, dusts, drosses, scraps, etc., where the content of non-ferrous metals is much higher. Though these hard waste products contain Cu and Zn in commensurate amounts, there are no data available in the literature reporting of attempts to electroextract them separately.

In the literature we have met only one paper concerning the influence of little amounts of Zn^{2+} on Cu electrodeposition. Muresan *et al.* [1] have observed that during electrowinning of Cu from wastes the deposits morphology slightly differs in the presence of Zn^{2+} . This suggests that Zn^{2+} ions are electrosorbed at the interface and slightly modify the effective surface of the copper deposits. The changes occur at small Zn^{2+} additions and there are no significant differences between the deposits obtained with Zn^{2+} concentrations of 0.05 and 0.5 g/L.

* To whom all correspondence should be sent:
E-mail: isivanov@ipc.bas.bg

Table 1.

Waste	Metal content, wt.%
“Blue powder” that results from condensing furnace gases during the thermometallurgical processing of non-ferrous ores.	Zn (25-41), Pb (20-25), Fe (3-5), Cu (0.5-1) [1, 2].
Cakes obtained during purification of the electrolytes for zinc electrowinning:	
1. Copper cake	Cu (36-54), Zn (5-10) [3].
2. Copper-cadmium cake	Cu (10), Zn (30), Cd (12) [3].
3. Collective cake	Cu (5.8), Zn (35.9), Cd (7.2) [3].
4. Cobalt-nickel cake	Cu (25), Zn (20), Cd (3) [3].
5. Lead-zinc cake	Zn (17-22), Pb (4.5-7), Cu (1.8-4.5), Fe (23-27) [3].
Flue dusts at a secondary copper smelter treated in the electrowinning zinc plant.	Zn (40-65), Cu (1-6), (Pb 6-20), Fe (0.1-1.5) [4].
Flue zinc dust in smelting processes.	Zn (19.4), Fe (24.6), Cu (0.42) [5].
Mixture of zinc scrap and zinc dross resulting from the zinc cathode industry.	Zn (51.01), Cu (2.7), Fe (1.6), Pb (4.28) [6].
Cake from a Waelz kiln processing zinc-lead carbonate ores.	Zn (11.3), Fe (8.3), Pb (24.6) [7].
Beta cake at the cadmium plant in the cobalt removing stage.	Zn (8.0-9.5), Co (0.5-1.4), Fe (2.3 – 5.6), Cu (1.1) [8].
Cementates obtained during the treatment of the Zn sulphate leach liquor with As ₂ O ₃ and Zn powder.	Cu (28.6), Zn (22.4) [9].

We found only three papers that discuss the influence of ferric and ferrous ions on the electroextraction of Cu from electrolytes with low metal concentration. Dew and Phillips [21] studied their effect on the cathodic and anodic reactions for dilute (5 g/L) acid CuSO₄ electrolytes with varying concentrations and mixtures of reacting species. The cathodic reduction of Fe³⁺ to Fe²⁺ leads to a significant decrease in current efficiency of deposition at high Fe³⁺ concentrations. Re-oxidation of Fe²⁺ to Fe³⁺ at the anode will compound the effect of Fe³⁺ concentration on the current efficiency. The same authors [22] also investigated the effect of Fe²⁺ and Fe³⁺ on the efficiency of Cu electrowinning from solutions containing less than 2 g dm⁻³ Cu²⁺, with an equivalent or higher concentration of iron as Fe²⁺ and Fe³⁺. Experiments showed that the current efficiency decreased in proportion to the increase in Fe³⁺ concentration. The work has shown that the Chemelec cell can achieve reasonable efficiencies for direct electrowinning from dilute leach liquors. Das and Gopala Krishna [23] studied the influence of Fe³⁺ concentration (varied from 0.5 to 6.0 g/L) on current efficiency, power consumption and cathode quality during Cu electrowinning in an open channel cell. A decrease in current efficiency started with increasing Fe³⁺ concentration at each of the flow rates studied. When Fe²⁺ was added to a Cu²⁺ - Fe³⁺ electrolyte, the harmful effect of Fe³⁺ on the current efficiency was reduced. More than 90% current efficiency

may be achieved if the Fe³⁺/ Fe²⁺ ratio is maintained ≤ 1. A marginal increase in the current efficiency was observed at an increase in Cu²⁺ concentration. This may be due to the fact that upon increasing Cu²⁺ concentration in the bath, the solution viscosity increases, which impedes the distribution of Fe³⁺ over the cathode surface. A decrease in current efficiency was observed when Fe³⁺ concentration was increased from 1.0 to 2.0 g/L at each H₂SO₄ concentration.

The literature review shows that the problem concerning the recovery of metals by electrolysis from hard wastes is neglected.

The aim of this paper is to study the influence of electrolyte composition and electrolysis conditions on the process of metal recovery from acidic sulphate electrolytes containing Cu²⁺, Zn²⁺ and Fe²⁺ ions in ratios close to the proportion of these metals in the solid metallurgical wastes.

EXPERIMENTAL

Galvanostatic deposition was carried out in a 0.5 dm³ bath on rolled copper cathodes (5.0 cm²) at current densities of 0.5, 1, 2 or 5 A/dm² using two Pb-Ag (1%) anodes. Cu cathodes were degreased in an ultrasonic bath and etched in dilute (1:1) solution of HNO₃. The potentials of deposition were measured using mercury/mercurous sulphate electrode in 0.5M H₂SO₄ (SSE), its potential vs. NHE being +0.720 V.

Table 2. Cathodic potentials, Cu and Zn content (in wt.%), phase composition and surface appearance of coatings obtained after 30 min deposition on copper cathodes.

Electrolyte composition, g/L	i, A/dm ²	E, V Cu cath.	Deposit composition, %		Coating appearance
			Cu	Zn	
Cu ²⁺ -1 Zn ²⁺ -50 H ₂ SO ₄ -130	1	-1.425	16.2	83.8	black powdery
	5	-1.665	12.0	88.0	black powdery
Cu ²⁺ -10 Zn ²⁺ -50 H ₂ SO ₄ -130	1	-0.460	100.0	0.0	orange smooth semi-bright
	5	-0.655	95.1	4.9	dark red spongy brittle

The applied current densities in this study are adequate to the conditions for industrial metals plating. Usually plant Cu electroextraction or electrorefining is carried out at current densities of 1 - 3 A/dm², whereas the current density (5 A/dm²) is a plant condition for Zn electroextraction. Cu²⁺, Zn²⁺ and Fe²⁺ concentrations were selected taking into account the ratio between these metals in waste products generated from nonferrous metallurgical industry.

Cu²⁺ ions (as CuSO₄·5H₂O) were added to electrolytes containing 220 g/L ZnSO₄·7H₂O (50 g/L Zn²⁺) and 130 g/L H₂SO₄. Fe²⁺ ions (as FeSO₄·7H₂O) were added to electrolytes containing 10 or 50 g/L Cu²⁺ and 130 g/L H₂SO₄. Both Cu²⁺ and Fe²⁺ ions were added to electrolytes containing 220 g/L ZnSO₄·7H₂O (50 g/L Zn²⁺) and 130 g/L H₂SO₄.

Metal deposition was carried out at a practically constant concentration of Cu²⁺, Zn²⁺ or Fe²⁺ ions. The Cu²⁺ concentration decreases only by 0.05 - 0.4% after 30 minutes and by 0.5 - 4% after 5 hours of deposition.

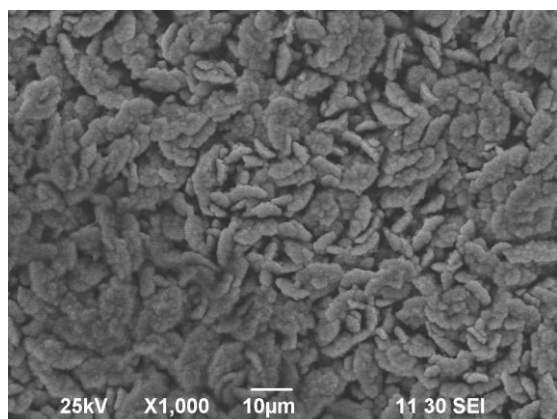
X-ray powder diffraction patterns for phase identification (characterization) of the deposits were recorded in the angle interval 20 - 110 (2θ) on a Philips PW 1050 diffractometer equipped with Cu Kα tube and scintillation detector. The surface morphology of the deposits was examined and EDX Analysis was performed by scanning electron microscopy (SEM) using a JEOL JSM 6390 microscope.

Electroextraction of Cu in the presence of Zn²⁺ ions.

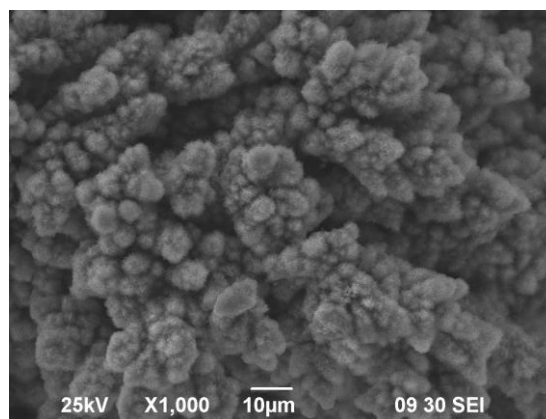
The data in Table 2 show that an increase in Cu²⁺ concentration in the electrolyte results in a decrease in the Zn content in the deposits. On the contrary, an increase in the current density yields an

increase in the content of Zn in the coatings. In electrolytes with low concentration of Cu²⁺ (1 g/L), the cathodic potentials are highly negative at both current densities, which facilitates the deposition of Zn. Besides, at the low Cu²⁺ concentration level, deposition of Cu occurs at a limiting diffusion current density (about 2 mA/cm²), which probably further decreases on longer deposition. This finding could explain the low content of Cu in the obtained coatings. There are no such diffusion limitations for the Zn²⁺ ions and hence this metal is deposited at the current density typical of electrochemical kinetics. At the higher Cu²⁺ concentration (10 g/L) the process of Cu deposition is not impeded by diffusion limitations and becomes predominating, as Cu is a more electropositive metal. At 1 A/dm², when the cathodic potential is between -0.460 and -0.485 V, a pure Cu coating is deposited, whereas at 5 A/dm², when the potential is more negative, the obtained coatings contain 4.9% Zn phase as well. Figures 1a and b show SEM pictures of coatings obtained after 30 min deposition at 1 (1a) or 5 (1b) A/dm² in electrolytes containing 1 g/L Cu²⁺, 50 g/L Zn²⁺ and 130 g/L H₂SO₄. In both cases the deposits are composed predominantly of Zn (between 80 and 90%). The coatings are black in color and powdery. Figures 2a and 2b show SEM pictures of coatings obtained after 30 min deposition from electrolytes containing 10 g/L Cu²⁺, 50 g/L Zn²⁺ and 130 g/L H₂SO₄. The coatings obtained at 1 A/dm² (2a) are light red in color with smooth and semi-bright surface. They are composed of pure Cu. The coatings deposited at 5 A/dm² (2b), however, are dark red, spongy and brittle. The coatings composition is 95.1% Cu and only 4.9% Zn.

Figures 3a and b show the SEM micrographs of pure copper coatings obtained after 30 min



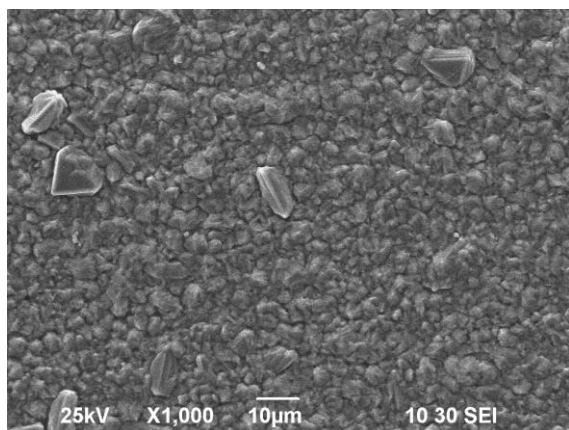
(a)



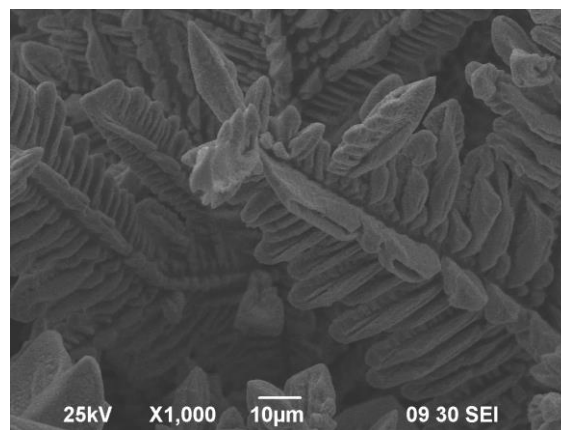
(b)

Fig. 1a. SEM micrographs of coatings obtained after 30 min deposition in an electrolyte, containing (g/L): Cu^{2+} - 1, Zn^{2+} - 50 and H_2SO_4 - 130 at 1 A/dm².

Fig. 1b. SEM micrographs of coatings obtained after 30 min deposition in an electrolyte, containing (g/L): Cu^{2+} - 1, Zn^{2+} - 50 and H_2SO_4 - 130 at 5 A/dm².



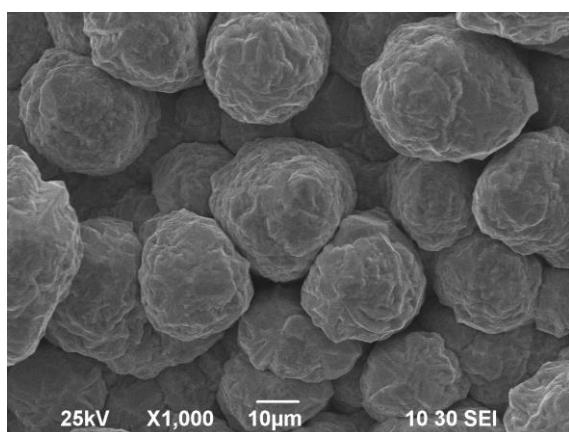
(a)



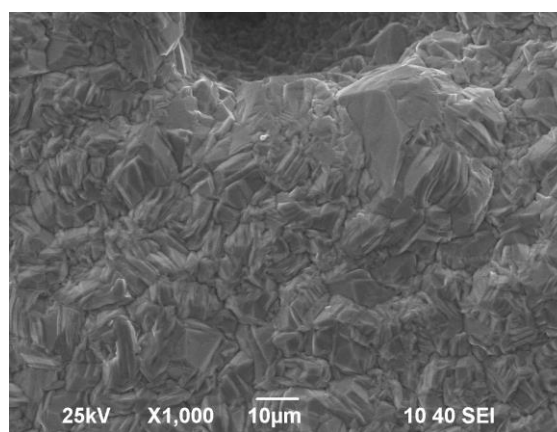
(b)

Figure 2a. SEM micrographs of coatings obtained after 30 min deposition in an electrolyte, containing (g/L): Cu^{2+} - 10, Zn^{2+} - 50 and H_2SO_4 - 130 at 1 A/dm².

Figure 2b. SEM micrographs of coatings obtained after 30 min deposition in an electrolyte, containing (g/L): Cu^{2+} - 10, Zn^{2+} - 50 and H_2SO_4 - 130 at 5 A A/dm².



(a)



(b)

Figure 3a. SEM micrographs of coatings obtained after 5 h deposition in an electrolyte, containing (g/L): Cu^{2+} - 10, Zn^{2+} - 50 and H_2SO_4 - 130 at 1 A/dm².

Figure 3b. SEM micrographs of coatings obtained after 5 h deposition in an electrolyte, containing (g/L): Cu^{2+} - 20, Zn^{2+} - 50 and H_2SO_4 - 130 at 1 A/dm².

deposition at current density 1 A/dm² and potentials between -0.430 and -0.530 V vs SSE in electrolytes containing (g/L) Cu²⁺ - 10 or 20 and H₂SO₄ - 130. The coating obtained in the electrolyte containing 10 g/L Cu²⁺ is dark red, rough and brittle (Figure 3a). The coating obtained in the electrolyte, containing 20 g/L Cu²⁺ is light red, smooth and semi-bright (Figure 3b). Light red, smooth and semi-bright coatings of pure Cu deposit are obtained at current density 0.5 A/dm² in electrolytes containing 10 or 20 g/L Cu²⁺. The current yield of Cu deposition is 97 – 99% in all cases.

Electroextraction of Cu in the presence of Fe²⁺ ions.

Figure 4 shows the dependence of current efficiency of Cu deposition (CE_{Cu}) on Fe²⁺ concentration. It is seen that CE_{Cu} sharply decreases with the increase in Fe²⁺ concentration during deposition in electrolytes containing 10 g/L Cu²⁺ and 130 g/L H₂SO₄ at a current density of 2 A/dm² (curve 1) and in electrolytes containing 50 g/L Cu²⁺ and 130 g/L H₂SO₄ at a current density of 1 A/dm² (curve 2). It is higher than 90% and is practically independent on Fe²⁺ concentration during deposition in electrolytes containing 50 g/L Cu²⁺ and 130 g/L H₂SO₄ at a current density of 2 A/dm² (curve 3). The very weak influence of Fe²⁺ on the electroextraction of Cu from electrolytes containing 50 g/L Cu²⁺ can be explained by the impeded access to the cathode of the Fe³⁺ ions formed on the anodes [23]. The reduction of ferric ions to ferrous ions on the cathode and the increased H₂ evolution may lead to a decrease in Cu current efficiency. This is, probably, the reason for the significantly

lower current efficiency when the concentrations of Cu²⁺ and Fe²⁺ are equal (10 g/L).

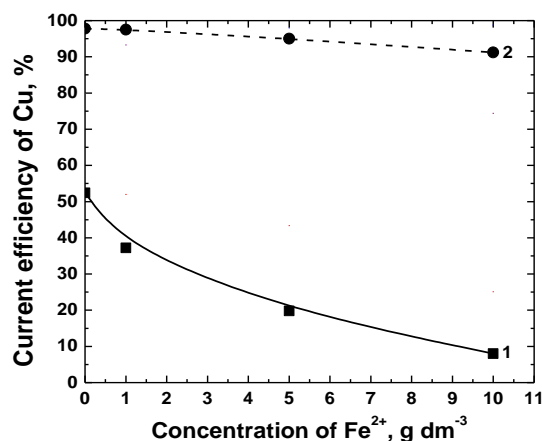
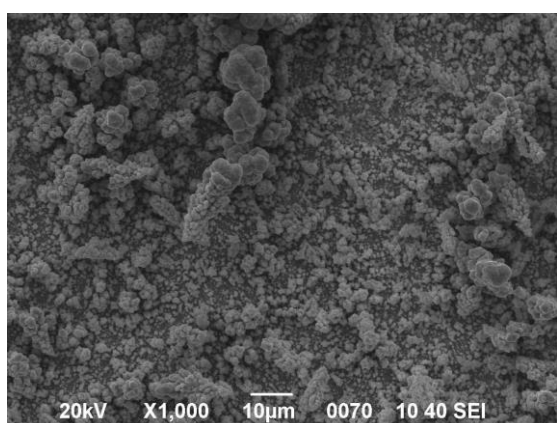
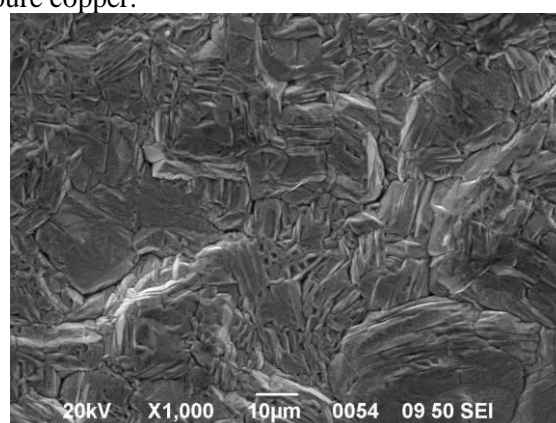


Figure 4. Dependence of the current efficiency of 5 hours galvanostatic deposition of copper as a function of Fe²⁺ concentration. Electrolytes: 1) 10 g/L Cu²⁺ and 130 g/L H₂SO₄, current density 2A/dm²; 2) 50 g/L Cu²⁺ and 130 g/L H₂SO₄, current density 1 A/dm²; 3) 50 g/L Cu²⁺ and 130 g/L H₂SO₄, current density 2 A/dm².

Figures 5a and b present SEM micrographs of copper coatings deposited for 5 h at 2 A/dm² in electrolytes containing 10 g/L Cu²⁺, 10 g/L Fe²⁺ and 130 g/L H₂SO₄ (Figure 5a) and 50 g/L Cu²⁺, 10 g/L Fe²⁺ and 130 g/L H₂SO₄ (Figure 5b). It is observed that coatings obtained from electrolytes containing 10 g/L Cu²⁺ in the presence of Fe²⁺ ions are dark red, rough and mat, probably, as a result of increased hydrogen evolution. The coatings obtained from electrolytes containing 50 g/L Cu²⁺ are light red, smooth and bright. The results of the microprobe analysis indicate that all coatings are of pure copper.



(a)



(b)

Figure 5a. SEM micrograph of Cu coating obtained in an electrolyte containing 10 g dm⁻³ Cu²⁺, 10 g dm⁻³ Fe²⁺ and 130 g dm⁻³ H₂SO₄. Current density 2A A/dm². Potential -0.615 V. Deposition time 5 h.

Figure 5b. SEM micrograph of Cu coating, obtained in an electrolyte, containing Cu²⁺ - 50 g dm⁻³, Fe²⁺ - 10 g dm⁻³ and H₂SO₄ - 130 g dm⁻³. Current density 2A/dm². Deposition time 5 h.

Electroextraction of Cu in the simultaneous presence of Zn²⁺ and Fe²⁺ ions.

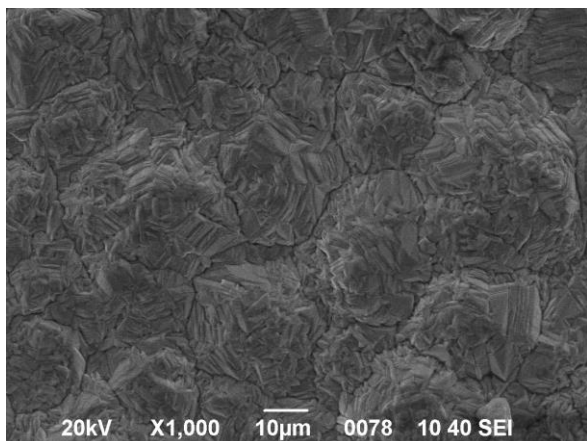


Figure 6. SEM micrograph of Cu coating, obtained in electrolytes, containing (g/L): Cu²⁺ - 50, Zn²⁺ - 50, Fe²⁺ - 10 and H₂SO₄ - 130. Current density 2 A/dm². Deposition time 5 h.

Figure 6 show deposit composition, surface appearance and SEM images of a copper coating deposited for 5 h at 2 A/dm² current density in an electrolyte containing 50 g/L Cu²⁺, 50 g/L Zn²⁺, 10 g/L Fe²⁺ and 130 g/L H₂SO₄. It is seen that the simultaneous presence of Zn²⁺ and Fe²⁺ ions leads to obtaining of a fine-grained coating similar to the coating obtained in the electrolyte containing only 50 g/L Cu²⁺ and 10 g/L Fe²⁺ (Figure 5b). The coating is light red in color, smooth and semi-bright. The microprobe analysis evidences that the coating is of pure copper.

CONCLUSION

Depending on the ratio between Cu²⁺ and Zn²⁺ ions in the electrolyte, conditions can be created favoring deposition of pure Cu and Zn phases, as well as an alloyed Cu-Zn phase with a different composition.

The coatings produced by means of galvanostatic deposition from electrolytes containing 1 g/L Cu²⁺, 50 g/L Zn²⁺ and 130 g/L H₂SO₄ are composed predominantly of Zn (80-90%). The coatings are black, smooth and powdery. Pure Cu coating is produced by deposition at 1 A/dm² in an electrolyte containing 10 g/L Cu²⁺, 50 g/L Zn²⁺ and 130 g/L H₂SO₄. Alloyed Cu-Zn coatings are produced at 5 A/dm² with Zn content of 4.9%. The coating deposited at 1 A/dm² is orange in color, smooth and semi-bright, while the coating obtained at 5 A/dm² is dark red, spongy and brittle.

To produce fine-grain, dense and smooth coatings of pure Cu in the presence of Zn²⁺ ions, the concentration of Cu²⁺ ions in the electrolyte should

be higher than 10 g/L and the current density should not exceed 1 A/dm².

On galvanostatic Cu deposition at 2 A/dm² from electrolytes containing 10 g/L Cu²⁺ and 130 g/L H₂SO₄, the current efficiency abruptly declines with the increase in Fe²⁺ concentration from 1 to 10 g/L. The coatings obtained at a current density of 2 A/dm² from electrolytes containing 10 g/L Cu²⁺ and 10 g/L Fe²⁺ are of pure copper, dark red in color, brittle and powdery.

The current efficiency of copper electrodeposition in electrolytes containing 50 g/L Cu²⁺ and 130 g/L H₂SO₄ is higher than 90% and slightly decreases with the increase in Fe²⁺ concentration. The coatings are of pure copper, light red in color, smooth and semi-bright in appearance.

On galvanostatic deposition at 2 A/dm² from electrolytes containing 50 g/L Cu²⁺, 50 g/L Zn²⁺, 10 g/L Fe²⁺ and 130 g/L H₂SO₄, the obtained coatings are of pure copper, light red in color, smooth and semi-bright.

REFERENCES

- 1.L. Muresan, A. Nicoara, S. Varvara, G. Maurin, *J Appl Electrochem.*, **29**, 719 (1999).
- 2.L. Muresan, S. Varvara, G. Maurin, S. Dorneanu, *Hydrometallurgy*, **54**, 1 (2000).
- 3.V.D. Karoleva, *Metallurgy of heavy non-ferrous metals, Part II*, c/o Jusautor, Sofia (1986).
- 4.R. Kammel, M. Goktepe, H. Oelmann, *Hydrometallurgy*, **19**, 11 (1987).
- 5.M.K. Jha, V. Kumar, R.J. Singh, *Resources, Conservation and Recycling*, **33**, 1 (2001).
- 6.L.J.L. Blanco, V.F.M. Zapata, D. De Juan Garcia, *Hydrometallurgy*, **54**, 41 (1999).
- 7.M.D. Turan, H.S. Altundogan, F. Tumen, *Hydrometallurgy*, **75**, 169 (2004).
- 8.R. Raghavan, R.N. Upadhyay, *Hydrometallurgy*, **51**, 207 (1999).
- 9.D. Melzner, J. Tilkowski, A. Mohrmann, W. Poppe, W. Halwachs, K. Schogerl, *Hydrometallurgy*, **13**, 105 (1984).
- 10.J.-S. Huang, I.-C. Lee, B.-J. Lin, *Water Sci. Technol.*, **28** (7), 223 (1993).
- 11.F.A. Lemos, L.G.S. Sobral, A.J.B. Dutra, *Minerals Engng*, **19**, 388 (2006).
- 12.A.J.B. Dutra, G.P. Rocha, F.R. Pombo, *J. Hazard. Mat.*, **152**, 648 (2008).
- 13.K. Scott, X. Chen, J.W. Atkinson, M. Todd, R.D. *Resources, Conservation and Recycling*, **20**, 43 (1997).
- 14.J.W. Evans, R. Ding, A. Neugebauer, F.M. Doyle, V. Jirichy, *Proc. Metal Separation Technologies III – Prof. Holappa Honorary Symposium, Copper Mountain, Colorado* (2004).

15. B. Zhang, 4th International Conference COPPER 99-COBRE 99, 669 (1999).
16. H.M. Veit, A. M. Bernardes, J. Z. Ferreira, J. A. S. Tenorio, C. de Fraga Malfatti, *J. Hazard. Mat.*, **B137**, 1704 (2006).
17. S. Roy, R. Buckle, *Separ. Purif. Technol.* **68**, 185 (2009).
18. M. Aghazadeh, A. Zakeri, M.Sh. Bafghi, *Hydrometallurgy*, **111–112**, 103 (2012).
19. L. Petkov, B. Spasov, *J. Environ. Protectn Ecol.*, **9**, 375 (2008).
20. L. Petkov, I. Dardanova, *J. Environ. Protectn Ecol.*, **9**, 384 (2008).
21. D.W. Dew, C.V. Phillips, *Hydrometallurgy*, **14**, 331 (1985).
22. D.W. Dew, C.V. Phillips, *Hydrometallurgy*, **14**, 351 (1985).
23. S.C. Das, P.G. Krishna, *Int.J. Mineral Process.*, **46**, 9 (1996).

ИЗВЛИЧАНЕ НА МЕТАЛИ ОТ ТВЪРДИ МЕТАЛУРГИЧНИ ОТПАДЪЦИ.
ГАЛВАНОСТАТИЧНА ЕЛЕКТРОЕКСТРАКЦИЯ НА МЕД ОТ СУЛФАТНИ
ЕЛЕКТРОЛИТИ, СЪДЪРЖАЩИ Zn^{2+} И Fe^{2+} ЙОНИ

Г. А. Ходжаоглу, Ив. С. Иванов

*Институт по физикохимия “Акад. Р. Каишев”, Българска академия на науките, ул. “Акад. Г. Бончев”,
блок 11, София 1113*

Постъпила на 2 август 2012 г.; приета на 26 септември, 2012 г.

(Резюме)

Посредством галваностатични методи е изследвана електроекстракцията на мед от сернокисели (130 g/L) сулфатни електролити в присъствието на Zn^{2+} или Fe^{2+} йони. Покритията, отложени от електролити, съдържащи 1 g/L Cu^{2+} и 50 g/L Zn^{2+} са съставени предимно от Zn (80-90%). Покритията са черни и прахообразни. Покрития от чиста мед се получават при 1 A/dm² от електролити, съдържащи 10 g/L Cu^{2+} и 50 g/L Zn^{2+} . Покритията са светлочервени на цвят, гладки и полублестящи. Добивът по ток на медното отлагане при 2 A/dm² от електролити, съдържащи 10 g/L Cu^{2+} рязко намалява с нарастването на концентрацията на Fe^{2+} . Добивът по ток е по-висок от 90% и практически не зависи от концентрацията на Fe^{2+} при отлагане от електролити, съдържащи 50 g/L Cu^{2+} . Покритията, получени от електролити, съдържащи 10 g/L Cu^{2+} в присъствието на Fe^{2+} йони са тъмночервени, грапави и матови, а тези получени от електролити, съдържащи 50 g/L Cu^{2+} са светлочервени, гладки и блестящи. И в двата случая покритията са от чиста мед.

Removal of detergents by zeolites and membranes

B. Tsyntsarski¹, B. Petrova¹, T. Budinova^{1*}, N. Petrov¹, A. Sarbu², T. Sandu²,
M. Ferhat Yardim³, A. Sirkecioglu³

¹*Institute of Organic Chemistry, Bulgarian Academy of Sciences, Acad. G. Bonchev str., BL.9, 1113 Sofia*

²*National Research and Development Institute for Chemistry and Petrochemistry-ICECHIM, Polymers Department, 202 Independentei Spl., Bucharest, Romania*

³*Istanbul Technical University, Department of Chemical Engineering, 34469 Maslak, Istanbul, Turkey*

Received January 16, 2013; Accepted February 12, 2013

The adsorption of sulfonic and phenolic substances in detergents by natural zeolites from Turkish and Romanian deposits was investigated. The zeolites were characterized by IR spectroscopy and surface measurements. The effects of contact time and pH on the adsorption process were investigated. It was established that the specific surface area is the determining factor which influences mostly on the adsorption of detergents. The removal of detergents was also investigated by applying different membranes. They have demonstrated higher adsorption capacity values than zeolites.

Key words: zeolite; membrane; adsorption; detergent; water

INTRODUCTION

The production of different washing materials has been always accompanied by regular accumulation of substantial quantities of detergents in waste waters. Currently used detergents generally consist of surfactants, bleaching agents, additives for secondary benefits, enzymes, etc. The effective removal of these hardly degradable pollutants from waste waters is a global problem of great importance. Many research efforts on the improvement of the adsorption process and adsorbent materials for removal of organic pollutants from waste water streams have been developed in the last years. Activated carbon is the most used adsorbent; however its regeneration is difficult and expensive. Recently many researchers are investigating new, efficient and regenerable adsorbents, such as inorganic materials, e.g. zeolites and clay materials [1-8]. An important benefit of zeolites is that they are stable and inclined to regeneration. Since the thermodynamics and kinetics of gas-phase adsorption of organic molecules by zeolites have been thoroughly investigated, the studies of adsorption of organic molecules by zeolites from aqueous solutions are relatively rare [7]. The adsorption from aqueous solution depends not only on the zeolite pore structure, but also on the competition between the

organic molecules and water molecules for the zeolite adsorption sites.

Advances in nano-scale science and engineering are providing unprecedented opportunities to develop low-cost and environmentally acceptable water purification processes. Besides, the adsorptive materials, membranes, membrane separation techniques are also promising as an effective alternative for water purification from various pollutants. The fundamental understanding of membrane performance is important for the suitable selection and application in industrial systems. There are many studies on the removal of organic substances from diluted solutions using membranes [9-14], but reports on separation of toxic detergents by membranes are rare in the literature. This paper gives a brief overview of the use of membranes in the purification of water, contaminated by toxic detergents.

This work aims to investigate the influence of structural and surface properties of zeolites and membranes on detergent removal (sulfonic and phenolic substances) in aqueous solution. This is a part of our efforts to develop an average scale module for purification of small factories waste waters from different pollutants, on the base of multi-layered filter containing natural zeolites and polymer membranes.

* To whom all correspondence should be sent:
E-mail: goriva@orgchm.bas.bg

EXPERIMENTAL

Characterization of the initial materials

In this study three zeolite samples and two membrane samples were investigated towards adsorption of sulfonic and phenolic substances. The first zeolite sample is from Romania (location: Marsid, Bocsă-Borla) and the other two zeolite samples are from Turkey (location: Bigadic and Gordes).

The membrane samples are prepared as follows:

Membrane M1 - from polymer mixture of 80 % C1 (prepared from monomer mixture of 90 % acrylonitrile (AN) and 10 % vinyl acetate (AcV) and 20 % polyvinyl alcohol (APV) , with coagulation bath composition of 70 % iso-propanol (IzOH) and 30% water.

Membrane M2 – polymer mixture of 80 % C2 (prepared from a monomer mixture of 80 % AN, 20% AcV) and 20 % APV.

Analytical methods for characterization of zeolites

The following methods were applied and equipment's were used for characterization of the zeolites:

- X-ray diffractometer BRUKER D8 ADVANCE, equipped with DIFFRA Cplus Commander XRD (Bruker AXS), and using Bragg-Brentano diffraction method, with coupling Θ - Θ in vertical configuration.

- Surface measurements were performed by porosimeter ASAP 2020 (Micromeritics).

- The samples were also analyzed by FTIR spectroscopy, using Bruker IFS 113V spectrophotometer, with resolution of 1 cm^{-1} . The samples were mixed with potassium bromide and the mixture was pressed into pellets to be used in the analysis.

Adsorption from aqueous solutions

Adsorption experiments were carried out by using a zeolite sample Marsid with two fractions: $\leq 0.09\text{ mm}$ and $0.10\text{-}0.14\text{ mm}$.

The adsorption capacity of the adsorbents for sulfonates and phenolic compounds were investigated by using Bulgarian commercial dishwashing liquid (pH 6.7). Adsorption experiments were conducted using aqueous solutions, containing different volumes of liquid detergent. Portions of adsorbents with amount of

0.1 g were used in the adsorption measurements. They were added to portions of the liquid detergent with volume of $5\text{-}30\text{ mL}$ and water was added in order to obtain final volume of 50 mL for each solution. Then the solutions were shaken for 5 min to 2 h . The amount of the sulfonates and phenolic compound were determined at wavelengths 220 and 269 cm^{-1} respectively, using UV spectrophotometer Pharo 300 [15, 16].

The factors affecting the sorption of the investigated detergents from aqueous solution, such as contact time, particle size distribution and effect of pH were studied.

The effect of pH of the solution on the equilibrium adsorption of sulfonate and phenolic compounds is investigated by using 0.1 g adsorbent and 50 mL solution (containing 20 mL liquid detergent) at 1 h contact time. The initial pH values of the solutions were adjusted with either HCl or NaOH.

RESULTS AND DISCUSSION.

Characterization of the natural zeolite samples

The results from XRD analysis (Fig.1) show that all the studied natural zeolites dominantly contain clinoptilolite.

Table 1 was prepared on the base of XRD results, which demonstrates the content of different minerals in the zeolite samples.

From XRD and atomic spectrophotometry results, the structural chemical phase composition of the samples were established and data are presented in Table 2.

The data in Table 2 show that the Turkish zeolites contain slightly higher amount of Al_2O_3 in comparison with zeolite sample Marsid. All the samples have high amount ($>60\%$) of silicon dioxide, whereas Gordes zeolite has the highest. The content of aluminium oxide in all samples is in between $12\text{-}13\%$. There are higher amounts of alkaline oxides in Bigadic and Gordes zeolites than Marsid zeolite. At the same time, the Bigadic zeolite contain more CaO and Fe_2O_3 than Marsid zeolite (contains half of the amount of Fe_2O_3 contained in Bigadic zeolite), and their content in Gordes zeolite (contains one-third of the amount of Fe_2O_3 contained in Bigadic zeolite) is the lowest.

Surface characterization results of Marsid, Bigadic and Gordes zeolites are presented in Table 3.

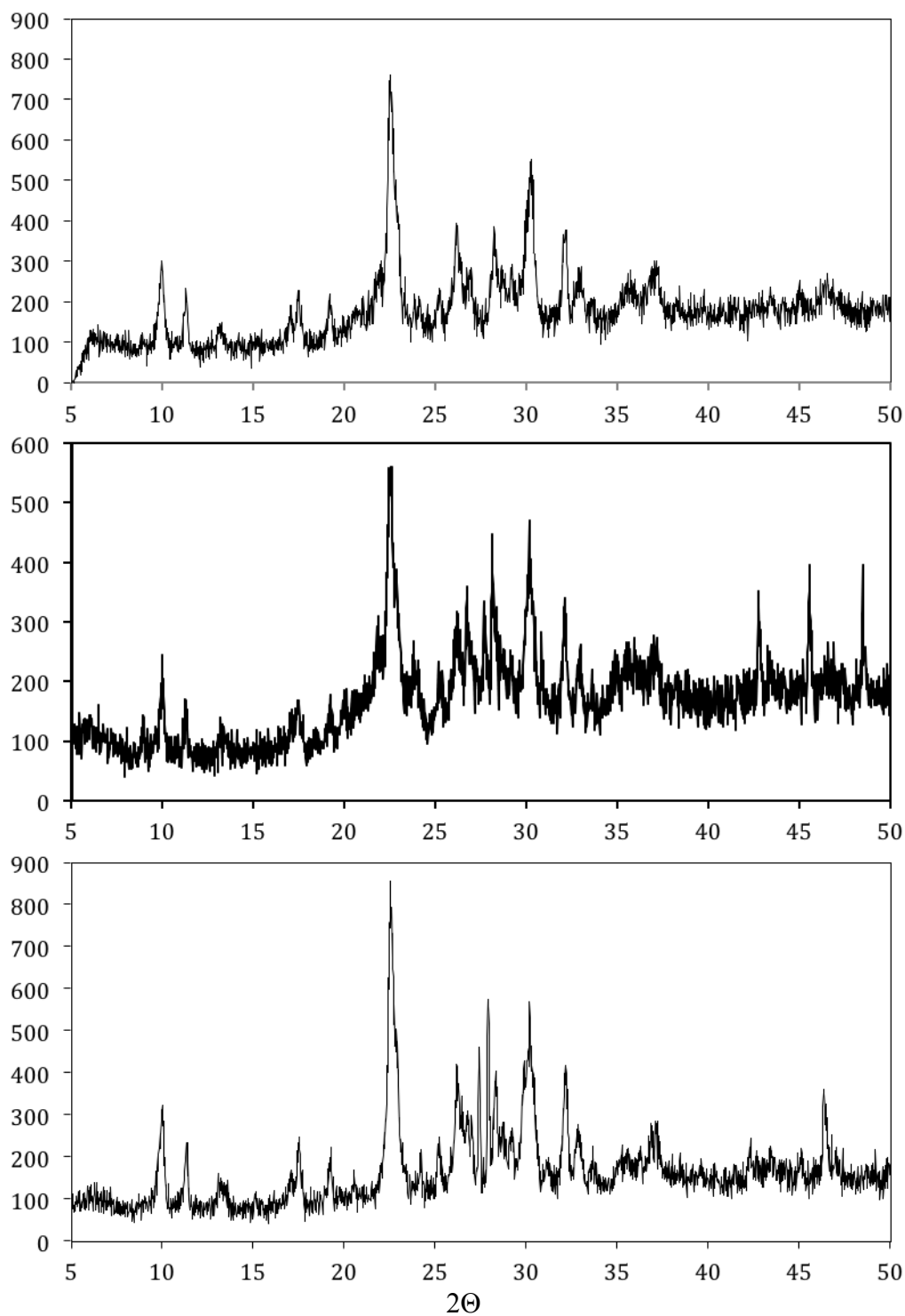


Fig 1. XRD patterns of Marsid, Gordes and Bigadic clinoptilolites

The data from Table 3 shows that the Marsid clinoptilolite has higher surface area and lower pore volume and pore radius than the other zeolites, as the average pore radius is lowest for the zeolite Marsid. Chemical character of the surface of Gordes and Marsid zeolites is probably due to the higher content of alkaline oxides.

The IR spectra of the zeolite Marsid is shown in Fig. 2. The bands are assigned to different vibration modes of the zeolite matrix were presented in Table 4 [17-19]. IR spectra (not shown) of Bigadic and Gordes zeolites are similar. IR results confirm that the investigated natural zeolites mainly contain the mineral clinoptilolite.

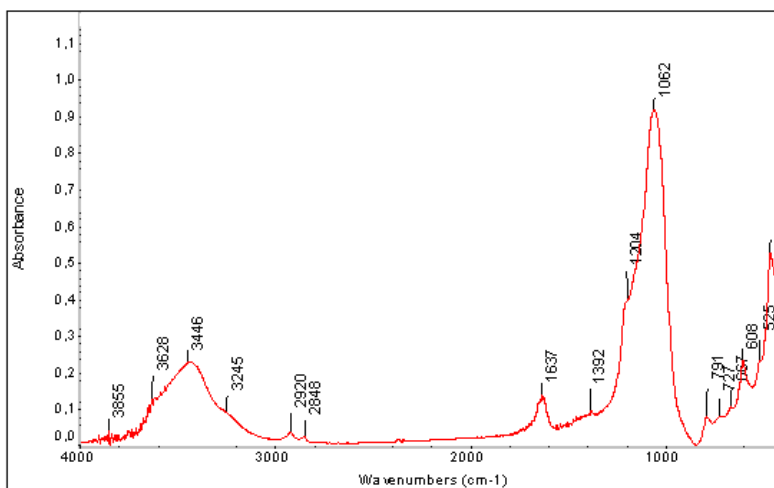


Fig. 2. IR spectra of clinoptilolite.

Table 1. Content of different minerals in zeolite samples

	Bigadic	Gordes	Marsid
Clinoptilolite content, %	@ 95	>96	75-80
Plagioclase	+	-	+
Cristobalite	+	-	+
Quartz	+	+	+
Biotite	+	+	-
Clays	+	-	-

Table 2. Chemical composition of the clinoptilolite samples, (wt. %).

	Bigadic	Gordes	Marsid
SiO ₂	64.00	71.98	66.21
Al ₂ O ₃	13.56	12.56	12.37
Na ₂ O	0.45	0.96	0.39
K ₂ O	3.61	4.28	2.43
CaO	3.61	1.99	2.44
Fe ₂ O ₃	1.35	0.45	0.74
MgO	-	0.42	0.86
H ₂ O	5.67	7.40	6.82
SiO ₂ /Al ₂ O ₃	4.72	6.32	5.35

Table 3. Surface characteristics of zeolites.

Clinoptilolite	Specific	Pore	Average	pH
	Area, m ² /g	Volume cm ³ /g	Pore Diameter Å	
Marsid	43.4	0.061	56.36	4.8
Gordes	30	0.165	42.12	7.5
Bigadic	28	0.075	111.2	7.3

Adsorption experiments for the zeolite samples

The results of the adsorption of detergents from aqueous solutions, containing different volumes of liquid detergent, 5, 10, 15, 20 and 30 mL (for each solution water was added in order to obtain final volume of 50 mL), are shown in Fig. 3, Fig. 4 and Fig. 5 for Marsid, Gordes and Bigadic zeolites, respectively. All the isotherms are type L of Giles classification, indicating that adsorption proceeds by the formation of a monolayer in the range of concentrations used [20].

Table 4. IR bands of clinoptilolite .

Hydroxy groups of basic nature	4000-3000 cm ⁻¹
CO ₂ (in the air)	2300 cm ⁻¹
H ₂ O (air+ads.)	1637 cm ⁻¹
Si-O asymmetric stretching	1204 cm ⁻¹
Si-O-Al asymmetrical stretching	1062 cm ⁻¹
O-Si-O symmetric stretching	791 cm ⁻¹
symmetric stretching of free SiO ₄	727 cm ⁻¹
symmetric stretching of free SiO ₄	667 cm ⁻¹
O-Si-O bending	608 cm ⁻¹
“pore opening” vibration of free SiO ₄	525 cm ⁻¹
Si-O bending	468 cm ⁻¹

The experimental data were fit to the Langmuir equation in linear form [21]:

$$C_e/Q_e = 1/Q_0b + C_e/Q_0 \quad (1)$$

where C_e is the equilibrium pollutant concentration remaining in solution after adsorption (mg L⁻¹), Q_e is the amount of pollutant adsorbed on the adsorbent (mg g⁻¹), Q₀ is the maximum amount of the pollutant per unit weight of adsorbent (mg g⁻¹), and b is a constant related to the affinity of adsorption sites (L mg⁻¹). The shape of the isotherms shows that the process of adsorption of detergents can be described by Langmuir theory, which states that adsorption proceeds via a monolayer formation.

Results (Fig. 3, Fig.4 and Fig. 5) show that Marsid zeolite with granulometric composition of ≤ 0.09 mm has the highest adsorption capacity. The samples with alkaline character of the surface - Bigadic and Gordes zeolites - show lower adsorption capacity towards both sulfonic and

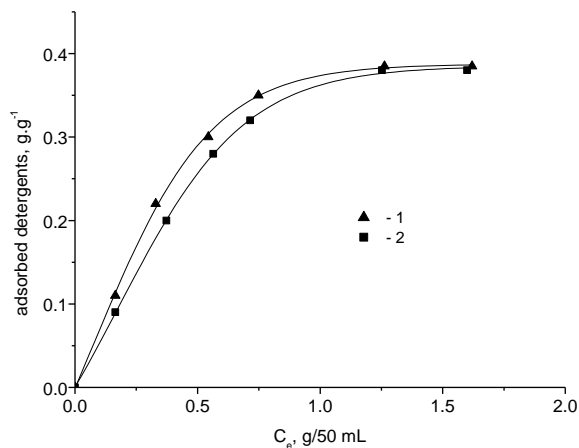


Fig. 3. Adsorption of detergents on Marsid zeolite: 1 - sulfonic compounds, 2 - phenolic compounds.

phenolic compounds (Fig. 4 and Fig. 5). These results indicate that the determining factors for their adsorption properties are the surface area and the pore size distribution of the samples, as well as the different chemical composition and chemical character of the surface.

Fig 6 shows the adsorption of sulfonic and phenolic compounds on the zeolite Marsid sample with particle size 0.10-0.14 mm. The enhancement of the particle size decreases the specific surface area, which causes reduction of the number of the active sites.

Comparing Fig 3 and Fig. 6 allows to understand the effect of the granulometric composition of the zeolites on the adsorption of both detergents (all zeolites show similar dependence).

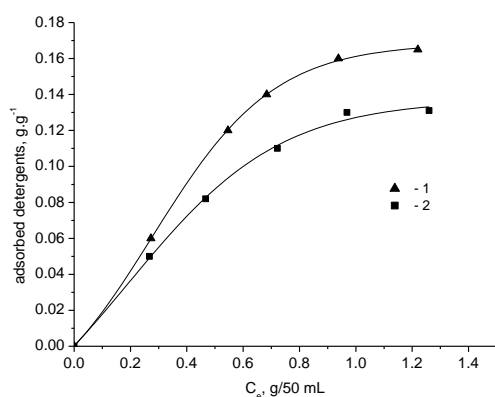


Fig. 4. Adsorption of detergents on Gordes zeolite: 1 - sulfonic compounds, 2 - phenolic compounds.

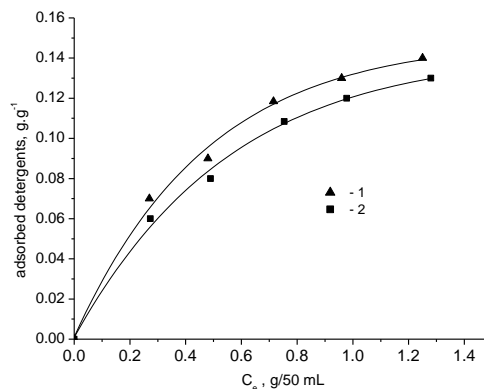


Fig. 5. Adsorption of detergents on Bigadic zeolite: 1 - sulfonic compounds, 2 - phenolic compounds.

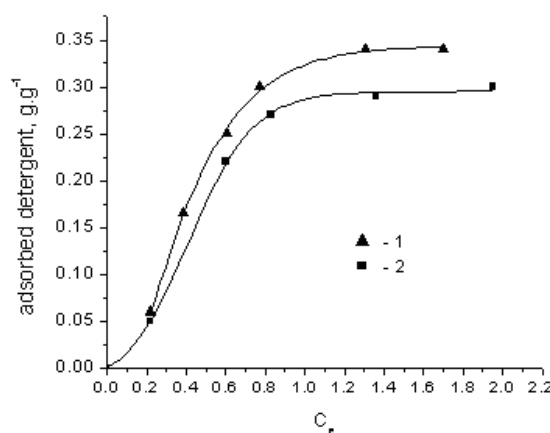


Fig. 6. Adsorption of detergents on Marsid zeolite samples with particle size 0.10-0.14 mm.

The increase of the size of the particles leads to decrease of the adsorption activity. Figure 7 shows the effect of the contact time on the removal of sulfonic compounds by Marsid zeolite. Data indicate that the removal of sulfonates increases with time and attains equilibrium in 30 minutes for all initial concentrations of the sulfonate solutions.

Sulfonate adsorption increases sharply for a short time and slows gradually when equilibrium is approaching. This behavior can be attributed to the decrease in the number of available sites on the zeolite surface during the process. The plot shows that the amount of sulfonate compounds adsorbed on the adsorbents (mg/g) vary in smooth and continuous curves, leading to saturation, which indicates the possibility for formation of monolayer coverage of sulfonates on the surface of the adsorbent. The kinetic curves (not shown) of the removal of sulfonates versus contact time for other zeolite samples show the same dependence.

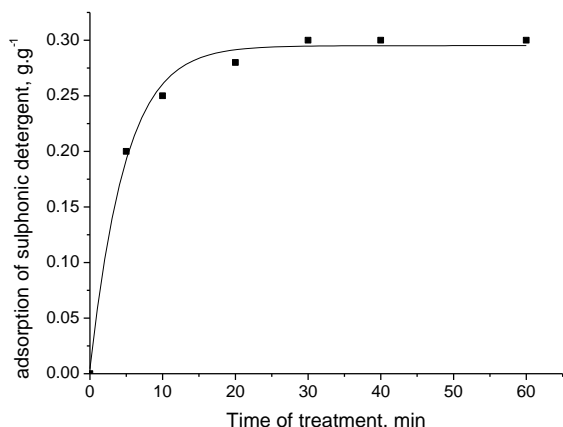


Fig. 7. Effect of contact time on adsorption at different concentrations of sulfonic compounds on zeolite Marsid.

Effect of pH on adsorption on zeolites

The pH of the aqueous solution has strong effects on the adsorption of different substances on the zeolite surface. pH is one of the key factor that control the adsorption in such processes, since it influences the electrostatic interactions between the adsorbent and the adsorbate.

The adsorption depends on the nature of the surface of the adsorbent and of the substances in the water solution. It was established that the Marsid zeolite has the lower pH value than other zeolites. Fig. 8 and Fig. 9 shows the effect of pH values on the adsorption of detergents on Gordes and Marsid zeolites. The target pH value was obtained by adding adequate amounts of NaOH or HCl diluted solutions to the initial non-buffered solution, containing sulfonic and phenolic compounds. The uptake of both compounds was found to be maximal at pH 6, independently with the fact that they have different pH values at initial conditions. As expected, these results confirm that both compounds are preferentially adsorbed from their neutral solutions. For both pollutants the amount adsorbed appeared to be much altered at neutral pH.

As the pH increases, the surface of zeolites is being negatively charged until solution $pH > pHPZC$, where the amount of negative charges becomes predominant in the zeolite surface. At this point, the fall in the uptake is probably due to the repulsive interactions, that appear between the anionic form of the adsorbates and the charges on the clinoptilolite surface. Other reason could be the competitive adsorption between sulfonate/phenolic and chlorine ions (probably present as impurities), which hinders detergent uptake.

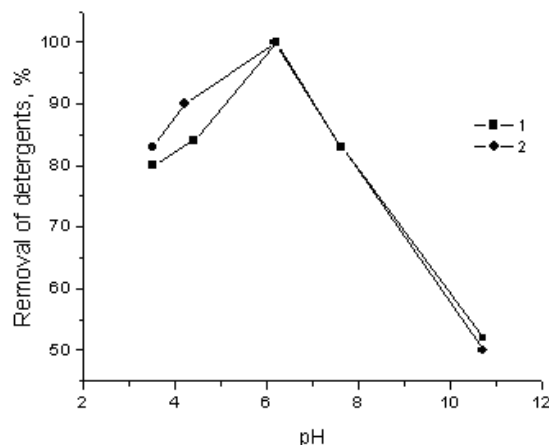


Fig. 8. Effect of pH on the retention of sulfonic and phenolic compounds on Gordes (pH 8.16) zeolite 1 - sulfonic compounds, 2 - phenolic compounds.

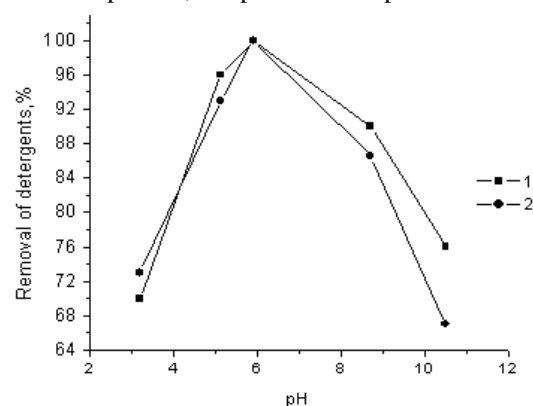


Fig. 9. Effect of pH on the retention of sulfonic and phenolic compounds on Marsid (pH 4.8) zeolite, 1 - sulfonic compounds, 2 - phenolic compounds.

Adsorption of detergents using membranes

Two types of membranes with different chemical composition are used in the experiments. The results are presented in Fig. 10 and Fig. 11.

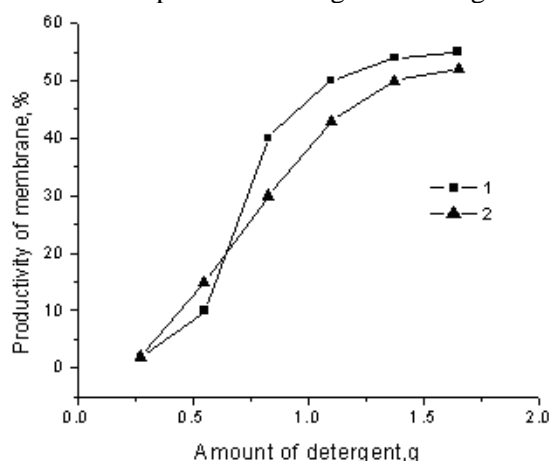


Fig. 10. Dependence of productivity of purification of detergents (1 - sulfonic; 2 - phenolic compounds) on membrane M1, at different amount of detergents in 50 mL solution.

As can be seen from Figure 10 and Figure 11, the removal of detergents from water increases sharply in the case of membrane M2 by attaining the highest value of 82 %, whereas the removal is 52 % for the membrane M1.

The differences in chemical composition of the acrylic copolymers affect the structure of the resulting membranes.

As can be seen from Fig.12, the membrane M1 is more compact (dense), with smaller pores, compared to the membrane M2, which is less compact, with more and larger pores.

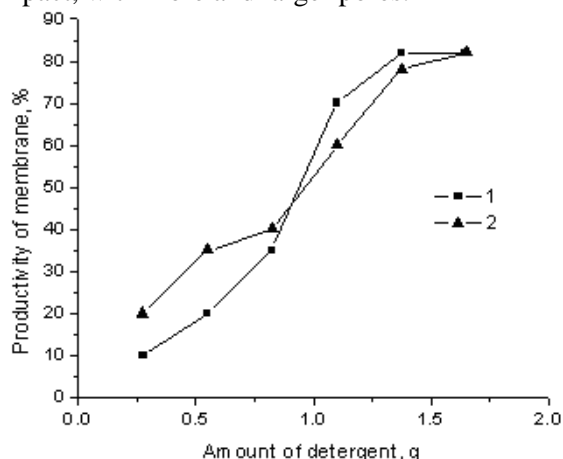


Fig. 11. Dependence of productivity of purification of detergents (1 – sulfonic; 2 -phenolic compounds) on membrane M2, at different amount of detergents in 50 mL solution.

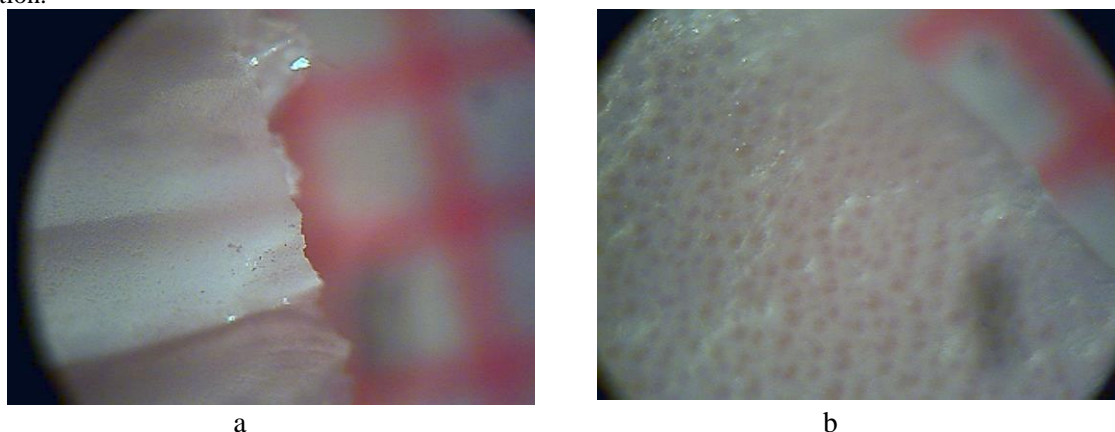


Fig.12. Optical microscope images of membranes M1 (a) and M2 (b).The red square has area of 1 mm².

REFERENCES

- 1.G.A. Garwood, M.M. Mortland, T.J. Pinnavaia, *J. Mol. Catal.* **22**, 153 (1983).
2. T.A. Wolfe, T. Demirel, E.R. Baumann, *J. Water Pollut. Control Fed.*, **58**, 68 (1986).
3. S.A. Boyd, M.M. Mortland, *Experientia* **41**, 1564 (1985).
4. S.A. Boyd., M.M. Mortland, *J. Mol. Catal.* **34**, 1 (1986).
5. K.R. Srinivasan, H.S. Fogler, *Clays Clay Miner.*, **38**, 287 (1990).
6. R.C. Zielke, T.J. Pinnavaia, *Clays Clay Miner.*, **36**, 403 (1988).
7. H.T. Shu, D. Li, A.A. Scala, Y.H. Ma, *Sep. Purif. Technol.*, **11**, 27 (1997).
8. Y.H. Shen, *Water Res.*, **36**, 1107 (2002).
9. L. Kastelan-Kunst, K. Kosutic, V. Dananic, B.F.T. Kunst, *Water Res.*, **31**, 2878 (1997).
10. W. Reimann, *Desalination*, **109**, 51 (1997,).

It seems that the differences in chemical composition and the morphology of the membranes lead to their different purification efficiency towards detergents.

CONCLUSIONS

The main factors, determining the adsorption properties towards detergents, are the surface area and the pore structure of the zeolites. Increasing the particle size leads to decrease in the adsorption capacity of the samples, due to reduced surface area. The uptake of both sulfonic and phenolic compounds was found to be maximal at pH 6. These results confirm that both compounds are preferably adsorbed from their water solutions in neutral forms.

The experiments conducted with membranes demonstrated that they have considerably higher adsorption capacities compared to zeolites. The chemical composition and morphology of the membranes is believed to be very important factor affecting the efficiency of the membrane for the removal of sulfonic and phenolic compounds from waste waters.

11. M.J. Rosa, M.N. De Pinho, *J. Membr. Sci.*, 1994, 89, 235-243.
12. F. Van Voorst Vader, *Trans. Faraday Soc.*, **56**, 1067 (1960).
13. J.-L. Rigaud, D. Levy, D. Mosser, O. Lambert, *Eur. Biophys. J.* **27**, 305 (1988).
14. S.M. El-Said, *Ass. Univ. Bull. Environ. Res.*, **7**, 137 (2004).
15. Y.L. Hoffman, H.P. Angstadt, *Chromatography*, **234**, 666 (1987).
16. B. Petrova, T. Budinova, B. Tsyntsarski, N. Petrov, C.O. Ania, J.-B. Parra, *Bulg. Chem. Commun.*, **42**, 141 (2010).
17. O. Korkuna, R. Lebeda, J. Skubiszewska-Zieba, T. Vrublevska, V.M. Gunko, J. Ryczkowski, *Microporous&Mesoporous Materials*, **87**, 243, (2006).
18. M. Akgul, A. Karabakan, *Microporous&Mesoporous Materials*, **145**,157 (2011).
19. M. Ostrooomov, P. Cappelletti, R. DeGennaro, *App. Clay Sci.*, **55**, 27 (2012).
20. G.H. Giles, T.H. MacEwan, S.N. Nakhwa, D. Smith, *J. Chem. Soc.*, 3973 (1960).
21. I. Langmuir, *J. Am. Soc.*, **409**, 161 (1916).

ИЗВЛИЧАНЕ НА ДЕТЕРГЕНТИ ЧРЕЗ ЗЕОЛИТИ И МЕМБРАНИ

Б. Цинцарски¹, Б. Петрова¹, Т. Будинова^{1*}, Н. Петров¹, А. Сарбу², Т. Санду²,
М. Ферхат Ярдим³, А. Серкичиоглу³

¹Институт по органична химия с Център по фитохимия, БАН, Акад. Г. Бончев, бл.9, София 1113

²Национален изследователски институт по химия и петрохимия, пл. Независимост 202, Букурещ, Румъния

³Истанбулски технически университет, Факултет по инженерна химия, 34469 Маслак, Истанбул, Турция

Постъпила 16 януари 2013 г.; Приета за печат 12 февруари 2013 г.

(Резюме)

Изследвана бе адсорбцията на сулфонати и фенолати, съдържащи се в детергенти, с помощта на природни зеолити от Турция и Румъния. Зеолитите бяха охарактеризирани посредством ИЧ спектроскопия и изучаване на повърхностните свойства. Изследвано бе влиянието на времето на контакт и на рН върху процеса на адсорбция. Установено бе, че специфичната повърхност е определящ фактор, който влияе в най-голяма степен върху адсорбцията на детергентите. Бе изследвано и извличането на детергенти с помощта на различни мембрани, които показаха по-висок адсорбционен капацитет в сравнение с изследваните зеолити.

Synthesis of 2,4,5-trisubstituted and 1,2,4,5-tetrasubstituted-1H-imidazole derivatives and or 2,4,5-Triaryloxazoles using of Silica-Supported Preyssler Nanoparticles

A. Gharib^{1,2*}, B. R.h Hashemipour Khorasani², M. Jahangir¹, M. Roshani¹,
L.Bakhtiari², S. Mohadeszadeh²

¹Department of Chemistry, Islamic Azad University, Mashhad, IRAN

²Agricultural Researches and Services Center, Mashhad, IRAN

Received: May 28, 2012; Revised: February 5, 2013

One-pot multi-component condensation of benzil and or benzoin, aldehydes, ammonium acetate and primary amines were used for synthesis of 2,4,5-trisubstituted and 1,2,4,5-tetrasubstituted-1H-imidazole derivatives under reflux conditions using Silica-supported Preyssler nanoparticles heteropolyacid as a catalysts. This catalyst has several advantages (simple work-up, inexpensive and reusability). These catalysts were also successfully employed in the synthesis of triaryloxazoles.

Keywords: substituted imidazole; silica-supported Preyssler nanoparticle; benzil; aromatic aldehyde; triaryloxazoles; multicomponent reaction

INTRODUCTION

Imidazole is a five-membered ring heteroaromatic compound with two nitrogen atoms at 1 and 3 [1]. This type of compound is known to exhibit a broad range of pharmaceutical and industrial applications. For instance, the imidazole core unity is present in many compounds with pronounced biologic activities such as angiotensin inhibitors [2], anti-inflammatory [3], glucagon antagonist [4], antiviral [5], fungicidal [6], and high cytotoxicity, which has indicated them as new candidates in cancer therapy [7]. Heterocyclic compounds with imidazole ring systems have many pharmaceutical activities and play important roles in biochemical processes [8]. Highly substituted imidazole derivatives are also the key intermediates in the synthesis of many therapeutic agents. Omeprazole, Pimobendan, Losarton, Olmesartan, Eprosartan and Triphenagrel are some of the leading drugs in the market with diverse functionality [9]. Triarylimidazoles are used in photography as photosensitive compound [10]. In addition, they are of interest due to their herbicidal [11], analgesic [12], fungicidal [13], antiinflammatory [14] and antithrombotic activities [15]. There are numerous methods in the literature for the synthesis of highly substituted imidazoles: (a) condensation of 1,2-diones, aldehydes, primary amines and ammonia [16], (b) *N*-alkylation of

trisubstituted imidazoles [17], (c) condensation of benzoin or benzoin acetate with aldehydes, primary amines and ammonia in the presence of copper acetate [18] (d) cyclization of sulfonamides with mesoionic 1,3-oxazolium-5-olates [19], (e) four component condensation of diones, aldehydes, primary amines and ammonium acetate in acetic acid under reflux conditions [20], (f) condensation of β -carbonyl *N*-acyl-*N*-alkylamines with ammonium acetate in refluxing acetic acid [21] and (g) conversion of *N*-(2-oxo)amides with ammonium trifluoroacetate under neutral conditions [22]. The synthesis of triarylimidazoles from the three component reaction of 1,2-dicarbonyl compounds, aldehyde and ammonia was independently discovered by Radziszewski [23]. However, long periods of time and harsh conditions were frequently associated with low yields of production. Davidson *et al.* [17] showed can reduce the reaction times using acetic acid as solvent and ammonium acetate instead of ammonia. This last protocol became usual and default procedure for the synthesis of triarylimidazoles [24]. Polyoxo-metalates (POMs) are metal-oxo anionic clusters whose chemical properties can be controlled by transition-metal substitution and the counteraction used. POMs have wide applications in many fields such as catalysis, medicine, magnetic properties, materials, surface chemistry, photochromism, and electrochromism, owing to their so-called "valueadding properties." These properties, combined with their ability to donate and accept

* To whom all correspondence should be sent:
E-mail: aligharib5@yahoo.com

electrons and their stability over a wide range of conditions, make them attractive candidates for catalysis. A new and efficient method for the preparation of 4(3*H*)-quinazolinones from the condensation of anthranilic acid, orthoester and substituted anilines, in the presence of catalytic amounts of silica-supported Preyssler nanoparticles is reported [25]. An efficient, improved, and environmentally benign procedure for catalytic oxidation of benzyl alcohols to the corresponding benzaldehydes was developed in the presence of nano-SiO₂-supported Preyssler heteropolyacid (HPA), both in thermal conditions and under microwave irradiation [26]. Silica-supported Preyssler nanoparticles appear to be a new and efficient solid acid catalyst for an economical, and environmentally benign one-pot synthesis of 3-substituted phthalides [27]. An efficient and environmentally benign procedure for the catalytic esterification of salicylic acid with aliphatic alcohols, C_nH_{2n+1}OH (*n* = 1–5) and benzylic alcohols, RC₆H₄CH₂OH (R = H, NO₂, OCH₃, Br, Cl, Me) was developed using nano-SiO₂-supported Preyssler heteropolyacid both under thermal conditions and microwave irradiation [28].

EXPERIMENTAL

Catalyst Preparation

Supported heteropolyacid catalyst was synthesized according to the literature [29,30] using a support in powder form (SiO₂) with an aqueous solution of the heteropolyacids. After stirring the mixture, the solvent was evaporated, dried at 120°C and calcined at 250°C in a furnace prior to use. Silica-supported Preyssler nano-structures were obtained through the microemulsion method [29].

Synthesis of 2,4,5-triaryl-1*H*-imidazoles (5*a*-Z4) from the benzils (1*a*-Z4):

General Procedure:

A mixture of benzils (1 mmol) and aromatic aldehyde (**2a-Z4**) (1 mmol), ammonium acetate (4 mmol) and EtOH (4 mL) was heated under reflux with magnetic stirring until the mixture melted. Silica-supported Preyssler nanoparticles (0.03 mmol) were added to this mixture and stirred under reflux for 3 h. The progress of the reaction was monitored by thin-layer chromatography (TLC). After completion of reaction, the reaction mixture was cooled to room temperature and poured on 100 ml ice water and diluted with dichloromethane, and separated from the catalyst by filtration. Pure products were obtained after the addition of water to the organic layer. Two phases of solution were

extracted and then the solvent was evaporated to afford 2,4,5-triaryl-1*H*-imidazoles (**5a-Z4**). The separated solid was filtered and washed with water. The residue was dried, and recrystallized from methanol: water (8:1) mixture.

Synthesis of 2,4,5-triarylimidazoles (5*a*-Z4) from the benzoin (5):

A mixture of benzoin (1 mmol) and aromatic aldehyde (**2a-Z4**) (1 mmol), ammonium acetate (5 mmol) and EtOH (4 mL) was heated under reflux with magnetic stirring until the mixture melted. Silica-supported Preyssler nanoparticles (0.03 mmol) were added to this mixture and stirred under reflux for 3 h. The progress of the reaction was monitored by thin-layer chromatography (TLC). After completion of reaction, the reaction mixture was cooled to room temperature and poured on 100 ml ice water and diluted with dichloromethane, and separated from the catalyst by filtration. Pure products were obtained after the addition of water to the organic layer. Two phases of solution were extracted and then the solvent was evaporated to afford 2,4,5-triaryl-1*H*-imidazoles (**5a-Z4**). The separated solid was filtered and washed with water. The residue was dried, and recrystallized from methanol: water (8:1) mixture.

Synthesis of 2,4,5-triaryloxazoles (9*a*-j):

A 10 mL round-bottom flask equipped with magnetic stirrer was charged with benzoin (**5**) and or benzils (**1a-Z4**) (1.0 mmol), aldehydes (**2a-j**) (1.0 mmol), NH₄OAc (**4**, 4.0 mmol) and Silica-supported Preyssler nanoparticles (0.05 mmol), followed by EtOH (4 mL). The reaction mixture was stirred and gently refluxed for 4 h. After the completion of the reaction with the monitoring of TLC, 4 mL of water were added. The solid was filtered under reduced pressure and washed with small portions of a mixture of cooled EtOH/H₂O (1:1, v:v). The crude product was recrystallized from acetone/water 9:1 or toluene.

Selected Spectra data:

2-(2,4-dichlorophenyl)-4,5-diphenyl-1*H*-imidazole (Table 1, entry 5):

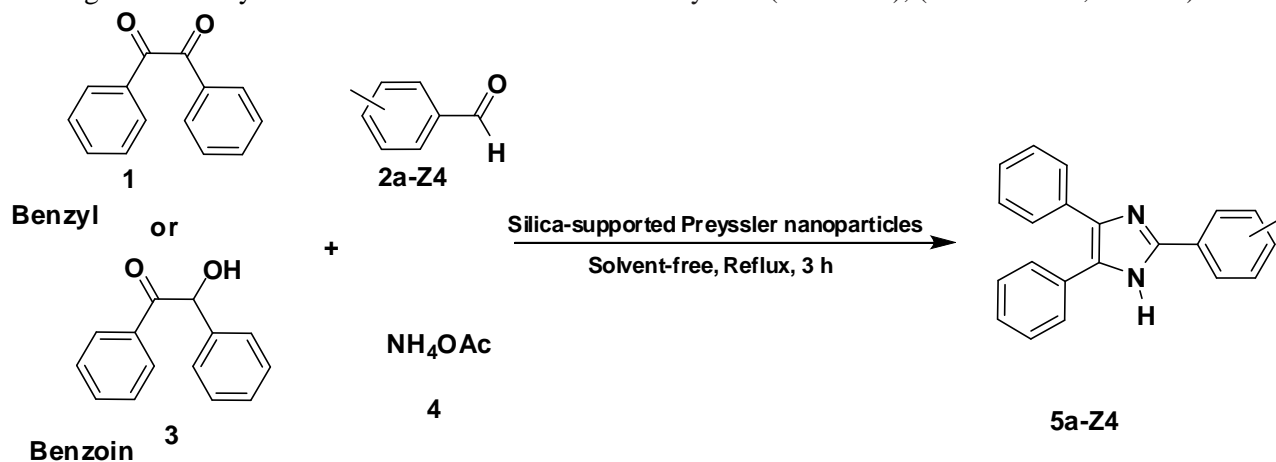
mp 175–176 °C. IR (KBr, cm⁻¹) ν_{max}: 3425, 3069, 1590, 824, 765, 698. ¹H NMR (300 MHz, DMSO-*d*₆) δ_H: 12.6 (s, 1H), 7.84 (d, *J* = 8.4 Hz, 1H), 7.80 (s, 1H), 7.45–7.65 (m, 12H). ¹³C NMR (100 MHz, DMSO-*d*₆) δ_C: 126.5, 127.4, 127.4, 127.8, 128.2, 128.5, 128.4, 128.7, 128.7, 129.55, 130.6, 132.4, 132.6, 133.9, 134.8, 137.1, 142.4. EIMS *m/z* 364 (M⁺-2, 100), 165, 123, 69, 55.

2-(4-methoxyphenyl)-4,5-diphenyl-1H-imidazole (Table 1, entry 17):

mp 231–232 °C. IR (KBr, cm^{-1}) ν_{max} : 3400, 3060, 1611, 1490, 1179, 1027, 830, 760. ^1H NMR (300 MHz, $\text{DMSO-}d_6$) δ_{H} : 12.47 (s, Br, 1H), 8.00 (dt, $J = 8.8\text{ Hz, } 2.0\text{ Hz, } 2\text{H}$), 7.50 (d, $J = 7.2\text{ Hz, } 4\text{H}$), 7.37 (t, $J = 7.2\text{ Hz, } 4\text{H}$), 7.28 (t, $J = 7.2\text{ Hz, } 2\text{H}$), 7.06 (dt, $J = 8.8\text{ Hz, } 2.0\text{ Hz, } 2\text{H}$), 3.82 (s, 3H). ^{13}C NMR (100 MHz, $\text{DMSO-}d_6$) δ_{C} : 55.2, 114.2, 122.9, 126.7, 127.1, 127.7, 128.4, 145.7, 159.5. EIMS: m/z (%) = 326 (M+, 100), 311, 283, 235, 97.

Reusing the Catalyst

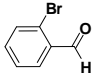
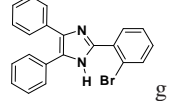
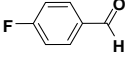
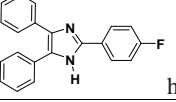
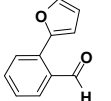
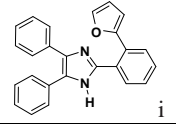
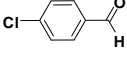
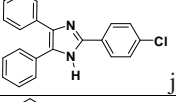
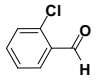
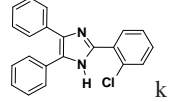
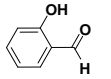
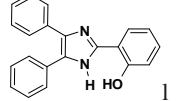
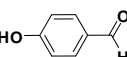
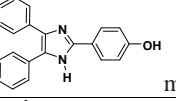
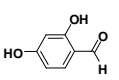
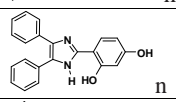
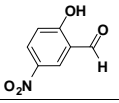
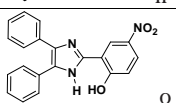
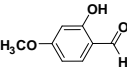
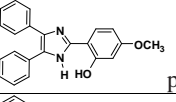
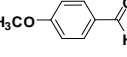
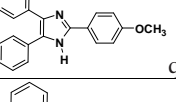
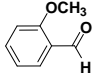
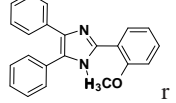
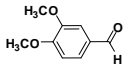
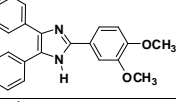
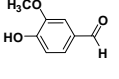
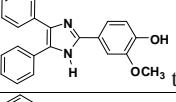
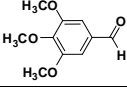
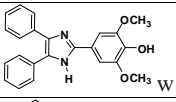
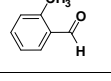
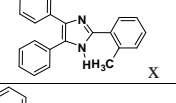
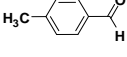
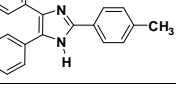
The reusability of the catalyst was also investigated. The synthesis of 3a was selected as



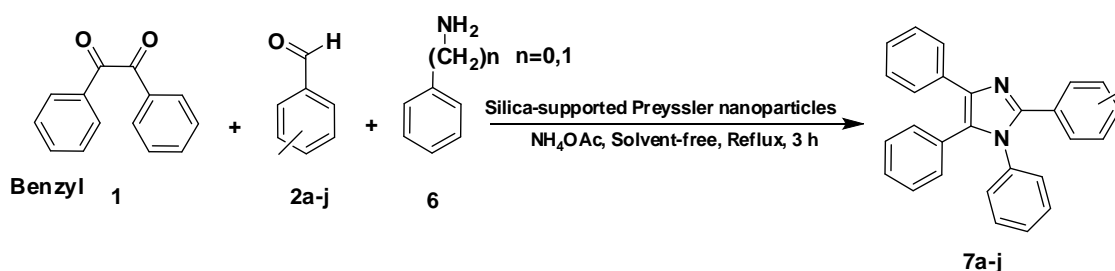
Scheme 1 Synthesis of 2,4,5-trisubstituted-1H-imidazole derivatives (5a-Z4) in the presence of Silica-Supported Preyssler Nanoparticles under Solvent-Free Conditions at reflux conditions and in proper times.

Table 1. Synthesis of 2,4,5-Trisubstituted Imidazoles via condensation of benzil, aldehydes, ammonium acetate and using silica-supported Preyssler nanoparticles under solvent-free conditions at reflux conditions and in proper times.

Entry	Substrate 2	Product 3	Time (h)		^a Yield (%)		MP (°C)	
			Benzil	Benzoin	Benzil	Benzoin	Found	Reported (lit.)
1			1	1.5	96	92	269-270	(274–276)[19]
2			1.5	2.5	98.5	96	240-241	240–242
3			1.5	2	93	96	>262	>260 [18]
4			1.5	2	96	92	180-182	(183–184)[20]
5			1	1.5	91	94	175-176	176.5-177 [31]
6			1	1.5	93	98	260-262	261.5-263.5 [21]

7			1	2	90	95	202-203	201-202 [32]
8			2	2.5	97	91	188-189	189-190 [33]
9			1.5	2	91	96	200-201	202-203 [32]
10			1.5	2	96	98	261-263	262-264 [21]
11			1.5	2	94	95	196-198	195-197 [31]
12			1	1.5	96	98	271	272 [17]
13			1.5	2	91	95	234	233 [19]
14			1.5	2	96	97	272	272 [17]
15			2	2.5	96	98	261-263	260.5-262 [24]
16			1.5	2	95	97	242	243 [17]
17			2	2.5	86	92	231-233	230-232 [21]
18			1	2	81	84	209-211	210-210.5 [21]
19			2	3	84	89	217-219	216-218 [22]
20			1	2	93	96	196	197 [34]
21			2	4	86	84	261-262	261 [17]
22			2	3	90	91	207-208	205-207 [21]
23			1	2	88	88	234-236	232-235 [20]

24			1	2	92	96	257-259	257-258 [33]
25			2	3	90	91	292-293	291.5-292 [21]
26			1	2.5	98	98	241-243	242-244 [35]
27			1.5	2.5	94	94	259-260	260-261 [33]
28			1	3	92	96	199-200	200-201 [33]

^aIsolated yield.

Scheme 2. Synthesis of 1,2,4,5-tetrasubstituted-1H-imidazole derivatives (7a-j) in the presence of Silica-Supported Preyssler Nanoparticles under Solvent-Free Conditions at reflux conditions and in proper times

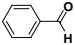
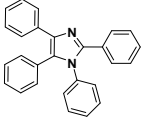
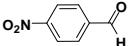
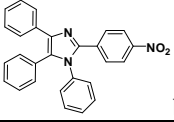
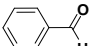
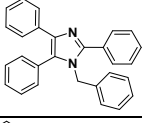

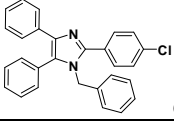
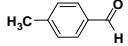
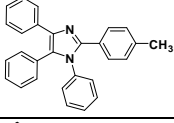
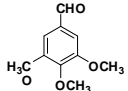
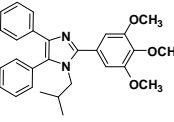

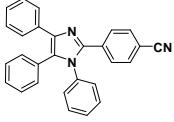
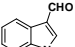
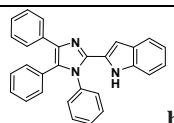
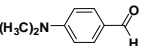
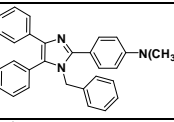
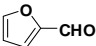
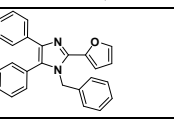
Similar methodology was applied for the synthesis of 1,2,4,5-tetrasubstituted-1H-imidazole derivatives (7a-j) which were also obtained in good to excellent yields by the condensation of benzil (1), aldehydes (2), aromatic amines (4) and ammonium acetate (Table 2) in presence of nano-structured Preyssler supported on silica as catalyst under solvent-free conditions. (Scheme 2).

The effect of solvent on the model reaction was studied by carrying out the reaction in a solvent-free system and in a variety of solvents including ethanol, methanol and acetonitrile at reflux conditions. As shown in Table 3 the best results in terms of yield and time have been achieved in free-solvent and ethanol conditions. Thus it was applied as solvent of choice. It is noteworthy to mention that in the absence of the catalyst and just refluxing the substrate in free-solvent and ethanol, no reaction took place.

To determine the most appropriate reaction conditions and evaluate the catalytic efficiency of silica-supported Preyssler nanoparticles, the synthesis of **5a** (as model reaction) was carried out in various conditions. First, we tried the reaction without catalyst. When a mixture of benzil, aromatic aldehyde and ammonium acetate was stirred under reflux conditions for 14 h in the

absence of silica-supported Preyssler nanoparticles, no conversion was detected. This observation indicated that a catalyst is necessary for this transformation. To study the effect of solvent on the yield of this reaction, the model reaction was carried out in various solvents and a solvent-free system using 0.03 mmol of silica-supported Preyssler nanoparticles as the catalyst. As shown in Table 1, the best results in terms of yield and time were achieved in solvent-free conditions and in the presence of EtOH as solvent, too. To investigate the effect of silica-supported Preyssler nanoparticles, we carried out comparative experiments with some silica-gel-supported heteropolyacids, and the comparative results are summarized in Tables 1 and 2 for the synthesis of 2,4,5-triphenyl-1H-imidazole (**5a**) and 1,2,4,5-tetrasubstituted-1H-imidazole (**7a**). We have performed aldehydes consisting electron withdrawing groups or electron donating groups at different positions but it did not show any remarkable difference in the yield of product and time of the reactions. Different mechanistic pathways have been proposed for this multicomponent reaction having the benzil or benzoin as starting materials [30]. The proposed rationale by Kokare *et al.* [31] seems to be in

Table 2. Synthesis of 1,2,4,5-tetrasubstituted-1*H*-imidazole via condensation of benzil, aldehydes, ammonium acetate and amine using Silica-Supported Preyssler Nanoparticles under reflux conditions and in proper times.

Entry	Substrate 2	Product 3	Time (min.)	^a Yielda (%)	MP (°C)	
			Benzil	Benzil	Found	Reported
1		 a	30	91	256–257	(261–262)[19]
2		 b	20	97	222–225	219–220 [33]
3		 c	25	91	161–163	158–160 [33]
4		 d	20	96	149–152	146–148 [24]
5		 e	30	81	192–193	189 [36]
6		 f	60	92	117–119	112–115 [33]
7		 g	25	93	205–207	198–201 [24]
8		 h	30	86	219–221	218–220 [24]
9		 i	30	94	180–182	183–185[23, 24]
10		 j	17	91	156–158	156–157 [24]

^aIsolated yield.

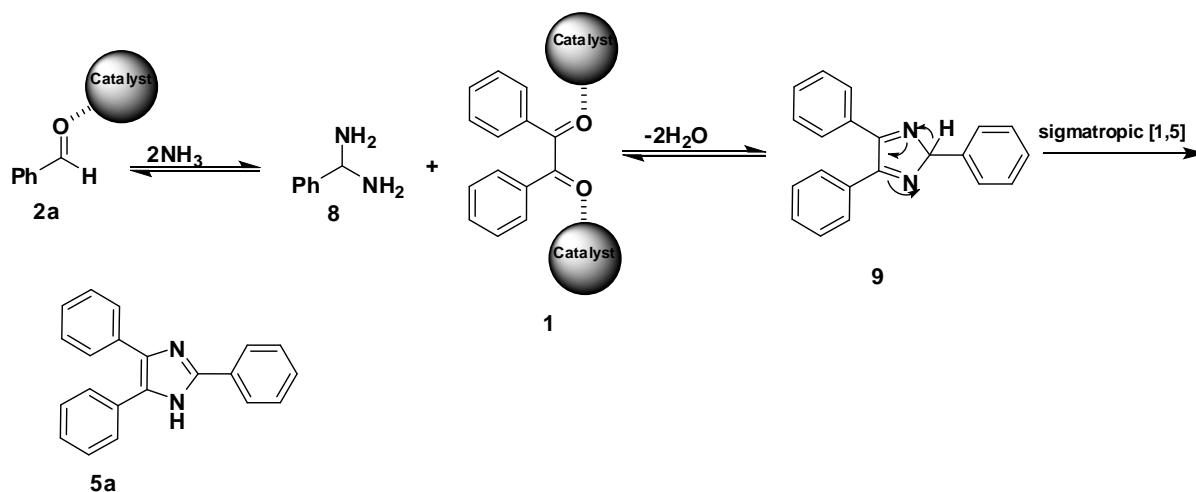
accordance with the results in Table 1 (Scheme 3). The authors suggested the initial formation of *N,N*-ketal (**10**) under heteropolyacid acidic catalysis from benzaldehyde (**2a**) and 2 equivalents of NH₄OAc (**4**). It was assumed that the same activation occurs in the heteropolyacid catalysis. Therefore, the condensation of **8** with benzil (**1**) after losing 2 equivalents of water, leads to the conjugate intermediate **9** which rearranges via a [1,5]-sigmatropic proton shift to afford the corresponding lophine (**5a**). On the other hand,

starting from benzoin, the cyclization of intermediate imino-alcohol (**10**) should occur by an intramolecular attack of nitrogen in a more hindered and saturated carbon to afford the dihydroimidazole intermediate (**11**) (Scheme 4). Additionally, the needed oxidation step to produce the conjugated intermediate (**12**) could explain the minor reactivity that is observed in the reactions starting from benzoin. The intermediate (**12**) is suggested as common specie in both mechanistic pathways.

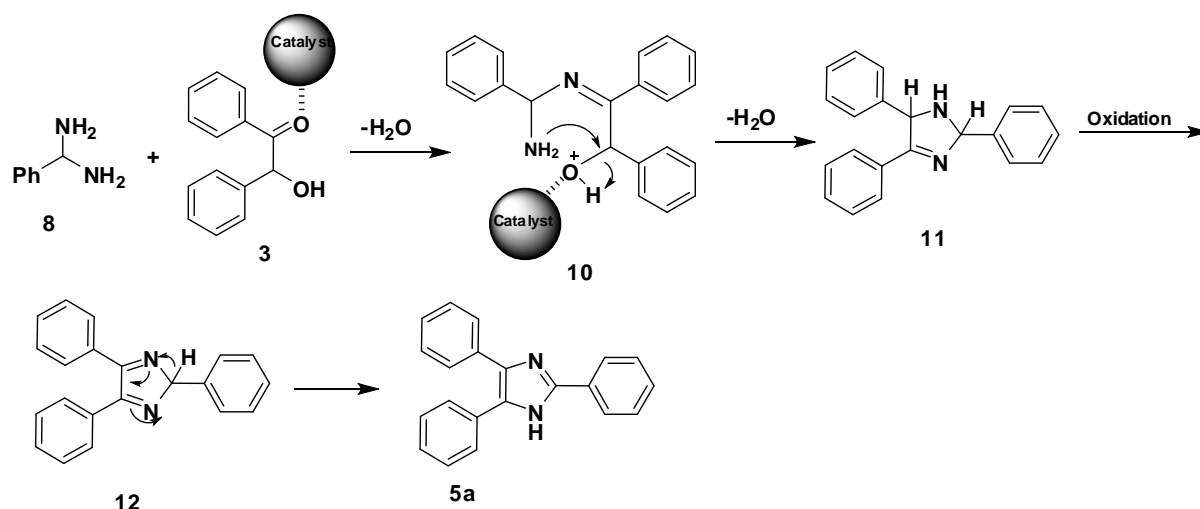
Table 3. Synthesis of 2,4,5-triphenyl-1H-imidazole (**3a**) in the presence of various silica-supported heteropolyacids in different solvents and proper times.

Entry	Solvent	Catalyst	Reaction Time (h)		^a Yield (%)	
			Benzil	Benzoin	Benzil	Benzoin
1	Free	H ₃ [PMo ₁₂ O ₄₀]/SiO ₂ (50%)	1.5	2	84	82
2	Free	H ₄ [PMo ₁₁ VO ₄₀]/SiO ₂ (50%)	1.5	2	91	88
3	Free	H ₃ [PW ₁₂ O ₄₀]/SiO ₂ (50%)	1.5	2	87	85
4	Free	H ₁₄ [NaP ₅ W ₃₀ O ₁₁₀]/SiO ₂ Nanoparticles	1	1.5	96	92
5	Free	H ₁₄ [NaP ₅ W ₃₀ O ₁₁₀]/SiO ₂ (50%)	1	1.5	94	90
6	EtOH	H ₃ [PMo ₁₂ O ₄₀]/SiO ₂ (50%)	1.5	2	83	80.5
7	EtOH	H ₄ [PMo ₁₁ VO ₄₀]/SiO ₂ (50%)	1.5	2	89.5	87
8	EtOH	H ₃ [PW ₁₂ O ₄₀]/SiO ₂ (50%)	1.5	2	85.5	84
9	EtOH	H ₁₄ [NaP ₅ W ₃₀ O ₁₁₀]/SiO ₂ Nanoparticles	1	1.5	95	91
10	EtOH	H ₁₄ [NaP ₅ W ₃₀ O ₁₁₀]/SiO ₂ (50%)	1	1.5	91.5	87.5
11	MeOH	H ₃ [PMo ₁₂ O ₄₀]/SiO ₂ (50%)	2	2	83	80
12	MeOH	H ₄ [PMo ₁₁ VO ₄₀]/SiO ₂ (50%)	2	2	88.5	86
13	MeOH	H ₃ [PW ₁₂ O ₄₀]/SiO ₂ (50%)	2	2	84.5	84
14	MeOH	H ₁₄ [NaP ₅ W ₃₀ O ₁₁₀]/SiO ₂ Nanoparticles	2	2	93	90
15	Acetonitrile	H ₁₄ [NaP ₅ W ₃₀ O ₁₁₀]/SiO ₂ (50%)	2	2	89.5	86
16	Acetonitrile	H ₃ [PMo ₁₂ O ₄₀]/SiO ₂ (50%)	2.5	3	80	77
17	Acetonitrile	H ₄ [PMo ₁₁ VO ₄₀]/SiO ₂ (50%)	2.5	3	85	84.5
18	Acetonitrile	H ₃ [PW ₁₂ O ₄₀]/SiO ₂ (50%)	2.5	3	82	82
19	Acetonitrile	H ₁₄ [NaP ₅ W ₃₀ O ₁₁₀]/SiO ₂ Nanoparticles	2	2.5	92	88.5
20	Acetonitrile	H ₁₄ [NaP ₅ W ₃₀ O ₁₁₀]/SiO ₂ (50%)	2	2.5	87.5	85

^aIsolated yield.



Scheme 3. Suggested mechanistic pathway starting from benzil (**5a**).



Scheme 4. Suggested mechanistic pathway starting from benzoin (**5a**).

Table 4. Comparative study of various supported heteropolyacid catalysts for the preparation of 2,4,5-trisubstituted (**5a**) under reflux conditions and solvent-free

Entry	Catalyst	Amount of catalyst (mmol)	Time (h)	Yield (%)
			Benzil	Benzil
1	H ₁₄ [NaP ₅ W ₃₀ O ₁₁₀]/SiO ₂ nanoparticles	0.08	8	96
2	H ₁₄ [NaP ₅ W ₃₀ O ₁₁₀]/SiO ₂ (50%)	0.09	10	94
3	H ₃ [PMo ₁₂ O ₄₀]/SiO ₂ (50%)	0.09	10	84
4	H ₄ [PMo ₁₁ VO ₄₀]/SiO ₂ (50%)	0.09	10	91
5	H ₃ [PW ₁₂ O ₄₀]/SiO ₂ (50%)	0.09	10	87
6	Free	-	-	-

The generality of this process was demonstrated by the wide range of substituted and structurally divers aldehydes to synthesize the corresponding products in high to excellent yields (Table 1). The high yield transformations were carried out without any significant amounts of undesirable side products. Unlike some previously reported methods, the present method does not require toxic or anhydrous organic solvents to produce the 2,4,5-trisubstituted imidazole derivatives. Comparison of silica-supported Preyssler nanoparticles, H₃[PMo₁₂O₄₀]/SiO₂ (50%), H₄[PMo₁₁VO₄₀]/SiO₂ (50%), H₁₄[NaP₅W₃₀O₁₁₀]/SiO₂ (50%) and H₃[PW₁₂O₄₀]/SiO₂ (50%) shows that silica-supported Preyssler nanoparticles led to greater yields and the higher activity. The results are represented in Table 3. Although it is difficult to offer an explanation for the different activity between these heteropolyacids, certainly there is a complex relationship between the activity and structure of polyanion. By changing the constituent elements of polyanion (both hetero and addenda atoms), the acid strength of HPA as well as its catalytic activity is able to vary in a wide range [34]. This observation can be explained by considering the reaction mechanism. As shown in Schemes 3, 4 the first stage of the reaction is the activation of the carbonyl group by an acidic catalyst. According to previous reports, the acidic property of the Preyssler type of heteropolyacids is greater than the Keggin [35].

The efficiency of H₁₄[NaP₅W₃₀O₁₁₀]/SiO₂(50%) and H₁₄[NaP₅W₃₀O₁₁₀]/SiO₂ nanoparticles as catalyst was also studied for this reaction, but the model reaction (reaction of benzil, aromatic aldehyde and ammonium acetate) did not go to completion in the presence of these catalysts even after long reaction times (8 h) and more amounts of catalyst (Table 4). The reactions were carried out as described in the synthesis of lophine (see Table 1). In the absence of the catalyst (Table 4, entry 6), **9** was only isolated in a poor yield. In H₁₄[NaP₅W₃₀O₁₁₀]/SiO₂ nanoparticles, the catalyst

is supported into silica nano-particles. As the particle size decreases, the relative number of surface atoms increases, and thus activity increases. Moreover, because of quantum size effects, nanometer-sized particles can exhibit unique properties. There are several advantages for the use of nano-structured Preyssler supported on silica as catalyst for this transformation, which include high conversions, low cost, and reusability of the catalyst. In addition, the use of supported catalyst under heterogeneous conditions facilitates ease of separation and recovery of the catalyst. The insolubility of the catalyst in different organic solvents provided an easy method for its separation from the product. The catalyst was easily separated by filtration and reused with only a gradual decrease in its activity. The synthesis of 2,4,5-trisubstituted and 1,2,4,5-tetrasubstituted-1H-imidazole derivatives using acetic acid for few hours is a well-established procedure [36,37]. However, this method suffering by several drawbacks such as drastic reaction conditions, difficult to handle, longer reaction time, tedious work-up, low yields, All such drawbacks were overcome in the present procedure as silica-supported Preyssler nanoparticles is easy to handle, short reaction time, yields are good, simple work-up procedure (Scheme 1). We have carried out aldehydes consisting electron withdrawing groups or electron donating groups at different positions but it did not show any remarkable difference in the yield of product and time of the reactions. All the reactions proceeded very efficiently and the results are summarized in Table 1. Similarly, we have studied the condensation of benzil, aldehydes, ammonium acetate with primary aromatic amines. The neat reactions were also attempted under conventional heating, keeping similar reaction conditions. The direct heating of reactants without solvent took more time for completion of reactions and gave the products with low yields. In some reactions decomposition of reactants took place.

CONCLUSION

In conclusion we have presented use of Silica-supported Preyssler nanoparticles as a catalyst for efficient synthesis of 2,4,5-triaryl-1H-imidazoles and 1,2,4,5-tetrasubstituted imidazoles with moderate to excellent yields from benzil as well as benzoin. For all the presented reactions, the ethanol-water solvent was used which is relatively environmentally benign and supporting to green Chemistry. The advantages of the reported method are the use of cheap, mild, and easily available catalyst, easy work-up, and better yields. Further studies on the application of this method for the synthesis of highly functionalized biologically active imidazoles are underway.

REFERENCES

- Grimmett, M. R. In *Comprehensive Heterocyclic Chemistry*, vol. 5; Katritzky, A. R.; Rees, C. W., eds.; Pergamon: Oxford, 1984; Grimmett, M. R. In *Science of Synthesis*, vol. 12; Neier R., ed.; Thieme: Stuttgart, 2002.
- J. I. Trujillo, J. R. Kiefer, W. Huang, A. Thorarensen, L. Xing, N. L. Caspers, J. E. Day, K. J. Mathis, K. K. Kretzmer, B. A. Reitz, R. A. Weinberg, R. A. Stegeman, A. Wrightstone, L. Christine, R. Compton, X. Li, *Bioorg. Med. Chem. Lett.*, **19**, 908 (2009).
- A. D. Palkowitz, M. I. Steinberg, K. J. Thrasher, J. K. Reel, K. L. Hauser, K. M. Zimmerman, S. A. Wiest, C. A. Whitesitt, R. L. Simon, W. Pfeifer, S. L. Lifer, D. B. Boyd, D. J. Barnett, T. M. Wilson, J. B. Deeter, K. Kakeuchi, R. E. Riley, W. D. Miller, W. S. Marshall, *J. Med. Chem.*, **37**, 4508 (1994).
- L. Linda, L. Chang, K. L. Sidler, M. A. Cascieri, S. Laszlo, G. Koch, B. Li, M. MacCoss, N. Mantlo, S. O'Keefe, M. Pang, A. Rolandoc, W. K. Hagmanna, *Bioorg. Med. Chem. Lett.*, **11**, 2549 (2001).
- D. Sharma, B. Narasimhan, P. Kumar, V. Judge, R. Narang, E. Clercq, J. Balzarini, *Eur. J. Med. Chem.* **44**, 2347 (2009).
- a) S. Laufer, P. Koch, *Org. Biomol. Chem.*, **6** (2008) 437 b) S. Kumar, J. Boehm, J. C. Lee, *Nat. Rev. Drug Disc.* **2**, 717 (2003).
- A. J. King, D. R. Patrick, R. S. Batorsky, M. L. Ho, H. T. Do, S. Y. Zhang, R. Kumar, A. K. Rusnak, D. M. Wilson, E. Hugger, L. Wang, F. Karreth, J. C. Loughheed, J. Lee, D. Chau, T. J. Stout, E. W. May, C. M. Rominger, M. D. Schaber, L. Luo, A. S. Lakdawala, J. L. Adams, R. G. Contractor, K. S. M. Smalley, M. Herlyn, M. M. Morrissey, D. A. Tuveson, P. S. Huang, *Cancer Res.*, **66**, 11100 (2006).
- R. J. Sundberg, R. B. Martin, *Chem. Rev.*, **74**, 471 (1974).
- M. Ghudamassi, J. Barasent, J. Imbach, P. Gayral, *Eup. J. Med. Chem.*, **23**, 225 (1988).
- H. Sensui, J. Ichikawa, S. Sato, *Japan Kokkai Tokyo Koho JP*, 62 **94** 841; *Chem Abstr.* **107** 187436q.
- R. Liebi, R. Randte, H. Mildenerger, K. Bauer, H. Bieringer, *Chem. Abst.* **108**, 6018 g (1987).
- S. E. Wolkenberg, D. D. Wisnosk, W. B. Liester, Y. Wang, Z. Zhao, C. W. Lindsley, *Org. Lett.*, **6**, 1453 (2004).
- A. F. Pozhershkii, A. T. Soldalenko, A. R. Katritzky, *Heterocycles in Life, Society*; (New York: Wiley) 179, 1997.
- J. G. Lombardino, E. H. Wiseman, *J. Med. Chem.*, **17**, 1182 (1974).
- A. P. Philips, H. L. White, S. Rosen, *Eur. Pat. Appl.*, **58**, 890 (1983).
- V. Stoczek, W. Schunack, *Arch. Pharmaz.*, **307**, 922 (1974).
- D. Davidson, M. Weiss, M. Jelling, *J. Org. Chem.*, **2**, 319 (1937).
- V. Stoczek, W. Schunack, *Arch. Pharmaz.*, **309**, 421 (1976).
- R. Consoni, P. D. Croce, R. Ferraccioli, R. Rosa, *J. Chem. Res.*, (s) 188 (1991).
- H. Schubert, J. Stodolka, *Prakt. Chem.*, **22**, 130 (1963).
- D. A. Evans, K. M. Lundy, *J. Am. Chem. Soc.*, **114**, 1495 (1992).
- C. F. Claiborne, N. J. Liverton, K. T. Nguyen, *Tetrahedron Lett.*, **39**, 8939 (1998).
- B. Radziszewski, *Ber. Dtsch. Chem. Ges.*, **15**, 1493 (1882).
- P. Lindberg, P. Nordberg, T. Alminger, A. Brandstorm, B. Wallmark, *J. Med. Chem.*, **29**, 1327 (1986).
- M. M. Heravi, S. Sadjadi, S. Sadjadi, H. A. Oskooie, R. H. Shoar, F. F. Bamoharram, *S. Afr. J. Chem.*, 2009, **62**, 1 (2009).
- F. F. Bamoharram, M. M. Heravi, H. Teymouri, M. Zebarjad, A. Ahmadpour, *Synthesis and Reactivity in Inorganic, Metal-Organic, and Nano-Metal Chemistry.*, **41**, 1221, (2011).
- M. M. Heravi, V. Rasmi, F. F. Bamoharram, S. Sadjadi, L. Fotouhi, S. Sadjadi, M. Bakavoli, *Synthetic Communications.*, **1**, 39, 4109 (2009).
- F. F. Bamoharram, M. M. Heravi, J. Ebrahimi, A. Ahmadpour, M. Zebarjad, *Chinese Journal of Catalysis.*, **32**, 5, 782 (2011).
- F. F. Bamoharram, M. M. Heravi, M. Roshani, A. Gharib, M. Jahangir, *J. Mol. Catal.*, **252**, 90 (2006).
- M. M. Heravi, S. Sadjadi, S. Sadjadi, H. A. Oskooie, R. Hekmat Shoar, F. F. Bamoharram, *S. Afr. J. Chem.*, **62**, 1 (2009).
- N. D. Kokare, J. N. Sangshetti, D. B. Shinde, *Synthesis.*, 2829 (2007).
- L.-M. Wang, Y.-H. Wang, H. Tian, Y.-F. Yao, J.-H. Shao, B. Liu, *J. Fluorine Chem.*, **127**, 1570 (2006).
- S. A. Siddiqui, U. C. Narkhed, S. S. Palimkar, T. Daniel, R. J. Lahoti, K. V. Srinivasan, *Tetrahedron.*, **61**, 3539 (2005).

34. M. M. Heravi, S. Sadjadi, H. A. Oskooie, R. Hekmat Shoar, F. F. Bamoharram, *Catal. Commun.* **9**, 470 (2008).
35. M. Misono, *Chem. Commun.*, 1141 (2001).
36. M. R. Grimmett, *In Comprehensive Heterocyclic Chemistry II*; A. R. Katritzky, C. W. Rees, E. F. Scriven, E. F. V. Eds. (New York: Pergamon) Vol. 3 P77, 1996.
37. D. Davidson, M. Weiss, M. Jelling, *J. Org. Chem.*, **2**, 328 (1937).

СИНТЕЗА НА 2,4,5-ТРИЗАМЕСТЕНИ И 1,2,4,5-ЧЕТИРИЗАМЕСТЕНИ-1Н-ИМИДАЗОЛОВИ ПРОИЗВОДНИ И/ИЛИ 2,4,5-ТРИАРИЛОКСАЗОЛИ С ПОМОЩТА НА НАНОЧАСТИЦИ ОТ PREYSSLER'ОВ КАТАЛИЗАТОР ВЪРХУ ПОДЛОЖКА ОТ СИЛИЦИЕВ ДИОКСИД

А. Гариб^{1,2*}, Б.Х. Хашемипур Хорасани², М. Джахангир¹, М. Рошаниа¹,
Л. Бахтиари², С. Мохадесзаде²

¹Департамент по химия, Ислямски университет Азад, Маишад, Иран

²Земеделски център за изследвания и услуги, Маишад, Иран

Получена на 28 май, 2012 г.; коригирана на 5 февруари, 2013 г.

(Резюме)

Използвана е едно-степенна синтеза на многокомпонентна кондензация на бензил (и/или бензоин), алдехиди, амониев ацетат и първични амини за получаването на 2,4,5-тризаместени и 1,2,4,5-четиризаместени-1Н-имидазолови производни при рефлукс катализирана от Preyssler'ова хетерополикиселина във вид на наночастици, фиксирани върху подложка от силициев диоксид. Този катализатор има няколко предимства: проста процедура, ниска цена и многократна употреба. Този катализатор е използван успешно и при синтезата на триарилноксазоли.

A facile synthesis of 1-(2, 4-dihydroxyphenyl)-3-aryl-propane-1,3-diones via Baker-Venkataraman rearrangement under solvent free conditions at room temperature

D. Sharma^{*1}, S. Kumar²

¹Department of Chemistry, BRCM College of Engineering & Technology, Bahal-127028, India

²Department of Chemistry, Technological Institute of Textile & Sciences, Bhiwani-127021, India

Received: December 17, 2012; Revised: February 4, 2013

A simple and highly efficient method for the synthesis of 1-(2,4-dihydroxyphenyl)-3-aryl-propane-1,3-diones via Baker-Venkataraman rearrangement involving grinding of 2-aryloxy-4-hydroxyacetophenones with pulverized potassium hydroxide at room temperature under solvent free conditions has been described. The structures of these compounds were identified from their spectral data (FT IR, ¹H NMR, ¹³C NMR, Mass). This protocol avoids the use of hazardous chemicals and organic solvents at any stage of the reaction.

Keywords: 2-aryloxy-4-hydroxyacetophenones, 1-(2,4-dihydroxyphenyl)-3-aryl-propane-1,3-diones, Baker-Venkataraman rearrangement, solvent free conditions, grinding technique

INTRODUCTION

1-(2,4-Dihydroxyphenyl)-3-aryl-propane-1,3-diones, commonly known as 2,4-dihydroxy dibenzoylmethanes are the required key intermediates for the synthesis of various naturally occurring compounds [1] such as flavones [2], pyrazoles [3], isoxazoles [4], pyrimidines [5], benzodiazepine [6] and also possess a broad spectrum of pharmacological activities like antibacterial [7], antiviral [8], insecticidal [9], antioxidant [10], antitumor [11] and antimutagenic [12] activity. Further these compounds have been found to be potent anticarcinogenic [13,14], antiestrogenic [15], breast cancer chemopreventive blocking agent [14] and also used as anti sunscreen agents [16]. In recent studies, β -ketoenols has been reported to be important pharmacophores for the HIV-1 integrase inhibitors [17]. Their metal complexes also exhibited good biological properties [18,19].

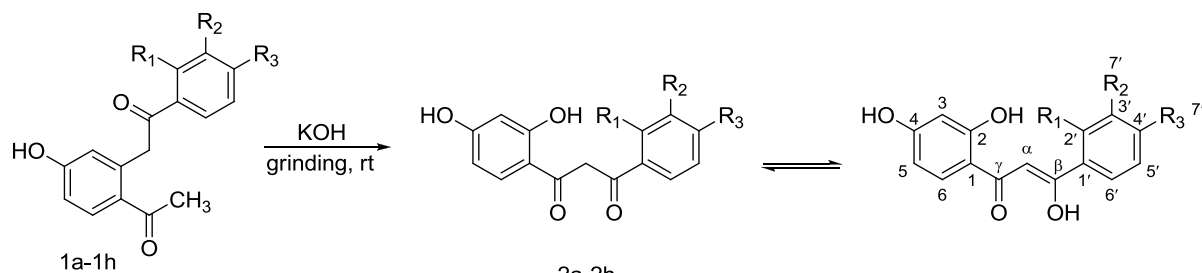
The most common method for the synthesis of these β -diketones is by Baker-Venkataraman rearrangement of 2-aryloxyacetophenones. Due to their important role in various fields, continuous efforts have been made to simplify

the procedures for their synthesis which include the use of potassium hydroxide in pyridine medium [20] or by heating with barium hydroxide in dimethylsulphoxide medium [21]. The above transformation has also been carried out in aqueous-benzene biphasic medium using phase transfer catalysis [22]. Other bases which have been used for this rearrangement include sodamide [23], sodium hydride [24], sodium hydroxide in dimethylsulphoxide [25], and potassium carbonate in aqueous medium under microwave irradiations [26].

Some of the above mentioned conditions possess shortcomings, such as use of harsh or hazardous chemicals, longer reaction time and elevated temperature. The shortcomings led us to develop a safe, environmentally benign, and more efficient condition for Baker-Venkataraman rearrangement.

In continuation of our work to develop eco-friendly procedures for the synthesis of organic compounds under solvent free conditions [27], we report herein a simple and efficient method for the synthesis of 1-(2,4-dihydroxyphenyl)-3-aryl-propane-1,3-diones via Baker-Venkataraman rearrangement under solvent free conditions using grinding technique (Scheme 1).

* To whom all correspondence should be sent:
E-mail: dksharma_84@rediffmail.com



2a-2h			
2	R ₁	R ₂	R ₃
a	H	H	OCH ₃
b	Cl	H	H
c	H	H	H
d	H	CH ₃	H
e	H	Cl	H
f	H	OCH ₃	H
g	H	H	CH ₃
h	H	H	Cl

EXPERIMENTAL

Melting points were determined in open capillary tubes and were uncorrected. IR spectra were recorded on Perkin-Elmer spectrum BX series FT-IR Spectrophotometer with KBr pellets. NMR spectra were recorded on Bruker Avance (400 MHz) instruments using TMS as an internal standard. Mass spectra were recorded on Bruker-Daltonich mass spectrometer. A mortar and pestle of porcelain was used for all the experiments. All the chemicals were obtained commercially and used as received. Resacetophenone was prepared by the Nencki reaction as reported in the literature [28].

General Procedure for the synthesis of 1-(2,4-dihydroxyphenyl)-3-aryl-propane-1,3-diones 2a-2g

The substituted 2-aryloxy-4-hydroxyacetophenones (1.95 mmol) was ground with pulverized potassium hydroxide (1.95 mmol) in a mortar by pestle for 5 minutes and the reaction mixture was left at room temperature for another 5-10 minutes. The completion of the reaction was checked by TLC. The reaction mixture was diluted with ice cold water and acidified with conc. HCl. The solid that separated out was filtered, washed with water and recrystallized from aqueous ethanol to afford 1-(2,4-dihydroxyphenyl)-3-aryl-propane-1,3-diones.

1-(2,4-Dihydroxyphenyl)-3-phenylpropane-1,3-dione 2a.

IR (KBr) $\nu_{\max}/\text{cm}^{-1}$: 3428 (OH), 1710 (C=O); ^1H NMR (CDCl_3) δ/ppm : 5.10 (s, 1H, Ar-OH), 6.35-6.65 (m, 2H, H-3, H-5), 6.75 (s, 1H, -CH=C-), 7.40-7.50 (m, 3H, H-3', H-4', H-5'), 7.85-8.0 (m, 2H, H-2', H-6'), 8.05 (d, 1H, $J=8.0$ Hz, H-6), 12.35 (s, 1H, Ar-OH), 15.50 (s, 1H, enolic OH); ^{13}C NMR (CDCl_3): δ/ppm : 94.0 (C- α), 104.3 (C-3), 109.1 (C-5), 115.1 (C-1), 126.1 (C-2'), 126.1 (C-6'), 128.1 (C-4'), 128.5 (C-3'), 128.5 (C-5'), 130.7 (C-1'), 132.5 (C-6), 163.4 (C-2), 165.5 (C-4), 184.6 (C- β), 190.1 (s, C- γ); MS (ESI): m/z 256.056 (M^+).

1-(2,4-Dihydroxyphenyl)-3-(3'-methoxyphenyl)propane-1,3-dione 2b.

IR (KBr) $\nu_{\max}/\text{cm}^{-1}$: 3422 (OH), 1708 (C=O); ^1H NMR (CDCl_3) δ/ppm : 3.95 (s, 3H, OCH₃), 5.20 (s, 1H, Ar-OH), 6.75 (s, 1H, -CH=C-), 6.80-7.45 (m, 4H, H-3, H-5, H-4', H-5'), 7.80 (dd, 1H, $J=8.0$ Hz & 2.0 Hz, H-6), 7.80-7.95 (m, 2H, H-2', H-6'), 12.35 (s, 1H, Ar-OH), 15.55 (s, 1H, enolic OH). ^{13}C NMR (CDCl_3): δ/ppm : 55.5 (C-7'), 93.6 (C- α), 104.0 (C-3), 109.5 (C-5), 110.0 (C-2'), 113.2 (C-4'), 115.5 (C-1), 118.2 (C-6'), 129.4 (C-5'), 131.1 (C-1'), 132.5 (C-6), 160.2 (C-3'), 163.5 (C-2), 164.0 (C-4), 184.6 (C- β), 190.1 (C- γ); MS (ESI): m/z 286.056 (M^+).

1-(2,4-Dihydroxyphenyl)-3-(4'-methoxyphenyl)propane-1,3-dione 2c.

IR (KBr) $\nu_{\max}/\text{cm}^{-1}$: 3420 (OH), 1705 (C=O); ^1H NMR (CDCl_3) δ/ppm : 3.9 (s, 3H, OCH_3), 5.15 (s, 1H, Ar-OH), 6.75 (s, 1H, $-\text{CH}=\text{C}-$), 6.85-7.48 (m, 4H, H-3, H-5, H-3', H-5'), 7.75 (dd, 1H, $J= 8.0$ Hz & 2.0 Hz, H-6), 7.85-7.95 (m, 2H, H-2', H-6'), 12.32 (s, 1H, Ar-OH), 15.52 (s, 1H, enolic OH); ^{13}C NMR (CDCl_3): δ/ppm : 56.0 (C-7'), 94.0 (C- α), 104.2 (C-3), 110.6 (C-5), 114.6 (C-3'), 114.6 (C-5'), 116.0 (C-1), 122.2 (C-1'), 127.9 (C-2'), 127.9 (C-6'), 131.4 (C-6), 159.4 (C-4'), 164.0 (C-2), 165.9 (C-4), 184.6 (C- β), 190.1 (C- γ); MS (ESI): m/z 286.071 (M^+).

1-(2,4-Dihydroxyphenyl)-3-(3'-methylphenyl)propane-1,3-dione 2d.

IR (KBr) $\nu_{\max}/\text{cm}^{-1}$: 3428 (OH), 1710 (C=O); ^1H NMR (CDCl_3) δ/ppm : 2.40 (s, 3H, CH_3), 5.12 (s, 1H, Ar-OH), 6.95-7.95 (m, 8H, H-3, H-5, H-6, $-\text{CH}=\text{C}-$, H-2', H-4', H-5', H-6'), 12.15 (s, 1H, Ar-OH), 15.60 (s, 1H, enolic OH); ^{13}C NMR (CDCl_3): δ/ppm : 24.6 (C-7'), 93.9 (C- α), 104.2 (C-3), 109.2 (C-5), 116.0 (C-1), 123.2 (C-6'), 126.4 (C-2'), 128.2 (C-4'), 128.6 (C-5'), 130.6 (C-1'), 131.8 (C-6), 138.1 (C-3'), 164.1 (C-4), 164.4 (C-2), 184.5 (C- β), 189.9 (C- γ); MS (ESI): m/z 270.056 (M^+).

1-(2,4-Dihydroxyphenyl)-3-(4'-methylphenyl)propane-1,3-dione 2e.

IR (KBr) $\nu_{\max}/\text{cm}^{-1}$: 3425 (OH), 1710 (C=O); ^1H NMR (CDCl_3) δ/ppm : 2.45 (s, 3H, CH_3), 5.15 (s, 1H, Ar-OH), 6.72 (s, 1H, $-\text{CH}=\text{C}-$), 6.82-7.45 (m, 4H, H-3, H-5, H-3', H-5'), 7.72 (dd, 1H, $J= 8.0$ Hz & 2.0 Hz, H-6), 7.80-7.92 (m, 2H, H-2', H-6'), 12.30 (s, 1H, Ar-OH), 15.48 (s, 1H, enolic OH); ^{13}C NMR (CDCl_3): δ/ppm : 24.2 (C-7'), 94.1 (C- α), 104.2 (C-3), 109.4 (C-5), 116.1 (C-1), 126.6 (C-2'), 126.6 (C-6'), 127.4 (C-1'), 129.4 (C-3'), 129.4 (C-5'), 131.8 (C-6), 137.4 (C-4'), 164.2 (C-2), 165.4 (C-4), 184.7 (C- β), 190.1 (C- γ); MS (ESI): m/z 270.071 (M^+).

1-(2,4-Dihydroxyphenyl)-3-(2'-chlorophenyl)propane-1,3-dione 2f.

IR (KBr) $\nu_{\max}/\text{cm}^{-1}$: 3435 (OH), 1715 (C=O); ^1H NMR (CDCl_3) δ/ppm : 5.05 (s, 1H, Ar-OH),

6.90-7.92 (m, 8H, H-3, H-5, H-6, $-\text{CH}=\text{C}-$, H-3', H-4', H-5', H-6'), 12.18 (s, 1H, Ar-OH), 15.57 (s, 1H, enolic OH); ^{13}C NMR (CDCl_3): δ/ppm : 93.4 (C- α), 104.1 (C-3), 109.2 (C-5), 115.8 (C-1), 126.6 (C-5'), 128.6 (C-3'), 129.6 (C-4'), 130.4 (C-6'), 131.1 (C-2'), 131.6 (C-1'), 133.2 (C-6), 163.8 (C-2), 165.1 (C-4), 185.4 (C- β), 190.3 (C- γ); MS (ESI): m/z 290.03 (M^+).

1-(2,4-Dihydroxyphenyl)-3-(3'-chlorophenyl)propane-1,3-dione 2g.

IR (KBr) $\nu_{\max}/\text{cm}^{-1}$: 3425 (OH), 1707 (C=O); ^1H NMR (CDCl_3) δ/ppm : 5.10 (s, 1H, Ar-OH), 6.85-8.0 (m, 8H, H-3, H-5, H-6, $-\text{CH}=\text{C}-$, H-2', H-4', H-5', H-6'), 12.17 (s, 1H, Ar-OH), 15.60 (s, 1H, enolic OH); ^{13}C NMR (CDCl_3): δ/ppm : 93.6 (C- α), 104.5 (C-3), 109.1 (C-5), 116.0 (C-1), 124.6 (C-6'), 126.4 (C-2'), 128.2 (C-4'), 131.0 (C-5'), 131.6 (C-1'), 132.5 (C-6), 134.2 (C-3'), 163.4 (C-2), 164.4 (C-4), 185.0 (C- β), 190.2 (C- γ); MS (ESI): m/z 290.03 (M^+).

1-(2,4-Dihydroxyphenyl)-3-(4'-chlorophenyl)propane-1,3-dione 2h.

IR (KBr) $\nu_{\max}/\text{cm}^{-1}$: 3425 (OH), 1712 (C=O); ^1H NMR (CDCl_3) δ/ppm : 5.20 (s, 1H, Ar-OH), 6.72 (s, 1H, $-\text{CH}=\text{C}-$), 6.88-7.45 (m, 4H, H-3, H-5, H-3', H-5'), 7.72 (dd, 1H, $J= 8.0$ Hz & 2.0 Hz, H-6), 7.85-7.95 (m, 2H, H-2', H-6'), 12.25 (s, 1H, Ar-OH), 15.45 (s, 1H, enolic OH); ^{13}C NMR (CDCl_3): δ/ppm : 94.2 (C- α), 104.3 (C-3), 109.4 (C-5), 116.2 (C-1), 127.2 (C-2'), 127.2 (C-6'), 128.2 (C-1'), 128.6 (C-3'), 128.6 (C-5'), 132.2 (C-6), 133.2 (C-4'), 163.3 (C-2), 164.6 (C-4), 185.1 (C- β), 190.1 (C- γ); MS (ESI): m/z 290.033 (M^+).

RESULTS AND DISCUSSION

2-Aroyloxy--4-hydroxyacetophenone prepared by esterification of resacetophenone with aromatic carboxylic acids was ground with pulverized potassium hydroxide in a mortar by pestle at room temperature in the absence of any solvent (Scheme 1). The progress of the reaction was checked by thin layer chromatography (TLC) when the reactants were found to have reacted almost completely in 5 minutes and it had to be kept at room temperature for another 5-10 minutes for the completion of the reaction. During grinding the

Table 1. Physical data of 1-(2,4-dihydroxyphenyl)-3-aryl-propane-1,3-diones synthesized

Compound	Yield / %	Time/min (a+b)	mp / °C	Lit. mp / °C [25]
2a	82	5+5	156-158	158-159
2b	80	5+10	190-192	189-190
2c	84	5+10	163-165	164-165
2d	90	5+5	135-136	136-137
2e	86	5+5	170-171	170-171
2f	80	5+5	149-151	151
2g	84	5+10	125	124-125
2h	80	5+10	210-212	210-211

a- Time for grinding

b- Time at which the reaction mixture was kept at room temperature

reaction mixture absorbed moisture which was found to be sufficient to make the reaction mixture homogeneous. The product is also recovered simply by acidification of the reaction mixture in ice-cold water and avoids the need for organic solvent extraction of the compound. Attempt was also made using other bases such as barium hydroxide, calcium hydroxide, and calcium oxide which proved to be futile.

The validity of the reaction was established by converting differently substituted 2-aryloxy-4-hydroxyaceto-phenones into 1-(2,4-dihydroxyphenyl)-3-aryl-propane-1,3-diones in high yield (Table 1).

CONCLUSION

In conclusion, it can be stated that the present protocol for the synthesis of 1-(2,4-dihydroxyphenyl)-3-aryl-propane-1,3-diones is highly efficient and eco-friendly as it avoids the use of organic solvents at any stage of the reaction.

REFERENCES

- J.N. Roitman, K. Mann, E. Wolenweber, *Phytochemistry*, **31**, 985 (1992).
- J. Staunton, H.D. Barton, W.D. Ollis *Comprehensive Organic Chemistry*, Pergamon Press, London, 1979.
- S. Heller, S. Natrajan, *Org. Lett.*, **8**, 2675 (2006).
- D. Simoni, F.P. Invidiata, R. Rondanin, S. Grimaudo, G. Cannizzo, E. Barbusca, F.D. Porretto, N. Alessandro, M. Tolomeo, *J. Med. Chem.*, **42**, 4961 (1999).
- O. Kuzueva, Y. Burgart, V. Saloutin, O. Chupakhin, *Chemistry of Heterocyclic Compounds*, Springer, Germany, 2001.
- R. Kumar, Y. Joshi, *Arkivoc*, **9**, 142 (2007).
- I. Bennett, N. Broom, R. Cassels, J. Elder, N. Masson, P. O'Hanlon, *Bioorg. & Med. Chem. Lett.*, **9**, 1847 (1999).
- G. Diana, P. Carabateas, R. Johnson, G. Williams, F. Pancic, J. Collins, *J. Med. Chem.*, **21**, 889 (1978).
- G. Crouse, M. McGowan, R. Boisvenue, *J. Med. Chem.*, **32**, 2148 (1989).
- T. Nishiyama, S. Shiotsu, H. Tsujita, *Polym. Degrad. & Stab.*, **76**, 435 (2002).
- N. Acton, A. Brossi, D. Newton, M. Sporn, *J. Med. Chem.*, **23**, 805 (1980).
- M. Huang, Y. Lou, J. Xie, W. Ma, Y. Lu, P. Yen, B. Zhu, H. Newmark, C. Ho, *Carcinogenesis*, **19**, 1697 (1998).
- K. Singletary, C. MacDonald, *Cancer Lett.*, **155**, 47 (2000).
- K. Singletary, C. MacDonald, M. Iovinelli, C. Fisher, M. Wallig, *Carcinogenesis*, **19**, 1039 (1998).
- C.C. Lin, Y.L. Tsai, M.T. Huang, Y.P. Lu, C.T. Ho, S.F. Tseng, S.C. Teng, *Carcinogenesis*, **27**, 131 (2006).
- I. Andrae, A. Bringhen, F. Bohm, H. Gonzenbach, T. Hill, L. Mulroy, T.A. Truscott, *J. Photochem. Photobiol. B: Biol.*, **37**, 147 (1997).
- L. Tchertanov, J.F. Mouscadet, *J. Med. Chem.*, **50**, 1133 (2007).
- J. Sheikh, H. Juneja, V. Ingle, P. Ali, T.B. Hadda, *J. Saudi Chem. Soc.*, **2**, 97 (2012).
- A. Rajbhoj, N. Korde, S. Gaikwad and J. Dargad, *Int. J. Green & Herb. Chem.*, **1**, 226 (2012).
- H.S. Mahal, K. Venkataraman, *Curr. Sci.*, **2**, 214 (1933).
- J.K. Makrandi, M.S. Lamba, S. Kumar, *J. Chem. Res.*, 133 (2006).
- S.K. Grover, J.K. Makrandi, S. Saxena, *Synthesis*, 697 (1985).
- S.V. Kostanecki, J. Tambor, *Chem. Ber.*, **33**, 330 (1900).

24. I. Hirao, M. Yamaguchi, M. Hamada, *Synthesis*, 1076 (1984).
25. J.I. Sheikh, I.N. Vishwas, H.D. Juneja, P. Ali, R. Dongre, *Der Pharma Chemica* **2**, 130 (2010).
26. J.K. Makrandi, A. Kumar, *Heteroletters*. **2**, 271 (2012).
27. D. Sharma, S. Kumar, J.K. Makrandi, *Green Chem. Lett. Rev.* **2**, 53 (2009).
28. V.K. Ahluwalia, R. Agarwal, *Comprehensive Practical Organic Chemistry: Preparation and Quantitative Analysis*, University Press, India, 2000.

ПРОСТА СИНТЕЗА НА 1-(2,4-ДИХИДРОКСИФЕНИЛ)-3-АРИЛ-ПРОПАН-1,3-ДИОНИ ЧРЕЗ ПРЕГРУПИРАНЕ НА ВАКЕР-VENKATARAMAN ПРИ ОБИКНОВЕНИ ТЕМПЕРАТУРИ БЕЗ РАЗТВОРИТЕЛ

Д. Шарма*¹, С. Кумар²

¹Департамент по химия, ВРСМ Колеж по инженерство и технология, Бахал, Индия

²Департамент по химия, Технологичен институт по текстил и наука, Бхивани, Индия

Получена на 17 декември, 2012 г.; коригирана на 4 февруари, 2013 г.

(Резюме)

Описан е прост и високоефективен метод за синтезата на 1-(2,4-дихидроксифенил)-3-арил-пропан-1,3-диони чрез прегрупирането на Baker-Venkataraman, включващ смилането на 2-ароилокси-4-хидроксиацетофенони с пулверизиран калиев хидроксид при стайна температура в отсъствие на разтворител. Структурата на тези съединения е идентифицирана от тяхните спектрални данни (FT IR, ¹H NMR, ¹³C NMR, мас-спектрометрия). Процедурата не избягва използването на опасни реактиви и органични разтворители при всеки етап от реакцията.

Kinetic study for formation of thiazole by cyclisation

B. H. Zaware^{1,*}, S. R. Kuchekar²

¹*Department of Chemistry, New Arts, Commerce & Science College, Ahmednagar
Maharashtra, India. 414 001*

²*Post Graduate Department of Chemistry, Arts Commerec Science College, At Post. Satral,
Taluka. Rahuri, District. Ahmednagar, Maharashtra, India, 413711*

Received: January 23, 2013; Revised: March 25, 2013

The kinetic study of 3-chloroacetyl acetone with various thioureas has been carried out in ethanol. In this study thioureas used are m-methyl phenylthiourea, m-methoxy phenylthiourea, methoxy phenylthiourea and m-chlorophenyl thiourea. The kinetic study reports second order rate constants for these reactions. The rate of reaction is first order with respect to thioureas and first order with respect to 3-chloroacetyl acetone. The effect of substituents on the rate of reaction is also studied. Thermodynamic parameters are used to explain the nature of reactions. The proposed reaction mechanism and details of Kinetics for various reactions were studied.

Keywords: Kinetics, Thiazole, Cyclisation

INTRODUCTION

Sulphur and nitrogen containing organic compounds are gaining importance in synthetic and pharmaceutical fields. Thiourea and their derivatives are well known intermediates in the synthesis of clinically important heterocycles like thiazoles, 4-thiozolidinones and benzothiozoles. Thioureas are commercially used in photographic films, plastics and textiles. Certain thiourea derivatives are insecticides, rhodenticides and pharmaceuticals. Some of the thioureas are screened for anticancer activity. Thioureas have shown antibacterial [1], antipyretic [2], hypnotic [3] and fungicidal [4] activity. Thiazoles are found in medicaments [5] like vitamin-B, sulphathiozoles, promizole, niridazole, aminotrizole and tetramisole. Kinetics and mechanism of reaction between thiourea and iodate in buffer medium has been studied [6]. The kinetic study of reaction of thiourea with formaldehyde is also reported [7]. Reaction kinetics of gold dissolution in acid thiourea solution using ferric sulphate as oxidant was investigated with rotating disk technique [8].

The kinetics of formation of chromium(III) – iminodiacetic acid complex has been studied in temperature range 35 – 55 °C spectrophotometrically. The study shows rate of reaction is first order with respect to chromium(III) and rate of increases with increase in temperature [9]. The kinetics of oxidation of thiourea and *N*-substituted thioureas and the corresponding formamidine disulfides by sodium *N*-chloro-*p*-toluenesulfonamide or chloramine-T (CAT) in the presence of HClO₄ has been studied at 278 K [10]. The kinetics of the reaction between vitamin C (L-ascorbic acid) and ferric chloride hexahydrate was investigated in acidic medium at pH 3 spectrophotometrically. The order of the reaction was established by applying different methods. The order of the reaction with respect to each reactant was found was first and the overall second order was recommended for the reaction [11]. Kinetic investigation in rhodium(III) catalyzed oxidation of D-Mannitol in an acidified solution of potassium bromate in the presence of Hg(OAc)₂ as a scavenger, have been studied in the temperature range of 300 - 450 °C [12]. Kinetic and thermodynamic study on the adsorption behavior of Rhodamine B dye on

* To whom all correspondence should be sent:
E-mail: zaware@india.com; shashi17@gmail.com

Duolite C-20 resin has been reported. The effects of various experimental factors; sorbent amount, contact time, dye concentration and temperature, were studied by using the batch technique [13].

We have reported kinetic study of reaction of chloroacetone with p-substituted phenyl thioureas [14]. We have also reported kinetics of reaction of 3-chloroacetyl acetone with p-substituted phenyl thioureas [15]. Literature survey reveals that there is no work on kinetic study of reaction of 3-chloroacetyl acetone with m-substituted phenyl thioureas.

EXPERIMENTAL

Apparatus

The pH of thiazole hydrochloride solution was measured by digital pH meter. (EQUIPTRONICS, EQ-614A)

Reagents

All the reagents used were of analytical reagent grade unless otherwise stated; double distilled water was used throughout the experimental work.

Aryl thioureas were prepared by Frank and Smith method [16]. The 3-chloroacetyl acetone (Merck India), diethyl ether (Qualigens) were used for this work. The standard solutions of 3-chloroacetyl acetone and thioureas were prepared in double distilled absolute alcohol.

General procedure

Kinetic measurements were carried out at different concentrations of reactants and temperatures. A solution containing appropriate amount of thiourea which is thermostated at particular temperature was added in the solution containing appropriate amount of 3-chloroacetyl acetone at same temperature. At different time intervals definite volume of aliquot was added to a mixture of diethyl ether and water. It was shaken immediately and aqueous layer containing thiazole hydrochloride was separated, diluted to definite volume with distilled water. The pH of thiazole hydrochloride solution formed was measured by digital pH meter. Equal amounts of thiourea and 3-chloroacetyl acetone were mixed under the similar experimental conditions and kept

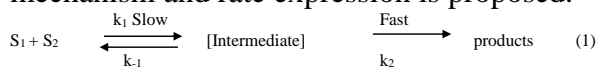
overnight. The reaction mixture was then cooled and poured on crushed ice. It was extracted with ether to remove the unreacted reactants. The aqueous layer was neutralized by sodium hydroxide. The white solid obtained was crystallized from ethanol.

RESULTS AND DISCUSSION

The stoichiometric study indicates that one mole of thiourea reacts with one mole of 3-chloroacetylacetone. The rates of reaction were measured at different concentration of thioureas at constant concentration of 3-chloroacetylacetone. The plot of $\log (dc/dt)$ against $\log [3\text{-chloroacetylacetone}]$ is also straight line by keeping concentration of thioureas constant. The slope of the graph is 1.0 (Fig. 1). The plot of $\log (dc / dt)$ against $\log [\text{thioureas}]$ by keeping concentration of 3-chloroacetylacetone constant it is also straight line and slope of the plot is one. The overall order of reaction is 2. By using Van't Hoff's differential method [17] the order of reaction with respect to 3-chloroacetylacetone and thioureas was also determined. Second order rate constants were determined at five different temperatures. The energy of activation (E_a^*) was determined by plotting graph of $\log k$ versus $1/T$ (Fig. 2) and other thermodynamic parameter were calculated, [Table.1]. The entropies of activation (ΔS^*) of these reaction are negative indicates rigid nature of the transition state. The negative value of entropies of activation (ΔS^*) also indicates that less stable noncyclic reactant convert into stable cyclic products [18]. Almost equal values of free energy of activation (ΔF^*) for all thioureas indicates that probably a similar type of mechanism prevails in all cases [18]. When rate constant for the reaction are compared, the thiourea is found to be more reactive than the substituted phenyl thioureas. This may be due to the presence of II-electron in benzene ring. The phenyl thiourea and m-methyl phenyl thiourea show nearly same rate constants. This may be due to small effect of methyl group due to hyper conjugation and inductive effect. The methoxy phenyl thiourea shows higher rate of reaction due to mesomeric effect. The m-chlorophenyl thiourea shows lower rate of

reaction due to negative inductive effect of chloro group [19-20]. It is found that, the reaction is second order, first order with respect to thioureas and first order with respect to 3-chloroacetylacetone. The rate constants calculated from second order rate law are fairly constant [Table. 2].

Based on these facts, the following general mechanism and rate expression is proposed.



S_1 stands for 3-chloroacetylacetone and S_2 stands for thioureas.

$$\text{Rate of reaction} = k_1 [S_1] [S_2] - k_{-1} [\text{Intermediate}] \quad (2)$$

On applying steady state approximation.

$$d / dt [\text{Intermediate}] = 0 = k_1 [S_1] [S_2] - k_{-1} [\text{Intermediate}] - k_2 [\text{Intermediate}] \quad (3)$$

$$[\text{Intermediate}] = \frac{k_1 [S_1] [S_2]}{k_{-1} + k_2} \quad (4)$$

Substituting the value of [Intermediate] in equation (2)

$$\text{Rate of reaction} = k_1 [S_1] [S_2] - \frac{k_{-1} k_1 [S_1] [S_2]}{k_{-1} + k_2} \quad (5)$$

$$\text{Rate of reaction} = \left\{ k_1 - \frac{k_{-1} k_1}{k_{-1} + k_2} \right\} [S_1] [S_2] \quad (6)$$

The order of reaction is two (Reaction mechanism). The derived rate law explains all the observed experimental facts.

CONCLUSION

The order of reaction between 3-chloroacetylacetone and thiourea is found to be two.

The proposed rate law also shows that the rate of reaction is two.

Nearly equal values of free energy (ΔF^*) indicates that same type of reaction mechanism prevails.

Decrease in entropy (ΔS^*) indicates that, from open chain reactants the cyclic product is formed.

Acknowledgment: The authors (BHZ) is thankful to authorities of A.J.M.V. Prasarak Samaj, Ahmednagar (M.S.) for their kind help and BCUD, University of Pune for financial assistance and (SRK) is thankful to management PRES Pravaranagar.

REFERENCES

1. M. Bockmuhl, W. Persh, E. Bartholomus, *Chem. Abs.*, **26**, 4683 (1932).
2. K. H. Slotta, *Chem Ber.*, **63B**, 208 (1930).
3. M. Shrimotani, *J. Pharma Soc, Jpn.*, **72**, 328 (1952).
4. E. J. Beer, *J. Pharma Exptl. Therap.*, **57**, 19 (1936).
5. A. G. Sehering, *Chem. Abst.*, 47, 1348 (1953).
6. S. Wang, J. Lin, F. Chun, *Sci. China B. Chem.*, **47**, 480 (2004).
7. K. Dusek, *J. Polymer Sci.*, **30**, 431 (2003).
8. J. Li, J. Millar, *Hydrometallurgy.*, **89**, 299 (2007).
9. A. E. Hassan, K. I. Mohamed, A. A. Ahemad, *J. Saudi Chem. Soc.*, **13**, 219 (2009).
10. J. P. Shubha, Puttaswamy, *J. Sulfur Chem.*, **30**, 490 (2009).
11. P. Sania, A. F. Muhammad, A. Rohana, A. Q. Fahim, *J. Saudi Chem. Soc.*, **16**, 63 (2012).
12. S. Sheila, S. Parul, *Der Chemi. Sinica.*, **1**, 13 (2010).
13. M. Al-Rashed Salwa, A. Al-Gaid Amani, *J. Saudi Chem. Soc.*, **16**, 209 (2012).
14. B. H. Zaware, R. A. Mane, D. B. Ingale, *J. Ind. Chem. Soc.*, **77**, 213 (2000).
15. B. H. Zaware, R. A. Mane, S. R. Kuchekar, *J. Pharm. and Chem. Res.*, **1**, 276 (2009).
16. R. L. Frank, P. V. Smith, *Org. Synth.*, **3**, 735 (1995).
17. Etudes de dynamique chimique, J. H. Van't Hoff, Myaller and Company, Amsterdam, 1984.
18. B. H. Zaware; R. A. Mane; D. B. Ingle, *J. Ind. Chem. Soc.*, **77**, 213(2000).
19. A Guide book to mechanism in organic Chemistry, Peter Sykes, 6th Edition, p. 150.
20. Advance Organic Chemistry, Carey and Sundberg, A, P.550-552.

B. H. Zaware, S. R. Kuchekar: Kinetic study for formation of thiazole by cyclisation

КИНЕТИЧНО ИЗСЛЕДВАНЕ НА ОБРАЗУВАНЕТО НА ТИАЗОЛ ЧРЕЗ ЦИКЛИЗАЦИЯ

Б.Х. Зауаре^{1*}, С.Р. Кучекар²

1 Департамент по химия, Колеж за нови изкуства, търговия и наука, Ахмеднагар Махаращра, Индия

*2 Департамент по химия – следдипломна квалификация, Колеж за нови изкуства, търговия и наука,
Ахмеднагар Махаращра, Индия*

Постъпила на 23 януари 2013 г.; коригирана на 25 март, 2013 г.

(Резюме)

Извършено е кинетично изследване на взаимодействието на 3-хлороацетилацетон с различни производни на тиокарбамида в етанол. Производните на карбамида са *m*-метил-фенилкарбамид, *m*-метоксифенилкарбамид, *m*-етоксифенилкарбамид и *m*-хлорофенилкарбамид. Порядъкът на реакциите е първи по отношение на тиокарбамидните производни, както и за 3- хлороацетилацетон. Изследван е и ефектът на заместителите върху скоростта на реакциите. Използвани са термодинамични параметри за обяснението на природата на реакциите. Изследван е предложеният механизъм на реакциите и подробности за кинетиката им.

Changes in structure of solid pyrolysis residue during slow pyrolysis of rice husk

S. Uzunova¹, D. Angelova¹, B. Anchev¹, I. Uzunov^{2*}, A. Gigova³

¹ University of Chemical Technology and Metallurgy Sofia, 8 St.Kl.Ohridski Blvd., 1756 Sofia, Bulgaria

² Institute of General and Inorganic Chemistry, Bulgarian Academy of Sciences, Acad. G.Bonchev Str., bl.11, 1113 Sofia, Bulgaria

³ Institute of Electrochemistry and Energy Systems, Bulgarian Academy of Sciences, Acad. G.Bonchev Str., bl.10, 1113 Sofia, Bulgaria

Received: September 17, 2012; Revised: February 12, 2013

The research provides the basis for development of a new environmental material with controllable characteristics, suitable for producing of value-added carbon/silica containing materials. The subject of the study is to determine the influence of the pyrolysis temperature on the specific surface area and porosity of charcoal obtained by slow pyrolysis in the temperature range 250-700°C of acid leached rice husks.

The char's structure was set out by the mercury porosimetry and Brunauer-Emmett-Teller method. The phase composition of the solid residue after pyrolysis and carbon/silica ratio therein has been determined by thermal analysis (TG/DTA/MS) and XRD. The morphology of the materials has been studied using scanning electron microscopy.

It was established that the slow pyrolysis in the investigated temperature range results in a solid residue with predominantly macro-porous structure and pore size distribution between 50 and 200 µm. The sample obtained at 480°C is characterized by the largest total pore volume and the largest average pore diameter. With increasing the pyrolysis temperature C:SiO₂ ratio in the solid pyrolysis residue decreased from 1.38 to 0.85 and specific surface area increased from 7.0 up to 440.0 m² g⁻¹.

Keywords: rice husk; pyrolysis; porosity; specific surface area; morphology

1. INTRODUCTION

In recent years, in relation with the periodical energy crises and the depletion of raw material stocks, particular attention is paid to obtaining energy and value-added products from renewable agricultural wastes. The rice husks, a by-product of the rice milling industry are produced in large quantities as a waste. The limited applicability of the rice husks as foodstuff for cattle is creating an ecological problem, connected with the storage and management of huge amounts of waste. On the other hand the specific phase composition, structure and properties of the husks renders them suitable for preparing different C/SiO₂ containing materials [1,2]. The rice husks possess, although a low, caloric effect. So they can be considered also as a renewable power source [3]. In recent years are offered different methods associated with the conversion of rice husks into the high-tech products [4-6].

Between the thermo-chemical conversion methods for processing of biomasses most often used pyrolysis. The process is related to obtaining a liquid phase, char and gaseous fractions (fuel gases). There are two approaches for the conversion

technology. So called conventional pyrolysis, is to maximum the yield of pyrolysis oil and/or fuel gas. The conditions are high temperature and high heating rate. The second enhanced the char production at the low temperature and low heating rate. One of the possible applications of solid pyrolysis residue is use it directly or after activation as biosorbents [5,7]. They are biodegradable and have high adsorption properties resulted from their morphology and surface functionalities [8]. There is no need to regenerate them because of the low production cost [5,9,10]. Their application is a good practice and has received much attention in sorption of various organic or inorganic pollutants from aqueous medium [11,12].

The use of the solid pyrolysis residue as adsorbent is related to obtaining of a material with suitable porous structure, high specific surface area and surface functionalities which providing a high adsorption capacity and selectivity [13,14]. Ways to get the carbon containing adsorbents with a developed porous structure are the use of suitable activating agents and/or controlling the pyrolysis conditions [15-17].

There have been several reports on the pyrolysis of rice husks which deal with the relation between the pyrolysis conditions with char structure. The development of advanced fast pyrolysis processes for bio-oil production has gained much attention

* To whom all correspondence should be sent:
E-mail: uzunov_iv@svr.igic.bas.bg

recently, because they offer a convenient way to convert agriculture wastes into biofuels and carbonaceous value-added products. That is why the studies are related to determination the impact of the temperature, heating rate and pressure on the quantity, phase composition and morphology of final products in fast pyrolysis. Hu et al. [18] determined the pyrolysis reactivity's of rice husk char and the evolution characteristics of char structure during rapid pyrolysis. Liou [19] investigated the effect of heating rates on the morphology and chemistry of the products from carbonization of rice husks. Kumagai et al. [20] and Bharadwaj et al. [21] also published data which dealt with the relationship between the fast pyrolysis conditions and char structure. The general conclusion is that the fast pyrolysis is associated with obtaining a small amount of solid pyrolysis residue with predominantly microporosity and narrow pore size distribution. These can be explained by the very fast decomposition of lignin-cellulose matter and evolution of volatiles during rapid pyrolysis, thus leaving a highly microporous structure.

It is reasonable to expect that the slow pyrolysis will lead to other, different phase and structural changes in solid pyrolysis residue.

In this study, the slow pyrolysis which provides a high yield of solid residue was used in a fixed bed induction heated reactor. In particular, the impact of pyrolysis temperature at a constant heating rate and retention time on the pore structure of rice husks char was investigated. The effect of the pyrolysis temperature on the carbon:SiO₂ ratio in solid pyrolysis residue was also discussed.

The results indicated that the slow pyrolysis temperature had an essential impact on the char's structure. The resulting solid pyrolysis products are characterized by a varied in size porous structure. The same is formed predominantly by meso- and macro pores with a wide range of pore size distribution. This fact is important when the solid residue from thermo-cracking of rice husks will be used as adsorbent [22-24].

2. EXPERIMENTAL

2.1 Materials

Rice husks (RH) were obtained by rice threshing performed in 2010 from Pazardjik region, Bulgaria. The husks with prevailing particle size above 5 mm were initially washed several times with water to remove any mechanical impurities. Determined amount of ash in the raw rice husks is 21 wt.%. Except the main quantity of amorphous silica, the

ash contains some other inorganic admixtures listed in Table 1. To reduce the content of these admixtures RH were treated with 12 N HCl, at hydro-module 3:1, for 3 hours at the boiling temperature of the acid. A reflux condenser was used. The acidified sample was washed with deionized water until pH 6.5 was reached and dried at 110° C to a moisture content less than 5 wt.%.

2.2 Pyrolysis

A weighted amount of the so pretreated husks were pyrolysed in a temperature interval 250-700° C. The following series of samples, designated as *B1* (250°C), *B2* (350°C), *B3*

(480°C) and *B4* (700°C) were obtained. The fixed bed slow pyrolysis experiments were performed in a vertical tube stainless steel electrically heated reactor, equipped with temperature controllers, under a residual pressure of 1.33 Pa. The reactor comprised a 240 mm (L) x 40 mm (ID) with 170 mm long heated zone. The liquid products were collected in a trap between the reactor and vacuum pump, maintained at the temperature of 2-3° C. The temperature in the reactor was increased linearly from room temperature up to the value needed for pyrolysis with a heating rate of 4° min⁻¹ and temperature retention for 4 hours. The time within which the temperature is maintained constant, is defined as "retention time". The sample was taken out after cooling the system down to room temperature, at atmospheric pressure. The yields of the solid pyrolysis residue were calculated based on the mass of raw rice husks fed.

2.3 Samples characterizations

The carbon/SiO₂ weight ratio in the solid pyrolysis residues has been determined applying thermal analysis (TG/DTA) accomplished with a SETARAM *LabsysEvo* device, in a corundum crucible, at a heating rate of 10° min⁻¹ in air. A mass spectrometer detector coupled to the device was used for the evolving gas analysis. The signals for mass numbers of 18 and 44 were continuously detected.

The phase composition of the samples has been carried out on the basis of the data, recorded by a diffractometer Philips ADP 15 with Cu K_α radiation.

Area of the pores as well as the bulk density was determined by mercury intrusion porosimetry on a MICROMERITICS Auto-Pore 9200 apparatus. Volume intrusion curves were obtained for every sample from 0.01 up to 34.84 MPa pressure, which

corresponded to a pore diameter range from 262.7 μm to 0.042 μm . Prior to

porosimetry analysis the samples were dried at 110° C for 48 h. The specific surface area was assessed by BET nitrogen adsorption measured in a static volumetric device Area Meter, Strolein.

The morphology of the surface of the raw rice husks and pyrolyzed ones was observed with SEM using JEOL- Superprobe 733 microscope, applying the appropriate magnification.

The total ash content into the raw RH was analyzed gravimetrically. The inorganic admixtures were determined by flame atomic absorption analysis (AAA) by spectrometer Solar M.

3. RESULTS AND DISCUSSION

3.1 Phase composition and morphology

The data of the inorganic admixture amount in the raw RH before and after treatment with hydrochloric acid evaluated by AAA are presented in Table 1.

Table 1. Inorganic admixture amount in the raw RH before and after acid treatment.

Element	Amount, wt. %
Carbon	38.4
Hydrogen	4.3
Oxygen	36.08

The low content of inorganic admixtures in the ash residue of leaching rice husks is reason hereafter to talk about phase of silica in solid pyrolysis residue.

The elemental microanalysis was used to investigate the carbon/silica weight ratio in the acid treated raw rice husks, Table 2. According to the results obtained the carbon/silica weight ratio in the acid leached raw rice husks amounted to 1.81 weight percent.

Table 2. Elemental composition of acid leached raw RH.

Element	In raw RH, $\mu\text{g g}^{-1}$	After leaching, $\mu\text{g g}^{-1}$
K	580	62
Na	370	60
Fe	330	38
Ca	103	*BDL
Cu	12	BDL
Mn	10	BDL
Zn	7	BDL
Mg	5	BDL

*BDL, below detection limit.

On the basis of the thermogravimetric analysis data, Fig. 1 (a) the weight C:SiO₂ ratio in the samples B1-B4 has been determined. The effect of pyrolysis temperature on the yield and carbon/silica ratio of the chars is shown in Table 3.

Table 3. Yield of the carbon-containing residue and C:SiO₂ weight ratio as a function of the pyrolysis temperature.

Sample	T _{pyrolysis} , °C	Yield, wt. %	Ratio C:SiO ₂
B1	250	58	1.38
B2	350	52	1.08
B3	480	49	0.96
B4	700	46	0.85

Actually the char represents a mixture of some quantity undecomposed residues of the lignin-cellulose material, highly carbonized rice husks and silica. The change of the C/SiO₂ ratio shows that with increasing of pyrolysis temperature the solid pyrolysis residue become increasingly less carbonaceous in nature and vice versa for the silica.

The thermal effects (DTA) and gas formation rates under conditions of linear temperature increase, in air medium for samples B1-B4 are presented on Figures 1(b) and (c).

The rice husks as a lignocelluloses' material is composed of various type biopolymers containing cellulose, hemicellulose, lignin and amorphous SiO₂ [4]. The chemical nature of biogenic silica in rice husks has discussed by a number of authors [25,26]. Upon pyrolysis condition in rice husks start some destruction processes. Hemicellulose started its decomposition easily; cellulose pyrolysis takes place at a higher temperature range while the lignin decomposes at a slow rate in the entire operating temperature interval [24]. The degradation reactions include depolymerization, dehydration, decarboxilation and oxidation of the lignocelluloses' matrix.

For example: sample B1, obtained at 250° C, contains in itself not completely decomposed residuals of cellulose and lignin. The exothermal effect in the interval 210 - 370° C is associated with the destruction of the remaining quantity of cellulose, contained in this sample. The process is accompanied by the evolving of the main quantity of water and a small amount of CO₂, as a consequence of the decomposition of the nuclei of the cellulose chain. The second exothermal effect with a maximum at 440° C corresponds to the full destruction of the lignin residuals and oxidation of the char, completed at 540° C. As a result of the decomposition of the condensed nuclei of the lignin mainly CO₂ is liberated.

The results from TA/MS analysis of samples B2-B4 confirmed the presence of undecomposed part of the lignin-cellulose material in the solid pyrolysis residue. According to the data of the TG analysis, the moisture content in carbonized rice husks amounted to 5 wt. %.

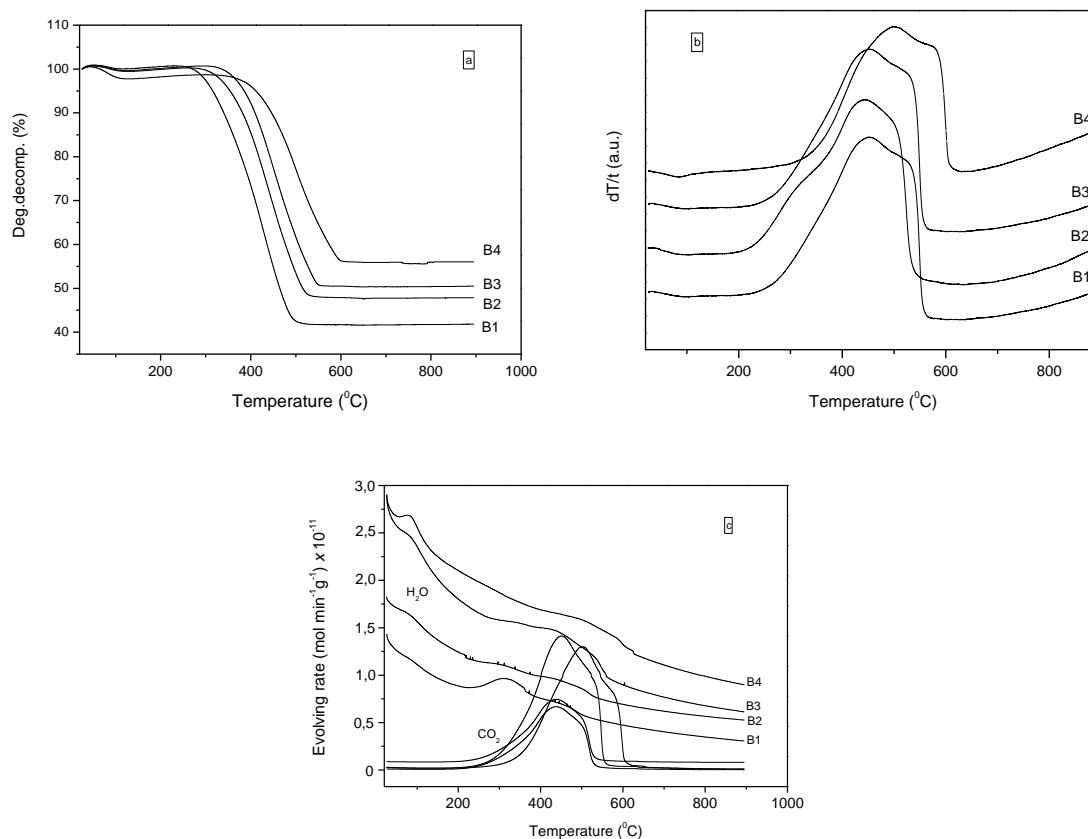


Fig.1. TG curves (a); DTA curves (b); gas formation rates and products distribution (c) during the thermal analysis of the samples in air atmosphere

The results from TA/MS analysis of samples B2-B4 confirmed the presence of undecomposed part of the lignin-cellulose material in the solid pyrolysis residue. According to the data of the TG analysis, the moisture content in carbonized rice husks amounted to 5 wt. %.

The X-ray diffraction patterns of the samples are presented in Fig. 2. The possible bonding of silicon with monosaccharides in rice husks has already been represented by Patel et al. [27]. The pyrolysis causes a decomposition of the organic material and breaking of the bonds between silicon and the organic matrix. The Si-O groups become attached to one another to produce a low form of cristobalite and tridimite. The resulting material, containing a mixture of amorphous silica and carbon show an XRD pattern with a broad maximum. The results also corroborate the formation of a porous network in the samples. The halo observed at about 2θ 22° corresponds to the presence of amorphous SiO₂ [28], but also shows the typical turbostratic structure with interlayer distances of graphenes substantially higher than those in graphite. The halo at 2θ 44° is typical for carbonized cellulose and reflects the initial formation of (100) planes, related to the graphite structure [29]. It becomes more

pronounced with increasing the temperature of pyrolysis.

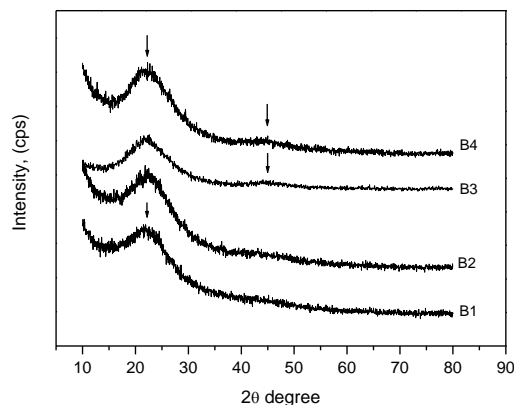


Fig.2. XRD patterns of the pyrolyzed RH

The cellulose and hemicellulose under conditions of pyrolysis degrade under cycloreversion and dehydration followed by transglycosylation. The mechanism of decomposition of lignin also occurs *via* dehydration [30]. The process is accompanied by intensive liberation of gases and liquid phase, containing different hydrocarbon compounds, CO, CO₂ and H₂O. The rapid mass transfer from the inside of the

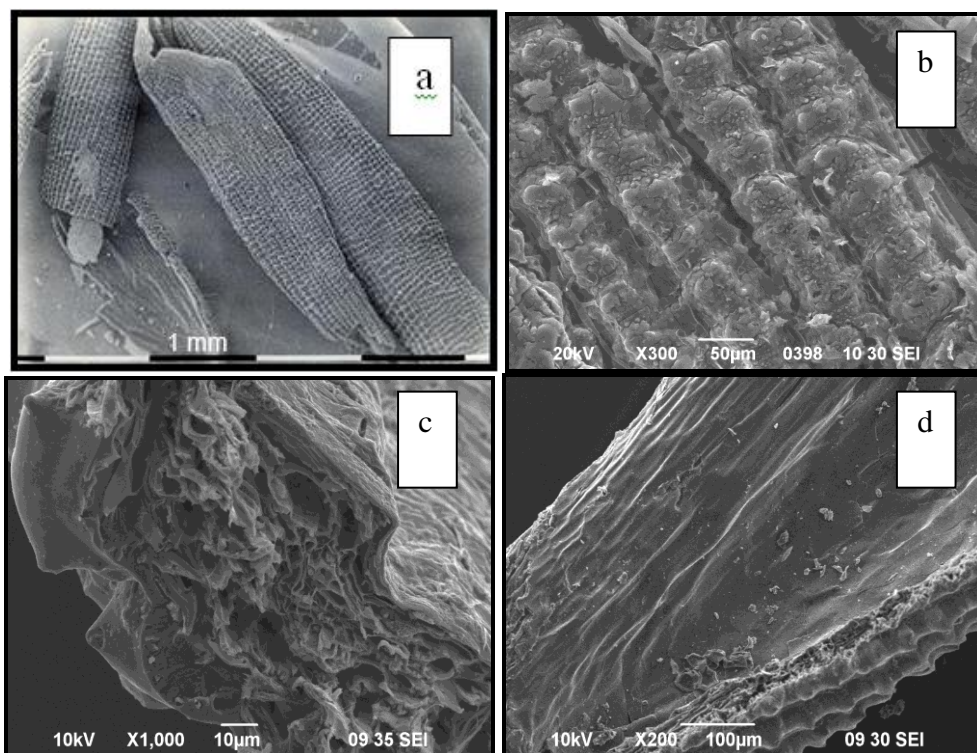


Fig.3. Micrographs of raw RH (a), outer epidermis (b), cross-section (c) and inner epidermis (d) of rice husks carbonized at 480° C.

particles to the surface caused structural evolution and morphological changes of the solid residue. Some part of fluids is being deposited on the char surface, determining its surface functionalities. Change in the morphology of rice husks in the pyrolysis process, studied by means of scanning electron microscopy, is demonstrated in Fig. 3.

A typical structure with granular formations located linearly on the outer epidermis as well as the fibrous structure of the inner epidermis can be seen in Fig. 3(a). It was established that the silica is concentrated predominantly in the outer surface and in a less amount in the inner surface of the RH [31]. After carbonization the rice husks appear to be cracked, Fig. 3(b). The size of small grains on the outer epidermis is reduced. Nevertheless the corrugated structure of the outer epidermis was kept in the solid pyrolysis residue. This means that after carbonization the solid pyrolysis residue retains skeleton of lignocelluloses' matrix, building the cell walls in which remains dispersed amorphous silica. After pyrolysis the lamellar inner epidermis remains undestroyed, Fig. 3(d). Evaporation of volatile matters creates in interior structure of the pyrolyzed RH many pores of different size with rough surface and irregular outlet, Fig. 3(c).

The increase of the pyrolysis temperature leads also to a change in the specific surface area of the obtained materials, varying in a range from 7 up to 440 square meters per gram, Fig. 4.

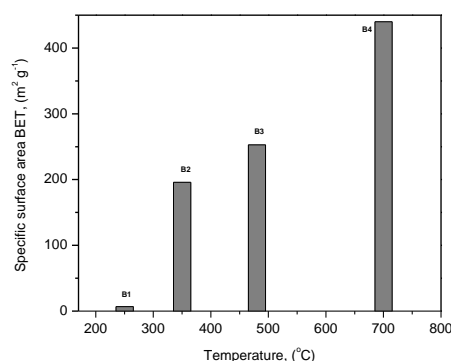


Fig.4. Dependence between BET specific surface area of the samples and the pyrolysis temperature.

3.2 The pore size distribution

The pore size distribution is a function of the pyrolysis temperature and phase composition of the lignocelluloses precursor. This is the most important dimension for characterizing the structural heterogeneity of the solid residue and is closely related to kinetic properties of porous materials [20].

The porosity characteristics of the samples, determined by mercury porosimetry are depicted in Table 4. The experimentally obtained data demonstrate that the porosity, respectively the total volume of the pores of samples B1, B2 and B4 have

similar values while the values for sample B3 are higher with about 9%. The sample B3 is characterized also by the greatest average pore diameter and the lowest bulk density.

Table 4. Porosity characteristics of the samples determined by mercury porosimetry.

Characteristics	B1	B2	B3	B4
Total pore volume, cm ³ g ⁻¹	0.898	0.814	1.053	0.778
Porosity, %	52.38	52.04	57.09	52.95
Total pore area, m ² g ⁻¹	6.652	6.369	5.869	5.164
Average pore diameter, μm	0.540	0.511	0.718	0.603
Bulk density, g cm ⁻³	0.583	0.640	0.542	0.680

The differential curves of the pore volume distribution with respect to diameter for the B1-B4 samples are exhibited in Fig. 5. All the porosity diagrams have a similar appearance, which shows that the analyzed samples possess pores with sizes varying within a wide range of values. The main share of all the pores belongs to the pores with large volumes and diameters within the interval 50-200 μm.

The maximum peak in the differential distribution curves for all four samples corresponds to the percentage of the total pore volume, as follows:

- For B1 - 14.9 %;
- For B2 - 14.6 %
- For B3 - 24.0 % and
- For B4 - 18.0 %.

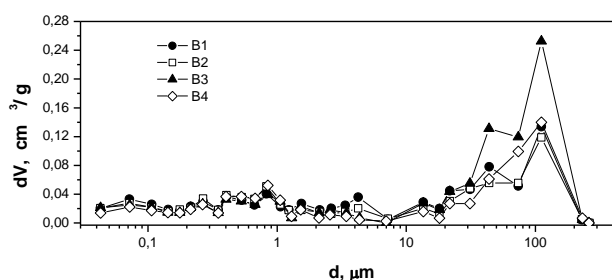


Fig.5. Pore volume distribution by pore diameter for samples B1-B4.

The results demonstrate that the prepared carbonized rice husks possess multi macroporous structure. The presence of the such structure, as a rule ensures high sorption ability of the material [32].

The theory of mercury porosimetry conditionally accepts that the diameter, determined by the integral dependence with respect to the pore volume and pore surface area at which there starts a steep increase is the value, dividing the pores in two kinds: “micro” pores, with pores diameter less than the value of the inflection point and “macro” pores, Fig. 6.

It should be noted that in according to IUPAC the classification of the pores as micro-, meso- and macropores is subject to certain requirements for the pore-width [33].

Table 5 represents the conditional dividing of pores in view of their size in the prepared samples.

Table 5. Provisionally pore size distribution in the pyrolyzed rice husks.

Characteristics	B1	B2	B3	B4
Value of the inflection point, μm	1.88	1.76	2.13	1.93
Volume of “micro” pores, cm ³ g ⁻¹	0.3676	0.3731	0.3424	0.3530
Percent of “micro” pores, %	40.9	45.9	32.5	45.4
Volume of “macro” pores, cm ³ g ⁻¹	0.5304	0.4406	0.7110	0.4252
Percent of “macro” pores, %	59.1	54.1	67.5	54.6

The porosity characteristics of sample B3 can be explained by the fact that the pyrolysis in this case has been carried out at temperature, which guarantees the destruction of all the components building up the cell walls of the rice husks. The volatile degradation products are in large amount and should escape from the char without delay. This leads to the obtaining of a material with a maximum quantity of the so-called closed type of pores. The temperatures lower than 480° C, cause as a result only a slow thermal cracking of the lignin-cellulose material, which does not ensure a sufficient development of a porous structure of the obtained composite. The increasing pyrolysis temperature enhances also the effect of dehydroxylation via conversion of silanol groups to siloxane bridges leading to opening of pores. However the pyrolysis at 700° C leads to a

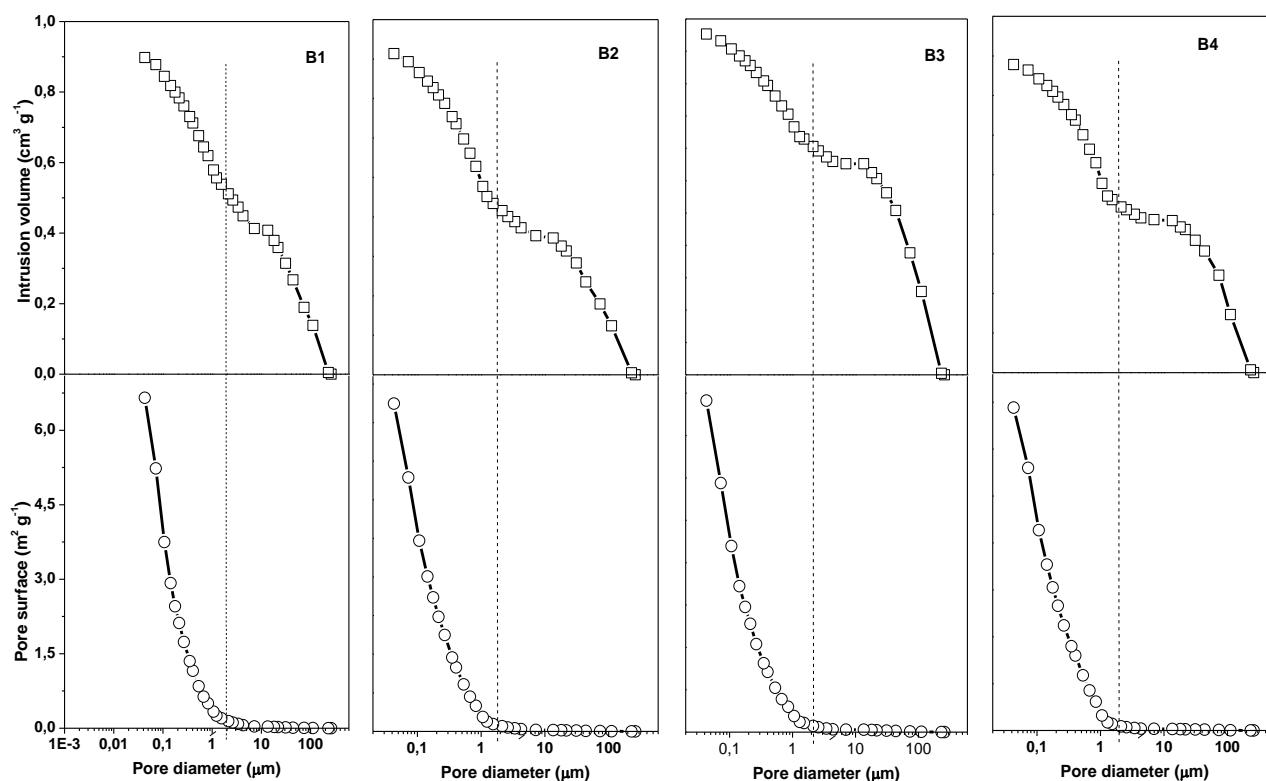


Fig.6. Characteristic integrated distribution curves of the volume and the surface area by the pore diameter for samples *B1-B4*.

complete decomposition of the organic matrix, associated with destroying of the organic-mineral structure. On the other hand thermal treatment at higher temperature causes modifications in the textural and structural characteristics of the carbon skeleton as a result of the sintering effects [34].

4. CONCLUSION

Summarizing, the results evidenced that in the conditions of slow pyrolysis of rice husks the pyrolysis temperature had a strong influence on the char's structure and phase composition.

The increasing pyrolysis temperature leads to produce of composite materials, possess multi porous structure in which main part occupies the pores with size distribution between 50 and 200 μm . While the volume of pores with a diameter less than 2.0 μm , for the investigated temperature range remains almost the same. The pyrolysis

temperature of 480°C could be pointed as optimal for obtaining C/SiO₂ containing materials by slow pyrolysis of rice husks. The charcoal, obtained at this temperature is characterized with high specific surface area and advanced meso- and macroporous structure. The texture characteristics and availability of appropriate surface functionalities of sample *B3* give us the reason to expect from the sample high adsorption activity in regard to adsorption of organic and inorganic pollutants from aqueous medium.

Acknowledgements: The authors gratefully acknowledge the financial support by the National Centre for Advanced Materials UNION (Contract No DCVP-02/2/2009) and the Science Research Branch of University of Chemical Technology and Metallurgy, Sofia (Contract No 10952/2012).

REFERENCES

- 1.B. Padhi, C. Patnaik, *Ceram. Int.*, **21**, 213 (1995).
- 2.A. Jain, R. Rao, S. Sambhi, P. Grover, *Biomass Bioenergy*, **7**, 285 (1995).
- 3.P.McKendry, *Bioresource Technol.*, **83**, 37 (2002).
- 4.O. Ioannidou, A. Zabaniotou, *Renew. Sustain. Energ. Rev.*, **11**, 1996 (2007).
- 5.S. Chandrasekhar, K. Satyanarayana, P. Pramada, P. Raghavan, T. Gupta, *J. Mater. Sci.*, **38**, 3159 (2003).

- 6.T. Watary, A.Nakata, Y. Kiba, T. Torikai, M. Yada, *J. Eur. Ceram. Soc.*, **26**, 797 (2006).
- 7.J. Dias, M. Alvim-Ferraz, M. Almeida, J. Rivera-Utrilla, M. Sanchez-Polo, *J. Environ.Manage*, **85**, 833 (2007).
- 8.W. Ngah, M. Hanafiah, *Bioresource Technol.*, **99**, 3935 (2008).
- 9.F.A. Kamenshchikov, E.I. Bogomolnii, Removal of oil products from water surface and soil, 1st edn., Moscow, 2006(in Russian).

10. M. Adebajo, R. Frost, J. Klopogge, O. Carmody, S. Kokot, *J. Porous Mat.*, **10**, 159 (2003).
11. S. Kumagai, K. Sasaki, Y. Shimizu, K. Takeda, *Sep. Pur. Tech.*, **61**, 398 (2008).
12. M. Akhtar, S. Iqbal, A. Kausar, M. Bhanger, M. Shaheen, *Colloid. Surf. B: Biointerfaces*, **75**, 149 (2010).
13. O. Carmody, R. Frost, Y. Xi, S. Kokot, *Surf. Sci.*, **601**, 2066 (2007).
14. T. Chuah, A. Jumariah, I. Azni, S. Katayon, S. Choong, *Desalination*, **175**, 305 (2005).
15. D. Kalderis, S. Bethanis, P. Paraskeva, E. Diamadopoulos, *Bioresource Technol.*, **99**, 6809 (2008).
16. Y. Guo, K. Yu, Z. Wang, H. Xu, *Carbon*, **41**, 1645 (2000).
17. C. Yun, Y. Park, C. Park, *Carbon*, **39**, 559 (2001).
18. S. Hu, J. Xiang, L. Sun, M. Xu, J. Qiu, P. Fu, *Fuel Process. Technol.*, **89**, 1096 (2008).
19. T.-H. Liou, *Carbon*, **42**, 785 (2004).
20. S. Kumagai, Y. Noguchi, Y. Kurimoto, K. Takeda, *Waste Manage.*, **27**, 554 (2007).
21. A. Bharadwaj, Y. Wang, S. Sridhar, V. Arunachalam, *Curr. Sci.*, **87**, 981 (2004).
22. K. Krishnani, X. Meng, C. Christodoulatos, V. Boddu, *J. Hazard. Mater.*, **153**, 1222 (2008).
23. D. Angelova, I. Uzunov, S. Uzunova, A. Gigova, L. Minchev, *Chem. Eng. J.*, **172**, 306 (2011).
24. H. Yang, R. Yan, H. Chen, D. Lee, C. Zheng, *Fuel*, **86**, 1781 (2007).
25. F. Lanning, B. Ponnaiya, C. Crumpton, *Plant Physiol.*, **33**, 339 (1958).
26. F. Lanning, *Agric. Food Chem.*, **11**, 435 (1963).
27. M. Patel, A. Karera, P. Prasanna, *J. Mater. Sci.*, **22**, 2457 (1987).
28. L. Kennedy, J. Vijaya, G. Sekaran, *Mater. Chem. Phys.*, **91**, 471 (2005).
29. S. Hanna, L. Farag, N. Mansour, *Thermochim. Acta*, **81**, 77 (1984).
30. A. Demirbaş, *Energy Conv. Manage.*, **41**, 633 (2000).
31. B.-D. Park, S. Wi, K. Lee, A. Singh, T.-H. Yoon, Y. Kim, *Biomass Bioenerg.*, **25**, 319 (2003).
32. L. Zemnukhova, A. Hohryakov, *Patent RU 2 304 559 C2* (2007).
33. J. Rouquerol, D. Avnir, C. Fairbridge, D. Everett, J. Haynes, N. Pernicone, J. Ramsay, K. Sing, K. Unger, *Pure Appl. Chem.*, **66**, 1739 (1994).
34. A. Rao, A. Fung, M. Dresselhaus, M. Endo, *J. Mater. Res.*, **7**, 1788 (1992).

ИЗМЕНЕНИЯ В СТРУКТУРАТА НА ТВЪРДИТЕ ОСТАТЪЦИ ОТ БАВНАТА ПИРОЛИЗА НА ОРИЗОВИ ЛЮСПИ

С. Узунова, Д. Ангелова, Б. Анчев, И. Узунов, А. Гигова

¹ Химикотехнологичен и металургичен университет, 1756 София

² Институте по обща и неорганична химия, Българска академия на науките, 1113 София

³ Институт по електрохимия и енергийни системи, 1113 София

Получена на 17 септември 2012 г.; коригирана на 12 февруари 2013 г.

(Резюме)

Изследването дава основата за разработването на нов екологично съобразен материал с контролирани характеристики, подходящи за производството на материали от въглерод и силициев диоксид с добавена стойност. Предмет на изследването е да се определи влиянието на температурата на пиролиза върху специфичната повърхност и порьозността на въглена, получен при бавна пиролиза в температурния интервал 250-700°C на оризови люспи, излужени с киселина. Структурата на въглена е определена с живачна порьозиметрия и BET-метода. Фазовият състав на твърдия остатък след пиролизата и отношението въглерод/силициев диоксид в него са определени чрез термичен анализ (TG/DTA/MS) и XRD. Морфологията на материала е изучен чрез сканираща електронна микроскопия. Установено е, че бавната пиролиза в изследвания температурен интервал дава твърд остатък с предимно макро-порьозна структура и разпределение на размера на порите между 50 и 200 µm. Образците, получени при 480°C се характеризират с най-голяма общ обем и най-голям среден диаметър на порите. С нарастване на температурата на пиролиза отношението C:SiO₂ в твърдия остатък намалява от 1.38 до 0.85, а специфичната повърхност нараства от 7.0 до 440.0 m² g⁻¹.

Liquid-phase synthesis of *N,N'*-diacetyl- β -chitobiosyl allosamizoline

H.-L. Huang¹, F. Liu², J. Chen², G.-L. Huang^{*2}

¹ Key Laboratory for Green Chemical Process of Ministry of Education, School of Chemical Engineering & Pharmacy, Wuhan Institute of Technology, Wuhan, 430073, P.R. China

² College of Chemistry, Chongqing Normal University, Chongqing, 401331, P.R. China

Received: Desember 23, 2013; Revised: February 11, 2014

Liquid-phase synthesis of *N,N'*-diacetyl- β -chitobiosyl allosamizoline **2** was studied. The *N*-benzyloxycarbonyl (Cbz) protected trichloroacetimidate donors **3** and **5** were prepared according to the routine method. The target allosamidin analogue **2** was high-efficiently synthesized by iterative glycosylation reactions, catalytic hydrogenation, acetylation, and deacetylation, respectively.

Keywords: *N,N'*-diacetyl- β -chitobiosyl allosamizoline, liquid-phase synthesis, trichloroacetimidate donors

INTRODUCTION

This pseudo-trisaccharide allosamidin **1** (Fig. 1) is a representative chitinase inhibitor, and it possesses high activities against insects and fungi [1-2]. The synthetic methodologies of compound **1** and its analogues were reported [3-5]. But the approach is more complicated, and the cost of mass production is high in every synthetic method, which restrict allosamidin **1** and its analogues to be widely utilized in agriculture. *N,N'*-Diacetyl- β -chitobiosyl allosamizoline **2** has been synthesized by solid-phase method [1,6], but the approach is still a bit longer, and this yield of introducing the solid-phase support is too low. Therefore, the allosamidin analogue **2** has been tried to synthesize by liquid-phase method in this paper, which is based on its reported solid-phase method, but the solid-phase support does not be introduced.

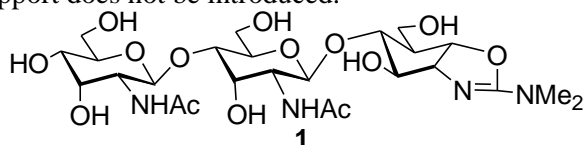


Fig. 1 Structure of allosamidin **1**.

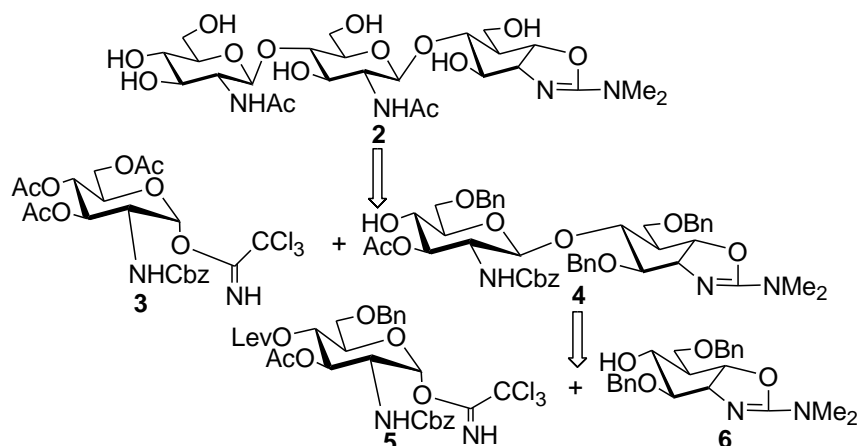
RESULTS AND DISCUSSION

The most important concept behind carbohydrate synthesis is glycosylation reaction to involve glycosyl donor and glycosyl acceptor. The retrosynthetic analysis of *N,N'*-diacetyl- β -chitobiosyl allosamizoline **2** was shown in Scheme 1. It indicated that the synthetic strategy for target compound **2** was in reverse order for the

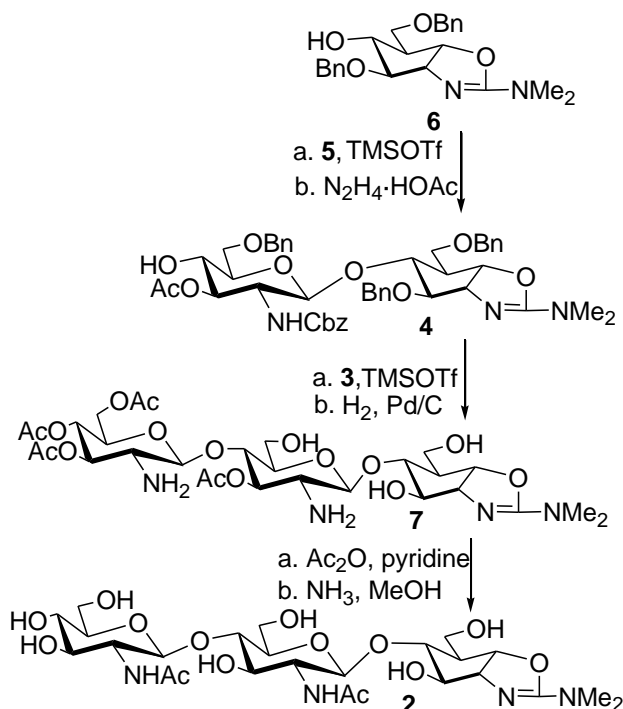
installation of subunits **3**, **5**, and **6**. It also has shown the effectiveness of glycosyl trichloroacetimidates as donors in the glycosidic bond formation. Levulinoyl ester is used as an orthogonal protecting group, which can be efficiently cleaved to liberate the free hydroxyl site for further glycosylation. The amino group is protected with benzyloxycarbonyl (Cbz). Due to the neighboring group participation of Cbz during glycosylation reaction, the β -linkage is easy to form. Cbz and Bn can be removed by catalytic hydrogenation.

The 3,6-di-*O*-benzylallosamizoline **6** (Scheme 2) was prepared according to the approach that described by Griffith and Danishefsky [7]. Glycosylation reactions were gone along using 3.0 equiv. of donor and 0.1 equiv. of trimethylsilyl trifluoromethanesulfonate (TMSOTf) as promoter to activate trichloroacetimidate donor. At low temperature, TMSOTf-promoted glycosylation of the *N*-Cbz protected trichloroacetimidate donor **5** [8-9] with intermediate **6** yielded the *O*-perprotected β -pseudodisaccharide in 83% yield. Cleavage of the levulinoyl ester was carried out with hydrazine acetate dissolved in MeOH to form the acceptor **4**. After acceptor **4** was glycosylated with the *N*-Cbz protected trichloroacetimidate donor **3** [8-9], the obtained pseudo-trisaccharide was catalytically hydrogenated for cleavage of Cbz and Bn to yield building block **7** in 96% yield. Then, the intermediate **7** was acetylated with Ac₂O/pyridine and deacetylated with NH₃/MeOH, respectively. After purification by column chromatography, the target compound **2** was obtained in 97% yield.

* To whom all correspondence should be sent:
E-mail: huangdoctor226@163.com



Scheme 1 Retrosynthetic analysis of *N,N'*-diacetyl- β -chitobiosyl allosamizoline **2**.



Scheme 2 The liquid-phase synthesis of *N,N'*-diacetyl- β -chitobiosyl allosamizoline **2**.

CONCLUSION

The liquid-phase synthesis of *N,N'*-diacetyl- β -chitobiosyl allosamizoline **2** was investigated. Compound **2** was obtained by iterative glycosylation reactions, catalytic hydrogenation, acetylation, and deacetylation, respectively.

Acknowledgments: The work was supported by Natural Science Foundation Project of CQ CSTC (No. cstc2012jjA10101), Science Research Foundation of Wuhan Institute of Technology (No.10122011), Open Foundation from Tertiary College of Chongqing Engineering Research Center of Bioactive Substance and Ministry of Education Engineering Research Center of Active Substance & Biotechnology (No. GCZX2012-2), Chongqing University Students' Training Project of

Innovation & Undertaking (Nos. 201210637015 and 201210637010), and Chongqing University Innovation Team Project (No. KJTD201309), China.

***N,N'*-Diacetyl- β -chitobiosyl allosamizoline **2**:**
¹H NMR (300 MHz, D₂O-CD₃COOD) δ 5.04 (dd, 1 H, H-1), 4.58 (d, 1 H, H-1''), 4.54 (d, 1 H, H-1'), 4.14 (dd, 1 H, H-2), 4.06 (dd, 1 H, H-3), 3.94 (dd, 1 H, H-6''b), 3.86 (dd, 1 H, H-6'b), 3.82 (dd, 1 H, H-6b), 3.75 (dd, 1 H, H-6'a), 3.74 (dd, 1 H, H-2''), 3.73 (dd, 1 H, H-2'), 3.72 (dd, 1 H, H-4), 3.70 (dd, 1 H, H-3'), 3.67 (dd, 1 H, H-6'a), 3.66 (dd, 1 H, H-6a), 3.61 (dd, 1 H, H-4'), 3.58 (dd, 1 H, H-3''), 3.56 (m, 1 H, H-5'), 3.51 (m, 1 H, H-5''), 3.47 (dd, 1 H, H-4''), 2.96 (d, 6 H, N(CH₃)₂), 2.38-2.34 (m, 1 H, H-5), 2.07-2.04 (d, 6 H, 2×NHCOCH₃).

REFERENCES

1. G.L. Huang, S.Q. Shu, *Synlett*, **23**(12), 1829-1831 (2012).
2. G.L. Huang, Y.P. Dai, *Synlett*, 21(10), 1554-1556 (2010).
3. G.L. Huang, *Curr. Org. Chem.*, **16**(1), 115-120 (2012).
4. A. Berecibar, C. Grandjean, A. Siriwardena, *Chem. Rev.*, **99**(3), 779-844 (1999).
5. G.L. Huang, *Mini-Rev. Med. Chem.*, **12**(7), 665-670 (2012).
6. G.L. Huang, *Lett. Org. Chem.*, **8**(9), 625-627 (2011).
7. D.A. Griffith, S.J. Danishefsky, *J. Am. Chem. Soc.*, **113**, 5863-5864 (1991).
8. G.L. Huang, *Lett. Org. Chem.*, **8**(1), 70-72 (2011).
9. G.L. Huang, F. Cheng, *Lett. Org. Chem.*, **9**(8), 577-579 (2012).

ТЕЧНОФАЗНА СИНТЕЗА НА N,N'-ДИАЦЕТИЛ- β - ХИТОБИОЗИЛ АЛОЗАМИЗОЛИН

Х.-Л. Хуанг¹, Ф. Лиу², Дж. Чен², Г.-Л. Хуанг*²

¹Лаборатория за зелени химични процеси на Министерство на образованието, Училище по инженерна химия и фармация, Ухански технологичен институт, Ухан, 430073, НР Китай

²Колеж по химия, Университет на Чунцин, Чунцин, 401331, НР Китай

Получена на 23 декември 2013 г.; коригирана на 11 февруари 2014 г.

(Резюме)

Иследвана беше течнофазната синтеза на N,N'-диацетил- β - хитобиозил алозамизолин **2**. Трихлоацетамидни донори **3** и **5**, защитени с N-бензоилкарбонил(Cbz), бяха приготвени по рутитен метод. Целевият алозамидинов аналог **2** беше синтезиран с висока ефективност чрез итеративни реакции на гликолизация, каталитично хидрогениране, ацетилиране и съответно деацетилизране.

Determination of heavy metal concentrations of most consumed fish species from Bulgarian Black Sea coast

M. Stancheva, L. Makedonski*, K Peycheva

Department of Chemistry, Medical University, 55 Marin Drinov, Str., 9002 Varna, Bulgaria

Received: October 29, 2012; Accepted: May 26, 2013

In this study some heavy metals (Cd, Ni, Cr, As, Hg, Cu, Fe, Mn, Pb and Zn) concentration in edible parts of five most consumed Bulgarian fish species - bluefish (*Pomatomus saltatrix*), gray mullet (*Mugil cephalus*), Mediterranean horse mackerel (*Trachurus mediterraneus ponticus*), shad (*Alosa pontica*) and sprat (*Sprattus sprattus sulinus*) collected from two stations across Bulgarian Black Sea coast were determined. The samples were digested with nitric acid followed by appropriate spectroscopic determination (Atomic Emission Spectroscopy with Inductively Coupled Plasma (AES-ICP), Flame Atomic Absorption Spectroscopy (FAAS) or Electrothermal Atomic Absorption Spectroscopy (ETAAS). The level of As in the edible part of gray mullet (*Mugil cephalus*) has shown a value higher than limits set from various health organizations (1.1 ± 0.1 mg/kg). On the contrary this fish species accumulates the other investigated heavy metals such as Hg, Zn, Fe and Pb to lower extend. The concentration of Zn and Fe showed the highest value for all fish species. With some exceptions the concentration of studied heavy metal elements was within the acceptable levels for food source for human consumption.

Keywords: heavy metals; fish; Black Sea; Bulgaria

INTRODUCTION

The heavy metal pollution of the marine environment has long been recognized as a serious environmental concern [1, 2].

Heavy metals can be accumulated by marine organisms through a variety of pathways, including respiration, adsorption and ingestion [3, 4]. Heavy metal contamination has been identified as a concern in coastal environment, due to discharges from industrial waste, agricultural and urban sewage [5, 6]. The levels of heavy metals are known to increase drastically in marine environment through mainly anthropogenic activities [7]. Heavy metals can be classified as potentially toxic (arsenic, cadmium, lead, mercury, nickel, etc.), probably essential (vanadium, cobalt) and essential (copper, zinc, iron, manganese, selenium) [8]. Fishes are good indicators for the long term monitoring of metal accumulation in the marine environment. Therefore, numerous studies have been carried out on metal accumulation in different fish species [9, 10].

There are limited data about heavy metals pollution of the Bulgarian Black Sea coast for the last twenty years [11]. Therefore the aim of this study was to determine the levels of cadmium, nickel, chromium, mercury, iron, manganese, copper, zinc, arsenic and lead in edible parts of five

most consumed Bulgarian fish species collected from the coast of Black Sea.

The Black Sea is the world's largest natural anoxic water basin below 180 m in depth. It is a closed sea with a very high degree of isolation from the world's oceans, but it receives freshwater inputs from some of the largest rivers in Europe; the Danube, the Dniester, and the Dnieper [12]. For this reason, Black Sea is considered one of the most polluted seas, and the increasing concentration of nutrients in recent years have led to a higher degree of eutrophication. The fishery yield has declined dramatically, and the tourism industry also suffers from serious pollution of the Black Sea.

EXPERIMENTAL

Sampling and sample treatment

Samples of fish were randomly acquired in local fishermen from cities across the coastal waters of Bulgarian Black Sea. All the fish species were sampled from February to November 2010. These sampling sites of two regions of Bulgarian Black Sea coast – Varna and Bourgas (Fig. 1).

The five species (34 samples) included in this study are shown in Table 1. Total length and weight of the sample brought to laboratory on ice after collection were measured to the nearest millimeter and gram before dissection. For small species (i.e. sprat and Mediterranean horse mackerel), the entire edible part of each individual was included for preparation of composite sample. However, for

* To whom all correspondence should be sent:
E-mail: lubomir60@yahoo.com

Table 1. Biometrics data (mean \pm SD) of fish from the coastal waters of the Bulgarian Black Sea

Sample	Sampling Location	Sampling season, year	N	Weight (g) \pm SD	Length (cm) \pm SD
Bluefish (<i>Pomatomus saltatrix</i>)	Bourgas	Autumn 2010	6	71.1 \pm 6.8	19.3 \pm 1.0
Gray mullet (<i>Mugil cephalus</i>)	Bourgas	Autumn 2010	6	335.0 \pm 1.2	32.1 \pm 0.8
Mediterranean horse mackerel (<i>Trachurus mediterraneus ponticus</i>)	Bourgas	Autumn 2010	6	10.8 \pm 5.3	9.7 \pm 1.4
Shad (<i>Alosa pontica</i>)	Varna	Spring 2010	6	195 \pm 3	29.5 \pm 1.3
Sprat (<i>Sprattus sprattus</i>)	Bourgas	Spring 2010	10	4.7 \pm 2.1	9.2 \pm 0.9



Fig. 1. The map of sampling locations in the Bulgarian Black Sea coast.

bigger species (i.e. gray mullet, bluefish and shad) only fillets of edible part of each individual were collected and included in the respective composite samples. Approximately 1 g sample of muscle from each fish were dissected, washed with distilled water, weighted, packed in polyethylene bags and stored at -18°C until chemical analysis.

Reagents and standard solutions

All solutions were prepared with analytical reagent grade chemicals and ultra-pure water (18 M Ω cm) generated by purified distilled water with the Milli-QTM PLUS system. HNO₃ was of superb quality was purchased from Fluka. All the plastic and glassware were cleaned by soaking in 2 M HNO₃ for 48 h, and rinsed five times with distilled water, and then five times with deionised water prior to use. The stock standard solutions of Cd, Cr, Cu, Fe, Mn and Pb 1000 $\mu\text{g mL}^{-1}$ were Titrisol, Merck in 2% v/v HNO₃ and were used for preparation calibration standards.

A DORM-2 (NRCC, Ottawa) certified dogfish tissues was used as the calibration verification

standard. Recoveries between 90.5 and 108% were accepted to validate the calibration.

Sample digestion

Fish samples (whole fish body or fish fillets) are thoroughly washed with MQ water. The fish specimens were dissected and samples of fish fillets quickly removed and washed again with MQ water. Each fish filletes (approximately 1 g) were analyzed after homogenization in small mixer. To assess the total metal contents, microwave assisted acid digestion procedure was carried out. Microwave digestion system “Multiwave”, “Anton Paar” delivering a maximum power and temperature of 800 W and 300 $^{\circ}\text{C}$, respectively, and internal temperature control, was used to assist the acid digestion process. Reactors were subjected to microwave energy at 800 W in five stages.

Instrumental

The samples were digested with nitric acid followed up by appropriate spectroscopy determination (Atomic Emission Spectroscopy with

Inductively Coupled Plasma (AES-ICP), Flame Atomic Absorption Spectroscopy (FAAS) or Electrothermal Atomic Absorption Spectroscopy (ETAAS)).

Determination of Cu, Fe and Zn: Flame atomic absorption spectrometric measurements were carried out on a Perkin Elmer (Norwalk, CT, USA) Zeeman 1100 B spectrometer with an air/acetylene flame. The instrumental parameters were optimized in order to obtain maximum signal-to-noise ratio.

Determination of As, Cd, Ni and Pb: Electrothermal atomic absorption spectrometric measurements were carried out on a Perkin Elmer (Norwalk, CT, USA) Zeeman 3030 spectrometer with an HGA-600 graphite furnace. Pyrolytic graphite-coated graphite tubes with integrated platforms were used as atomizers. The spectral bandpass, the wavelengths and instrumental parameters used were as recommended by the manufacture. Only peak areas were used for qualification. Pd as (NH₄)₂PdCl₄ was used as modifier for ETAAS measurements of As and Cd.

Determination of Hg was performed by Milestone DMA-80 direct Mercury Analyzer. The sample size is between 0.020 and 0.0060 g, with drying temperature at 300°C for 60 sec, decomposition time -180 sec and waiting time 60 sec.

Statistical analysis

The whole data were subjected to a statistical analysis. Student's-test was employed to estimate the significance of values.

RESULTS AND DISCUSSION

Levels of heavy metal in the muscle of fish species from coastal waters of Bulgarian Black Sea are shown in Table 2.

Table 2. The mean heavy metal concentration (mg/kg f.w.) in the tissues of the examined species from Bulgarian Black Sea coast

Species	Cd		Ni		Cr		As		Hg		Zn		Cu		Fe		Mn		Pb	
	mean	SD	mean	SD	mean	SD	mean	SD	mean	SD	mean	SD	mean	SD	mean	SD	mean	SD	mean	SD
Bluefish fillet	0.008	0.001	0.009	0.001	0.06	0.01	0.77	0.06	0.09	0.01	10	1	0.8	0.1	5.0	0.4	0.08	0.01	0.03	0.01
Gray mullet fillet	0.012	0.002	0.009	0.001	0.07	0.01	1.1	0.1	0.05	0.01	5.2	0.3	0.34	0.02	2.2	0.2	0.17	0.01	0.05	0.01
Medi-terranean horse mackerel whole fish	0.008	0.001	0.008	0.001	0.03	0.01	0.73	0.05	0.16	0.02	8.5	0.6	0.56	0.04	4.2	0.3	0.06	0.01	0.06	0.01
Shad fillet	0.007	0.001	0.07	0.01	0.05	0.01	0.38	0.02	0.08	0.01	9	1	0.45	0.03	9	1	0.11	0.01	0.05	0.01
Sprat whole fish	0.005	0.001	0.028	0.003	0.04	0.01	0.73	0.04	0.12	0.02	11.0	0.7	1.40	0.08	9	1	0.11	0.01	0.08	0.02

At p < 0.05

The summarized results of this study are expressed as means (mg/kg) fresh weight.

Cadmium is a non-essential, highly toxic metal. Chronic effects on human health may occur as a result of its accumulation in liver, bones, blood, kidney and muscle [13]. About 50% of the Cd that reaches the sea comes from human activities (industrial waste, fertilizers containing phosphate or animal origin, etc.). The European Community [14] established the maximum levels permitted of cadmium in a fish as 0.05 mg/kg f.w. Moreover, the Joint Food and Agriculture Organization and World Health Organization (FAO/WHO) [15] has recommended the provisional tolerable weekly intake (PTWI) as 0.007 mg/kg body weight for cadmium. The maximum Cd level permitted for fish samples is 0.10 mg/kg according to Turkish Food Codex [16]. The Bulgarian Food Regulation recommends a 0.05 mg/kg f.w. for sea fish [17]. Cadmium levels in analyzed fish species were below 0.010 mg/kg fresh weight for muscle except gray mullet – 0.012 mg/kg f.w. Cadmium concentration in literature has been reported as follow: 0.02-0.24 mg kg⁻¹ for gray mullet [18]; from 0.10 µg/g in *Psetta maxima*; up to 0.35 µg/g in *Mugil cephalus*; 0.23 µg/g for *Pomatomus Saltator*; 0.13 µg/g for *Sarda Sarda*; 0.32 µg/g for *Trachurus trachurus*; 0.30 µg/g for *Sprattus sprattus* from the Black Sea, Turkey [19]; 0.02-0.37 mg kg⁻¹ for edible part of fishes caught from Marmara, Aegean and Mediterranean seas in Turkey [20] and 0.002-0.02 mg Cd kg⁻¹ fresh weight for species from Adriatic Sea [21]. In the present study, cadmium levels (Fig. 2) were in good agreement with

reported literature data and with the data from the international organizations.

The highest total lead content was found in sprat (*Sprattus sprattus*), 0.08 ± 0.02 mg Pb kg⁻¹ fresh weight, while the lead content for the other fish samples were below 0.06 mg/kg (Fig. 3).

Lead is one of the most ubiquitous and useful metal known to humans and it is detectable in practically all phases of the inert environment and in all biological systems [22]. The Joint FAO/WHO

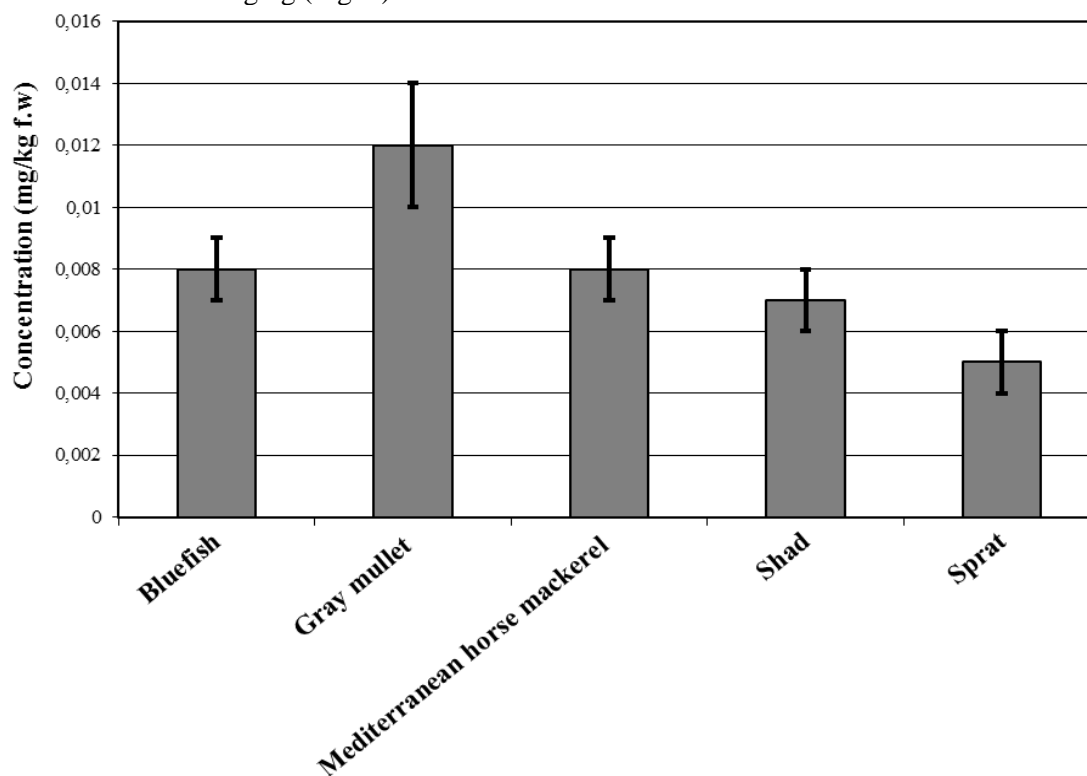


Fig. 2. Distribution of Cd in fish species from Bulgarian Black Sea coast.

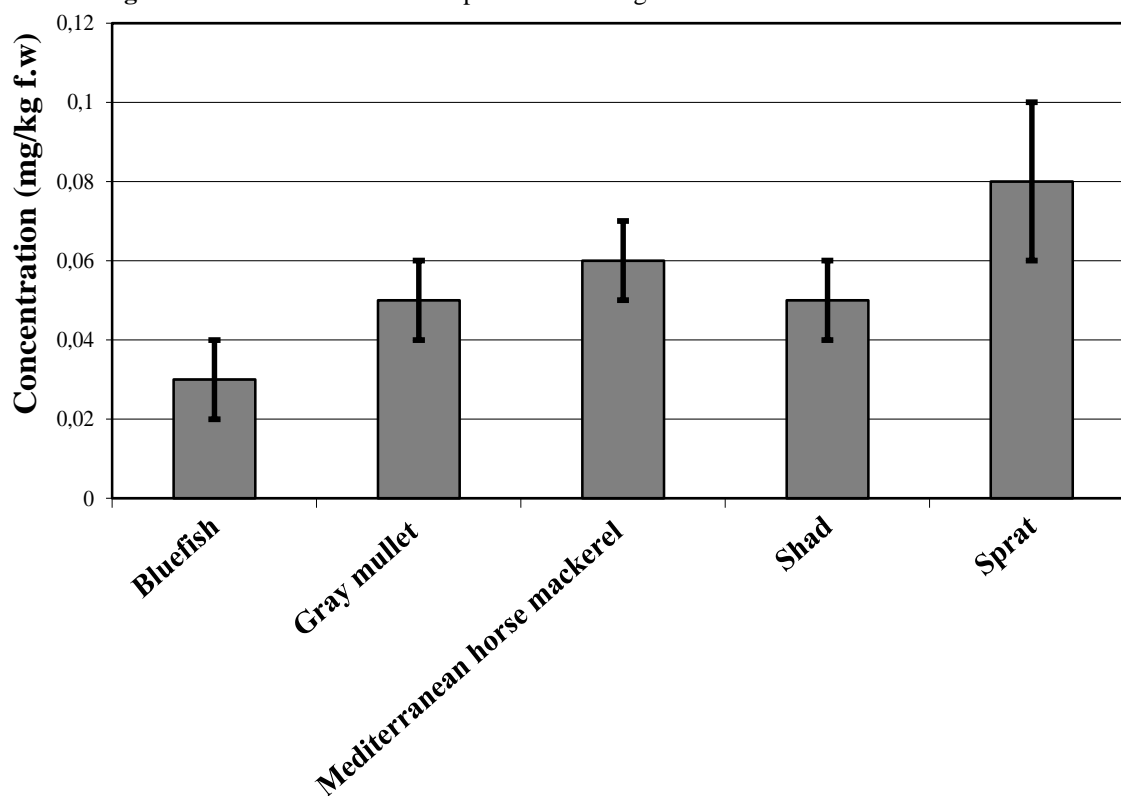


Fig. 3. Distribution of Pb in fish species from Bulgarian Black Sea coast.

[23] Expert Committee on Food Additives establishes a provisional tolerable weekly intake (PTWI) for lead as 0.025 mg/kg body weight. Whereas the maximum level of lead in seafood establishes by the European Community [14] is 0.2 mg/kg f.w in fish. According to Turkish Food Codex, the maximum lead level permitted for sea fishes is 0.3 mg/kg [16] while Bulgarian Food Regulation sets this level as 0.4 mg/kg fresh weight (for sea fish) [17]. Lead levels in the literature have been reported in the range of 0.22-0.85 mg kg⁻¹ for muscle of fish from the middle Black Sea [24], 0.28 µg/g in *Psetta maxima* and 0.87 µg/g in *Pomatomus Saltator* from the Black Sea, Turkey [19], 0.33-0.93 µg kg⁻¹ for muscle of fish from Black and Aegean seas [25] and in between 0.14 and 1.28 µg kg⁻¹ for fish muscle from Aegean and Mediterranean seas [26]. The values obtained from the analyzed samples showed good agreement with values reported in the literature and below the level set by various health organizations.

Arsenic, a naturally occurring element, is a worldwide contaminant that is found in rock, soil, water, air and food. Arsenic is highly toxic element. Humans can be exposed to arsenic through the intake of food and drinking water, but for most people, the major exposure source is the diet, mainly fish and seafood [22]. Arsenic concentration

in this study ranged between 0.38 mg kg⁻¹ in shad (*Alosa pontica*) from north up to 1.1 mg kg⁻¹ in gray mullet (*Mugil cephalus*) from south.

There are limited data about the arsenic content in fish species in the literature. The Joint FAO/WHO [27] Expert Committee on Food Additives (JECFA) establishes a provisional tolerable weekly intake (PTWI) for inorganic arsenic as 0.015 mg/kg body weigh/week and 0.05 mg/kg body weigh/week for organic-arsenic intakes. The maximum arsenic level permitted for fishes is 1.0 mg/kg according to Australian standards [28]. The concentration of arsenic reported in fish species from Adriatic Sea ranged of 0.56 to 10.03 mg As kg⁻¹ fresh weight [21] and in Lake Kasumigaura, Japan was around 13.3 µg g⁻¹ dry wt for fish food [29]. Tuzen [19] had measured an arsenic concentration in different fish species from Black Sea as follows: 0.15 ± 0.01 µg/g for *Psetta maxima*; 0.27 ± 0.02 µg/g for *Pomatomus Saltator*, 0.23 ± 0.01 µg/g for *Mugil cephalus*, 0.14 ± 0.01 µg/g for *Sarda Sarda*, 0.18 ± 0.02 µg/g for *Trachurus trachurus* and 0.17 ± 0.01 µg/g for *Sprattus sprattus*. The concentration of As in this study (Fig. 4) was generally low in all the species compared with both the data in the literature and world food standards except the value for gray mullet (*Mugil cephalus*).

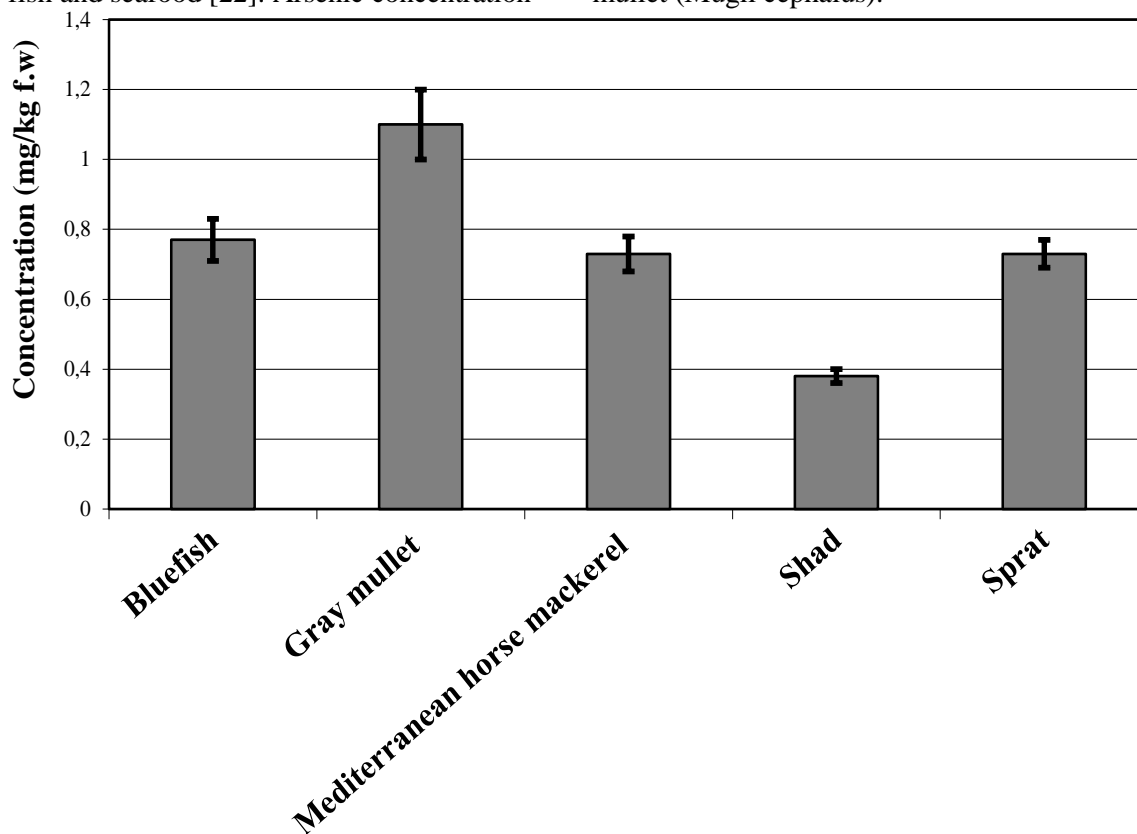


Fig. 4. Distribution of As in fish species from Bulgarian Black Sea coast.

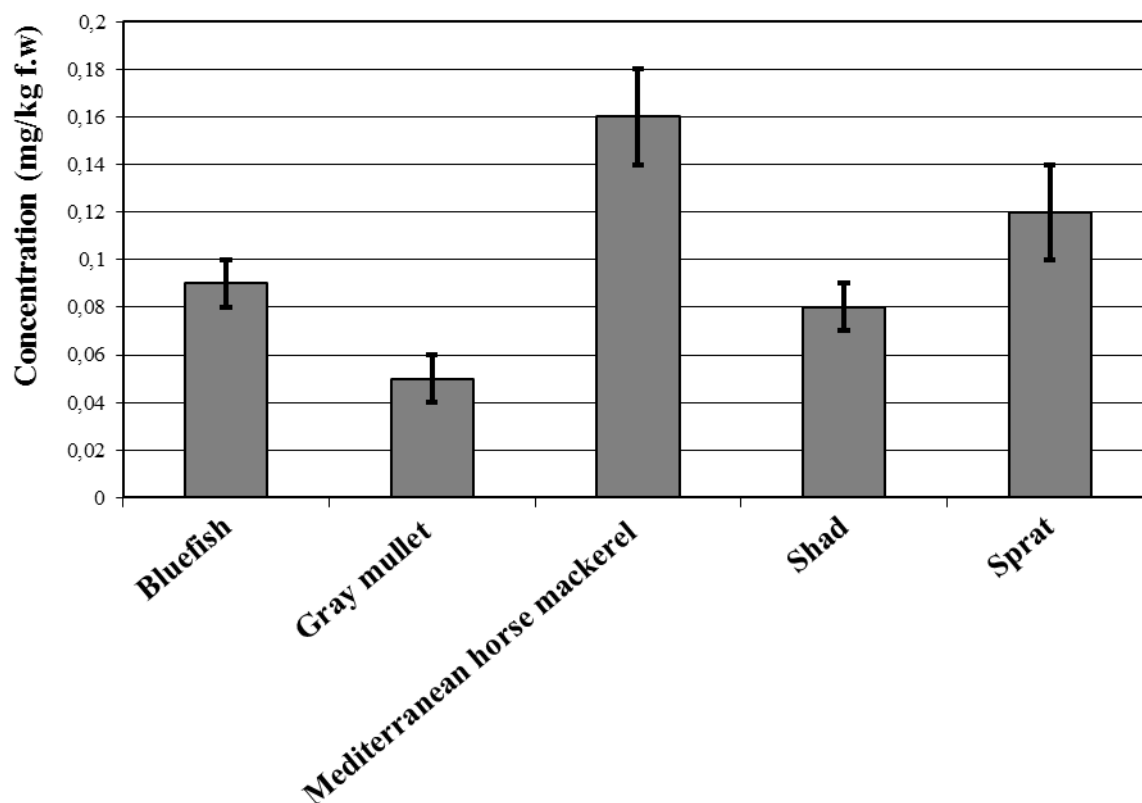


Fig. 5. Distribution of Hg in fish species from Bulgarian Black Sea coast.

The lowest and highest mercury levels in fish species were found as 0.05 mg/kg in *Mugil cephalus* and 0.16 mg/kg in *Trachurus mediterraneus ponticus* (Fig. 5). The maximum Hg level permitted for fishes is 0.5 mg/kg according to Turkish Food Codex [16] and Bulgarian Food Codex [17]. The PTWI is 5 mg total mercury kg⁻¹ body weight (bw) and 3.3 mg methylmercury kg⁻¹ bw [30] was reduced to 1.6 mg methylmercury kg⁻¹ bw [31] and could be exceeded depending on the species and quantity consumed. Mercury levels in analyzed fish samples were found to be lower than legal limits. In the literature mercury levels in fish samples have been reported in the range of 0.01-0.50 µg/g in marine fishes in Malaysia [32], 0.02-0.74 mg/kg wet weight in canned fishes [33], 25-84 µg/kg for fishes from Black Sea [19]. In humans, mercury is toxic to the developing fetus and considered a possible carcinogen [34]. Mercury is a known human toxicant and the primary sources of mercury contamination in man are through eating fish [35].

Copper is essential for good health but very high intake can cause adverse health problems such as liver and kidney damage [36]. The copper concentration found in this study was in the range of 0.34 up to 1.4 mg kg⁻¹. Copper in the literature range from 0.23 to 9.49 mg kg⁻¹ for muscle of fish

from Marmara Sea [37], 0.32-6.48 mg kg⁻¹ for muscle of fish from Marmara, Aegean and Mediterranean seas in Turkey [20] and 0.34-7.05 mg kg⁻¹ wet weight for fish muscle from central Aegean and Mediterranean Sea [26]. The minimum and maximum copper levels in fish species from Black Sea, Turkey were found as 0.65 µg/g in *Trachurus trachurus* and 2.78 µg/g in *Pomatomus Saltator* [19]. The maximum copper level permitted for sea fishes is 10 mg/kg according to Bulgarian Food Authority [17] and 20 mg/kg according to Turkish Food Codex [16]. The Joint FAO/WHO [23] Expert Committee on Food Additives established the provisional tolerable weekly intake (PTWI) for copper of 3.5 mg/kg body weight/week. Our values were lower than the values from the literature.

Zinc is known to be involved in most metabolic pathways. Deficiency of this essential element most often occurs when intake of zinc is inadequate or if there is poor absorption by the body. The minimum and maximum zinc levels in fish were found as 5.2 mg Zn kg⁻¹ in *Mugil cephalus* and 11 mg Zn kg⁻¹ in *Sprattus sprattus* from Bourgas station.

The concentration for zinc reported in the literature range of 9.5-22.9 mg kg⁻¹ for muscle of fish from the Black Sea coast [18], 16.1-31.4 mg

kg⁻¹ for muscles of fish from Mediterranean sea [38], 3.51-53.5 mg kg⁻¹ for species from Aegean and Mediterranean Sea [26], 9.50-22.94 µg/g dry weight for fish muscle from middle Black sea [24], and 38.8 µg/g - 93.4 µg/g for different types of fishes from Black Sea, Turkey [19]. The maximum zinc level permitted for fishes is 50 mg/kg according to Bulgarian Food Codex [17] and Turkish Food Codex [16]. The Joint FAO/WHO [23] Expert Committee on Food Additives established the PTWI for zinc of 7 mg/kg body weight/week. Maximum Zn level in edible parts of fish in this research was found to be below than both the Turkish permissible standards and levels reported in the literature.

Manganese is an essential element for all known living organisms. Manganese deficiency diseases are very striking ranging from severe birth defects, asthma, convulsions and etc. The lowest and highest levels in fish species were found in Mediterranean horse mackerel (0.06 mg/kg) and in Mugil cephalus. Manganese contents in the literature have been reported in the range of 1.56-3.76 µg/g dry weight in fish samples of the middle Black Sea (Turkey) [24], 0.05-4.64 µg/g dry weight in fish species from Iskenderun Bay, Northern East Mediterranean Sea, Turkey [39] and 0.69-3.56 mg kg⁻¹ for muscles of fish from the Black Sea coasts [18]. According to both FAO [40] and Bulgarian standards [17] there is no information on the carcinogenicity of manganese. The concentration of manganese in our study was generally in agreement with the literature.

Iron levels ranged from 2.2 mg/kg fresh weight in *Trachurus mediterraneus ponticus* up to 9.0 mg/kg fresh weight for *Alosa pontica* and *Sprattus sprattus*. Iron concentration in the literature were reported between 59.6 and 73.4 mg kg⁻¹ for muscles of fish from Mediterranean sea [38], 30-160 mg kg⁻¹ for muscles of fish from the Black Sea coasts [18] and 9.52-32.40 µg/g dry weight in fish samples of the middle Black Sea (Turkey) [24]. The US National Academy of Science [41] recommends a Recommended Dietary Allowance (RDA) for iron in elderly women and men - 10 mg/day. There is no information about the maximum permissible iron concentration in fish tissues in Bulgarian standards [17]. Iron is an essential mineral that plays an important role in the human physiology. High Fe absorption causes excessed Fe to be stored in the organs, eventually leading to iron overload. Results achieved in this study were in good agreement with other reported data from the literature.

The lower chromium content was 0.03 mg/kg in *Trachurus mediterraneus ponticus* while the highest chromium content was 0.07 mg/kg in *Mugil cephalus*. Chromium is an essential mineral in humans and has been related to carbohydrate, lipid, and protein metabolism. The recommended daily intake is 50-200 µg [41]. The amount of chromium in the diet is of great importance as Cr is involved in insulin function and lipid metabolism [42]. The maximum Cr level permitted for fishes is 0.3 mg/kg according to Bulgarian Food Codex [17] and 0.1 mg/kg according to Brazil Standard [43]. Chromium contents in the literature have been reported in the range of 0.07-6.46 µg/g dry weight in fish species from Iskenderun Bay, Northern East Mediterranean Sea, Turkey [39], 0.04-1.75 µg/g in seafood from Marmara, Aegean and Mediterranean seas in Turkey [20], 1.42 µg/g in fish feed [34]. Our values are under those reported in the literature.

The lowest and highest nickel levels in fish species were 0.008 mg/kg in *Sprattus sprattus* and 0.07 mg/kg in *Alosa pontica*. Nickel contents have been reported in the range of 0.11-12.9 µg/g dry weight in fish species from Iskenderun Bay [39], 0.93-2.77 µg/g dry weight in fish samples from Dhanmondi Lake, 0.42-0.85 µg/g in canned fish [25], 1.14-3.60 µg/g in fishes from Black Sea, Turkey [19] and 0.02-3.97 µg/g in seafood from Marmara, Aegean and Mediterranean seas in Turkey [20]. The World Health Organization [13] recommends 100-300 µg nickel for daily intake. The maximum nickel level permitted for fishes is 0.5 mg/kg according to Bulgarian Food Codex [17]. The results from this study were below the limits sets by various health organizations and the data in the literature.

CONCLUSION

Heavy metals (Cd, Pb, As, Hg, Ni, Cu, Mn, Zn, Fe and Cr) were determined in five most consumed Bulgarian fish species collected from Bulgarian coastal of Black Sea. Among the ten metals under study, iron and zinc showed the highest level of accumulation. None the less this value was in the range stated in the literature. The levels of arsenic in gray mullet were higher than the other fish species but in within the recommended legal limits. In the analyzed fishes, there were no health risks in respect to the concentration of cadmium, copper, lead, mercury and other elements' level.

Acknowledgments: *The authors would like to thank the National Science Fund, Ministry of Education and Science of Bulgaria for their financial support (Project DVU 440 / 2008).*

REFERENCES

1. I. T. Blakas, S. Tugrel & I. Salhoglu, Trace metal levels in fish and crustaceans from Northeastern Mediterranean coastal waters. *Marine Environmental Research*. **6**, 281-289 (1982).
2. J. Tariq, M. Jaffar & M. Moazzam, Concentration correlations between major cations and heavy metals in fish from the Arabian Sea, *Marine Pollution Bulletin*. **22** (11), 562-565 (1991).
3. J. L. Zhou, S. M. Salavador, Y. P. Liu, M. Sequeria, Heavy metals in the tissues of common dolphins (*Delphinus delphis*) stranded on the Portuguese coast. *Science of the Total Environment*. **273**, 61 (2001).
4. M. Boran, H. Karacam, M. S. Celikkale, S. Kose, M. Feyzioglu, S. Kutlu, Levels of heavy metals in blue whiting caught from the eastern Black Sea area of Turkey. *Toxicological & Environmental Chemistry*. **75**, 67-73 (2000).
5. T. Hung, Ch. Huang, Pei-Jie, A. Chuang, Sh. Wu, Heavy metals in fish tissues and different species of fish from the southern coast of Taiwan. *Chemistry and Ecology*. **16**, 283-296 (1999).
6. Z. Valova, P. Jurajda, M. Janač, I. Bernardova, H. Hudcova, Spatiotemporal trends of heavy metal concentrations in Fish of the River Morava (Danube basin). *Journal of Environmental Science and Health, Part A: Toxic/Hazardous Substances and Environmental Engineering*. **45**, 1892-1899 (2010).
7. E. M. Seco-Gesto, A. Moreda-Piñeiro, A. Bermejo-Barrera & P. Bermejo-Barrera, Multi-element determination in raft mussels by fast microwave-assisted acid leaching and inductively coupled plasma-optical emission spectrometry, *Talanta*. **72**, 1178 (2007).
8. R. Munoz-Olivas, C. Camara, Speciation related to human health, In: L. Ebdon, L. Pitts, R. Cornelis, H. Crews, O. F. X. Donad, P. Quevauviller, (Eds.), Trace Element Speciation for Environment, Food and Health. *The Royal Society of Chemistry*, pp.331-353 (2001).
9. M. Türkmen, A. Türkmen, Y. Tepe, Metal contaminations in five fish species from Black, Marmara, Aegean and Mediterranean seas, Turkey. *Journal of the Chilean Chemical Society*. **52**, 4, 1314-1318 (2007).
10. H. Al-Sayed, J. Al-Saad, I. Madany, D. Al-Hooti, Heavy metals in the grouper fish *Epinephelus coioides* from the coast of Bahrain: an assessment of monthly and spatial trends. *International Journal of Environmental Studies*. **50**, 237-246 (1996).
11. F. Görür, R. Keser, N. Akçay, S. Dizman, Radioactivity and heavy metal concentrations of some commercial fish species consumed in the Black Sea Region of Turkey. *Chemosphere*. **87**, 356-361 (2012).
12. T. Stoichev, L. Makedonski, T. Trifonova, M. Stancheva, F. Ribarova, DDT in fish from the Bulgarian region of the Black Sea, *Chemistry and Ecology*. **23** (3), 191-200 (2007).
13. WHO (World Health Organization), Cadmium. Environmental Health Criteria, Volume **134** (Geneva: WHO) (1992).
14. EEC, Regolamento no 466/2001 della Commissione dell'8 marzo 2001 che definisce i tenori massimi di taluni contaminanti presenti nelle derrate alimentari. *Gazzetta Ufficiale delle Comunità Europee*, L 77 (2001).
15. FAO/WHO, Expert Committee on Food Additives, Cadmium (2005a). http://www.inchem.org/documents/jecfa/jecval/jec_297.htm.
16. Anonymous, Regulation of Settings Maximum Level for Certain Contaminants in Foodstuffs, *Official Gazette*, 17 may, 2008, Issue 26879 (2008).
17. Anonymous, Regulation of Setting Maximum Levels of Certain Contaminants in Foodstuff Number 31, *Darjaven Vestnik*, 08 October 2004, Issues 88 (2004).
18. S. Topcuoğlu, Ç. Kırbaçoğlu, and N. Güngör, Heavy metals in organisms and sediment from Turkish Coast of the Black Sea, 1997-1998. *Environment International*. **27**, 7, 521-526 (2002).
19. M. Tuzen, Toxic and essential trace elemental contents in fish species from the Black Sea, Turkey, *Food and Chemical Toxicology*. **47**, 1785-1790 (2009).
20. M. Türkmen, A. Türkmen, Y. Tepe, A. Ateş, and K. Gökkuş, Determination of metal contamination in sea food from Marmara, Aegean and Mediterranean seas: Twelve fish species, *Food Chemistry*. **108**, 2, 794-800 (2008).
21. D. Jureša, M. Blanuša, Mercury, arsenic, lead and cadmium in fish and shellfish from the Adriatic Sea, *Food Additives and Contaminants*. **20**, 3, 241-246 (2003).
22. M. I. Castro-Gonzales, M. Méndez-Armenta, Heavy metals: Implication associated to fish consumption, *Environmental Toxicology and Pharmacology*. **26**, 3, 263-271 (2008).
23. FAO/WHO, "Summary of Evaluations Performed by the Joint FAO/WHO Expert Committee on Food Additives (JECFA 1956-2003)", ILSI Press International Life Sciences Institute 2004 (2004).
24. M. Tuzen, Determination of heavy metals in fish samples of the middle Black Sea (Turkey) by graphite furnace atomic absorption spectrometry. *Food Chemistry*. **80**, 1, 119-123 (2003).
25. O. D. Uluozlu, M. Tuzen, D. Mendil & M. Soylak, Trace metal content in nine species of fish from the Black and Aegean Seas, Turkey, *Food Chemistry*. **104**, 2, 835-840 (2007).
26. M. Türkmen, A. Türkmen, Y. Tepe, Y. Töre and A. Ateş, Determination of metals in fish species from Aegean and Mediterranean Sea, *Food Chemistry*. **113**, 233-237 (2009).
27. FAO/WHO, Expert Committee on Food Additives, Arsenic. http://www.inchem.org/documents/jecfa/jecval/jec_159.htm (2005b).
28. Australia New Zealand Food Authority, Food Standards Code. Standard A12, Issue 37 (1998).

29. M. G. M. Alam, A. Tanaka, G. Allinson, L. J. Laurenson, F. Stagnitti & E. T. Snow, A comparison of trace element concentrations in cultured and wild carp (*Cyprinus Carpio*) of lake Kasamigaura, Japan. *Ecotoxicology and Environmental Safety*. **53**, 348-354 (2002).
30. JECFA, Summary of Evaluations Performed by the Joint FAO/WHO Expert Committee on Food Additives: Mercury. Available: http://www.inchem.org/documents/jecfa/jecval/jec_1285.htm. Accessed: 10 March 2007 (1978).
31. JECFA, Summary of Evaluations Performed by the Joint FAO/WHO Expert Committee on Food Additives: Cadmium. Available: http://www.inchem.org/documents/jecfa/jecval/jec_276.htm. Accessed 10 March 2007 (2003).
32. P. Hajeb, S. Jinap, A. Ismail, A. B. Fatimah, B. Jamilah, M. A. Rahim, Assessment of mercury level in commonly consumed marine fishes in Malaysia. *Food Control*. **20**, 79-84 (2009).
33. A. Ikem, N. O. Egiebor, Assessment of trace elements in canned fishes (mackerel, tuna, salmon, sardines and herrings) marketed in Georgia and Alabama (United States of America). *Journal of Food Composition and Analysis*. **18**, 771-787 (2005).
34. A. Ikem, J. Egilla, Trace element content of fish feed and bluegill sunfish (*Lepomis macrochirus*) from aquaculture and wild source in Missouri. *Food Chemistry*. **110**, 301-309 (2008).
35. F. Emami Khansari, M. Ghazi-Khansari, M. Abdollahi, Heavy metals content of canned tuna fish. *Food Chemistry*. **93**, 293-296 (2005).
36. A. Ikem, N. O. Egiebor, Assessment of trace elements in canned fishes (mackerel, tuna, salmon, sardines and herrings) marketed in Georgia and Alabama (United States of America). *Journal of Food Composition and Analysis*. **18**, 771-787 (2005).
37. Y. Keskin, R. Baskaya, O. Özyaral, Y. Yurdun, N. E. Lüleci and O. Hayran, Cadmium, lead, mercury and copper in fish from Marmara Sea, Turkey, *Bulletin of Environmental Contamination and Toxicology*. **78**, 258-261 (2007).
38. M. Kalay, Ö. Ay, M. Canli, Heavy metal concentration in fish tissues from the northeast Mediterranean Sea, *Bulletin of Environmental Contamination and Toxicology*. **3**, 5, 673-681 (1999).
39. A. Türkmen, M. Türkmen, Y. Tepe, I. Akyurt, Heavy metals in three commercially valuable fish species from Iskenderun Bay, Northern East Mediterranean Sea, Turkey. *Food Chemistry*. **91**, 167-172 (2005).
40. FAO (Food and Agricultural Organization), Compilation of legal limits for hazardous substances in fish and fishery products. FAO Fishery Circular No464, 5-10. Food and Agricultural organization of the United Nations, Rome 1989, WHO Technical report Series (1983).
41. RDA, Recommended dietary allowance (10th ed.). Washington, DC: National Academic Press (1989).
42. M. S. Bratakos, E. S. Lazos, S. M. Bratakos, Chromium content of selected Greek foods. *The Science of the Total Environment*. **290**, 47-58 (2002).
43. C. R. T. Tarley, W. K. T. Coltro, M. Matsushita, N. E. de Souza, Characteristic levels of some heavy metals from Brazilian canned sardines (*Sardinella brasiliensis*). *Journal of Food Composition and Analysis*. **14**, 611-617 (2001).

ОПРЕДЕЛЯНЕ НА КОНЦЕНТРАЦИИТЕ НА ТЕЖКИ МЕТАЛИ В НАЙ-КОНСУМИРАНИТЕ РИБНИ ВИДОВЕ В БЪЛГАРСКОТО ЧЕРНОМОРСКО КРАЙБРЕЖИЕ

М. Станчева, Л. Македонски*, К. Пейчева

Департамент по химия, Медицински университет, 9002 Варна

Получена на 29 октомври 2012 г.; приета на 26 май 2013 г.

(Резюме)

В настоящата работа са определени концентрациите на някои тежки метали (Cd, Ni, Cr, As, Hg, Cu, Fe, Mn, Pb and Zn) в едливите части на пет най-разпространени рибни видове - лефер (*Pomatomus saltatrix*), кефал (*Mugil cephalus*), средиземноморски сафрид (*Trachurus mediterraneus ponticus*), карагьоз (*Alosa pontica*) и цаца (*Sprattus sprattus sulinus*), събирани на две станции по българското черноморско крайбрежие. Пробите са третираны с азотна киселина със следващо спектроскопско определяне (атомно-емисионна спектрометрия с индуцирана плазма (AES-ICP), пламъкова атомна абсорбционна спектрометрия (FAAS) или електротермична атомна абсорбционна спектрометрия (ETAAS). Нивото на арсена в едливите части на кефала (*Mugil cephalus*) показват стойности, по-високи от допустимите според различните здравни организации (1.1 ± 0.1 mg/kg). Този рибен вид натрупва в по-ниска степен други изследвани метали, като Hg, Zn, Fe и Pb. Концентрациите на Zn и Fe показват най-високи стойности за всички рибни видове. С някои изключения концентрациите на изследваните тежки метали са в границите на приемливите нива за храна за консумация.

BULGARIAN CHEMICAL COMMUNICATIONS

Instructions about Preparation of Manuscripts

General remarks: Manuscripts are submitted in English by e-mail or by mail (in duplicate). The text must be typed double-spaced, on A4 format paper using Times New Roman font size 12, normal character spacing. The manuscript should not exceed 15 pages (about 3500 words), including photographs, tables, drawings, formulae, etc. Authors are requested to use margins of 3 cm on all sides. For mail submission hard copies, made by a clearly legible duplication process, are requested. Manuscripts should be subdivided into labelled sections, e.g. **Introduction, Experimental, Results and Discussion, etc.**

The title page comprises headline, author's names and affiliations, abstract and key words.

Attention is drawn to the following:

a) **The title** of the manuscript should reflect concisely the purpose and findings of the work. Abbreviations, symbols, chemical formulas, references and footnotes should be avoided. If indispensable, abbreviations and formulas should be given in parentheses immediately after the respective full form.

b) **The author's** first and middle name initials, and family name in full should be given, followed by the address (or addresses) of the contributing laboratory (laboratories). **The affiliation** of the author(s) should be listed in detail (no abbreviations!). The author to whom correspondence and/or inquiries should be sent should be indicated by asterisk (*).

The abstract should be self-explanatory and intelligible without any references to the text and containing not more than 250 words. It should be followed by key words (not more than six).

References should be numbered sequentially in the order, in which they are cited in the text. The numbers in the text should be enclosed in brackets [2], [5, 6], [9–12], etc., set on the text line. References, typed with double spacing, are to be listed in numerical order on a separate sheet. All references are to be given in Latin letters. The names of the authors are given without inversion. Titles of journals must be abbreviated according to Chemical Abstracts and given in italics, the volume is typed in bold, the initial page is given and the year in parentheses. Attention is drawn to the following conventions:

a) The names of all authors of a certain publications should be given. The use of “*et al.*” in

the list of references is not acceptable.

b) Only the initials of the first and middle names should be given.

In the manuscripts, the reference to author(s) of cited works should be made without giving initials, e.g. “Bush and Smith [7] pioneered...”. If the reference carries the names of three or more authors it should be quoted as “Bush *et al.* [7]”, if Bush is the first author, or as “Bush and co-workers [7]”, if Bush is the senior author.

Footnotes should be reduced to a minimum. Each footnote should be typed double-spaced at the bottom of the page, on which its subject is first mentioned.

Tables are numbered with Arabic numerals on the left-hand top. Each table should be referred to in the text. Column headings should be as short as possible but they must define units unambiguously. The units are to be separated from the preceding symbols by a comma or brackets.

Note: The following format should be used when figures, equations, *etc.* are referred to the text (followed by the respective numbers): Fig., Eqns., Table, Scheme.

Schemes and figures. Each manuscript (hard copy) should contain or be accompanied by the respective illustrative material as well as by the respective figure captions in a separate file (sheet). As far as presentation of units is concerned, SI units are to be used. However, some non-SI units are also acceptable, such as °C, ml, l, etc.

The author(s) name(s), the title of the manuscript, the number of drawings, photographs, diagrams, etc., should be written in black pencil on the back of the illustrative material (hard copies) in accordance with the list enclosed. Avoid using more than 6 (12 for reviews, respectively) figures in the manuscript. Since most of the illustrative materials are to be presented as 8-cm wide pictures, attention should be paid that all axis titles, numerals, legend(s) and texts are legible.

The authors are asked to submit **the final text** (after the manuscript has been accepted for publication) in electronic form either by e-mail or mail on a 3.5” diskette (CD) using a PC Word-processor. The main text, list of references, tables and figure captions should be saved in separate files (as *.rtf or *.doc) with clearly identifiable file names. It is essential that the name and version of

the word-processing program and the format of the text files is clearly indicated. It is recommended that the pictures are presented in *.tif, *.jpg, *.cdr or *.bmp format, the equations are written using "Equation Editor" and chemical reaction schemes are written using ISIS Draw or ChemDraw programme.

The authors are required to submit the final text with a list of three individuals and their e-mail addresses that can be considered by the Editors as potential reviewers. Please, note that the reviewers should be outside the authors' own institution or organization. The Editorial Board of the journal is not obliged to accept these proposals.

EXAMPLES FOR PRESENTATION OF REFERENCES

REFERENCES

1. D. S. Newsome, *Catal. Rev.–Sci. Eng.*, **21**, 275 (1980).
2. C.-H. Lin, C.-Y. Hsu, *J. Chem. Soc. Chem. Commun.*, 1479 (1992).
3. R. G. Parr, W. Yang, *Density Functional Theory of Atoms and Molecules*, Oxford Univ. Press, New York, 1989.
4. V. Ponec, G. C. Bond, *Catalysis by Metals and Alloys* (Stud. Surf. Sci. Catal., vol. 95), Elsevier, Amsterdam, 1995.
5. G. Kadinov, S. Todorova, A. Palazov, in: *New Frontiers in Catalysis* (Proc. 10th Int. Congr. Catal., Budapest, 1992), L. Guzzi, F. Solymosi, P. Tetenyi (eds.), Akademiai Kiado, Budapest, 1993, Part C, p. 2817.
6. G. L. C. Maire, F. Garin, in: *Catalysis. Science and Technology*, J. R. Anderson, M. Boudart (eds), vol. 6, Springer-Verlag, Berlin, 1984, p. 161.
7. D. Pocknell, *GB Patent 2 207 355* (1949).
8. G. Angelov, PhD Thesis, UCTM, Sofia, 2001.
9. JCPDS International Center for Diffraction Data, Power Diffraction File, Swarthmore, PA, 1991.
10. *CA* **127**, 184 762q (1998).
11. P. Hou, H. Wise, *J. Catal.*, in press.
12. M. Sinev, private communication.
13. <http://www.chemweb.com/alchem/articles/1051611477211.html>.

CONTENTS

<i>S. Stanchev, I. Manolov</i> , Aldol condensation of 3-acetylcoumarin derivatives and extraordinary side reactions ...	5
<i>Raghavendra Rao, K. Ramakrishna Reddy, K.N. Mahendra</i> , Synthesis, characterization, antibacterial, antifungal and anthelmintic activities of a new 5 - nitroisatin Schiff base and its metal complexes.....	11
<i>A. Gharib, N. Noroozi Pesyan, L. Vojdani Fard, M. Roshani</i> , Silica-bonded N-propyl sulfamic acid: a recyclable catalyst for microwave-assisted synthesis of various dihydropyrano[3,2-c]chromenes	18
<i>S.S. Muvvala, V.N. Ratnakaram</i> , Antibacterial activity of some newer 1,2,3 – benzotriazole derivatives synthesized by ultrasonication in solvent – free conditions	25
<i>S. Ali Beyramabadi</i> , DFT Study on the Fe, Cu and Zn Complexes of 4-(2-Thiazolylazo) Resorcinol	31
<i>F. Jafari, S. Khodabakhshi</i> , MnSO ₄ .H ₂ O: A highly efficient and inexpensive catalyst for the synthesis of benzo-2-pyrones and benzopyrazines	36
<i>H. Moghanian, A. Mohamadi</i> , Imine-enamie tautomerism in bicyclic systems in gas phase and solution: a computational study	43
<i>L. V. Kabaivanova, G. E. Chernev, P. V. Markov, I. M. Miranda Salvado</i> , Hybrid materials parameters influencing the enzyme activity of immobilized cells	50
<i>R. Harizanova, L. Vladislavova, C. Bocker C. Rüssel, I. Gugov</i> , Phase composition and microstructure of sodium - alumoborosilicate glasses and glass-ceramics in the system Na ₂ O/BaO/TiO ₂ /Al ₂ O ₃ /B ₂ O ₃ /SiO ₂ /Fe ₂ O ₃ ..	56
<i>M. Hadzhilazova, J.-F. Ganghoffer</i> , Membrane fusion based on the stalk model	62
<i>J. Mouhovski, O. Vitov, V. Dimov, B. Kostova, S. Gechev</i> , High vacuum phase transformation of fluorspar vapors to crystal aggregates	68
<i>A. Bamoniri, B. F. Mirjalili, S. Nazemian, N. Yaghmaeiyan Mahabadi</i> , Nano silica phosphoric acid as an efficient catalyst for one-pot synthesis of 2,4,5-tri-substituted imidazoles under solvent free condition	79
<i>N.S. Dighe, R.B. Saudagar, D.A. Jain</i> , Design, synthesis and pharmacological screening of some [3-benzoyl-5-(4-substituted)-2, 3-dihydro-1,3,4-oxadiazol-2-yl] and [5-(4-substituted)-4H-1, 2, 4-triazol-3-yl] derivatives	85
<i>M. Montazerzohori, H. Tavakol, S. Kheiri, S. A. Musavi and S. Joohar</i> , Synthesis, spectral characterization and theoretical investigation of some new mercury four coordinated complexes	96
<i>S. Atashrouz, H. Mirshekar</i> , Phase equilibrium modeling for binary systems containing CO ₂ using artificial neural networks	104
<i>D. Tekin, S. Yörük and Y. K. Bayhan</i> , The Effect of Temperature on Rate of Bacterial Oxidation of Fe(II).....	117
<i>Bl. V. Itoua, C. Vladov, P. Ongoka, L. Petrov</i> , Hydrodesulfurization of thiophene on the CoMo/Al ₂ O ₃ catalyst modified by coking pretreatment.....	120
<i>S.R. Pattan, P.V. Patel, G.S. Athare, A.B. Jagnar, S.A. Nirmal, J.S.Pattan</i> , Synthesis and evaluation of some substituted pyrazole derivatives of biological interest	125
<i>B. Mikhova, V. Janevska, B. Stamboliyska, G. Draeger, E. Popovski</i> , Synthesis and structure of some novel dicoumarinamines	135
<i>P. L. Meena, N. Kumar, A. S. Meena, K. S. Meena</i> , Comparative Studies on Russell-Saunders Atomic Term Symbols (Terms) for Equivalent Electrons of nf ⁴ and nf ¹⁰ Configurations	141
<i>G. A. Hodjaoglu, I. S. Ivanov</i> , Metal recovery of solid metallurgical wastes. Galvanostatic electroextraction of copper from sulphate electrolytes containing Zn ²⁺ and Fe ²⁺ ions	150
<i>B. Tsyntsarski, B. Petrova, T. Budinova, N. Petrov, A. Sarbu, T. Sandu, M. Ferhat Yardim, A. Sirkecioglu</i> , Removal of detergents by zeolites and membranes	157
<i>A. Gharib, B. R. Hashemipour Khorasani, M. Jahangir, M. Roshani, L. Bakhtiari, S. Mohadeszadeh</i> , Synthesis of 2,4,5-trisubstituted and 1,2,4,5-tetrasubstituted-1H-imidazole derivatives and or 2,4,5-Triaryloxazoles using of Silica-Supported Preyssler Nanoparticles.....	165
<i>D. Sharma, S. Kumar</i> , A facile synthesis of 1-(2, 4-dihydroxyphenyl)-3-aryl-propane-1,3-diones via Baker-Venkataraman rearrangement under solvent free conditions at room temperature	175
<i>B. H. Zaware, S. R. Kuchekar</i> , Kinetic study for formation of thiazole by cyclisation	180
<i>S. Uzunova, D. Angelova, B. Anchev, I. Uzunov, A. Gigova</i> , Changes in structure of solid pyrolysis residue during slow pyrolysis of rice husk	184
<i>H.-L. Huang, F. Liu, J. Chen, G.-L. Huang</i> , Liquid-phase synthesis of N,N ² -diacetyl-β-chitobiosyl allosamizoline	192
<i>M. Stancheva, L. Makedonski, K. Peycheva</i> , Determination of heavy metal concentrations of most consumed fish species from Bulgarian Black Sea coast	195
INSTRUCTIONS TO THE AUTHORS.....	204

СЪДЪРЖАНИЕ

<i>Ст. Станчев, И. Манолов</i> , Алдолна кондензация на производни на 3-ацетилкумарина с неочаквани странични реакции.....	10
<i>Р. Рао, К.Р. Реди, К.Н. Махендра</i> , Синтеза, охарактеризиране, антибактериални, противогъбични и антихелминтни свойства на 5-нитроизатин шифова база и нейните комплекси.....	17
<i>А. Гариб, Н. Норузи Песян, Л. Вождани Фард, М. Рошани</i> , N-пропил-сулфаминова киселина върху носител от силициев диоксид: рециклируем катализатор за синтези на различни дихидропропанол [3,2-с] – хромени при микровълново лъчение.....	24
<i>С.С. Муввала, В.Н. Ратнакар</i> , Антибактериална активност на някои нови производни на 1,2,3 – бензотриазола, синтезирани при ултразвуково въздействие без разтворители.....	30
<i>С. Али Бейрамабади</i> , DFT-изследване на комплексите на желязото, медта и цинка с 4-(2-тиазолилазо)резорцинол.....	35
<i>Ф. Джафари, С. Ходабахши</i> , MnSO ₄ .H ₂ O: високоефективен и евтин катализатор за синтеза на бензо-2-пирони и бензопиразини.....	42
<i>Х. Моганиан, А. Мохамеди</i> , Имино-енаминна тавтомерия при би-циклични системи в газова фаза: изчислително изследване.....	49
<i>Л. В. Кабаиванова, Г. Е. Чернев, П. В. Марков, И. М. Миранда Салвадо</i> , Параметри на хибридни материали, влияещи върху ензимната активност на имобилизирани клетки.....	55
<i>Р. Харизанова, Л. Владиславова, Кр. Бокър, Кр. Рюсел, И. Гугов</i> , Фазов състав и микроструктура на натриево-алумоборосиликатни стъкла и стъклокерамики в системата Na ₂ O/VaO/TiO ₂ /Al ₂ O ₃ /V ₂ O ₃ /SiO ₂ /Fe ₂ O ₃	61
<i>М. Хаджилазова, Ж.-Фр. Гангхофер</i> , Стеблови модел на сливане на мембрани.....	67
<i>Й. Муховски, О. Витов, В. Димов, Б. Костова, С. Гечев</i> , Високовакуумни фазови превръщания на флуоритови пари в кристални агрегати.....	78
<i>А. Бамонири, Б.Ф. Мирджалили, С. Наземиан, Н.Я. Махабади</i> , Нано-силициево-фосфорна киселина като ефективен катализатор при едностепенната синтеза на 2,4,5-три-заместени имидазоли в отсъствие на разтворител.....	84
<i>N.S. Dighe, R.B. Saudagar, D.A. Jain</i> , Design, synthesis and pharmacological screening of some [3-benzoyl-5-(4-substituted)-2, 3-dihydro-1,3,4-oxadiazol-2-yl] and [5-(4-substituted)-4H-1, 2, 4-triazol-3-yl] derivatives.....	95
<i>М. Монтезрозохори, Х. Тавакол, С. Хеури, С.А. Мусави, С.Джухари</i> , Синтеза, спектрално охарактеризиране и теоретично изследване за някои живачни комплекси с координационно число четири.....	103
<i>С.Аташруз, Х. Мишекар</i> , Моделиране чрез изкуствени невронни мрежи на бинарни системи, съдържащи въглероден диоксид.....	116
<i>Д. Текин, С. Йорюк, Й.К. Байхан</i> , Влияние на температурата върху скоростта на бактериално окисление на Fe(II).....	119
<i>Бл. В. Итѝа, Ч. Владов, П. Онгока, Л. Петров</i> , Хидроочистка на тиофен върху CoMo/Al ₂ O ₃ катализатор, модифициран чрез предварителна коксуваща обработка.....	124
<i>S.R. Pattan, P.V. Patel, G.S. Athare, A.B. Jagnar, S.A. Nirmal, J.S.Pattan</i> , Synthesis and evaluation of some substituted pyrazole derivatives of biological interest.....	134
<i>В. Mikhova, V. Janevska, B. Stamboliyska, G. Draeger, E. Popovski</i> , Synthesis and structure of some novel dicoumarinamines.....	140
<i>P. L. Meena, N. Kumar, A. S. Meena, K. S. Meena</i> , Comparative Studies on Russell-Saunders Atomic Term Symbols (Terms) for Equivalent Electrons of nf ⁴ and nf ¹⁰ Configurations.....	149
<i>Г. А. Ходжаоглу, Ив. С. Иванов</i> , Извличане на метали от твърди металургични отпадъци. Галваностатична електроекстракция на мед от сулфатни електролити, съдържащи Zn ²⁺ и Fe ²⁺ йони.....	156
<i>Б. Цинцарски, Б. Петрова, Т. Будинова, Н. Петров, А. Сарбу, Т. Санду, М. Ферхат Ярдим, А. Серкичиоглу</i> , Извличане на детергенти чрез зеолити и мембрани.....	164
<i>А. Гариб, Б.Х. Хашемипур Хорасани, М. Джахангир, М. Рошаниа, Л. Бахтиари, С. Мохадесзаде</i> , Синтеза на 2,4,5-тризаместени и 1,2,4,5-четиризаместени-1H-имидазолви производни и/или 2,4,5-триарилоксазоли с помощта на наночастици от Preyssler'ов катализатор върху подложка от силициев диоксид.....	174
<i>Д. Шарма, С. Кумар</i> , Проста синтеза на 1-(2,4-дихидроксифенил)-3-арил-пропан-1,3-диони чрез прегрупиране на Baker-Venkataraman при обикновени температури без разтворител.....	179
<i>Б.Х. Зауаре, С.Р. Кучекар</i> , Кинетично изследване на образуването на тиазол чрез циклизация.....	183
<i>С. Узунова, Д. Ангелова, Б. Анчев, И. Узунов, А. Гигова</i> , Изменения в структурата на твърдите остатъци от бавната пиролиза на оризови люспи.....	191

<i>Х.-Л. Хуанг, Ф. Луу, Дж. Чен, Г.-Л. Хуанг, Течнофазна синтеза на N,N'-диацетил- β - хитобиозил алозамизолин</i>	194
<i>М. Станчева, Л. Македонски, К. Пейчева, Определяне на концентрациите на тежки метали в най-консумираните рибни видове в българското черноморско крайбрежие</i>	203
<i>ИНСТРУКЦИЯ ЗА АВТОРИТЕ</i>	204